1995
XVI Brazilian National Meeting on Particles and Fields

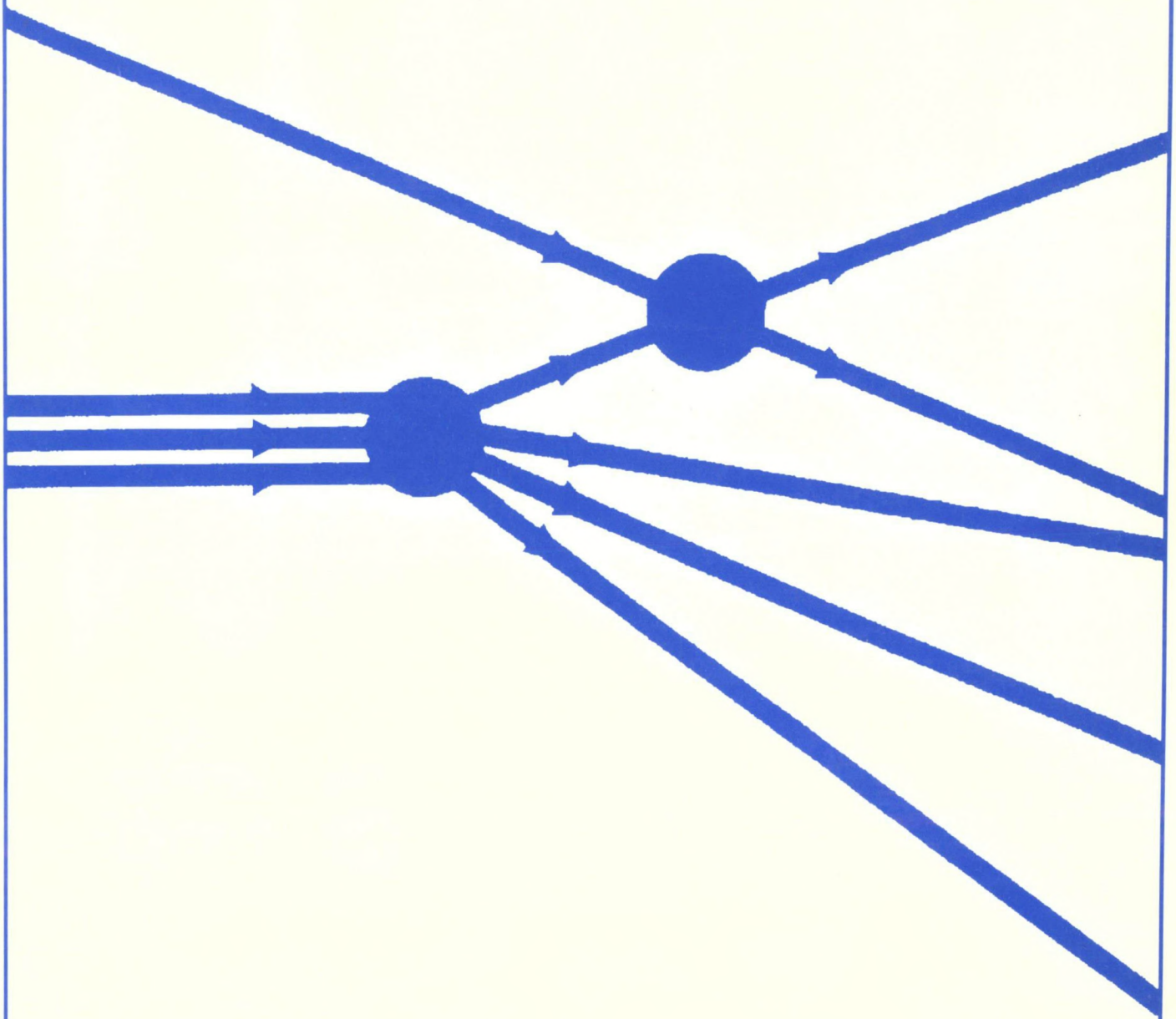

SBF
SOCIEDADE BRASILEIRA DE FÍSICA

XVI Encontro Nacional de Física de Partículas e Campos

(XVI Brazilian National Meeting on Particles and Fields)

October 24–28, 1995

Caxambu, Brazil

Editors

G. A. Alves, CBPF
F. T. Brandt, IFUSP
H. O. Girotti, UFRGS
V. Rivelles, IFUSP
M. E. de Araújo, UnB
C. O. Escobar, IFUSP
M. Gleiser, Dartmouth
A. Santoro, CBPF
N. R. F. Braga, UFRJ
E. Ferreira, UFRJ
M. Novello, CBPF
J. W. F. Valle, IFIC

Sociedade Brasileira de Física

The Brazilian National Meeting on Particles and Fields

High Energy Physics is one of the most traditional areas of research in Physics in Brazil. It started in the 30's with the important contribution of G. Wataghin and the next generations, which included J. Tiomno, J. Leite Lopes, C. M. G. Lattes, J. A. Swieca, J. J. Giambiagi and G. Bollini.

The Brazilian National Meeting on Particles and Fields (Encontro Nacional de Física de Partículas e Campos) is a scientific meeting held every year that assembles the Brazilian Physics community working in Field Theory, Cosmology and Gravitation, Particle Physics Phenomenology, and Experimental High Energy Physics. The most important aim of this meeting is to enable the interchange of information among the whole community through invited review talks of wide interest. An overview of the research in the area is achieved through the presentation of short communications of the submitted papers and the panel session.

The first of these meetings was held in 1978 and had about 80 participants. In the following years this number has grown considerably and in 1995 we have more than 300 participants, including Master and Ph.D. graduated students, and 215 submitted papers.

The meeting is organized under the auspices of Sociedade Brasileira de Física (SBF) with the support of Coordenação de Aperfeiçoamento de Pessoal de Nível Superior (CAPES), Centro Latino–Americano de Física (CLAF), Conselho Nacional de Desenvolvimento Científico e Tecnológico (CNPq), Fundação de Amparo à Pesquisa do Estado de São Paulo (FAPESP), do Rio de Janeiro (FAPERJ), do Rio Grande do Sul (FAPERGS), and Financiadora de Estudos e Projetos (FINEP).

We would like to thank the SBF staff for all their efforts, in particular to Neusa M. L. Martin for organizing these Proceedings.

June 1996

The Organizing Committee

ÍNDICE

PALESTRAS DE REVISÃO E SEMINÁRIOS

CONTRIBUIÇÕES CIENTÍFICAS

A. COSMOLOGIA E GRAVITAÇÃO

B. FÍSICA EXPERIMENTAL DE ALTAS ENERGIAS

C. FENOMENOLOGIA DE PARTÍCULAS ELEMENTARES

D. TEORIA DE CAMPOS

The Top Quark and More: Some Highlights of Physics from the DØ Experiment

Hugh E. Montgomery*
Fermi National Accelerator Laboratory
P.O. Box 500
Batavia, Il 60510, U.S.A

Representing the DØ Collaboration

Received March, 1996

In this paper we describe some highlights of recent physics results from the DØ experiment at the Tevatron $\bar{p}p$ collider. One aspect of recent QCD experimentation has been the emphasis on studies of events with rapidity gaps; the characteristics of such events in the DØ data are described. The non-abelian nature of the electroweak interaction is a well defined property of the standard model. The very high energies available at the Tevatron have opened a new window which permits the testing of this aspect of the standard model. *THE* highlight among recent results was the observation of the top quark and this result is discussed. At the highest energy available, DØ is conducting numerous searches for phenomena which might indicate the structure of the world beyond the electroweak scale. We discuss searches for the sparticles of supersymmetry. The luminosity of the collider will increase dramatically over the next five years. This will open new fields of investigation for an upgraded DØ detector.

This paper is a description, necessarily brief, of a very few selected topics pertaining to the physics results and the future program of the DØ experiment. It is neither intended to review those results exhaustively[1] nor to make any comparison with results from the other Tevatron Collider experiment, CDF[2]. No attempt is made to update the content for information which has become public since the conference. Nevertheless, I hope that I convey some measure of the excitement of an experiment on the discovery frontier.

DØ is a large international collaboration of more than 400 physicists from 44 institutions worldwide including two Brazilian institutions and three other South American institutions. The DØ detector[3] is shown in Fig. 1. A compact central tracking system is surrounded by a highly segmented liquid Argon and depleted Uranium calorimeter. The calorimeter is in turn surrounded by a muon detection system of solid iron toroids and chambers which together provide identification of muons and a measure of their momenta. Electrons are distinguished from hadrons primarily by the shape of the energy deposition, both in depth and breadth, in the calorimeter and from photons by the presence of an associated track. The acceptance in pseudorapidity extends beyond $\eta = \pm 3$ for the leptons and hadrons. This makes the determination of the missing transverse energy, through the energy imbalance, rather good. It is from this measurement that the transverse energy of a neutrino may be inferred. The detector is thus capable of detecting and measuring the relevant parameters of all the objects resulting from high energy interactions.

In this paper we will first very briefly summarise measurements of the b quark production cross-section. This subject is covered in an extensive parallel session paper at this conference. As an example of an advanced QCD analysis we describe a measurement of events with substantial regions of rapidity in which there are *no* particles. Such events have generated interest in the last couple of years both in hadron-hadron collisions and in lepton-hadron collisions. We then discuss diboson production which permits the investigation of the couplings of gauge bosons

*Presented at the XVI Encontro Nacional de Física de Partículas e Campos, Caxambu, MG, Brazil, Outubro 24-28, 1995.

and in which we have demonstrated the non-abelian nature of the electroweak interaction. In 1995 it would be a sin to omit a description of the observation of the sixth and possibly last quark. The standard model is not thought to be the ultimate description of nature. At DØ we have a program of searches for indications of physics beyond such confines and we will describe a small selection. Finally we will briefly indicate the directions and sensitivities that can be expected from an upgraded detector running with the Tevatron at much higher luminosity in the Main Injector era.

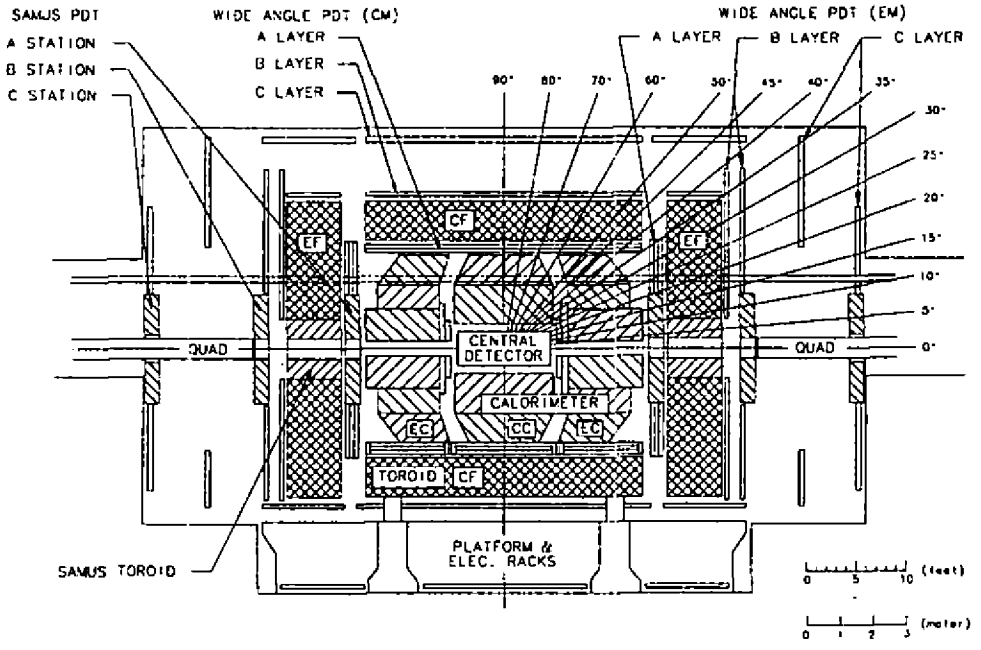

Figure 1. The DØ Detector in a side view showing the location of the component systems.

I Strong Interactions and *b* Quark Production

The strong interaction is probed in $\overline{p}p$ colliders using many different experimental techniques involving the detection of the different species of quarks and of gluons or generic jets with different multiplicities, or of gauge bosons such as photon or W and Z boson. We confine ourselves to two aspects here.

I.1 *b* Quark Production

DØ has measured the b quark production cross-section using a number of methods[1, 4, 5]. In general we have used final state muons, in or near jets to indicate the presence of b jets. Backgrounds from π and K decay, and from charm quarks are controlled by the intrinsic properties of the detector and by cuts on the relative kinematics of the detected muons and jets. The subject was covered in considerable detail by Gilvan Alves[5] in a major parallel session presentation at this conference. A comparison of different measurements with the theoretical expectations is given in Figure 2. The data lie somewhat above the central expectations of the theory, but not incompatibly so. The uncertainties on the latter are indicated by the dashed lines.

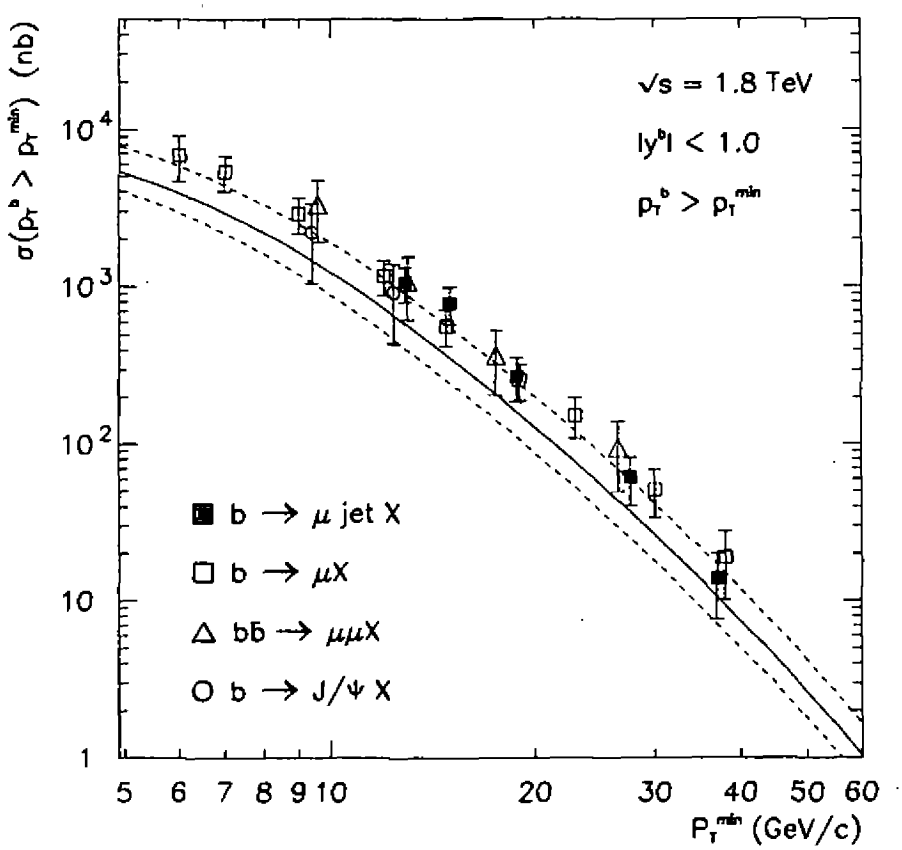

Figure 2: b-quark production cross sections for $| y^b | < 1$ from the inclusive muon, muon plus jet, dimuon and J/ψ data samples.

I.2 Color Singlet Exchange

In this analysis[6, 7] we measure strongly interacting color singlet exchange by tagging events with a low multiplicity of particles between jets. Few particles are expected in the space between the leading jets in color singlet events. In contrast the presence of a color string connecting the scattered partons in color octet events (gluon exchange) gives rise to a smooth distribution of particles between the leading jets. In QCD the absence of particles as a result of strong color singlet exchange is a manifestation of the destructive interference between the emissions of gluons from two colored objects, the gluon components of the pomeron.

Two different data sets were used to study this effect: one selected events with the two jets on opposite sides, in η, of the calorimeter ($\eta_1 \cdot \eta_2 < 0$) while the other selected events with jets on the same side ($\eta_1 \cdot \eta_2 > 0$). The same side sample is expected to be dominated by color octet exchange and is used as a control. Figure 3 shows the number of electromagnetic calorimeter towers above threshold (n_{cal}) versus the number of central drift chamber tracks (n_{trk}) for the (a) opposite side and (b) same side samples. Each of these measures is sensitive to a different fraction of the total particles produced. The two distributions are similar in shape except at very low multiplicities, where the opposite side sample has a striking excess of events in the region where the multiplicity of both electromagnetic calorimeter cells, and tracks is close to zero. One can perform fits in one or other of these variables. Except for the lowest bins, the multiplicities are well described by negative binomial distributions, or modified negative binomial distributions. In the opposite side sample there is an excess in the low multiplicities consistent with the existence

of a color singlet exchange process. We measure the fractional excess of color singlet above color octet exchange to be 1.07 ± 0.10 (stat) $^{+0.25}_{-0.13}$ (syst)%. The probability of such an excess has been estimated for both electroweak and strong color singlet (pomeron) exchange. The former is expected to be at a level much below that observed. On the other hand, the estimations for pomeron exchange are at approximately the level observed.

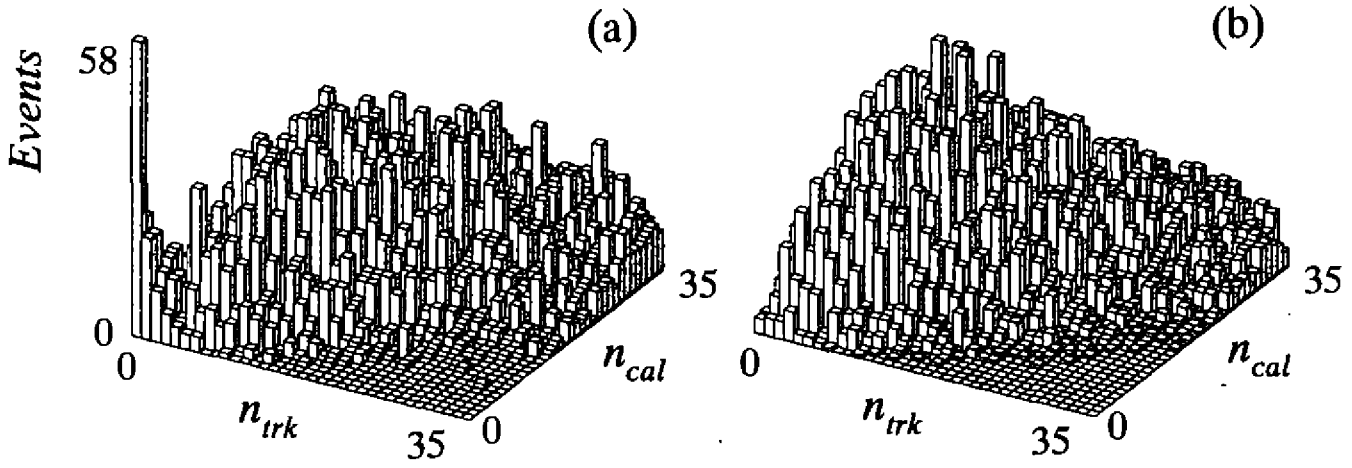

Figure 3: The calorimeter tower multiplicity (n_{cal}) vs. the charged track multiplicity (n_{trk}) in the pseudorapidity region $|\eta| < 1.3$ for the (a) opposite-side and (b) same-side samples described in the text.

II Electroweak Interactions: The Boson Couplings

Tests of the electroweak sector of the Standard Model have concentrated on the consistency between, and the radiative corrections to, the basic parameters of the model. One aspect which has received relatively little attention until recently is the examination of the vertex functions, the couplings between the vector bosons themselves. The very fact of their mutual interaction is a feature of the non-abelian nature of the theory which in turn is related to its local gauge invariance. A straightforward way to examine such interactions is through the production of pairs of gauge bosons. Given the high masses of the W and Z, there is a premium on high energy. Consequently the advances from the Tevatron data have been remarkable.

II.1 Diboson production

In the standard electroweak model, the self-couplings of the W, Z, and γ bosons are completely specified and so consequently, are the gauge boson pair production cross sections. $W\gamma$[8], $Z\gamma$[9], WW[10] and WZ[11] production have all been studied by DØ . The ZZ production cross section is extremely small.

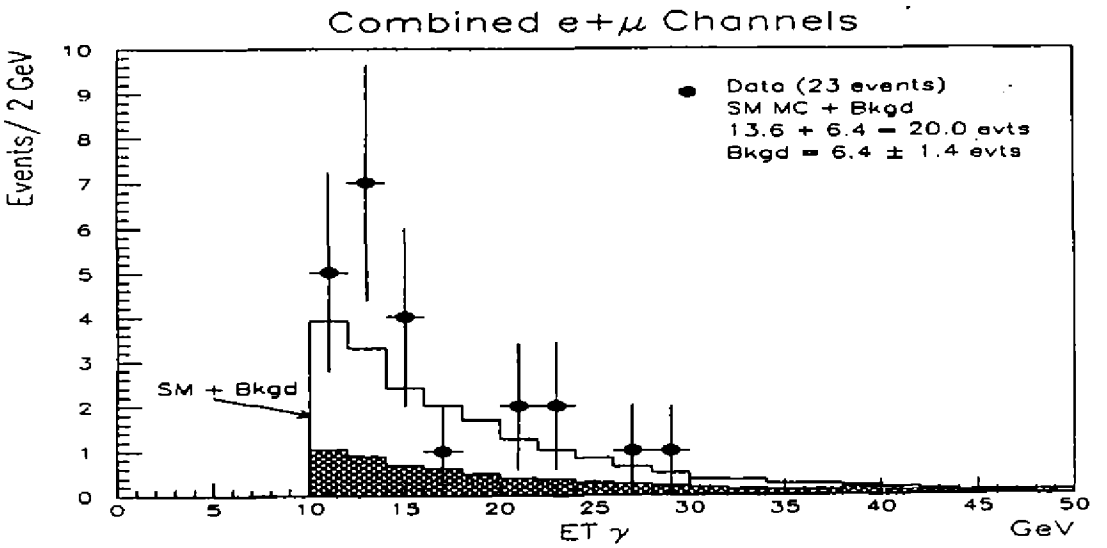

Figure 4: Transverse energy spectrum of the photon produced in $p\bar{p} \to W\gamma + X \to \ell\nu\gamma + X$, $\ell = e, \mu$. The points are data, the shaded area represents the estimated background, and the solid histogram is the sum of the SM prediction and estimated background.

The production mechanisms include both t-channel quark exchange diagrams and the direct s-channel diagram with a third virtual vector boson in that channel. The latter diagram involves the trilinear vector boson couplings. Deviation from the standard model predictions could imply new physics entering through loop corrections to this vertex. Any non-Standard Model contributions to the $WW\gamma$ vertex, can be interpreted as an anomalous contribution to the electromagnetic dipole and quadrupole moments of the W. This is analogous to the contributions to $g-2$ of the muon from the "new physics" in the weak and hadronic loop diagrams.

A useful feature from the experimental point of view is that any anomalous couplings enter quadratically in the expression for the cross section and hence would lead to an increase in the cross section. A limit measurement therefore necessarily constrains the anomalous components. In addition the enhancement occurs with a weaker dependence on p_T than the standard form so that examination of the p_T dependence of any observed signal provides further discrimination.

Generally, each trilinear vertex can be described by a set of four coupling constants. The $WW\gamma$ (WWZ) couplings are usually referred to as $\kappa_{\gamma(Z)}$, $\lambda_{\gamma(Z)}$, $\tilde{\kappa}_{\gamma(Z)}$, $\tilde{\lambda}_{\gamma(Z)}$, with the first two couplings being CP-conserving and the other two being CP-violating. For $ZZ\gamma$ ($Z\gamma\gamma$) vertices the corresponding couplings are denoted $h_i^{Z(\gamma)}$, $i = 1...4$, with $h_{1,2}$ being CP-violating and $h_{3,4}$ CP-conserving. In the Standard Model $\kappa_{\gamma,Z} = 1$; all others are zero. The convention $\Delta\kappa = \kappa - 1$ will be used below.

The admission of non-standard values for the couplings is an ad hoc procedure and does not necessarily lead to a consistent theory. In particular, unless modifications through form factors with scale Λ are introduced, S-matrix unitarity is violated at high sub-process energies. A simplified way to look at the plotted unitarity bounds, Fig. 6, is to consider that if the measured limits fit within the bound for a higher Λ, they are more stringent than if they fit only within the bound for a smaller Λ. As the limits approach more closely the standard model values, the Λ scale, which can be accommodated, approaches infinity.

Using $W\gamma$ production data with both electron and muon decays of the W, the γ transverse energy distribution is shown in Fig. 4, there are 23 candidates and a background of 6.4 ± 1.4 events. The corresponding limits are shown in Fig. 5 for both 68% and 95% confidence level. The star indicates the expectation for purely electromagnetic coupling of the W and photon, and a gyromagnetic ratio of unity for the W boson. Thus, at 80% confidence level, the weak-electromagnetic unification of the couplings is required.

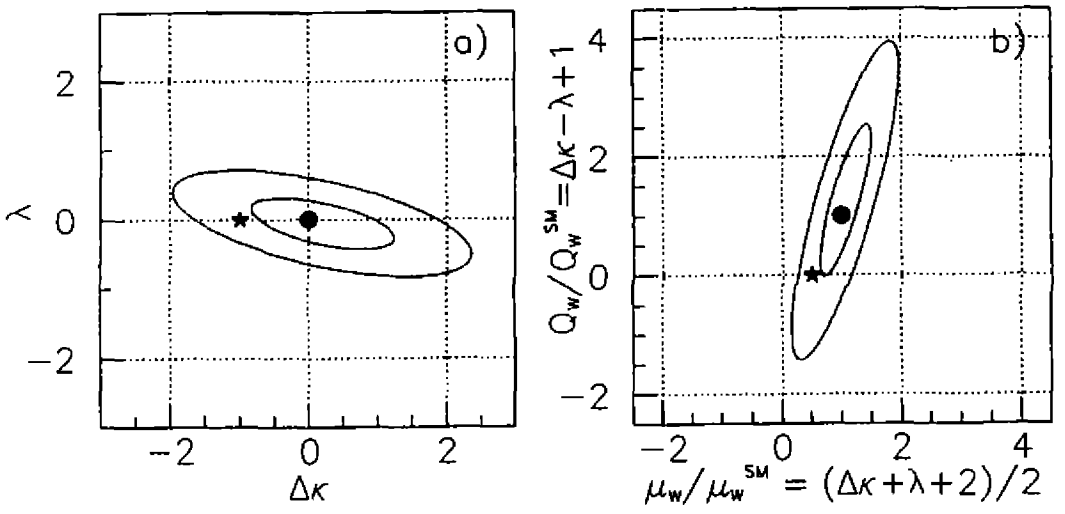

Figure 5: Limits on (a) *CP*-conserving anomalous coupling parameters $\Delta\kappa$ and λ, and on (b) the magnetic dipole μ_W and electric quadrupole Q_W^e moments of the W boson. The ellipses represent the 68% and 95% CL exclusion contours. The dot represents the SM values, while the star indicates the $U(1)_{EM-only}$ coupling of the W boson to a photon. Form-factor scale $\Lambda = 1.5$ TeV.

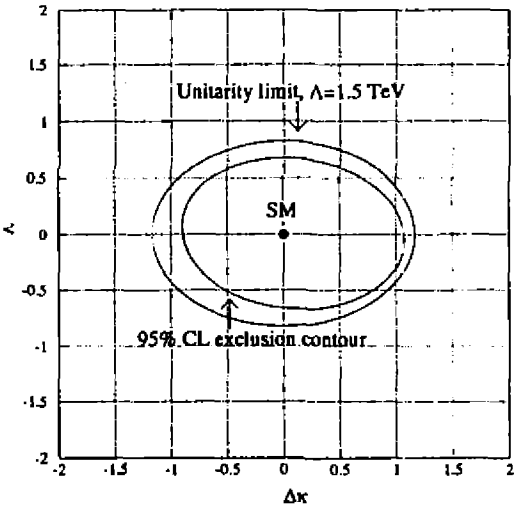

Figure 6: 95% CL limits on the *CP*-conserving anomalous couplings $\Delta\kappa$, λ assuming $\Delta\kappa_\gamma = \Delta\kappa_Z; \lambda_\gamma = \lambda_Z$ derived from $WW/WZ \to e\nu jj$. The dashed line shows the S-matrix unitarity limits. Form-factor scale $\Lambda = 1500$ GeV.

In the $Z - \gamma$ final state six events are observed with an expected background of 0.48 ± 0.06 events and a fit to the transverse momentum spectrum of the γ is used to obtain limits. For WW production only one candidate is observed with an expected background of 0.56 ± 0.13 events. Besides the lepton-only channels, one can look for the case where one of the bosons decays into a pair of hadronic jets. Again the transverse momentum of the objects is a key discriminator. The limits obtained are shown in Fig. 6. In this case a unitarity bound of 1.5 TeV can be accommodated by any values of the coupling constants in the allowed region.

The limits resulting from these analyses are collected in Table 1. The corresponding CP-violating limits in all the above analyses the limits are numerically the same. With this rather large number of independent measurements available, and with comparable sensitivity, the next step will be to combine the limits and obtain an overall constraint on the deviations of the couplings from the standard model expectations.

CP-conserving coupling limits		Channel
$-1.6 < \Delta\kappa_\gamma < 1.8$,	$-0.6 < \lambda_\gamma < 0.6$	($W\gamma$, $\Lambda = 1500$ GeV)
$-1.8 < h_{30}^Z < 1.8$,	$-0.5 < h_{40}^Z < 0.5$	($Z\gamma$, $\Lambda = 500$ GeV)
$-1.9 < h_{30}^\gamma < 1.9$,	$-0.5 < h_{40}^\gamma < 0.5$	($Z\gamma$, $\Lambda = 500$ GeV)
$-2.6 < \Delta\kappa_\gamma = \Delta\kappa_Z < 2.8$,	$-2.1 < \lambda_\gamma = \lambda_Z < 2.1$	($WW \to \ell^+\ell^-\nu\nu$, $\Lambda = 900$ GeV)
$-0.9 < \Delta\kappa_\gamma = \Delta\kappa_Z < 1.1$,	$-0.7 < \lambda_\gamma = \lambda_Z < 0.7$	($WW/WZ \to e\nu jj$, $\Lambda = 1500$ GeV)

Table 1: Limits on the *CP*-conserving couplings. Limits for the *CP*-violating couplings are the same within 5%.

Decay Mode	Number of Events	Background	Significance
Dilepton	3	0.65 ± 0.15	0.03 (1.9σ)
Lepton plus jets (topological)	8	1.9 ± 0.5	0.002 (2.9σ)
Lepton plus jets (b–tag)	6	1.2 ± 0.2	0.002 (2.9σ)
All	17	3.8 ± 0.6	2.0×10^{-6} (4.6σ)

Table 2: The number of events observed, background predicted, and the probability that the background fluctuated up to the observed data for each channel.

III The Top Quark

III.1 Observation of the Top Quark

In the spring of 1995, CDF[12] and DØ[13] published papers describing the observation of the top quark. The high top mass had retarded progress[14] but led to a clear experimental signature. Two large mass objects decay each into a W boson and a b quark. In turn, the former can decay either leptonically or hadronically, the latter results in a jet in which there may be an embedded muon as a result of the semi-leptonic decay of the b or its daughter c quark. If both W bosons decay leptonically a final state with two high p_T, isolated charged leptons and two jets results. If one of the W bosons decays hadronically there are 4 jets in the final state. The former case is generically labelled "dilepton", the latter "lepton plus jets". In both cases there is substantial missing transverse energy as a result of the presence of one or more neutrinos.

In the dilepton case the backgrounds are dominantly physics processes which can lead to the same final states. For example Z production leads to $\mu\mu$ and ee final states.

In the case of the lepton plus jets channels the dominant backgrounds are those with a real or false W boson and multiple jets. The false W boson is generated by mis-identification of one of the jets in a multi-jet event in conjunction with a mismeasurement of the missing transverse energy. To reduce the background two approaches are used.

One approach applies kinematic cuts to the observed events such as to reduce the W- plus-jets background while maintaining acceptance for top production. The event shape for top is typically spherical with all objects having large transverse momenta. The W-plus-jets background tends to derive several of its jets due to gluon radiation from a primary two parton final state configuration. The planar characteristics of that two-body state often survive, even after gluon radiation, since the radiated jets tend to be at low relative transverse momenta.

The second approach relies on the presence of two b jets in top events. The probability that a muon from either direct or cascade decays of one or other of these b jets exists is about 45% . The probability that the μ is detected in DØ is about 50% , so about 22% of top events should have an observed soft muon. In contrast, the probability that a generic mixture of jets will lead to the same is approximately 0.5% per jet (dependent on jet p_T). The jet μ tag rate has been measured using various samples of data and, at the level of precision needed, is independent of the data sample. It is therefore taken to be true for both the principle backgrounds, true and false W bosons with

multiple jets.

The observed numbers of events are summarized in Table 2. Also shown is the predicted background for each $t\bar{t}$ decay channel along with the probabilities for the predicted background to fluctuate up to account for the observed data. The combined probability that the observed events be a background fluctuation is

$$\mathcal{P} = 2.0 \times 10^{-6}.$$

The corresponding cross-section, for a top quark of mass m_t= 200 GeV/c^2, is $\sigma_{t\bar{t}} = 6.3 \pm 2.2$ pb. These results were based on an integrated luminosity of about 50 pb^{-1}.

III.2 Top Quark Mass

In the simplest situation the final state with $t\bar{t}$ consists of six final state fermions. There are therefore 18 momentum components to be determined. Under the $t\bar{t}$ production hypothesis there are two constraints from the known W masses and a further constraint from the equality of the masses of the t and $\bar{t}$. Provided that the different decay components are unambiguously identified, fifteen of the momentum components must be measured to completely describe the event. With more, a constrained fit for the mass of the top can be attempted.

III.2.1 The Lepton plus Jets Channel

In the lepton plus jets channel, an attempt is made to identify the the decay $t\bar{t} \rightarrow \ell\nu b\, q\bar{q}\bar{b}$. This demands at least four quark jets in the event. Complications can arise since primary quark jets may escape detection, be merged with other jets, or jets arising from gluon radiation may increase the jet multiplicity. The momenta of the four most energetic jets, the lepton, and the missing energy, for which we measure only the two transverse components, give a total of 17 measurements. If the b jets are not identified the number of possible permutations of assignments is twelve. Taking into account the ambiguity for the longitudinal momentum of the neutrino gives a total of 24 possible combinations for each event.

With the mass constraints, a fit to the $t\bar{t}$ system is performed. We apply a cutoff in the fit quality (χ^2); events which do not have a jet assignment combination with a χ^2 below the cutoff are dropped from the m_t results. Finally, the central mass is obtained from the weighted average of the best three χ^2 fits for each event. The result is termed the 'fitted mass'.

A number of template distributions from a $t\bar{t}$ Monte Carlo is generated for a range of top masses and for each distinct decay channel. A similar template is prepared for the background processes. All detector effects and biases from the fitting procedures are accounted for by the simulation. The top mass is then obtained using a likelihood fit of the signal and background templates to the observed distribution of fitted masses.

The result is:

$$m_t = 199^{+19}_{-21}(\text{stat})^{+14}_{-21}(\text{syst})\ \text{GeV/c}^2$$

Jet combinatorics contribute strongly to the bias in mapping between observed and true masses and also to the width of that distribution. This and other effects were extensively examined using Monte Carlo studies and are included in the systematic error assignment.

Figure 7(a) shows the fitted mass distribution for the DØ lepton plus jets events, taken with loose selection criteria. The histogram represents the fitted masses of the observed events, and the solid curve represents the background and the top Monte Carlo combined. Figure 7(a) is the distribution of central mass values, Fig. 7(b) shows the resulting likelihood fit, with an arrow indicating the best fit value. Note that the clear separation of background and signal events, permits a good top mass determination.

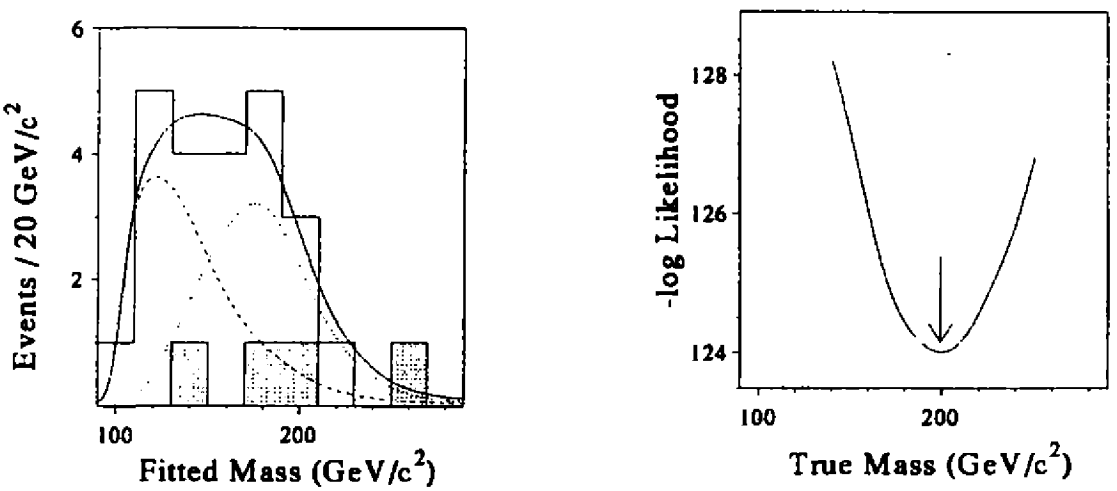

Figure 7: The fitted mass distribution (a) for events is shown as the line histogram, the dashed line is the background distribution and the dotted line is the best fit Monte Carlo fitted mass distribution. The solid line is the combination of the best fit Monte Carlo plus background. The shaded histogram represent events that were bottom quark tagged. The top mass is extracted from the fitted mass distribution using a likelihood method (b).

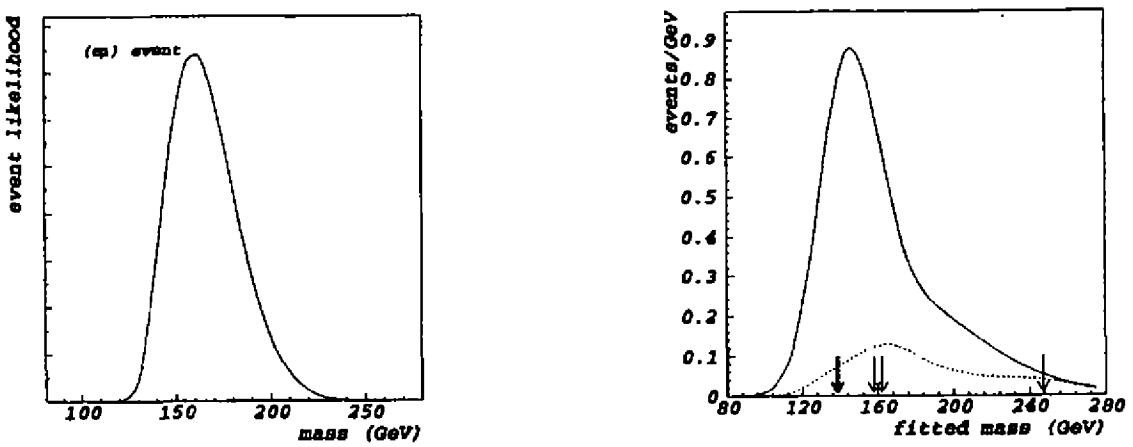

Figure 8: The dilepton mass fit method. The likelihood as a function of top mass for a particular event is shown in (a). The peak represents one of the arrows in (b), which is the fitted mass for all the dilepton events (arrows). The background fitted mass distribution is shown as the dashed line, and the best fit for background and Monte Carlo is shown as the solid line. The likelihood curve for the best mass has a broad minimum (not shown), leading to large errors on the mass.

III.2.2 The Dilepton Channel

The dilepton channel is more difficult as we have less information, an extra neutrino in the final state reduces the constraints by three. In order to provide additional information, a model of the initial state parton momentum distributions and the expected decay characteristics of the standard model top quark are used.

We use a method[15] inspired by Dalitz, Goldstein and Kondo[16], but which takes into account all the measured information and reduces the theoretical assumptions. For a given event a top quark mass is chosen and a weight is assigned based on known distributions of the transverse momentum of the lepton and the distribution functions for the valence quarks. The result is a likelihood curve for each event as a function of m_t, as shown in Figure 8(a). Analogously to the lepton plus jets analysis, the most likely value of mass is retained as a characteristic parameter for each event.

Templates for the distributions of most likely masses are prepared from $t\bar{t}$ Monte Carlo and background samples. The best true mass is extracted using a likelihood method analogous to that used in the lepton plus jets analysis. Figure 8(b) shows the resulting best fit, where the arrows denote the peak of each individual event's likelihood

curve, the dashed histogram is the background Monte Carlo distribution, and the solid is the fit for the best value of the true mass. The likelihood is broad, and gives the result:

$$m_t \approx 145 \text{ GeV/c}^2 \text{ (preliminary)}$$

The statistical error deduced by examining the behavior of Monte Carlo samples of the same size is 25 GeV/c^2 , the systematic error is approximately 20 GeV/c^2, dominated by jet energy resolutions.

IV Beyond the Standard Model: SUSY Searches

Although the standard model is a useful framework, the search for physics beyond the standard model is a necessity for the highest energy experiments.

Supersymmetric extensions of the standard model, which relate bosons and fermions, are theoretically attractive. However they lead to a second array of fundamental particles dubbed "sparticles" . In the *Minimal Supersymmetric Standard Model* , unstable sparticles must decay into a lighter sparticle (*plus other* ordinary particles); there must then be one sparticle which does not decay. This is referred to as the LSP. Most models have the $\tilde{Z}_1$ as the LSP.

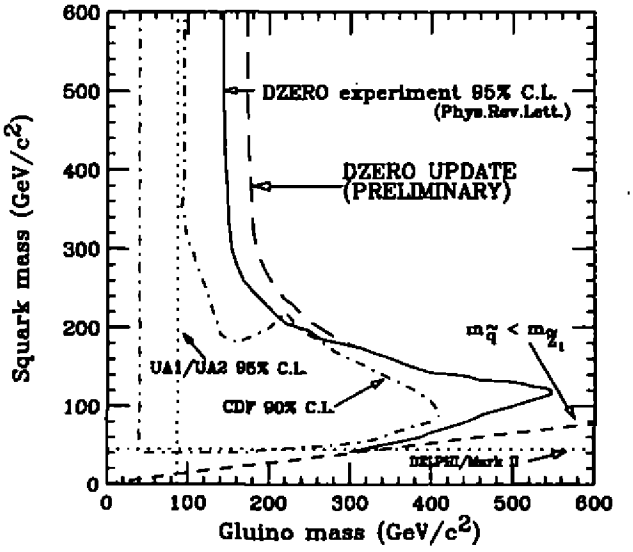

Figure 9: The squark and gluino mass limits. The long dashed line marks the *preliminary* DØ 95% confidence level excluded region from the combination of the three jet and four jet analyses. The solid line indicates the DØ three jet search result. The region below the dashed line labeled $m_{\tilde{q}} < m_{\tilde{Z}}$ is excluded since there the squark becomes lighter than the LSP. Other published limits from CDF, UA1, UA2, and DELPHI are displayed as well.

IV.1 Squarks and Gluinos

The most copiously produced SUSY particles should be squarks ($\tilde{q}$) and gluinos ($\tilde{g}$). In previous searches, the $\tilde{q}$ and $\tilde{g}$ were assumed to decay directly into quarks and the lightest supersymmetric particle. The event signature for which we have searched[17] is three or more jets and missing transverse energy ($\not\!\!E_T$). One measurement searched for events with three or more high E_T jets and very large $\not\!\!E_T$, and another for events with at least four jets but slightly less $\not\!\!E_T$.

The major backgrounds to these searches are vector boson production with associated jets and QCD events with mismeasured jet energies. After analysis cuts, 14 events survived in the three jet analysis and 5 events in the four jet sample.

Backgrounds from vector bosons plus jets backgrounds were estimated. The detector response was simulated using the DØ detector simulation program. A total of 14.2 ± 4.4 W/Z events are expected to pass the three jet

analysis cuts. For the four jet search, 5.5 ± 2.2 events are predicted. The contribution from multijet production was estimated using data from jet triggers. We predict 0.42 ± 0.37 events for the three jet analysis and 1.6 ± 0.9 events for the four jet search.

Since the number of events seen in the squark/gluino data sample is consistent with these standard model backgrounds no signal is observed. 95% CL lower mass limits of $m_{\tilde{g}} > 173$ GeV/c^2 for large squark mass, $m > 229$ GeV/c^2 for the case of equal mass squarks and gluinos, are obtained. The limits are shown in Fig. 9.

IV.2 The Top Squark

The squark/gluino search assumed that the squarks are mass degenerate. The large top mass can drive the mass of its SUSY partner, the top squark or stop ($\tilde{t}$) to lower masses than the other squarks. Mixing between the left- and right-handed top squarks can also leave one of the two $\tilde{t}$ lighter than the top quark itself. A light top squark mass is popular in view of recent measurements of the $Z \to b\bar{b}$ branching fraction at LEP[18].

The top squark[19] is expected to decay via $\tilde{t}_1 \to b\tilde{W}_1$. If $m_{\tilde{W}_1} > m_{\tilde{t}_1} + m_b$ the three-body decays $\tilde{t}_1 \to bl\bar{\nu}$ and $\tilde{t}_1 \to b\nu\tilde{l}$ will predominate *unless* sleptons and sneutrinos are also much heavier than the $\tilde{t}_1$. In this second case the top squark will decay via $\tilde{t}_1 \to c\tilde{Z}_1$ producing final states with two acollinear jets and $\not\!\!E_T$. In either case, the expected signature of the top squark events is two energetic jets and large $\not\!\!E_T$ from the two LSP's.

The top squark production occurs via gluon fusion and $q\bar{q}$ annihilation and is thus fixed by QCD in terms of $m_{\tilde{t}_1}$. The decay topology is solely determined by $m_{\tilde{t}_1}$ and $m_{\tilde{Z}_1}$. Our background subtracted 95% CL exclusion limit contour is shown in Fig. 10. This contour intersects the $m_{\tilde{t}_1} = m_{\tilde{\chi}_1^0} + m_b + m_W$ line at $m_{\tilde{Z}_1} = 8$ GeV/c^2 and $m_{\tilde{t}_1} = 93$ GeV/c^2, the highest $m_{\tilde{t}_1}$ value we exclude. The maximum excluded value for $m_{\tilde{Z}_1}$ is 44 GeV/c^2 for $m_{\tilde{t}_1} = 85$ GeV/c^2.

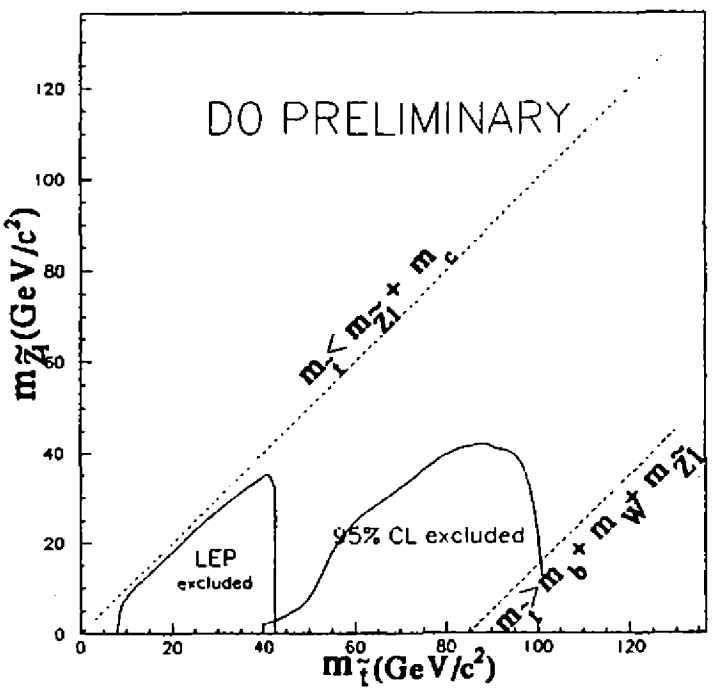

Figure 10: The DØ 95% Confidence Level top squark exclusion contour. Also shown is the result from LEP (OPAL experiment).

IV.3 Gaugino Searches

The largest gaugino production cross section is for a $\widetilde{W}_1\widetilde{Z}_2$ pair. The decays of the $\widetilde{W}_1$ and $\widetilde{Z}_2$ can lead to final states similar to those from virtual W and Z bosons plus missing E_T from the LSP's. The possible event signatures are: four jets + $\not\!\!E_T$, lepton + two Jets + $\not\!\!E_T$, two leptons + two jets + $\not\!\!E_T$, and three leptons + $\not\!\!E_T$. The last channel has few standard model backgrounds and is relatively clean in terms of hadronic activity. We see no candidate events[20] consistent with $\widetilde{W}_1\widetilde{Z}_2$ pair production and subsequent decay into trilepton final states.

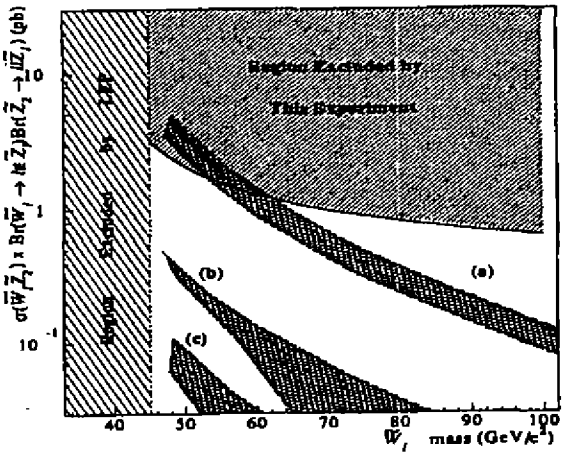

Figure 11: The 95% CL limit on cross section times branching ratio into any one trilepton final state, as a function of $m_{\widetilde{W}_1}$, along with the region of $m_{\widetilde{W}_1}$ excluded by LEP. Also shown are bands of theoretical predictions, as described in the text.

Detection efficiencies were determined using a combination of data and Monte Carlo simulations. The main sources of background are single lepton and dilepton events with one or more misidentified leptons. These were estimated from data and Monte Carlo.

The results from the four channels trilepton channels were combined in the calculation of the limit, with the assumption that $BR(eee) = BR(ee\mu) = BR(e\mu\mu) = BR(\mu\mu\mu)$. In Fig. 11 we show the resulting 95% c.l. limit in the region above the LEP limit. For comparison, we also show three bands of theoretical curves. Band (a) shows the ISAJET production cross section obtained with a wide range of input parameters, multiplied by a branching ratio of $\frac{1}{9}$. The value of $\frac{1}{9}$ for a single trilepton channel is obtained when the $\widetilde{W}_1$ and $\widetilde{Z}_2$ decay purely leptonically. Branching ratios of this order are predicted in models with very light sleptons. Bands (b) and (c) show the $\sigma \cdot BR$ values from ISAJET obtained with the unification scale parameters $m_0 = [200, 900]\mathrm{GeV/c^2}$, $m_{\frac{1}{2}} = [50, 120]\mathrm{GeV/c^2}$, $A_0 = 0$ and the sign of μ negative. Band (b) is for $\tan\beta = 2$ and band (c) for $\tan\beta = 4$.

V Future Prospects

The approved DØ upgrade retains the strengths of the existing detector, including hermetic coverage in finely segmented liquid argon calorimetry and large acceptance muon detection using magnetized iron toroids, and combines these with a new magnetic central tracking system based upon scintillating fibers and silicon strip technologies in a 2 Tesla solenoidal field.

The Tevatron Collider Luminosity has increased tenfold between 1989 and 1996. The Main Injector is currently under construction and a further factor of ten may be anticipated by the first years of the next decade. Initial running, starting in 1999 with the new machines, is expected to yield an integrated luminosity of $2pb^{-1}$. This would be about a factor twenty more than the current data sample and opens new windows on physics.

V.1 Components of the DØ Upgrade

A key element of the upgraded DØ detector is the introduction of a 2 Tesla solenoidal field to enable improved b quark tagging and to provide added calibration and precision for lepton measurements. The central tracking region is instrumented with several new detector systems. Surrounding the collision region at radii less than 10 cm and covering $|\eta| < 3$ is a silicon vertex tracker.

Surrounding the silicon tracker is a central scintillating fiber tracker which covers the radial interval $20\,\text{cm} < r < 50\,\text{cm}$, and pseudorapidity interval $|\eta| < 2$. The scintillating fibers are 830 μm in diameter and are read out with light sensing visible light photon counters (VLPC's). This leads to a compact fast tracker with high efficiency, good resolution, and excellent trigger and pattern recognition capabilities.

The present liquid argon calorimetry system is expected to operate very well at the proposed luminosities after upgrade of the readout electronics. The effects of pileup due to the shorter Tevatron bunch crossing times will be offset by new, lower noise, front end electronics and reduced sampling times. The existing intercryostat detector will be reworked to operate in a magnetic field.

The iron toroids and the drift chambers for the central muon system will be retained, but the front-end electronics for the chambers will be modified. For the region $|\eta| < 1$, new scintillation counters will be installed to reduce the muon trigger p_T threshold to about 1.5 GeV/c. For $1 < |\eta| < 2.2$, new scintillator and "pad-pixel" proportional drift tube chambers will be installed.

The multi-level trigger system will be reworked to increase the flexibility and the bandwidth and help reduce the rates as the luminosity increases. Some of this upgrade will involve completely new filtering and data acquisition software. The world of computing has evolved tremendously since the original design of DØ and converting fitting the old and new analysis code into a framework of Object Oriented software is one of several areas where we expect the LAFEX group to play a major role.

V.2 The DØ Upgrade Physics Program

A central goal of the upgraded DØ program is the substantial improvement of our knowledge of the standard model electroweak parameters. Measurement of the top quark and W boson masses to much better precision than available now will be possible and will permit incisive tests of the validity of the model and indirectly constrain the Higgs boson mass. The study of forward-backward asymmetries in Z leptonic decays will also complement the precision information from LEP on heavy quark and leptonic asymmetries and will provide high precision information on $\sin^2\theta_W$ for light quarks. These measurements will allow consistency checks of the standard model within a single experiment, complementary to the direct searches for new phenomena, which will continue to be a major part of the DØ high p_T physics program.

A reconstructed sample of ~ 1000 $t\bar{t}$ candidates is expected with a signal to background ratio of $> 5:1$. With this sample, one can measure m_t to a precision of better than 5 GeV/c^2, corresponding to an uncertainty in the SM Higgs mass of $\delta m_h/m_h \sim 0.8$. Roughly half of the uncertainty in m_t is of statistical origin, and the remainder is due to systematics such as uncertainties in the energy scale and in Monte Carlo simulation of the effects of gluon radiation. The presence of W decays to two jets in the top decays themselves offers a powerful tool for *in situ* calibration of the multijet mass scale.

Possible signals	Production cross sections (over accessible mass range)	Mass limit (model dependent)	Discovery reach 1 fb^{-1}
$t\bar{t}$	6.3 ± 2.2 pb	199 ± 30 GeV (measured)	discovered!
W_R	0.5-1000 pb	720 GeV	
W'	0.5-0.0001 x σ_W	610 GeV	~ 1 TeV
Z'	0.1-0.001 x σ_Z	480 GeV	~ 1 TeV
scalar 1st generation leptoquarks	1.0-100. pb	133 GeV	~ 240 GeV
scalar 2nd generation leptoquarks	1.0-100. pb	119 GeV	~ 240 GeV
$\tilde{q}$ and $\tilde{g}$ pairs	5-1000 pb	170-230 GeV	~ 200-320 GeV
gaugino pairs	0.5-10.0 pb	~ 60 GeV[1]	~ 90 GeV
$\tilde{t}$	0.1-100 pb	~ 90 GeV [2]	
b'	10-1000 pb	not yet reported	
q*	0.1-100 pb	not yet reported	~ 700 GeV

Table 3: Summary of DØ's current limits and mass reach for the discovery of new particles (10 events required for discovery).

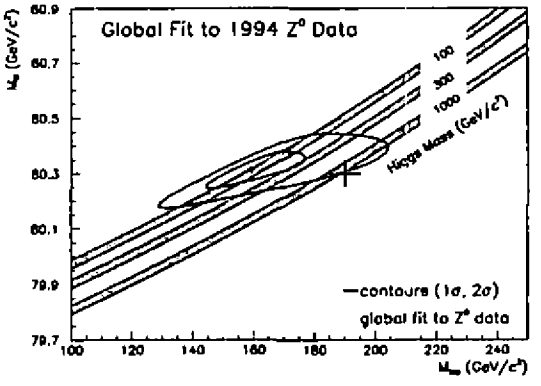

Figure 12: m_t–m_W contours from a global standard model fit to all e^+e^- and νN data, with m_h a free parameter. A hypothetical Run II measurement is shown.

Improved measurements of the W boson mass m_W (accompanied by a measurement of m_t) provides a constraint on the Higgs mass as shown in Fig. 12. For e and μ channels, a W mass measurement with $\delta m_W = 40\,\mathrm{MeV/c^2}$ is expected.

We will also be able to begin the Higgs search in the WH^0 channel in the mass region near 100 GeV/c^2. Table 3 contains a summary of current and future possible search limits from DØ[1].

The approved upgrade DØ detector provides a versatile experimental platform with significant capabilities for the study of top, electroweak symmetry breaking, QCD, b-physics, and new phenomena. The upgrade maintains

the excellent performance characteristics of the present detector and significantly improves the capabilities for b-tagging, and electron, muon and tau identification and measurement. The detector is well matched to the accelerator environment and the physics goals and provides a solid foundation for any additional enhancements needed for operation at higher luminosities.

VI Conclusions

Over the last year or so, DØ has observed the top quark, has numerous interesting results in the basic standard model physics that rules our everyday lives and has shown several unique results of searches for the most likely of possible extensions of the standard model. In particular SUSY scenarios have received some concerted attention. For the future, beyond the doubling of the present data set which is yet to be exploited during the present run we look forward to a bright and exciting future with an upgraded detector and a factor of twenty increase in integrated luminosity.

VII Acknowledgements

I would like to thank all my colleagues on DØ who obtained the results described herein. I would also like to thank the organisers of the conference whose invitation gave me the chance to discuss physics in a wonderful setting on my first trip south of the equator. The hospitality has been superb.

References

[1] A list of DØ journal and conference publications is maintained on the World Wide Web at *http : //d0sgi0.fnal.gov/publications_talks/publications_talks.html*. Fermilab Note 640, "The Standard Model and Beyond: Physics with the DØ Experiment" Editor: Paul Quintas, Contributors: Stefan Gruenendahl, Terry Heuring, Thorsten Huehn, Greg Landsberg, Lee Sawyer, Gordon Watts.

[2] The collected reprints of publications in Physical Review and Physical Review Letters from the CDF Collaboration can be obtained as Fermilab-Pub-95/248-E (1995)

[3] S. Abachi *et al.*, Nucl. Instr. and Meth. A338, 185 (1994).

[4] S. Abachi *et al.*, Phys. Rev. Letters 74, 3548 (1995).

[5] Gilvan Alves, "b Quark Physics at DØ ." Talk presented at this conference.

[6] S. Abachi *et al.*, Phys. Rev. Letters 72, 2332 (1994).

[7] S. Abachi *et al.*, to be published in Phys. Rev. Letters.

[8] S. Abachi *et al.*, Phys. Rev. Letters 75, 1034 (1995).

[9] S. Abachi *et al.*, Phys. Rev. Letters 75, 1028 (1995).

[10] S. Abachi *et al.*, Phys. Rev. Letters 75, 1023 (1995).

[11] Phys. Rev. Letters 75, 1456 (1995).

[12] F. Abe *et al.*, Phys Rev. Letters 74, 2626 (1995).

[13] S. Abachi *et al.*, Phys Rev. Letters 74, 2632 (1995).

[14] S. Abachi *et al.*, Phys. Rev. D52, 4877 (1995).

[15] DØ Collaboration, S. Snyder, in International Europhysi Europhysics Conference on High Energy Physics (HEP 95), Brussels, 1995.

[16] K. Kondo, J. Phys. Soc. Japan 57, 4126(1988), R. H. Dalitz and G. R. Goldstein, Phys. Rev. D45, 1531 (1992).

[17] S. Abachi *et al.*, Phys. Rev. Letters 75 618 (1995).

[18] OPAL Collaboration, OPAL Physics Note 181(Jul 1995), submitted to the EPS-HEP Conference, Brussels, 27 July- 2 August 1995(EPS0278) and The Lepton Photon Symposium, Beijing, 10-15 August, 1995. DELPHI Collaboration, DELPHI Note 95-89-PHYS-524 (Jul 1995), submitted to the EPS-HEP Conference, Brussels, 27 July- 2 August 1995(EPS0570)

[19] S. Abachi *et al.*, to be published in Phys. Rev. Letters. (FERMILAB-PUB-95/380-E)

[20] S. Abachi *et al.*, to be published in Phys. Rev. Letters. (FERMILAB-PUB-95/385-E)

The Origin of Matter in the Universe: A Brief Review

Marcelo Gleiser
Department of Physics and Astronomy, Dartmouth College, Hanover, NH 03755

Received March, 1996

In this talk I briefly review the main ideas and challenges involved in the computation of the observed baryonic excess in the Universe.

I Evidence for Baryonic Asymmetry

One of the outstanding challenges of the interface between particle physics and cosmology is the explanation for the observed baryonic asymmetry in the Universe [1]. It is by now quite clear that there is indeed an excess of baryons over antibaryons in the Universe. A strong constraint on the baryonic asymmetry comes from big-bang nucleosynthesis, setting the net baryon number density (n_B) to photon entropy density (s) ratio at about $n_B/s \equiv \frac{n_b - n_{\bar{b}}}{s} \sim 8 \times 10^{-11}$. Within our solar system, there is no evidence that antibaryons are primordial. Antiprotons found in cosmic rays at a ratio of $N_{\bar{p}}/N_p \sim 10^{-4}$ are secondaries from collisions with the interstellar medium and do no indicate the presence of primary antimatter within our galaxy [2].

We could imagine that in clusters of galaxies there would be antimatter galaxies as well as galaxies. However, this being the case we should observe high energy γ-rays from nucleons of galaxies annihilating with antinucleons of "antigalaxies". The fact that these are not detected rules out the presence of both galaxies and antigalaxies on nearby clusters, which typically have about $10^{14}\ M_\odot$ or so of material. For scales larger than galactic clusters there is no observational evidence for the absence of primordial antimatter.

We could also imagine a baryon-symmetric Universe with large domains of matter and antimatter separated over vast distances. However, a simple cosmological argument rules out this possibility. In a locally baryon-symmetric Universe, nucleons remain in chemical equilibrium with antinucleons down to temperatures of about $T \sim 22$ MeV or so, when $n_b/s \sim n_{\bar{b}}/s \sim 7 \times 10^{-20}$. Annihilation is so efficient as to become catastrophic! To avoid this annihilation, and still obey the nucleosynthesis bound with a baryon-symmetric Universe, we need a mechanism to separate nucleons and antinucleons by $T \sim 38$ MeV, when $n_b/s \sim n_{\bar{b}}/s \sim 8 \times 10^{-11}$. However, at $T \sim 38$ MeV, the horizon contained only about $10^{-7} M_\odot$, making separation of matter and antimatter on scales of $10^{14} M_\odot$ causally impossible. It seems that we must settle for a primordial baryon asymmetry.

II The Sakharov Conditions and GUT Baryogenesis

Given that the evidence is for a Universe with a primordial baryon asymmetry, we have two choices; either this asymmetry is the result of an initial condition, or it was attained through dynamical processes that took place in the early Universe. In 1967, just a couple of years after the discovery of the microwave background radiation, Sakharov wrote a ground-breaking work in which he appealed to the drastic environment of the early stages of the hot big-bang model to spell out the 3 conditions for dynamically generating the baryon asymmetry of the Universe [3]. Here they are, with some modifications:

i) Baryon number violating interactions: Clearly, if we are to generate any excess baryons, our model must have interactions which violate baryon number. However, the same interactions also produce antibaryons at the same rate. We need a second condition;

ii) C and CP violating interactions: Combined violation of charge conjugation (C) and charge conjugation combined with parity (CP) can provide a bias to enhance the production of baryons over antibaryons. However, in thermal equilibrium $n_b = n_{\bar{b}}$, and any asymmetry would be wiped out. We need a third condition;

iii) Departure from thermal equilibrium: Nonequilibrium conditions guarantee that the phase-space density of baryons and antibaryons will not be the same. Hence, provided there is no entropy production later on, the net ratio n_B/s will remain constant.

Given the above conditions, we have to search for the particle physics models that both satisfy them and are capable of generating the correct asymmetry. The first models that attempted to compute the baryon asymmetry dynamically were Grand Unified Theory (GUT) models [4]. GUT models naturally satisfy conditions i) and ii);

by construction, as strong and electroweak interactions are unified, quarks and leptons appear as members of a common irreducible representation of the GUT gauge group. Thus, gauge bosons mediate interactions in which baryons can decay into leptons, leading to baryon number violation. C and CP violation can be built into the models to at least be consistent with the observed violation in the standard model. C is maximally violated by weak interactions and CP violation is observed in the neutral kaon system. One expects that C and CP violation will be manifest in all sectors of the theory including the superheavy boson sector (*e.g.*, $X \to qq$ with branching ratio r, and $\bar{X} \to \bar{q}\bar{q}$, with branching ratio $\bar{r} \neq r$).

Condition iii), departure from thermal equilibrium is provided by the expansion of the Universe. In order for local thermal equilibrium to be maintained in the background of an expanding Universe, the reactions that create and destroy the heavy bosons X and $\bar{X}$ (decay, annihilation, and their inverse processes) must occur rapidly with respect to the expansion rate of the Universe, $H = \frac{\dot{R}}{R} \simeq T^2/M_{\rm pl}$, where $R(t)$ is the scale factor (the dot means time derivative), T is the temperature, and $M_{\rm pl} = 1.2 \times 10^{19}$ GeV is the Planck mass. A typical mechanism of GUT baryogenesis is known as the "out-of-equilibrium decay scenario"; one insures that the heavy X bosons have a long enough lifetime so that their inverse decays go out of equilibrium as they are still abundant. Baryon number is produced by the free decay of the heavy Xs, as the inverse rate is shut off.

Interesting as they are, GUT models of baryogenesis have serious obstacles to overcome. An obvious one is the lack of experimental confirmation for the main prediction of GUTs, the decay of the proton. One can, however, build models (invoking -or not- supersymmetry) in which the lifetime surpases the limits of present experimental sensitivity. A second obstacle is the production of magnetic monopoles predicted to happen as the GUT semi-simple group is broken into subgroups that involve a $U(1)$. The existence of such monopoles was one of the original motivations for inflationary models of cosmology. As is well known, the existence of an inflationary, or superluminal, expansion of the Universe will efficiently dilute any unwanted relics from a GUT-scale transition (and before). Unfortunately, inflation would also dilute badly wanted relics, such as the excess baryons produced, say, by the out-of-equilibrium decay scenario mentioned above. One way of bypassing this diluting effect is to have inflation followed by efficient reheating to temperatures of about 10^{14} GeV, so that the processes responsible for baryogenesis could be reignited. Unfortunately, reheating temperatures are usually much lower than this ($T_{\rm reh} < 10^{12}$ GeV, and $< 10^9$ GeV for supersymmetric models due to nucleosynthesis constraints on gravitino decays), posing a serious problem for GUT baryogenesis.

Finally, a third obstacle to GUT baryogenesis comes from nonperturbative electroweak processes. The vacuum manifold of the electroweak model exhibits a very rich structure, with degenerate minima separated by energy barriers (in field configuration space). Different minima have different baryon (and lepton) number, with the net difference between two minima being given by the number of families. Thus, for the standard model, each jump between two adjacent minima leads to the creation of 3 baryons and 3 leptons, with net $B - L$ conservation and $B + L$ violation. At $T = 0$, tunneling between adjacent minima is mediated by instantons, and, as shown by 't Hooft [5], the tunneling rate is suppressed by the weak coupling constant ($\Gamma \sim e^{-4\pi/\alpha_{\rm W}} \sim 10^{-170}$). That is why the proton is stable. However, as pointed out by Kuzmin, Rubakov, and Shaposhnikov, at finite temperatures ($T \sim 100$ GeV), one could hop over the barrier, tremendously enhancing the rate of baryon number violation [6]. The height of the barrier is given by the action of an unstable static solution of the field equations known as the sphaleron [7].

Being a thermal process, the rate of baryon number violation is controlled by the energy of the sphaleron configuration, $\Gamma \sim \exp[-\beta E_{\rm S}]$, with $E_{\rm S} \simeq M_{\rm W}/\alpha_{\rm W}$, where $M_{\rm W}$ is the W-boson mass. Note that $M_{\rm W}/\alpha_{\rm W} = \langle\phi\rangle/g$, where $\langle\phi\rangle$ is the vacuum expectation value of the Higgs field. For temperatures above the critical temperature for electroweak symmetry restoration, it has been shown that sphaleron processes are not exponentially suppressed, with the rate being roughly $\Gamma \sim (\alpha_{\rm W} T)^4$ [8]. Even though this opens the possibilty of generating the baryonic asymmetry at the electroweak scale, it is bad news for GUT baryogenesis. Unless the original GUT model was $B - L$ conserving, any net baryon number generated then would be brought to zero by the efficient anomalous electroweak processes. There are several alternative models for baryogenesis invoking more or less exotic physics. The interested reader is directed to the review by Olive, listed in Ref. 1. I rather move on to discuss the promises and challenges of electroweak baryogenesis.

III Electroweak Baryogenesis

As pointed out above, temperature effects can lead to efficient baryon number violation at the electroweak scale. Can the other two Sakharov conditions be satisfied in the early Universe so that the observed baryon number could be generated during the electroweak phase transition? The short answer is that in principle yes, but probably not in the context of the minimal standard model. Let us first see why it is possible to satisfy all conditions for baryogenesis in the context of the standard model.

Departure from thermal equilibrium is obtained by invoking a first order phase transition. After summing over matter and gauge fields, one obtains a temperature corrected effective potential for the magnitude of the Higgs field, ϕ. The potential describes two phases, the symmetric phase with $\langle\phi\rangle = 0$ and massless gauge and matter fields, and the broken-symmetric phase with $\langle\phi\rangle = \phi_+(T)$, with massive gauge and matter fields. The loop contributions from the gauge fields generate a cubic term in the effective potential, which creates a barrier separating the two phases. This result depends on a perturbative evaluation of the effective potential, which presents problems for large Higgs masses as I will discuss later. At 1-loop, the potential can be written as [9]

$$V_{\rm EW}(\phi, T) = D\left(T^2 - T_2^2\right)\phi^2 - ET\phi^3 + \frac{1}{4}\lambda_T\phi^4, \tag{1}$$

where the constants D and E are given by

$$D = \left[6(M_W/\sigma)^2 + 3(M_Z/\sigma)^2 + 6(M_T/\sigma)^2\right]/24 \ \sim \ 0.17 \ ,$$

and

$$E = \left[6(M_W/\sigma)^3 + 3(M_Z/\sigma)^3\right]/12\pi \ \sim \ 0.01 \ ,$$

where I used, $M_W = 80.6$ GeV, $M_Z = 91.2$ GeV, $M_T = 174$ GeV [10], and $\sigma = 246$ GeV. The (lengthy) expression for λ_T, the temperature corrected Higgs self-coupling, can be found in Ref. [9]. Here T_2 is the temperature at which the origin becomes an inflection point (*i.e.*, below T_2 the symmetric phase is unstable), given by $T_2 = \sqrt{(M_H^2 - 8B\sigma^2)/4D}$, where the physical Higgs mass is given in terms of the 1-loop corrected λ as $M_H^2 = (2\lambda + 12B)\sigma^2$, with $B = \left(6M_W^4 + 3M_Z^4 - 12M_T^4\right)/64\pi^2\sigma^4$. For high temperatures, the system will be in the symmetric phase with the potential exhibiting only one minimum at $\langle\phi\rangle = 0$. As the Universe expands and cools, an inflection point will develop away from the origin at $\phi_{\rm inf} = 3ET_1/2\lambda_T$, where $T_1 = T_2/\sqrt{1 - 9E^2/8\lambda_T D}$. For $T < T_1$, the inflection point separates into a local maximum at $\phi_-(T)$ and a local minimum at $\phi_+(T)$, with $\phi_\pm(T) = \left\{3ET \pm \left[9E^2T^2 - 8\lambda_T D(T^2 - T_2^2)\right]^{1/2}\right\}/2\lambda_T$. At the critical temperature, $T_C = T_2/\sqrt{1 - E^2/\lambda_T D}$, the minima have the same free energy, $V_{\rm EW}(\phi_+, T_C) = V_{\rm EW}(0, T_C)$. As $E \to 0$, $T_C \to T_2$ and the transition is second order. Since E and D are fixed, the strength of the transition is controlled by the value of the Higgs mass, or λ.

Assuming that the above potential (or something close to it) correctly describes the two phases, as the Universe cools belows T_C the symmetric phase becomes metastable and will decay by nucleation of bubbles of the broken-symmetric phase which will grow and percolate completing the transition. Departure from equilibrium will occur in the expanding bubble walls. This scenario relies on the assumption that the transition is strong enough so that the usual homogeneous nucleation mechanism correctly describes the approach to equilibrium. As I will discuss later this may not be the case for "weak" transitions. For now, we forget this problem and move on to briefly examine how to generate the baryonic asymmetry with expanding bubbles.

The last condition for generating baryon number is C and CP violation. It is known that C and CP violation are present in the standard model. However, the CP violation from the Kobayashi-Maskawa (KM) phase is too small to generate the required baryon asymmetry. This is because the KM phase is multiplied by a function of small couplings and mixing angles, which strongly suppresses the net CP violation to numbers of order 10^{-20} [12], while successful baryogenesis requires CP violation of the order of 10^{-8} or so. A dynamical mechanism to enhance the net CP violation in the standard model was developed in detail by Farrar and Shaposhnikov [13]. It is based on a phase separation of baryons via the scattering of quarks by the expanding bubble wall. This scenario has been criticized by the authors of Ref. [14] who claim that QCD damping effects reduce the asymmetry to a negligible amount. Even though the debate is still going on, efficient baryogenesis within the standard model is a remote possibility.

For many, this is enough motivation to go beyond the standard model in search of extensions which have an enhanced CP violation built in. Several models have been proposed so far, although the simplest invoke either more generations of massive fermions, or multiple massive Higgs doublets with additional CP violation in this sector of the theory. Instead of looking into all models in detail, I will just briefly describe the essential ingredients common to most models.

The transition is assumed to proceed by bubble nucleation. (For alternative mechanisms based on topological defects, see Ref. [11].) Outside the bubbles the Universe is in the symmetric phase, and baryon number violation is occurring at the rate $\Gamma \sim (\alpha_W T)^4$. Inside the bubble the Universe is in the broken symmetric phase and the rate of baryon number violation is $\Gamma \sim \exp[-\beta E_S]$. Since we want any net excess baryon number to be preserved in the broken phase, we must shut off the sphaleron rate inside the bubble. This imposes a constraint on the strength of the phase transition, as $E_S \simeq \langle\phi(T)\rangle/g$; that is, we must have a large "jump" in the vacuum expectation value of ϕ during the transition, $\langle\phi(T)\rangle/T \gtrsim 1$, as shown by Shaposhnikov [12].

Inside the bubble wall the fields are far from equilibrium and there is CP violation, and thus a net asymmetry can be induced by the moving wall. In practice, computations are complicated by several factors, such as the dependence on the net asymmetry on the bubble velocity and on its thickness [15]. Different charge transport mechanisms based on leptons as opposed to quarks have been proposed, which enhance the net baryonic asymmetry produced [16]. However, the basic picture is that as matter traverses the moving wall an asymmetry is produced. And since baryon number violation is suppressed inside the bubble, a net asymmetry survives in the broken phase. Even though no compelling model exists at present, and several open questions related to the complicated nonequilibrium dynamics remain, it is fair to say that the correct baryon asymmetry may have been generated during the electroweak phase transition, possibly in some extension of the standard model. However, I would like to stress that this conclusion has two crucial assumptions built in it; that we know how to compute the effective potential reliably, and that the transition is strong enough to proceed by bubble nucleation. In the next Section I briefly discuss some of the issues involved and how they may be concealing interesting new physics.

IV Challenges to Electroweak Baryogenesis

IV.1 The Effective Potential

A crucial ingredient in the computation of the net baryon number generated during the electroweak phase transition is the effective potential. In order to trust our predictions, we must be able to compute it reliably. However, it is well known that perturbation theory is bound to fail due to severe infrared problems. It is easy to see why this happens. At finite temperatures, the loop expansion parameter involving gauge fields is $g^2T/M_{\rm gauge}$. Since $M_{\rm gauge} = g\langle\phi\rangle$, in the neighborhood of $\langle\phi\rangle = 0$ the expansion diverges. This behavior can be improved by summing over ring, or daisy, diagrams [17]. However, the validity of the ring-improved effective potential for the temperatures of interest relies on cutting off higher-order contributions by invoking a nonperturbative magnetic plasma mass, $M_{\rm plasma}$, for the gauge bosons such that the loop expansion parameter, $g^2T/M_{\rm plasma}$, is less than 1. Since this nonperturbative contribution is not well understood at present, one should take the results from the ring-improved potentials with some caution. Recent estimates show that perturbation theory breaks down for Higgs masses above 70 GeV [18]. These estimates are confirmed by nonperturbative methods based on the subcritical bubbles method [19].

Another problem that appears in the evaluation of the effective potential is due to loop corrections involving the Higgs boson. For second order phase transitions, the vanishing of the effective potential's curvature at the critical temperature leads to the existence of critical phenomena characterized by diverging correlation lengths. Even though there is no infrared-stable fixed point for first order transitions, for large Higgs masses the transition is weak enough to induce large fluctuations about equilibrium; the mean-field estimate for the correlation length $\xi(T) = M^{-1}(T)$ is certainly innacurate. The loop expansion parameter of the effective static 3d theory is $\lambda T/M_{\rm H}(T)$, which diverges as $T_{\rm C} \to T_2$ [20]. This behavior has led some authors [20, 21] to invoke ϵ-expansion methods to deal with the infrared divergences. Although this is a promising line of work, it relies on the success these methods have on different systems. Another alternative is to go to the computer and study the equilibrium properties of the standard model on the lattice [22]. Recent results are encouraging inasmuch as they seem to be consistent with perturbative results in the broken phase for fairly small Higgs masses. Furthermore, they indicate how the transition becomes weaker for large values of the Higgs mass, $M_{\rm H} \gtrsim 60$ GeV; physical quantities, which characterize the strength of the transition, such as the bubble's surface tension and the released latent heat, turn out to be quite small. Let me move on to discuss nonequilibrium aspects of the transition.

IV.2 Weak vs. Strong First Order Transitions

In order to avoid the erasure of the produced net baryon number inside the broken-symmetric phase, the sphaleron rate must be suppressed within the bubble. As mentioned earlier, this amounts to imposing a large enough "jump" on the vacuum expectation value of ϕ during the transition. In other words, the transition cannot be too weakly first order. But what does it mean, really, to be "weakly" or "strongly" first order? Looking into the literature, the most obvious distinction between weak and strong is the thickness of the bubble. A "strong" transition has thin-wall bubbles, that is, the bubble wall is much thinner than the bubble radius (hence the name "bubble"), while "weak" transitions have thicker walls. It is implicitly assumed that weak transitions proceed by the usual bubble nucleation mechanism which, nevertheless, is derived only for the case of strong transitions.

This is a very important point which must not be overlooked (although it often is!); the vacuum decay formalism used for the computation of decay rates relies on a semi-classical expansion of the effective action. That is, we assume we start at a *homogeneous* phase of false vacuum, and evaluate the rate by summing over small amplitude fluctuations about the metastable state [23]. This approximation must break down for weak enough transitions, when we expect

large fluctuations to be present within the metastable phase. An explicit example of this breakdown was recently presented by Gleiser and Heckler, where the extra free energy available due to the presence of large-amplitude fluctuations was incorporated into the computation of the decay rate [24].

Gleiser and Kolb [25] suggested that weak transitions may evolve by a different mechanism, characterized by substantial mixing of the two phases as the critical temperature is approached from above (*i.e.* as the Universe cools to T_C). They estimated the fraction of the total volume occupied by the broken-symmetric phase by assuming that the dominant fluctuations about equilibrium are subcritical bubbles of roughly a correlation volume which interpolate between the two phases. Their approach was later refined by the authors of Ref. [26] who found, within their approximations, that the 1-loop electroweak potential shows considerable mixing for $M_H \gtrsim 55$ GeV. Clearly, the presence of large-amplitude, nonperturbative thermal fluctuations compromises the validity of the effective potential, since it does not incorporate such corrections.

In order to understand the shortcomings of the mean-field approximation in this context, numerical simulations in 2d [27] and 3d [28] were performed, which focused on the amount of "phase mixing" promoted by thermal fluctuations. The idea was to simulate the nonequilibrium dynamics of a self-interacting real scalar field, which is coupled to a thermal bath at temperature T. In order to study the approximate behavior relevant to the electroweak phase transition, the field was chosen to have a potential given by Eq. 1. (Note that the temperature dependence of the potential can be scaled away with a proper redefinition of the couplings.) The coupling to the bath was modelled by a Markovian Langevin equation, which assumes that the bath thermalizes much faster than any relevant dynamical time-scale for the scalar field. Thus, the equation represents a coarse-grained description of the dynamics, with faster modes with $\lambda << \xi(T)$ integrated out, where $\xi(T) = m^{-1}(T)$ is the mean field correlation length.

The results show that the problem boils down to how well localized the system is about the symmetric phase as it approaches the critical temperature. If the system is well localized about the symmetric phase, it will become metastable as the temperature drops below T_C and the transition can be called "strong". In this case, the mean-field approximation is reliable. Otherwise, large-amplitude fluctuations away from the symmetric phase rapidly grow, causing substantial mixing between the two phases. This will be a "weak" transition, which will not evolve by bubble nucleation. Defining $\langle\phi\rangle_V$ as the volume averaged field and ϕ_{inf} as the inflection point nearest to the $\phi = 0$ minimum, the criterion for a strong transition can be written as [27]

$$\langle\phi\rangle_V < \phi_{inf} \quad . \tag{2}$$

Recently, an analytical model, based on the subcritical bubbles method, was shown to qualitatively and *quantitatively* describe the results obtained by the 3d simulation [29]. The fact that subcritical bubbles successfully model the effects of thermal fluctuations promoting phase mixing and the breakdown of the mean-field approximation with subsequent symmetry restoration, supports previous estimates which showed that the assumption of homogeneous nucleation is incompatible with standard model baryogenesis for $M_H \lesssim 55$ GeV [26, 19]. It is straightforward to adapt these computations to extensions of the standard model. Thus, the requirement that the transition proceeds by bubble nucleation can be used, together with the subcritical bubbles method, to constrain the parameters of the potential.

In conclusion, the past few years saw encouraging progress towards the goal of computing the baryon asymmetry of the Universe. Likewise, it has also become clear that serious challenges lie ahead if we are to finally achieve this goal. The need for enhanced CP violation probably calls for physics beyond the standard model. Although this is an exciting prospect for many, we need guidance from experiments in order to point us in the right direction. We must also be able to compute the effective potential reliably for a wider range of Higgs masses. And finally, we must understand several nonequilibrium aspects of the phase transition, be it within the context of expanding critical bubbles for strong transitions or the dynamics of phase separation for weak transitions. Judging from what has happened in the past few years, progress will keep coming fast, and the goal will keep getting closer.

I am grateful to my collaborators Rocky Kolb, A. Heckler, Graciela Gelmini, M. Alford and R. Ramos for the many long discussions on bubbles and phase transitions. I am also grateful to Fernando Brandt and the local organizing committee for their warm hospitality during this Conference. This work was partially supported by the National Science Foundation through a Presidential Faculty Fellows Award no. PHY-9453431 and by a NASA grant no. NAGW-4270.

References

[1] For reviews see, L. Yaffe, hep-ph/9512265, A. G. Cohen, D. B. Kaplan, and A. E. Nelson, Annu. Rev. Nucl. Part. Sci. **43**, 27 (1993); A. Dolgov, Phys. Rep. **222**, 311 (1992); K. A. Olive, in "Matter under extreme conditions", eds. H. Latal and W. Schweiger (Springer-Verlag, Berlin, 1994).

[2] G. Steigman, Ann. Rev. Astron. Astrophys. **14**, 339 (1976).

[3] A. D. Sakharov, JETP Lett. **5**, 24 (1967).

[4] For a review see E. W. Kolb and M. S. Turner, Ann. Rev. Nucl. Part. Sci. **33**, 645 (1983); *ibid.* The Early Universe, (Addison-Wesley, Redwood, CA, 1990).

[5] G. t'Hooft, Phys. Rev. Lett. **37**, 8 (1976); Phys. Rev. **D14**, 3432 (1976).

[6] V. A. Kuzmin, V. A. Rubakov, and M. E. Shaposhnikov, Phys. Lett. **B155**, 36 (1985).

[7] N. S. Manton, Phys. Rev. **D28**, 2019 (1983); F. R. Klinkhammer and N. S. Manton, Phys. Rev. **D30**, 2212 (1984).

[8] P. Arnold and L. McLerran, Phys. Rev. **D36**, 581 (1987); *ibid.* **D37**, 1020 (1988); J. Ambjorn and A. Krasnitz, Phys. Lett. **B362**, 97 (1995).

[9] G. W. Anderson and L. J. Hall, Phys. Rev. D **45**, 2685 (1992); M. Dine, P. Huet, and R. Singleton, Nucl. Phys. **B375**, 625 (1992).

[10] F. Abe et al. (CDF Collaboration), Phys. Rev. Lett. **73**, 225 (1994).

[11] R. Brandenberger and A.-C. Davis, Phys. Lett. **B308**, 79 (1993); R. Brandenberger, A.-C. Davis, and M. Trodden, Phys. Lett. **B335**, 123 (1994).

[12] C. Jarlskog, Z. Physik **C29**, 491 (1985); Phys. Rev. Lett. **55**, 1039 (1985); M. E. Shaposhnikov, Nucl. Phys. **B287**, 757 (1987); **B299**, 797 (1988).

[13] G. R. Farrar and M. E. Shaposhnikov, Phys. Rev. Lett. **70**, 2833 (1993); Phys. Rev. **D50**, 774 (1994).

[14] M. B. Gavela, P. Hernández, J. Orloff, O. Pène, and C. Quimbay, Nucl. Phys. **B430**, 382 (1994) P. Huet and E. Sather, preprint SLAC-PUB-6479 (1994).

[15] B. Liu, L. McLerran, and N. Turok, Phys. Rev. **D46**, 2668 (1992); M. Dine and S. Thomas, Phys. Lett. **B328**, 73 (1994); G.D. Moore and T. Prokopec, Phys. Rev. Lett. **75**, 777 (1995).

[16] A. G. Cohen, D. B. Kaplan, and A. E. Nelson, Phys. Lett. **B245**, 561 (1990); Nucl. Phys. **B349**, 727 (1991); **B373**, 453 (1992); Phys. Lett. **B336**, 41 (1994); M. Joyce, T. Prokopec, and N. Turok, Phys. Rev. Lett. **75**, 1695 (1995); hep-ph/9410281.

[17] P. Arnold and O. Espinosa, Phys. Rev. **D47**, 3546 (1993); M. Dine, P. Huet, R.G. Leigh, A. Linde, and D. Linde, Phys. Rev. **D46**, 550 (1992); C.G. Boyd, D.E. Brahm, and S. Hsu, Phys. Rev. **D48**, 4963 (1993); M. Quiros, J.R. Spinosa, and F. Zwirner, Phys. Lett. **B314**, 206 (1993); W. Buchmüller, T. Helbig, and D. Walliser, Nucl. Phys. **B407**, 387 (1993); M. Carrington, Phys. Rev. **D45**, 2933 (1992).

[18] W. Buchmüller and Z. Fodor, Phys. Lett. **B331**, 124 (1994).

[19] M. Gleiser and R. Ramos, Phys. Lett. **B300**, 271 (1993).

[20] M. Gleiser and E.W. Kolb, Phys. Rev. **D48**, 1560 (1993).

[21] P. Arnold and L. Yaffe, Phys. Rev. **D49**, 3003 (1994).

[22] K. Farakos, K. Kajantie, K. Rummukainen, and M. Shaposhnikov, hep-lat/9510020; Nucl. Phys. **B407**, 356 (1993); *ibid.* **B425**, 67 (1994); *ibid.***B442**, 317 (1995); B. Bunk, E.-M. Ilgenfritz, J. Kripfganz, and A. Schiller, Phys. Lett. **B284**, 372 (1992); Nucl. Phys. **B403**, 453 (1993); Z. Fodor et al. Nucl. Phys. **B439**, 147 (1995).

[23] J. S. Langer, Ann. Phys. (NY) **41**, 108 (1967); *ibid.* **54**, 258 (1969); M. B. Voloshin, I. Yu. Kobzarev, and L. B. Okun', Yad. Fiz. **20**, 1229 (1974) [Sov. J. Nucl. Phys. **20**, 644 (1975); S. Coleman, Phys. Rev. **D15**, 2929 (1977); C. Callan and S. Coleman, Phys. Rev. **D16**, 1762 (1977); A. D. Linde, Nucl. Phys. **B216**, 421 (1983); [Erratum: **B223**, 544 (1983)]; M. Gleiser, G. Marques, and R. Ramos, Phys. Rev. **D48**, 1571 (1993); D. Brahm and C. Lee, Phys. Rev. **D49**, 4094 (1994).

[24] M. Gleiser and A. Heckler, hep-ph/9509347. In press, Physical Review Letters.

[25] M. Gleiser and E. W. Kolb, Phys. Rev. Lett. **69**, 1304 (1992); M. Gleiser, E. W. Kolb, and R. Watkins, Nucl. Phys. **B364**, 411 (1991); N. Tetradis, Z. Phys. **C57**, 331 (1993).

[26] G. Gelmini and M. Gleiser, Nucl. Phys. **B419**, 129 (1994).

[27] M. Gleiser, Phys. Rev. Lett. **73**, 3495 (1994).

[28] J. Borrill and M. Gleiser, Phys. Rev. **D51**, 4111 (1995).

[29] M. Gleiser, A. Heckler, and E.W. Kolb, cond-mat/9512032, submitted to Physical Review Letters.

The Auger Project: Highest Energy Cosmic Rays

Alberto Etchegoyen
Tandar-CNEA and CONICET
Argentina

Received March, 1996

More than 30 years ago in Volcano Ranch, U.S.A. an extensive air shower (EAS) with an energy in excess of 10^{20} eV was detected. Since then, the observatories placed in Haverath Park in the United Kingdom, Yakutsk in Russia, AGASA in Japan, and Dugway in U.S.A., also observed EAS with ascribed energies above 10^{20} eV. Little is known about such rays and in particular, where they come from, how are they accelerated, and what are they, but their ultrarelativistic energy precludes most answers and reduces them to a set amenable to experimental research. Groups of physicists from approximately 20 countries are working in an effort to build two giant observatories, one in each hemisphere spread over an area of 3000 km^2 each. Such giant arrays are needed due to a roughly estimated flux of 1 cosmic ray/km^2/century/sr yielding approximately 60 events per year per stern radian.

The project was named after the French physicist, Pierre Auger, who first detected cosmic showers back in 1938 and the observatories construction will start in 1998. The project focuses on the highest energy cosmic rays, i.e., above 10^{19} eV.

1. Introduction

Up to date, there are 8 events with measured energies above 10^{20} eV. As mentioned above, the first one was detected in Volcano Ranch in April 1962 with an energy of 1.3×10^{20} eV while the two more energetic are from AGASA ($2.0^{+0.6}_{-0.3}$) $\times10^{20}$ eV and Dugway (3.2 $\pm$ 0.9) 10^{20} eV. Although very little is known and understood about the process we do not have any doubt that such EAS energies exist and therefore it is appropriate to undertake the task of building giant detector arrays. Several group of physicists with different levels of commitment, from Argentina, Armenia, Australia, Bolivia, Brazil, China, France, Germany, India, Italy, Japan, Russia, South Africa,Spain, Sweden, Switzerland, United Kingdom, United States of America, and Vietnam, are currently involved in the Auger Project and the collaboration is led by J. W. Cronin (Spokesperson) and A. Watson.

The EAS starts to develop at the entrance of the primary particle to the Earth atmosphere. At these very high energies the first collisions will be hadronic (quark-quark collisions) and as the shower proceeds the number of particles in it will increase getting as large as 10^{11} as estimated for the (3.2 $\pm$ 0.9) 10^{20} eV primary. Apart from muons, electrons and gammas reaching the surface, there will be fluorescence light from the excitation of the atmospheric nitrogen electrons and therefore a hybrid detector is envisaged: a surface component of detectors spread over the 3000 km^2 and an optical component to measure the fluorescence light covering the same sky range as the surface detectors. The main advantage of such a hybrid detection is that it will measure independently and with totally different systems, mechanisms, and parameters, the same showers allowing to contrast, for instance the energy calibrations.

The scientific motivation is to understand the origin, acceleration mechanism and chemical composition of these primaries. Very little is known about cosmic rays but these ultra high energies impose severe restrictions as we shall see during the talk and therefore there is confidence that the Auger Project will cast light on the three issues.

2. Scientific Motivation

Although there are only 8 events with E > 10^{20} eV, there are much more with lower energies. Some trends can therefore be motivated by them, but final answers await further experimental results since at these ultrarelativistic energies the behaviour might change very abruptly.

2.1 Chemical Composition of the Primary

The conventional candidates are protons (or neutrons), gammas, neutrinos, and heavier nuclei. We can assess the chemical composition by the large amount of data that has been collected over the last decades and in particular by the dependence of the cosmic ray flux on the incident energy. The spectrum is displayed in Fig. 1 where it is seen to be a smooth curve over 26 orders of magnitude in the flux and 9 in the energy, and described in first order by a power law in energy with an exponent close to -3. In Fig. 2 there is a blow up of the higher energy region of Fig. 1, normalized by E^3. Inspection of Fig. 1 shows there is a break in the spectrum slope at about $10^{15} - 10^{16}$ eV, from roughly $E^{-2.7}$to $E^{-3.0}$, and this feature is often referred as the '*knee* '. This knee is close to the theoretical limit of the supernova blast wave acceleration for protons. In Fig. 2 two further slope changes can be seen. The spectrum steepens at $10^{17.6}$eV and flattens at $10^{18.5}$ eV [1]. This flatting is generally called '*ankle* ' and is related to the chemical composition of the primaries at the energies of interest. In ref. 1 they measured the altitude at shower maximum as a function of energy. This altitude is expressed as the atmospheric depth maximum X_M, and they compared the experimental results with the calculated X_M for iron nuclei and protons. They found that the composition is getting lighter, going from heavy masses below $10^{17.5}$ eV to light composition near 10^{19} eV. They also performed a simple two-component fit (pure iron and pure proton) to Fig. 2 and with the result reproduced the X_M experimental energy dependence. Also, the measured longitudinal development of the shower for the highest energy event is not compatible with a photon as a primary.

In summary, there is evidence of a migration to lower masses as the energy increases beyond $10^{17.5}$ eV.

2.2 Source Identification

The main issue here is the so-called GZK cut-off (Greisen, Zatsepin, and Kuz'min cut-off). The particles as they travel through the space will interact with the 2.7°K background radiation, and very energetic particles will quickly loose energy and approach an asymptotic value around 4 × 10^{19} eV, as shown in Fig. 3. In this figure the degradation of energy is displayed for a proton due to collisions with $\gamma_{2.7}$ (e.g., $\gamma_{2.7}+p \rightarrow n+\pi^+$, or $\gamma_{2.7}+p \rightarrow p+\pi^o$). The source is at the coordinate origin and at approximately 100 Mpc the different initial energies approach 10^{20} eV. Heavier nuclei will disintegrated and will fall below 10^{20} eV at closer distances from the source [2], which is in line with the observation described in section 2.1.

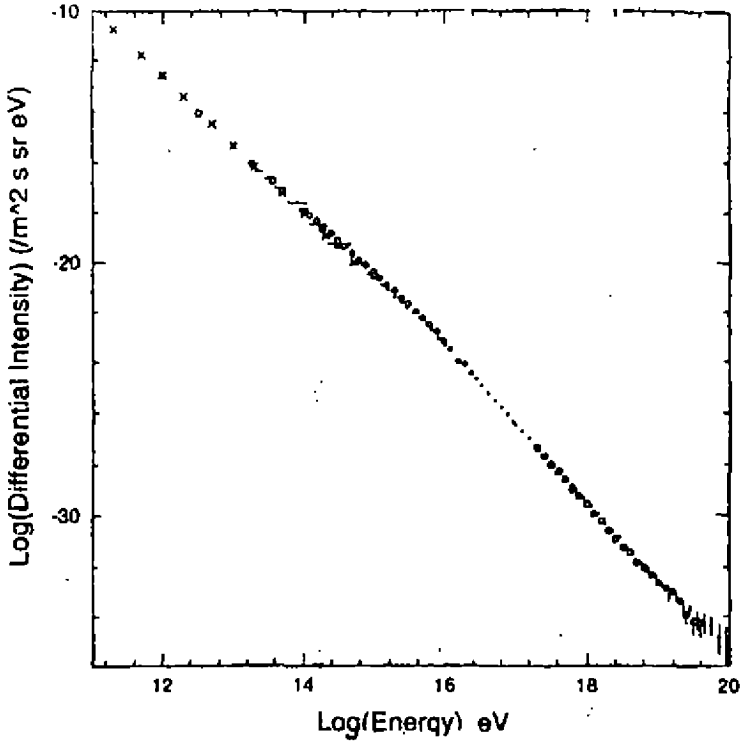

Figure 1. Cosmic ray spectrum, flux vs. energy.

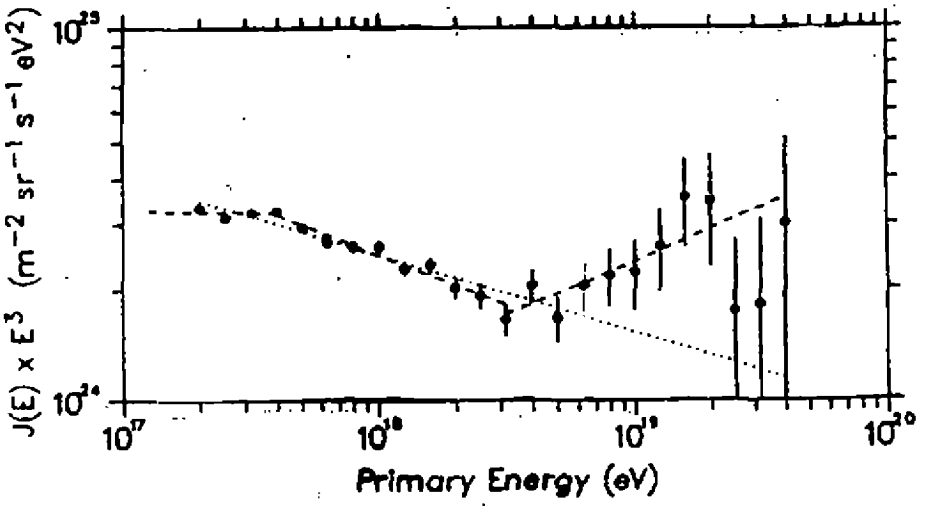

Figure 2. Higher energy cosmic ray spectrum multiplied by E^3.

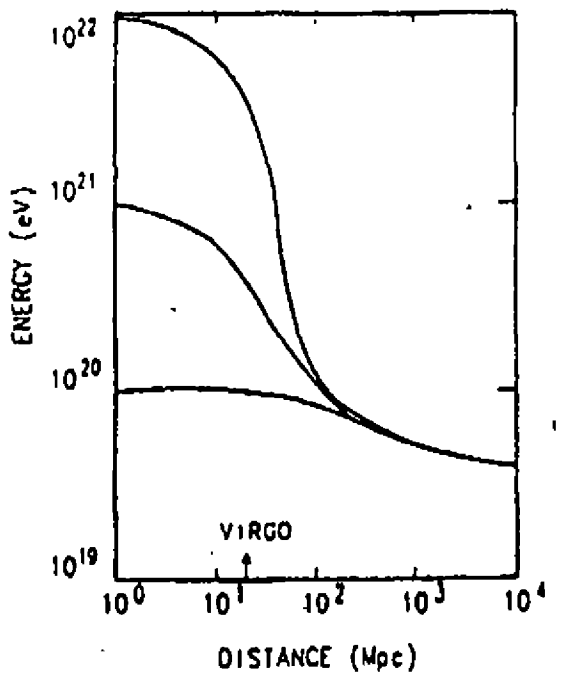

Figure 3. Proton energy vs. the distance travelled from the source. The proton looses energy by photo-pion production with collision with the background radiation.

Assuming a proton primary, it is seen that the 3.2 x 10^{20} eV event should not have originated farther away than 50 Mpc, which is close in cosmological distances. Added to this, the large magnetic rigidity of these ultrarelativistic particles, make it easier to identify possible sources

2.3 Possible Acceleration Sources

An extensive study of possible acceleration sites was performed by Hillas in 1984 [3] and the results are displayed in Fig. 4. In the axes are plotted the magnetic field B, in which the acceleration region is embedded and the size L of this region. (the energy E is proportional to $B \times L$, as in a cyclotron accelerator). The diagonal, drawn as a full line, correspond to a proton accelerated to 10^{20} eV, and therefore celestial objects below this line will fail to accelerate protons to this value (note in particulars that our galaxy falls below the line). It is seen that few possible sources remain, namely neutron stars, white dwarfs, active galactic nuclei and radiogalaxies. These calculations where done for $\beta = 1$ for the accelerator, a more realistic $\beta = \frac{1}{300}$ moves the line somewhere up, within the shaded area, mostly forbidden all sources. These calculations are a guidance as to the difficulty in achieving energies above 10^{20} eV. There are more recent theoretical work concentrating in radio galaxies [4] or in Centaurus A [5] according to which higher energies are attained.

As a final remark to this section, it is mentioned that there are also theoretical models of exotic sources [6]. Assuming that after some years of data taking by the Auger Project, some cumulative data do not point to any known source, we will seriously considered exotic sources. A suggested one is a decay into quarks of a super massive X particle with an energy associated of the order of the GUT scale, 10^{24} eV. Sources of such particles could be topological defects of the universe, remnants of the early stages of the Big Bang. Also a gap above 2-3 x10^{20} will point in the direction of these processes, since conventional mechanism would produce events filling such an energy gap. Another exotic possibility is an unknown particle with a very low $\gamma_{2.7}$ cross section. Most of these discussions

are very useful predictions, some 'ad hoc ' proposals, awaiting for experimental data to guide us in the research.

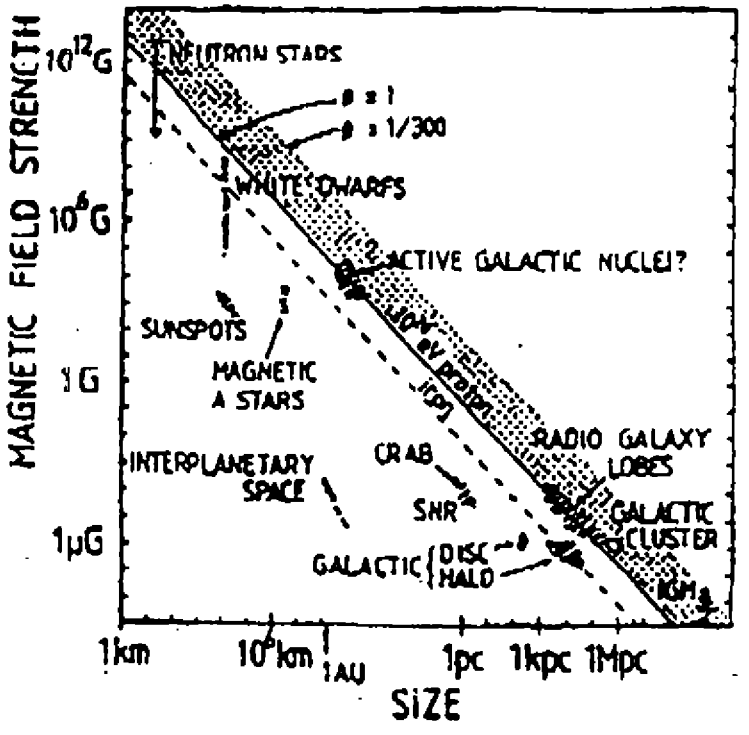

Figure 4. Magnetic fields and sizes of possible acceleration sites. Sites below the full diagonal line can not accelerate protons to 10^{20} eV.

3. The Hybrid Detector

The most important restriction arises from the extremely EAS low fluxes which force a giant size for the detector array. The Auger Project consists in two observatories, one in each hemisphere. Argentina has been chosen as the preferred country for installation of the southern hemisphere observatory and in mid 1996 the northern preferred country will be elected.

We have on one hand, as the shower develops, electromagnetical excitation of atmospheric atoms which eventually decay by emission of fluorescence light and on the other hand, a large number of muons, electrons and gammas will collide with the Earth surface. So, a hybrid system is planned to detect both the fluorescence light and the impinging particles.

The fluorescence detector will be an optical telescope of the fly's eye type using the technique developed at the Fly's Eye observatory at Dugway, Utah. It has mirrors that look at different regions of the sky and focus the light on photomultipliers. This segmentation gives rise to the name. It has a duty cycle of 10% working only in clear moonless nights. The main goal of this component is to measure the shower as it develops in the sky given its longitudinal profile, which in turn yields the energy of the primary by integration. Also, the atmospheric depth maximum, X_M, depends on the chemical composition of the primary given thus information on the primary mass composition (see Fig. 5).

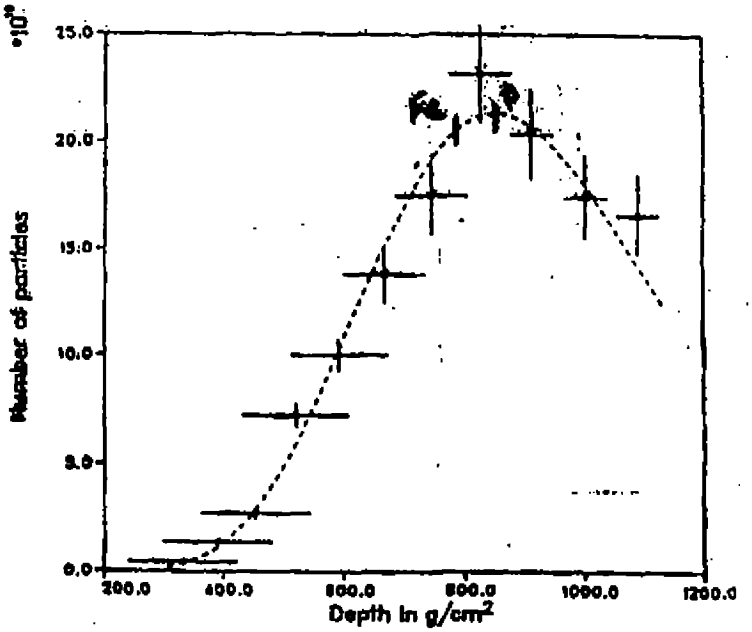

Figure 5. The longitudinal profile of the most energetic cosmic ray detected. Model calculated X_M for iron and proton are shown.

The impinging particles will be observed by an array of 1650 surface detectors, placed in a triangular grid, with 1.5 km spacing between detectors over the total area of 3000 km^2. These detectors need to identify the muonic from the electromagnetic components of the shower since this ratio depends on the mass composition of the primary ($[\frac{\mu}{\gamma e}]_{iron} > [\frac{\mu}{\gamma e}]_p > [\frac{\mu}{\gamma e}]_\gamma$). There are two proposed systems: the leadburger and water cerenkov tanks (WTC). The leadburger is a sandwich of scintillator, lead, and scintillator and the idea is that electrons will produce a signal in the first scintillator, muons in both and gammas, through convertion in lead, only in the second scintillator. But the currently preferred design is the WTC. An artistic view of such a tank is displayed in Fig. 6. The WTC's need to be autonomous since it would be impractical to wire an area of 3000 km^2. The power will be provided by solar panels and they will communicate among first neighbours via cellular phones. Timing information will be from the Global Positioning Satellite system, GPS, which will be used for both generating a trigger and for reconstructing the direction of arrival of the primary. Intense research in being carried out with WCT prototypes, there is one operational in Fermilab, one near complexion in Buenos Aires and one being constructed in Tokyo. There plans to built a unitary cell of 7 detectors in Dugway this year, fully equipped with solar panels and communication system. Although the grid is triangular, since the detectors 'listen' to first neighbours the unitary cell is an hexagon with WTC's in the vertices and in the centre.

The prototype we have at Buenos Aires is a cylinder tank built of stainless steel, 0.65 cm thick, 1.80 m high and 10 m^2 of surface area. The photomultipliers. are not placed in the lid but are mounted inside the tank on movable aluminum rods, as to allow different geometries on the plane and different heights inside the tank. The photocatodes are embedded in the water. The water was demineralized with a resistivity of approximately 1 MΩ/cm. The prototype lid is not welded and can be raised and lowered for planning different experiments. The tank walls are currently polished but will be either painted or, more probable, covered with a diffusing plastic (as done in Haverath Park). Simulations done with the GEANT code from the CERN library show that totaling reflecting surfaces produce more than one peak for 1 GeV muons due to multiple reflections of the cerenkov light. There are also two scintillators counters one on top and the other one below the tank as a way of identifying muons. Bacteria growth has just started to be monitored every couple of weeks. There are plans to use smaller tanks for quick testing of wave shifters, salt in water for diminishing the freezing point (that might occur in the site), paints and

plastics, and bacteria grows under different conditions (e.g. tests of the efficiency as a bacteria killer of ultraviolet light by bathing with it the tank prior to filling, or germicides as copper or zinc in contact or spread in the water).

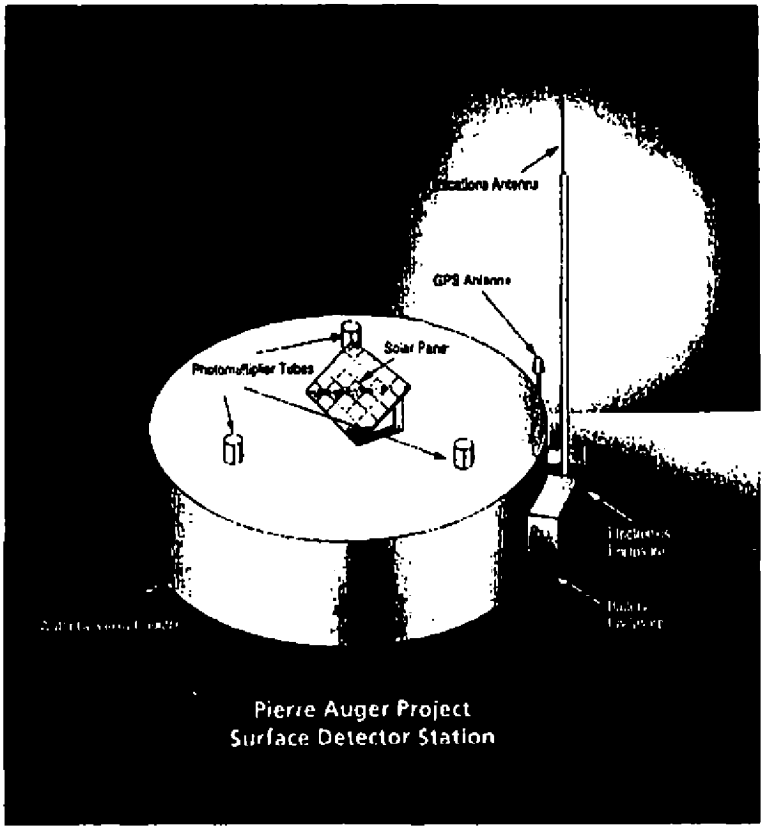

Figure 6. Artistic view of the preferred surface detector, a water cerenkov tank.

As mentioned, a hybrid detector has the enormous advantage that it measures the same showers (within the duty cycle of the fly's eye) with totally different apparatus, given confidence due to this redundancy. For instance, the energy calibration: the fly's eye obtains it though integration of the shower profile, while the WTC by counting particles at the Earth surface.

4. Conclusions

The schedule for the Auger Project encompasses two years of research and development, 1996 and 1997. The constructions of the observatories will start in 1998 and will last for four years, but still data taking can start well before the complete array is mounted.

Eight cosmic rays with energies above 10^{20} eV has been detected insofar and therefore we are convinced that they exist. Due to the very low fluxes we need giant detectors arrays and 6000 km^2 of detection area are envisaged, split in two identical observatories in each hemisphere.

The source identification is simplified due to the GZK cut-off and the magnetic rigidity of the primary. Also the primary characterization may be achieved in an statistical way by measuring the muon and electromagnetic contents of the shower and the X_M of the shower profiles.

The main questions arising from ultra high energy cosmic rays await for higher statistics, not much further can be advanced without it. In particular, identification of sources are needed in order to test the different theoretical models for acceleration to these energies.

Note: A complete document on both the physics and the detector design is presented in the Auger Project Design Report [7].

References

[1] D.J. Bird et al., Phys. Rev. Lett. **71**, 3401 (1993).

[2] J. W. Cronin, Nucl. Phys. **B28**, 213 (1992).

[3] A. M. Hillas, Ann. Rev. Astron. Astrophys. **22**, 425 (1984).

[4] J. Rachen, Todor Stanev, and P.L. Biermann, Astron. Astrophys. **273**, 377 (1993).

[5] G. E. Romero, J. A. Combi, L. A. Anchordoqui, S. E. Perez Bergliaffa, submitted to publication.

[6] G. Sigl, S.Lee, D. N. Scharamm, P. Bhattacharjee, Fermilab-Pub 95/148-A, astroph/9506118.

[7] *The Pierre Auger Project*, Design Report, October 1995.

Screening in High-t QCD*

R. Jackiw†

Center for Theoretical Physics,

Department of Physics and Laboratory for Nuclear Science

Massachusetts Institute of Technology

Cambridge, MA 02139 U.S.A.

MIT-CTP #2513

Received January, 1996

These days, as high energy particle colliders become unavailable for testing speculative theoretical ideas, physicists are looking to other environments that may provide extreme conditions where theory confronts physical reality. One such circumstance may arise at high temperature T, which perhaps can be attained in heavy ion collisions or in astrophysical settings. It is natural therefore to examine the high-temperature behavior of the standard model, and here I shall report on recent progress in constructing the high-T limit of QCD.

My presentation will be unified by the theme of **screening**, a familiar phenomenon in electrodynamical plasmas. I shall explore how similar effects can be described in QCD at a sufficiently high temperature (above the putative confinement - deconfinement phase transition) so that we may speak of unconfirmed quarks and gluons forming a plasma. But first let me review briefly the screening phenomena in plasmas of electromagnetically charged particles. We begin with Poisson's equation, which relates the scalar electric potential ϕ to a charge density ρ.

$$-\nabla^2\phi = \rho$$

For the charge density we take a statistical distribution of positive-charged $(+q)$ and negative-charged $(-q)$ particles, each carrying the energy $\pm q\phi$, respectively, and described by the same density n. Then

$$\rho = n(qe^{-q\phi/T} - qe^{q\phi/T})$$

*To be published in: The Proceedings of *XVI National Meeting on Particles and Fields*, Caxambu, Brazil, October 1995

†This work is supported in part by funds provided by the U.S. Department of Energy (D.O.E.) under cooperative agreement # DF-FC02-94ER40818.

For large T, this becomes

$$\rho_{(\widetilde{\text{large } T})} -2nq^2\phi/T$$

so that the Poisson equation reads

$$-\nabla^2\phi + \left(\frac{2nq^2}{T}\right)\phi = O$$

Evidently, a screening mass $\propto \left(\frac{nq^2}{T}\right)^{\frac{1}{2}}$ has been induced for the electric potential ϕ; the inverse is called the **Debye screening length**. Again at high T and for a relativistic plasma, one expects $n \sim (1/\text{volume}) \sim T^3$, hence the induced **electric** screening mass is

$$m \propto |q|T$$

We shall see a similar result emerging in the non-Abelian theory as well. Note that Debye screening occurs for the electric (temporal) component of the gauge potential. There is no electrodynamical magnetic screening, because there are no magnetic resources.

$$\boldsymbol{\nabla} \cdot \mathbf{B} = O$$

In the non-Abelian theory, the corresponding equation involves the covariant divergence.

$$\boldsymbol{\nabla} \cdot \mathbf{B}^a = g f^{abc} \mathbf{A}^b \cdot \mathbf{B}^c$$

(Here g is the gauge coupling constant.) So the issue of magnetic sources is not so clear in the Yang-Mills case, and one of the topics that we shall address later is whether in the non-Abelian theory there exists magnetic screening.

The above argument – it is essentially Debye's – makes little use of field theoretical formalism. But to carry through analogous calculations in the standard model, we shall begin with quantum field theory. Let me explore how finite-temperature calculations are performed in that context.

When studying a field theory at finite temperature, the simplest approach is the so-called imaginary-time formalism. We continue time to the imaginary interval $[0, 1/iT]$ and consider bosonic (fermionic) fields to be periodic (anti-periodic) on that interval. Perturbative calculations are performed by the usual Feynman rules as at zero temperature, except that in the conjugate energy-momentum, Fourier-transformed space, the energy variable p^0 (conjugate to the periodic time variable) becomes discrete – it is $2\pi nT$, (n integer) for bosons. From this one immediately sees that at high temperature – in the limiting case, at infinite temperature – the time direction disappears, because the temporal interval shrinks to zero. Only zero-energy processes survive, since "non-vanishing energy" necessarily means high energy owing to the discreteness of the energy variable $p^0 \sim 2\pi nT$, and therefore all modes with $n \neq 0$ decouple at large T. In this way a Euclidean three-dimensional field theory becomes effective at high temperatures and describes essentially static processes.[1]

Let me repeat in greater detail. Finite-T, imaginary-time perturbation theory makes use of conventional diagrammatic analysis in "momentum" space, with modified "energy" variables, as indicated above. Specifically a spinless boson propagator is

$$D(p) = \frac{i}{p_0^2 - \mathbf{p}^2 - m^2} \qquad p_0 = i\pi(2n)T$$

while a spin-$\frac{1}{2}$ fermion propagator reads

$$S(p) = \frac{i}{\gamma^0 p_0 - \gamma \cdot \boldsymbol{p} - m} \qquad p_0 = i\pi(2n+1)T$$

The zero-temperature integration measure $\int \frac{d^4p}{(2\pi)^4}$ becomes replaced by $iT\sum_{n=-\infty}^{\infty}\int\frac{d^3p}{(2\pi)^3}$. Thus it is seen that Bose exchange between two $O(g)$ vertices contributes $iT\sum_{n=-\infty}^{\infty}\int\frac{d^3p}{(2\pi)^3}g\frac{i}{-4\pi^2n^2T^2-\boldsymbol{p}^2-m^2}g$ where g is the coupling strength. In the large T limit, all $n \neq 0$ terms (formally) vanish as T^{-1} and only the $n = 0$ term survives. One is left with $\int\frac{d^3p}{(2\pi)^3}g\sqrt{T}\frac{1}{\boldsymbol{p}^2+m^2}g\sqrt{T}$. This is a Bose exchange graph in a Euclidian 3-dimensional theory, with effective coupling $g\sqrt{T}$. Similar reasoning leads to the conclusion that fermions decouple at large T.

While all this is quick and simple, it may be physically inadequate. First of all, frequently one is interested in non-static processes in real time, so complicated analytic continuation from imaginary time needs to be made before passing to the high-T limit, which in imaginary time describes only static processes. Also one may wish to study amplitudes where the real external energy is neither large nor zero, even though virtual internal energies are high.

Another reason that the above may be inadequate emerges when we consider massless fields (such as those that occur in QCD). We have seen that the $n = 0$ mode leaves a propagator that behaves as $\frac{1}{\boldsymbol{p}^2}$ when mass vanishes, and a phase space of d^3p. It is well known that this kind of kinematics at low momenta leads to infrared divergences in perturbation theory even for off-mass-shell amplitudes — Green's functions in massless Bosonic field theories possess infrared divergences in naive perturbation theory.[2] Since physical QCD does not suffer from off-mass-shell infrared divergences, perturbation theory must be resummed.

A final shortcoming of the above limiting procedure is that it is formal: the limit is taken before the integration/summation is carried out. But the latter need not converge uniformly; indeed owing to ultraviolet divergences, it may not converge at all and must be renormalized. As a consequence the $n \neq 0$ contributions in single Boson exchange graphs may not decrease as T^{-1}.

Thus the formal arguments for the emergence of a 3-dimensional theory at high-T need be re-examined for QCD. Nevertheless, even if unreliable, the arguments alert us to the possibility that 3-dimensional field theoretic structures may emerge in the high-T regime. Indeed this occurs, although not in a direct, straightforward fashion; this will be demonstrated presently.

Here is a graphical argument to the same end discussed above: *viz.* The need to resum perturbation theory. Consider a one-loop amplitude $\Pi_1(p)$,

$$\Pi_1(p) \equiv \int dk\ I_1(p,k)\ ,$$

given by the graph in the figure.

$\Pi_1(p) =$ 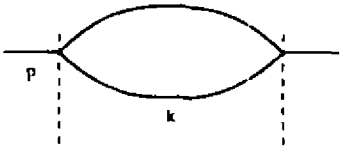

$$\equiv \qquad \int dk\, I_1(p,k)$$

Compare this to a two-loop amplitude $\Pi_2(p)$,

$$\Pi_2(p) \equiv \int dk\, I_2(p,k) \ ,$$

in which Π_1 is an insertion, as in the figure below.

$$\Pi_2(p) =$$

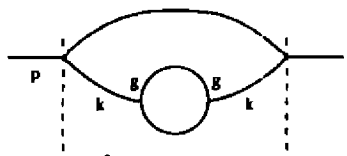

$$\equiv \qquad \int dk\ I_2(p,k)$$

Following Pisarski,[3] we estimate the relative importance of Π_2 to Π_1 by the ratio of their integrands,

$$\frac{\Pi_2}{\Pi_1} \sim \frac{I_2}{I_1} = g^2\, \frac{\Pi_1(k)}{k^2} \ ,$$

Here g is the coupling constant, and the k^2 in the denominator reflects the fact that we are considering a massless field, as in QCD. Clearly the $k^2 \to 0$ limit is relevant to the question whether the higher order graph can be neglected relative to the lower order one. Because one finds that for small k and large T, $\Pi_1(k)$ behaves as T^2, the ratio Π_2/Π_1 is g^2T^2/k^2. As a result when k is $O(gT)$ or smaller the two-loop amplitude is not negligible compared to the one-loop amplitude. Thus graphs with "soft" external momenta [$O(gT)$ or smaller] have to be included as insertions in higher order calculations.

A terminology has arisen: graphs with generic/soft external moment [$O(gT)$ where g is small and T is large] and large internal momenta [the internal momenta are integration variables in an amplitude; when T is large they are $O(T)$, hence also large] are called "hard thermal loops."[3,4] Much study has been expended on them and finally a general picture has emerged. Before presenting general results, let us look at a specific example — a 2-point Green's function.

It needs to be appreciated that in the imaginary-time formalism the correlation functions are unique and definite. But passage to real time, requires continuing from the integer-valued "energy" to a continuous variable, and this cannot be performed uniquely. This reflects the fact that in real time there exists a variety of correlation functions: time ordered products, retarded commutators, advanced commutators, *etc.* Essentially one is seeing the consequence of the fact that a Euclidean Laplacian possesses a unique inverse, whereas giving an inverse for the Minkowskian d'Alembertian requires specifying temporal boundary conditions, and a variety of answers can be gotten with a variety of boundary conditions. Thus, when presenting results one needs to specify precisely what one is computing.

We shall consider a correlation function for two fermionic currents, in the 1-loop approximation.

$$\Pi^{\mu\nu}(x,y) \ = \ -i\,\langle j^\mu(x) j^\nu(y)\rangle$$

$$= \int \frac{d^4k}{(2\pi)^4} e^{-ik(x-y)} \Pi^{\mu\nu}(k)$$

The QCD result differs from the QED result by a group theoretical multiplicative factor, so we present high-T results only for the latter, in real-time, and consider the time-ordained product $\Pi^{\mu\nu}_T$ as well as the retarded commutator $\Pi^{\mu\nu}_R$.

$\Pi^{\mu\nu}$ possesses a real and an imaginary part. It is found that at large T, the real parts of $\Pi^{\mu\nu}_T$ and $\Pi^{\mu\nu}_R$ coincide.

$$-\mathrm{Re}\Pi^{\mu\nu}(k) = \frac{T^2}{6} P_2^{\mu\nu} + \frac{T^2 k^2}{|\boldsymbol{k}^2|} \left[1 + \frac{k^0}{2|\boldsymbol{k}|} \ln \left| \frac{k^0 - |\boldsymbol{k}|}{k^0 + |\boldsymbol{k}|} \right| \right] \left[\frac{1}{3} P_1^{\mu\nu} + \frac{1}{2} P_2^{\mu\nu} \right]$$

where the projection operators are

$$\begin{aligned} P_1^{\mu\nu} &= g^{\mu\nu} - k^\mu k^\nu / k^2 \\ P_2^{\mu\nu} &= \begin{cases} 0 & \text{if } \mu \text{ or } \nu = 0 \\ \delta^{ij} - k^i k^j / |\boldsymbol{k}^2| & \text{otherwise} \end{cases} \end{aligned}$$

For the imaginary part, which is present only for space-like arguments, different expressions are found.

$$\begin{aligned} -\mathrm{Im}\Pi^{\mu\nu}_R(k) &\equiv -\pi \rho^{\mu\nu}(k) \\ &= \frac{\pi k^2}{|\boldsymbol{k}|^3} \frac{k^0}{2} T^2 \theta(-k^2) \left[\frac{1}{3} P_1^{\mu\nu} + \frac{1}{2} P_2^{\mu\nu} \right] \\ -\mathrm{Im}\Pi^{\mu\nu}_T(k) &= \frac{\pi k^2}{|\boldsymbol{k}|^3} \left[\frac{k^0}{2} T^2 + T^3 \right] \theta(-k^2) \left[\frac{1}{3} P_1^{\mu\nu} + \frac{1}{2} P_2^{\mu\nu} \right] \end{aligned}$$

A unified presentation of these formulas is achieved in a dispersive representation. For the retarded function this reads

$$\Pi^{\mu\nu}_R(k) = \Pi^{\mu\nu}_{SUB}(k) + \int dk'_0 \frac{\rho^{\mu\nu}(k'_0, \boldsymbol{k})}{k'_0 - k_0 - i\epsilon}$$

while the time-ordered expression is

$$\Pi^{\mu\nu}_T(k) = \Pi^{\mu\nu}_{SUB}(k) + \int dk'_0 \frac{\rho^{\mu\nu}(k'_0, \boldsymbol{k})}{k'_0 - k_0 - i\epsilon} + \frac{2\pi i}{e^{k_0/T} - 1} \rho^{\mu\nu}(k_0, \boldsymbol{k})$$

The dispersive expressions may also be used to give the imaginary-time formula.

$$\Pi^{\mu\nu}_{\substack{\text{imaginary} \\ \text{time}}}(k) = \Pi^{\mu\nu}_{SUB}(k) + \int dk'_0 \frac{\rho^{\mu\nu}(k'_0, \boldsymbol{k})}{k'_0 - 2\pi i n T}$$

In all the above formulas, $\Pi^{\mu\nu}_{SUB}$ is a real subtraction term.

Note that a universal statement about high-T behavior can be made only for the absorptive part $\rho^{\mu\nu}$: it is $O(T^2)$. This also characterizes $\Pi^{\mu\nu}_R$, but $\Pi^{\mu\nu}_T$ possesses an additional $O(T^3)$ imaginary part, which is seen to arise from the additional term in $\Pi^{\mu\nu}_T$ involving the bosonic distribution function $\frac{1}{e^{k_0/T}-1}$. Finally, the $\Pi^{\mu\nu}_{\substack{\text{imaginary} \\ \text{time}}}$ amplitude has a temperature

behavior determined by its external "energy" $= 2\pi inT$. If this is replaced by a fixed k_0 (T-independent) or if only the $n = 0$ mode is considered, then one may assign an $O(T^2)$ behavior to this quantity as well.

In conclusion, we assert that the 2-point correlation function behaves as $O(T^2)$, where it is understood that this statement is to be applied to the retarded amplitude, or to the imaginary time amplitude with its "energy" argument continued away from $2\pi inT$.[5]

Similar analysis has been performed on the higher-point functions and this work has culminated with the discovery (Braaten, Pisarski, Frenkel, Taylor)[3,4,6] of a remarkable simplicity in their structure. To describe this simplicity, we do not discuss the individual n-point functions, but rather their sum multiplied by powers of the vector potential, *viz.* we consider the generating functional for single-particle irreducible Green's functions with gauge field external lines in the hard thermal limit. (Effectively, we are dealing with continued imaginary-time amplitudes.) We call this quantity $\Gamma_{\rm HTL}(A)$ and it is computed in an $SU(N)$ gauge theory containing N_F fermion species of the fundamental representation. $\Gamma_{\rm HTL}$ is found (i) to be proportional to $(N + \frac{1}{2}N_F)$, (ii) to behave as T^2 at high temperature, and (iii) to be gauge invariant.

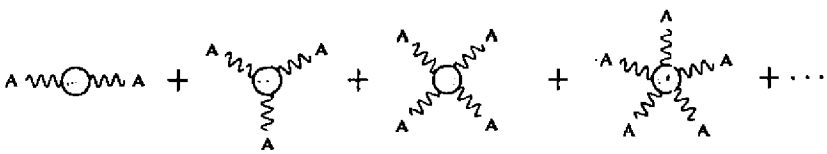

$$= (N + \tfrac{1}{2}N_F)\,\frac{g^2T^2}{12\pi}\,\Gamma_{\rm HTL}(A)$$

$$\Gamma_{\rm HTL}(U^{-1}\,A\,U + U^{-1}\,dU) \quad = \Gamma_{\rm HTL}(A)$$

(Henceforth g, the coupling constant, is scaled to unity.) A further kinematical simplification in $\Gamma_{\rm HTL}$ has also been established. To explain this we define two light-like four-vectors $Q^\mu_\pm$ depending on a unit three-vector $\hat{q}$, pointing in an arbitrary direction.

$$Q^\mu_\pm = \frac{1}{\sqrt{2}}(1,\ \pm\hat{q})$$

$$\hat{q}\cdot\hat{q} = 1\ , \qquad Q^\mu_\pm Q_{\pm\mu}\ =\ 0\ , \qquad Q^\mu_\pm Q_{\mp\mu} = 1$$

Coordinates and potentials are projected onto $Q^\mu_\pm$.

$$x^\pm \equiv x_\mu Q^\mu_\pm\ , \qquad \partial_\pm \equiv Q^\mu_\pm \frac{\partial}{\partial x^\mu}\ , \qquad A_\pm \equiv A_\mu Q^\mu_\pm$$

The additional fact that is now known is that (iv) after separating an ultralocal contribution from $\Gamma_{\rm HTL}$, the remainder may be written as an average over the angles of $\hat{q}$ of a functional W that depends only on A_+; also this functional is non-local only on the two-dimensional $x^\pm$ plane, and is ultralocal in the remaining directions, perpendicular to the $x^\pm$ plane. ["Ultralocal" means that any potentially non-local kernel $k(x,y)$ is in fact a δ-function of the difference $k(x,y) \propto \delta(x-y)$.]

$$\Gamma_{\rm HTL}(A) = 2\pi \int d^4x\ A^a_0(x)A^a_0(x) + \int d\Omega_{\hat{q}}\, W(A_+)$$

These results are established in perturbation theory, and a perturbative expansion of $W(A_+)$, *i.e.* a power series in A_+, exhibits the above mentioned properties. A natural question is whether one can sum the series to obtain an expression for $W(A_+)$.

Important progress on this problem was made when it was observed (Taylor, Wong)[6] that the gauge-invariance condition can be imposed infinitesimally, whereupon it leads to a functional differential equation for $W(A_+)$, which is best presented as

$$\frac{\partial}{\partial x^+}\frac{\delta}{\delta A^a_+}\left[W(A_+)+\tfrac{1}{2}\int d^4x\; A^b_+(x)A^b_+(x)\right] - \frac{\partial}{-\partial x^-}\left[A^a_+\right]+f^{abc}A^b_+\frac{\delta}{\delta A^c_+}\left[W(A_+)+\tfrac{1}{2}\int d^4x\; A^d_+(x)A^d_+(x)\right]=0$$

In other words we seek a quantity, call it

$$S(A_+)\equiv W(A_+)+\frac{1}{2}\int d^4x\, A^a_+(x)A^a_+(x)\ ,$$

which is a functional on a two-dimensional manifold $\{x^+,x^-\}$, depends on a single functional variable A_+, and satisfies

$$\partial_1\frac{\delta}{\delta A^a_1}S-\partial_2 A^a_1+f^{abc}A^b_1\frac{\delta}{\delta A^c_1}S=0$$

$$\text{“1”}\equiv x^+\ ,\qquad \text{“2”}\equiv -x^-\ ,\qquad A^a_1\equiv A^a_+$$

Another suggestive version of the above is gotten by defining $A^a_2\equiv\frac{\delta S}{\delta A^a_1}$.

$$\partial_1 A^a_2-\partial_2 A^a_1+f^{abc}A^b_1A^c_2=0$$

To solve the functional equation and produce an expression for $W(A_+)$, we now turn to a completely different corner of physics, and that is Chern-Simons theory at zero temperature.

The Chern-Simons term is a peculiar gauge theoretic topological structure that can be constructed in odd dimensions, and here we consider it in 3-dimensional space-time.

$$I_{\rm CS}\propto\int d^3x\,\epsilon^{\alpha\beta\gamma}\,{\rm Tr}\,(\partial_\alpha A_\beta A_\gamma+\tfrac{2}{3}A_\alpha A_\beta A_\gamma)$$

This object was introduced into physics over a decade ago, and since that time it has been put to various physical and mathematical uses. Indeed one of our originally stated motivations for studying the Chern-Simons term was its possible relevance to high-temperature gauge theory.[7] Here following Efraty and Nair,[8] we shall employ the Chern-Simons term for a determination of the hard thermal loop generating functional, $\Gamma_{\rm HTL}$.

Since it is the space-time integral of a density, $I_{\rm CS}$ may be viewed as the action for a quantum field theory in (2+1)-dimensional space-time, and the corresponding Lagrangian would then be given by a two-dimensional, spatial integral of a Lagrange density.

$$I_{\rm CS}\ \propto\ \int dt\ L_{\rm CS}$$

$$L_{\rm CS}\ \propto\ \int d^2x\,\left(A^a_2\dot{A}^a_1+A^a_0F^a_{12}\right)$$

I have separated the temporal index (0) from the two spatial ones (1,2) and have indicated time differentiation by an over dot. F^a_{12} is the non-Abelian field strength, defined on a two-dimensional plane.

$$F^a_{12} = \partial_1 A^a_2 - \partial_2 A^a_1 + f^{abc} A^b_1 A^c_2$$

Examining the Lagrangian, we see that it has the form

$$L \sim p\dot{q} - \lambda H(p,q)$$

where A^a_2 plays the role of p, A^a_1 that of q, F^a_{12} is like a Hamiltonian and A^a_0 acts like the Lagrange multiplier λ, which forces the Hamiltonian to vanish; here A^a_0 enforces the vanishing of F^a_{12}.

$$F^a_{12} = 0$$

The analogy instructs us how the Chern-Simons theory should be quantized.

We postulate equal-time computation relations, like those between p and q.

$$\left[A^a_1(\boldsymbol{r}),\, A^b_2(\boldsymbol{r}')\right] = i\,\delta^{ab}\delta(\boldsymbol{r} - \boldsymbol{r}')$$

In order to satisfy the condition enforced by the Lagrange multiplier, we demand that F^a_{12}, operating on "allowed" states, annihilate them.

$$F^a_{12}|\ \rangle = 0$$

This equation can be explicitly presented in a Schrödinger-like representation for the Chern-Simons quantum field theory, where the state is a functional of A^a_1. The action of the operators A^a_1 and A^a_2 is by multiplication and functional differentiation, respectively.

$$\begin{aligned} |\ \rangle &\sim \Psi(A^a_1) \\ A^a_1|\ \rangle &\sim A^a_1\,\Psi(A^a_1) \\ A^a_2|\ \rangle &\sim \frac{1}{i}\frac{\delta}{\delta A^a_1}\Psi(A^a_1) \end{aligned}$$

This, of course, is just the field theoretic analog of the quantum mechanical situation where states are functions of q, the q operator acts by multiplication, and the p operator by differentiation. In the Schrödinger representation, the condition that states be annihilated by F^a_{12}

$$\left(\partial_1 A^a_2 - \partial_2 A^a_1 + f_{abc} A^b_1 A^c_2\right)\Big|\ \Big\rangle = 0$$

leads to a functional differential equation.

$$\left(\partial_1 \frac{1}{i}\frac{\delta}{\delta A^a_1} - \partial_2\, A^a_1 + f_{abc} A^b_1 \frac{1}{i}\frac{\delta}{\delta A^c_1}\right)\Psi(A^a_1) = 0$$

If we define S by $\Psi = e^{iS}$ we get equivalently

$$\partial_1 \frac{\delta}{\delta A^a_1} S - \partial_2 A^a_1 + f_{abc} A^b_1 \frac{\delta}{\delta A^c_1} S = 0$$

This equation comprises the entire content of Chern-Simons quantum field theory. S is the Chern-Simons eikonal, which gives the exact wave functional owing to the simple dynamics of the theory. Also the above eikonal equation is recognized to be precisely the equation for the hard thermal loop generating functional, given above.

Let me elaborate on the connection with eikonal-WKB ideas. Let us recall that in particle quantum mechanics, when the wave function $\psi(q)$ is written in eikonal form

$$\psi(q) = e^{iS(q)}$$

then the WKB approximation to $S(q)$ is given by the integral of the canonical 1-form pdq

$$S(q) = \int^q p(q')dq'$$

where $p(q)$, the momentum, is taken to be function of the coordinate q, by virtue of satisfying the equation of motion.

$$\begin{aligned} \frac{p^2(q)}{2} + V(q) &= E \\ p(q) &= \sqrt{2E - 2V(q)} \end{aligned}$$

Analogously, in the present field theory application, the eikonal $S(A_1)$ may be written as a functional integral,

$$S(A_1) = \int^{A_1} A_2^a(A_1')\mathcal{D}A_1'^a$$

where $A_2^a(A_1)$ is functional of A_1 determined by the equation of motion

$$\partial_1 A_2^a - \partial_2 A_1^a + f^{abc}A_1^b A_2^b = 0$$

Since, by construction $\frac{\delta S}{\delta A_1^a} = A_2^a$, it is clear that as a consequence S satisfies the required equation. However, we reiterate that in the Chern-Simons case there is no WKB approximation: everything is exact owing to the simplicity of Chern-Simons dynamics.

The gained advantage for thermal physics is that "acceptable" Chern-Simons states, *i.e.* solutions to the above functional equations, were constructed long ago,[9] and one can now take over those results to the hard thermal loop problem. One knows from the Chern-Simons work that Ψ and S are given by a 2-dimensional fermionic determinant, *i.e.* by the Polyakov-Wiegman expression. While these are not described by very explicit formulas, many properties are understood, and the hope is that one can use these properties to obtain further information about high-temperature QCD processes. We give two applications.

The Chern-Simons information allows presenting the hard-thermal loop generating functional as

$$\Gamma_{\rm HTL} = \frac{1}{2}\int d\Omega_{\hat{q}}[A_+^a A_-^a + S(A_+) + S(A_-)] \ .$$

Using the known properties of S, one can give a very explicit series expansion for $\Gamma_{\rm HTL}$ in terms of powers of A

$$\Gamma_{\rm HTL} = \frac{1}{2!}\int \Gamma^{(2)}_{\rm HTL} AA + \frac{1}{3!}\int \Gamma^{(3)}_{\rm HTL} AAA + \cdots$$

where the non-local kernels $\Gamma^{(i)}_{\rm HTL}$ are known explicitly. This power series may be used to systematize the resummation procedure for the pertubative theory. Here is what one does: perturbation theory for Green's functions may be organized with the help of a functional integral, where the integrand contains (among other factors) $e^{iI_{\rm QCD}(A)}$ where $I_{\rm QCD}$ is the QCD action. We now rewrite that as

$$e^{i\left\{I_{\rm QCD}(A)+\frac{m^2}{4\pi}\Gamma_{\rm HTL}(A)-\frac{m^2}{4\pi}\Gamma_{\rm HTL}(A)\right\}}$$

where $m = T\sqrt{\frac{N+N_F/2}{3}}$. Obviously nothing has changed, because we have merely added and subtracted the hard-thermal-loop generating functional. Next we introduce a loop counting parameter l: in an l-expansion, different powers of l correspond to different numbers of loops, but at the end l is set to unity. The resummed action is then taken to be

$$e^{iI_{\rm resummed}} = e^{i\left\{\frac{1}{l}\left[I_{\rm QCD}(\sqrt{l}A)+\frac{m^2}{4\pi}\Gamma_{\rm HTL}(\sqrt{l}A)\right]-\frac{m^2}{4\pi}\Gamma_{\rm HTL}(\sqrt{l}A)\right\}}$$

One readily verifies that an expansion in powers of l describes the resummed perturbation theory, and this then represents the first application of the present Chern-Simons formalism.

For a second application, we note that even though the closed form for $\Gamma_{\rm HTL}$ is not very explicit, a much more explicit formula can be gotten for its functional derivative $\frac{\delta\Gamma_{\rm HTL}}{\delta A^a_\mu}$. This may be identified with an induced current, which is then used as a source in the Yang-Mills equation. Thereby one obtains a non-Abelian generalization of the Kubo equation, which governs the response of the hot quark gluon plasma to external disturbances.[5]

$$D_\mu F^{\mu\nu} = \frac{m^2}{2} j^\nu_{\rm induced}$$

From the known properties of the fermionic determinant — hard thermal loop generating functional — one can show that $j^\mu_{\rm induced}$ is given by

$$j^\mu_{\rm induced} = \int \frac{d\Omega_{\hat q}}{4\pi}\left\{Q^\mu_+\left(a_-(x)-A_-(x)\right)+Q^\mu_-\left(a_+(x)-A_+(x)\right)\right\}$$

where $a_\pm$ are solutions to the equations

$$\begin{aligned}\partial_+ a_- - \partial_- A_+ + [A_+, a_-] &= 0\\ \partial_+ A_- - \partial_- a_+ + [a_+, A_-] &= 0\end{aligned}$$

Evidently $j^\mu_{\rm induced}$, as determined by the above equations, is a non-local and non-linear functional of the vector potential A_μ.

There now have appeared several alternative derivations of the Kubo equation. Blaizot and Iancu[10] have analyzed the Schwinger-Dyson equations in the hard thermal regime; they truncated them at the 1-loop level, made further kinematical approximations that are justified in the hard thermal limit, and they too arrived at the Kubo equation. Equivalently the argument may be presented succinctly in the language of the composite effective action,[11] which is truncated at the 1-loop (semi-classical) level — two-particle irreducible graphs are omitted. The stationarity condition on the 1-loop action is the gauge invariance constraint

on $\Gamma_{\rm HTL}$. Finally, there is one more, entirely different derivation — which perhaps is the most interesting because it relies on classical physics.[12] We shall give the argument presently, but first we discuss solutions for the Kubo equation.

To solve the Kubo equation, one must determine $a_\pm$ for arbitrary $A_\pm$, thereby obtaining an expression for the induced current, as a functional of $A_\pm$. Since the functional is non-local and non-linear, it does not appear possible to construct it explicitly in all generality. However, special cases can be readily handled.

In the Abelian case, everything commutes and linearizes. One can determine $a_\pm$ in terms of $A_\pm$.

$$a_\pm = \frac{\partial_\pm}{\partial_\mp} A_\mp$$

(Incidentally, this formula exemplifies the kinematical simplicity, mentioned above, of hard thermal loops: the nonlocality of $1/\partial_\pm$ lies entirely in the $\{x^-, x^-\}$ plane.) With the above form for $a_\pm$ inserted into the Kubo equation, the solution can be constructed explicitly. It coincides with the results obtained by Silin long ago, on the basis of the Boltzmann-Vlasov equation.[13] One sees that the present theory is the non-Abelian generalization of that physics; in particular m, given above, is recognized as the Debye screening length, which remains gauge invariant in the non-Abelian context.

It is especially interesting to emphasize that Silin did not use quantum field theory in his derivation; rather he employed classical transport theory. Nevertheless, his final result coincides with what here has been developed from a quantal framework. This raises the possibility that the non-Abelian Kubo equation can also be derived classically, and indeed such a derivation has been given, as mentioned above.

We now pause in our discussion of solutions to the non-Abelian Kubo equation in order to describe its classical derivation.

Transport theory is formulated in terms of a single-particle distribution function f on phase space. In the Abelian case, f depends on position $\{x^\mu\}$ and momentum $\{p^\mu\}$ of the particle. For the non-Abelian theory it is necessary to take into account the fact that the particle's non-Abelian charge $\{Q^a\}$ also is a dynamical variable: Q^a satisfies an evolution equation (see below) and is an element of phase space. Therefore, the non-Abelian distribution function depends on $\{x^\mu\}$, $\{p^\mu\}$ and $\{Q^a\}$, and in the collisionless approximation obeys the transport equation $\frac{d}{d\tau} f = 0$, *i.e.*

$$\frac{\partial f}{\partial x^\mu}\frac{dx^\mu}{d\tau} + \frac{\partial f}{\partial p^\mu}\frac{dp^\mu}{d\tau} + \frac{\partial f}{\partial Q^a}\frac{dQ^a}{d\tau} = 0$$

The derivatives of the phase-space variables are given by the Wong equations, for a particle with mass μ.

$$\begin{aligned}
\frac{dx^\mu}{d\tau} &= \frac{p^\mu}{\mu} \\
\frac{dp^\mu}{d\tau} &= F^{\mu\nu}_a \frac{dx_\nu}{d\tau} Q^a \\
\frac{dQ^a}{d\tau} &= -f^{abc}\frac{dx^\mu}{d\tau} A^b_\mu Q^c
\end{aligned}$$

In order to close the system we need an equation for $F^{\mu\nu}$. In a microscopic description (with a single particle) one would have $(D_\mu F^{\mu\nu})^a = \int d\tau Q^a(\tau)\frac{p^\nu(\tau)}{\mu}\delta^4(x - x(\tau))$ and consistency would require covariant conservation of the current; this is ensured provided Q^a satisfies the equation given above. In our macroscopic, statistical derivation, the current is given in terms of the distribution function, so the system of equations closes with

$$(D_\mu F^{\mu\nu})^a = \int dp\, dQ\, Q^a p^\nu f(x, p, Q)$$

(One verifies that the current – the right side of the above – is covariatly conserved.) The collisionless transport equation, with the equations of motion inserted, is called the Boltzmann equation. The closed system formed by the latter supplemented with the Yang-Mills equation is known as the non-Abelian Vlasov equations. To make progress, this highly non-linear set of equations is approximated by expanding around the equilibrium form for f,

$$f^{\text{free}}_{\substack{\text{boson}\\\text{fermion}}} \propto \left(e^{\frac{1}{T}\sqrt{\mathbf{p}^2+\mu^2}} \mp 1\right)^{-1}$$

This comprises the Vlasov approximation, and readily leads to the non-Abelian Kubo equation.[12]

One may say that the non-Abelian theory is the minimal elaboration of the Abelian case needed to preserve non-Abelian gauge invariance. The fact that classical reasoning can reproduce quantal results is presumably related to the fact that the quantum theory makes use of the (resummed) 1-loop approximation, which is frequently recognized as an essentially classical effect. Evidently, the quantum fluctuations included in the hard thermal loops coincide with thermal fluctuations.

Returning now to our summary of the solutions to the non-Abelian Kubo equation that have been obtained thus far, we mention first that the static problem may be solved completely.[11] When the *Ansatz* is made that the vector potential is time independent, $A_\pm = A_\pm(\mathbf{r})$, one may solve for $a_\pm$ to find $a_\pm = -A_\pm$ and the induced current is explicitly computed as

$$\frac{m^2}{2} j^\mu_{\text{induced}} = \begin{pmatrix} -m^2 A^0 \\ \mathbf{0} \end{pmatrix}$$

This exhibits gauge-invariant electric screening with Debye mass m. One may also search for localized static solutions to the Kubo equation, but one finds only infinite energy solutions, carrying a point-magnetic monopole singularity. Thus there are no plasma solitons in high-T QCD.[11] Specifically, upon selecting the radially symmetric solution that decreases at large distances, there arises a magnetic monopole-like singularity at the origin.

Much less is known concerning time-dependent solutions. Blaizot and Iancu[14] have made the *Ansatz* that the vector potentials depend only on the combination $x \cdot k$, where k is an arbitrary 4-vector: $A_\pm = A_\pm(x \cdot k)$. Once again $a_\pm$ can be determined; one finds $a_\pm = \frac{Q_\pm \cdot k}{Q_\mp \cdot k} A_\mp$, and the induced current is computable. For $k = \begin{pmatrix} 1 \\ \mathbf{0} \end{pmatrix}$, where there is no space dependence (only a dependence on time is present) one finds

$$\frac{m^2}{2} j^\mu_{\text{induced}} = \begin{pmatrix} 0 \\ -\frac{1}{3} m^2 \boldsymbol{A} \end{pmatrix}$$

More complicated expressions hold with general k. The Kubo equation can be solved numerically; the resulting profile is a non-Abelian generalization of a plasma plane wave.

The physics of all these solutions, as well as of other, still undiscovered ones, remains to be elucidated, and I invite any of you to join in this interesting task.

We see that Debye electric screening is reproduced in essentially the same form as in an Abelian plasma (to leading order). How about magnetic screening? It is important to appreciate that the above time-independent, space-independent induced current, with $\mathbf{j}$ proportional to $\mathbf{A}$, does **not** describe magnetic screening because screening is determined by static configurations. Thus we conclude that the hard-thermal-loop limit of hot QCD does not show magnetic screening. Indeed it appears that if one proceeds perturbatively, beyond the resummed perturbation expansion of hard thermal loops, no direct evidence for magnetic screening can be found.

However, there is indirect evidence: although the hard thermal loop resummation cures some of the perturbative infrared divergences, as one calculates to higher perturbative orders, they reappear essentially due to the non-linear interactions between electric (temporal) and unscreened magnetic (spatial) degrees of freedom as well as among the magnetic degrees of freedom due to their self-interaction. (Such interactions are absent in an Abelian theory.) Consequently it is believed that non-perturbative magnetic screening arises in the non-Abelian theory, and it is recalled that, as mentioned in the Introduction, there is something akin to a magnetic source in Yang-Mills theory.

Another qualitative argument can be offered to make plausible the idea that a magnetic mass should arise. Although I have argued that high-temperature dimensional reduction from four to three dimensions can not be carried out reliably for a gauge theory, one may speculate that there is **some** truth in the idea, when restricted to magnetic (spatial) components of the non-Abelian potential. So one is led, as preliminary to studying the full QCD problem, to an analysis of three-dimensional Euclidean Yang-Mills theory at zero temperature. One quickly discovers that infrared divergences are present in perturbation theory for this model as well, so here again arises the question of a dynamically induced mass. In three dimensions, the coupling constant squared $g^2_{(3)}$ carries dimensions of mass. (Recall that in a high-temperature reduction $g_{(3)}$ is related to the four-dimensional coupling g by $g_{(3)} = g\sqrt{T}$.) Therefore it is plausible that three-dimensional Yang-Mills theory generates an $O(g^2_{(3)})$ mass, which eliminates its perturbative infrared divergences and suggests the occurrence of an $O(g^2T)$ magnetic mass in the four-dimensional theory at high T. Unfortunately thus far no analysis of the three-dimensional Yang-Mills model has led to a proof of such mass generation.

Since the mass is not seen in perturbative expansions, even resummed ones, one attempts a non-perturbative calculation, based on a gap equation. Of course an exact treatment is impossible; one must be satisfied with an approximate gap equation, which effectively sums a large, but still incomplete set of graphs. At the same time, gauge invariance should be maintained; gauge non-invariant approximations are not persuasive.

Deriving an approximate, but gauge invariant gap equation is most efficiently carried out in a functional integral formulation. We begin by reviewing how a one-loop gap equation is gotten from the functional integral, first for a non-gauge theory of a scalar field φ, then we indicate how to extend the procedure when gauge invariance is to be maintained for a gauge field A_μ.

Consider a self-interacting scalar field theory (in the Euclidean formulation) whose potential $V(\varphi)$ has no quadratic term, so in direct perturbation theory one may encounter infrared divergences, and one enquires whether a mass is generated, which would cure them.

$$\begin{aligned} \mathcal{L} &= \tfrac{1}{2}\partial_\mu\varphi\partial^\mu\varphi + V(\varphi) \\ V(\varphi) &= \lambda_3\varphi^3 + \lambda_4\varphi^4 + \ldots. \end{aligned}$$

The functional integral for the Euclidean theory involves the negative exponential of the action $I = \int \mathcal{L}$. Separating the quadratic, kinetic part of I, and expanding the exponential of the remainder in powers of the field yields the usual loop expansion. As mentioned earlier, the loop expansion may be systematized by introducing a loop-counting parameter ℓ and considering $e^{-\frac{1}{\ell}I(\sqrt{\ell}\varphi)}$: the power series in ℓ is the loop expansion. To obtain a gap equation for a possible mass μ, we proceed by adding and subtracting $I_\mu = \frac{\mu^2}{2}\int\varphi^2$, which of course changes nothing.

$$I = I + I_\mu - I_\mu$$

Next the loop expansion is reorganized by expanding $I + I_\mu$ in the usual way, but taking $-I_\mu$ as contributing at one loop higher. This is systematized as in the hard-thermal-loop application with an effective action, I_ℓ, containing the loop counting parameter ℓ, which organizes the loop expansion in the indicated manner:

$$I_\ell = \frac{1}{\ell}\left(I(\sqrt{\ell}\varphi) + I_\mu(\sqrt{\ell}\varphi)\right) - I_\mu(\sqrt{\ell}\varphi)$$

An expansion in powers of ℓ corresponds to a resummed series; keeping all terms and setting ℓ to unity returns us to the original theory (assuming that rearranging the series does no harm); approximations consist of keeping a finite number of terms: the $O(\ell)$ term involves a single loop.

The gap equation is gotten by considering the self energy Σ of the complete propagator. To one-loop order, the contributing graphs are depicted in the Figure.

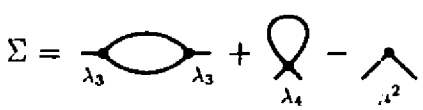

Self energy resummed to one-loop order.

Regardless of the form of the exact potential, only the three- and four- point vertices are needed at one-loop order; the "bare" propagator is massive thanks to the addition of the mass term $\frac{1}{\ell}I_\mu(\sqrt{\ell}\varphi) = \frac{\mu^2}{2}\int\varphi^2$; the last $-\mu^2$ in the Figure comes from the subtraction of the same mass term, but at one-loop order: $-I_\mu(\sqrt{\ell}\varphi) = -\ell\frac{\mu^2}{2}\int\varphi^2$.

The gap equation emerges when it is demanded that Σ does not shift the mass μ. In momentum space, we require

$$\Sigma(p)\Big|_{p^2=-\mu^2} = 0$$

$$\Big|_{p^2=-\mu^2} = \mu^2$$

Graphical depiction of above equation.

While these ideas can be applied to a gauge theory, it is necessary to elaborate them so that gauge invariance is preserved. We shall discuss solely the three-dimensional non-Abelian Yang-Mills model (in Euclidean formulation) as an interesting theory in its own right, and also as a key to the behavior of spatial variables in the physical, four-dimensional model at high temperature.

The starting action I is the usual one for a gauge field.

$$I = \int d^3x \ \mathrm{tr}\ \tfrac{1}{2} F^i F^i$$
$$F^i = \tfrac{1}{2}\epsilon^{ijk} F_{jk}$$

While one may still add and subtract a mass-generating term I_μ, it is necessary to preserve gauge invariance. Thus we seek a gauge invariant functional of A_i, $I_\mu(A)$, whose quadratic portion gives rise to a mass. Evidently

$$I_\mu(A) = -\frac{\mu^2}{2} \int d^3x \ \mathrm{tr}\ A_i \left(\delta_{ij} - \frac{\partial_i \partial_j}{\nabla^2}\right) A_j + \ldots$$

The transverse structure in the above equation guarantees invariance against Abelian gauge transformations; the question then remains how the quadratic term is to be completed in order that $I_\mu(A)$ be invariant against non-Abelian gauge transformations. [In fact for the one-loop gap equation only terms through $O(A^4)$ are needed.]

A very interesting proposal for $I_\mu(A)$ was given by Nair[15,16] who also put forward the scheme for determining the magnetic mass, which we have been describing. By modifying in various ways the hard thermal loop generating functional (which gives a four-dimensional, gauge invariant but Lorentz non-invariant effective action with a transverse quadratic term), he arrived at a gauge and rotation invariant three-dimensional structure, which can be employed in the derivation of a gap equation.*

Let me describe Nair's modification. Recall that the hard-thermal-loop generating functional, which I record here again,

$$\Gamma_{\mathrm{HTL}} = \frac{1}{2} \int d\Omega_{\hat{q}} [Q_+^\mu Q_-^\nu A_\mu^a A_\nu^a + S(Q_+^\mu A_\mu) + S(Q_-^\mu A_\mu)]$$

*A gap equation for the full gauge-field propagator, rather than just for the mass, has been put forward and analyzed by Cornwall *el al.*; see *Phys. Lett.* **B153**, 173 (1985) and *Phys. Rev. D* **34**, 585 (1986).

is gauge invariant because $Q^\mu_\pm = (0, \pm\hat{q})$ is light-like and S is the Chern-Simons eikonal. Before averaging over $\Omega_{\hat{q}}$ one is dealing with a functional of only $A_\pm$; after averaging all four components of A_μ enter. With Nair,[15,16] we observe that another choice for $Q^\mu_\pm$ can be made, where those vectors remain light-like, but have vanishing time component. This is achieved when the spatial components of $Q^\mu_\pm$ are complex and of zero length; for example:

$$Q^\mu_+ = (0, \mathbf{q}) \qquad Q^\mu_- = (0, \mathbf{q}^*)$$

$$\mathbf{q} = (-\cos\theta\cos\varphi - i\sin\varphi, -\cos\theta\sin\varphi + i\cos\varphi, \sin\theta) = \hat{\theta} + i\hat{\varphi}$$

Evidently $\mathbf{q}^2 = 0$, $Q^2_+ = 0$ and $Q_- = Q^*_+$. Using these forms for $Q^\mu_\pm$ in $\Gamma_{\rm HTL}$ still leaves it gauge invariant. Also it is clear that $\Gamma_{\rm HTL}$ is real and depends only on the spatial components of the vector potential. Hence this is an excellent candidate for $I_\mu(A)$, which therefore, following Nair, we take it to be

$$\frac{\mu^2}{4\pi}\Gamma_{\rm HTL}(A)\Big|_{\substack{\text{evaluated}\\ \text{as above}}}$$

The scheme proceeds as in the scalar theory, except that $I_\mu(A)$ gives rise not only to a mass term for the free propagator, but also to higher-point interaction vertices. At one loop only the three- and four- point vertices are needed, and to this order the subtracting term uses only the quadratic contribution. Thus the gap equation reads, pictorially

The first three graphs are as in ordinary Yang-Mills theory, with conventional vertices, but massive gauge field propagator (solid line);

$$D_{ij}(p) = \delta_{ij}\frac{1}{p^2+\mu^2}$$

the first graph depicting the gauge compensating "ghost" contribution, has massless ghost propagators (dotted line) and vertices determined by the quantization gauge, conveniently chosen, consistent with the above form for the propagator, to be

$$\mathcal{L}_{\substack{\text{gauge}\\ \text{fixing}}} = \tfrac{1}{2}\nabla\cdot\mathbf{A}(1-\mu^2/\nabla^2)\nabla\cdot\mathbf{A}$$

The remaining three graphs arise from Nair's form for the hard thermal loop-inspired $I_\mu(A)$, with solid circles denoting the new non-local vertices. As it happens, the last graph with the four-point vertex vanishes, while the three-point vertex reads

$$^{N}V^{abc}_{ijk}(\mathbf{p},\mathbf{q},\mathbf{r}) =$$
$$-\frac{i\mu^2 f^{abc}}{3!(\mathbf{p}\times\mathbf{q})^2}\left\{\frac{1}{3}\left(\frac{\mathbf{p}\cdot\mathbf{q}}{p^2}+\frac{\mathbf{r}\cdot\mathbf{q}}{r^2}\right)p_ip_jp_k - \frac{\mathbf{r}\cdot\mathbf{p}}{3r^2}(q_iq_jp_k + q_ip_jq_k + p_iq_jq_k)\right\} + \text{5 permutations}$$

$$p+q+r=0$$

The permutations ensure that the vertex is symmetric under the exchange of any pair of

index sets $(a\ i\ p), (b\ j\ q), (c\ k\ r)$. Inverse powers of momenta signal the non-locality of the vertex. [We discuss the $SU(N)$ theory, with structure constants f^{abc}.]

The result of the computation is

$$
\begin{aligned}
{}^{N}\Pi_{ij}^{ab} &= \delta^{ab}\Pi_{ij}^{N} \\
\Pi_{ij}^{N} &= \Pi_{ij}^{YM} + \overline{\Pi}_{ij}^{N}
\end{aligned}
$$

Π_{ij}^{YM} is the contribution from the first three Yang-Mills graphs and $\overline{\Pi}_{ij}^{N}$ sums the graphs from $I_\mu(A)$. The reported results are[17]

$$
\begin{aligned}
\Pi_{ij}^{YM}(p) &= N(\delta_{ij} - \hat{p}_i\hat{p}_j)\left[\left(\frac{-13p^2}{64\pi\mu} + \frac{5\mu}{16\pi}\right)\frac{2\mu}{p}\tan^{-1}\frac{p}{2\mu} - \frac{\mu}{16\pi} - \frac{p}{64}\right] \\
&\quad + N\hat{p}_i\hat{p}_j\left[\left(\frac{p^2}{32\pi\mu} + \frac{\mu}{8\pi}\right)\frac{2\mu}{p}\tan^{-1}\frac{p}{2\mu} + \frac{\mu}{8\pi} - \frac{p}{32}\right] \\
\overline{\Pi}_{ij}^{N}(p) &= N(\delta_{ij} - \hat{p}_i\hat{p}_j)\left[\left(\frac{3p^2}{64\pi\mu} + \frac{3\mu}{16\pi}\right)\frac{2\mu}{p}\tan^{-1}\frac{p}{2\mu} - \frac{p^2}{3\pi\mu}\left(\frac{\mu^2}{p^2}+1\right)^2\frac{\mu}{p}\tan^{-1}\frac{p}{\mu} + \frac{\mu}{16\pi} + \frac{\mu^3}{8\pi p^2}\right. \\
&\quad \left. - N\hat{p}_i\hat{p}_j\left[\left(\frac{p^2}{32\pi\mu} + \frac{\mu}{8\pi}\right)\frac{2\mu}{p}\tan^{-1}\frac{p}{2\mu} + \frac{\mu}{8\pi} - \frac{p}{32}\right]\right.
\end{aligned}
$$

The Yang-Mills contribution Π_{ij}^{YM} is not separately gauge-invariant (transverse) owing to the massive gauge propagators. [At $\mu = 0$, Π_{ij}^{YM} reduces to the standard result[18]: $N(\delta_{ij} - \hat{p}_i\hat{p}_j)\left(-\frac{7}{32}p\right)$.] The longitudinal terms in Π_{ij}^{YM} are canceled by those in $\overline{\Pi}_{ij}^{N}$, so that the total is transverse.

$$
\Pi_{ij}^{N}(p) = N(\delta_{ij} - \hat{p}_i\hat{p}_j)\left[\left(\frac{-5p^2}{32\pi\mu} + \frac{1}{2\pi}\mu\right)\frac{2\mu}{p}\tan^{-1}\frac{p}{2\mu} - \frac{p^2}{8\pi\mu}\left(\frac{\mu^2}{p^2}+1\right)^2\frac{\mu}{p}\tan^{-1}\frac{p}{\mu} + \frac{\mu^3}{8\pi p^2}\right]
$$

[Dimensional regularization is used to avoid divergences.]

Before proceeding, let us note the analytic structures in the above expressions, which are presented for Euclidean momenta, but for the gap equation have to be evaluated at the Minkowski value $p^2 = -\mu^2 < 0$. Analytic continuation for the inverse tangent is provided by

$$
\frac{1}{x}\tan^{-1}x = \frac{1}{2\sqrt{-x^2}}\ln\frac{1+\sqrt{-x^2}}{1-\sqrt{-x^2}}
$$

Evidently $\Pi_{ij}^{N}(p)$ possesses threshold singularities, at various values of $-p^2$.

There is a singularity at $p^2 = -4\mu^2$ (from $\tan^{-1}\frac{p}{2\mu}$) arising because the graphs in the Figure containing massive propagators describe the exchange of two massive gauge "particles". Moreover, there is singularity at $p^2 = -\mu^2$ (from $\tan^{-1}\frac{p}{\mu}$) and also, separately in Π_{ij}^{YM} and $\overline{\Pi}_{ij}^{N}$, at $p^2 = 0$ (from the $\pm\frac{p}{64}, \pm\frac{p}{32}$ terms). These are understood in the following way. Even though the propagators are massive, the non-local three-point function contains $\frac{1}{p^2}$,

$\frac{1}{q^2}$, $\frac{1}{r^2}$ contributions, which act like massless propagators. Thus the threshold at $p^2 = -\mu^2$ arises from the exchange of a massive line (propagator) together with a massless line (from the vertex). Similarly the threshold at $p^2 = 0$ arises from the massless lines in the vertex (and also from massless ghost exchange). The expressions acquire an imaginary part when the largest threshold, $p^2 = 0$, is crossed: Π_{ij}^{YM} and $\overline{\Pi}_{ij}^{N}$ are complex for $p^2 < 0$.

In the complete answer, the $p^2 = 0$ thresholds cancel, and the singularity at the $p^2 = -\mu^2$ threshold is extinguished by the factor $(\frac{\mu^2}{p^2} + 1)^2$. Consequently Π_{ij}^{N} becomes complex only for $p^2 < -\mu^2$, and is real, finite at $p^2 = -\mu^2$.

$$\Pi_{ij}^{N}(p)\Big|_{p^2=-\mu^2} = (\delta_{ij} - \hat{p}_i\hat{p}_j)\,\frac{N\mu}{32\pi}\,(21\ln 3 - 4)$$

From the gap equation in the last Figure, the result for the mass is[17]

$$\mu = \frac{N}{32\pi}\,(21\ln 3 - 4) \sim 2.384\,\frac{N}{4\pi}$$

[in units of the coupling constant $g_{(3)}^2$ (or g^2T), which has been scaled to unity].

Before accepting this plausible answer for μ, it is desirable to assess higher order corrections, for example two-loop contributions. Unfortunately, an estimate[17] indicates that 79 graphs have to be evaluated, and the task is formidable.

An alternative test for the reliability of the above approach and for assessing the stability of the result against corrections has been proposed.[19]

It is suggested that the gap equation be derived with a gauge invariant completion different from Nair's. Rather than taking inspiration from hard thermal loops (which after all have no intrinsic relevance to the three-dimensional gauge theory†), the following formula for I_μ is taken

$$I_\mu(A) = \mu^2 \int d^3x\ \mathrm{tr}\ F^i \frac{1}{D^2} F^i$$

where D^2 is the gauge covariant Laplacian. While ultimately there is no *a priori* way to select one gauge-invariant completion over another, we remark that expressions like the above appear in two-dimensional gauge theories (Polyakov gravity action, Schwinger model) and are responsible for mass generation. If two- and higher- loop effects are indeed ignorable, this alternative gauge invariant completion, which corresponds to an alternative resummation, should produce an answer close to the previously obtained one.

With the alternative I_μ, the graphs are as before, where the propagator is still given by the previous expression. However, the three- and four- point vertices in $I_\mu(A)$ are different. One now finds for the non-local three-point vertex

$$V_{ijk}^{abc}(\mathbf{p},\mathbf{q},\mathbf{r}) = \frac{-i\mu^2}{3!} f^{abc}\,(\delta_{ij}\mathbf{q}\cdot\mathbf{r} + q_i p_j)\,\frac{p_k}{p^2 q^2} + \text{ 5 permutations}$$

† Recall that the hot thermal loop generating functional is related to the Chern-Simons eikonal. Since the Chern-Simons term *is* a three-dimensional structure, this fact may provide a basis for establishing the relevance of the hard thermal loop generating functional to three-dimensional Yang Mills theory. The point is under investigation by D. Karabali and V. P. Nair.

$$p+q+r=0$$

and the non-local four-point vertex reads

$$V^{abcd}_{ijkl}(\mathbf{p},\mathbf{q},\mathbf{r},\mathbf{s}) = \frac{-\mu^2}{4!} f^{abe} f^{cde} \left\{ \frac{1}{2}\delta_{jk}\,\epsilon_{imn}\,\epsilon_{\ell on}\,\frac{p_m}{p^2}\,\frac{s_0}{s^2} \right.$$
$$\left. -\frac{1}{2r^2}\left(\frac{1}{4}\epsilon_{ijm}\epsilon_{k\ell m} - \epsilon_{imn}\epsilon_{k\ell n}\frac{p_m}{p^2}(p-r-s)_j + \epsilon_{imn}\epsilon_{\ell on}\frac{p_m}{p^2}\frac{s_0}{s^2}(p-r-s)_j(p+q-s)_k\right)\right\}$$
$$+ \text{ 23 permutations}$$

$$p+q+r+s=0$$

These vertices do not affect the first three graphs in the Figure so that Π^{YM}_{ij} is as before. However, in the last three graphs the alternative non-local vertices produce the following result, with the help of dimensional regularization,

$$\overline{\Pi}_{ij}(p) = N(\delta_{ij}-\hat{p}_i\hat{p}_j)\left(\left(\frac{p^6}{128\pi\mu^5}+\frac{p^4}{32\pi\mu^3}+\frac{7p^2}{64\pi\mu}+\frac{27\mu}{64\pi}-\frac{\mu^3}{16\pi p^2}\right)\frac{2\mu}{p}\tan^{-1}\frac{p}{2\mu}\right.$$
$$-\left(\frac{p^6}{32\pi\mu^5}+\frac{p^4}{16\pi\mu^3}-\frac{p^2}{16\pi\mu}+\frac{\mu}{32\pi}\right)\left(\frac{\mu^2}{p^2}+1\right)^2\frac{\mu}{p}\tan^{-1}\frac{p}{\mu}$$
$$\left.-\frac{p^2}{32\pi\mu}-\frac{3\mu}{16\pi}+\frac{49\mu^3}{96\pi p^2}+\frac{\mu^5}{32\pi p^4}+\frac{p^5}{128\mu^4}+\frac{p^3}{32\mu^2}-\frac{p}{16}\right)$$
$$-N\hat{p}_i\hat{p}_j\left(\left(\frac{p^2}{32\pi\mu}+\frac{\mu}{8\pi}\right)\frac{2\mu}{p}\tan^{-1}\frac{p}{2\mu}+\frac{\mu}{8\pi}-\frac{p}{32}\right)$$

A check on this very lengthy calculation is that summing it with Yang-Mills contributions yields a transverse expression.

$$\Pi_{ij}(p) = N(\delta_{ij}-\hat{p}_i\hat{p}_j)\left(\left(\frac{p^6}{128\pi\mu^5}+\frac{p^4}{32\pi\mu^3}-\frac{3p^2}{32\pi\mu}+\frac{47\mu}{64\pi}-\frac{\mu^3}{16\pi p^2}\right)\frac{2\mu}{p}\tan^{-1}\frac{p}{2\mu}\right.$$
$$-\left(\frac{p^6}{32\pi\mu^5}+\frac{p^4}{16\pi\mu^3}-\frac{p^2}{16\pi\mu}+\frac{\mu}{32\pi}\right)\left(\frac{\mu^2}{p^2}+1\right)^2\frac{\mu}{p}\tan^{-1}\frac{p}{\mu}$$
$$\left.-\frac{p^2}{32\pi\mu}-\frac{\mu}{4\pi}+\frac{49\mu^3}{96\pi p^2}+\frac{\mu^5}{32\pi p^4}+\frac{p^5}{128\mu^4}+\frac{p^3}{32\mu^2}-\frac{5p}{64}\right)$$

Another check on the powers of $\frac{p}{\mu}$ is that the above reduces to the Yang-Mills result at $\mu = 0$.[18]

Just as Nair's expression, the present formula exhibits threshold singularities: at $-p^2 = 4\mu^2$, which are beyond our desired evaluation point $-p^2 = \mu^2$; there are also threshold singularities at $-p^2 = \mu^2$, which are extinguished by the factor $(\frac{\mu^2}{p^2}+1)^2$; however, those at $p^2 = 0$ do *not* cancel, in contrast to the previous case — indeed $\Pi_{ij}(p)$ diverges at $p^2 = 0$, and is complex for $p^2 < 0$. [It is interesting to remark that the last graph in the last Figure, involving the new four-point vertex, which vanishes in Nair's evaluation, here gives a transverse result with unextinguished threshold singularities at $-p^2 = \mu^2$ and at $p^2 = 0$. The

protective factor of $(\frac{\mu^2}{p^2}+1)^2$ arises when the remaining two graphs are added to form $\overline{\Pi}_{ij}$, and these also contain non-canceling $p^2=0$ threshold singularities, as does the Yang-Mills contribution.]

Although $\Pi_{ij}(p)\Big|_{p^2=-\mu^2}$ is finite, it is complex and the gap equation has no solution for real μ^2, owing to unprotected threshold singularities at $p^2=0$, which lead to a complex $\Pi_{ij}(p)$ for $p^2<0$.

$$\begin{aligned}\mu &= \frac{N}{32\pi}\left(29\tfrac{1}{4}\ln 3 - 22\tfrac{1}{3}\right) \pm iN\frac{13}{128}\\ |\mu| &\sim 1.769\frac{N}{4\pi}\end{aligned}$$

It may be that the hot thermal loop-inspired completion for the mass term is uniquely privileged in avoiding complex values for $-\mu^2 \le p^2 \le 0$, but we see no reason for this.[‡] Absent any argument for the disappearance of the threshold at $p^2=0$, and reality in the region $-\mu^2 \le p^2 < 0$, we should expect that also the hot thermal loop-inspired calculation will exhibit such behavior beyond the 1-loop order.[§]

Thus until the status of threshold singularities is clarified, the self-consistent gap equation for a magnetic mass provides inconclusive evidence for magnetic mass generation. Moreover, if there exist gauge invariant completions for the mass term, other than the hard thermal loop-inspired one, that lead to real Π_{ij} at $p^2=-\mu^2$, it is unlikely that they all would give the same μ at one loop level, which is further reason why higher orders must be assessed.

[‡] We note that Nair's hot thermal loop-inspired vertex ${}^{N}Vijk^{abc}$ is less singular than the alternative V_{ijk}^{abc}, when any of the momentum arguments vanish. Correspondingly $\Pi_{ij}^{N}(p)$ is finite at $p^2=0$, in contrast to $\Pi_{ij}(p)$ which diverges at $\frac{1}{p^2}$. However, we do not recognize that this variety of singularities at $p^2=0$ influences reality at $p^2=-\mu^2$; indeed the individual graphs contributing to Π_{ij}^{N} are complex at that point, owing to non-divergent threshold singularities at $p^2=0$ that cancel in the sum.

[§] V.P. Nair states that at the two loop level, there is evidence for $\ln(1+\frac{p^2}{\mu^2})$ terms, but it is not known whether they acquire a protective factor of $(\frac{p^2}{\mu^2}+1)$.

References

1. For a summary, see R. Jackiw and G. Amelino-Camelia, "Field Theoretical Background for Thermal Physics" in *Banff CAP Workshop on Thermal Field Theory*, F. Khanna, R. Kobes, G. Kunstatter, and H. Umezawa eds. (World Scientific, Singapore, 1994).
2. R. Jackiw and S. Templeton, "How Super-Renormalizable Interactions Cure their Infrared Divergences," *Phys. Rev. D* **23** (1981) 2291.
3. R. Pisarski, "How to Compute Scattering Amplitudes in Hot Gauge Theories," *Physica* **A158** (1989) 246.
4. E. Braaten and R. Pisarski, "Soft Amplitudes in Hot Gauge Theory: a General Analysis," *Nucl. Phys.* **B337** (1990) 569; J. Frenkel and J. C. Taylor, "High-Temperature Limit of Thermal QCD," *Nucl. Phys.* **B334** (1990) 199.
5. R. Jackiw and V. P. Nair, "High Temperature Response Function and the Non-Abelian Kubo Formula," *Phys. Rev. D* **48** (1993) 4991.
6. J. C. Taylor and S. M. Wong, "The Effective Action of Hard Thermal Loops in QCD," *Nucl. Phys.* **B346** (1990) 115.
7. R. Jackiw, "Gauge Theories in Three Dimensions ($\approx$ at Finite Temperature)" in *Gauge Theories of the Eighties*, R. Ratio and J. Lindfors, eds. Lecture Notes in Physics **181** (1983) 157 (Springer, Berlin).
8. R. Efraty and V. P. Nair, "Action for the Hot Gluon Plasma Based on the Chern-Simons Theory," *Phys. Rev. Lett.* **68** (1992) 2891, "Chern-Simons Theory and the Quark-Gluon Plasma," *Phys. Rev. D* **47** (1993) 5601.
9. D. Gonzales and A. Redlich, "A Gauge Invariant Action for 2+1 Dimensional Topological Yang-Mills Theory," *Ann. Phys.* (NY) **169** (1986) 104; G. Dunne, R. Jackiw and C. Trugenberger, "Chern-Simons Theory in the Schrödinger Representation," *Ann. Phys.* (NY) **149** (1989) 197.
10. J.-P. Blaizot and E. Iancu, "Kinetic Equations for Long-Wavelength Excitation of Quark-Gluon Plasma," *Phys. Rev. Lett.* **70** (1993) 3376, "Soft Collective Excitations in Hot Gauge Theories," *Nucl. Phys.* **B 417** (1994) 608.
11. R. Jackiw, Q. Liu, and C. Lucchesi, "Hard Thermal Loops, Static Response and Composite Effective Action," *Phys. Rev. D* **49** (1994) 6787.
12. P. Kelly, Q. Liu, C. Lucchesi, and C. Manuel, "Deriving the Hard Thermal Loops of QCD from Classical Transport Theory," *Phys. Rev. Lett.* **72** (1994) 3461, "Classical Transport Theory and Hard Thermal Loops in the Quark-Gluon Plasma," *Phys. Rev. D* **50** (1994) 4209.
13. E. M. Lifshitz and L. P. Pitaevskii, *Physical Kinetics* (Pergamon, Oxford UK, 1981).
14. J.-P. Blaizot and E. Iancu, "Non-Abelian Excitation of the Quark-Gluon Plasma," *Phys. Rev. Lett.* **72** (1994) 3317, "Non-Abelian Plane Waves in the Quark-Gluon Plasma," *Phys. Lett.* **B326** (1994) 138.
15. V.P., Nair, "Hard Thermal loops on a Moving Plasma and a Magnetic Mass Term," *Phys. Lett.* **B352** (1995) 117.
16. For a summary, see V.P. Nair, "Chern-Simons and WZNW theories and the quark-gluon plasma," Lectures at Mt. Sorak symposium, Korea, June 1994.
17. G. Alexanian and V.P. Nair, "A self-consistent inclusion of magnetic screening for the quark-gluon plasma," *Phys. Lett.* **B352** (1995) 435.
18. S. Deser, R. Jackiw and S. Templeton, "Topologically Massive Gauge Theories," *Ann. Phys.* (NY) **140** (1982) 372 (E) **185** (1988) 406.

19. R. Jackiw and S.-Y. Pi, "Threshhold Singularities and the Magnetic Mass in Hot QCD" *Phys. Lett.* **B368**, 131 (1996).

The Higgs Boson : Why, Where, How and When

Rogerio Rosenfeld
Instituto de Física Teórica, Universidade Estadual Paulista
Rua Pamplona, 145; 01405-900 - São Paulo,SP, Brazil

Received March, 1996

A brief non-technical review about the Standard Model Higgs boson and its discovery possibilities at future planned colliders is presented. Plenary talk presented at the Brazilian Meeting on Particles and Fields, Caxambu, October 1995.

I Motivation (Why)

The Standard Model (SM) [1] has been tested to an unprecedent degree of accuracy of 0.1% in some of the physical observables at LEP1, with many implications to physics beyond the SM [2]. However, we still have very little information about the Higgs sector of the SM, which is responsible for the spontaneous breaking of the electroweak symmetry.

The Higgs field (and the Higgs potential) is a necessary ingredient of the SM for three reasons :

- It generates all the fermion masses ;
- It generates masses for the electroweak gauge bosons $W^{\pm}$ and Z^0 ;
- It ensures the renormalizability (*i.e.*, the good high energy behaviour of the scattering amplitudes) of the SM model.

Any alternative model to the Higgs sector as a mechanism for electroweak symmetry breaking must also include the above features (the renormalizability condition may refer to a more fundamental model that has the SM as its low energy limit).

The Higgs sector of the SM predicts the existence of a "witness" to the process of symmetry breaking, the now famous Higgs boson. Finding the Higgs boson and studying its properties has become the foremost priority in particle physics. There is even a whole book dedicated to the problem of "hunting" for the Higgs boson [3]. I can't do justice to this vast subject in an one-hour talk but I'll try my best. For the interested reader, I recommend some recent detailed reviews that will be used throughout this talk [3, 4, 5, 6].

Besides the Higgs boson, there is another witness to the process of symmetry breaking, namely the longitudinal components of the electroweak gauge bosons. We'll see below that by studying the scattering of longitudinally polarized $W^{\pm}$ and Z^0 we can also obtain information on the symmetry breaking mechanism.

The Higgs boson mass is a free parameter in the SM and in the next section we review some educated guesses about how heavy the Higgs boson can be.

II Theoretical Prejudices About the Higgs Boson

II.1 Perturbative Unitarity

If one considers the s-wave projection of the scattering amplitude of $W_L^+W_L^- \to Z_LZ_L$ (the subscript L denotes the longitudinal component of the vector boson) in the SM one finds that it is independent of the c.m. energy (has a good high energy behaviour) and it is proportional to the square of the Higgs boson mass :

$$a_0(W_L^+W_L^- \to Z_LZ_L) \propto G_F M_H^2 \tag{1}$$

where G_F is the Fermi constant and M_H is the Higgs boson mass. Perturbative unitarity requires that for any partial wave J, $|a_J(s) < 1|$ and this implies an upper limit on M_H. A coupled channel analyses results in [7] :

$$M_H < 700 \text{ GeV} \tag{2}$$

If $M_H > 700$ GeV, higher order (loops) corrections to the scattering amplitude become important since we believe the theory to be unitary. This means that the theory is *strongly coupled* and we can't trust perturbation theory to compute scattering amplitudes (more on that later).

II.2 Triviality

In the SM, the Higgs boson mass is given by :

$$M_H^2 = 2\lambda v^2 \tag{3}$$

where λ is the unknown Higgs self-coupling and v is the vacuum expectation value of the Higgs field and is determined experimentally to be $v = 246$ GeV.

The Higgs self-coupling λ depends on the energy scale via the renormalization group equations. It turns out that the self-coupling *grows* with energy (it is not asymptotically free) and we can relate λ at two energy scales v and Λ ($\gg v$) by :

$$\frac{1}{\lambda(v)} - \frac{1}{\lambda(\Lambda)} = \frac{3}{4\pi^2} \ln(\Lambda^2/v^2) \tag{4}$$

One finds that the self-coupling has an infinity (known as Landau pole) at an energy scale

$$\Lambda = v e^{\frac{2\pi^2}{3\lambda(v)}} \tag{5}$$

What this means is that the theory does not make sense at these high energies. We are dealing with an *effective* theory, valid for energy scales $E \ll \Lambda$.

The so-called triviality of the theory appears if we insist that the theory is well defined up to arbitrarily large energies, *i.e.* if we take $\Lambda \to \infty$, which implies that theory is free (trivial), since $\lambda(v) \to 0$ from equation (5).

Equation (4) combined with equation (3) results in an *upper* limit for the Higgs boson mass in terms of Λ [8] :

$$M_H^2 < \frac{8\pi^2 v^2}{3 \ln(\Lambda^2/v^2)} \tag{6}$$

If we decide that the SM is valid all the way up to the Planck energy $M_{Pl} = 10^{19}$ GeV, where one has to incorporate gravity in the SM, we find $M_H < 150$ GeV. However, if we are more modest and decide that the Higgs mass itself may be the scale where new physics comes about we would have $M_H < 800$ GeV.

One could rightly argue that these arguments are based on perturbative calculations that are not valid when the Higgs self-coupling constant gets large. However, non-perturbative lattice calculations tend to agree with this naive estimation [9].

Let's pause here for a brief digression that is somewhat beyond the scope of this talk, which is intended to concentrate mainly on the SM Higgs boson. We saw that the SM is an effective theory valid for energy scales $E \ll \Lambda$. We are now in a position to understand the two major contestants to superseed the SM, depending on what we choose for Λ :

- $\Lambda = M_{Pl} \Rightarrow M_H = \mathcal{O}(100)$ GeV

In this case one has to impose a tremendous amount of fine tuning in order to explain why $M_H/M_{Pl} \ll 1$ (the so-called naturalness problem). This problem is solved if one invokes the idea of supersymmetry (SUSY), a global symmetry relating fermions and bosons. Therefore, a minimal supersymmetric extension of the SM (denoted MSSM in the literature) has become a favorite candidate to be *the* new physics beyond the SM. It has received indirect experimental support from the unification of coupling constants that occur in SUSY extensions of grand unified

theories [10]. In the MSSM model, the particle spectrum is doubled with the introduction of supersymmetric partners to all particles already present in the SM. If SUSY were an unbroken symmetry, the SUSY partners would have the same mass as the original particles. Since this is not observed, SUSY must be broken and the SUSY partners must have masses of $\mathcal{O}(1\text{TeV})$ to avoid the naturalness problem to be reintroduced. The MSSM model also possesses an extended scalar sector, with five scalar bosons instead of the single Higgs boson of the SM and a firm prediciton of the model is that the lightest scalar must have a mass $M_S < 150$ GeV [11]. Hence, the MSSM has a very rich phenomenology around the TeV scale that will not be discussed here.

- $\Lambda = M_H \Rightarrow M_H = \mathcal{O}(1\text{TeV})$

In this case the SM breaks down at around 1 TeV and the prototypical model that describes the new physics is called Technicolor model (TC), that contains new fermions (technifermions) interacting via a QCD-like interaction (technicolor). This new interaction becomes strong at the weak scale provoking the condensation of technifermions whereby the symmetry of the SM is dynamically broken. This class of models can easily generate masses for the electroweak gauge bosons but in order to generate masses for the fermions one has to extend the model by introducing a broken gauge interaction called Extended Technicolor (ETC). To date no realistic TC and ETC models have been constructed and the minimal ones run into problems with precision measurements at LEP1. However, the idea is appealling and must be kept alive. There are also common features of the various TC and ETC models that have interesting phenomenological consequences at future accelerators and should be investigated. [12].

II.3 (Meta)Stability

The effective potential of the SM Higgs sector can develop a non-standard minimum for values of the Higgs field much larger than the weak scale, depending also on the Higgs boson and top quark masses (M_H and m_t) [13]. By requiring that the SM vacuum is metastable, *i.e.* it doesn't decay to the non-standard vacuum one finds a *lower* limit to M_H that depends on m_t and on the energy scale Λ up to which the the effective potential remains valid.

Assuming a common scale Λ and $m_t = 175$ GeV, the upper limits from triviality and the lower limits from metastability are roughly :

$$\begin{aligned} \Lambda &= 10^{19}\,\text{GeV} \quad \Rightarrow 130 < M_H < 180\,\text{GeV} \\ \Lambda &= 10\,\text{TeV} \quad \Rightarrow 70 < M_H < 700\,\text{GeV} \end{aligned} \tag{7}$$

III Physical Properties of the SM Higgs Boson

The Higgs boson couples to fermions via Yukawa couplings that are proportional to the fermion mass. Therefore, the Higgs boson decays preferentiably to the heaviest fermion such that the decay $H \rightarrow f\bar{f}$ is kinematically allowed. It also couples to the electroweak gauge bosons $W^{\pm}$ and Z^0 and once the W^+W^- and Z^0Z^0 channels open up they dominate the Higgs decay rate. There are also one loop induced couplings like $H\gamma\gamma$, $H\gamma Z$ and Hgg, where g is the gluon field. Albeit small, these couplings are very important for Higgs boson production at hadron colliders (Hgg) and for a clean detection of a light Higgs boson ($H\gamma\gamma$), as will be seen below.

IV Where, How and When I : LEP1

The electron-positron accelerator LEP1 at CERN has finished this year its long run with center-of-mass energy on the Z boson peak, collecting approximately 10^7 Z's in its four detectors. They were able to set limits on the Higgs boson mass M_H in two different ways that we briefly describe below.

IV.1 Direct Searches

They have searched for the decay $Z \to H + Z^*$, with the subsequent decays $H \to b\bar{b}$ and $Z^* \to q\bar{q}, l\bar{l}, \nu\bar{\nu}$, where Z^* is an off-mass-shell Z boson. The branching ratio for this decay decreases very fast for large M_H, being of the order of 10^{-6} for $M_H \simeq 70$ GeV. With approximately 10^7 Z's they haven't found any events and consequently they are able to place lower limits on M_H. The combined 95% C.L. lower limit on M_H is 64.5 GeV [14].

IV.2 Indirect Searches

Due to the large number of events accumulated, LEP1 experiments were able to perform very precise measurements of electroweak observables. These observables $\mathcal{O}$ are sensitive to M_H and m_t via one loop effects :

$$\mathcal{O} = \mathcal{O}(\alpha_{em}, G_\mu, M_Z, m_t, M_H, \alpha_s) \tag{8}$$

where α_{em}, G_μ and α_s are the electromagnetic coupling constant, the muon decay constant and the strong coupling constant respectively.

Just to give an idea of the sensitivity of these measurements, we recall that before the announcement of the top quark last year from the Tevatron with a mass of $m_t = 181 \pm 12$ GeV (combined from CDF and D0), the precision measurements from LEP1 data already had $m_t = 176 \pm 20$ GeV. Unfortunately, the sensitivity to M_H is only logarithmic instead of quadratic as in the case of m_t. Therefore, the limits are much poorer in the Higgs case. From a global fit to the electroweak precision data one has [15] :

$$M_H = 76^{+152}_{-50}\text{GeV} \quad \Rightarrow \quad M_H < 700 \text{ GeV } @2\sigma \tag{9}$$

V Where, How and When II : LEP2

The LEP2 upgrade of LEP1 will begin operation this year, with a planned center-of-mass energy of $\sqrt{s} = 175$ GeV and luminosity $\mathcal{L} = 500$ pb^{-1} for the first year.

The four detectors will look for the Higgs boson produced primarily in the so-called Bjorken or Higgs-strahlung process :

$$e^+e^- \to Z^* \to HZ \to b\bar{b}f\bar{f} \tag{10}$$

The various possible final state channels with different fermion-antifermion pairs were studied. In all cases tagging the b-quarks with microvertex detectors is crucial in order to reject background.

The conclusion of several studies [5] is that a SM Higgs boson with mass up to 82 GeV can be found in the first year of LEP2 operation. In the subsequent years the center-of-mass energy will be incresed and the 5σ discovery limit for $\mathcal{L} = 500$ pb^{-1} is $M_H = 95(103)$ GeV for $\sqrt{s} = 192(205)$ GeV.

There is an interesting possibility to increase the discovery limits for the Higgs boson if there exist anomalously large $H\gamma\gamma$ and $HZ\gamma$ couplings. In the SM these couplings are very small since they are generated only at the 1-loop level. However, in an effective theory describing new physics beyond the SM, these couplings can be large and preliminary results show that a Higgs boson with mass up to 150 GeV could be found in the first year of LEP2 operation [16].

VI Where, How and When III : LHC

The LHC (Large Hadron Collider), a proton-proton accelerator with planned center-of-mass energy of $\sqrt{s} = 14$ TeV , has been approved for construction in the LEP tunnel at CERN and will probably begin operation around the year 2004. There will be two main experiments named ATLAS and CMS that will look for the Higgs boson.

There are four mechanisms for producing the Higgs boson at the LHC :

- gluon-gluon fusion ;
- W^+W^- and ZZ fusion;
- $q\bar{q}$ fusion ;
- Associated WH, ZH and $t\bar{t}H$ production.

Some of these processes have been computed at next-to-leading order in QCD [17] and at LHC energies the gluon-gluon fusion, in spite of being a 1-loop process, is the dominant mechanism.

The strategy to be adopted in searching for the Higgs boson at the LHC depends on its mass. Usually, three mass regions are considered and we summarize the results taken from ATLAS [18] below.

VI.1 Light Higgs, $80 < M_H < 120$ GeV

This is the most difficult case, since the dominant Higgs decay , $H \to b\bar{b}$, is swamped by QCD background. The strategy is to concentrate on the rare 1-loop induced decay $H \to \gamma\gamma$, with branching ratio of the order of 0.1%−0.2%. The low end of the mass range is the most challenging due to the small branching ratio and the large background. For a yearly luminosity of $\mathcal{L} = 100$ fb^{-1}, the number of LHC years necessary for a 5σ discovery at ATLAS for $M_H = 80(90)(100)(110)(120)(130)(150)$ GeV are respectively [18] 4.3(2.9)(1.3)(0.8)(0.6)(0.6)(1.1) years.

The associated WH and $t\bar{t}H$ processes are also useful in this mass range. The significance of the combined $\gamma\gamma$, WH and $t\bar{t}H$ processes can reach 6.4σ in a third of a LHC year for $M_H = 80$ GeV [18].

VI.2 Intermediate Higgs, $130 < M_H < 180$ GeV

In this mass range the branching ratio for $H \to ZZ^*$ can be as large as 8%, providing a clean signature for the Higgs boson. For a one year of LHC running at $\mathcal{L} = 100$ fb^{-1}year^{-1}, the significances of the Higgs signal for $M_H = 120(130)(150)(170)(180)$ are respectively [18] $2.4(8.5)(21.7)(6.5)(17.3)\sigma$, indicating that a Higgs boson in the intermediate mass range can be found in this channel.

VI.3 Heavy Higgs, $180 < M_H < 800$ GeV

In this mass range, the decay channel $H \to ZZ$ is fully open, with a branching ratio of approximately 30%. The subsequent decays $Z \to l^+l^-$ for both Z's provide a striking signature of four leptons (the so-called gold-plated mode) in the final state with a small background. Tha ATLAS collaboration claims detection of this mode up to a Higgs mass of 800 GeV for a one year of LHC running at $\mathcal{L} = 100$ fb^{-1}year^{-1} [18].

VII What if the Higgs boson is not found ?

It will be difficult to make the case for an elementary Higgs boson if it has a mass $M_H > 800$ GeV. In particular, SUSY extensions of the SM would be discarded. The Higgs boson's width becomes very large , $\Gamma_H \simeq 250$ GeV and one is reaching the triviality bound discussed previously, such that new physics should appear at around M_H. How can one study the electroweak symmetry breaking sector in this case ?

One of the signatures of electroweak symmetry breaking is the fact that the electroweak gauge vector bosons have masses, and hence they have a longitudinal component $V_L = (W_L, Z_L)$. Therefore, the interactions among V_L's carry some information about the electroweak symmetry breaking sector. In particular, in the case of a very heavy Higgs, the V_L's are strongly coupled and their interactions can be described by effective lagrangians [19], very much akin to pion physics. These effective lagrangians may contain scalar (Higgs-like) and/or vector (techni-rho -like) resonances.

Because of the strong couplings, there is an enhancement in the cross section $\sigma(pp \to V_L V_L X)$ that can be measured at LHC. These measurements can be used to distinguish different models of strongly interacting V_L's [20].

VIII Conclusions

It is clear that the the Higgs hunting season is open. Our weapons are the combination of accelerators & detectors & ingenuity.

LEP2 will be able to find a Higgs boson with mass up to 82 GeV in its first phase, maybe reaching up to $\simeq 100$ GeV at later stages. The LHC will probably detect the Higgs boson in the mass range $80 < M_H < 800$ GeV in the first decade of the next century. Detailed study of the Higgs boson properties will have to wait for the next generation of e^+e^- colliders, like the NLC (Next Linear Collider).

If the Higgs boson is not found at the LHC, one should be able to see the consequences of a strongly interacting $V_L V_L$ system, indicating the existence of new dynamics.

Therefore, we are bound to learn something interesting in the next 10 years !

References

[1] See, *e.g.*, C. Quigg, *Gauge Theories of strong, Weak and Electromagnetic Interactions*, (Benjamin/Cummings, 1983).

[2] See, *e.g.*, K. Hagiwara, talk presented at the *XVII International Symposium on Lepton and Photon Interactions at High Energies, 10-15 August 1995, Beijing, China*, KEK preprint 95-184, hep-ph/9512425.

[3] J.F. Gunion, H.E. Haber, G.L. Kane and S. Dawson, *The Higgs Hunter's Guide*, (Addison-Wesley, 1989).

[4] A. Djouadi, Int. J. Mod. Phys. **A10**, 1 (1995).

[5] Higgs Physics at LEP2, M. Carena and P. Zerwas (conveners), to appear in *Reports of the Workshop on Physics at LEP2*, G. Altarelli, T. Sjostrand and F. Zwirner (editors), CERN 96-01, hep-ph/9602250.

[6] J.F. Gunion, A. Stange and S. Willenbrock, preprint UCD-95-28, hep-ph/9602238.

[7] B.W. Lee, C. Quigg and H. Thacker, Phys. Rev. **D16**, 1519 (1977).

[8] N. Cabbibo, L. Maiani, G. Parisi and R. Petronzio, Nucl. Phys. **B158**, 295 (1979).

[9] U. Heller, M. Klomfass, H. Neuberger and P. Vranas, Nucl. Phys. **B405**, 555 (1993).

[10] J. Ellis, S. Kelley and D. Nanopoulos, Phys. Lett. **B260**, 131 (1991); U. Amaldi, W. de Boer and H. Furstenau, Phys. Lett. **B260**, 447 (1991); P. Langacker and M. Luo, Phys. Rev. **D44**, 817 (1991).

[11] See, *e.g.*, M. Carena, J.R. Espinosa, M. Quiros and C.E.M. Wagner, Phys. Lett. **B355**, 209 (1995).

[12] R.S. Chivukula, R. Rosenfeld, E.H. Simmons and J. Terning, Subgroup report for the "Electroweak Symmetry Breaking and Beyond the Standard Model" working group of the DPF Long Range Planning Study. To appear in "Electroweak Symmetry Breaking and Beyond the Standard Model", edited by T. Barklow, S. Dawson, H.E. Haber, and J. Siegrist, to be published by World Scientific. Preprint BUHEP-95-7, hep-ph/9503202.

[13] G. Altarelli and G. Isidori, Phys. Lett. **B337**, 141 (1994); J.A. Casas, J.R. Espinosa and M. Quirós, Phys. Lett. **B342**, 171 (1995); J.R. Espinosa and M. Quirós, Phys. Lett. **B353**, 257 (1995).

[14] F. Richard, presented at the 27^{th} International Conference on High Energy Physics, Glasgow, July 20-27, 1994, preprint LAL 94-50 (1994).

[15] J. Ellis, G.L. Fogli and E. Lisi, preprint CERN-TH/95-202, hep-ph/9507424; P.H. Chankowski and S. Pokorski, preprint MPI-PH-95-39, hep-ph/9509207.

[16] S.M. Lietti, S.F. Novaes and R. Rosenfeld, work in progress.

[17] M. Spira, A. Djouadi, D. Graudenz and P.M. Zerwas, Nucl. Phys. **B453**, 17 (1995); T. Han, G. Valencia and S. Willenbrock, Phys. Rev. Lett. **69**, 3274 (1992); T. Han and S. Willenbrock, Phys. Lett. **B273**, 167 (1990).

[18] E. R.-Was, D. Froidevaux, F. Gianotti, L. Poggioli, D. Cavalli and L. Cozzi, ATLAS internal note Phys-NO-048 (1995).

[19] See, *e.g.*, S. Weinberg, Physica **96A**, 327 (1979); J.F. Donoghue, E. Golowich and B.R. Holstein, *Dynamics of the Standard Model* (Cambridge University Press, 1992).

[20] J. Bagger, V.D. Barger, K. Cheung, J. Gunion, T. Han, G. Ladinsky, R. Rosenfeld and C.P.- Yuan, Phys. Rev. **D49**, 1246 (1994), Phys. Rev. **D52**, 3878 (1995)

BRS Cohomology of Zero Curvature Systems*

M. Carvalho, L.C.Q. Vilar, C.A.G. Sasaki
C.B.P.F
Centro Brasileiro de Pesquisas Físicas,
Rua Xavier Sigaud 150, 22290-180 Urca
Rio de Janeiro, Brazil

S.P. Sorella
Universidade do Estado do Rio de Janeiro
Departamento de Física Teórica
Instituto de Física, UERJ
Rua São Francisco Xavier, 528
20550-013, Rio de Janeiro, Brazil

Received March, 1996

The computation of the BRS cohomology classes associated to the Wess-Zumino consistency condition in local field theories is presented within a zero curvature formalism. This approach relies on the existence of an operator δ which decomposes the exterior space-time derivative as a BRS commutator. As explicit examples, the three dimensional Chern-Simons gauge model and the B-C string ghost system will be discussed in detail.

I Introduction

Nowadays it is an established fact that the search of the possible anomalies and of the counterterms which arise at the quantum level in local field theories can be done in a purely algebraic way [1]. Following the standard general BRS procedure, a local field theory is characterized by a set of fields $\{\phi\}$ (gauge fields, ghosts, matter...), a set of anti-fields $\{\phi^*\}$ (the BRS sources needed to properly quantize systems with non-linear symmetries) and a set of transformations described by means of a nilpotent operator b whose action on the fields and on the anti-fields can be generically written as

$$\begin{aligned} b\phi &= \mathcal{Q}(\phi,\phi^*)\ , \\ b\phi^* &= \mathcal{P}(\phi,\phi^*)\ , \\ b^2 &= 0\ , \end{aligned} \tag{I.1}$$

with $\mathcal{Q},\mathcal{P}$ local polynomials in (ϕ,ϕ^*). In addition, if

$$S = \int d^D x\, \mathcal{L}(\phi,\phi^*)\ , \tag{I.2}$$

*Talk given at the XVI Encontro Nacional Física de Partículas e Campos, CAXAMBU, MG, Brazil, October 1996

denotes the fully quantized classical action, we have the Slavnov-Taylor (or Master Equation) identity

$$bS = 0 \,, \tag{I.3}$$

summarizing the symmetry content of the model, i.e. the invariance of S under the transformations (I.1). At the quantum level, the radiative corrections lead to an effective action

$$\Gamma = S + \hbar\Gamma^{(1)} + \hbar^2\Gamma^{(2)} + \dots \,, \tag{I.4}$$

which obeys the broken Slavnov-Taylor identity

$$b\Gamma = \hbar^n \mathcal{A} + O(\hbar^{n+1}) \,, \qquad n \geq 1 \,, \tag{I.5}$$

where, according to the Quantum Action Principle, $\mathcal{A}$ is an integrated local polynomial in (ϕ, ϕ^*) and their derivatives whose ultraviolet dimensions are bounded by power counting requirements [1]. As it is well known, the breaking term $\mathcal{A}$, due to the nilpotency of the operator b, obeys the Wess-Zumino consistency condition, i.e.

$$b\mathcal{A} = 0 \,. \tag{I.6}$$

Supposing now that the most general soultion of (I.6) can be written as a $b-$variation of a local polynomial $\hat{\Delta}$,

$$\mathcal{A} = b\hat{\Delta} \,, \tag{I.7}$$

then it is very easy to check that the redefined quantum action

$$\bar{\Gamma} = \Gamma - \hbar^n \hat{\Delta} \,, \tag{I.8}$$

turns out to be symmetric up to the order $\hbar^{n+1}$,

$$b\bar{\Gamma} = O(\hbar^{n+1}) \,. \tag{I.9}$$

This equation tells us that if the breaking $\mathcal{A}$ is a pure $b-$variation, then it is always possible to extend the invariance of the classical action S at the quantum level by means of the introduction of appropriate local counterterms. The procedure can be iterated by induction, allowing ourselves to prove that the Slavnov-Taylor identity (I.3) can be maintained at all orders of perturbation theory. Otherwise, if $\mathcal{A}$ cannot be written as a $b-$variation of a local polynomial,

$$\mathcal{A}^n \neq b\hat{\Delta} \,, \tag{I.10}$$

then the symmetry cannot be restored and the theory displays an anomaly. In particular, equations (I.6), (I.10) show that the existence of an anomaly is related to a nonvanishing cohomology of the operator b in the space of integrated local polynomials. It is apparent then that the knowledge of the cohomology classes of b is of great importance in order to establish if a given model is anomalous or not.

As a first step in the computation of the cohomology of b, let us translate the integrated consistency condition (I.6) at the nonintgrated level. Writing

$$\mathcal{A} = \int \omega^1_D \,, \tag{I.11}$$

[1] We shall consider here only power counting renormalizable models.

ω^1_D denoting a local polynomial in the fields of ghost number 1 and form degree D, the integrated condition (I.6) is equivalent to

$$b\omega^1_D + d\omega^2_{D-1} = 0 \,, \tag{I.12}$$

$d = dx^\mu \partial_\mu$ being the exterior space-time derivative which together with the operator b satisfies the algebraic relations

$$b^2 = d^2 = bd + db = 0 \,. \tag{I.13}$$

For the sake of generality, equation (I.12) is usually referred to an arbitrary value G of the ghost number, i.e.

$$b\omega^G_D + d\omega^{G+1}_{D-1} = 0 \,, \tag{I.14}$$

the values $G = 0, 1$ correspond respectively to invariant counterterms and anomalies. Acting now with the operator b on the equation (I.14) and making use of the algebraic relations (I.13), we get

$$db\omega^{G+1}_{D-1} = 0 \,, \tag{I.15}$$

which, from the algebraic Poincare Lemma [2], i.e.

$$d\Delta^Q_{D-1} = 0 \quad \Rightarrow \quad \Delta^Q_{D-1} = d\hat{\Delta}^Q_{D-2} \,, \tag{I.16}$$

implies the new equation

$$b\omega^{G+1}_{D-1} + d\omega^{G+2}_{D-2} = 0 \,, \tag{I.17}$$

with ω^{G+2}_{D-2} local polynomial of ghost number $G+2$ and form degree $D-2$. Iteration of this procedure yields a system of equations usually called descent equations (see [1] and refs. therein):

$$\begin{aligned}
&b\omega^G_D \quad + d\omega^{G+1}_{D-1} = 0 \,, \\
&b\omega^{G+1}_{D-1} + d\omega^{G+2}_{D-2} = 0 \,, \\
&\quad \cdots\cdots\cdots \\
&\quad \cdots\cdots\cdots \\
&b\omega^{G+D-1}_1 + d\omega^{G+D}_0 = 0 \,, \\
&b\omega^{G+D}_0 = 0 \,,
\end{aligned} \tag{I.18}$$

where the $\omega^{G+D-j}_j (\, 0 \le j \le D)$ are local polynomials in the fields of ghost number $(G+D-j)$ and form degree j. The problem of solving the descent equations (I.18) is a problem of cohomology of b modulo d, the corresponding cohomology classes being given by solutions of (I.18) which are not of the type

$$\begin{aligned}
&\omega^{G+D-m}_m = b\hat{\omega}^{G+D-m-1}_m + d\hat{\omega}^{G+D-m}_{m-1} \,, \qquad 1 \le m \le D \,, \\
&\omega^{G+D}_0 = b\hat{\omega}^{G+D-1}_0 \,,
\end{aligned} \tag{I.19}$$

with $\hat{\omega}$'s local polynomials. Notice also that at the nonintegrated level one looses the property of making integration by parts. This implies that the fields and their derivatives have to be considered as independent variables.

Of course, the knowledge of the most general nontrivial solution of the descent equations (I.18) immediately yields the integrated cohomology classes of the operator b. Indeed, once the full system (I.18) has been solved, integration on space-time of the equation (I.14) will give the general

solution of the consistency condition (I.6). The problem of finding the solutions of the equations (I.18) will be the main subject of this talk.

It should be remarked that the last equation of the system (I.18) is a problem of local cohomology instead of a modulo d one. Actually the latter can be handled by means of several tools as, for instance, the spectral sequences technique. We shall therefore assume that the most general solution of the last of the equations (I.18) is known.

For instance, in the case of the standard renormalizable Yang-Mills theory for which the BRS transformations of the gauge field $A = A^a T^a$ (T^a being the generators of the gauge group) and of the Faddeev-Popov ghost $c = c^a T^a$ are

$$bA = -dc - i[A, c] , \qquad bc = ic^2 , \tag{I.20}$$

the cocycle ω_0^{G+D} is given by polynomials in the ghost field c built up with invariant monomials of the type [3, 4, 5, 6, 7, 8]

$$\mathrm{Tr}\,\frac{c^{G+D}}{(G+D)!} , \qquad (G+D) \text{ odd} . \tag{I.21}$$

II Solution of the Descent Equations

We face now the problem of finding the solution of the full system of descent equations (I.18). To this purpose we introduce an operator δ which decomposes the exterior derivative d as a BRS commutator [9], i.e.

$$d = -[b, \delta] . \tag{II.1}$$

Although not necessary, we shall also suppose for simplicity that

$$[d, \delta] = 0 . \tag{II.2}$$

It is easily proven now that, once the decomposition (II.1) has been found, repeated applications of the operator δ on the polynomial ω_0^{G+D} which solves the last of the equations (I.18) will give an explicit nontrivial solution for the higher cocycles ω_j^{G+D-j}

$$\omega_j^{G+D-j} = \frac{\delta^j}{j!}\omega_0^{G+D} , \qquad j = 1, ..., D. \tag{II.3}$$

This very simple and elegant formula displays the usefulness of the introduction of the operator δ whose existence turns out to be quite general. In fact the decomposition (II.1) is actually present in a large class of field theory models such as

1. Yang-Mills type theories [9, 10]
2. Gravity [11]
3. Topological models (BF models, Chern-Simons, Witten's type models, ..) [12, 13, 14]
4. String theory [15, 16]

5. W_3 - gravity [17]

6. $N = 1$ four dimensional supersymmetric Yang-Mills theories in superspace [18].

III The Zero-Curvature Condition

Recently we have found [19] an interesting connection between the existence of the operator δ and the possibility of encoding the full set of BRS transformations into a unique equation which takes the form of a generalized zero curvature condition

$$\tilde{\mathcal{F}} = \tilde{d}\tilde{\mathcal{A}} - i\tilde{\mathcal{A}}^2 = 0 \,, \tag{III.1}$$

the operator $\tilde{d}$ and the generalized gauge connection $\tilde{\mathcal{A}}$ being respectively the transformations under δ of the BRS operator b and of the Faddeev-Popov ghost, i.e.

$$\tilde{d} = e^{\delta}\, b\, e^{-\delta} \,, \qquad \tilde{\mathcal{A}} = e^{\delta}\, c \,. \tag{III.2}$$

In particular, in the case in which eq.(II.2) holds, we have

$$\tilde{d} = b + d \,. \tag{III.3}$$

Notice that, as a consequence of eq.(III.1), the operator $\tilde{d}$ turns out to be nilpotent

$$\tilde{d}^2 = 0 \,. \tag{III.4}$$

The zero curvature condition (III.1) has a very simple interpretation and its origin is deeply related to the existence of the operator δ entering the decomposition (II.1). Indeed, acting with the operator e^{δ} on the equation (I.20) expressing the BRS transformation of the Faddeev-Popov ghost we obtain

$$e^{\delta} b e^{-\delta} e^{\delta} c = i\, e^{\delta}\, c^2 \qquad \Rightarrow \qquad \tilde{d}\tilde{\mathcal{A}} = i\tilde{\mathcal{A}}^2 . \tag{III.5}$$

This is not surprising since, as it is well known, the ghost field c identifies the so called Maurer-Cartan form of the gauge group G and its BRS transformation is nothing but the corresponding Maurer-Cartan equation [20] which is in fact a zero curvature condition.

Turning now to the cohomology of the operator $\tilde{d}$, it is apparent to see that the cohomology classes of $\tilde{d}$ are obtained by δ—transforming the corresponding cohomology classes of the BRS operator b. In other words, it is very easy to check that the generalized cocycles

$$\mathrm{Tr}\,\frac{\tilde{\mathcal{A}}^{2n+1}}{(2n+1)!} = e^{\delta}\mathrm{Tr}\,\frac{c^{2n+1}}{(2n+1)!} \,, \tag{III.6}$$

identify cohomology classes of $\tilde{d}$.

Introducing now the generalized cocycle

$$\tilde{\omega}^{G+D} = \sum_{j=0}^{D} \omega_j^{G+D-j} \,, \tag{III.7}$$

the full system of descent equations (I.18) can be cast in the compact form

$$\tilde{d}\tilde{\omega}^{G+D} = 0 \,, \tag{III.8}$$

from which one sees that $\tilde{\omega}^{G+D}$ belongs to the cohomology of $\tilde{d}$. It follows then that $\tilde{\omega}^{G+D}$ is simply given by polynomials of the type (III.6), i.e.

$$\tilde{\omega}^{G+D} = e^{\delta}\omega_0^{G+D} \,. \tag{III.9}$$

This equation shows that the solution of the descent equations (I.18) are related to the cohomology of the operator $\tilde{d}$ entering the zero curvature equation (III.1). Moreover, the cohomology of the operator $\tilde{d}$ is given by δ–transforming the cohomology of the BRS operator b. It is clear thus that the existence of the operator δ as well as the zero curvature condition (III.1) give a complete and very elegant algebraic set up in order to deal with the solutions of the descent equations. Let us conclude by remarking that, although referred to a nonabelian type theory, the zero curvature condition can be generalized to gauge theories whose ghost content is different from the usual Yang-Mills Faddeev-Popov fields. An example of this will be provided later on by the so called $B-C$ string ghost system.

IV Example I : D = 3 Chern-Simons Gauge Theories

For a better understanding of the previous construction let us discuss in details the case of the three dimensional Chern-Simons theory, corresponding to $G = 0$ and $D = 3$.

The relevant fields here are the one form gauge field and the zero form Faddeev-Popov ghost

$$\begin{aligned} A &= T^a A^a_\mu dx^\mu \,, \\ c &= T^a c^a \,, \end{aligned} \tag{IV.1}$$

and the corresponding antifields, respectively a two form γ (associated to the nonlinear transformation of A) and a three form τ (associated to c)

$$\begin{aligned} \gamma &= \frac{1}{2} T^a \gamma^a_{\mu\nu} dx^\mu \wedge dx^\nu \,, \\ \tau &= \frac{1}{3!} T^a \tau^a_{\mu\nu\rho} dx^\mu \wedge dx^\nu \wedge dx^\rho \,. \end{aligned} \tag{IV.2}$$

The invariant quantized action can be written as

$$S = \int \mathrm{Tr}\,(AF + i\frac{A^3}{3} + \gamma Dc + i\tau c^2) \,, \tag{IV.3}$$

F being the two-form gauge field strength $F = dA - iA^2$ and Dc the covariant derivative

$$Dc = dc - i[A, c] \,. \tag{IV.4}$$

The action (IV.3) is invariant under the following set of transformations:

$$\begin{aligned} b\,c &= ic^2 \,, \\ b\,A &= -dc + i\,[c, A] \,, \\ b\,\gamma &= -F + i\,[c, \gamma] \,, \\ b\,\tau &= -d\gamma + i\,[c, \tau] + i\,[A, \gamma] \,, \\ b^2 &= 0 \,. \end{aligned} \tag{IV.5}$$

Introducing now the operator δ [13] defined as

$$\begin{aligned} \delta c &= A \ , \\ \delta A &= 2\gamma \ , \\ \delta \gamma &= 3\tau \ , \\ \delta \tau &= 0 \ , \end{aligned} \tag{IV.6}$$

one easily checks that equations (II.1) and (II.2) are verified, i.e. δ decomposes the exterior derivative d as a BRS commutator. For the generalized connection of eq. (III.2) we get

$$\widetilde{A} = e^{\delta} c = c + A + \gamma + \tau \ . \tag{IV.7}$$

Remark that the generalized connection $\widetilde{A}$ collects all the relevant fields, meaning that the external sources γ and τ are naturally included in the zero curvature formalism.

The zero curvature condition

$$\widetilde{d}\widetilde{A} = i\widetilde{A}^2 \tag{IV.8}$$

reads now

$$(b+d)(c+A+\gamma+\tau) = i(c+A+\gamma+\tau)^2 \ , \tag{IV.9}$$

which is easily seen to reproduce the transformations (IV.5).

As explained before, in order to find a solution of the descent equations

$$\begin{aligned} & b\,\omega^j_{3-j} + d\,\omega^{j+1}_{2-j} = 0 \ , \qquad 0 \le j \le 2 \ , \\ & b\omega^3_0 = 0 \ , \end{aligned} \tag{IV.10}$$

it is sufficient to expand the generalized cocycle of total degree three

$$\widetilde{\omega}^3 = \frac{1}{3!}\mathrm{Tr}\,\widetilde{A}^3 \ . \tag{IV.11}$$

After an easy computation we get

$$\frac{1}{3!}\mathrm{Tr}\,\widetilde{A}^3 = \omega^0_3 + \omega^1_2 + \omega^2_1 + \omega^3_0 \ , \tag{IV.12}$$

with

$$\begin{aligned} \omega^3_0 &= \frac{1}{3!}\mathrm{Tr}\,c^3 \ , \\ \omega^2_1 &= \frac{1}{2}\mathrm{Tr}\,c^2 A \ , \\ \omega^1_2 &= \frac{1}{2}\mathrm{Tr}\,\left(c^2\gamma + cA^2\right) \ , \\ \omega^0_3 &= \frac{1}{2}\mathrm{Tr}\,\left(c^2\tau + cA\gamma + c\gamma A + \frac{A^3}{3}\right) \ . \end{aligned} \tag{IV.13}$$

From

$$-i\mathrm{Tr}\,\left(c^2\tau + cA\gamma + c\gamma A\right) = -\mathrm{Tr}\,AF + b\,\mathrm{Tr}\,(c\tau + A\gamma) + d\,\mathrm{Tr}\,c\gamma \ , \tag{IV.14}$$

the three-form ω^0_3 can be rewritten as

$$\omega^0_3 = \frac{-i}{2}\mathrm{Tr}\,(AF + i\frac{A^3}{3}) + \frac{i}{2}b\,\mathrm{Tr}\,(c\tau + A\gamma) + \frac{i}{2}d\,\mathrm{Tr}\,c\gamma \ , \tag{IV.15}$$

yielding thus the invariant action

$$S = i\int \omega_3^0 = \frac{1}{2}\int \mathrm{Tr}\,(AF + i\frac{A^3}{3}) - \frac{1}{2}b\int \mathrm{Tr}\,(c\tau + A\gamma)\,, \tag{IV.16}$$

which is easily recognized as the action of the fully quantized Chern-Simons gauge theory (IV.3).

V Example II: the Bosonic String

Let us discuss now, as the second example of the zero curvature construction, the so called $B-C$ model whose action is given by

$$S_{B-C} = \int dzd\bar{z}\, B\,\bar{\partial}C\,. \tag{V.1}$$

The fields $B = B_{z\,z}$ and $C = C^z$ are anticommuting and carry respectively ghost number -1 and $+1$. The action (V.1) is recognized to be the ghost part of the quantized bosonic string action. It is usually accompanied by its complex conjugate. However, the inclusion of the latter in the present framework does not require any additional difficulty.

As it is well known, the action (V.1) is left invariant by the following nonlinear BRS transformations

$$\begin{aligned} s\,C &= C\,\partial C\,, \\ s\,B &= -(\partial B)\,C - 2\,B\,\partial C\,. \end{aligned} \tag{V.2}$$

Transformations (V.2) being nonlinear, one needs to introduce two external invariant sources $\mu = \mu^z{}_z$ and $L = L_{z\,z\,z}$ of ghost number respectively 0 and -2

$$S_{ext} = \int dzd\bar{z}\,(\mu\, s\,B + L\,s\,C)\,. \tag{V.3}$$

The complete action

$$S = S_{B-C} + S_{ext} \tag{V.4}$$

obeys thus the classical Slavnov-Taylor identity

$$\int dzd\bar{z}\left(\frac{\delta S}{\delta B}\frac{\delta S}{\delta \mu} + \frac{\delta S}{\delta L}\frac{\delta S}{\delta C}\right) = 0 = \frac{1}{2}b\,S\,, \tag{V.5}$$

b denoting the nilpotent linearized operator

$$b = \int dzd\bar{z}\left(\frac{\delta S}{\delta B}\frac{\delta}{\delta \mu} + \frac{\delta S}{\delta \mu}\frac{\delta}{\delta B} + \frac{\delta S}{\delta L}\frac{\delta}{\delta C} + \frac{\delta S}{\delta C}\frac{\delta}{\delta L}\right)\,. \tag{V.6}$$

The operator b acts on the fields and on the external sources in the following way

$$\begin{aligned} b\,C &= s\,C = C\,\partial C\,, \\ b\,\mu &= \bar{\partial}C + (\partial\mu)\,C - \mu\,(\partial C)\,, \end{aligned} \tag{V.7}$$

and

$$\begin{aligned} b\,B &= s\,B = -(\partial B)\,C - 2\,B\,\partial C\,, \\ b\,L &= \bar{\partial}\,B - (2\,B)\,\partial\mu - \mu\partial B + (\partial L)\,C + 2\,L\,\partial C\,. \end{aligned} \tag{V.8}$$

Introducing now the two functional operators [15]

$$\mathcal{W} = \int dz d\bar{z} \frac{\delta}{\delta C} , \qquad \overline{\mathcal{W}} = \int dz d\bar{z} \left(\mu \frac{\delta}{\delta C} + L \frac{\delta}{\delta B} \right) , \tag{V.9}$$

one easily proves that

$$\delta = dz\, \mathcal{W} + d\bar{z}\, \overline{\mathcal{W}} \tag{V.10}$$

obeys to

$$d = -[b, \delta] , \qquad [d, \delta] = 0 , \tag{V.11}$$

d being the exterior derivative $d = dz\partial + d\bar{z}\bar{\partial}$. We have thus realized the decomposition (II.1). In order to derive the transformations (V.7), (V.8) from a zero curvature condition, we proceed as before and we define the generalized field

$$\tilde{C}^z = e^b C^z = C^z + dz + d\bar{z}\mu^z_{\bar{z}} , \tag{V.12}$$

so that introducing the holomorphic generalized vector field $\tilde{C} = \tilde{C}^z \partial_z$, it is easily checked that equations (V.7) can be cast in the form of a zero curvature condition

$$\tilde{d}\tilde{C} = \frac{1}{2}\left[\tilde{C}, \tilde{C}\right] = \mathcal{L}_{\tilde{C}} \tilde{C} , \tag{V.13}$$

where, as usual, $\tilde{d}$ is the operator

$$\tilde{d} = e^b\, b\, e^{-b} = b + d , \tag{V.14}$$

and $\mathcal{L}_{\tilde{C}}$ denotes the Lie derivative with respect to the vector field[2] $\tilde{C}$.

Concerning now the second set of transformations (V.8), we define a second generalized field $\tilde{B}_{zz}$ as

$$\tilde{B}_{zz} = e^b B_{zz} = B_{zz} + d\bar{z} L_{zzz} . \tag{V.15}$$

To expression (V.15) one can naturally associate the generalized holomorphic quadratic differential

$$\tilde{B} = \tilde{B}_{zz} dz \otimes dz . \tag{V.16}$$

Therefore, transformations (V.8) can be rewritten as

$$\tilde{d}\tilde{B} - \mathcal{L}_{\tilde{C}} \tilde{B} = 0 . \tag{V.17}$$

Let us consider now the problem of identifying the anomalies which affect the Slavnov-Taylor identity (V.5) at the quantum level. We look then at the solution of the descent equations

$$\begin{aligned} & b\omega_2^1 + d\omega_1^2 = 0 , \\ & b\omega_1^2 + d\omega_0^3 = 0 , \\ & b\omega_0^3 = 0 . \end{aligned} \tag{V.18}$$

As it has been proven in refs. [15, 21], the cohomology of the BRS operator in the sector of the zero-forms with ghost number three contains, in the present case, a unique element given by

$$\omega_0^3 = C\, \partial C\, \partial^2 C . \tag{V.19}$$

[2] Of course, the bracket $[\tilde{C}, \tilde{C}]$ in eq.(V.14) refers now to the Lie bracket of vector fields.

From the zero curvature condition (V.13), it follows then that the generalized cocycle of total degree three

$$\tilde{\omega}^3 = \tilde{C}\,\partial\,\tilde{C}\,\partial^2\,\tilde{C}\ , \tag{V.20}$$

belongs to the cohomology of $\tilde{d}$. The expansion of $\tilde{\omega}^3$ will give thus a solution of the ladder (V.18), *i.e.*

$$\tilde{\omega}^3 = \omega_0^3 + \omega_1^2 + \omega_2^1\ , \tag{V.21}$$

with ω_1^2, ω_2^1 given respectively by

$$\begin{aligned} \omega_1^2 &= \left(C\,\partial\,C\partial^2\,\mu - C\,\partial^2\,C\,\partial\mu + \mu\,\partial\,C\partial^2\,C\right)d\bar{z} + \left(\partial C\right)\left(\partial^2\,C\right)dz\ , \\ \omega_2^1 &= \left(-\partial\,C\partial^2\,\mu + \partial\,\mu\partial^2\,C\right)dz\wedge d\bar{z}\ . \end{aligned} \tag{V.22}$$

In particular,

$$\int \omega_2^1 = 2\int dz d\bar{z}\,C\partial^3\mu \tag{V.23}$$

is recognized to be the well known two-dimensional diffeomorphism anomaly characterizing the central charge of the energy-momentum current algebra.

Conclusion

We have shown that the zero curvature formulation can be obtained as a consequence of the existence of the operator δ realizing the decomposition (II.1). This formalism enables us to encode into a unique equation all the relevant informations concerning the BRS cohomology classes.

References

[1] O. Piguet and S.P. Sorella, *Algebraic Renormalization*, Monographs Series, m 28, Springer-Verlag, Berlin, 1995;

[2] F. Brandt, N. Dragon and M. Kreuzer, *Nucl. Phys.* B340 (1990) 187;
F. Brandt, *Structure of BRS Invariant Local Functionals*, NIKHEF-H-93-12, hep-th/9310123;
G. Barnich, F. Brandt and M. Henneaux, *Local BRST cohomology in Einstein-Yang-Mills theory*, KUL-TF-95/16, ULB-TH-95/07, hep-th/9505173;

[3] J.A. Dixon, *Comm. Math. Phys.* 139 (1991) 495;

[4] J. Thierry-Mieg, *J. Math. Phys.* 21 (1980) 2834; *Nuovo Cim.* 56A (1980) 396;
L. Baulieu, *Nucl. Phys.* B241 (1984) 557;
L. Baulieu and J. Thierry-Mieg, *Phys. Lett.* B145 (1984) 53;
J. Manes, R. Stora and B. Zumino, *Comm. Math. Phys.* 102 (1985) 157;
R. Stora, *Algebraic Structure and Topological Origin of Anomalies*, in " *Progress in Gauge Field Theory* ", ed. 't Hofft et al. Plenum Press, New York, 1984;
R.D. Ball, *Phys. Rev.* 182 (1989) 1;

[5] M. Dubois-Violette, M. Talon and C.M. Viallet, *Comm. Math. Phys.* 102 (1985) 105;

[6] F. Brandt, N. Dragon and M. Kreuzer, *Phys. Lett.* B231 (1989) 263; *Nucl. Phys.* B332 (1990) 224, 250;

[7] M. Dubois-Violette, M. Henneaux, M. Talon and C.M. Viallet, *Phys. Lett.* B289 (1992) 361;

[8] G. Barnich, F. Brandt and M. Henneaux, *Local BRST cohomology in the antifield formalism: I. General theorems*, ULB-TH-94/06, NIKHEF-H 94-13, hepth/9405109;
G. Barnich, F. Brandt and M. Henneaux, *Local BRST cohomology in the antifield formalism: II. Application to Yang-Mills theory*, ULB-TH-94/07, NIKHEF-H 94-15;

[9] S.P. Sorella, *Comm. Math. Phys.* 157 (1993) 231;

[10] S.P. Sorella and L.Tataru, *Phys. Lett.* B324 (1994) 351;

[11] M. Werneck de Oliveira and S.P. Sorella, *Int. J. Mod. Phys.* A9 (1994) 2979;
O. Moritsch, M. Schweda and S.P. Sorella, *Class. Quantum Grav.* 11 (1994) 1225;
O. Moritsch and M. Schweda, *Helv. Phys. Acta* 67 (1994) 289;
P.A. Blaga, O. Moritsch, M. Schweda, T. Sommer, L. Tataru and H. Zerrouki, *Algebraic structure of gravity in Ashtekar variables*, REP.TUW 94-19;
O. Moritsch, M. Schweda, T. Sommer, L. Tataru and H. Zerrouki, *BRST cohomology of Yang-Mills gauge fields in the presence of gravity in Ashtekar variables*, REP.TUW 94-17;

[12] E. Guadagnini, N. Maggiore and S.P. Sorella, *Phys. Lett.* B255 (1991) 65;
C. Lucchesi, O. Piguet and S. P. Sorella, *Nucl. Phys.* B395 (1993) 325;
D. Birmingham and M. Rakowski, *Phys. Lett.* B275 (1992) 289;
D. Birmingham and M. Rakowski, *Phys. Lett.* B289 (1992) 271;

[13] C. Lucchesi, O. Piguet and S.P. Sorella, *Nucl. Phys.* 395 (1993) 325;
O. Piguet, *On the Role of Vector Supersymmetry in Topological Field Theory*, UGVA-DPT 1995/02-880, hep-th/9502033;

[14] A Brandhuber, O. Moritsch, M.W. de Oliveira, O. Piguet and M. Schweda, *Nucl. Phys.* B341 (1994) 173;

[15] M. Werneck de Oliveira, M. Schweda and S.P. Sorella, *Phys. Lett.* B315 (1993) 93;
G. Bandelloni and S. Lazzarini, *J. Math. Phys.* 34 (1993) 5413;

[16] A. Boresch, M. Schweda and S.P. Sorella, *Phys. Lett.* B328 (1994) 36;

[17] M. Carvalho, L.C. Queiroz Vilar and S.P. Sorella, *Int. J. Mod. Phys.* A10 (1995) 3877;

[18] L. C. Queiroz Vilar, C.A.G. Sasaki aand S.P.Sorella, *work in progress*;

[19] M. Carvalho, L.C. Queiroz Vilar, C.A.G. Sasaki and S.P. Sorella, *BRS Cohomology of Zero Curvature Systems I. The Complete Ladder Case*, CBPF-NF-062/95; *BRS Cohomology of Zero Curvature Systems II. The Noncomplete Ladder Case*, CBPF-NF-063/95;

[20] T. Eguchi, B. Gilkey and J. Hanson, *Phys. Rev.* 6 (1980) 213;

[21] F. Brandt, W. Troost and A. Van Proeyen, NIKHEF-H 94-16, KUL-TF 94/17, hep-th/9407061, proceedings of the workshop *Geometry of Constrained Dynamical Systems*, Isaac Newton Institute for Mathematical Sciences, Cambridge, june 1994;

Extending the Use of the Zeta Function

D. G. C. McKeon*
Department of Applied Mathematics
University of Western Ontario, London
CANADA, N6A 5B7
email: TMLEAFS@APMATHS.UWO.CA
Telephone: (519)679-2111, ext. 8789
Fax: (519)661-3523

Received March, 1996

The ζ-function technique is a useful device for regulating the functional determinant occurring in one-loop generating functionals [1-4]. It is possible to use the fundamental idea in this approach, that of regulating a functional logarithm through the equation

$$\ln\ H = \lim_{s\to 0}\left(-\frac{d}{ds}H^{-s}\right)\ , \tag{1}$$

in order to compute Green's functions in perturbation theory [5]. The fact that the initial Lagrangian is unaltered in this approach means that symmetries present in the initial Lagrangian are not violated explicitly by the insertion of a regulating parameter (such as n, the dimension of space-time) into the initial action. This is particularly useful in supersymmetric models [6], non-linear sigma models with torsion [7], chiral theories [8] and gravitational theory [9]. No explicit divergences arise at any stage of a calculation when one employs operator regularization, eliminating the need for performing explicit renormalization; however one still can recover the renormalization group functions by examining the dependence of Green's functions on a mass scale parameter μ^2 that arises [10]. An additional advantage of this approach is that one can circumvent having to perform the analogue of the loop-momentum integral by use of the quantum mechanical path integral [11]; this approach is also useful in thermal field theory [12].

To illustrate this technique, let us consider a ϕ_6^3 model whose action is

$$S = \int d^6x\left[-\frac{1}{2}\phi(p^2+m^2)\phi - \frac{\lambda}{3!}\phi^3\right]\ \ (p=-i\partial)\ . \tag{2}$$

Employing operator regularization is contingent upon splitting ϕ into the sum of a classical background field (f) and a quantum field (h) so that

$$\phi = f + h\ . \tag{3}$$

To one- and two-loop order, the unregulated generating functional is given by

$$\Gamma^{(1)}[f] = -\frac{1}{2}\ln\ det\left(\frac{p^2+m^2+\lambda f}{\mu^2}\right) \tag{4}$$

and

$$\Gamma^{(2)}[f] = \frac{\lambda^2}{12}\mu^{-6}\int d^6x\ d^6y\left[\langle x\mid\left(\frac{p^2+m^2+\lambda f}{\mu^2}\right)^{-1}\mid y\rangle\right]^3 \tag{5}$$

*Caxambu, M.G. October 26, 1995

respectively. (Here μ^2 is an arbitrary scale parameter that comes into play when considering the renormalization group equations.)

We now regulate $\Gamma^{(1)}$ in (4) using (1). If $H = p^2 + m^2 + \lambda f$, then

$$\Gamma^{[1]} = \frac{1}{2} \lim_{s\to 0} \frac{d}{ds}\, str(H/\mu^2)^{-s} \tag{6}$$

$$\equiv \zeta'(0)$$

where

$$\zeta(s) = str(H/\mu^2)^{-s}$$

$$= \frac{\mu^{2s}}{\Gamma(s)} \int_0^\infty dt\ t^{s-1} str\, e^{-Ht} . \tag{7}$$

(The supertrace, str, in (6) must be used if H is a superoperator containing both Bosonic and Fermionic sectors.) The divergence in the integral over t in (7) arising when $s = 0$ is the analogue of the usual ultraviolet divergence; it is cancelled by the explicit factor of $1/\Gamma(s)$ that occurs.

It is possible to extract one-loop Green's functions from (7) by use of the Schwinger expansion [13] with $H_0 = p^2 + m^2$, $H_1 = \lambda f$,

$$e^{-(H_0+H_1)t} = e^{-H_0 t} + \int_0^1 du\, e^{-(1-u)H_0 t}(-t\ H_1)e^{-uH_0 t} + \ldots \tag{8}$$

or, upon taking the trace of (8),

$$str\, e^{-(H_0+H_1)t} = str\left[e^{-H_0 t} + (-tH_1)e^{-H_0 t} + \frac{1}{2}\int_0^1 du\, e^{-(1-u)H_0 t}(-t\ H_1)e^{-uH_0 t}(-tH_1) + \ldots\right] . \tag{9}$$

Green's functions correspond to particular terms in this expansion; explicit forms are determined by evaluating the functional trace in momentum space using the convention [13,5]

$$(2\pi)^3 \langle p \mid f \mid q\rangle = f(p-q) . \tag{10}$$

For example, the contribution to the ζ-function corresponding to the two-point function at one-loop order is

$$\zeta_{ff}(s) = \frac{\lambda^2\mu^{2s}}{\Gamma(s)} \int_0^\infty dt\, t^{s-1}\left[\frac{(-t)^2}{2}\int_0^1 du \int \frac{d^6p}{(2\pi)^6}\frac{d^6q}{(2\pi)^6} e^{-(1-u)p^2 t} f(p-q)\right.$$

$$\left. e^{-uq^2 t} f(q-p) e^{-m^2 t}\right] , \tag{11}$$

which, upon evaluating the integrals over t and q, gives

$$\zeta'_{ff}(0) = \lambda^2 \frac{\Gamma(s-1)}{\Gamma(s)} \int \frac{d^6p}{(4\pi)^3} \int_0^1 du \left\{\ln\left[(u(1-u)p^2 + m^2)/\mu^2\right]\right.$$

$$\left. -[u(1-u)p^2 + m^2]\right\} . \tag{12}$$

At two-loop order, it is the inverse of operators that must be regulated, not their logarithm. This can be done in a way that is consistent with (1),

$$H^{-1} = \frac{d}{dH} \ln\ H = \lim_{s\to 0} \frac{d}{ds}(sH^{-s-1}) , \tag{13}$$

or, more generally,

$$H_1^{-1} \ldots H_p^{-1} = \lim_{s\to 0} \frac{d^n}{ds^n}\left(\frac{s^n}{n!} H_1^{-s-1} \ldots H_p^{-s-1}\right) \quad (n = 0, 1, \ldots) . \tag{14}$$

Particular Green's functions can be considered by using the exponential representation used in (7), and then expanding the exponential in powers of the background field as in the one-loop case using the Schwinger expansion of (8). In particular, the generating function $\Gamma^{(2)}$ in (5) when regulated becomes

$$\Gamma^{(2)} = \frac{\lambda^2}{12}\mu^{-6}\int dxdy\left\{\lim_{s\to 0}\frac{d^2}{ds^2}\,\frac{s^2}{2!}\prod_{i=1}^{3}\int_0^\infty \frac{dt_i t_i^s}{\Gamma(s+1)}\langle x \mid \exp-\left(\frac{p^2+m^2+\lambda f}{\mu^2}\right)t_i \mid y\rangle \right. \tag{15}$$

$$\left. + [\text{"Parts from subdivergences"}]\ \right\}.$$

(The "parts from subdivergences" in (15) are regulated forms of zero needed to ensure unitarity. Their form is constructed in analogy with the BPHZ procedure [10,7].) Expanding the exponential in powers of f in order to determine Green's functions is now a straightforward exercise. We use $n = 2$ in (14) in the regulated generating function of (15) in order to ensure finiteness as s approaches zero.

Matrix elements of the form $\langle x \mid e^{-Ht} \mid y\rangle$ that arise in the regulated generating functional (e.g. (7) and (15)) can be written using the path integral provided $H = \frac{1}{2}(p-A)^2 + V$ [14]

$$\langle x \mid e^{-Ht} \mid y\rangle = \mathbb{P}\int_{q(0)=y}^{q(t)=x} Dq(\tau)\exp\int_0^t d\tau\left[-\frac{\dot{q}^2(\tau)}{2} + i\dot{q}(\tau)\cdot A(q(\tau)) - V(q(\tau))\right].$$

($\mathbb{P}$ - path ordering)

By systematically using the standard result [15]

$$\int_{q(0)=y}^{q(t)=x} Dq(\tau)\exp\int_0^t d\tau\left[-\frac{\dot{q}^2(\tau)}{2} - \gamma(\tau)\cdot q(\tau)\right]$$

$$= (2\pi t)^{-D/2}\exp\left\{-\frac{(x-y)^2}{2t} - \frac{1}{t}\int_0^t d\tau\,[x\tau + y(t-\tau)]\cdot\gamma(\tau)\right. \tag{16}$$

$$\left. -\frac{1}{2}\int_0^t d\tau d\tau' G(\tau,\tau')\gamma(\tau)\cdot\gamma(\tau')\right\}$$

$$(G(\tau,\tau') \equiv \frac{1}{2}\mid \tau-\tau' \mid -\frac{1}{2}(\tau+\tau') + \frac{\tau\tau'}{t})$$

Green's functions can be evaluated without encountering loop-momentum integrals [11]. This approach also has been used in [16-18] but with a different Green's function G.

For example, let us consider how the contribution of the two-point function to the ζ-function in (7) can be computed from the path integral. We have

$$\zeta(s) = \frac{\mu^{2s}}{\Gamma(s)}\int_0^\infty dt\, t^{s-1}\int dx\, dy\,\delta(x-y)\left[\langle x \mid e^{-\frac{1}{2}(p^2+\lambda f)t} \mid y\rangle\right]. \tag{17}$$

The matrix element in (17) can be written in terms of a path integral

$$\langle x \mid e^{-\frac{1}{2}(p^2+\lambda f)t} \mid y\rangle = \int_{q(0)=y}^{q(t)=x} Dq(\tau)\exp\int_0^t d\tau\left(-\frac{\dot{q}^2(\tau)}{2} - \frac{\lambda}{2}f(q(\tau))\right) \tag{18}$$

which, to second order in f, becomes

$$= \int_{q(0)=y}^{q(t)=x} Dq(\tau)\frac{(-\lambda/2)^2}{(2\pi)^6}\int_0^t d\tau_1\int_0^{\tau_1} d\tau_2\,\epsilon_1\epsilon_2$$

$$\exp\int_0^t d\tau\left[-\frac{\dot{q}^2(\tau)}{2} - i\,(k_1\delta(\tau-\tau_1) + k_2\delta(\tau-\tau_2))\cdot q(\tau)\right] \tag{19}$$

provided $f(q(\tau_i))$ is represented by a plane wave field. Applying (16) to (19) we obtain when $x = y$

$$= \frac{(-\lambda/2)^2}{(2\pi)^6}\int_0^t d\tau_1\int_0^{\tau_1} d\tau_2\,\epsilon_1\epsilon_2\, e^{i(k_1+k_2)\cdot x} \tag{20}$$

$$\exp\frac{1}{2}\left[k_1^2 G(\tau_1,\tau_1)+k_2^2 G(\tau_2,\tau_2)+2k_1\cdot k_2 G(\tau_1,\tau_2)\right]\ .$$

The ζ-function consequently becomes

$$\zeta_{ff}(s)=\frac{\mu^{2s}}{\Gamma(s)}\int_0^\infty dt\, t^{s+1}\left[\frac{(-\lambda/2)^2}{(2\pi)^3}\frac{\epsilon_1\epsilon_2}{2}\int_0^1 du\, e^{-\frac{1}{2}u(1-u)k^2 t}\right], \tag{21}$$

yielding the same result as (12) but without ever encountering any loop-momentum integrals.

Background Fermions and vectors can also be accommodated in this approach. For example, let us consider quantum electrodynamics in the presence of a background spinor field η. The classical and gauge fixing Lagrangians are

$$\mathcal{L}_{cl}=\bar\psi(\not p-e\not A-m)\psi-\frac{1}{4}(\partial_\mu A_\nu-\partial_\nu A_\mu)^2 \tag{22}$$

$$\mathcal{L}_{gf}=-\frac{1}{2}(\partial\cdot A)^2$$

so that the term in the effective Lagrangian bilinear in the quantum fields is

$$\mathcal{L}^2=\frac{1}{2}(\chi^T,\bar\chi,Q_\mu)\begin{pmatrix}0 & -(\not p-m)^T & e(i\gamma_\nu)^T\\ \not p-m & 0 & -e\gamma_\nu\eta\\ -e\bar\eta\gamma_\mu & e(\gamma_\mu\eta)^T & -p^2 g_{\mu\nu}\end{pmatrix}\begin{pmatrix}\chi\\ \bar\chi^T\\ Q_\nu\end{pmatrix}. \tag{23}$$

If M is the supermatrix in (23), then the one-loop generating functional is given by

$$i\Gamma^{(1)}=\ln\ sdet^{-\frac{1}{2}}M \tag{24}$$

which we will replace by

$$i\Gamma^{(1)}=\ln\ sdet^{-\frac{1}{2}}Y\ M \tag{25}$$

where Y is the field-independent supermatrix

$$Y=\frac{1}{2}\begin{pmatrix}0 & \not p+m & 0\\ -(\not p+m)^T & 0 & 0\\ 0 & 0 & -\eta_{\mu\nu}\end{pmatrix} \tag{26}$$

that is chosen so that YM is in the standard for $\frac{1}{2}(p-A)^2+V$ with

$$A_\lambda=\begin{pmatrix}0 & 0 & -(e/2)\gamma_\lambda\gamma_\nu\eta\\ 0 & 0 & (e/2)(\bar\eta\gamma_\nu\gamma_\lambda)^T\\ 0 & 0 & 0\end{pmatrix} \tag{27}$$

and, if $m=0$

$$V=\begin{pmatrix}0 & 0 & (ie/2)\gamma_\lambda\gamma_\nu\eta_{,\lambda}\\ 0 & 0 & -(ie/2)(\bar\eta_{,\lambda}\gamma_\nu\gamma_\lambda)^T\\ e\bar\eta\gamma_\mu & -e(\gamma_\mu\eta)^T & 0\end{pmatrix}. \tag{28}$$

In Minkowski space (with $g_{\mu\nu}=diag(+\ +\ +\ -)$), the ζ-function is given by

$$\zeta(s)=\frac{1}{\Gamma(s)}\int_0^\infty dit(it)^{s-1}str\langle x\mid e^{-i[\frac{1}{2}(p-A)^2+V]t}\mid y\rangle \tag{29}$$

with the matrix element in (29) to second order in the background fields given by

$$\langle x\mid e^{-[\frac{1}{2}(p-A)^2+V]t}\mid y\rangle\approx\int_0^t d\tau_1\int_0^{\tau_1}d\tau_2\int_{q(0)=y}^{q(t)=x}Dq(\tau)\left[\exp\ i\int_0^t d\tau\frac{\dot q^2(\tau)}{2}\right] \tag{30}$$

$$i\left[\dot q(\tau_1)\cdot A(q(\tau_1))-V(q(\tau_1))\right]i\left[\dot q(\tau_2)\cdot A(q(\tau_2))-V(q(\tau_2))\right].$$

The background field in (30) can be taken to be a plane wave field, so that upon using (16) we find that

$$str\langle x\mid e^{-iYMt}\mid y\rangle\approx\frac{e^2}{(2\pi it)^2}\frac{t^2}{2}\int_0^1 dx\, e^{-\frac{1}{2}ik^2x(1-x)}\bar u(-1-2x)\not k u. \tag{31}$$

Again, no loop-momentum integral is encountered at any stage. In general, computations with vector theories in this approach are simplified by virtue of the fact that the vector field A_μ enters only linearly in the Lagrangian occuring the path integral.

The path integral can be modified to accommodate background fields that are not necessarily local or plane waves [19,20]. It is also possible to treat situations in which there are different boundary conditions, in particular, the periodic boundary conditions that arise in thermal field theory [12].

Let us consider the thermal field theory of a ϕ^3_D model. We are necessarily working in Euclidean space with $\phi(x_0,\vec{x}) = \phi(x_0+n\beta,\vec{x})$ where $\pm n = 1,2,3\ldots$ and $\beta = 1/T$. The same ζ-function as in (6) is encountered, so that we now must deal with

$$M^{\beta}_{(x;y)} = \langle x \mid e^{-\frac{1}{2}(p^2+\lambda f)t} \mid y\rangle = \int_{per} Dq(\tau)\exp -\frac{1}{2}\int_0^t d\tau\left[\dot{q}^2(\tau)+\lambda f(q(\tau))\right] \tag{32}$$

where "per" now means that $q(0) = y$, $q(t) = x$ with invariance under $q_0 \to q_0 + n\beta$ (viz we are doing the path integral on a cylinder). It has been shown [21] that

$$M^{\beta}_{(x;y)} = \sum_{n=-\infty}^{\infty} e^{i\delta_n} M^{\infty}_{(x_0+n\beta,\vec{x};y)} \tag{33}$$

where

$$\begin{aligned} \delta_n &= 0 \quad \text{(Bosons)} \\ &= n\pi \quad \text{(Fermions)}, \end{aligned} \tag{34}$$

so that by (16) and (33),

$$\begin{aligned} &\int_{per} Dq(\tau)\exp -\int_0^t d\tau\left(\frac{\dot{q}^2(\tau)}{2}+\gamma(\tau)\cdot q(\tau)\right) \\ &= \sum_{n=-\infty}^{\infty}\frac{e^{i\delta n}}{(2\pi t)^{D/2}}\exp\left\{-\frac{(x_0+n\beta-y_0)^2+(\vec{x}-\vec{y})^2}{2t} - \frac{1}{t}\int_0^t d\tau\left[((x_0+n\beta)\tau+y_0(t-\tau))\,\gamma_0(\tau)\right.\right. \\ &\qquad \left.\left.+(\vec{x}\tau+\vec{y}(t-\tau))\cdot\vec{\gamma}(\tau)\right] - \frac{1}{2}\int_0^t d\tau d\tau' G(\tau,\tau')\gamma(\tau)\cdot\gamma(\tau')\right\}. \end{aligned} \tag{35}$$

If, in (32),

$$\sqrt{\beta}(2\pi)^{(D-1)/2} f(q(\tau_i)) = \exp -i\left\{\omega_n q_0(\tau_i) + \vec{k}_i\cdot\vec{q}_i(\tau_i)\right\} \tag{36}$$

$$(\omega_n = \tfrac{2n\pi}{\beta} \text{ - Matsubara Frequency})$$

then by (35), (32) becomes

$$\begin{aligned} Tr\, M^{\beta}_{(x;y)} = \sum_{N=0}^{\infty}\int_0^t d\tau_1\ldots\int_0^{\tau_{N-1}} d\tau_N \int \frac{dx}{((2\pi)^{D-1}\beta)^{\frac{N}{2}}}\sum_{n=-\infty}^{\infty}{}'\frac{e^{i\delta n}}{(2\pi t)^{D/2}}\exp\left\{-\frac{(n\beta)^2}{2t}\right. \\ \left. -ix\cdot\sum_{j=1}^{N}k_j - \frac{in\beta}{t}\sum_{j=1}^{N}k_{j_0}\tau_j + \frac{1}{2}\sum_{i,j=1}^{N}G(\tau_i,\tau_j)k_i\cdot k_j\right\}. \end{aligned} \tag{37}$$

If $D = 3$, then systematic use of the Poisson resummation formula

$$\sum_{m=-\infty}^{\infty} A(m) = \sum_{m=-\infty}^{\infty}\int_{-\infty}^{\infty} d\mu\, e^{2\pi i m\mu} A(\mu) \tag{38}$$

and of the representation

$$2\pi i\sum_{m=-\infty}^{\infty} f(n) = \left(\int_{-\infty-ie}^{\infty-ie} d\lambda + \int_{\infty+ie}^{-\infty+ie} d\lambda\right)\frac{f(\lambda)}{e^{2\pi i\lambda}-1} \tag{39}$$

(f - well behaved on Re)

shows that the only Green's function with β dependence in the static limit $k_{i0} = 0$ is the two-point function [12],

$$\frac{4\pi^2\epsilon_1\epsilon_2}{(2\pi\sqrt{\beta})^2}\int_0^1 d\sigma \frac{1}{e^{[m^2+\vec{k}^2\sigma(1-\sigma)]^{\frac{1}{2}}}-1}\ \frac{1}{[m^2+\vec{k}^2\sigma(1-\sigma)]^{\frac{1}{2}}}. \tag{40}$$

It is also convenient to employ the DeWitt expansion [22]

$$\langle x \mid e^{-[\frac{1}{2}(p-A)^2+V]t} \mid y\rangle = \frac{e^{-\Delta^2/2t}}{(2\pi t)^{D/2}}\sum_{n=0}^{\infty} a_n(x_0,\Delta)t^n \tag{41}$$

$$(\Delta \equiv x-y, \quad x_0 \equiv (x+y)/2)$$

when discussing renormalization of a model, as the region t near zero controls the ultraviolet behaviour of a theory. At one-loop order, one needs only the diagonal elements $a_n(x_0,0)$, and these have been computed a number of ways [22]. Beyond one-loop order, the off diagonal elements are required. These have been examined using recursion formulae [23], the Schwinger expansion [24] and the path integral [25].

Using this approach, it has been possible to show that to two-loop order, the renormalization group functions vanish in both non-Abelian Chern Simons theory [26] and a renormalizable model for Abelian gauge Bosons in three dimensions [27]. In this latter case, we have a classical action

$$\mathcal{L} = \frac{1}{2}\left[\epsilon^{\mu\alpha\nu}A_\mu\partial_\alpha A_\nu + \mu(A_\mu+\partial_\mu\phi)^2\right] + \bar{\psi}(\not{p}+g\not{A}-m)\psi \tag{42}$$

which is gauge invariant under the transform

$$A_\mu \to A_\mu + \partial_\mu\Lambda, \quad \phi \to \phi - \Lambda, \quad \psi \to e^{-ig\Lambda}\psi. \tag{43}$$

The fields ϕ and A_μ decouple if we have the gauge fixing Lagrangian

$$\mathcal{L}_{gf} = \frac{1}{2a\mu}(\partial\cdot A + a\mu^2\phi)^2, \tag{44}$$

leaving us with the propagator

$$\langle A_\mu A_\nu\rangle = \frac{1}{\partial^2-\mu^2}\epsilon_{\mu\alpha\nu}\partial^\alpha - \frac{\mu}{\partial^2-\mu^2}g_{\mu\nu} + \frac{\mu(1-a)}{(\partial^2-\mu^2)(\partial^2-a\mu^2)}\partial_\mu\partial_\nu \tag{45}$$

demonstrating that this theory is renomalizable.

The generating functional at two-loop order is

$$\Gamma^{(2)}[A] = \frac{-ie^2}{2}\int dx\, dy \langle x \mid (-i\epsilon_{\mu\rho\nu}p^\rho + \mu g_{\mu\nu})(p^2+\mu^2)^{-1} \mid y\rangle \tag{46}$$

$$Tr\left\{\gamma^\mu\langle x \mid (\not{p}+g\not{A})\left[(p+gA)^2 - \frac{g}{2}\epsilon_{\alpha\beta\lambda}F_{\alpha\beta}\gamma_\lambda\right]^{-1} \mid y\rangle\right.$$

$$\left.\gamma^\nu\langle y \mid (\not{p}+g\not{A})\left[(p+gA)^2 - \frac{g}{2}\epsilon_{\lambda\delta\sigma}F_{\gamma\delta}\gamma_\sigma\right]^{-1} \mid x\rangle\right\}$$

so that upon applying operator regularization as in (14), we need to consider

$$N_{xy} = \langle x \mid e^{-is[(p+gA)^2 - \frac{g}{2}\epsilon_{\mu\nu\lambda}F_{\mu\nu}\gamma_\lambda]t} \mid y\rangle\,. \tag{47}$$

It is possible to show that the only contributions at $s = 0$ to the divergences in the integrals over the proper time integrals in the regulated form of (46) come from a_0 and a_1 to Δ^2 and Δ respectively. It is possible to show that to this order [24]

$$N_{xy} = \frac{e^{i\Delta^2/4t}}{(4\pi it)^{\frac{3}{2}}}\left[\left(1 - igA\cdot\Delta - \frac{g^2}{2}(\Delta\cdot A)^2\right)\right. \tag{48}$$

$$+it\,(1-ig\Delta\cdot A)\left(\frac{g}{2}\epsilon_{\mu\lambda\nu}F_{\mu\lambda}A_{\nu}\right)\Big].$$

Explicit calculation shows that remarkably the contributions of these terms to the possible divergence at $s=0$ all cancel, and hence in this model the renormalization group functions all are zero to two-loop order.

The quantum mechanical path integral can be used to compute $a_n(x_0,\Delta)$. In the path integral one writes

$$q(\tau)=x_0+\delta(\tau) \tag{49}$$

and then makes the expansions

$$A_{\mu}(x_0+\delta(\tau))=\sum_{N=0}^{\infty}\frac{1}{N!(N+2)}(\delta(\tau)\cdot D)^N\,\delta^{\lambda}(\tau)F_{\lambda\mu}(x_0) \tag{50}$$

(which follows from the gauge condition $\delta(\tau)\cdot A(x_0+\delta(\tau))=0$ [28]) and

$$V(x_0+\delta(\tau))=\sum_{N=0}^{\infty}\frac{1}{N!}(\delta(\tau)\cdot D)^N V(x_0). \tag{51}$$

Simple power counting arguments can be used to show that $a_0(x_0,\Delta)$ is proportional to 1 while those contributions to $a_1(x_0,\Delta)$ are of the form $(\Delta\cdot D)^k V$, $(\Delta\cdot D)^k(\Delta^{\alpha}D^{\beta}F_{\alpha\beta})$, and $(\Delta\cdot D)^k(\Delta^{\alpha}\Delta^{\beta}F_{\alpha\lambda}F_{\beta}{}^{\lambda})(k=0,1,2\ldots)$ while $a_k(x_0,\Delta)$ has thirteen separate possible contributions. Systematic application of (16) can be used to determine to coefficients of each of these terms. This technique can also be applied in curved space-time.

We see that there is indeed a wide variety of problems in perturbative field theory to which the ζ-function and its generatlizations can be applied.

Acknowledgements

The author would like to thank the organizers of the meeting in Caxambu, especially F.T. Brandt, for all they did to make it such a pleasant and productive event.

References

[1] A. Salam and J. Strathdee, Nucl. Phys. B90 (1975) 203.

[2] J.S. Dowker and R. Critchley, Phys. Rev. D13 (1976) 3224.

[3] S. Hawking, Comm. Math. Phys. 55 (1977) 133.

[4] E. Elizalde, S.D. Odinstov, A. Romeo, A.A. Bytsenko and S. Zerbini, Zeta Regularization Techniques with Applications (World Scientific, Singapore 1994).

[5] D.G.C. McKeon and T.N. Sherry, Phys. Rev. D35 (1987) 3854
D.G.C. McKeon and T.N. Sherry, Ann. of Phys. (NY) 218 (1992) 325.

[6] D.G.C. McKeon, S. Rajpoot and T.N. Sherry, Phys. Rev. D35 (1987) 3873
D.G.C. McKeon and T.N. Sherry, J. Mod. Phys. A2 (1987) 785
D.G.C. McKeon, S.S. Samant and T.N. Sherry, J. Mod. Phys. A5 (1990) 1919.

[7] M. Leblanc, R.B. Mann, D.G.C. McKeon and M. Wehlau, Ann. of Phys. 212 (1991) 156
M. Leblanc, R.B. Mann, D.G.C. McKeon and T.N. Sherry, Nucl. Phys. B349 (1991) 494
M. Leblanc, R.B. Mann, P. Madsen and D.G.C. McKeon, J. Mod. Phys. A5 (1990) 2031.

[8] D.G.C. McKeon and T.N. Sherry, Can. J. Phys. 66 (1988) 580
L. Culumovic and D.G. McKeon, Can. J. Phys. 68 (1990) 1166.

[9] R.B. Mann, D.G.C. McKeon, T. Steele and L. Tarasov, Nucl. Phys. B311 (1989) 630.

[10] L. Culumovic, R. B. Mann, M. Leblanc, D.G.C. McKeon and T.N. Sherry, Phys. Rev. D41 (1990) 514
L. Culumovic, D.G.C. McKeon and T.N. Sherry, Ann. of Phys. (NY) 197 (1989) 94
A. Kotikov and D.G.C. McKeon, Can. J. Phys. (in press).

[11] D.G.C. McKeon, Can. J. Phys. 70 (1992) 652
D.G.C. McKeon, Ann. of Phys. (NY) 224 (1993) 139
D.G.C. McKeon and A. Rebhan, Phys. Rev. D48 (1993) 2891.

[12] D.G.C. McKeon and A. Rebhan, Phys. Rev. D47 (1993) 5487; ibid D49 (1994) 1047
D.G.C. McKeon (UWO report 1995).

[13] J. Schwinger, Phys. Rev. 82 (1951) 664.

[14] R.P. Feynman, Rev. Mod. Phys. 20 (1948) 367
R.P. Feynman and A.R. Hibbs, Quantum Mechanics and Path Ingegrals (McGraw-Hill, New York 1965).

[15] C. Itzykson and J.B. Zuber, Quantum Field Theory, pg. 432 (McGraw-Hill, New York 1980).

[16] A.M. Polyakov, Gauge Fields and Strings (Harwood Academic Publishers, Chur 1987).

[17] M. Strassler, Nucl. Phys. B385 (1992) 145.

[18] M.G. Schmidt and C. Schubert, Phys. Lett. 318B (1993) 438.

[19] D.G.C. McKeon, Can. J. Phys. (in press).

[20] D.G.C. McKeon and T.N. Sherry, Mod. Phys. Lett. A (to be published).

[21] L. Schulman, Techniques and Applications of Path Integration (John Wiley, New York 1981).

[22] B. DeWitt, Dynamical Theory of Groups and Fields (Gordon and Breach, New York 1965)
R.T. Seeley, Amer. Math. Soc. 10 (1967) 288.

[23] M. Lüscher, Ann. Phys. 142 (1982) 359.

[24] L. Culumovic and D.G.C. McKeon, Phys. Rev. D38 (1988) 3831.

[25] F.A. Dilkes and D.G.C. McKeon, Phys. Rev. D (to be published).

[26] D.G.C. McKeon and S.K. Wong, J. Mod. Phys. (in press).

[27] F.A. Dilkes and D.G.C. McKeon, Phys. Rev. D (in press).

[28] C. Crönstrom, Phys. Lett. 90B (1980) 267
M.A. Shifman, Nucl. Phys. B173 (1980) 13
A. Fock, Phys. Z. Sowjetunion 12 (1937) 404.

Numerical Simulations and Lattice Field Theories

Marcia G. do Amaral
Departamento de Física, Universidade Federal Fluminense
Niterói, Rio de Janeiro, RJ

Received March, 1996

I Introduction

One of the main motivations for field theoreticians to begin studying Quantum Field Theories (QFT) on a lattice was the fact that with the introduction of the lattice, one could probe, non-perturbatively, regions where the QCD coupling constant is greater than unity, that is, regions inacessible to perturbative expansions. But why specifically the lattice? In perturbation theory calculations, we know how to handle ultraviolet divergences that appear in QFT. This usually involves a redefinition of variable parameters like masses, coupling constants ... . A non-perturbative way of defining the theory and taming ultraviolet divergences is automatically achieved when one approximates the continuous space-time by a lattice, since it involves the introduction of a lattice parameter a, which is the smallest distance between any two lattice sites. There is, now, a maximum momentum , $\Lambda \approx \frac{1}{a}$ for the lattice, and, as a consequence, the theory is now automatically ultraviolet finite without ever pre-supposing any perturbative expansion.

II The Lattice Regularization of QFT-The Euclidean Method:

Nearly all numerical simulations os QFT are based on the Euclidean Path Integral Formulation of those theories. Feynman's path integral formulation of Quantum Mechanics reveals a deep connection between classical mechanics and quantum Theory. Indeed, in an Imaginary time formulation, the Feynman integral is mathematically equivalent to a partition function. Using this analogy, particle physicists have used a well known technique to study gauge theories. The formulation of field theories through Feynman's path integral is very similar to that of Quantum Mechanics. We can define the analogous in QFT of the partition function which is given by,

$$Z_E = \int D\phi(x)\ \exp\left(-S_E(\phi(x))\right) \tag{1}$$

where S_E is the Euclidean action defining the QFT.

$$S_E = \int d^N x\ L(\phi(x)) \tag{2}$$

We have made a Wick rotation, from Minkowski space to the Euclidean one, through the following transformations,

$$\begin{aligned} t &\longmapsto -it \\ iS(\phi) &\longmapsto -S_E(\phi) \end{aligned} \tag{3}$$

in order to replace mathematically difficult-to-handle, oscillating, complex exponentials by well behaved falling exponentials, making it easier to distinguish important paths from unimportant ones.

When performing a numerical simulation, one has to deal with finite volumes, since infinite lattices would imply in infinite CPU time. In this way, when we approximate continous space-time for a discrete set of points and, we reduce the number of degrees of freedom from infinity to a large but finite number.

In principle, the discretization procedure should preserve all the basic symmetries of the continuum theory. The problem is that this is not always possible. The only requirement one imposes on the lattice action - apart from gauge invariance in the case of lattice gauge theories- is that it yields the correct continuum action in the so called continuum limit, $a \to 0$.

Following the same point of view, when we introduce finite temperature effects on the lattice we must simulate a lattice of infinite lenght on the spatial directions and of finite directions in the temporal direction, that is,

$$N_S \quad a \gg \quad N_T \quad a \tag{4}$$

where N_S and N_T are the number of sites in the spatial and temporal directions, respectively.

As we cannot simulate lattices with infinite volumes, we consider as zero temperature lattices as those which have the same number of lattice sites in all directions, that is,

$$N_S \; a \; = N_T \; a \Rightarrow N_S = N_T \tag{5}$$

If we work with a large number of sites N_S and N_T we can simulate the thermodynamical limit. On the other hand, the larger the asymmetry among the number of lattice sites, the higher the temperature, since $N_T \; a = \tau \simeq \frac{1}{KT}$.

It is worth to mention that the critical point in the formulation of a Lattice Field Theory is the discretization procedure. This procedure can lead to different actions on the lattice as will be seen below.

When one discretizes the problem, the lattice Eucidean partition function version of eq. is given by,

$$Z_E = \int \prod_n d\phi(n) \; \exp\{-S_E(\phi(n))\} \tag{6}$$

We can now identify our QFT as a Statistical Mechanics Problem where $\exp(-S_E(\phi(n)))$ is the Boltzmann factor.

Finite temperature QFT can be also be easily simulated on the lattice. In the continuum, to calculate a field theory at a finite temperature T, one simply takes the Euclidean Field Theory and makes it periodic in time with period $t = \tau = \frac{1}{KT}$.

The fundamental quantities in Quantum field theories are the expctation values or Green Functions,

$$< \phi(x_1) \; \phi(x_2) ..... >= \; \frac{1}{Z_E} \int D\phi \; \phi(x_1) \; \phi(x_2) .... \exp(-S_E) = G(x_1, x_2, ..) \tag{7}$$

III Scalar Field Theories:

Scalar field theories are the most simple examples of QFT on a lattice. The best example os such theories is the $\lambda\phi^4$ theory on a lattice. Even though this theory is the simplest of interesting field theories, it has eluded a complete analytical understanding for quite sometime, and it provides an excellent laboratory for the study of more complete field theories.

Scalar fields are easy to be studied on a lattice. In the discrete version of this theory, the scalar fields are defined at lattice sites, labelled by the number vector $\vec{n}$ and field derivatives are substituted by finite differences,

$$\partial_i(\varphi(x)) = \frac{\left[\varphi(\vec{n} + \hat{e}_i) - \varphi(\vec{n})\right]}{a} \tag{8}$$

where a is the lattice spacing and $\hat{e}_i$ is a unit vector in the direction i.

The continuum action for a $\lambda\phi^4$ theory in 4 dimensions is given by,

$$S = d^4x \left\{ \frac{1}{2} (\partial\phi(x))^2 + \frac{1}{2} m_0^2 \phi^2(x) + \frac{1}{4} \lambda \phi^4(x) \right\} + \frac{m^4}{\lambda} \tag{9}$$

which, when discretized, reduces to,

$$S = \beta a^4 \sum_n \left\{ \begin{array}{c} -\frac{1}{2a^2}\theta(n) \sum_{i=1}^{\mu} (\theta(n+\mu) + \theta(n-\mu)) + \frac{4}{a^2}\theta^2(n) \\ +\frac{1}{4}\left(\theta^2(n) - 1\right)^2 \end{array} \right\} \tag{10}$$

where the first sum is over all lattice sites, μ is an unitary vector,

$$\theta = \sqrt{\lambda}\, \frac{\phi}{m} \tag{11}$$

is a dimensionless field and

$$\beta = \frac{1}{\lambda} \tag{12}$$

plays the role of a temperature in a statistical mechanics problem. We must pay attention to the fact that although we may do this kind of connection between λ and the " "temperature ", as long as we work with a square lattice we will be studying QFT at zero temperature.

Adding an external current term $J\phi$ to the action, and defining the connected partition function in the usual way,

$$Z(J) = \exp\left(-W(J)\right) \tag{13}$$

where $W(J)$ is the connected Green function functional generator, we can easily obtain expressions for the average of a functional of the fields in the presence of an external current,

$$< A(\theta(n)) >_J = \frac{\int D\theta(n)\ A(\theta(n))\ \exp(-\beta H\ )}{\int D\theta(n)\ \exp(-\beta H\ )} \tag{14}$$

such as magnetization Φ, susceptibility χ and the Binder-Challa-Landau cumulant U_L.

$$\Phi = \sum_n \left\langle \frac{\theta(n)}{N} \right\rangle_J = \frac{1}{\beta N a^4}\, \frac{\delta W(J)}{\delta J} \tag{15}$$

$$\chi(J,\beta) = -\frac{\delta\Phi}{\delta J} = \beta N a^4 \left\{ \left\langle \left(\sum_n \frac{\theta(n)}{N} \right)^2 \right\rangle_J - \Phi^2 \right\} \tag{16}$$

$$U_L = 1 - \frac{< S^4 >^c}{3\,\chi} \tag{17}$$

where

$$< S^4 >^c = \left\langle \left(\sum_n \frac{\theta(n)}{N} \right)^4 \right\rangle - 3 \left\langle \left(\sum_n \frac{\theta(n)}{N} \right)^2 \right\rangle^2 - 4\Phi \left\langle \left(\sum_n \frac{\theta(n)}{N} \right)^3 \right\rangle +$$

$$+ 12\Phi^2 \left\langle \left(\sum_n \frac{\theta(n)}{N} \right)^2 \right\rangle - 6\Phi^4 \tag{18}$$

Other very useful quantities are the internal energy density ϵ and the specific heat C,

$$\epsilon = \left\langle \frac{H}{Na^4} \right\rangle_J = -\frac{1}{Na^4}\, \frac{\partial}{\partial\beta} \{\ln Z(J)\} \tag{19}$$

$$C = -\beta^2\, \frac{\partial\epsilon}{\partial\beta} = \beta^2 N a^4 \left\{ \left\langle \left(\frac{1}{N} h(n) \right)^2 \right\rangle_J - \epsilon^2 \right\} \tag{20}$$

IV Gauge Fields:

When we have studied quantum fields on a lattice we have defined our operators at each point of the lattice and have replaced the derivatives by finite differences. However, we must modify this prescription because if we repeat the same procedure for gauge fields, we will verify that the resulting lattice action does not preserve gauge invariance, and as it was pointed out by Wilson, [1] exact gauge invariance may be a crucial ingredient for quark confinement. So, in order to guarantee the preservation of gauge invariance we must replace,

$$idx_\nu \; eA_\nu(\vec{x},t) \; \rightarrow \exp\left[i \; e \; aA_\nu(n)\right] \equiv U_\nu(n) \tag{21}$$

and redefine the gauge transformation on the lattice by[1]

$$U_\nu(\alpha) \rightarrow G(\alpha)U_\nu(\alpha)G^{-1}(\alpha+\nu) \tag{22}$$

where α labels a point in space time, G =exp $(i\chi)$ and e is the dimensionless electric charge. $U_\nu(n)$ is a link variable defined on a link, that is on a bond that links the site n to the site $n+\nu$, where ν is an unitary vector in any of the four lattice directions.

The simplest example of a gauge invariant object that can be constructed with gauge fields $U_\nu(n)$ is the smallest closed Wilson Loop or a plaquette variable- a 1×1 loop.

$$P_{\mu\nu}(n) = Re\left[U_\nu(n)U_\mu(n+\nu)U_\nu^{-1}(n+\mu)U_\mu^{-1}(n)\right] \tag{23}$$

and the Wilson action on the lattice is written in terms of this plaquette variable,

$$S_{QED} = \beta \sum_{\nu>\mu} \sum_n P_{\mu\nu}(n) \tag{24}$$

where $\beta = 1/e^2$. The above equation reduces to ,

$$S_{QED} = \frac{1}{4} \sum_{\mu\nu} \int d^4x \; F_{\nu\mu}F_{\nu\mu} \tag{25}$$

in the continuum limit $a \rightarrow 0$. In the case of non-abelian gauge fields the action has the same form as that of 24 except that now $\beta = 6/g^2$ where g is the gauge coupling constant. The fields U_ν are now matrices and a trace has to appear in 24.

The observables to be measured must be gauge invariants , otherwise the expectation value will be equal to 0.

V Lattice Fermions:

Until now we have not verified the existence of any prpblems in the definition of gauge fields or scalar fields on the lattice. The free Euclidean fermion action in the continuum (in 4 dimensions) is given by,

$$S_F^N(\psi,\overline{\psi}) = \int d^4x \; \overline{\psi}(x)\left(\gamma_\mu\partial_\mu + m\right)\psi(x) \tag{26}$$

If we follow the prescription used in the discretization of gauge and scalar fields, we will replace the derivatives by symmetric differences,

$$S_F^N(\psi,\overline{\psi}) = \sum_{n,\mu} \frac{1}{2a} \overline{\psi}(n)\gamma_\mu\left(\psi(n+\mu) - \psi(n-\mu)\right) + m\sum_n \overline{\psi}(n)\psi(n) \tag{27}$$

This action suffers from the well known problem of doubling of fermionic species. This problem can be easily understood if we write down the propagator,

$$G(p) = \left(i\gamma_\mu \sin\; p_\mu\, a \; + ma\right)^{-1} \tag{28}$$

If we consider the massless theory, we can observe that besides the pole at $p = (0,0,0,0)$, there are other fifteen unwanted poles at $p = (\pi,0,0,0)$, ... (π,π,π,π). This is a model describing sixteen massless fermions instead of the expected one.

It had been shown that [2] the individual contribution of these poles to thye triangle graph alternate in sign and add up to zero. One may ask if this unexpected property of the lattice Dirac equation is general in character or tight to this specific action. A no-go theorem by Nielsen and Ninomiya [3] tells us that if one do not sacrifice continuous chiral symmetry, it will end up with many fermions in the continuum limit (2^D) . The only way of evading species doubling is by using a non local lattice derivative [4]. The problem with that approach is that those kind of theories have severe problems in the continuum limit.

There are many ways of dealing with this kind of problem, and we will mention here two methods mostly used by physicists.

V.1 Wilson Fermions:

In this treatment one adds an irrelevant operator to the action in such a way that it has only one pole at $p = (0,0,0,0)$ and, hence, describes one massless particle. Actually, the 15 unwanted fermionic species are still there, but as they are given a large mass $\sim \frac{1}{a}$, they disappear from the theory as $a \to 0$. The irrelevant term is irrelevant in the sense that it vanishes $\sim a$ in the continuum limit.

The simplest version of this solution is due to Wilson ,and , in this case, a second order derivative-like term S^W is added to the naive fermion action, S_F^N ,

$$S^W = -\frac{r}{2a}\sum_{n\ \mu}\overline{\psi}(n)\ \{\psi(n+\mu) - 2\psi(n) + \psi(n-\mu)\} \tag{29}$$

in which r is a parameter that lies between 0 and 1 even though usually $r = 1$ is more commonly used.. With Wilson fermions, it is conventional not to use the mass, but the hopping parameter $K = \frac{1}{2}(ma + 4r)^{-1}$ and to rescale the fields $\psi \to \sqrt{2K}\psi$. In this way, the fermion action for the interacting theory is now given by,

$$S \ = \ \sum_n \overline{\psi}(n)\psi(n) -$$

$$- K\sum_{n\mu}\ \{\overline{\psi}(n)(r-\gamma_\mu)U_\mu(n)\psi(n+\mu) + \overline{\psi}(n)(r+\gamma_\mu)U_\mu^\dagger\psi(n-\mu)\} \tag{30}$$

What are the main advantages of this formulation? First of all, the Wilson formulation is very similar to the continuum formulation, since there is a four component spinor on every lattice site for every colour and/or flavour of quarks, and the γ matrices also are present.

Construction of currents and states are just like the continuum. The main disavantage is that chiral invariance of the action is lost at finite lattice spacing and is to be recovered in the continuum limit.

V.2 Staggered fermions:

This approach is due to Kogut and Susskind [5]. In this formulation the number of additional species is reduced by the distribution of each of the four components of the continuum spinor over different sites of the lattice. With this formulation, if one introduces different staggered fermion species on the lattice, the staggered fermion action will lead to $n_f = 4\ f$ fermion species in the continuum.

The staggered fermion action obtained after a diagonalization in the Dirac indices is given by,

$$S_{KS} = \sum_{i=1}^{f}\sum_{nm}\overline{\chi}_i(n)M^{-1}(n,m)\chi_i(m) \tag{31}$$

where $\chi, \overline{\chi}$ are anticommuting Grassman variables defined on the sites of the lattice and the fermionic matrix $M^{i}(n,m)$ is given by,

$$M^{i}(n,m) = \sum_{\mu=0}^{3} D_{\mu}(n,m) + m_i \delta(n,m) \tag{32}$$

where

$$D_{\mu}(n,m) = \frac{1}{2}\eta_{\mu}(n)\left[U_{\mu}(n)\delta(n,m-\mu) - U_{\mu}^{-1}(n)\delta(n,m+\mu)\right] \tag{33}$$

The phase factors

$$\eta_{\mu}(n) = (-1)^{n0+\cdots n\mu-1} \qquad para \quad \mu > 0 \qquad \eta_0(n) = 1 \tag{34}$$

are remnants of the γ_{μ} matrices.

Staggered fermions preserve an explicit chiral symmetry as $m \to 0$ even for finite lattice spacing, as long as all 4 flavors are degenerate. For studies of chiral symmetry breaking and of deconfining transition at high temperatures it is convenient to work with such a lattice. Another advantage is that numerical simulations with staggered fermions are computationally less CPU demanding than those with Wilson fermions, since they involve less variables. On the other hand, flavor symmetry and translational symmetry are all mixed together and the construction of meson and baryon states are much more complicated than for Wilson fermions.

VI Simulation Methods:

As we have seen the relevant physical quantities can be extracted from expectation values like,

$$< A >= \frac{\int \prod_i dx_i \; A(x_i) \exp\{-S(x_i)\}}{\int \prod_i dx_i \exp\{-S(x_i)\}} \tag{35}$$

On a finite lattice, this integral is a well defined multidimensional integral. Monte Carlo simulation is a numerical method to evaluate these kind of integrals. With the advent of powerful computers, this method became practical for investigations relevant to QFT.

If we represent the integrals in the above equation by a sum over sufficiently many points, the multidimensional integral becomes a summation. Each term is represented by a set of field variables on the sites or links, called a field configuration. The contribution of a given field configuration to $< A >$ is given by,

$$< A > \simeq A(\{\psi_i\}) \exp(-S\{\psi_i\}) \tag{36}$$

The number of configurations is so large (for continuous groups it is infinite) that is impossible to sum over all configurations exactly. This would not also be a wise procedure, anyway, since most of the configurations have a very small Boltzmann factor, making their contribution to the total sum negligible. The above equation suggests a sampling over configurations, where the probability that a configuration $\{\psi_i\}$ is included in this set is proportional to the Boltzmann weight factor $\exp(-S(\{\psi_i\}))$. This procedure is called importance sampling.

Let us assume that a sequence M of configurations is generated with the equilibrium probability,

$$P_{eq}(\{\psi_i\}) \simeq \exp(-S(\{\psi_i\})) \tag{37}$$

then, the expectation value of $< A >$ can be approximated by,

$$< A > \simeq \overline{A} = \frac{1}{M}\sum_{\nu=1}^{M} A(\{\psi_\nu\}) \tag{38}$$

Configurations with the equilibrium distribution P_{eq} can be generated by a Markov process, where the elements of the Markov chain are configurations. These configurations are generated subsequently, each configuration from

the previous one. The transitions probability of creating a configuration $\{\psi\}_{\nu'}$ from $\{\psi\}_{\nu}$ in a step is given by $W\ (\nu \rightarrow \nu')$, which must obey the following properties,

a) $\sum_{\nu'} W\ (\nu \rightarrow \nu') = 1$

b) Any finite action configuration should be reachable in a finite number of steps.

c) A Detailed Balance condition must hold,

$$P_{eq}(\nu)\ W(\nu \rightarrow \nu') = P_{eq}(\nu')\ W(\nu' \rightarrow \nu)$$

There are many ways of constructing $W(\nu \rightarrow \nu')$ satisfying the above conditions. The method developed by Metropolis and collaborators [6] is the most commonly used. In this method, first, a new candidate value $\widehat{\psi}_\nu$ is selected with an arbitrary probability distribution P_o obeying,

$$P_o(\psi_\nu \rightarrow \widehat{\psi}_\nu) = P_o(\widehat{\psi}_\nu \rightarrow \psi_\nu) \tag{39}$$

Then, the change in the action ΔS caused by the replacement of $\psi_\nu \rightarrow \widehat{\psi}_\nu$ is computed, where,

$$\Delta S = S(\widehat{\psi}_\nu) - S(\psi_\nu) \tag{40}$$

If $\Delta S \leq 0$ the change is accepted and $\widehat{\psi}_\nu = \psi_{\nu'}$ is the next member of the Markov chain. If $\Delta S > 0$ the change is accepted with a conditional probability $\exp(-\Delta S)$. For that, a random number $r \in (0, 1)$ is chosen and the next element of the Markov chain is taken to be $\widehat{\psi}_\nu$ if $r < \exp(-\Delta S)$, otherwise it remains given by ψ_ν.

In general, the configurations are changed locally and the new configuration is nearly equal to the old one, except for the value of the field at a given site (or link), where $\psi_j \rightarrow \psi'_j$. Only when one has updated all sites or links of a given lattice, one can say that a Monte Carlo step has been completed. Generally the number of Monte Carlo steps needed in a simulation is of the order of millions of steps. Usually, one has to wait until the system reaches equilibrium before starting to calculated the desired averages. This number N of steps required before the calculation of the mean values is called thermalization number and depends on the lattice volume, the model and the phase space parameters.

Even after we have made a sweep through the system updating every variable, it may happen that the new configuration is correlated to the previous one. This means that sucessive measurements of the interesting observables are correlated. This correlation can be described as,

$$\Gamma(t) = \frac{< O(\tau)O(t+\tau) > - < O(\tau) >^2}{< O(\tau)^2 > - < O(\tau) >^2} \tag{41}$$

For very large values of t , $\Gamma(t)$ behaves like

$$\exp\left(-\frac{t}{t_C}\right) \tag{42}$$

where t_C is the autocorrelation time for the operator O. In principle, we should only perform measurements among non-correlated configurations. Close to a critical point, that is, when the continuum limit is approached and the correlation length diverges, the autocorrelation also diverges. Both quantities are related through a scaling law and a dynamical critical exponent Z.

$$\tau_C \sim \xi_L^Z \tag{43}$$

The divergence of τ_C near the continuum limit is called critical slowing down. In the case of a standard Metropolis algorithm, $Z = 2$. In an ideal algorithm $Z = 0$. Much research is now being done in order to improve methods to reduce the critical slowing down.For Ising systems and other models with global symmetry, it is known that cluster algorithms are able to give $Z = 0$ [7][8][9]. In the case of gauge theories the situation is more complicated and one has to search for other algorithms.

VI.1 Fermion Simulations:

When one deals with fermion fields life is much more complicated. Instead of ordinary numbers in the path integral we have anticommuting numbers or Grassmann variables. Thus, the action is not an ordinary number and we cannot use its exponential as a probability density. However, in many field theories, including QCD, the action is quadractic in the fermion fields,

$$\int [d\psi d\overline{\psi}]\ \exp(-S_F) = \int [d\psi d\overline{\psi}]\ \exp\left\{-\int d^3x\ dt\ \overline{\psi}(\gamma_\mu \partial_\mu - m)\psi\right\} \simeq$$
$$\simeq \int [d\psi d\overline{\psi}]\ \exp\left\{-\sum_{i,j} \overline{\psi}_i\ M_{ij}\ \psi_j\right\} \tag{44}$$

where M_{ij} is the discrete interaction matrix on the lattice. If we integrate out the fermion variables we will verify that the above integral is equal to $\det(M)$ times some unimportant normalization factor.

Let us consider a more general problem that includes both fermionic and bosonic fields and where fermions and bosons interact via the fermion matrix M , If we represent the real bosonic fields by φ, then the expectation values will have the form,

$$< O(\varphi) >= \frac{1}{Z}\int [d\overline{\psi}d\psi]\,[d\varphi]\ O(\varphi)\ \exp\left(-S_E^O(\varphi) - \sum \overline{\psi}_i M_{ij}(\varphi)\psi_j\right) =$$
$$= \frac{1}{Z}\int [d\varphi]\ O(\varphi)\ \det(M(\varphi))\exp\left(-S_E^O(\varphi)\right) \simeq$$
$$\simeq \frac{1}{Z}\int [d\varphi]\ O(\varphi)\ \exp\left\{-S_E^O(\varphi) + Tr\ln(M(\varphi))\right\} \tag{45}$$

where Z is the theory partition function. If the fermion determinat is a positive real number, we can use $\det(M(\varphi))\exp\left(-S_E^O\right)$ as a probability.

In principle, there is nothing that forbids the evaluation of the fermion determinant in a Monte Carlo simulation, but an exact calculation of $\det(M(\varphi))$ involves N^3 operations (where N is the dimensionality of $M(\varphi)$,which is equal to the total number of lattice sites). As each Monte Carlo sweep involves the update of all lattice sites, this means that the total number of operations required by the fermion determinant is equal to $N * N^3 = N^4$. For example if we have a lttice with 32^4 sites, the number of operations required by the determinant, for each Monte Carlo sweep is given by,$[32^4] \simeq 1208 \times 10^{24}$. As a consequence, it turns out that Monte Carlo calculations are pratically forbidden in the case of fermions. This fact led to the use of the so called quenched approximation, in which the fermion detreminant is set to 1 . This approximation amounts to neglecting virtual fermion loops and treating fermions as static degrees of freedom.

All fermions algorithms in use, which try to take into account the dynamical effects of fermions in the generation of field configurations make use of the following relation,

$$\int d\overline{\psi}d\psi d\varphi\ \exp\left\{-S_O(\varphi) - \overline{\psi}M(\varphi)\psi\right\} = \int d\varphi\ \exp\left(-S_O(\varphi)\right)\det(M(\varphi)) =$$
$$= \int d\chi\ \exp\left\{-S_O(\varphi) - \chi^T\ \left(M^T(\varphi)M(\varphi)\right)^{-1}\chi\right\} \tag{46}$$

where we have assumed that M is a real matrix and the χ are real pseudofermionic fields, that is, bosonic fields that interact via the fermion matrix [10][11].If the interaction matrix was complex, we would have to use complex pseudofermionic fields and one would have to pay the cost of simulating twice the number of fermion species. This extra doubling can be eliminated in the case of Kogut-Susskind fermions by the use of the prescriptions suggested by Polonyi[12] . If we observe the above relation we will verify that we have traded the determinant for the inverse of the Dirac matrix, but as we now have pseudofermionic fields, in principle, we can use a standard Monte Carlo simulation. The problem now is that because the inverse of a sparse matrix is not a sparse matrix, any local

updating scheme would be prohibitively CPU time consuming. On the other hand, if we try to do a global updating the acceptance rate would drop to zero very quickly.

More recently, some algorithms based on the solution of differential equations were proposed. The Microcanonical method was first formulated to investigate scalar and gauge models by Callaway and Rahman [13] and was later modified to include ferions by Polonyi and Wyld [12]. In this method,, as in all other methods that will be mentioned below, an artificial time parameter (which can be thought as the computer time) is introduced. A Hamiltonian is built, the Hamiltonian equations of motion are integrated out and one obtains a deterministic evolution of the fields in the phase space at fixed energy. The Langevin method [14][15][16] is very similar, in principle, to the microcanonical method, the difference being that a differential stochastic equation, the Langevin equation, is used to simulate the equilibrium configurations in the phase space. In the case of those two methods, there are some drawbacks that should be mentioned. The probelms arises from the necessity of discretizing the equations of motion by the introduction of an artificial time parameter τ in order to evaluate them in the computer. This means that we must work wth a finite value of τ and, in the end, make a careful extrapolation of the results to the limit where $\tau \to 0$. Besides this problem, the microcanonical method may suffer from ergodicity problems. If these problems are true, phase space is not swept uniformly and the results may be incorrect. The Langevin method, in the other hand, sweeps phase spcae randomly instead of following classical trajectories. As a consequence, the Langevin equation evolution in phase space is very slow and a great number of Langevin steps is required to obtain the correct results.

The Hybrid Monte Carlo Method [17] is by far one of the most used fermion algorithms nowadays. This method, was introduced with the idea that it would be an efficient and exact way of introducing dynamical fermions in Monte Carlo methods. Although this method has all the statistical errors associated to any Monte Carlo simulation, it does not contain non controllable systematical errors.

The central idea behind the Hybrid Monte Carlo method is to combine the good qualities of both Microcanonical and Langevin methods, that is, ergodicity and fast progress through phase space together with those of a Monte Carlo simulation.

One of the main advantages of the HMC method is that the fields are updated in a parallel way over all the lattice sites and later the new configuration generated is accepted or rejected globally. As there are no truncation errors coming from the discretization of the equiations of motion, one can work with a diecrete time step as large as possible, the only limitation being the Monte Carlo acceptation rate, which shall be kept high if one wants the method to be efficient and fast.

In the HMC algorithm an artificial time parameter τ is introduced together with a Hamiltonian dynamics specifying the evolution of the scalar fields as a function of τ.

Let us consider the case of a fermion field coupled to a scalar field through an interaction matrix $M(\varphi)$ and let us add a quadratic termto the Kogut-Susskind action.,

$$H = \frac{1}{2}\sum_n \pi^2 + S_O(\varphi) + \chi^T \left(M^T(\varphi)M(\varphi)\right)^{-1}\chi \tag{47}$$

where χ and χ^T are pseudofermionic fields, $S_O(\varphi)$ is some action that governs the behavior of the scalar field φ and the π fields are canonical momenta conjugate to the bosonic φ fields are are located over the lattice sites. The above equiation can be thought as the Hamiltonian from which equiations of motion in a ficticious time τ can be derived. The equations of motion are given by,

$$\dot{\varphi} = \pi \tag{48}$$

$$\dot{\pi} = -\frac{\delta S_O(\varphi)}{\delta\varphi} -$$

$$-\chi^T \left(M^T(\varphi)M(\varphi)\right)^{-1}\left\{\frac{\delta}{\delta\varphi}\left(M^T(\varphi)M(\varphi)\right)\right\}\left(M^T(\varphi)M(\varphi)\right)^{-1}\chi \tag{49}$$

and a new configuration (φ', χ') is generated in the following way. supposing that an old configuration (φ, χ) already exists.

1) A set of initial conjugate momenta $\pi(\tau)$ are randomly generated, from a gaussian distribution of mean zer and dispersion 1,

$$P_G(\pi) \approx \exp\left(-\frac{\pi^2}{2}\right) \tag{50}$$

2) The interaction matrices $M(\varphi)$, $M^T(\varphi)$ and $M^T(\varphi)M(\varphi)$ are constructed.

3) The pseudofermionic fields are generated according to,

$$\chi = M^T \eta \tag{51}$$

where η is a vector whose elements are generated in a random way by means of a Gaussian distribution of mean zero and dispersion 1. Ergodicity of the process is assured in this way.

4) Once the χ fields are known, we build an auxiliar vector,

$$\Phi = \left(M^T(\varphi)M(\varphi)\right)^{-1}\chi \tag{52}$$

by way of an specific solver (Gauss Seidel, Conjugate Gradient ....)

5) While the pseudofermionic fields are kept fixed , we perform the evolution of the π and φ fields using eqs 4849 and the Leap Frog algorithm, which can be easily adopted to this specific problem [17][18].

6) After a complete (π, φ) Molecular Dynamics evolution, the new configuration will be accepted or rejected by a Global Monte Carlo with a probability,

$$P_{AC} = P_{AC}\left((\pi, \varphi) \rightarrow \left(\pi', \varphi'\right)\right) = \min(1, \exp(-\delta H)) \tag{53}$$

where $\delta H = H(\pi', \varphi') - H(\pi, \varphi)$ and H is given by eq 46.

If the integration of the equations of motion could be carried out exactly, the acceptance probability for a configuration at the end of a trajectory would be unity. However, the necessity of discretizing the equations of motion numerically introduces integration errors which lead to small variations of energy conservation. The Hybrid Monte Carlo method compensates for these errors by performing the global acceptation/rejection

7) After each accept/reject Monte Carlo step we generate new values of the momenta according to eq 48 and new values of the pseudofermionic fields χ according to eq. 49.

It can be shown that the transition probability restricted only to the fields φ obey the Detailed Balance Principle if the Dynamics is reversible. This can be achieved by letting evolve the fields and their conjugate momenta according to a Leapfrog discretization scheme. In this integration scheme, the phase space volume is preserved for all values of $\delta\tau$ (satisfies the Liouville Theorem). The errors involved are $O(\delta\tau^3)$ and $O(\delta\tau^5)$ for the second and fourth order algorithms.

References

[1] K.G. Wilson ; Phys.Rev. D10 (1974) 2445.

[2] Karsten and smit; Nucl. Phys. B183 (1981) 103.

[3] H.R. Nielsen and M. Ninomiya; Nucl. Phys. B193 (1981) 173.

[4] S. Drell , M. Weinstein and S. Yankielowicz; Phys. Rev. D24 (1976) 487.

[5] J.B. Kogut and L. Susskind; Phys. Rev. D11 (1975) 395.

[6] N. Metropolis et al ; J. Chem. Phys. 21 (1953) 1087.

[7] R.H. Swendsen and J. S. Wang; Phys. Rev Lett 58 (1987) 86.

[8] U. Wolff; Nucl. Phys. B322 (1989) 759.

[9] M. Hasenbusch ; Nucl. Phys. B333 (1990) 581.

[10] D. N. Petcher and D.H Weingarten; Phys. Lett. B99 (1981) 333.

[11] F. Fucito et al ; Nucl. Phys. B180 (1981) 369.

[12] J. Polonyi and H. Wyld; Phys. Rev. Lett 51 (1983) 2257

[13] D.J. Callaway and A. Rahman; Phys. Rev. Lett 49 (1982) 613.

[14] C.G. Batrouni, G.R.Katz, A. S. Kronfeld, G. Lepage, B, Svetisky and K. G Wilson; Phys. Rev.D32 (1985) 2736.

[15] A. Ukawa and M. Fukugita; Phys. Rev. Lett 55 (1985) 1854.

[16] M. Creutz and R. Gavai; Nucl. Phys. B280 (1987) 181.

[17] S. Duane, A.D. Kennedy, B.J. Pendleton and D. Roweth; Phys. Lett B195 (1987) 216.

[18] M. Campostrini and P. Rossi; Nucl. Phys. B329 (1990) 753

Noncommutative Geometry and the Standard Model: An overview

José M. Gracia-Bondía
Department of Mathematics, Universidad de Costa Rica,
2060 San José, Costa Rica

Received March, 1996

Introduction

As it is usually presented in textbooks, the Standard Model of "fundamental interactions" is, mathematically speaking, a hideous construction. We can summarize its content thus:

1 The interaction fields are gauge fields with a $SU(3)_c \times SU(2)_L \times U(1)_Y$ symmetry. In other words, there are three systems of gauge bosons $A_\nu^{SU(3)}$, $A_\nu^{SU(2)}$, $A_\nu^{U(1)}$. They contribute terms $(F \mid F) := \mathrm{tr} \int F_{\mu\nu} F^{\mu\nu} d^4x$ to the Action, where F is the gauge field, which is obtained from the gauge potential by the recipe $F = dA + A \wedge A$.

2 The (fermionic) matter fields ψ contribute terms $\int \psi_1 D\psi_2 = \int \psi_1 \partial\!\!\!/ \psi_2 + \int \psi_1 A\!\!\!/ \psi_2$.

3 Unfortunately, in order to give mass to the electroweak gauge bosons, there is the need to add a colorless scalar "matter" field, called the Higgs particle, with dynamics given by $\int L^\nu \phi^\dagger D_\nu \phi + V(\phi)$ where $V(\phi) = -\mu^2 \phi^\dagger \phi + \lambda(\phi^\dagger \phi)^2$. The "negative mass" μ is needed for symmetry breakdown to work. The introduction of the Higgs is justified on a technical basis: it preserves unitarity and renormalizability of the quantized theory and ... it works. It also gives mass to the fermions through the seemingly ad hoc and apparently non gauged ...

4 ... Yukawa interaction terms, $\int \bar{\psi}_1 \phi \psi_2$.

5 We summarize thus the several aesthetically unpleasant features of the SM:

1. The Higgs sector is introduced by hand.
2. The link between the parity violating and the symmetry breaking sector remains mysterious.
3. There is no explanation for the observed number of fermionic generations.
4. The choice of gauge groups and hypercharge assignments seems rather arbitrary, although it has the felicitous result that the model, despite being chiral, is anomaly-free.
5. There is an apparent juxtaposition of gauged and non-gauged interaction sectors.
6. There is no explanation for the huge span of fermionic masses.

Noncommutative geometry goes a good bit of the way to solving these questions —except the last.

A new framework for thinking about the SM

In noncommutative geometry (NGC) all the complexities and idiosyncrasies of the SM stem from a "pure QCD-like theory" with a unified noncommutative gauge boson $\mathbb{A}$ for the $SU(3)_c \times SU(2)_L \times U(1)_Y$ symmetry. Thus the Lagrangian:

$$\mathcal{L}_{\rm NCG} = -\tfrac{1}{4}(\mathbb{F} \mid \mathbb{F}) + (\bar{\Psi} \mid D(\mathbb{A})\Psi)$$

on a *noncommutative space*, to wit, the *product of M_4 by the space of the internal degrees of freedom*: colour, weak isospin and hypercharge. Here

$$\mathbb{A} = \mathbb{A}(A^{SU(3)}, A^{SU(2)}, A^{U(1)}, \phi).$$

That is to say, the Higgs is seen as a gauge boson (this helps to explain its quartic kinetic energy and its pointlike coupling to fermions). We still have $\mathbb{F} = d\mathbb{A} + \mathbb{A}^2$, and therefore

$$\mathbb{F} = \mathbb{F}(F^{SU(3)}, F^{SU(2)}, F^{U(1)}, D\phi, |V|^{1/2}).$$

The spaces of noncommutative geometry

The mathematical framework hinges on two related ideas: (1) geometrical properties of spaces of points (e.g., spacetime without chirality) are determined by their c-number functions; (2) other geometrical settings (e.g., spacetime with chirality) can be accommodated by allowing noncommutative algebras of q-number functions; both are thought of as algebras of operators on Hilbert spaces.

Many structures arising in classical geometry are thus replaced by their quantum counterparts. For instances, measure spaces are replaced by von Neumann algebras, topological spaces by C^*-algebras, vector bundles by projective modules, Lie groups by smooth groupoids, de Rham homology by cyclic cohomology, and spin manifolds by spectral triples.

Think of functions as forming an algebra $\mathcal{A}$ of multiplication operators on a Hilbert space $\mathcal{H} = \mathcal{H}^+ \oplus \mathcal{H}^-$. If Γ is the sign operator ($= \pm 1$ on $\mathcal{H}^\pm$), then $\delta f = [\Gamma, f]$ is an "infinitesimal" operator. Differential calculus is done with a "spectral triple" consisting of the algebra $\mathcal{A}$, the Hilbert space $\mathcal{H}$ and an odd selfadjoint operator D on $\mathcal{H}$ (e.g., the Dirac operator on the space of spinors $L^2(S_M)$). Integration of functions is effected by the Dixmier trace of operators: if T has eigenvalues $\mu_n(T) \geq 0$, then

$$\int T = \lim_{n-\infty} \frac{\mu_0(T) + \cdots + \mu_n(T)}{\log n}, \qquad \text{where} \quad \int f = \int f|D|^{-d}.$$

Other classical geometrical objects have their quantum counterparts. A complex variable becomes an operator in $\mathcal{H}$, a real variable is a selfadjoint operator, and an infinitesimal is a compact operator. An infinitesimal of order k is seen to be a compact operator whose singular values μ_n are $O(n^{-k})$ as $n \to \infty$. The differential of real or complex variable is replaced by $\delta f \equiv [\Gamma, f] = \Gamma f - f\Gamma$; and the integral of a first-order infinitesimal is given by the Dixmier trace.

The spectral triple $(\mathcal{A}, \mathcal{H}, D)$ determines the geometry completely. For example, here is the formula for computing distances between points (i.e., pure states of $\mathcal{A}$) on a conventional Riemannian manifold:

$$d(p,q) = \sup\{\, |f(p) - f(q)| : f \in \mathcal{A};\ \|[D, f]\| \leq 1 \,\},$$

where $D = \partial\!\!\!/$ is the usual Dirac operator. Thus, we now have a fully quantum formalism for the classical world, and we notice that distances are better measured by neutrinos than by scalar particles!

The reconstruction of the SM

We need to have more details on the noncommutative differential calculus. One can embed $\mathcal{A}$ in the "universal differential algebra" $\Omega^*\mathcal{A} = \bigoplus_{n \geq 0} \Omega^n \mathcal{A}$, generated by symbols $a_0\, da_1 \ldots da_n$ with a formal antiderivation d satisfying

$d(a_0\,da_1\ldots da_n) = da_0\,da_1\ldots da_n$, $d1 = 0$ and $d^2 = 0$. Having a spectral triple allows us to condense this large algebra to a more useful one. We first represent the whole of $\Omega^\bullet\mathcal{A}$ on the Hilbert space $\mathcal{H}$ by taking:

$$\pi(a_0\,da_1\ldots da_n) := a_0\,[D,a_1]\ldots[D,a_n].$$

The algebra of operators $\pi(\Omega^\bullet\mathcal{A})$ is not a differential algebra, in general. This problem is handled by a standard trick: the differential ideal of "junk" $J := \{\,c' + dc'' \in \Omega^\bullet\mathcal{A} : \pi c' = \pi c'' = 0\,\}$ is factored out, thereby obtaining a new graded differential algebra of "noncommutative differential forms" by

$$\Omega^\bullet_D\mathcal{A} := \pi(\Omega^\bullet\mathcal{A})/\pi(J).$$

The quotient algebra $\Omega^\bullet_D C^\infty(M;\mathbb{C})$ for the standard commutative spectral triple is an algebra of operators on $L^2(S_M)$ isomorphic to the de Rham complex of differential forms. The Connes model is given by

$$\mathcal{A} := C^\infty(M,\mathbb{R})\otimes\mathcal{C}_F \simeq C^\infty(M,\mathbb{C})\oplus C^\infty(M,\mathbb{H})\oplus M_3(C^\infty(M,\mathbb{C})),$$
$$\mathcal{H} := L^2(S_M)\otimes(\mathcal{H}_F^+\oplus\mathcal{H}_F^-), \qquad D := (\partial\!\!\!/\otimes 1)\oplus(1\otimes D_F).$$

The D_F operator holds information about the Yukawa–Kobayashi–Maskawa couplings. The mimimal coupling recipe leads then to the usual fermionic action plus the mass terms. The noncommutative gauge potential $\mathbb{A}$ and field $\mathbb{F}$, on the boson side, are selfadjoint elements respectively of:

$$\begin{aligned}\Omega^1_D\mathcal{A} &\simeq \Lambda^1(M,\mathbb{C})\oplus\Lambda^0(M,\mathbb{H})\oplus\Lambda^0(M,\mathbb{H})\oplus\Lambda^1(M,\mathbb{H})\oplus M_3(\Lambda^1(M,\mathbb{C}))\\ \Omega^2_D\mathcal{A} &\simeq \Lambda^2(M,\mathbb{C})\oplus\Lambda^0(M,\mathbb{H})\oplus\Lambda^0(M,\mathbb{H})\oplus\Lambda^1(M,\mathbb{H})\\ &\quad\oplus\Lambda^1(M,\mathbb{H})\oplus\Lambda^2(M,\mathbb{H})\oplus M_3(\Lambda^2(M,\mathbb{C})),\end{aligned}$$

from which the Yang–Mills Action and thus the (classical) Lagrangian are obtained by a noncommutative procedure strictly parallel to the usual one. To avoid a $U(3)\times SU(2)\times U(1)$ theory, however, an ingredient is missing. Following Connes we impose the "unimodularity condition"

$$\mathrm{Str}(\mathbb{A} + J\mathbb{A}J) = 0,$$

where the supertrace is taken with respect to particle-antiparticle splitting; here J is the conjugation operator that interchanges particles and antiparticles. One gets the reduction to the SM gauge group and the correct hypercharges; this happens now irrespectively of whether neutrinos are massive or not. We have recently shown that the unimodularity condition is strictly equivalent, within the NCG framework, to anomaly cancellation: a first exciting hint at a deeper relationship between quantum physics and NCG than was known before.

Recapitulation

The picture that emerges is that of a "doubling" of the space stemming from chirality, with gauge bosons corresponding to the displacements in continuous directions and the Higgs boson corresponding to the exchange of quanta in the discrete direction

There are 18 free parameters in the SM (leaving aside the vacuum angle θ): the strong coupling constant α_3; the electroweak parameters α_2, $\sin^2\theta_W$, m_W; the Higgs mass; the nine (or twelve, if neutrinos are massive) fermion masses; and four Kobayashi–Maskawa parameters. One has as inputs the fermionic constants only; one can treat α_2 as an adjustable parameter. When all computations are done, one obtains the *constrained* classical SM Lagrangian:

$$\begin{aligned}\mathcal{L} &= -\tfrac{1}{4}AB_{\mu\nu}B^{\mu\nu} - \tfrac{1}{4}EF^a_{\mu\nu}F^{\mu\nu}_a - \tfrac{1}{4}CG^a_{\mu\nu}G^{\mu\nu}_a + SD_\mu\phi\,D^\mu\phi\\ &\quad -L(\|\phi_1\|^2+\|\phi_2\|^2)^2 + 2L(\|\phi_1\|^2+\|\phi_2\|^2),\end{aligned}$$

where B, F, G denote respectively the $U(1)$, $SU(2)$, $SU(3)$ gauge fields and the coefficients A, E, C, S, L are given in function of four *unknown* parameters $C_{\ell\jmath}$, $C_{\ell e}$, $C_{q\jmath}$, C_{qe}, which play the role of coupling constants in NCG.

The appearance of parameter restrictions is only natural, as all gauge fields now are part of a unique field. As only the ratios among those NCG parameters are important, there would remain only one "prediction", i.e., the Higgs particle mass. We can be a little more explicit if we take the values which are more natural in the NCG framework: $C_{\ell\jmath} = C_{\ell e}$, $C_{q\jmath} = C_{qe}$. Introduce the parameter $x := (C_{\ell\jmath} - C_{\ell\jmath})/(C_{\ell\jmath} + C_{q\jmath})$, with range $-1 \leq x \leq 1$. The most natural value is $x = 0.5$. When one identifies the previous constrained Lagrangian to the usual SM Lagrangian, it yields:

$$m_W = m_{\text{top}} \sqrt{\frac{3}{N_F} \frac{1-x}{4-2x}}.$$

Then $m_{\text{top}} \geq \sqrt{3} m_W$. Similarly, $g_3 = \frac{1}{2} g_2 \sqrt{(4-2x)/(1-x)}$.

For the Weinberg angle, in the massive neutrino case, one gets $\sin^2 \theta_W := (12-6x)/(32-8x)$. Then one obtains the constraint $\sin^2 \theta_W \leq 0.45$. Finally, for the mass of the Higgs:

$$m_H = m_{\text{top}} \sqrt{3 - \frac{3}{N_F} \frac{1-x}{2-x}} = m_{\text{top}} \sqrt{3 - \frac{6 m_W^2}{N_F m_{\text{top}}^2}};$$

from which we get the relatively tight constraint $\sqrt{7/3}\, m_{\text{top}} \leq m_H \leq \sqrt{3}\, m_{\text{top}}$.

Open problems

One can accommodate the experimental values of the strong coupling constant and the Weinberg angle by choosing $C_{\ell e} \gg C_{qe}$. Thus, NCG offers no real predictions for the ratio of the coupling constants to the Weinberg angle. Though $m_W \leq m_{\text{top}}/\sqrt{N_F}$ is a suggestive constraint —it gives at once the right ballpark— there is no true prediction for the mass of the top quark, either. Rather, the experimentally determined top mass helps to fix the more important parameter of the theory, namely x. Once the top mass is pinned down, the model seems to fix the value of the Higgs mass. For instance, if $m_{\text{top}} = 2.5\, m_W \simeq 200\,\text{GeV}$, we get $x = 0.53$, and then $m_H = 328.3$ GeV. Note that for $x \gtrsim 0.8$, we are outside the perturbative regime in Quantum Field Theory. If there were a compelling reason to adopt Connes' relations on-shell, the theory would stand or fall by the value of the Higgs mass.

On the other hand, unless and until someone comes out with a quantization procedure specific to NCG that does the trick, there seems to be no such compelling reason. It is only reasonable to apply the standard renormalization procedures of present-day QFT to Connes' version of the SM Lagrangian. The constraints are not preserved under the renormalization flow, i.e., they do not correspond to a hidden symmetry of the SM. The view that any constraints can be imposed only in a fully renormalization group invariant way is, nevertheless, theoretically untenable.

It is just conceivable that Nature has chosen for us a scale μ_0 at which to impose Connes' restrictions. If we choose $x = 0.5$, the present experimental values for the strong interaction coupling and Weinberg angle are regained on imposing Connes' relations at the energy scale $\mu_C \approx 5 \times 10^8$ GeV (in the massive case). This "intermediate unification scale" would mark the limit of validity of the present, phenomenological NCG model, essentially corresponding to an ordinary, but disconnected, manifold; at higher energy scales, the regime of truly noncommutative geometries would begin. On imposing the mass relations at μ_C, and running the renormalization equations at one loop, we get $m_{\text{top}} \simeq 215$ GeV (within the error bars of the D0 experiment) and $m_H \simeq 235$–240 GeV. The 1-loop approximation is not very accurate; inclusion of quantum corrections at 2nd order would give somewhat higher Higgs masses.

There is also a direct relation between NCG and gravitation: the noncommutative integral $\oint D^{-2}$ gives the Einstein–Hilbert action of general relativity. However, there seems to be at present no unambiguous unification strand, within NCG, of gravitation and the subatomic forces.

Some sources

The original groundbreaking paper was [1]. For the "old scheme" of NCG (as presented in the 1992–94 period), and the introduction of the "new scheme", see [2]. For the mathematics of NCG, see [2] and [3]. The parameter relations were derived in [4]. Renormalization of NCG models, and the rôle of anomalies in NCG schemes, have been explored in [5]. A noncommutative geometry model with massive neutrinos was proposed in [6]. Links between gravitation and NCG have been studied in [7]. For the philosophy of the whole thing, see [8].

References

[1] A. Connes and J. Lott, Nucl. Phys. B (Suppl.) 18 (1990) 29.

[2] A. Connes, *Noncommutative Geometry* (Academic Press, London, 1994); J. Math. Phys. **36**, 6194 (1995).

[3] J. C. Várilly and J. M. Gracia-Bondía, J. Geom. Phys. 12 (1993) 223.

[4] D. Kastler and T. Schücker, Theor. Math. Phys. 92 (1993) 1075; B. Iochu n, D. Kastler and T. Schücker, **hep-th/9507150**, CPT, Luminy, 1995.

[5] E. Alvarez, J. M. Gracia-Bondía and C. P. Martín, Phys. Lett. B306 (1993) 55; Phys. Lett. B329 (1994) 259; Phys. Lett. B364 (1995) 33.

[6] J. M. Gracia-Bondía, Phys. Lett. B351 (1995) 510.

[7] D. Kastler, Commun. Math. Phys. 166 (1995) 633;
M. Walze, "Nicht-kommutative Geometrie und Gravitation", thesis, Universität Mainz, 1996.

[8] J. M. Gracia-Bondía, in *A Gift of Prophecy, Essays in Celebration of the life of Robert Eugene Marshak*, ed. E. C. G. Sudarshan (World Scientific, Singapore, 1994) p. 208;
R. E. Marshak, *Conceptual Foundations of Modern Particle Physics* (World Scientific, Singapore, 1993);
G. Cammarata and R. Coquereaux, preprint **hep-th/9505192**, CPT, Luminy, 1995.

O Paradoxo de Perda de Informações no interior de um Buraco Negro

M. Schiffer*
Instituto de Matemática Estatística e Ciências da Computação
Universidade Estadual de Campinas
Cx. Postal 6065, SP 01183-090, Brazil

Received March, 1996

Nesse seminário apresentamos uma introdução ao paradoxo de perda de informação devida a buracos negros com a consequente quebra regra de evolução unitária da Mecânica Quântica, na qual estados originalmente puros são convertidos em estados mistos (Radiação de Hawking).

Baseando a discussão em argumentos envolvendo a mecânica quântica, teoria de informações e experimentos mentais, analisamos as varias sugestões para a resolução do paradoxo existentes no mercado. Mostramos a impossibilidade quântica de que a informação absorvida pelo buraco negro seja copiada nos estados finais. Tambem pudemos excluir um cenário envolvendo buracos negros remanescentes. Discutimos a opção radical em que a Mecânica Quântica é modificada na presença de campos gravitacionais para acomodar uma evolução não unitária e vimos que implicaria em sérios problemas como a não conservação de energia/momento.

Finalmente, concluimos que para a resolução do paradoxo faz-se necessário que efeitos quânticos da gravitação entrem em ação já no processo de formação do horizonte de eventos do buraco negro, mesmo que esse seja macroscópico.

Referências

[1] S. Hawking, *Phys. Rev.* **D14** (1976) 2460.
[2] G. 't Hooft, *Nucl. Phys.* **B335** (1990) 138.
[3] C.G. Callan, S.B. Giddings, J.A. Harvey, A. Strominger,*Phys. Rev.* **D-15** (1992) R1005.
[4] W. K. Wootters and W. H. Zurek, *Nature* **299** (1982) 802.
[5] S. Coleman, J. Preskill and F. Wilczek, *Nucl. Phys.* **B378** (1991) 175.
[6] J. Preskill, "Do Black Holes Destroy Information?", *Proceedings of the International Symposium on Black Holes, Membranes, Wormholes and Superstrings*, Texas, January 1992.
[7] T. Banks, A. Dabholkar, M. R. Douglas and M. O'Loughlin, *Phys. Rev.***D45** (1992) 3607.
[8] Danielsson, U. H. and Schiffer, M. *Phys. Rev.***D48** (1993) 4779.

*e.mail: schiffer@ime.unicamp.br

Field theoretic approach for systems of composite hadrons*

G. Krein
Instituto de Física Teórica, Universidade Estadual Paulista
Rua Pamplona, 145 - 01405-900 São Paulo-SP, Brazil

Received March, 1996

Effective chiral Lagrangians involving constituent quarks, Goldstone bosons and long-distance gluons are believed to be able to describe the strong interactions in an intermediate energy region between the confinement scale and the chiral symmetry breaking scale. Baryons and mesons in such a description are bound states of constituent quarks. In this talk we discuss the combined use of techniques of effective chiral field theory and of the field theoretic method known as Fock-Tani representation to derive effective hadron interactions. The Fock-Tani method is based on a change representation by means of a unitary transformation such that the composite hadrons are redescribed by elementary-particle field operators. Application of the unitary transformation on the microscopic quark-quark interaction derived from a chiral effective Lagrangian leads to chiral effective interactions describing all possible processes involving hadrons and their constituents. The formalism is illustrated by deriving the one-pion-exchange potential between two nucleons from the quark-gluon effective chiral Lagrangian of Manohar and Georgi at tree level.

1. Introduction.

The quark-gluon description of the interactions among hadrons and the properties of high temperature and/or density hadronic matter is one of the most central problems of contemporary nuclear physics. Such problems are characterized by processes that involve the simultaneous presence of hadrons and their constituents. The mathematical description of the processes requires approximations where a drastic reduction of the degrees of freedom is unavoidable. In this sense, one would expect simplifications by describing the hadrons participating in the processes in terms of macroscopic hadron field operators, instead of the microscopic constituent ones. At low energies the hadron-hadron interaction can be described by an effective chiral field theory in which the quarks and gluons are "integrated out" in favor of hadrons and Goldtone bosons [1, 2]. At higher energies it is very likely that the substructure of the hadrons will play a role and another effective field theory involving these degrees of freedom must be introduced.

There is a widespread belief that there exists an intermediate energy region in which it makes sense to describe the strong interactions in terms of an effective field theory of *constituent quarks* subject to weak color forces that become strong only at large separations and keep the quarks confined. The u and d constituent quarks have a mass of $m \sim 300$ MeV, which are believed to be the result of the spontaneous breakdown of the $SU(2) \otimes SU(2)$ chiral symmetry. If this is so, the Golstone bosons of the spontaneous symmetry breakdown (pions in the case of u and d quarks only) must be included among the degrees of freedom of the effective theory. The lowest order terms of the Lagrangian of such an effective field theory were written down by Manohar and Georgi [3]. Many of the successes of the simple nonrelativistic quark model can be understood in this framework with a chiral symmetry breaking scale $\Lambda_{\chi SB} \sim 1$ GeV, which is significantly larger than the confinement scale Λ_{conf}. This scenario of weakly interacting constituent quarks has recently been shown [4] to provide a nice interpretation of lattice calculations. Also it has been shown recently that the Manohar and Georgi model can be derived from QCD models of the Nambu–Jona-Lasinio type and QCD effective action calculations [5].

*Talk at the XVI Particles and Fields, 24-28 October 1995, Caxambu-MG, Brazil

The description of the hadron-hadron interaction in such a theory becomes complicated because hadrons are not the basic degrees of freedom of the theory; hadrons are composites and in general cannot be described by field operators of the sort used to describe elementary particles. In this talk we discuss a method we believe can be very useful for treating composite hadron interactions at the quark-gluon level. The method is known as Fock-Tani representation and was invented independently by Girardeau [3],[7] and Vorob'ev and Khomkin [8] to deal with atomic systems where atoms and electrons are simultaneously present in the system and the internal degrees of freedom of atoms cannot validly be neglected. The method is based on a change representation by introducing fictitious elementary hadrons in close correspondence to the real hadrons. The change of representation is implemented by means of a unitary transformation such that the composite hadrons are redescribed by elementary-particle field operators. In the new representation the microscopic interquark forces change, they become weaker, in the sense they cannot bind the quarks into hadrons, they describe only truly scattering processes. In the new representation, in addition to the modified interquark forces, one obtains effective interactions describing all possible processes between hadrons and their constituents. In the new representation all field operators representing quarks, antiquarks, gluons and *hadrons* satisfy canonical commutation relations and therefore the traditional methods of quantum field theory can be readily applied.

The use of the Fock-Tani representation for studying hadronic interactions at the quark-gluon level shares some similarities with the program outlined by Weinberg in the last section of his 1979 paper on effective Lagrangians [1]. Weinberg makes the suggestion of using the "quasiparticle" approach [10] for making perturbative calculations in QCD at low energies. The quasiparticle approach is a formalism developed by Weinberg in the 60's to deal with potentials that are too strong to allow the use of perturbation theory. In the quasiparticle approach the bound states of the theory are redescribed by fictitious elementary particles and, in order not to change the physics of the problem, the original potential is modified in such a way that the new potential does not produce the elementary particles as bound states of the theory. With such a modification the potential becomes sufficiently weak that scattering amplitudes can be calculated perturbatively. Weinberg imagines the possibility of implementing a quasi-particle approach to QCD. The program would start by weakening the forces of QCD with the introduction of an infrared cut-off. In order to preserve the physical content of the theory, the bound states (hadrons) are introduced as fictitious elementary particles which should be described by an effective chirally invariant Lagrangian. The parameters of the effective Lagrangian would have to be functions of the cut-off, defined by differential equations which guarantee the cut-off independence of the S-matrix, with the boundary condition that for higher enough energies one recovers pure QCD, where there is no cut-off. The program would work in practice if the solutions of the equations could be continued at low energies to cutoff values sufficiently small that perturbation theory could be employed.

The use of the Fock-Tani representation in connection with an effective quark-gluon Lagrangian involves a two-step process implementation of a similar program as Weinberg's one outlined above. In the first step the QCD forces are weakened by the introduction of an infrared cutoff Λ, which we choose to be $\Lambda_{\rm conf} < \Lambda < \Lambda_{\chi SB}$, and the QCD Lagrangian is replaced by an effective Lagragian, as for example the one of Manohar and Georgi. In the next step, fictitious elementary particles with the quantum numbers of hadrons are introduced and their effective interactions are derived from the microscopic effective quark-gluon Lagrangian through the Fock-Tani unitary transformation. The parameters of the resulting effective hadronic interactions are functions of those of the quark-gluon Lagrangian. The program will be completed, in the sense of Weinberg's program, when the cutoff independence of the S-matrix elements is enforced. Of course, this is the most difficult part of the entire program and not much progress can be made without a better understanding of the underlying mechanisms which govern the confinement and dynamical chiral symmetry breaking phenomena of QCD. While such an understanding is not reached, progress in the study of the hadronic interactions at the quark-gluon level can be made by fixing the parameters of the effective quark-gluon theory experimentally.

Recently the original Fock-Tani formalism was extended to hadronic physics for deriving effective meson and

baryon Hamiltonians in constituent quark models [9]. Here we discuss ts application in the context of the effective chiral field theory of Manohar and Georgy. In the next section we explain the formalism using a simple example. We consider mesons as bound states of a quark-antiquark pair and use a simple microscopic quak model. We derive the effective Hamiltonians describing the quark-antiquark, quark- and antiquark-meson, and meson-meson interactions. We discuss the properties of the effective Hamiltonians and make contact with the quasiparticle approach of Weinberg. In section 3 we consider baryons in the Georgi-Manohar model and derive an effective chiral Hamiltonian for baryons. One particularly important component present in the effective nucleon-nucleon interaction is the one-pion exchange interaction. In the last section we present conclusions and discuss future perspectives.

2. Fock-Tani representation: real and ideal particles.

In this section we use a simple example to explain the Fock-Tani formalism. In the next section we use the formalism to derive effective Hamiltonians in the chiral quark model. We start specifying the model microscopic Hamiltonian in Fock space ($\mathcal{F}$). We consider a Hamiltonian where quarks and antiquarks interact by two-body forces:

$$\begin{aligned} H &= T(\mu)\, q_\mu^\dagger q_\mu + T(\nu)\, \bar{q}_\nu^\dagger \bar{q}_\nu + \frac{1}{2} V_{qq}(\mu\nu;\tau\rho)\, q_\mu^\dagger q_\nu^\dagger q_\rho q_\sigma \\ &\quad + \frac{1}{2} V_{\bar{q}\bar{q}}(\mu\nu;\sigma\rho)\, \bar{q}_\mu^\dagger \bar{q}_\nu^\dagger \bar{q}_\rho \bar{q}_\sigma + V_{q\bar{q}}(\mu\nu;\sigma\rho)\, q_\mu^\dagger \bar{q}_\nu^\dagger \bar{q}_\rho q_\sigma \,, \end{aligned} \tag{1}$$

where a summation over repeated indices is implied, and the quark and antiquark creation and annihilation operators obey standard anticommutation relations:

$$\{\bar{q}_\mu, \bar{q}_\nu^\dagger\} = \{q_\mu, q_\nu^\dagger\} = \delta_{\mu\nu}, \qquad \{q_\mu, q_\nu\} = \{\bar{q}_\mu, \bar{q}_\nu\} = \{\bar{q}_\mu, q_\nu^\dagger\} = 0. \tag{2}$$

The indices $\mu, \nu, \cdots$ represent spatial, color, spin, and flavor quantum numbers of the quarks and antiquarks.

We consider mesons as bound states of a quark-antiquark pair. In Fock space $\mathcal{F}$ the state of a meson composed by a quark-antiquark pair, $|\alpha\rangle$, where α represents the meson quantum numbers (c.m. momentum, internal energy, spin and flavor), can be represented as:

$$|\alpha\rangle = M_\alpha^\dagger |0\rangle \equiv \Phi_\alpha^{\mu\nu} q_\mu^\dagger \bar{q}_\nu^\dagger |0\rangle, \tag{3}$$

where $|0\rangle$ is the vacuum state, defined as $q_\mu|0\rangle = \bar{q}_\nu|0\rangle = 0$, $M_\alpha^\dagger$ is the meson creation operator, and $\Phi_\alpha^{\mu\nu}$ is the meson wave function. The meson wave-functions Φ's are taken to be orthonormalized:

$$\Phi_\alpha^{*\mu\nu} \Phi_\beta^{\mu\nu} = \delta_{\alpha\beta}. \tag{4}$$

In free space, the equation of motion for the single meson state is given by:

$$H(\mu\nu;\mu'\nu')\, \Phi_\alpha^{\mu'\nu'} = \left\{ \delta_{\mu[\mu']} \delta_{\nu[\nu']} [T(\mu) + T(\nu)] + V_{q\bar{q}}(\mu\nu;\mu'\nu') \right\} \Phi_\alpha^{\mu'\nu'} = E_{[\alpha]} \Phi_{[\alpha]}^{\mu\nu}, \tag{5}$$

where E_α is the total energy of the meson. Here we are using the convention that there is no sum over repeated indices inside square brackets.

Using the quark anticommutation relations of Eq. (2), and the orthonormalization condition for the Φ's, Eq. (4), one can show that the meson operators satisfy the following *noncanonical* commutation relations:

$$[M_\alpha, M_\beta^\dagger] = \delta_{\alpha\beta} - \Delta_{\alpha\beta}, \qquad [M_\alpha, M_\beta] = 0, \tag{6}$$

where

$$\Delta_{\alpha\beta} = \Phi_\alpha^{*\mu\nu} \Phi_\beta^{\mu\sigma} \bar{q}_\sigma^\dagger \bar{q}_\nu + \Phi_\alpha^{*\mu\nu} \Phi_\beta^{\rho\nu} q_\rho^\dagger q_\mu \,. \tag{7}$$

In addition, one can easily show:

$$[\bar{q}_\nu, M_\alpha^\dagger] = -\delta_{\nu\nu'} \Phi_\alpha^{\mu\nu'} q_\mu^\dagger \,, \qquad [q_\mu, M_\alpha^\dagger] = \delta_{\mu\mu'} \Phi_\alpha^{\mu'\nu} \bar{q}_\nu^\dagger \,, \qquad [q_\mu, M_\alpha] = [\bar{q}_\nu, M_\alpha] = 0 \,. \tag{8}$$

One observes that the composite nature of the mesons is manifested by the term $\Delta_{\alpha\beta}$ in Eq. (6). Eq. (8) indicates that mesons and quarks are not independent degrees of freedom. The presence of these terms complicates the direct application of field theoretic techniques such as Wick's theorem and Feynman graphs for the $M_\alpha^\dagger$ and M_α operators, since these techniques are set up for canonical field operators.

The change to the FT representation is implemented by means of a unitary transformation U, such that a *single* composite meson state $|\alpha) = M_\alpha^\dagger|0)$ is transformed into a *single* ideal-meson state $|\alpha) = m_\alpha^\dagger|0) \equiv U^{-1}|\alpha)$, where U is of the general form:

$$U = \exp(-\pi/2F), \qquad F = \sum_\alpha \left(m_\alpha^\dagger O_\alpha - O_\alpha^\dagger m_\alpha\right). \tag{9}$$

The $m_\alpha^\dagger$ and m_α are the ideal-meson creation and annihilation operators and the $O_\alpha^\dagger$ and O_α operators are functionals of the $M_\alpha^\dagger$, M_α and $\Delta_{\alpha\beta}$. By definition, the m's and O's satisfy canonical commutation relations:

$$[m_\alpha, m_\beta^\dagger] = [O_\alpha, O_\beta^\dagger] = \delta_{\alpha\beta}, \qquad [m_\alpha, m_\beta] = [m_\alpha^\dagger, m_\beta^\dagger] = [O_\alpha, O_\beta] = [O_\alpha^\dagger, O_\beta^\dagger] = 0, \tag{10}$$

and, by definition, the $m^\dagger$ and m commute with the quark and antiquark operators.

The operator U acts on an enlarged Fock space $\mathcal{I}$, which is the graded direct product of $\mathcal{F}$ and an *ideal* state space $\mathcal{M}$, the space with the new degrees of freedom described by the ideal meson operators $m_\alpha^\dagger$ and m_α. The vacuum state of $\mathcal{M}$ is denoted by $|0)_\mathcal{M}$ and so, the vacuum state of $\mathcal{I}$ is

$$|0) = |0) \times |0)_\mathcal{M}. \tag{11}$$

In $\mathcal{I}$ the physical states, $|\psi)$, constitute a subspace $\mathcal{I}_0$ isomorphic to $\mathcal{F}$ and satisfy the constraint equation:

$$m_\alpha|\psi) = 0. \tag{12}$$

Now, the new degrees of freedom acquire physical content when the unitary operator U transforms the physical states $|\psi)$ of $\mathcal{I}_0$ to states $|\psi) = U^{-1}|\psi)$. The image states $|\psi)$ span the FT space $\mathcal{F}_{FT} = U^{-1}\mathcal{I}_0$, and satisfy the transformed constraint equation:

$$U^{-1}m_\alpha U|\psi) = O_\alpha|\psi) = 0. \tag{13}$$

Although the physical content of the Fock spaces $\mathcal{F}$ and $\mathcal{F}_{FT}$ is the same, the mathematical representation of states and operators in $\mathcal{F}_{FT}$ involves only canonical field operators. A more detailed discussion of these and other formal aspects of the mapping procedure can be found in the original publications [7], [11].

The operators $O_\alpha^\dagger$ and O_α are constructed by an iterative procedure as a power series in the Φ's:

$$O_\alpha = \sum_n O_\alpha^{(n)}, \tag{14}$$

where n identifies the power of Φ in the expansion. The expansion starts at zeroth order with:

$$O_\alpha^{(0)} = M_\alpha. \tag{15}$$

The construction of the higher order terms $O_\alpha^{(n)}$, $n \geq 1$, involves addition of a series of counterterms such that commutation relations of $O^\dagger$ and O are satisfied order by order. Since at zeroth order one has:

$$[O_\alpha^{(0)}, O_\beta^{(0)\dagger}] = \delta_{\alpha\beta} - \Delta_{\alpha\beta}, \tag{16}$$

and $\Delta_{\alpha\beta}$ is of second order [see Eq. (7)], one has that

$$O_\alpha^{(1)} = 0. \tag{17}$$

The next nonzero term is then of order $n = 2$. It is not difficult to show that the second order counterterm that has to be added to $O_\alpha^{(0)}$ to cancel the $\Delta_{\alpha\beta}$ in $[O_\alpha^{(0)}, O_\beta^{(0)\dagger}]$ is equal to:

$$\frac{1}{2}\Delta_{\alpha\beta}M_\beta. \tag{18}$$

Then, up to $n = 2$,

$$O_\alpha = B_\alpha + \frac{1}{2}\Delta_{\alpha\beta}B_\beta, \tag{19}$$

and one obtains

$$\begin{aligned}[O_\alpha, O_\beta^\dagger] &= \delta_{\alpha\beta} - \frac{1}{2}[\Delta_{\alpha\gamma}, M_\beta]M_\gamma - \frac{1}{2}M^\dagger[M_\alpha, \Delta_{\gamma\beta}] \\ &= \delta_{\alpha\beta} + \mathcal{O}(\Phi^3).\end{aligned} \tag{20}$$

A third order counterterm has to be added such that the $\mathcal{O}(\Phi^3)$ piece cancels, and so on to higher orders. However, for our purposes here one needs O_α up to $n = 3$ only:

$$O_\alpha = M_\alpha + \frac{1}{2}\Delta_{\alpha\beta}M_\beta - \frac{1}{2}M_\beta^\dagger[\Delta_{\beta\gamma}, M_\gamma]M_\gamma\,. \tag{21}$$

The transformation of the Hamiltonian is made by transforming initially the quark and antiquark operators. Since the O operators are given by a power series, the transformed quark operators are also obtained as a power series, which can be obtained by expanding the exponential in Eq. (9) to the desired order or, equivalently, by means of the "equation of motion" technique [7]. Up to third order, one obtains:

$$\begin{aligned}
q_\mu^{(0)} &= q_\mu, \quad \bar{q}_\nu^{(0)} = \bar{q}_\nu, \quad q_\mu^{(1)} = \Phi_\alpha^{\mu\nu_1}\bar{q}_{\nu_1}^\dagger\,(m_\alpha - M_\alpha), \quad \bar{q}_\nu^{(1)} = \Phi_\alpha^{\mu_1\nu}q_{\mu_1}^\dagger\,(M_\alpha - m_\alpha), \\
q_\mu^{(2)} &= -\frac{1}{2}\Phi_\alpha^{*\mu_2\nu_1}\Phi_\beta^{\mu\nu_1}\left(m_\alpha^\dagger m_\beta + M_\alpha^\dagger M_\beta + 2M_\alpha^\dagger m_\beta\right)q_{\mu_2}, \\
\bar{q}_\nu^{(2)} &= -\frac{1}{2}\Phi_\alpha^{*\mu_1\nu_2}\Phi_\beta^{\mu_1\nu}\left(m_\alpha^\dagger m_\beta + M_\alpha^\dagger M_\beta + 2M_\alpha^\dagger m_\beta\right)\bar{q}_{\nu_2}, \\
q_\mu^{(3)} &= \frac{1}{2}\Phi_\alpha^{*\rho\sigma}\Big[\Phi_\beta^{\mu\sigma}\Phi_\gamma^{\rho\sigma_1}\bar{q}_{\sigma_1}^\dagger\left(-m_\alpha^\dagger m_\beta m_\gamma - M_\alpha^\dagger m_\beta M_\gamma + m_\alpha^\dagger m_\beta M_\gamma + M_\alpha^\dagger M_\beta M_\gamma\right) \\
&\quad + \Phi_\alpha^{\mu\nu_1}\left(\Phi_\beta^{\rho\sigma_1}\bar{q}_{\nu_1}^\dagger\bar{q}_{\sigma_1}^\dagger\bar{q}_\sigma + \Phi_\beta^{\rho_1\sigma}\bar{q}_{\nu_1}^\dagger q_{\rho_1}^\dagger q_\rho\right)(m_\beta - 2M_\beta)\Big] \\
\bar{q}_\nu^{(3)} &= -\frac{1}{2}\Phi_\alpha^{*\rho\sigma}\Big[\Phi_\beta^{\rho\nu}\Phi_\gamma^{\rho_1\sigma}q_{\rho_1}^\dagger\left(-m_\alpha^\dagger m_\beta m_\gamma - M_\alpha^\dagger m_\beta M_\gamma + m_\alpha^\dagger m_\beta M_\gamma + M_\alpha^\dagger M_\beta M_\gamma\right) \\
&\quad + \Phi_\alpha^{\mu_1\nu}\left(\Phi_\beta^{\rho\sigma_1}q_{\mu_1}^\dagger\bar{q}_{\sigma_1}^\dagger\bar{q}_\sigma + \Phi_\alpha^{\mu_1\nu}\Phi_\beta^{\rho_1\sigma}q_{\mu_1}^\dagger q_{\rho_1}^\dagger q_\rho\right)(m_\beta - 2M_\beta)\Big].
\end{aligned} \tag{22}$$

The transformation of the microscopic Hamiltonian is obtained by using the transformed quark operators of Eq. (22) in Eq. (2). This is done [7] by considering all possible combinations of the form $T(\mu)q_\mu^{(n)\dagger}q_\mu^{(m)}$, $V_{q\bar{q}}(\mu\nu;\sigma\rho)q_\mu^{(n)\dagger}q_\nu^{(m)\dagger}q_\rho^{(k)}q_\sigma^{(l)}$, etc. where $n, m, k, l = 1, 2, 3$. One obtains that the general structure of the transformed Hamiltonian is:

$$H_{\rm FT} = H_q + H_m + H_{mq}\,, \tag{23}$$

where the subindices identify the operator content of each term. The quark Hamiltonian H_q has an identical structure to the one of the microscopic quark Hamiltonian of Eq. (2), except that the term corresponding to the quark-antiquark interaction is modified to:

$$\begin{aligned}V_{q\bar{q}}(\mu\nu;\sigma\rho) \to \quad &[V_{q\bar{q}}(\mu\nu;\sigma\rho) - \Delta(\mu\nu;\mu'\nu')H(\mu'\nu';\sigma\rho) - H(\mu\nu;\sigma'\rho')\Delta\,(\sigma'\rho';\sigma\rho) \\ &+ \Delta(\mu\nu;\mu'\nu')H(\mu'\nu';\sigma'\rho')\Delta(\sigma'\rho';\sigma\rho)]\;q_\mu^\dagger\bar{q}_\nu^\dagger\bar{q}_\rho q_\sigma,\end{aligned} \tag{24}$$

where $\Delta\,(\mu\nu;\mu'\nu') = \Phi_\alpha^{\mu\nu}\Phi_\alpha^{*\mu'\nu'}$ is the "bound state kernel". When Φ is an eigenstate of the microscopic Hamiltonian, Eq. (5), the quark-antiquark interaction is then modified to:

$$V_{q\bar{q}}(\mu\nu;\sigma\rho) \to [V_{q\bar{q}}(\mu\nu;\sigma\rho) - E_\alpha\Phi_\alpha^{\mu\nu}\Phi_\alpha^{*\sigma\rho}]\;q_\mu^\dagger\bar{q}_\nu^\dagger\bar{q}_\rho q_\sigma, \tag{25}$$

It is not difficult to show (see Appendix C of Ref. [7]) that this modified interaction does not produce the quark-antiquark bound states. This feature leads to the same effect of curing the bound state divergences of the Born series as in Weinberg's quasi-particle method [10] discussed in the Introduction: the modified quark-antiquark interaction is unable to form mesons, the mesons are redescribed by the H_m part of the effective Hamiltonian.

H_{mq} describes quark-meson processes as meson breakup into a quark-antiquark pair, meson-quark scattering, meson-meson total break up into two quark-antiquark pairs, etc. In models where quarks are truly confined, these terms contribute to free-space meson-meson processes as intermediate states only. However, in high temperature and/or density systems hadrons and quarks can coexist and the breakup and recombination processes can play important role.

The term involving only ideal meson operators has a component that represents an effective meson-meson interaction. This meson-meson interaction is of the general form:

$$H_m = E_\alpha m_\alpha^\dagger m_\alpha + \frac{1}{2} V_{mm}(\alpha\beta;\gamma\delta)\, m_\alpha^\dagger m_\beta^\dagger m_\delta m_\gamma \,, \tag{26}$$

where the effective meson-meson potential V_{mm} can be divided into a sum of *direct*, *exchange*, and *intra-exchange* parts:

$$V_{mm} = V_{mm}^{int} + V_{mm}^{dir} + V_{mm}^{ex}, \tag{27}$$

where:

$$\begin{aligned} V_{mm}^{dir}(\alpha\beta;\gamma\delta) &= 2\Phi_\alpha^{*\mu\sigma}\Phi_\beta^{*\rho\nu} V_{q\bar{q}}(\mu\nu;\mu'\nu')\Phi_\delta^{\rho\nu'}\Phi_\gamma^{\mu'\sigma} + \Phi_\alpha^{*\mu\sigma}\Phi_\beta^{*\rho\nu} V_{qq}(\mu\rho;\mu'\rho')\Phi_\delta^{\rho'\nu}\Phi_\gamma^{\mu'\sigma} \\ &\quad + \Phi_\alpha^{*\mu\sigma}\Phi_\beta^{*\rho\nu} V_{\bar{q}\bar{q}}(\sigma\nu;\sigma'\nu')\Phi_\delta^{\rho\nu'}\Phi_\gamma^{\mu\sigma'}, \end{aligned} \tag{28}$$

$$\begin{aligned} V_{mm}^{exc}(\alpha\beta;\gamma\delta) &= -\frac{1}{2}\Big[\Phi_\alpha^{*\mu\nu}\Phi_\beta^{*\rho\sigma} V_{q\bar{q}}(\mu\nu;\mu'\nu')\Phi_\delta^{\mu'\sigma}\Phi_\gamma^{\rho\nu'} + \Phi_\alpha^{*\rho\sigma}\Phi_\beta^{*\mu\nu} V_{q\bar{q}}(\mu\nu;\mu'\nu')\Phi_\delta^{\rho\nu'}\Phi_\gamma^{\mu'\sigma} \\ &\quad + \Phi_\alpha^{*\mu\sigma}\Phi_\beta^{*\rho\nu} V_{q\bar{q}}(\mu\nu;\mu'\nu')\Phi_\delta^{\mu'\nu'}\Phi_\gamma^{\rho\sigma} + \Phi_\alpha^{*\rho\nu}\Phi_\beta^{*\mu\sigma} V_{q\bar{q}}(\mu\nu;\mu'\nu')\Phi_\delta^{\rho\sigma}\Phi_\gamma^{\mu'\nu'} \\ &\quad + 2\Phi_\alpha^{*\mu\sigma}\Phi_\beta^{*\rho\nu} V_{qq}(\mu\rho;\mu'\rho')\Phi_\delta^{\mu'\nu}\Phi_\gamma^{\rho'\sigma} + 2\Phi_\alpha^{*\mu\sigma}\Phi_\beta^{*\rho\nu} V_{\bar{q}\bar{q}}(\sigma\nu;\sigma'\nu')\Phi_\delta^{\mu\nu'}\Phi_\gamma^{\rho\sigma'}\Big], \end{aligned} \tag{29}$$

$$\begin{aligned} V_{mm}^{int}(\alpha\beta;\gamma\delta) &= -\frac{1}{2}\Big[\Phi_\alpha^{*\mu\nu}\Phi_\beta^{*\rho\sigma} H(\mu\nu;\mu'\nu')\Phi_\delta^{\mu'\sigma}\Phi_\gamma^{\rho\nu'} + \Phi_\alpha^{*\rho\sigma}\Phi_\beta^{*\mu\nu} H(\mu\nu;\mu'\nu')\Phi_\delta^{\rho\nu'}\Phi_\gamma^{\mu'\sigma} \\ &\quad + \Phi_\alpha^{*\mu\sigma}\Phi_\beta^{*\rho\nu} H(\mu\nu;\mu'\nu')\Phi_\delta^{\mu'\nu'}\Phi_\gamma^{\rho\sigma} + \Phi_\alpha^{*\rho\nu}\Phi_\beta^{*\mu\sigma} H(\mu\nu;\mu'\nu')\Phi_\delta^{\rho\sigma}\Phi_\gamma^{\mu'\nu'}\Big]. \end{aligned} \tag{30}$$

The higher order terms in Φ which are neglected in the above expressions give rise to many-meson (higher than two-meson) forces, and also introduce orthogonality corrections. The orthogonality corrections have the effect, among others, of weakening the "intra-exchange" interactions [11], and appear in powers of the bound state kernel $\Delta(\mu\nu;\sigma\rho)$. To lowest order in Δ, the orthogonality corrections exactly cancel V_{mm}^{int} of Eq. (30). The cancellation of the intra-exchange terms to lowest order is the dominant effect of the orthogonalization terms and higher order corrections are small.

3. Effective chiral Hamiltonian for baryons.

Now we discuss the application of the FT formalism to the effective QCD field theory of Manohar and Georgi. The lowest order Lagrangian density is given by:

$$\mathcal{L} = \bar{\psi}\left(i\not{\partial} + \not{V} - m_q + g_A \not{A}\gamma_5\right)\psi + \frac{1}{4} f_\pi^2 \mathrm{tr}\partial^\mu \Sigma^\dagger \partial_\mu \Sigma - \frac{1}{2}\mathrm{tr} G_{\mu\nu} G^{\mu\nu} \tag{31}$$

where the $SU(3)_{\text{flavor}}$ vector V_μ and axial-vector A_μ fields are given by

$$V_\mu = \frac{1}{2}\left(\xi^\dagger \partial_\mu \xi + \xi \partial_\mu \xi^\dagger\right), \tag{32}$$

$$A_\mu = \frac{1}{2} i \left(\xi^\dagger \partial_\mu \xi - \xi \partial_\mu \xi^\dagger\right), \tag{33}$$

where ξ is given in terms of the Goldstone boson fields as

$$\xi = e^{i\pi/f}, \tag{34}$$

and

$$\pi = \frac{1}{\sqrt{2}} \begin{bmatrix} \frac{1}{\sqrt{2}}\pi^0 + \frac{1}{\sqrt{6}}\eta & \pi^+ & K^+ \\ \pi^- & -\frac{1}{\sqrt{2}}\pi^0 + \frac{1}{\sqrt{6}}\eta & K^0 \\ K^- & \overline{K}^0 & -\frac{2}{\sqrt{6}}\eta \end{bmatrix}. \tag{35}$$

The Σ field is simply

$$\Sigma = e^{2i\pi/f} \equiv \xi\xi. \tag{36}$$

D is the covariant derivative involving the gluon field G_μ,

$$D_\mu = \partial_\mu + igG_\mu, \tag{37}$$

$G_{\mu\nu}$ is the gluon field-strength tensor

$$G_{\mu\nu} = \partial_\mu G_\nu - \partial_\nu G_\mu + ig[G_\mu, G_\nu], \tag{38}$$

with the gluon field normalized as

$$\mathrm{tr}\, T^a T^b = \frac{1}{2}\delta^{ab}, \tag{39}$$

where $T^a, a = 1, \cdots, 8$ are the $SU(3)_{\mathrm{color}}$ generators. The four-quark Lagrangian is:

$$\mathcal{L}_{4-q} = \frac{C_\alpha}{2f^2}(\overline{\psi}\Gamma_\alpha\psi)(\overline{\psi}\Gamma^\alpha\psi). \tag{40}$$

where Γ_α stands for $1, \gamma_5, \gamma_\mu, \gamma_\mu\gamma_5$ and $\sigma_{\mu\nu}$. m_q is the constituent quark mass matrix and f is the Goldstone boson decay constant ($f_\pi = 93$ MeV).

As discussed in the Introduction, since the effects of dynamical chiral symmetry breaking are included in the constituent quark mass the interquark forces become weaker in the effective theory. This allows to identify the low-lying hadrons with nonrelativistic bound states of the constituent quarks. The quarks are presumably bound by the confining QCD interactions, along with effects of multiquark and multigluon operators that appear in high orders of $1/\Lambda_{\mathrm{conf}}$ in the effective Lagrangian.

Calculations of matrix elements of strong and electroweak couplings of quarks are performed using perturbation theory or large N_c expansion techniques, where N_c is the number of colors. For the calculation of matrix elements involving hadrons, such as the calculation of baryon magnetic moments and the G_A/G_V ratio in β-decay, the usual nonrelativistic quak-model wave functions are used for the hadron bound states. The nonrelativistic wave functions are obtained by solving the Schrödinger equation for three quarks (baryons) or a quark-antiquark pair (mesons) using a phenomenological confining interaction.

The combined use of an effective chiral field theory of the type of Manohar and Georgi and the Fock-Tani representation for the study of hadronic interactions seems interesting and would proceed as follows. From the Lagrangian of the effective quark-gluon theory one derives an effective quark-quark interaction by means of the techniques of effective field theory up to a certain order in the chiral expansion . Given the quark-quark interaction one solves a Schrödinger-like equation for the bound-state hadrons. This would proceed in a similar way as the calculation of the deuteron properties from a nucleon-nucleon interaction derived from a nucleon-pion chiral Lagrangian [2]. Once one has the microscopic quark-quark potential and the hadron bound-states, one implements the Fock-Tani transformation to obtain effective hadron-hadron interactions. The lowest order Lagrangian density of Eq. (31) would be appropriate for low enough scattering energies, and higher dimensional terms are introduced as higher scattering energies are considered. Of course, there remains the problem of the confining forces which are

difficult to access in such an approach. Perhaps the simplest assumption one can make is to invoke previous studies of the hadron-hadron interaction in nonrelativistic constituent quark models. The great majority of such studies have been performed using the Resonating Group Method (RGM) [12]. The microscopic quark-quark interaction is composed of one-gluon-exchange between the constituent quarks and a phenomenological two-body confining interaction of the form

$$V_{conf} = \sum_{i>j} T_i^a T_j^a V(\mathbf{r}_i - \mathbf{r}_j), \tag{41}$$

where $V(\mathbf{r}_i - \mathbf{r}_j)$ is a linear ou harmonic confining potential. More recently, π and σ (chiral partner of the π) exchange between quarks have been considered [13]. Perhaps one of the most interesting results of these studies is that the confining interaction of the form of Eq. (41) contributes very little to the hadron-hadron interaction; in particular a harmonic confining interaction gives no contribution to the scattering.

From this it seems that at the moment the simplest assumption one can make is to invoke previous RGM results and postulate that confining forces are not relevant for the hadron-hadron scattering. The situation can possibly be improved if the effects of the gluon degrees of freedom for the quark-quark interaction are treated in a lattice gauge theory formulation similarly to the nonrelativistic QCD (NRQCD) technique for the heavy quarks [14].

Let us consider just the pion-quark interaction piece of the Lagrangian of Eq. (31). The corresponding pion-quark Hamiltonian at tree level is the standard pseudovector coupling:

$$\mathcal{H}_{\pi q} = \frac{1}{f_\pi} g_A \bar{\psi} \gamma_5 t^a \alpha \cdot \nabla \pi^a \psi, \tag{42}$$

where $t^a = 1/2\,\tau^a$. This leads to an effective nonrelativistic quark-quark interaction of the form

$$V_{\pi q} = -\left(\frac{g_A}{f_\pi}\right)^2 t^{a(1)} t^{a(2)} \frac{\boldsymbol{\sigma}^{(1)} \cdot \mathbf{q}\, \boldsymbol{\sigma}^{(2)} \cdot \mathbf{q}}{\mathbf{q}^2 + m_\pi^2}. \tag{43}$$

The three-quark baryon states are of the form:

$$B_\alpha^\dagger = \frac{1}{\sqrt{3!}} \Phi_\alpha^{\mu_1 \mu_2 \mu_3} q_{\mu_1}^\dagger q_{\mu_2}^\dagger q_{\mu_3}^\dagger, \tag{44}$$

where Φ is the baryon wave function. Given this and the quark-quark interaction, one obtains through the lowest-order Fock-Tani transformation the following effective baryon Hamiltonian [9]:

$$H_b = \Phi_\alpha^{*\mu\nu\lambda} H(\mu\nu;\sigma\rho) \Phi_\beta^{\sigma\rho\lambda} b_\alpha^\dagger b_\beta + \frac{1}{2} V_{bb}(\alpha\beta;\gamma\delta)\, b_\alpha^\dagger b_\beta^\dagger b_\delta b_\gamma, \tag{45}$$

where V_{bb} is the effective two-baryon interaction, which we write as a sum of a direct and quark-exchange parts:

$$V_{bb} = V_{bb}^{dir} + V_{bb}^{exc}. \tag{46}$$

The direct term V_{bb}^{dir}, represented in Figure 1 below, is given by:

$$V_{bb}^{dir}(\alpha\beta;\delta\gamma) = 9\, V_{qq}(\mu\nu;\sigma\rho) \Phi_\alpha^{*\mu\mu_2\mu_3} \Phi_\beta^{*\nu\nu_2\nu_3} \Phi_\gamma^{\rho\nu_2\nu_3} \Phi_\delta^{\sigma\mu_2\mu_3}. \tag{47}$$

When the baryons are nucleons and the microscopic quark-quark interaction is the one of Eq. (43), the explicit form of this term is the familiar one-pion-exchange potential in momentum space:

$$V_{NN}^{dir}(q) = -9\,\frac{25}{81}\left(\frac{g_A}{f_\pi}\right)^2 \tau_N^{a(2)} \tau_N^{a(1)} F(q^2) \frac{\boldsymbol{\sigma}_N^{(1)} \cdot \mathbf{q}\, \boldsymbol{\sigma}_N^{(2)} \cdot \mathbf{q}}{\mathbf{q}^2 + m_\pi^2} F(q^2), \tag{48}$$

where the $\tau_N^a, a = 1, \cdots, 3$ and $\boldsymbol{\sigma}_N$ are respectively the nucleon isospin and spin Pauli matrices, and $F(q^2)$ is the nucleon (matter) form factor.

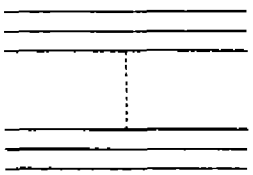

Figure 1. Graph of V_{bb}^{dir}.

The exchange term V_{bb}^{exch} involves simultaneous exchange of pions between two quarks and the exchange of quarks between the baryons. The different contributions to V_{bb}^{exch} are represented in Figure 2. below and are given by:

$$V_{bb}(\alpha\beta;\delta\gamma) = 9\, V_{qq}(\mu\nu;\sigma\rho)\left[\Phi_\alpha^{*\mu\mu_2\mu_3}\Phi_\beta^{*\nu\nu_2\nu_3}\left(-\Phi_\gamma^{\sigma\nu_2\nu_3}\Phi_\delta^{\rho\mu_2\mu_3} - 4\Phi_\gamma^{\rho\nu_2\mu_3}\Phi_\delta^{\sigma\mu_2\nu_3}\right)\right.$$
$$\left. + 2\Phi_\alpha^{*\mu\nu\mu_3}\Phi_\beta^{*\nu_1\nu_2\nu_3}\Phi_\gamma^{\rho\nu_2\nu_3}\Phi_\delta^{\nu_1\sigma\mu_3} - 2\Phi_\alpha^{*\mu\mu_2\mu_3}\Phi_\beta^{*\nu_1\nu_2\nu}\Phi_\gamma^{\nu_1\nu_2\mu_3}\Phi_\delta^{\sigma\mu_3\rho}\right]. \qquad (49)$$

Because these terms involve quark exchange between the baryons, they are of shorter range than the one of V_{bb}^{exch}.

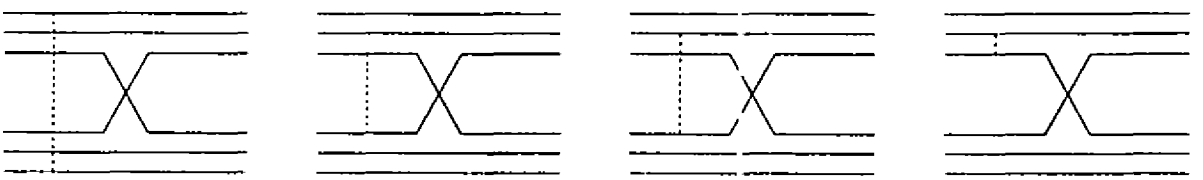

Figure 2. Graph of the terms in V_{bb}^{exch}.

The multidimensional integral over the quark coordinates in V_{bb}^{exch} cannot in general be done explicitly. However, when the baryon wave functions are of a gaussian form, V_{bb}^{exch} can be expressed in terms of a single integral. For illustration we present the final expression of the first term in Eq. (49) [First graph of Figure 2.] for quarks in the s-state of nucleons:

$$V_{1^{st}\,term}^{exch}(\mathbf{p},\mathbf{p}') = \mathcal{O}^{ij}(\sigma,\tau)\left(\frac{g_A}{f_\pi}\right)^2\left(\frac{3b^2}{4\pi}\right)^{3/2} e^{-b^2[5(\mathbf{p}^2+\mathbf{p}'^2)/12-\mathbf{p}\cdot\mathbf{p}'/2]}$$
$$\times \int d^3q\, \frac{q^i q^j}{\mathbf{q}^2+m_\pi^2}\, e^{-b^2[\mathbf{q}^2-\mathbf{q}\cdot(\mathbf{p}'-\mathbf{p})]}, \qquad (50)$$

where $\mathcal{O}^{ij}(\sigma,\tau)$ is given by:

$$\mathcal{O}^{ij}(\sigma,\tau) = \frac{1}{9}\left\{\left[25 + \frac{1}{3}\tau_N^{a(2)}\tau_N^{a(1)}\left(1 + 18\sigma_N^{(1)}\cdot\sigma_N^{(2)}\right)\right]\delta^{ij} + \left(1 + 19\tau_N^{a(2)}\tau_N^{a(1)}\right)\sigma_N^{i(1)}\sigma_N^{j(2)}\right\} \qquad (51)$$

The other terms in Eq. (49) can be expressed in a similar form as Eq. (50).

Work is in progress where the the four-point interactions and the one gluon-exchange at the tree level are summed to the tree-level pion exchange just discussed. The aim is to calculate phase-shifts of the nucleon-nucleon scattering and compare with the traditional one-boson exchange models [15].

4. Conclusions and future perspectives

The combined use of the techniques of effective chiral field theory and the Fock-Tani representation seems to provide great opportunities to study the role of quarks and gluons in hadronic interactions. The fact that in the Fock-Tani representation all operators satisfy canonical (anti)commutation relations allows the direct use of the known field theoretic techniques such as Feynman diagrams and Green's functions which have proven to be very useful in the study of processes involving elementary particles. Particularly interesting applications of these techniques are the study of short-range hadron-hadron interactions and the problem of hadron properties in a hot and/or dense medium.

References

[1] S. Weinberg, Physica **96A**, 341 (1979).

[2] S. Weinberg, Phys. Lett. B **251**, 288 (1990); Nucl. Phys. B **363**, 3 (1991).

[3] A. Manohar and H. Georgi, Nucl. Phys. B **234**, 189 (1984).

[4] A. Gocksch, Phys. Rev. Lett. **67**, 1701 (1991).

[5] J. Bijnens, Ch. Bruno and E. de Rafael, Nucl. Phys. B **390**, 501 (1993); D. Espriu, E. de Rafael and J. Taron, Nucl. Phys. B **345**, 22 (1990); **355**, 278 (E).

[6] M.D. Girardeau, Phys. Rev. Lett. **27**, 1416 (1971).

[7] M.D. Girardeau, J. Math. Phys. **16**, 1901 (1975).

[8] V.S. Vorob'ev and A.L. Khomkin, Teor. i Mat. Fiz. **8**, 109 (1971) (in Russian). English translation: Consultants Bureau, Plenum Publ. Co., New York, 1972.

[9] D. Hadjimichef, G. Krein, S. Szpigel and J.S. da Veiga, Phys. Lett. B **367**, 317 (1996); S. Szpigel, G. Krein, D. Hadjimichef, J.S. da Veiga, submitted to publication.

[10] S. Weinberg, Phys. Rev. **130**, 776 (1963); **131**, 440 (1963); **133**, B232 (1964).

[11] J.C. Straton and M.D. Girardeau, Phys. Rev. A **40**, 2991 (1989).

[12] For a review see: K. Shimizu, Rep. Prog. Phys. **52**, 1 (1989).

[13] A. Valcarce, A. Buchmann, F. Fernandez, and A. Faßler, Phys. Rev. C **51**, 1480 (1995).

[14] For a recent discussion on NRQCD see: G.P. Lepage, AIP Conference Proceedings **334**, 210 (1995).

[15] R. Machleidt, K. Holinde and Ch. Elster, Phys. Rep. **149**, 1 (1987).

Intrinsic and Leading Charm in Hadronic Collisions

F. S. Navarra[‡] , F. O. Durães[†] and M. Nielsen[§]
Instituto de Física, Universidade de São Paulo
C.P. 66318, 5389-970 São Paulo, SP, Brazil

Received March, 1996

We discuss leading charm production and the intrinsic charm model. Using a $\overline{D}$ meson cloud model we calculate the squared charm radius of the nucleon . The ratio between this squared radius and the ordinary baryon squared radius is identified with the probability of "seeing" the intrinsic charm component of the nucleon. Our estimate is compatible with those used to successfully describe the charm production phenomenology. The connection between leading charm and energy deposition in the central rapidity region is considered. Attention is given to the correlation between production in central and fragmentation regions. If the fraction of the reaction energy released in the central region increases the asymmetry in the x_F distributions of charmed mesons will become smaller. We illustrate this quantitatively with simple calculations performed using the Interacting Gluon Model.

1. Introduction

In the early eighties there was a hope to understand charm production solely in terms of perturbative QCD. Inspite of all uncertainties in defining the scale, it would be in any case of the order of a few GeV and therefore the coupling constant would be smaller than one. As more and more data became available it became clear that perturbative QCD alone was not enough to properly account for the measured differential cross sections. Higher order corrections improved the results but did not solve the problems. The main difficulty was that the produced charmed particles were too fast. In other words, there was a remarkable excess of particles with large Feynman x (x_F). In adition a "leading particle" effect has been observed, i.e., charmed mesons carrying one of the valence quarks of the projectile are faster than those carrying no projectile valence quark. This is very hard to explain on the basis of parton fusion alone and is considered as an evidence of some non perturbative production mechanism.

Several new experiments have reported [1] a significant difference between the x_F dependence of leading and nonleading charmed mesons. It is still not possible to explain these data with the usual perturbative QCD [2] or with the string fragmentation model contained in PYTHIA [3] and some alternative mechanisms have been advanced.

Already over ten years ago, the idea was advanced [4], that the hadron wave function contains a charm component even before undergoing a collision. This component is originated in higher twist QCD interactions inside the hadron. The so called "intrinsic" charmed pairs produced by these interactions are different from usual sea quark pairs. The crucial difference between them is that the intrinsic charm is part of the valence system and therefore very fast in contrast to the sea charm, which is slow. During the last years, an intrinsic charm component was added to the perturbative QCD component in a quantitative and systematic way [5]. As a result, a very good description of data was achieved. In order to obtain such good agreement with experimental data the crucial point was the normalization of the intrinsic charm component, σ_{ic} of the hadron + nucleon $\rightarrow c-\bar{c}$ X cross section. The quantity σ_{ic} is related to the probability of observing the intrinsic charm component of the hadron, P_{ic} [6]. It is very difficult to calculate this quantity from first principles. It was estimated from a phenomenological analysis to be less than 1% [7]. In fact, $P_{ic} = 0.3\%$ seems to be the best value to describe recent data on charm production [5].

A very important question is, of course, whether this 1% of intrinsic charm can be supported by any model based calculation. In ref. [8], such a calculation was done using the MIT bag model. It was found that the probability of

finding a five-quark component $|uudc\bar{c}\rangle$ configuration bound within the nucleon bag is of 1 or 2%, in good agreement with the above mentioned phenomenological estimate. The first purpose of this work is to calculate P_{ic} using an approach, which is completely different and independent from that used in refs. [4, 5, 6, 7, 8] and can therefore be used as a cross-check to those estimates.

The intrinsic charm model (ICM) can make predictions for asymmetry and leading particle effect at higher energies. In the ICM another essential ingredient (apart from P_{ic}) for a good description of asymmetries is the recombination mechanism which binds together the intrinsic (fast) charm quarks and the valence quarks of the projectile. Toghether with this fast component there is a slow one , which populates predominantly the central rapidity (low x_F) region and is given by perturbative QCD. The ICM is thus a two-component model where the central (parton fusion) and fragmentation regions (containing intrinsic charm) components are completely independent and added in a simple way. In particular, there is *no energy conservation constraint* imposed on both components, which would obviously result in some simple kinematical correlations between them. The second purpose of this work is to show that such kinematical correlations between central and non-central production is relevant for the study of the observed asymmetries in the production of charmed mesons and that it is also connected to another characteristic of high energy multiparticle production processes, namely to the inelasticity K of reaction. It defines the fraction of the initial energy $\sqrt{s}$ which is released and deposited in the central region of reaction. In particular its energy ($\sqrt{s}$) dependence will be important here. All models that adress charm production in the central region predict that there is no asymmetry in this region. Asymmetry comes from the fragmentation (large rapidity y) region. Therefore, if K increases with energy there will be less energy available in the large y region and this will result in a softening of the leading x_F distributions. Notice that this is independent of all ingredients of the hadronization process since they are universal and energy independent (like, for example, the fragmentation functions). The x_F distributions of the leading charmed particles will thus eventually merge with the distribution of the centrally produced charmed particles, which will then become broader. The asymmetry will then not be observed! The opposite might also be true if K decreases with energy. In this case the leading system will carry proportionally more and more energy, implying a faster leading charm and resulting in stronger asymmetry [10].

The asymmetry problem can therefore be well formulated just in terms of kinematical considerations. All dynamics will show itself only in the way through which initial energy of projectiles will be distributed in rapidity space. For example, one would naively expect that, if perturbative QCD becomes more important at higher energies (due to, for example, increased minijet activity), the central production (and also energy deposition in central region) will become dominant and the asymmetry will decrease or even disappear. This goes along with the expected increase with energy of inelasticity deduced from the analysis of accelerator and cosmic ray data [11].

2. The meson cloud and the charm form factor

The existence of intrinsic charm is here associated with low momentum components of a virtual c-$\bar{c}$ pair in the nucleon. At low momentum scales, the virtual pair lives a sufficiently long time to permit the formation of charm hadronic components of the nucleon wave function. It is this component that, when the nucleon is boosted, will move as fast as the valence quarks.

Generally speaking, we can say that the proton is a fluctuating object, being sometimes a neutron plus a pion, sometimes a strange hyperon plus kaon and so on. It can be any combination of virtual hadrons possessing the right quantum numbers. In particular, if charmed pairs pre-exist inside the nucleon, it can fluctuate into a charmed hyperon plus a $\overline{D}$ meson, as e.g., by the process

$$p \rightarrow \Lambda_c + \overline{D} \rightarrow p \,. \tag{1}$$

We calculate the intrinsic charm contribution to the matrix element $\langle N|\bar{c}\gamma_\mu c|N\rangle$ arising from this virtual $\overline{D}$ meson cloud. The idea that intrinsic quark contributions to nucleon matrix elements can be given by meson clouds

is not new. It was used in refs.[12, 13, 14, 15] to estimate the intrinsic strangeness content of the nucleon and it was suggested in ref [4] as a picture to understand the existence of intrinsic charm in the nucleon.

As in ref.[12], we compute the $\overline{D}$ meson loops using an effective meson-nucleon vertex characterized by a monopole form factor

$$F(k^2) = \frac{m^2 - \Lambda^2}{k^2 - \Lambda^2}\,, \tag{2}$$

and we introduce "seagull" terms in order to satisfy the Ward-Takahashi (WT) identity. In Eq.(2) m is the meson mass and Λ is the effective cut-off. The inclusion of the meson-nucleon form-factors is important to properly take into account the underlying nucleon structure and its spatial extension. As shown in ref.[14], when the sub-structure of the nucleon is considered, it is the size of the proton, rather than the masses involved in the loop, that determines the effective momentum cut-off. We expect therefore the effective cut-off in the $\overline{D}$ meson-nucleon form factor to be approximately the same used in the pion-nucleon or kaon-nucleon form factors.

The pseudoscalar meson-baryon coupling for extended hadrons is schematically given by

$$\mathcal{L}_{BBM} = -ig_{BBM}\bar{\Psi}\gamma_5\Psi F(-\partial^2)\phi\,, \tag{3}$$

where Ψ and ϕ are baryon and meson fields respectively, $F(k^2)$ is the form factor at the meson-baryon vertices and k is the momentum of the meson. The fact that the nucleon-$\overline{D}$-Λ_c coupling constant is not known is not important here because we are mostly interested in arriving at some upper limit to the intrinsic charm content of the nucleon and not at definitive numerical predictions. Accordingly we will use the pion-nucleon coupling constant as an upper limit to the nucleon-$\overline{D}$-Λ_c coupling constant.

We employ pointlike couplings between the current and the intermediate meson and baryon. For the vector current one has

$$\langle\Lambda_c(p')|\bar{c}\gamma_\mu c|\Lambda_c(p)\rangle = \overline{U}(p')\gamma_\mu U(p) \tag{4}$$

and

$$\langle\overline{D}(p')|\bar{c}\gamma_\mu c|\overline{D}(p)\rangle = -(p+p')_\mu \tag{5}$$

in a convention where the c-quark has charm charge=+1.

The effective lagrangian Eq.(3) is non-local and this induces an electromagnetic vertex current if the photon is present. In order to maintain gauge invariance we have to take into account the "seagull vertex"

$$i\Gamma_\mu(k,q) = \pm g_{N\Lambda_c\overline{D}}\gamma_5(q \pm 2k)_\mu \frac{F(k^2) - F((q\pm k)^2)}{(q\pm k)^2 - k^2}\,, \tag{6}$$

which is generated via minimal substitution [16]. The upper and lower signs in Eq.(6) correspond to an incoming or outgoing meson respectively.

The three distinct contributions to the intrinsic form factors, associated with processes in which the current couples to the baryon line (B) (figure 1a), to the meson line (M) (figure 1b) or to the meson-baryon vertex (V) (figure 1c and 1d) in the loop are given by

$$\Gamma^B_\mu(p',p) = -ig^2_{N\Lambda_c\overline{D}}\int\frac{d^4k}{(2\pi)^4}\Delta(k^2)F(k^2)\gamma_5 S(p'-k)\gamma_\mu S(p-k)\gamma_5 F(k^2)\,, \tag{7}$$

$$\Gamma^M_\mu(p',p) = ig^2_{N\Lambda_c\overline{D}}\int\frac{d^4k}{(2\pi)^4}\Delta((k+q)^2)(2k+q)_\mu\Delta(k^2)F((k+q)^2)\gamma_5 S(p-k)\gamma_5 F(k^2)\,, \tag{8}$$

$$\begin{aligned}\Gamma^V_\mu(p',p) \;=\; & ig^2_{N\Lambda_c\overline{D}}\int\frac{d^4k}{(2\pi)^4}F(k^2)\Delta(k^2)\left[\frac{(q+2k)_\mu}{(q+k)^2-k^2}\left(F(k^2) - F((k+q)^2)\right)\times\right.\\ & \left.\gamma_5 S(p-k)\gamma_5 - \frac{(q-2k)_\mu}{(q-k)^2-k^2}\left(F(k^2) - F((k-q)^2)\right)\gamma_5 S(p'-k)\gamma_5\right]\,.\end{aligned} \tag{9}$$

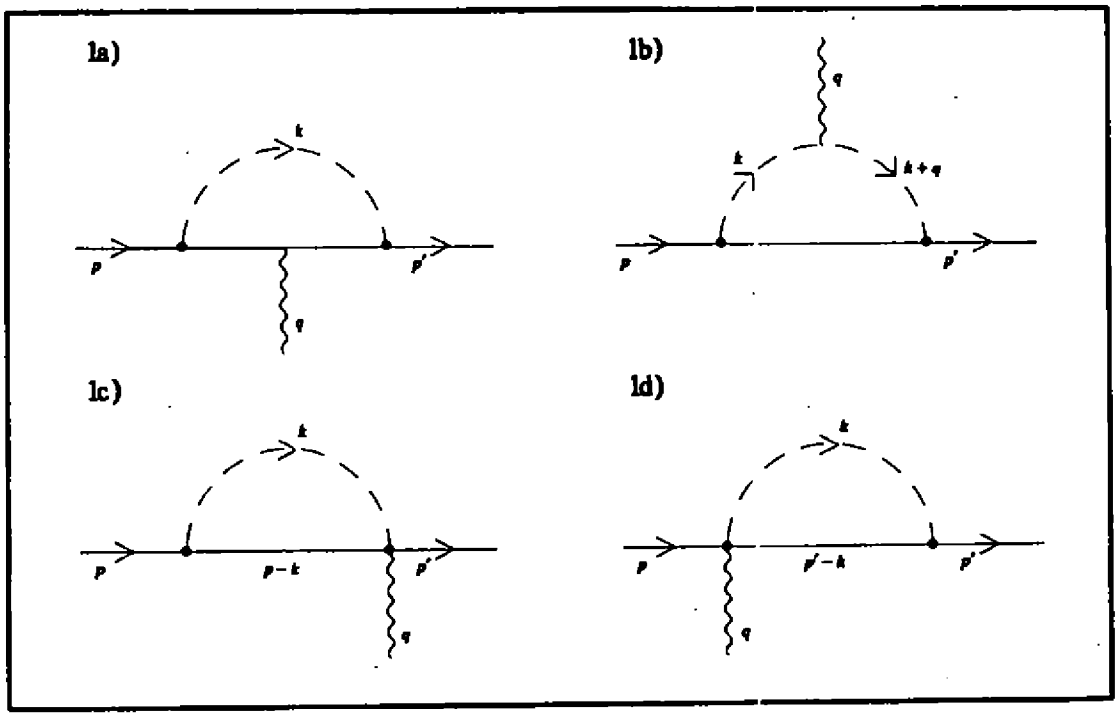

Figure 1

Figure 1. Diagrams which contribute to the calculation of the vertex function. Solid external lines represent the proton and solid internal lines represent the Λ_c. Dashed and wavy lines represent the $\overline{D}$ and the vector current respectively.

In the above equations

$$\Delta(k^2) = \frac{1}{k^2 - m^2 + i\epsilon} \tag{10}$$

is the meson propagator and

$$S(p-k) = \frac{1}{\not{p} - \not{k} - M_\Lambda + i\epsilon} \tag{11}$$

is the Λ_c propagator and $p' = p + q$ with q being the photon momentum. In figure 1 we show all momentum definitions.

With these amplitudes it is easy to show that the Ward-Takahashi identity

$$q^\mu(\Gamma^B_\mu(p',p) + \Gamma^M_\mu(p',p) + \Gamma^V_\mu(p',p)) = Q_c(\Sigma(p) - \Sigma(p')) \,, \tag{12}$$

is satisfied. In Eq.(12) Q_c is the nucleon charm charge, $Q_c = 0$, and $\Sigma(p)$ is the self-energy of the nucleon related to the $\overline{D}\,\Lambda_c$ loop. The sum of the three amplitudes also ensures the charge non-renormalization (or the Ward Identity)

$$(\Gamma^B_\mu + \Gamma^M_\mu + \Gamma^V_\mu)_{q=0} = Q_c\left(-\frac{\partial}{\partial p^\mu}\Sigma(p)\right) = 0 \,. \tag{13}$$

The intrinsic charm form factors are obtained by writing these amplitudes in terms of the Dirac and Pauli form factors

$$\Gamma_\mu(p',p) = \gamma_\mu F_1^c(q^2) + i\frac{\sigma_{\mu\nu}q^\nu}{2M_N} F_2^c(q^2) \,. \tag{14}$$

The intrinsic squared charm radius of the nucleon is defined as

$$r_c^2 = 6\frac{\partial G_E^c(q^2)}{\partial q^2}\bigg|_{q^2=0} \,, \tag{15}$$

where $G_E^c(q^2)$ is the electric form factor introduced by Sachs [17]

$$G_E^c(q^2) = F_1^c(q^2) + \frac{q^2}{4M_N^2} F_2^c(q^2) \,. \tag{16}$$

The numerical results for $|r_c^2|$ are shown in figure 2, as a function of the form factor cut-off Λ. The value of the coupling and masses used are $M_N = 939\,\mathrm{MeV}$, $M_{\Lambda_c} = 2285\,\mathrm{MeV}$, $m_{\overline{D}} = 1865\,\mathrm{MeV}$ and $g_{N\Lambda_c\overline{D}}/\sqrt{4\pi} = g_{N\pi N}/\sqrt{4\pi} = -3.795$

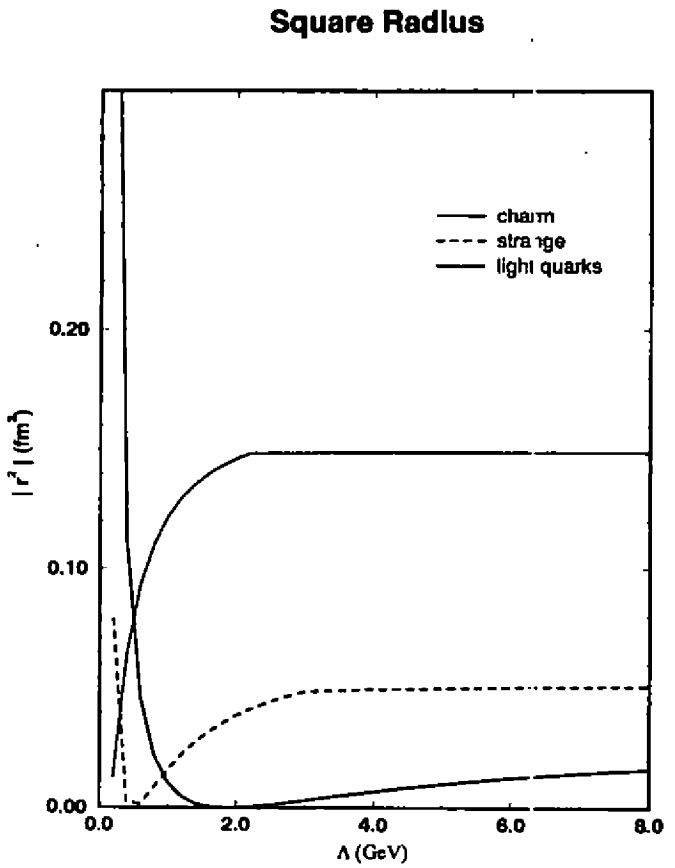

Figure 2

The intrinsic charm mean square radius of the nucleon as a function of the cut-off Λ in the baryon-meson form factor.

As it can be seen the results depend very strongly on the value of Λ. The region of very small values of Λ does not give realistic results for $|r_c^2|$ because it corresponds to a very large proton size. The region with values of Λ around the meson mass is also not reliable because it gives results which are just an artifact of the parametrization of the form factor. The asymptotic region of large Λ is interesting because it provides results which are weakly dependent on the cut-off.

3. The intrinsic charm probability

The probability P_{ic} which is relevant for the calculations done in [9] is the square of the coefficient of the corresponding Fock state. Since we have no access to this quantity we shall estimate it in a geometrical way. In terms of the wave function, we shall make use of its shape instead of its (unknown) normalization.

The intensity of a given proton fluctuation may be associated with its average squared radius $|r^2|$. The larger is $|r^2|$, the more frequently we will find the proton in that particular fluctuation and the larger will be the probability of "seeing " it.

We shall assume that the average barionic radius of the proton ($r_p = [< r_B^2 >]^{\frac{1}{2}}, \sim 0.72fm$) associated with the isoscalar part of the electromagnetic current is a good measure of the proton "total size", i.e., the size which takes into account all possible fluctuations that couple to isoscalar currents. The intrinsic charm probability is then given by

$$P_{ic} = \frac{|r_c^2|}{r_p^2} = 0.9\% \tag{17}$$

where $|r_c^2| = 0.0047fm^2$ is the average charm squared radius calculated above with a cut-off $\Lambda = 1.2$ GeV. P_{ic} is the ratio between the charm "area" and the total proton "area".

We want to compare our results with those obtained by Donoghue and Golowich in ref. [8] for the five quark components of the proton wave function, $|uuds\bar{s}>$ and $|uudq\bar{q}>$, where q represents a light quark. We repeat then the calculations for kaon and pion loops (with the same cut-off Λ), obtaining the average strange radius $|r_s^2| = 0.025fm^2$ and the average light quark radius $|r_q^2| = 0.130fm^2$. Dividing these radii by the barionic squared radius used above we obtain the probabilities $P_{is} = 5$ % and $P_{iq} = 25$ % The calculations done in ref. [8] arrive at $P_{is} = 16$ % and $P_{iq} = 31$ %. The discrepancy in the strange sector suggests that the vector meson dominance model contribution coming from the $\omega - \phi$ mixing (see ref. [15]) is really important. In fact, it will change the result from $P_{is} = 5$ % to $P_{is} = 10$ % [15]. As there is no experimental evidence for a $\omega - J/\Psi$ mixing, the vector meson model will not contribute in the charm sector. With the inclusion of the $\omega - \phi$ mixing our results agree with those obtained in ref. [8] within 6 %.

The charm squared radius increases with Λ (as it can be seen in figure 2) reaching $|r_c^2| = 0.016fm^2$ at asymptotically large values of Λ. In this limit we would have $P_{ic} = 3.0$ %. Considering that we are overestimating the coupling constant in the charm loop, this number can be taken as an upper limit for the intrinsic charm probability in the context of our calculation scheme. Our result seems to be consistent with previous estimates [4, 5, 6, 7, 8].

As a further point we would like to compare our predictions for the x_F distributions of Λ_c and $\overline{D}$ in the meson cloud model with distributions obtained by Brodsky and collaborators. Following ref. [4] we make a Fock state decomposition of the proton. The difference is now that instead of, for example, five quarks ($uudc\bar{c}$) our state will contain a baryon plus a meson ($\overline{D}$-Λ_c). The probability distribution corresponding to this two particle Fock state is, as in [4] and [6], assumed to have the form

$$P(x_{\Lambda_c}, x_D) = \frac{N\delta(1 - x_{\Lambda_c} - x_D)}{(m_p^2 - \frac{\hat{m}_{\Lambda_c}^2}{x_{\Lambda_c}} - \frac{\hat{m}_D^2}{x_D})^2} \tag{17}$$

where $\hat{m}_i^2 = m_i^2 + < k_T >_i^2$ are the effective transverse masses, with $< k_T >$ being the average transverse momentum. Since $m_{\Lambda_c}^2, m_D^2 >> m_p^2, < k_T >^2$ we can write

$$P(x_{\Lambda_c}, x_D) = \frac{N' x_{\Lambda_c}^2 x_D^2 \delta(1 - x_{\Lambda_c} - x_D)}{(x_{\Lambda_c} + (\frac{m_{\Lambda_c}}{m_D})^2 x_D)^2} \tag{18}$$

where $N' = 50.68$ is determined by imposing a normalization condition on $P(x_{\Lambda_c}, x_D)$. Integrating the equation above in x_D (x_{Λ_c}) we find the Λ_c ($\overline{D}$) x_F distribution, which is shown in figure 4(3) (solid lines). For the sake of comparison we also show in these figures the corresponding distributions obtained in ref.[4] for Λ_c and $\overline{D}$ (dashed lines), by combining respectively the u, d and c and the u and $\bar{c}$ quarks in the $|uudc\bar{c}>$ Fock state. It is interesting to notice that the x_F distributions look very similar in the two approaches. The results obtained here have a mass scale whereas there is no information about the Λ_c and $\overline{D}$ masses in the calculations of ref.[4]. The existence of mass scales is responsable for the slight differences between the x_F distributions. From the phenomenological point of view the differences will not be noticeable. The resemblance between these curves is a strong indication that the idea of intrinsic charm can be well understood in terms of the meson cloud model.

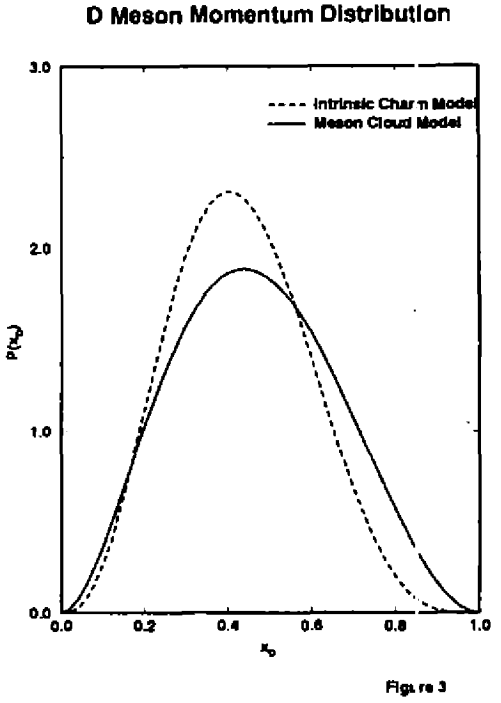

Figure 3

Feynman x distribution of $\overline{D}$ mesons in the meson cloud model (solid line) and in the intrinsic charm model (dashed line).

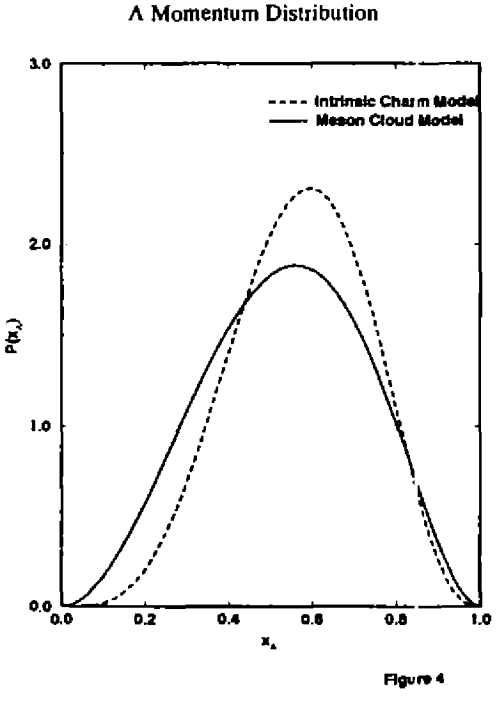

Figure 4

Feynman x distribution of the charmed baryon Λ in the meson cloud model (solid line) and in the intrinsic charm model (dashed line).

Another straightforward extension of our calculations is the estimate of the beauty content of the proton. Assuming $g_{N\Lambda_b B} = g_{N\Lambda_c D} = g_{\pi NN}$, the only differences will be the masses of the baryon and meson. In the asymptotic limit we get $P_{ib}/P_{ic} \sim 1/3$, which is different from the scaling proposed in ref.[4]: $P_{ib}/P_{ic} \sim (m_c/m_b)^2 \sim 1/9$. However, this should not be taken as a discrepancy between the two approaches, since a very strong approximation about the value of the coupling constants was done by us to get the value $P_{ib}/P_{ic} \sim 1/3$.

In this work we have only considered loops involving the particular combination $\overline{D}$-Λ_c. In principle we could include loops with $\overline{D}$-Σ_c and also with vector mesons. However, due to the lack of knowledge of the relevant couplings and cut-offs, no attempt is made to go beyond the $\overline{D}$-Λ_c loop. We expect this contribution to be the most significant, specially in view of the very large values of the coupling constant and cut-off used here. This might be sufficient for an estimate of the order of magnitude of P_{ic}.

4. Leading charm and the IGM

In this section we shall study leading charm production in terms of the Interacting Gluon Model (IGM) [18], which has been invented to describe the inelasticity and its energy behaviour and recently used also to successfuly describe many aspects of multiparticle production (including its semi-hard minijets component, which can be important for charm production at high energies).

Since the IGM has already been described previously in great detail [18] we shall provide here, for completeness, only the most basic formulas and concentrate our attention on the specific mechanisms of charm production and on the calculation of the asymmetries between leading and nonleading charm mesons. The asymmetry has been most accurately measured in the πp scattering, therefore we shall start discussing this process first [19]. In Fig. 5a we show the IGM description of the energy flow in a hadron- hadron collision at high energies. Through the cooperative action of a certain number of soft gluons, carrying an overall momentum fraction x_1 of the incoming pion, colliding with a similar bunch of gluons coming from the target nucleon and carrying fraction x_2 of its momentum , an object called central fireball (CF) is formed. It will decay later on producing observed secondaries. In the IGM [18] the probability for this to happen is given by the function $\chi(x_1, x_2)$. The pion remnants leaving the central region (i.e., their valence quarks plus some gluons which did not interact) carrying momentum x_L are called in the IGM the *leading jet* (LJ) and, being themselves excited objects, may also produce particles (including D mesons) . From the basic function $\chi(x_1, x_2)$ we can compute the Feynman momentum distributions of the CF , $\chi(x_{CF})$, where $x_{CF} = x_1 - x_2$, and of the LJ , $f_{LJ}(x_L)$, by a simple change of variables :

$$\chi(x_{CF}) = \int_0^1 dx_1 \int_0^1 dx_2\, \delta(x_{CF} - x_1 + x_2)\, \chi(x_1, x_2)\, \theta(x_1 x_2 s - 4m_D^2) \tag{19}$$

$$f_{LJ}(x_L) = \int_0^1 dx_1 \int_0^1 dx_2\, \delta(1 - x_1 - x_L)\, \chi(x_1, x_2)\, \theta(x_1 x_2 s - m_0^2) \tag{20}$$

where m_D (1.8 GeV) and m_0 are the masses of the D meson and of the lightest state produced in such collisions [18] . In the above equations we clearly see the connection between central and fragmentation production. The momentum distributions of the systems which will later give origin to charmed particles are derived from the same quantity $\chi(x_1, x_2)$. Moreover , $\chi(x_{CF})$ and $f_{LJ}(x_L)$ carry all the energy ($\sqrt{s}$) dependence of the process , which is both explicit , in the theta functions , and implicit , since $\chi(x_1, x_2)$ depends on $\sqrt{s}$. In Fig. 5b we show central $D\overline{D}$ meson production where $D(\overline{D})$ is any D meson carrying a $c(\bar{c})$ quark. Notice that, in the spirit of IGM, the central production ignores the valence quarks of target and projectile (defined here as those which carry the essential quantum numbers of the colliding pions and protons) which, in the first approximation, just "fly through". Because of this, the centrally produced D's will not show any leading particle effect. There are two distinct ways to produce D mesons out of LJ's: fragmentation and recombination. It is assumed here that, whenever energy allows, we shall have also $\bar{c}c$ pairs in the LJ (produced, for example, from the remnant gluons present there). These charmed quarks may undergo fragmentation into D mesons, as shown in Fig. 5c, but may also as well recombine with the valence quarks as depicted in Fig. 5d. It turns out that only this last process will produce asymmetry.

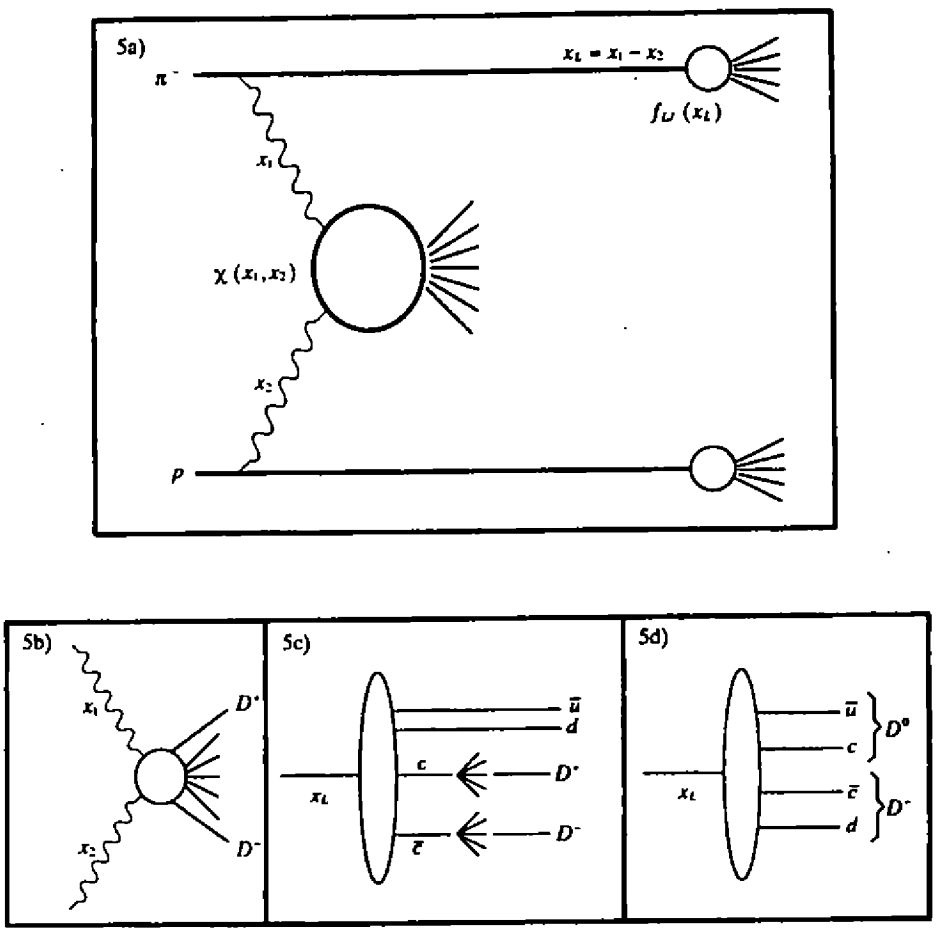

Figure 5

(*a*) Illustration of a pion-nucleon collision: fractions x_1 and x_2 of the incoming hadrons momenta form a central fireball (CF) with probability $\chi(x_1, x_2)$. Fraction $1 - x_1 = x_L$ is carried by the leading jet (LJ). The leading jet momentum spectrum is $f_{LJ}(x_L)$; (*b*) Nonleading D meson production by central fireball fragmentation; (*c*) Nonleading D meson production by leading jet fragmentation; (*d*) Leading D meson production by leading jet recombination.

In the case of pion-nucleon scattering, the measured leading charmed mesons are D^- and the nonleading are D^+. We shall now write the Feynman x_F single inclusive distribution of D^- mesons produced by the CF, by the fragmentation in the LJ (F) and by the recombination there (R):

$$\frac{d\sigma^{CF}}{dx_{D^-}} = \int_{x_{D^-}}^{1} dx_{CF}\, \chi(x_{CF}) \int_{x_{D^-}}^{x_{CF}} dx_{\bar{c}}\, g(x_{\bar{c}})\, D\left(\frac{x_{D^-}}{x_{\bar{c}}}\right) \quad , \tag{21}$$

$$\frac{d\sigma^{F}}{dx_{D^-}} = \int_{x_{D^-}}^{1} dx_L f_{LJ}(x_L) \int_{x_{D^-}}^{x_L} dx_{\bar{c}}\, g(x_{\bar{c}})\, D\left(\frac{x_{D^-}}{x_{\bar{c}}}\right) \quad , \tag{22}$$

$$\frac{d\sigma^{R}}{dx_{D^-}} = \int_{x_{D^-}}^{1} dx_L f_{LJ}(x_L) \int dx_c \int dx_{\bar{c}} \int dx_{\bar{u}} \int dx_d\, g(x_c)\, g(x_{\bar{c}})\, f(x_{\bar{u}})\, f(x_d)$$

$$\delta(x_{D^-} - x_{\bar{c}} - x_d)\, \delta(x_L - x_{\bar{c}} - x_c - x_d - x_{\bar{u}}) \quad , \tag{23}$$

where $f(x)$ and $g(x)$ are distribution functions of valence and charm quarks respectively and the $D(z)$'s are charm quark fragmentation functions [9]. The D^+ momentum distributions are given by (21) and (22) with the replacements: $D^- \to D^+$, $\bar{c} \to c$. These nonleading mesons will not be produced by recombination (eq. (23)). The functions $f(x)$ and $g(x)$ are essentially unknown since they are momentum distributions of partons inside the CF

and inside the LJ after the collision. Following our assumption that the valence quarks interact weakly we shall approximate $f(x)$ by the initial state valence quark distributions and take them from reference [20] . As for the charm quark distribution , $g(x)$, the situation is less clear. The $c-\bar{c}$ pairs do not come directly from the sea : in the CF they are produced and in the LJ they may be excited. It is therefore reasonable to think that the charm quarks will be somewhat faster than ordinary sea quarks. Accordingly we shall use for $g(x)$ the ansatz proposed by Barger and collaborators [21] :

$$g(x) = \left(\frac{1-x}{x}\right)^{1/2} \tag{24}$$

which is less singular than $1/x$ but still much softer than an intrinsic charm distribution which behaves typically like $x(1-x)$. The fragmentation functions have the Peterson form [22] :

$$D_{c\to D}(z) = \frac{N}{z[1-1/z-\varepsilon/(1-z)]^2} \tag{25}$$

where $\varepsilon \simeq \frac{(m_q^2+p_{qT}^2)}{(m_Q^2+p_{QT}^2)}$, m_q, p_{qT} , m_Q , p_{QT} are mass and transverse momentum of the light and of the heavy quark respectively and N is a normalization constant. In the present case $\varepsilon \simeq 0.06$. In Fig. 6a we show the (unnormalized) contributions coming from the three processes above (eqs. (21), (22) and (23)). As expected , central production (solid line) leads to the softest D meson x_F distribution , recombination in the leading jet (dotted line) leads to the hardest final distribution and leading jet fragmentation (dashed line) lies in between. This is so because $\chi(x_{CF})$ is softer than $f_{LJ}(x_L)$ and because recombination adds momenta whereas fragmentation causes always some deceleration. Note that , although flat , the dashed and dotted curves have a pronounced maximum at very low x_D . This is a direct consequence of the behaviour of $g(x)$. If instead of the form (24) we use an intrinsic charm distribution we will obtain a strong suppression at low x and a maximum around $x_D = 0.4-0.6$. A final comment on this figure is that our distribution of centrally produced D's (solid line) is broader than the one obtained from perturbative QCD. This is so because the cooperative mechanism adds together soft gluons, increasing the energy released in the central region , favouring higher values of x_1 and x_2 (in Fig. 5a) and allowing for fluctuations with higher x_{CF} . Considering all that was said above we can conclude that the IGM (like the ICM) is a two component model in which the components are not very much different in shape from each other (in sharp contrast to what happens with the components of the ICM) and have some overlap. Because of this we expect to find smaller asymmetries than those found in ref. [9] ,but this depends, of course, on how one mixes the different components.

5. Momentum distributions, asymmetries and energy dependence

In what follows we write the differential cross section as the sum of a central fireball (CF) and leading jet (LJ) component and the last one as the sum of a fragmentation (F) and a recombination (R) component , using a similar notation as in ref. [9] :

$$\frac{1}{\sigma}\frac{d\sigma}{dx_{D^-}} = (1-\eta)\,\frac{1}{\sigma^{CF}}\frac{d\sigma^{CF}}{dx_{D^-}} + \eta\,\frac{1}{\sigma^{LJ}}\frac{d\sigma^{LJ}}{dx_{D^-}} \quad , \tag{26}$$

$$\frac{1}{\sigma^{LJ}}\frac{d\sigma^{LJ}}{dx_{D^-}} = (1-\xi)\,\frac{1}{\sigma^{F}}\frac{d\sigma^{F}}{dx_{D^-}} + \xi\,\frac{1}{\sigma^{R}}\frac{d\sigma^{R}}{dx_{D^-}} \tag{27}$$

where the mixture parameters are ξ $(0 \le \xi \le 1)$ and

$$\eta = \frac{\sigma^{LJ}}{\sigma^{CF}+\sigma^{LJ}} \tag{28}$$

In the case of the D^+ distribution, the expressions above are the same but $\xi = 0$.

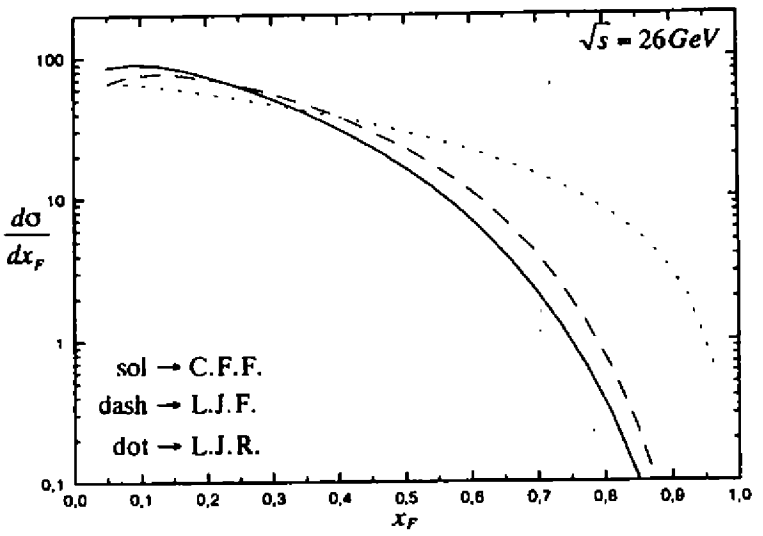

Figure 6

x_F distributions of D mesons calculated with the IGM. The solid line shows the contribution of the central fireball fragmentation. The dashed line shows the contribution of the leading jet fragmentation and the dotted line shows the contribution of the leading jet recombination.

The ICM parameter η has been chosen 0.2 because of an analogy between σ_{ic} (our σ^{LJ}) and the diffractive charm cross section. On the other hand , in the Valon Model [23] the same data are adressed without any central component. This would correspond to taking $\eta = 1$. Here , because of the kinematical mixing between CF and LJ the value of η is essentially free. In what follows we will choose it to be $\eta = 0.7$. Note also that , in our case ,$\xi = 0$ corresponds to no asymmetry. Since existing data on open charm production [1] apparently do not show nuclear effects [24], we use here (as all other models which address these data) the IGM for hadron-nucleon collisions [25].

In Fig. 7 we compare our calculations with WA82 data. Fig. 7a and 7b show the x_F spectrum of D^+ and D^-, respectively, and Fig. 7c shows the asymmetry which is given by :

$$A(x_F) = \frac{\frac{d\sigma}{dx_{D^-}} - \frac{d\sigma}{dx_{D^+}}}{\frac{d\sigma}{dx_{D^-}} + \frac{d\sigma}{dx_{D^+}}} \tag{29}$$

In Fig. 7b and 7c solid , dashed and dotted lines correspond to $\xi = 0.8, 0.5$ and 0.2 respectively. Data points are from the WA82 , E769 and E791 [26] collaborations. As it can be seen, a satisfactory description of data can be obtained with the IGM . The best description can be obtained with a large ammount of recombination ($\xi = 0.8$) . This is ultimately due to our choice of $g(x)$. We have checked that the choice of an ordinary sea distribution for the charm quarks in the CF and LJ requires $\eta = 1.0$ and $\xi = 1.0$ for a reasonable fit. The choice of an intrinsic charm distribution allows for small values of η and ξ . The conclusion seems to be that although data do not rule out usual sea distributions as an input , good fits with more reasonable values of the parameters can be obtained using harder charm quark distributions like (24) or the one used in ref. 4.

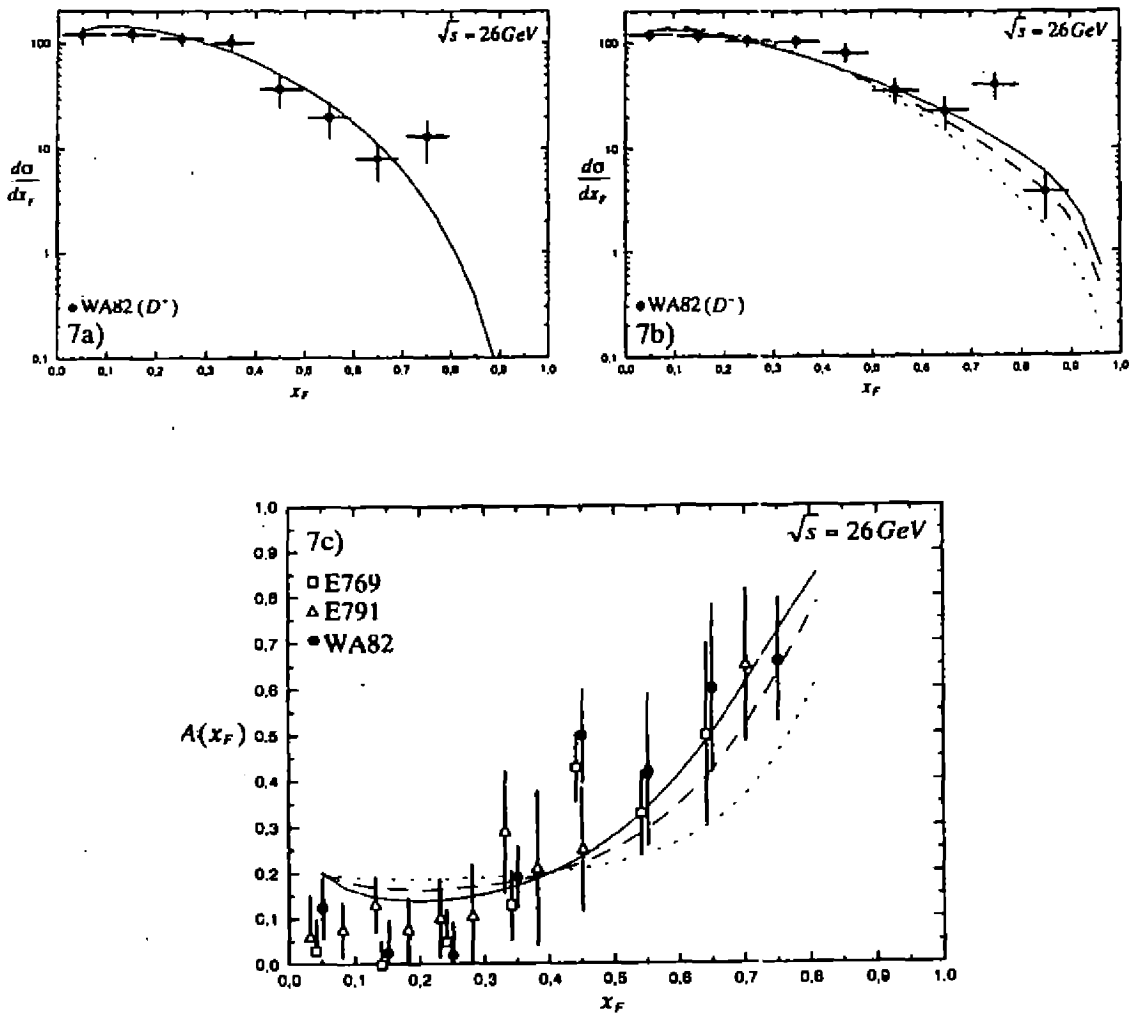

Figure 7

(*a*) x_F distribution of D^+ mesons calculated with our model and compared with WA82 data; (*b*) x_F distribution of D^- mesons calculated with our model and conpared with WA82 data. Solid line corresponds to $\xi = 0.8$ in eq. (27) while dashed and dotted lines correspond to $\xi = 0.5$ and $\xi = 0.2$ respectively; (*c*) the asymmetry calculated with the IGM and compared with WA82 (solid circles) , with E769 (open squares) and E791 (open triangles) data. Solid , dashed and dotted lines correspond to the same choices of ξ of 7b).

We consider now the energy dependence of the asymmetry. All details concerning the particularities of charm production are energy independent. In equations (26) and (27) η , ξ and the differential distributions , i.e. , respectively normalization and shape of the curves, can depend on $\sqrt{s}$. For simplicity we shall assume that ξ does not change with the energy. The distributions $\frac{d\sigma}{dx_{D^-}}$ will depend on $\sqrt{s}$ through $\chi(x_{CF})$ and $f_{LJ}(x_L)$. The behaviour of these last functions with $\sqrt{s}$ is shown in Fig. 8a and 8b respectively. We observe a very modest broadening of $\chi(x_{CF})$ implying a small increase of $\langle x_{CF} \rangle$ and a more pronounced softening of $f_{LJ}(x_L)$ with the corresponding reduction of $\langle x_L \rangle$. As for η , an extensive analysis [18] of charged particle production up to Tevatron energies has shown that it decreases by a factor 3 when we go from ISR to Tevatron energies. Assuming a similar reduction for the case of charmed particle production η will change from 0.7 to 0.25. Considering what was said above we evaluate again all the expressions (19)-(27) at $\sqrt{s} = 1800$ GeV. The resulting asymmetry is shown in Fig. 8c with a dashed line. For comparison we show in the same figure (with a solid line) the asymmetry at $\sqrt{s} = 26$ GeV calculated with the same parameters. It decreases 20% in the region $x_F \geq 0.5$. Although this is not a very impressive change it illustrates the trend. Moreover, we know that the asymmetry goes asymptotically

to zero since $\eta \to 0$. We emphasize that this is so because the IGM (in its version [18]) predicts that at higher energies, because of the action of minijets, the energy deposition in the central region will increase implying two effects : a growth of the central multiplicity (implying thus an increase of $1-\eta$) and a softening of the leading jet momentum distribution. We can therefore conclude that, irrespective of details of charm production, these both effects combined will reduce the asymmetry. It is interesting to mention that the data collected in Fig. 7c come from three different collaborations E769 , WA82 and E791 with beam energies of 250, 340 and 500 GeV respectively. In the CMS this corresponds to a variation of $\sqrt{s} = 23$ GeV to $\sqrt{s} = 33$ GeV. This energy change is small, the error bars are large and therefore no change in the asymmetry is visible yet. At higher energies there is a chance to experimentally verify this behaviour at RHIC or LHC.

6. Leading beauty

As a straightforward extension of our analysis we calculate now the asymmetry in B meson production. This is done by simply replacing m_D by $m_B = 4.75$ GeV in (19) and $\varepsilon = 0.06$ by $\varepsilon = 0.006$ in (25). In principle we should also change $g(x)$ but in a first estimate we keep the ansatz (24). If we would use an intrinsic distribution for $g(x)$ it would be very weakly dependent on the heavy quark mass [9]. In Fig. 9 we show the $\chi(x_{CF})$ distribution for charm (dashed line) and for beauty production (solid line) with the proper change in eq. (19) . The energy is $\sqrt{s} = 26$ GeV . The effect of increasing the production threshold ($m_D \to m_B$ in the theta function in eq.(19)) is to select events with a more massive CF and with larger lower limits for x_1 and x_2, suppressing thus larger values of $x_{CF} = x_1 - x_2$ with respect to charm production (in the limit of total energy deposition, i.e., $x_1 = x_2 = 1$, the CF would be at rest). This effect is however very small. This is expected and seen in Fig. 9. In Fig. 10a (10b) we show the x_F distributions of nonleading (leading)D and B mesons. The energy is the same as in Fig. 9 and the parameters are the same as before ($\eta = 0.7$ and $\xi = 0.8$). Nonleading spectra are calculated with eqs. (21) and (22). The Peterson fragmentation functions , appearing in those equations, are very sensitive to the value of ε. In the case of beauty, the strong reduction of ε makes the fragmentation function strongly peaked at very large values of z. The emerging B's will therefore be much less decelerated than the D's . This effect compensates the previous one and the final nonleading B distribution is harder than the nonleading D one. The leading distributions include recombination , given by eq. (23) , which is not affected by the change in the heavy quark mass. Because of this , the spectra in Fig. 10b exhibit the same qualitative behaviour (B's faster than D's) seen in Fig. 10a but the difference between B's and D's is smaller. The asymmetries of B^-/B^+ and D^-/D^+ are shown in Fig. 11 with solid and dashed lines respectively for $\sqrt{s} = 26$ and 1800 GeV. The asymmetry in beauty is about 50% weaker than in charm at $x_F = 0.8$ and both show a similar decrease with energy.

In conclusion: the IGM describes the energy flow in high energy hadron collisions. It takes properly into account the correlation between energy deposition in the central region and the leading particle momentum distribution. It accounts for charmed meson production in a natural and satisfactory way and makes the prediction that at higher energies the increase of inelasticity K (see [18]) will lead to the decrease of the asymmetry in heavy quark production. It also predicts a weaker asymmetry for beauty. We believe that this point should also be adressed by other models which deal with asymmetry in heavy flavour production [27].

Acknowledgements

This work was supported partially by FAPESP, by CNPq.

References

[1] M.Adamovich et al. (WA82 Collab.), *Phys. Lett.* **B306** (1993) 402; G.A.Alves et al. (E769 Collab.), *Phys. Rev. Lett.* **72** (1994) 812.

[2] S.Frixione et al., *Nucl. Phys.* **B431** (1994) 453. P.Nason, S.Dawson and K.Ellis, *Nucl. Phys.* **B327** (1989) 49.

[3] T.Sjöstrand, *Comp. Phys. Commun.* **39** (1986) 344; T.Sjöstrand and Bengtsson, *Comp. Phys. Commun.* **43** (1987) 367.

[4] S.J. Brodsky, C. Peterson and N. Sakai, Phys. Rev. **D23** (1981) 2745;S. J. Brodsky, P. Hoyer, C. Peterson and N. Sakai, Phys. Lett.**B93** (1980) 451.

[5] R. Vogt, S. J. Brodsky, P. Hoyer, Nucl. Phys. B383 (1992) 643 and references therein.

[6] R. Vogt, S. J. Brodsky, LBL Report LBL-35380, 1994.

[7] E. Hoffmann and R. Moore, Z. Phys. **C20** (1983) 71.

[8] J.F. Donoghue and E. Golowich, Phys. Rev. **D15** (1977) 3421.

[9] R.Vogt and S.J.Brodsky, *Nucl. Phys.* **B438** (1995) 261.; R.Vogt, S.J.Brodsky and P.Hoyer, *Nucl. Phys.* **B383** (1992) 643.

[10] The energy dependence of the leading particle effect in charm production is relevant also for experimental reasons. The experiment E781, scheduled to run in the near future at Fermilab, is strongly based on the existence of this effect. Since it will use a pion beam of higher energies than presently available, predictions for the corresponding leading charm distributions are in order here.

[11] Cf., for example, J.Bellandi, R.J.M.Covolan and A.L.Godoi, *Phys. Lett.* **B343** (1995) 410 and references therein. However, one should also stress here that the problem of energy dependence of K is essentially still open, cf., Z.Wlodarczyk, **23 ICRC**, Calgary (1993), eds. D.A.Leahy et al., World Scientific, Singapore (1994), p. 355.

[12] M.J. Musolf and M. Burkardt, Z. Phys. **C61** (1994) 433.

[13] W. Koepf, E.M. Henley and S.J. Pollock, Phys. Lett. **B288** (1992) 11; W. Koepf and E.M. Henley, Phys. Rev. **C49** (1994) 2219.

[14] W. Koepf, E.M. Henley and M. Alberg, "Mesons and the Structure of Nucleons", preprint DOE/ER/40427-08-N94.

[15] T.D. Cohen, H. Forkel and M. Nielsen, Phys. Lett. **B316** (1993) 1; H. Forkel, M. Nielsen, X. Jin and T.D. Cohen, Phys. Rev. **C50** (1994) 3108.

[16] K. Ohta, Phys. Rev. **D35** (1987) 785.

[17] R.G. Sachs, Phys. Rev. **126** (1962) 2256.

[18] F.O.Durães, F.S.Navarra and G.Wilk, *Phys. Rev.* **D50** (1994) 6804 and references therein.

[19] Note that so far IGM has been applied only to reactions with nucleons. In order not to introduce new parameters when applying it to pion beams we are changing only the relevant cross sections entering it, namely $\sigma_{NN}^{inel} \to \sigma_{\pi N}^{inel}$, and gluon distributions.

[20] P.J.Sutton, A.D.Martin, R.G.Roberts and W.S.Stirling, *Phys. Rev.* **D45** (1992) 2349.

[21] V. Barger, F. Halzen and W. Y. Keung ,*Phys. Rev.* **D25** (1982) 112.

[22] C. Peterson et al. ,*Phys. Rev.* **D27** (1983) 105.

[23] R.C.Hwa, *Phys. Rev.* **D51** (1995) 85.

[24] Recent (but still preliminary) high statistics data (K.Rybicki, *Charm production in hadronic collisions*, invited talk at *XXV Int. Symp. on Multip. Dynamics*, Stará Lesná, Slovakia, 12-16 September 1995, to be published in the proceedings) reveal that in the parametrization $\sigma^A/\sigma^N = A^\alpha$ exponent $\alpha \simeq 1$ in the whole range of x_F and p_T measured.

[25] One should, however, keep in mind the fact that nuclear effects in the x_F dependence of differential cross sections have been observed in hidden charm hadroproduction . See for example : D. M. Alde et al. ,*Phys. Rev. Lett.* 66 (1991) 133 and references therein.

[26] T. Carter , Fermilab Report FNAL-CONF-94/383 (1994).

[27] "Firetube Model: strangeness and charm production", C.E.M. Aguiar, T. Kodama, R.A.M.S. Nazareth and G. Pech , proceedings on Relativistic Aspects of Nuclear Physics, Rio de Janeiro (1993), World Scientific Publishing (1994)27-48 ; " Leading/Nonleading Charm Hadroproduction in the Quark-Gluon String Model" , O. I. Piskounova, Dubna Report (1995).

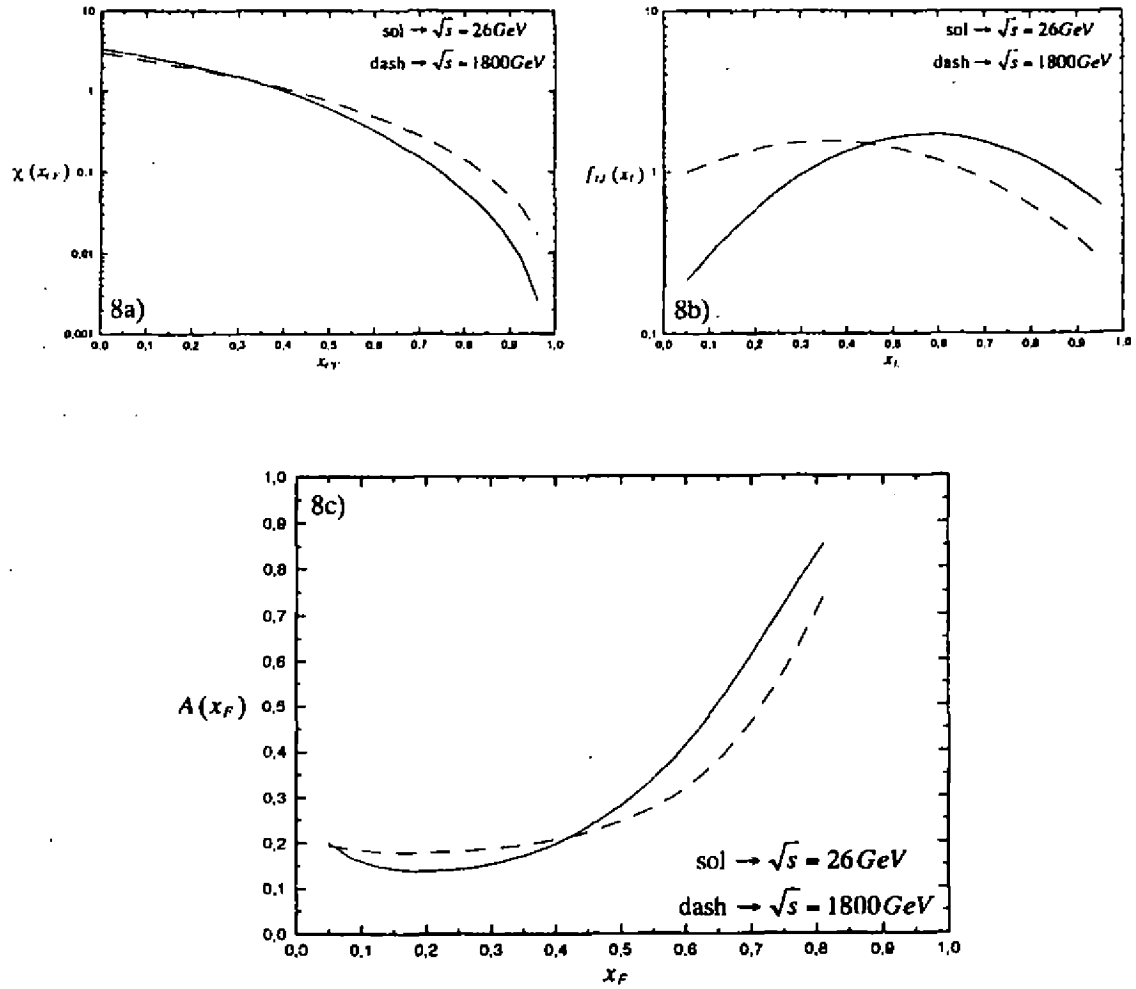

Figure 8

(*a*) Momentum distribution $\chi(x_{CF})$ of the central fireball at $\sqrt{s} = 26$ GeV (solid line) and at $\sqrt{s} = 1800$ GeV (dashed line) ; (*b*) momentum distribution $f_{LJ}(x_L)$ of the leading jet at $\sqrt{s} = 26$ GeV (solid line) and at $\sqrt{s} = 1800$ GeV (dashed line) ; (*c*) the asymmetry in pion- proton collision calculated with the IGM : solid line corresponds to $\sqrt{s} = 26$ GeV with $\eta = 0.7$ and dashed line corresponds to $\sqrt{s} = 1800$ GeV with $\eta = 0.25$. In both cases $\xi = 0.8$.

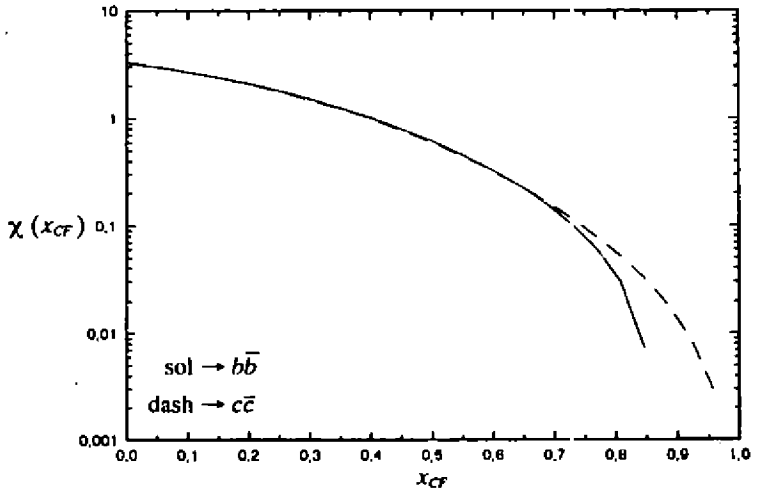

Figure 9

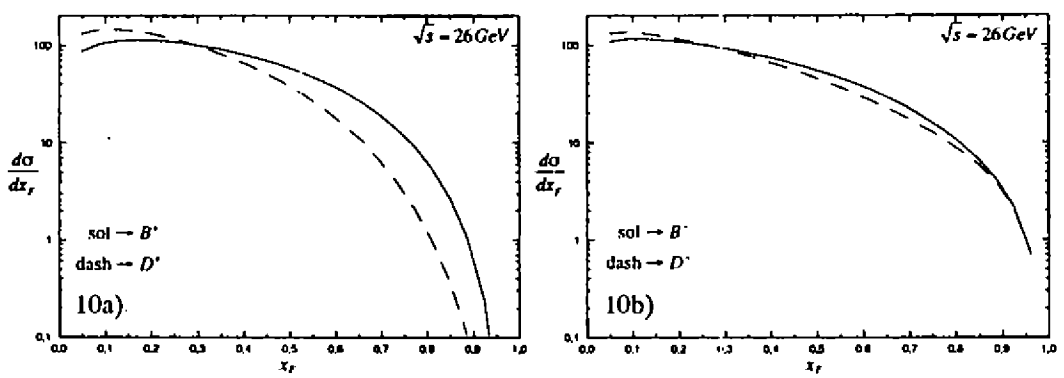

Figure 10

Figure 9. x_F distribution ($\chi(x_{CF})$) of centrally produced $b - \bar{b}$ (solid line) and $c - \bar{c}$ (dashed line) quark pairs.

Figure 10. (*a*) x_F distribution of nonleading B (solid line) and D (dashed line) mesons; (*b*) the same as (*a*) for leading B (solid line) and D (dashed line) mesons. The energy is in both cases $\sqrt{s} = 26$ GeV.

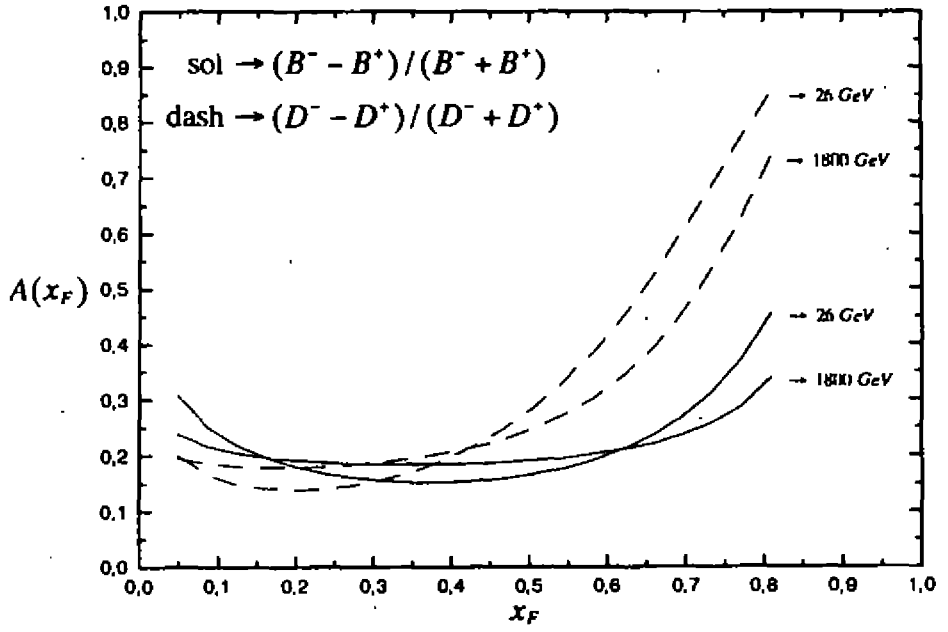

Figure 11

B^-/B^+ (solid lines) and D^-/D^+ (dashed lines) asymmetries at $\sqrt{s} = 26$ and 1800 GeV.

B-Physics at Fermilab DØ Experiment Present and Prospects

G. A. Alves
LAFEX/CBPF
Rua Dr. Xavier Sigaud 150, Rio de Janeiro, RJ
(Representing the D0 Collaboration*)

Received March, 1996

We present the first B-Physics results from the 1992/93 collider run at Fermilab, using the DØ detector. Results are given for the b-quark production cross section using inclusive single muons and J/ψ to tag the heavy flavor production. Preliminary results on $B^0 - \bar{B}^0$ Mixing are also presented. We compare the results with theoretical predictions where appropriated and present the prospects for future runs.

1 Introduction

Although the DØ experiment is optimized for high p_T physics, its extensive muon detection system capable on triggering on muons in a large pseudorapidity range, combined with the large $b\bar{b}$ cross section at $\sqrt{s} = 1.8$ TeV make it possible to study the b production in single muon and multimuon channels. The inclusive single muon and J/ψ cross sections, measured as a function of muon transverse momentum p_T^μ and pseudorapidity η, can be used to infer the $b\bar{b}$ cross section for which QCD predictions have been calculated in the in next-to-leading (NLO) order [1]. Measurement of heavy quark production at large pseudorapidity provides information on the gluon structure function at small x.

2 DØ Detector

The DØ detector [2] is a large general purpose facility with no central magnetic field. The detector consists of central drift chambers, a transition radiation detector, a highly segmented liquid-argon uranium calorimeter with good energy resolution and a muon system.

The muon detector consists of five magnetized iron toroids between the first two of the three layers of proportional drift tubes. It provides a measurement of a muon momentum over a pseudorapidity range $|\eta| < 3.3$. The momentum resolution is limited by the Multiple Coulomb scattering to $\geq 20\%$. Test beam data indicate that the intrinsic diffusion limit on the spacial resolution is ≈ 200 μm. The resolution is currently limited to 700 μm by the accuracy of the geometric alignment. The central tracking system helps in identifying muons associated with the interaction vertex. The calorimeter coverage extends down to $|\eta|$ of ≈ 4.4 and is used in this analysis to detect jets associated with the muons. The total thickness for the calorimeter plus the toroid varies from 13 to 18 λ and reduce the hadron punchthrough to a negligible level.

The DØ detector design was optimized keeping in mind three main objectives:

*Universidad de los Andes (Colombia), University of Arizona, Brookhaven National Laboratory, Brown University, University of California, Davis, Irvine, Riverside, Centro Brasileiro de Pesquisas Físicas (Brasil), CINVESTAV (Mexico), Columbia University, Delhi University (India), Fermilab, Florida State University, University of Hawaii, University of Illinois, Chicago, Indiana University, Iowa State University, Korea University (Korea), Lawrence Berkeley Laboratory, University of Maryland, University of Michigan, Michigan State University, Moscow State University (Russia), New York University, Northeastern University, Northern Illinois University, Northwestern University, University of Notre Dame, Panjab University (India), Institute for High Energy Physics (Russia), Purdue University, Rice University, University of Rochester, CEN Saclay (France), State University of New York,Stony Brook, SSC Laboratory, Tata Institute of Fundamental research (India), University of Texas, Arlington, Texas A&M University

- Provide excellent identification and energy measurement for electrons and muons, as one expects that new phenomena generally have large branching fractions into final states with one or more leptons. On the other hand, those processes typical of QCD, which are much more frequent, have comparatively lower semileptonic branching fractions.
- Allow the observation of parton jets with excellent energy resolution. Emphasis was given to the observation of parton jets instead of the individual particles, because the jets as a whole are more directly related to the fundamental processes occurring in a high energy collision than each isolated particle.
- Provide a good measurement of $\not\!\!E_T$, the missing energy necessary to transverse energy-momentum balance, as an indirect means of detecting neutrinos and other neutral particles with low interaction rate with matter.

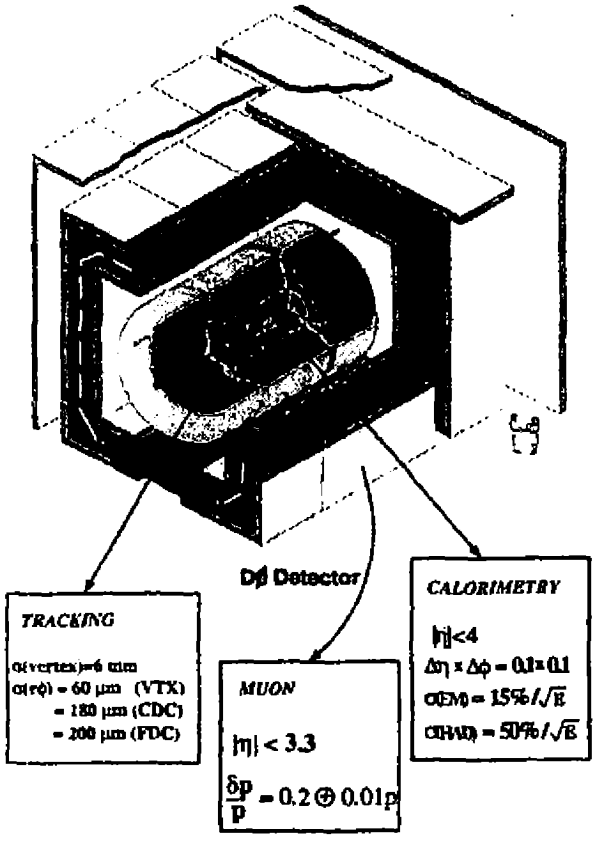

Figure 1. Isometric view of the DØ Detector showing its subcomponents

3 Inclusive muon Cross Section

3.1 Event Selection

The DØ event selection consists of 3 levels of trigger [2] which reduces $\approx$ 43 *mb* [3] of inelastic cross section to 2 Hz of data written to magnetic tape. The Level 0 trigger selects inelastic collisions from beam-beam scintillator coincidences and measures the vertex position. Level 1 hardware muon trigger requires 2 hits in either 2 or 3 layers of the muon system, depending on the geometric region, in a coarse road of 60 cm width. The efficiency of the Level 1 muon trigger for high p_T muons is $\approx$ 60%, the losses being mostly geometric. The Level 2 software muon trigger requires a good quality muon track with the reconstructed transverse momentum $p_T^{\mu} >$ 3 GeV.

3.2 Data Analysis

The inclusive muon cross section measurements are based on special runs taken at low luminosity. These runs used single muon triggers for two regions of pseudorapidity, central ($|\eta| < 1$) and forward ($2.2 < |\eta| < 3.3$), with integrated luminosities of $73.3nb^{-1}$, and $37.7nb^{-1}$, respectively. The data presented here comes from the 1992/93 collider run. The results for the forward region are still preliminary.

For the offline analysis the muon was required to have $p_T^{\mu} > 5$ GeV. Quality cuts require: hits in all the three layers of the muon system; a matching central detector track; at least 1 GeV energy deposition in the calorimeter; good impact parameter vertex projection in both bend and non-bend views; the muon track passing cosmic ray rejection cuts and synchronized within $100ns$ with the beam crossing time.

For the single muon analysis the overall efficiency was evaluated using ISAJET [4] $b\bar{b} \rightarrow \mu X$ Monte Carlo events. These events were put through a complete GEANT detector simulation Level 1 and Level 2 trigger simulators and the offline event reconstruction. As shown in Figure 2, the overall efficiency is 26% for $p_T^{\mu} > 5$ GeV and $|\eta| < 1$. For muons in $2.2 < |\eta| < 3.3$, it is $\approx 17\%$.

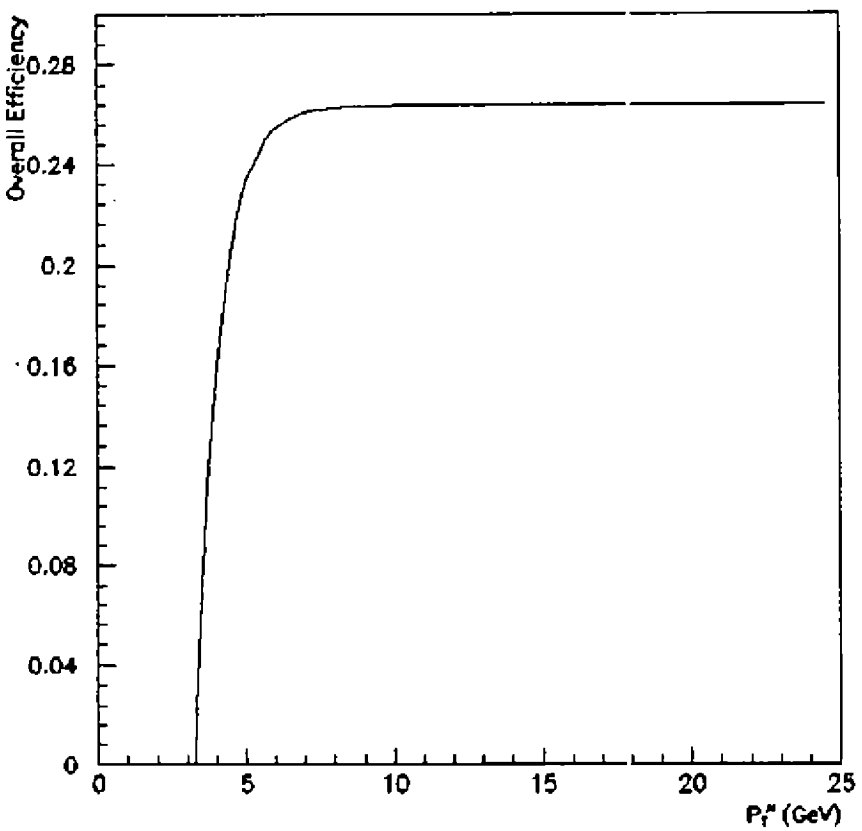

Figure 2. Overall efficiency for muons with $|\eta| < 1$.

3.3 Results and Discussion

The inclusive muon cross section for $|\eta| < 1$ and $2.2 < |\eta| < 3.3$, is shown in Figures 3(a) and 3(b), respectively. The main sources of systematic error are the uncertainty in the luminosity measurement (12%) and the cosmic ray and combinatoric backgrounds ($\approx 10\%$ for $|\eta| < 1$). The data have been compared to

(NLO) ISAJET Monte Carlo predictions. Figures 3(a) and 3(b) show the predicted contributions to the cross section from b→ μX , c→ μX, and π or K decays summed together.

The shape of the p_T^μ spectrum is in good agreement with expectation. Although no jet was required either in the trigger or the analysis, it was found that nearly 60% of the events have jets associated with them, suggesting that most of the events are indeed from b decays as expected.

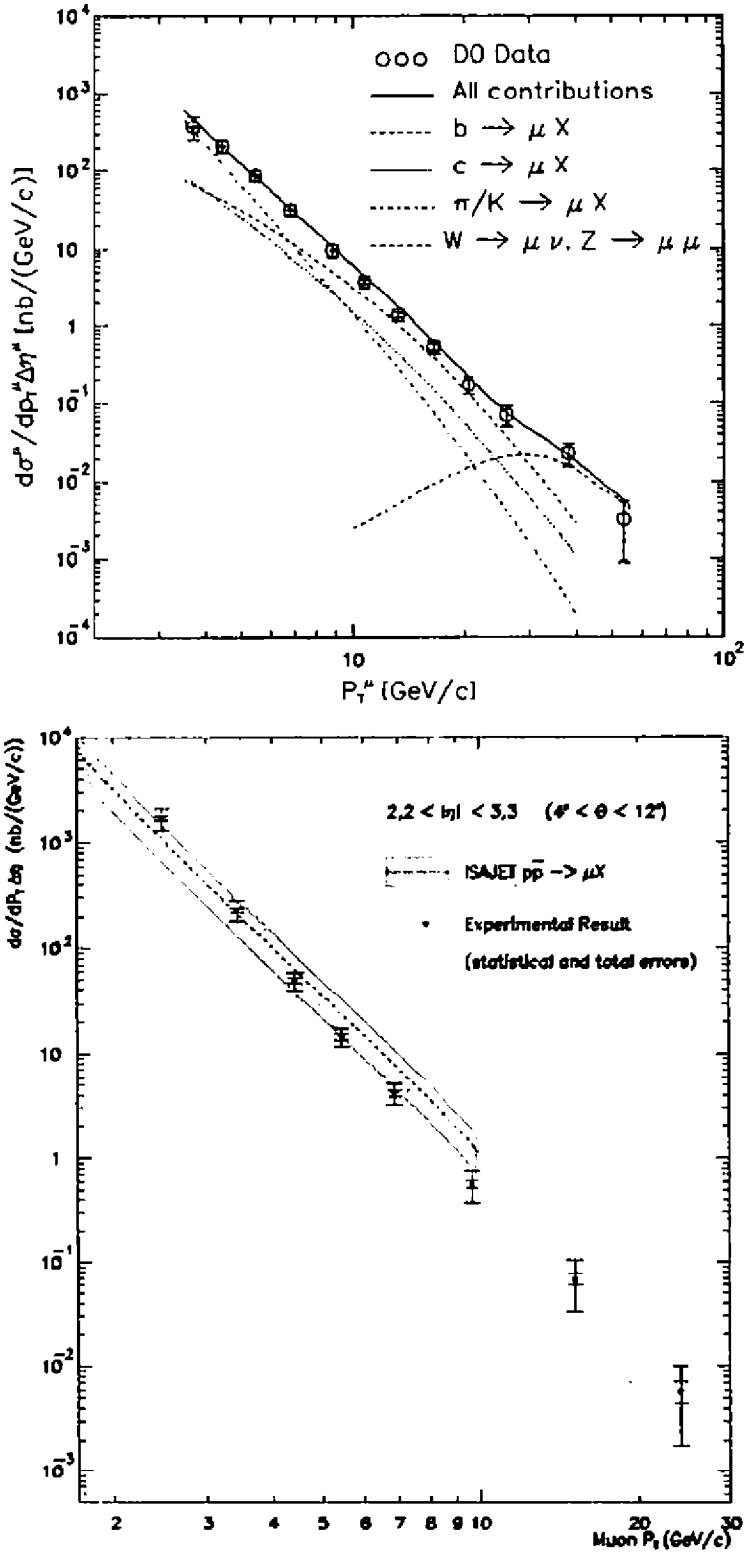

Figure 3. Inclusive muon cross sections compared to Monte Carlo predictions from ISAJET

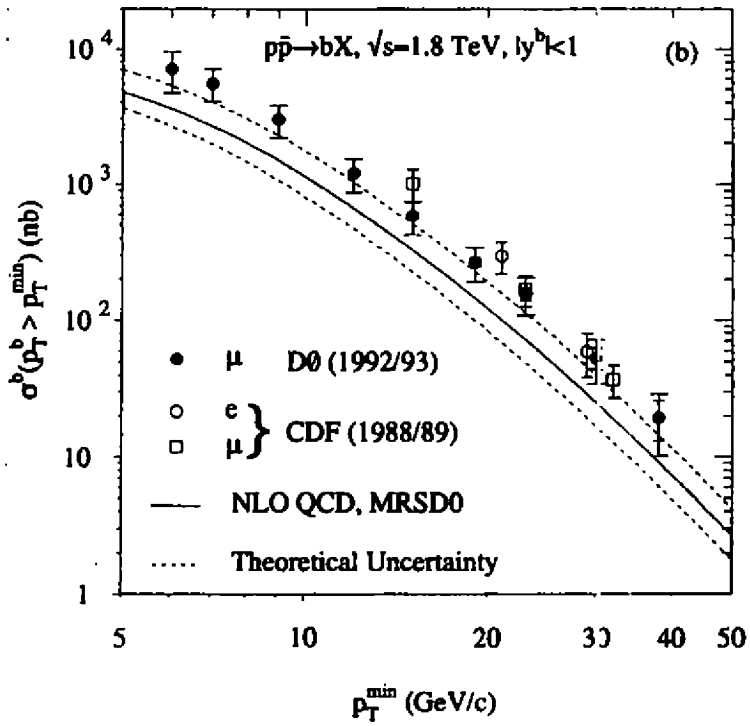

Figure 4. b-quark production cross section compared to NLO QCD predictions of NDE using MRSD0 structure functions, Ref. [1].

Work is in progress to decrease the systematic uncertainties and to extract the $b\bar{b}$ cross section in the forward region. In the central region, the $b\bar{b}$ cross section was extracted folowing a general procedure developed by the UA1 collaboration [5].The relation between the b-quark cross section and the experimental muon spectrum is given by:

$$\sigma^b(p_T^b > p_T^{min}) = \frac{1}{2}\,\sigma_b^\mu(p_T^{\mu 1}, p_T^{\mu 2})\,\frac{\sigma_{MC}^b}{\sigma_{MC}^\mu}\quad , \tag{1}$$

where $\sigma_b^\mu(p_T^{\mu 1}, p_T^{\mu 2})$ is the muon cross section integrated over the interval $p_T^{\mu 1} < p_T^\mu < p_T^{\mu 2}$. The resulting cross section as a function of p_T^{min} is shown in Figure 4, where similar CDF [6] measurements using inclusive leptons are shown for comparison. Details of this work can be found in ref. [7] and in the Ph.D. thesis of V. Oguri and J.G.R. Lima [8]

4 Inclusive J/ψ Cross Section

4.1 Event Selection

For the J/ψ study it was required that the events have at least two muons at both Level 1 and Level 2 trigger, with $p_T^\mu > 3$ GeV at Level 2. The data for this analysis were taken during normal high luminosity runs, and correspond to a total integrated luminosity of $6.6pb^{-1}$. It represents a totally independent sample from the one used for the single muon analysis.

4.2 Data Analysis

In the offline analysis two good quality muons were required in the fiducial volume $|\eta| < 1.0$ with a dimuon transverse momentum $p_T^{\mu\mu} > 8$ GeV. In addition, both muons were required to be consistent with the recon-

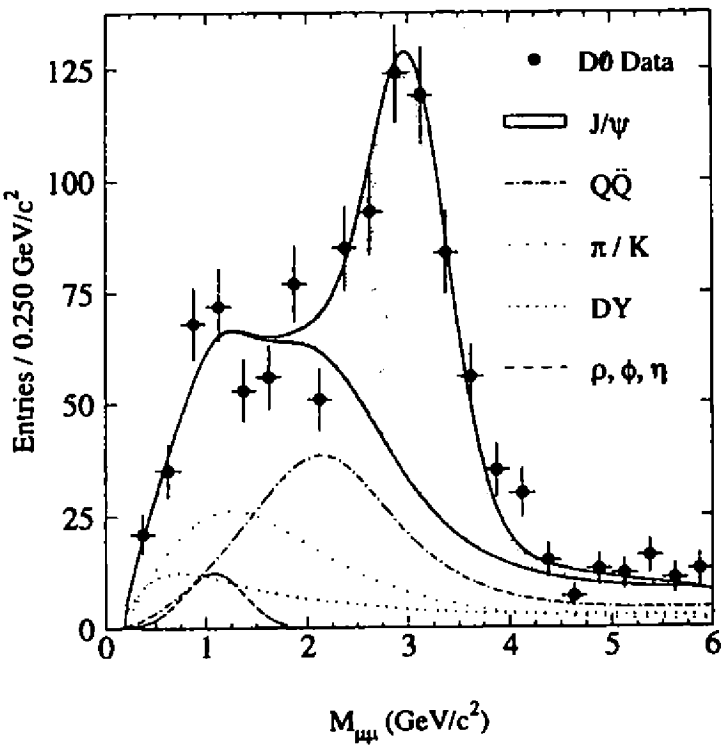

Figure 5. The mass spectum for opposite sign muon pairs. The solid curve is the fitted sum of the J/ψ signal and background contributions.

structed vertex position, to have a calorimeter energy deposition consistent with a minimum ionizing particle and not be back to back in η and ϕ ($\Delta\theta <$ 170° and $\Delta\phi <$ 160°) to avoid cosmic background contamination. In view of our modest dimuon mass resolution, $\approx$ 12% at the J/ψ mass, we limit the invariant mass of this analysis to $M_{\mu\mu} < 6GeV/c^2$

4.3 Results and Discussion

Muons coming from leptonic decays of b quarks are associated with jets, while Drell-Yan processes and direct charmonium production yield muons isolated from jets. Other mechanism that generate isolated dimuons is the decay of light quark mesons, such as ρ, ϕ, and η.

Isolated dimuons are defined such that neither muon is associated with a jet with $E_T > 8$ GeV, within 0.7 in η,ϕ space. If one or both of the muons are within a jet, the muon pair is defined to be non-isolated. For non-isolated dimuons we define $p_T^{\mu\mu}{}_{\rm rel}$ as the transverse momentum of the dimuon with respect to the associated jet.
For each of the dimuon production processes mentioned above, we generated a sample of Monte Carlo events using the ISAJET program. To estimate the relative contribution of each process we applied a maximum likelihood fit to the invariant mass($M_{\mu\mu}$), Isolation and $p_T^{\mu\mu}{}_{\rm rel}$ distributions. The results are shown in Fig. 5. The total estimated number of J/ψ events is 407±28, of which 147±33 are isolated.

The inclusive J/ψ production cross section as a function of transverse momentum is shown in Fig. 6. The data points are shown with statistical and p_T dependent systematic errors added in quadrature. Also plotted are theoretical predictions [9]. They agree with our measurement within the total experimental and theoretical uncertainty but tend to be less steeply falling with p_T.

To determine the fraction f_b of J/ψ from B meson decays, we have examined the distribution of the impact

parameter of the muons relative to the event vertex, in the $r - \phi$ plane. We have performed a simultaneous mass and impact parameter maximum likelihood fit to the opposite sign dimuon data. The resulting value of the J/ψ b fraction from this fit is $f_b = 0.35 \pm 0.09(stat) \pm 0.10(syst)$. Using this fraction, we determine the b quark cross section using the same method explained for the single muon data. The resulting integrated cross section as a function of p_T^{min} is shown in Fig. 7 together with the inclusive muon results.

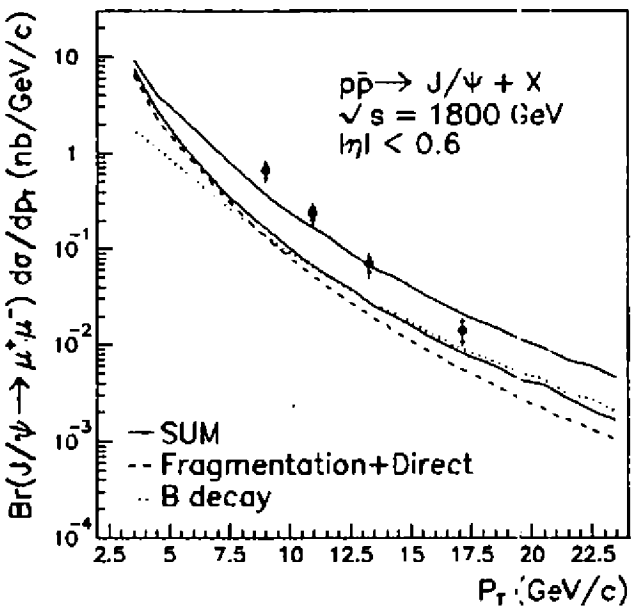

Figure 6. Inclusive J/ψ cross section times Branching Ratio into muons.

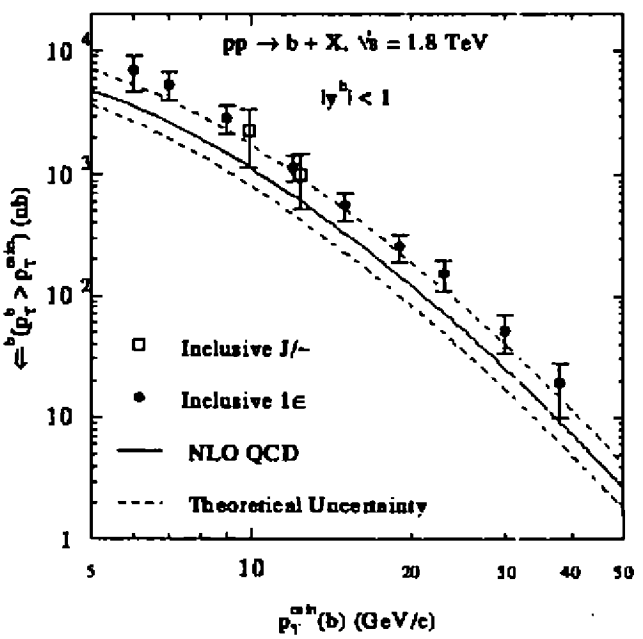

Figure 7. Integrated b quark production cross section vs p_T^{min}. The curve represents the QCD NLO prediction of NDE, Ref. [1].

5 $B^\circ - \bar{B}^\circ$ Mixing

$B^\circ - \bar{B}^\circ$ mixing can occur in the Standard Model through the well-known box diagrams, which result from the non-conservation of quark flavor in the weak interaction.

In the case of semileptonic decay of B mesons into muons, the time averaged mixing probability χ can be writen as

$$\chi = \frac{P(B^0 \to \overline{B^0} \to \mu^- X)}{P(B^0 \to \mu^+ X) + P(B^0 \to \overline{B^0} \to \mu^- X)} \tag{2}$$

which is an average over both B_d^0 and B_s^0 mesons.

Experimentally, one measures the ratio R of like to unlike sign dimuons. In order to extract χ from R it is necessary to model the relative contributions of all processes which contribute to dimuon production.

5.1 Event Selection

The data set used in this preliminary analysis was collected using both a dimuon and a single muon plus jet trigger. The dimuon trigger was the same used for the J/ψ analysis, while the muon plus jet trigger required one muon candidate in $|\eta| < 1.7$ with $p_T^\mu > 3$ GeV/c, and one reconstructed jet in $|\eta| < 3.5$ with $E_T^{jet} \geq 10$ GeV. The corresponding integrated luminosity for these triggers was 10.3 pb^{-1} .

5.2 Data Analysis

The offline requirements for this analysis were essentially the same as for the J/ψ case, except for the dimuon invariant mass, required to be between 6 GeV and 40 GeV, in order to remove events from J/ψ and Z^0 decay. Correcting for the estimated cosmic ray background, we find the ratio of like to unlike sign dimuons to be

$$R = \frac{likesign}{unlikesign} = 0.43 \pm 0.07(stat) \pm 0.05(syst) \tag{3}$$

The relative contributions of the different dimuon production processes were determined using ISAJET Monte Carlo plus the full DØ detector and trigger simulations. Sources of systematic error to the relative fractions given by Monte Carlo were investigated using checks from the data wherever possible.

5.3 Results and Discussion

Combining the experimental parameter R, as given above, with the relative fractions of the dimuon production processes, we determine the time and flavor averaged mixing probability to be

$$\chi = 0.09 \pm 0.04(stat) \pm 0.03(syst) \tag{4}$$

The measured value for χ is in agreement with other recent experimental results from UA1, CDF and LEP [10] as shown in Fig. 8.

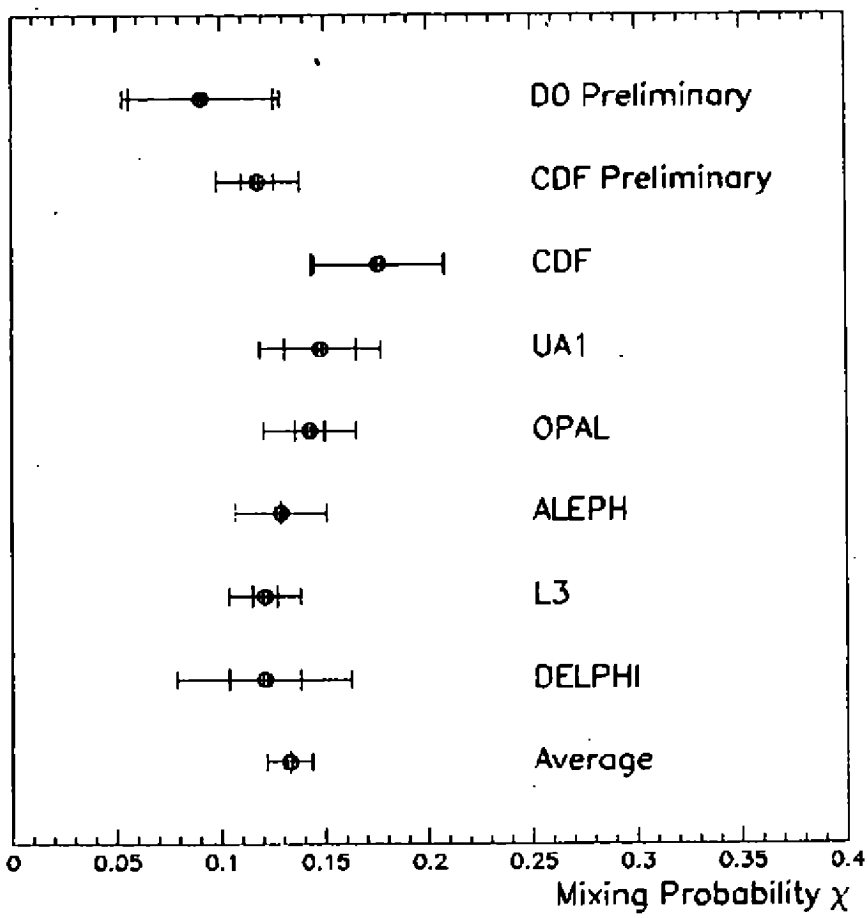

Figure 8. Mixing probability measurements. The average does not include the preliminary DØ and CDF results.

6 Summary

The DØ experiment has completed several analysis with data from its first run, using nearly 15 $pb^{-1}$of data. We have measured the inclusive muon and the inclusive J/ψ cross-sections, and extracted from them the b quark cross section. The cross section results in both cases are in general agreement with the values expected from QCD calculations in the next to leading order. Preliminary results for $B^0 - \bar{B}^0$ mixing were also obtained using muons to tag the heavy flavor decay. The measured value for the averaged mixing probability is in agreement with recent results from other experiments. Searches for Υ, χ states, as well as for additional particles such as K^0_S and Λ associated with the J/ψ are in progress. We expect to increase our statistics by a factor of 5-10 using new data coming from the second run (Run 1b) scheduled to end by february 1996.

Several upgrades of the DØ detector are scheduled for the Main Injector era, near 1998, including a new Silicon Vertex Detector and a central magnetic field, which will improve both the momentum resolution and the capability to detect the secondary vertex from beauty decays. These improvements will enhance our B-Physics program for the future, with the addition of exclusive decay channels, search for rare B decays, CP violation and much more.

7 Acknowledgements

We would like to thank the technical staff of Fermilab and other collaborating institutions for their support. Funding has been provided by the U.S. Department of Energy, the U.S. National Science Foundation, the CNPQ in Brazil, the Colciencias in Columbia, the Commissariat a l' Energie in France, the State Committee for Atomic Energy in Russia and the Department of Energy in India.

References

[1] P. Nason, S. Dawson and R. K. Ellis, Nucl. Phys. **B303** (1988) 607; **B327** (1989) 49. W. Beenaker, H. Kuijf, W. L. van Neervan and J. Smith, Phys. Rev. **D40** (1989) 54. W. Beenaker, W. L. van Neervan, R. Meng, G. Schuler and J. Smith, Nucl. Phys. **B351** (1991) 507.

[2] S. Abachi *et al.*, "The DØ Detector", NIM **A338** (1994) 185

[3] K. Hikasa *et al.*, Review of Particle Properties, Particle Data Group Phys. Rev. **D45** (1992) III.84.

[4] F. Paige and S. Protopopescu, BNL Report no. BNL38034, 1986 (unpublished), release v 7.0.

[5] UA1 Collaboration, C. Albajar *et. al.*, Phys. Lett. **B213**, 405 (1988); **B256**, 121 (1991).

[6] CDF Collaboration, F. Abe *et. al.* , Phys. Rev. Lett. **68**, 3403 (1992); **69**, 3704 (1992); **71**, 500, 2396, 2537 (1993); Phys. Rev. D **50**, 4252 (1994).

[7] S. Abachi *et al.*, Phys. Rev. Lett., **74** (1995) 3548

[8] V. Oguri, Ph.D. Thesis, Centro Brasileiro de Pesquisas Físicas, August 1995(unpublished)
J.G.R. Lima, Ph.D. Thesis, Centro Brasileiro de Pesquisas Físicas, May 1995(unpublished)

[9] M. Mangano, P. Nason and G. Ridolfi, Nucl. Phys. **B373** (1992) 295

[10] C. Albajar *et al.*, Phys. Lett **B262** (1991) 171
F. Bedeschi (CDF collaboration), *Proc. of the 10th Topical Workshop on Proton-Antiproton Collider Physics*, Fermilab (1995)
P. Abreu *et al.*, Phys. Lett. **B301** (1993) 145

Geometrical sketch for an extended Einstein-Cartan theory

M. F. Borges
UNESP - Campus de São José do Rio Preto
DCCE - Caixa Postal 136
15.054-000 - São José do Rio Preto - SP

Received March, 1996

Extended gravity theories are an embedding of Einstein's theory of gravity in a broader framework. In such theories the internal symmetries (gauge groups of Yang-Mills) and the space-time symmetries (gauge groups of Poincaré) are unified in an algebraic structure. In this way also the internal symmetries show a geometrical feature that extend the geometrical interpretation of pure gravity. In this letter geometrical structure from an extended Einstein-Cartan theory sketched on the group manifold $G = \mathcal{G} \otimes \overline{SU(2,2/1)}$ ($\mathcal{G}$, is the Yang-Mills group, a general gauge group and $\overline{SU(2,2/1)}$ is the appropriate contracted supergravity group).

I Geometrical Einstein-Cartan Theory

The group manifold of our extended Einstein-Cartan Theory (ECT) is determided by the fact that this theory is directly coupling to the supergravity. The group of the theory turns out then to be the diret product between that of supergravity and a general gauge group , with r parameters:

$$G = \mathcal{G} \otimes \overline{SU(2,2/1)}$$

In the supergravity case it is shown that exists a gauge invariance of the theory with respect to:

$$H = SO(1,4) \otimes U(1)$$

Then, the coupling between ECT and supergravity acquires a bundle structure, where,

$$H' = \mathcal{G} \otimes SO(1,4) \otimes U(1)$$

will be the fibre, and the quocient space

$$\frac{G}{H'}$$

the base space of the principal fibre bundle.

As the ECT in five dimensions has a gauge invariance with respecto to H', then by expressing the 2-form (curvature associated to the gauge group $\mathcal{G}$) in the whole multiplet of 1-forms, we obtain that:

$$\begin{aligned} F &= F_{BC}\mu^B \wedge \mu^C \\ &= F_{ab,G}\omega^{ab} \wedge \mu^G + F_{\gamma,G}\psi^\gamma \wedge \mu^G + F_{ij}V^i \wedge V^j + F_{\Theta,G}B \wedge \mu^G \end{aligned}$$

then

$$F = F_{\gamma,G}\psi^\gamma \wedge \mu^G + F_{ij}V^i \wedge V^j, \qquad (1)$$

as consequence of,

$$F_{ab,G} = 0 \tag{2}$$

and

$$F_{\Theta,G} = 0 \tag{3}$$

We have also, as a starting point, that,

$$F_{\alpha,G} = C^{B}_{\alpha Gi,j} F^{ij}_{B}; \tag{4}$$

$C^{B}_{\alpha Gi,j}$ are constants.

The condition (4) is called Rheonomy, and it is the compatibility requirement to establish the curvature F. It is worthwhile to come back once again to N = 2 - d = 5 supergravity. For this theory the components "in" of the curvature (that is, those components with respect to the basis VV) are related to the components "out" (with respect to the basis ψV or $\psi\psi$).

From the way it has been formulated, our theory lies in superspace, that is, the fields depends on χ^{μ} and θ_A (pseudo-Majorana fermionic coordinates). We can consider the space-time M^5 as a hypersurface embedded in superspace.

The components "in" of the curvature are substantially the derivatives of the pseudo-connection along M^5, the componeuts "out" being those along orthonormal directions. The Rheonomy thereforeis equivalent to the possibility of developing all the dynamics in space-time, giving to the the theory a physical meaning. In order that the ECT, formulated in superspace, also acquires a physical meaning, it will be necessary that the derivatives "out" may be expressed in terms of the derivatives "in".

We may try to express, so, a hypothesis for the explicit relations for Θ_A ("curvatures" defined in a generalized way [1, 2]):

$$\begin{aligned}
\Theta_1 &= F \\
\Theta_2 &= D\lambda_A \\
\Theta_3 &= D\sigma \\
\Theta_4 &= DF^{ab}
\end{aligned}$$

A general hypothesis will be the following:

$$\begin{aligned}
F &= d\Lambda = F_{ab} V^a \wedge V^b + ic\overline{\lambda_A} \wedge \Gamma_m \psi_A \wedge V^m + \\
&\quad + id\epsilon_{AB}\overline{\lambda_A} \wedge \Gamma_m \psi_B \wedge V^m + if\sigma \wedge \overline{\psi_A} \wedge \psi_A; \qquad (5) \\
D\lambda_A &= \Lambda_{mA} \wedge V^m + igF_{ab} \wedge \Sigma^{ab}\psi_A + \\
&\quad + h\phi_a \wedge \Gamma^a \psi_A + itF_{ab} \wedge \epsilon_{AB}\Sigma^{ab}\psi_B + \\
&\quad + Z\phi_a \wedge \Gamma^a \epsilon_{AB}\psi B; \qquad (6) \\
D\sigma &= \phi_a \wedge V^a + ik\overline{\lambda_A} \wedge \psi_A + il\epsilon_{AB}\overline{\lambda_A} \wedge \psi_B; \qquad (7) \\
DF^{ab} &= G^{ab}_{m} \wedge V^m + in\overline{\Lambda_A}^{[a} \wedge \Gamma^{b]}\psi_A + ip\epsilon_{AB}\overline{\Lambda_A}^{[a} \wedge \Gamma^{b]}\psi_B \qquad (8)
\end{aligned}$$

where $\phi_a = \partial_a \sigma$ and $G^{ab}_{m} = \partial_m I^{ab}$.

The Rheonomy requirement (4) suggests that $C = f$, so we will make both of them egual to one.

II Conclusion

To find the remaining free parameters the integrability conditions for the equations (5 - 8) have to be apllied. Such conditions on a manifold are usually called Bianchi identities. The determination through the analysis of the Bianchi identities of a compatible system of equations for the parameters of the theory would be important for the explicit construction of ECT Lagrangean, which I expect to present in a future report.

References

[1] CASTELLANI, L.: D'AURIA, R.; FRÉ, P., "Supergravity and Superstrings. A geometric perspective", vol. 1, Mathematical Foundations, World Scientific Publishing, New Jersey, 1991.

[2] BORGES, M.F., Cartan Connexion and Curvature of a five dimensional estended gravity theory, Proceedings of the XVII CNMAC, Annual Conference on Applied Mahtematics, Vitoria, Brazil, 420-425, 1994.

Bianchi Identities for an extended five dimensional Cartan gravity theory

M. F. Borges and J. Longhi
UNESP - Campus de São José do Rio Preto
DCCE - Caixa Postal 136
15.054-000 - São José do Rio Preto - SP

Received March, 1996

In this work the explicit determination of the parameters for the curvatures of a five dimensional theory sketched in a early paper is possible through the solution of the Bianchi identities.

I Bianchi Identities

From criteria, such as, consideration of the degree of the forms, Lorentz covariance, respect of the charater of reality, dimensional analysis and factorization wich is associated to the use of the restricted basis V^a and ψ_A, a general hypothesis proposed [1] for the exterior covariant derivatives $D\lambda_A$, $D\sigma$ and DF^{ab} of a 5-dimensional manifold is the following:

$$\begin{aligned} D\lambda_A &= \Lambda_{mA}\wedge V^m + igF_{ab}\wedge\Sigma^{ab}\psi_A + \\ &\quad + h\phi_a\wedge\Gamma^a\psi_A + itF_{ab}\wedge\epsilon_{AB}\Sigma^{ab}\psi_B + \\ &\quad + Z\phi_a\wedge\Gamma^a\epsilon_{AB}\psi B; \end{aligned} \tag{1}$$

$$D\sigma = \phi_a\wedge V^a + ik\overline{\lambda_A}\wedge\psi_A + il\epsilon_{AB}\overline{\lambda_A}\wedge\psi_B; \tag{2}$$

$$DF^{ab} = G^{ab}_m\wedge V^m + in\overline{\Lambda_A}^{[a}\wedge\Gamma^{b]}\psi_A + ip\epsilon_{AB}\overline{\Lambda_A}^{[a}\wedge\Gamma^{b]}\psi_B \tag{3}$$

where $\phi_a = \partial_a\sigma$ and $G^{ab}_m = \partial_m F^{ab}$. Rheonomic symmetry and the property of factorizatiom imply that

$$\begin{aligned} dA &= F_{ab}V^a\wedge V^b + ic\overline{\lambda_A}\wedge\Gamma_m\psi_A\wedge V^m + \\ &\quad + id\epsilon_{AB}\overline{\lambda_A}\wedge\Gamma_m\psi_B\wedge V^m + if\sigma\wedge\overline{\psi_A}\wedge\psi_A; \end{aligned} \tag{4}$$

To find the remaining free parameters the integrability conditions for the equations above will be applyed [2]. Such a kind of identities on a manifold are usually called Bianchi identities. We shall adopt this nomenclature for the preceding equations, even though the last three have more than one covariant derivative. By solving the Bianchi identities for the system of equations we will find that:

$$\begin{aligned} DDF^{ab} &= D(G^{ab}_m)\wedge V^m + \frac{i}{2}G^{ab}_m\wedge\wedge\overline{\psi_A}\wedge\Gamma^m\psi_A - \\ &\quad - inD\overline{\Lambda_A}^{[a}\wedge\Gamma^{b]}\psi_A + ipD\overline{\Lambda_A}^{[a}\wedge\Gamma^{b]}\psi_B = 0 \end{aligned} \tag{5}$$

where we have already used the fact that $DV^m = \frac{1}{2}\psi_A\wedge\Gamma^m\psi_A$ and $D\psi_A = 0$ if the curvatures of SU(2,2/1) vanish.

Upon substitution of the expressions of $D(G^{ab}_m)$ and $D\overline{\Lambda}^a_A$ we obtain

$$\begin{aligned} D_nG^{ab}_m\quad & \wedge V^n\wedge V^m + inD_m\overline{\Lambda_a}^{[a}\wedge\Gamma^{b]}\psi_A\wedge V^m + \\ & + ipD_m\overline{\Lambda_B}^{[a}\wedge\Gamma^{b]}\psi_B\wedge V_m + \frac{i}{2}G^{ab}_m\wedge\overline{\psi}_A\wedge\Gamma^m\psi_A + \\ & + inD^{[a}\Lambda_{mA}\wedge V^m\wedge\Gamma^{b]}\psi_A + ngD^{[a}F_{lm}\wedge\overline{\psi}_A\wedge\Sigma^{lm}\Gamma^{b]}\psi_A + \\ & + inhD^{[a}\phi_l\wedge\psi_A\Gamma^l\Gamma^{b]}\psi_A + nt\epsilon_{AB}D^{[a}F_{lm}\wedge\psi_B\Sigma^{lm}\Gamma^{b]}\psi_A + \\ & + inz\epsilon_{AB}D^{[a}\phi_l\wedge\psi_B\Gamma^l\Gamma^{b]}\psi_A + ip\epsilon_{AB}D^{[a}\overline{\Lambda}_{mA}\wedge V^m\wedge\Gamma^{b]}\psi_A + \\ & + pg\epsilon_{AB}D^{[a}F_{lm}\wedge\overline{\psi_A}\wedge\Sigma^{lm}\Gamma^{b]}\psi_B + iph\epsilon_{BC}D^{[a}\phi_l\wedge\overline{\psi_A}\wedge\Gamma^l\Gamma^{b]}\psi_C + \\ & + pt\epsilon_{AB}\epsilon_{AC}D^{[a}F_{lm}\wedge\psi_B\wedge\Sigma^{lm}\Gamma^{b]}\psi_C + \\ & + ipz\epsilon_{AB}\epsilon_{AC}D^{[a}\phi_l\wedge\psi_B\wedge\Gamma^l\Gamma^{b]}\psi_C = 0 \end{aligned}$$

The projection on two fünfbeins leads to

$$D_{[n}D_{m]}F^{ab} = 0 \tag{6}$$

By picking those terms containing $\Sigma\Gamma$ and $\Gamma\Gamma$ and developing them in the basis of Dirac matrices, one finds that

$$D^m F^{ab} - 2(ng + pk)D^{[a}F^{b]m} = 0 \tag{7}$$

which coincides with the homogeneous Maxwell equations

$$G_{[ab/m]} = 0, \tag{8}$$

and one then has $ng + pt = 1$ and

$$\frac{1}{2}(pg - nt)\epsilon^{cdlm[b}D^{a]}F_{cd} + 2(ph - nz)\eta^{n[b}D^{a]}\phi^l = 0 \tag{9}$$

In order that the relationship (9) be satisfied without requiring the validity of non-physically acceptable relations betwwen the derivatives of different fields, it is necessary that; $pg - nt = 0$ and $ph - nz = 0$

We have therefore obtained the first three relations among the parameters of the curvatures. By using (2) and working in zero supergravity, one has

$$\begin{aligned} DD\sigma \;=\; & D_a\phi_b \wedge V^a \wedge V^b + ikD_a\overline{\lambda}_A \wedge \psi_A \wedge V^a + \\ & + il\epsilon_{AB}D_a\overline{\lambda}_A \wedge \psi_B \wedge V_a + \frac{i}{2}\phi_a \wedge \overline{\psi}_A \wedge \Gamma^a\psi_A + \\ & + ik\overline{\Lambda}_{mA} \wedge V^m \wedge \psi_A + kgF_{ab} \wedge \overline{\psi}_A \wedge \Sigma^{ab}\psi_A + \\ & + ikh\phi_a \wedge \overline{\psi}_A\Gamma^a\psi_A + kt\epsilon_{AB}F_{ab} \wedge \overline{\psi}_B \wedge \Sigma^{ab}\psi_A + \\ & + ikz\epsilon_{AB}D^{[a}\phi_a \wedge \overline{\psi}_B\Gamma^a\psi_A + il\epsilon_{AB}\overline{\Lambda}_{mA} \wedge V^m \wedge \psi_B + \\ & + lg\epsilon_{AB}F_{ab} \wedge \overline{\psi_A} \wedge \Sigma^{ab}\psi_B + ilh\epsilon_{AB}\phi_a \wedge \overline{\psi_A} \wedge \Gamma^a\psi_B + \\ & + lt\epsilon_{AB}\epsilon_{AC}F_{ab} \wedge \overline{\psi}_B \wedge \Sigma^{ab}\psi_C + \\ & + il z\epsilon_{AB}\epsilon_{AC}\phi_a \wedge \overline{\psi}_B \wedge \Gamma^a\psi_C = 0 \end{aligned}$$

Where use has been made of the developments for $D\phi^a$ and $D\overline{\Lambda}_A$. As in the preceding case, one does not get any information from the projections over VV and ϕV. We have only to examine the terms containing two ϕ's. By separating those with $\overline{\psi_A}\Gamma_a\psi_A$ and $\overline{\psi_A}\Sigma^{ab}\Psi_A$, one gets

$$\frac{i}{2}\phi_a \wedge \overline{\psi_A} + ikh\phi_a \wedge \overline{\psi}_A \wedge \Gamma^a\psi_A + ilz\epsilon_{AB}\phi_a \wedge \overline{\psi}_B \wedge \Gamma^a\psi_A = 0 \tag{10}$$

Whereby it follows that $1/2 + kh + lz = 0$ and

$$kt\epsilon_{AB}F_{ab} \wedge \overline{\psi}_B \wedge \Sigma^{ab}\psi_A + lg\epsilon_{AB}F_{ab} \wedge \overline{\psi}_A \wedge \Sigma^{ab}\psi_B = 0 \tag{11}$$

and then a new equation for the parameters $kt - g = 0$.

By following a reasoning analogous to the previous two which we have presented, we develop the Bianchi identities for DA and $D\lambda_A$, and we can thereby find the remaining equations for the parameters of the curvatures. There will be compatibility among the equations. Therefore the hypothesis made for the curvatures is acceptable: a more restrictive hypothesis could imply the non-solvability of the system.

II Conclusions

The determination, through the analysis of the Bianchi Identities, of a compatible system of equations for the parameters of the theory indicates that the hypotesis made for them is acceptable, and that Rheonomy can infact be regarded, in this case, as an underlying symmetry; Some calculations in supergravity [3] may be performed by using a simbolic manipulation package, written in Reduce. A program called SUPERGRAV, written in Reduce 3.2 for the manipulation of differential forms of arbitrary degrees, in arbitrary representations of the Lorentz group, and in whatever space-time dimension, can assist in computing the step by step intermediate results. A further development of this present work can be that of verifying if SUPERGRAV can be used to implement The Bianchi identities in theories of Yang-Mills type.

References

[1] CASTELLANI, L., D'AURIA, P., FRE, R. Supergravity and superstrings, vol. 2, Supergravity, World Scientific Publishing, New Jersey, 1991.

[2] D'AURIA, R. and FRE, P. Geometric supergravity in d=11 and its hidden supergroup. Nucl. Phys. B201, 101, 1982.

[3] CASTELLANI, L. Supergrav-A reduce package for bose-fermi exterior calculus and the construction of supergravity actions. International Journal of Modern Physics A,3,6,1.435, 1988.

Density perturbations in Kaluza–Klein theory during a de Sitter phase

Júlio César Fabris* and Mairi Sakellariadou**

**Departamento de Física*

Universidade Federal do Espírito Santo - UFES, Av. Fernando Ferrari s/n, CEP 29060-900, Vitória - ES, Brazil

**Institut für Theoretische Physik*

der Universität Zürich, Winterthurerstr. 190, CH-8057 Zürich, Switzerland

June 21, 1996

The Einstein evolution equations for linear perturbations on a background consisting of a homogeneous isotropic universe filled with a perfect fluid, which is described by a barotropic equation of state of the form $p = -\rho$ and obeying conservation of energy-momentum tensor, lead to the vanishing of density fluctuations. This basically means that, in the Standard Cosmological Scenario, within the framework of general relativity, there are no density perturbations during de Sitter phase. There are three ways that one can attempt to get non-zero density perturbations during a de Sitter phase of the evolution of the universe, namely, either to consider theories where the energy–momentum is not conserved, or to remove the condition of a perfect fluid, or, as in our approach, to work with multi-dimensional theories. We will consider here the third choice.

The Lagrangian density in a n–dimensional spacetime, coupling gravity to ordinary matter, is

$$L = \frac{1}{16\pi\tilde{G}}\sqrt{-\tilde{g}}(R) - L_m \ , \tag{1}$$

where a tilde refers to the multidimensional quantities. From this expression, we can deduce the field equations in higher dimensions

$$R_{AB} - \frac{1}{2}g_{AB}R = 8\pi\tilde{G}T_{AB} \ , \tag{2}$$

$$T^{AB}{}_{;B} = 0 \ . \tag{3}$$

It will be supposed that each spatial section is divided into two spaces, the external one of dimension d_1 and the internal one of dimension d_2, such that $n = 1 + d_1 + d_2$. We assume the metric to be of the form

$$ds^2 = -dt^2 + a(t)^2\gamma_{ij}dx^i dx^j + b(t)^2\gamma_{ab}dx^a dx^b \ , \tag{4}$$

where γ_{ij} is the external metric and γ_{ab} the internal one, and both spatial sections have a constant curvature, not necessarily zero. Normalizing the curvature, we write $k_1 = -1$, 0 or 1 and $k_2 = -1$, 0 or 1 for the curvatures of the spaces with dimensions d_1 and d_2 respectively.

We consider an anisotropic energy–momentum tensor, with different pressures in each subspace. Thus, it takes the

*Current address: Université de Genève, Département de Physique Théorique, 24 quai Ernest Ansermet, CH-1211 Genève, Switzerland; e-mail address: mairi@karystos.unige.ch

form

$$T^{AB} = (\rho+\bar{p})u^A u^B - p_1 u^i u^{(A}\delta_i^{B)} - p_2 u^a u^{(A}\delta_a^{B)} - \bar{p}g^{AB} + \frac{p_1}{2}g^{i(A}\delta_i^{B)} + \frac{p_2}{2}g^{a(A}\delta_a^{B)} , \quad (5)$$

where $i = 1,\ldots,d_1$; $a = 1,\ldots,d_2$; $\bar{p} = \frac{1}{2}(p_1+p_2)$; $u^{(A}u^{B)} = \frac{1}{2}(u^A u^B + u^B u^A)$. We consider that both pressures have a barotropic equation of state: $p_1 = \alpha_1\rho$ and $p_2 = \alpha_2\rho$.

Then, the differential equations we obtain from Eqs. (2) and (3), relating $a(t)$, $b(t)$ and ρ are

$$d_1\frac{\ddot{a}}{a} + d_2\frac{\ddot{b}}{b} = -\frac{8\pi G}{d_1+d_2-1}\left[d_1(1+\alpha_1) + d_2(1+\alpha_2) - 2\right]\rho \quad ; \quad (6)$$

$$\frac{\ddot{a}}{a} + (d_1-1)(\frac{\dot{a}}{a})^2 + d_2\frac{\dot{a}}{a}\frac{\dot{b}}{b} + (d_1-1)\frac{k_1}{a^2} = \frac{8\pi G}{d_1+d_2-1}\left[1-\alpha_1+d_2(\alpha_1-\alpha_2)\right]\rho \quad ; \quad (7)$$

$$\frac{\ddot{b}}{b} + (d_2-1)(\frac{\dot{b}}{b})^2 + d_1\frac{\dot{a}}{a}\frac{\dot{b}}{b} + (d_2-1)\frac{k_2}{b^2} = \frac{8\pi G}{d_1+d_2-1}\left[1-\alpha_2+d_1(\alpha_2-\alpha_1)\right]\rho \quad ; \quad (8)$$

$$\dot{\rho} + d_1(1+\alpha_1)\frac{\dot{a}}{a}\rho + d_2(1+\alpha_2)\frac{\dot{b}}{b}\rho = 0 . \quad (9)$$

Some special solutions for these equations were found by Sahdev [1].

We now proceed with the perturbative level. We introduce in Eqs. (2) and (3) the quantities $\tilde{g}_{AB} = {}^0g_{AB} + h_{AB}$, $\tilde{\rho} = {}^0\rho + \delta\rho$, $\tilde{p} = {}^0p + \delta p$, where ${}^0g_{AB}$, ${}^0\rho$ and ${}^0p$ represent the background solutions while h_{AB}, $\delta\rho$ and δp are small perturbations around them. We will also impose that the perturbations behave spatially like plane waves. Due to the anisotropy of the space, the equations take a tractable form only if the wave is defined in just one space. So, we will consider that all perturbed functions depend only on the coordinate of the external space, *i.e.*, $\delta(x_i,t) = \delta(t)\exp(i\vec{q}\cdot\vec{x})$, where x_i denote the coordinates in the space of dimension d_1.

We will impose the synchronous coordinate condition [2],

$$h_{A0} = 0 . \quad (10)$$

We define $h = h_k{}^k/a^2$, $H = h_a{}^a/b^2$, $\Delta = \delta\rho/\rho$. After a long but straightforward calculation, we obtain from Eqs. (6) – (9) the following system of differential equations

$$\ddot{h} + 2\frac{\dot{a}}{a}\dot{h} + \ddot{H} + 2\frac{\dot{b}}{b}\dot{H} = 2\left(d_1\frac{\ddot{a}}{a} + d_2\frac{\ddot{b}}{b}\right)\Delta \quad ; \quad (11)$$

$$\ddot{H} + (d_1\frac{\dot{a}}{a} + 2d_2\frac{\dot{b}}{b})\dot{H} + \left[\frac{q^2}{a^2} - 2(d_2-1)\frac{k_2}{b^2}\right]H = -d_2\frac{\dot{b}}{b}\dot{h} + 2d_2\left[\frac{\ddot{b}}{b} + (d_2-1)(\frac{\dot{b}}{b})^2 + d_1\frac{\dot{a}}{a}\frac{\dot{b}}{b} + (d_2-1)\frac{k_2}{b^2}\right]\Delta \quad ; \quad (12)$$

$$\dot{\Delta} + (1+\alpha_1)\delta u^i{}_{,i} + \frac{1}{2}(1+\alpha_1)\dot{h} + \frac{1}{2}(1+\alpha_2)\dot{H} = 0 ; \quad (13)$$

$$(1+\alpha_1)\delta\dot{u}^i + (1+\alpha_1)\left[(2-d_1\alpha_1)\frac{\dot{a}}{a} - d_2\alpha_2\frac{\dot{b}}{b}\right]\delta u^i = -\frac{1}{2}(\alpha_1-\alpha_2)H^{,i} - \alpha_1\Delta^{,i} \quad . \quad (14)$$

These equations describing the evolution of scalar perturbations, are too complicated to be solved in the general case. We will solve them in two particular cases, where the external space is in a de Sitter phase. The two cases are the following:

(i) The external space is a de Sitter flat space filled with a perfect fluid described by $p_1 = -\rho$. Both the external and the internal spaces have scale factors with a power-law behaviour, $a \propto t^r$ $(r > 0)$ and $b \propto t^s$, respectively. The internal space is also flat. To get a non-vanishing $\delta\rho/\rho$, the set of equations describing the evolution of density perturbations requires $\alpha_2 \neq -1$. On the other hand, the background equations and the energy conservation equation imply

$$s = \frac{2}{d_2(1+\alpha_2)} ; \tag{15}$$

$$r = \frac{d_2 s(s-1)}{d_2 s + d_1 - 1} . \tag{16}$$

One can easily check that Eqs. (11) - (14) imply

$$\Delta = -\frac{1}{2}(1+\alpha_2)H + const \tag{17}$$

and lead to the following third order equation for H :

$$\begin{aligned} H''' + H''\frac{1}{\eta(1-r)}\Big[d_1 r + d_2 s - r + 1\Big] \\ + H'\left[q^2 + \frac{1}{[\eta(1-r)]^2}\{d_1(r^2+2r) + d_2 s(2+3r-2s) - r^2 - 2\}\right] \\ + H\left[\frac{q^2}{\eta(1-r)} + \frac{2}{[\eta(1-r)]^3}\{d_1 r^2 + d_2 s(2r-s) - 2r + 1\}\right] = 0, \end{aligned} \tag{18}$$

where primes denote partial derivatives w.r.t. conformal time η, defined by $a d\eta = dt$. After some manipulations, we obtain that, as far as time evolution is concerned, Eq. (18) reduces to the second order equation

$$\begin{aligned} \frac{d^2 g}{d\tau^2} + \frac{1}{\tau}\frac{dg}{d\tau} + g\Big[1 - \frac{1}{\tau^2}\frac{1}{4(1-r)^2}\{1 + r^2(d_1^2 - 4d_1 + 4) \\ + s^2 d_2(d_2+8) - r(6d_1 - 4) - 6d_2 s + 2rs d_2(d_1 - 6)\}\Big] = 0 , \end{aligned} \tag{19}$$

where

$$g = \Big[H\eta^{1/(1-r)}\Big]' \tau^\gamma ; \tag{20}$$

$$\gamma = \frac{3 - d_1 r - d_2 s}{2(r-1)} ; \tag{21}$$

$$\tau^2 = q^2\eta^2 . \tag{22}$$

Equation (19) is a Bessel equation, whose solutions are Bessel functions of order

$$\nu = \frac{d_2^4 s^4 + 2d_2^3 s^3(s+2) + d_2^2 s^3(s+4) + 8d_2^2 s^2 + 4d_2 s(s+2) + 4}{4[d_2 s(2-s) + 2]^2} . \tag{23}$$

This expression simplifies a lot if $d_1 = 3$ and $d_2 s = -1$, which means that the external space grows like t^r with $r > 1$, while the internal one goes like t^s where $s < 0$. In that case,

$$\nu = \frac{r}{2(1-r)} = -\frac{1+d_2}{2} . \tag{24}$$

The general solution of Eq. (19) is

$$g(\tau) = uJ_\nu(\tau) + vJ_{-\nu}(\tau) , \tag{25}$$

where u and v are arbitrary constants. For the sign in the argument of the Bessel functions we choose $\tau = +q\eta$.

In terms of the density contrast, we find

$$\Delta = -\frac{1}{2}(1+\alpha_2)\eta^{\frac{1}{\gamma-1}} q^\gamma \int \eta^{-\gamma}\Big(uJ_\nu(q\eta) + vJ_{-\nu}(q\eta)\Big)d\eta. \tag{26}$$

For the particular case we are considering here, and reexpressing the solutions in terms of the cosmic time t, we find the asymptotic behaviour for Δ, for $t \to 0$ ($\eta \to \infty$) and $t \to \infty$ ($\eta \to 0$), namely

$$t \to 0 \Longrightarrow \Delta \to t^{-\frac{d_2+2}{2d_2}}(c_1 \cos t^{-\frac{1}{d_2}} + c_2 \sin t^{-\frac{1}{d_2}}), \tag{27}$$

$$t \to \infty \Longrightarrow \Delta \to t^{\frac{-d_2-6\pm 2(d_2+1)}{2d_2}}. \tag{28}$$

So, initially the density contrast has an oscillatory behaviour with decreasing amplitude, while asymptotically it tends only to decreasing modes.

(ii)The external space is a de Sitter flat space filled with a perfect fluid described by $p_1 = -\rho$, and its scale factor goes like $a \propto e^{rt}$, where r is a constant. The internal space has dimensions $d_2 > 3$, constant non-zero curvature and constant scale factor. The energy conservation equation implies $\rho = const$ and the background equations lead to $d_2 < 2/(1+\alpha_2)$. To get a non-zero $\delta\rho/\rho$, the perturbation equations require $\alpha_2 \neq -1$. The system of equations describing the evolution of the scalar perturbations simplifies to :

$$\ddot{h} + 2r\dot{h} + \ddot{H} = 6r^2\Delta\ ; \tag{29}$$

$$\ddot{H} + d_1 r\dot{H} - \left[2(d_2-1)\frac{k_2}{b_2} - \frac{q^2}{e^{2rt}}\right]H = (d_2-1)\frac{k_2}{b^2}\Delta d_2\ ; \tag{30}$$

$$\dot{\Delta} + \frac{1}{2}(1+\alpha_2)\dot{H} = 0\ ; \tag{31}$$

$$\Delta_{,i} + \frac{1}{2}(1+\alpha_2)H_{,i} = 0\ . \tag{32}$$

Clearly, Eqs. (30) - (32) again imply

$$\Delta = -\frac{1}{2}(1+\alpha_2)H + const\ . \tag{33}$$

To get a growing solution of Eq. (30), assuming that the (q^2/e^{2rt})-term will soon become negligible, we find the same requirement as the one imposed by the energy conservation equation, namely

$$d_2 < \frac{2}{1+\alpha_2}\ . \tag{34}$$

Then, the solution for the density perturbation is

$$\Delta = -\frac{1}{2}(1+\alpha_2)\exp\left\{\left[-d_1\frac{r}{2} + \sqrt{(d_1\frac{r}{2})^2 + (d_2-1)\frac{K_2}{b^2}\{2-(1+\alpha_2)d_2\}}\right]t\right\}\ , \tag{35}$$

which exhibits an exponential growth.

References

[1] D. Sahdev, *Phys. Rev.* D30, 2495 (1984).

[2] E.M. Lifshitz and I.M. Khalatnikov, *Advances Phys.*, 12, 185 (1963).

Universo Primordial com Fase de Contração

Flávio Gimenes Alvarenga e Júlio César Fabris
Departamento de Física
Universidade Federal do Espírito Santo - UFES
CEP 29060-900, Vitória, ES, Brazil

June 21, 1996

1 Introdução

Os problemas do Modelo Padrão (problemas do horizonte e entropia) são normalmente tratados através de uma fase inflacionária, onde a condição da energia forte é violada durante um breve período de tempo após o big bang, enquanto o fator de escala do Universo aumenta exponencialmente.

Um cenário completamente diferente pode ser traçado se a condição da energia forte for violada desde o começo. Tal violação pode ser efetuada mediante o acoplamento não trivial da gravitação a dois campos escalares. Neste caso, o Universo exibe uma singularidade inicial, mas a distância própria entre quaisquer dois pontos do espaço-tempo é infinita. Existe inicialmente uma breve fase de contração, que persiste até o momento em que o fator de escala do Universo atinja um valor mínimo a partir do qual segue uma fase de expansão que resgata a cosmologia padrão. Este cenário cosmológico primordial, o qual denominamos de cenário anti-big bang, é obtido para valores negativos do "parâmetro de Brans-Dicke" ω em uma teoria de gravitação acoplada a dois campos escalares.

2 Descrição do Modelo

A extensão da ação de Brans-Dicke a fim de incluir o efeito de um segundo campo escalar acoplado minimamente à gravitação, mas não minimamente ao primeiro campo escalar, pode ser escrita como

$$A = \int d^4x\sqrt{-g}\left(\frac{\phi}{16\pi G}R - \frac{\omega}{16\pi G}\frac{\phi_{;\rho}\phi^{;\rho}}{\phi} - \frac{1}{16\pi G}\frac{\Psi_{;\rho}\Psi^{;\rho}}{\phi} + L_m\right); \tag{1}$$

onde L_m é a densidade lagrangeana para todos os campos de matéria.

Desta ação extraímos as equações de campo:

$$R_{\mu\nu} - \frac{1}{2}g_{\mu\nu}R = \frac{8\pi}{\phi}T_{\mu\nu} + \frac{\omega}{\phi^2}(\phi_{;\mu}\phi_{;\nu} - \frac{1}{2}g_{\mu\nu}\phi_{;\rho}\phi^{;\rho})$$

$$+ \frac{1}{\phi}(\phi_{;\mu;\nu} - g_{\mu\nu}\Box\phi) + \frac{1}{\phi^2}(\Psi_{;\mu}\Psi_{;\nu} - \frac{1}{2}g_{\mu\nu}\Psi_{;\rho}\Psi^{;\rho}); \tag{2}$$

$$\Box\phi + \beta\frac{\Psi_{;\rho}\Psi^{;\rho}}{\phi} = 4\pi\beta T, \beta = \frac{2}{3+2\omega}; \tag{3}$$

$$\Box\Psi - \frac{\phi_{;\rho}\Psi^{;\rho}}{\phi} = 0 \tag{4}$$

Considerando a métrica de Robertson-Walker e o tensor fluido-perfeito, obtemos como equações de movimento:

$$3(\frac{a'}{a})^2 + 3ka^4 = 8\pi\frac{\rho a^6}{\phi} + \frac{\omega}{2}(\frac{\phi'}{\phi})^2 - 3\frac{a'}{a}\frac{\phi'}{\phi} + \frac{1}{2}(\frac{\Psi'}{\phi})^2; \tag{5}$$

$$\phi'' + \beta\frac{(\Psi')^2}{\phi} = 4\pi\beta(\rho - 3p)a^6; \tag{6}$$

$$\Psi'' - \frac{\phi'}{\phi}\Psi' = 0; \tag{7}$$

$$\rho' + 3\frac{a'}{a}(\rho + p) = 0 \tag{8}$$

Aqui a coordenada tempo foi reparametrizada:

$$dt = a^3 d\theta \tag{9}$$

Podemos agora através dos parâmetros ω e β determinar e classificar as diferentes soluções cosmológicas para este modelo.

3 Soluções Cosmológicas

A equação (7) nos fornece facilmente uma integral primeira para o campo escalar Ψ

$$\Psi' = C\phi \tag{10}$$

A obtenção de a e ϕ depende da natureza do conteúdo material do Universo. Estudaremos as soluções correspondentes a um Universo vazio e as relativas ao Universo dominado pela radiação.

3.1 Vácuo - ($\rho = 0$, $p = 0$)

Fazendo $C = 1$ e introduzindo (10) nas equações de movimento, somos levados a diferentes classes de soluções conforme o sinal do parâmetro β.

3.1.1 $\beta < 0$ $(\omega < -\frac{3}{2})$

Desacoplando as equações de movimento obtemos as seguintes soluções para ϕ e a:

$$\phi = \phi_o cosh(\sqrt{-\beta}\theta); \tag{11}$$

$$a = \frac{a_o}{\sqrt{cosh(\sqrt{-\beta}\theta)}} \frac{exp\left(\frac{\pm 1}{\sqrt{-6\beta}} tan^{-1}|sinh(\sqrt{-\beta}\theta)|\right)}{\left(1 + kexp(\pm\sqrt{\frac{8}{-3\beta}} tan^{-1}|sinh(\sqrt{-\beta}\theta)|)\right)^{\frac{1}{4}}} \tag{12}$$

Como características principais observamos que:

a) o Universo começa com um valor finito para seu fator de escala a; expande inicialmente em seus momentos iniciais, mas acaba por colapsar.

b) o campo escalar ϕ é inicialmente constante ($\theta = 0$), e cresce continuamente até explodir em tempos maiores. Este é um resultado bastante indesejável, visto que, o efeito dos campos escalares deve ter sido relevante apenas no Universo primordial.

3.1.2 $\beta > 0$ $(\omega > -\frac{3}{2})$

Novamente obtemos soluções analíticas para ϕ e a

$$\phi = \phi_o sen(\sqrt{\beta}\theta); \tag{13}$$

$$a = \frac{a_o}{\sqrt{sin(\sqrt{\beta}\theta)}} \frac{tan^{\frac{\pm 1}{\sqrt{6\beta}}}\left(\frac{\sqrt{\beta}\theta}{2}\right)}{\left(1 + ktan^{\pm\sqrt{\frac{8}{3\beta}}}\left(\frac{\sqrt{\beta}\theta}{2}\right)\right)^{\frac{1}{4}}}. \tag{14}$$

Estas soluções revelam que:

a) A evolução do Universo segundo seu fator de escala apresenta dependência do parâmetro ω. Quando $\beta > 0$ temos $\omega > -\frac{3}{2}$, contudo ω pode ser positivo ou negativo, o que pode vir a gerar cenários cosmológicos bastante distintos.

a.1) $\beta > 0 \quad (\omega > 0)$

Neste caso, o Universo está em expansão desde o seu início. Está caracterizado então um cenário do tipo big-bang.

a.2) $\beta > 0 \quad (-\frac{3}{2} < \omega < 0)$

Temos um Universo que começa infinito, contrai até que seu fator de escala atinja um valor mínimo, e então entra em uma fase de expansão. Este comportamento do Universo define um cenário do tipo anti-big bang.

b) A evolução do campo escalar mostra que o mesmo cresce nos momentos iniciais do Universo, até atingir um valor máximo e então começar a decrescer, cessando seu efeito em tempos posteriores.

Existe a possibilidade de encontrarmos dentre estas soluções tipo anti-big bang, soluções de caráter não singular na origem ($t = 0$) do Universo. Assim sendo, é conveniente realizarmos um estudo assintótico de (14) acerca do tempo $\theta \to 0$:

$$a \sim (\sqrt{\beta}\theta)^{\frac{2-\sqrt{6\beta}}{2\sqrt{6\beta}}} \quad (\theta \to 0) \tag{15}$$

O tempo cósmico t pode ser escrito como função do tempo θ

$$t \sim \frac{2\sqrt{6}}{(6-\sqrt{6\beta})} \ (\sqrt{\beta}\theta)^{\frac{6-\sqrt{6\beta}}{2\sqrt{6\beta}}} \quad (\theta \to 0); \tag{16}$$

o que nos permitirá revelar a natureza singular ou não desta solução.

Em termos do tempo cósmico t:

$$a \sim [\ \frac{6-\sqrt{6\beta}}{2\sqrt{6}}\ t\ ]^{\frac{2-\sqrt{6\beta}}{6-\sqrt{6\beta}}} \quad (\theta \to 0) \tag{17}$$

Podemos agora classificar os possíveis cenários cosmológicos segundo o parâmetro ω:

a) $\quad (2-\sqrt{6\beta}) > 0$

Temos neste caso uma classe de soluções relativa a $\beta < \frac{2}{3}$, ou ainda $\omega > 0$.

Como $(2-\sqrt{6\beta})$ é positivo, $(6-\sqrt{6\beta})$ também o será, de modo que o expoente de t em (17) é sempre positivo. Por outro lado, (16) mostra que o momento $\theta = 0$ corresponde à $t = 0$, ou seja, a singularidade inicial está presente nesta classe de soluções. Conclui-se então que para $\omega > 0$ prevalece o cenário big bang singular.

b) $\quad (2-\sqrt{6\beta}) < 0$

Existem duas possibilidades:

b.1) $\quad (2-\sqrt{6\beta}) < 0 \quad$ e $\quad (6-\sqrt{6\beta}) < 0$

Neste caso $\beta > 6$ implica em $\omega < -\frac{4}{3}$, entretanto, ω é necessariamente maior que $-\frac{3}{2}$ quando $\beta > 0$, restringindo assim uma classe de soluções para $-\frac{3}{2} < \omega < -\frac{4}{3}$.

Observe em (16) que para $\beta > 6$ o expoente em θ é negativo, o que faz o valor do tempo conforme $\theta = 0$ corresponder ao tempo cósmico $t = -\infty$. Este fato implica que para $-\frac{3}{2} < \omega < -\frac{4}{3}$ a singularidade inicial está deslocada para tempos t negativos infinitos, de modo que não existe singularidade em um tempo próprio finito. Tem-se soluções anti-big bang não singulares.

b.2) $\quad (2-\sqrt{6\beta}) < 0 \quad$ e $\quad (6-\sqrt{6\beta}) > 0$

O parâmetro β está agora restrito aos valores $\frac{2}{3} < \beta < 6$, como consequêcia temos $-\frac{4}{3} < \omega < 0$.

De (16) nós notamos que o momento inicial $\theta = 0$ corresponde à $t = 0$. Pode ser visto ainda, (17), que o fator de escala do Universo evolui segundo um expoente sempre negativo. Portanto, para $-\frac{4}{3} < \omega < 0$ temos novamente o cenário anti-big bang, mas agora o Universo tem uma origem singular em $t = 0$.

Table 1: Classificação das soluções cosmológicas.

Parâmetro β	Parâmetro ω	Cenário	
$\beta < 0$	$\omega < -\frac{3}{2}$	solução não física	
$0 < \beta < \frac{2}{3}$	$\omega > 0$	big bang	singular
$\frac{2}{3} < \beta < 6$	$-\frac{4}{3} < \omega < 0$	anti-big bang	singular
$\beta > 6$	$-\frac{3}{2} < \omega < -\frac{4}{3}$	anti-big bang	não singular

3.2 Fluido de Radiação - ($p = \rho/3$)

Ao considerarmos um Universo preenchido com um fluido de radiação somos conduzidos às seguintes soluções:

3.2.1 $\beta < 0 \quad (\omega < -\frac{3}{2}) \quad (k = 0)$

$$\phi = \phi_o cosh(\sqrt{-\beta}\theta); \tag{18}$$

$$a = \frac{a_o}{\sqrt{cosh(\sqrt{-\beta}\theta)}} \frac{exp\left(\frac{\pm 1}{\sqrt{-6\beta}} tan^{-1}|sinh(\sqrt{-\beta}\theta)|\right)}{\left(1 - exp(\pm\sqrt{\frac{2}{-3\beta}} tan^{-1}|sinh(\sqrt{-\beta}\theta)|)\right)} \tag{19}$$

3.2.2 $\beta > 0 \quad (\omega > -\frac{3}{2}) \quad (k = 0)$

$$\phi = \phi_o sin(\sqrt{\beta}\theta) \tag{20}$$

$$a = \frac{a_o}{\sqrt{sin(\sqrt{\beta}\theta)}} \frac{tan^{\frac{\pm 1}{\sqrt{6\beta}}}(\frac{\sqrt{\beta}\theta}{2})}{\left(1 - tan^{\pm\sqrt{\frac{2}{3\beta}}}(\frac{\sqrt{\beta}\theta}{2})\right)} \tag{21}$$

Uma análise detalhada destas soluções revela um comportamento semelhante ao caso vácuo, no que concerne aos parâmetros da teoria. Contudo, para um Universo radiativo podemos traçar a história térmica do Universo.

A definição da temperatura do Universo como

$$T(\theta) \propto \frac{1}{a(\theta)};$$

nos permite descrever o seu comportamento térmico, durante a evolução da solução (21), em função dos parâmetros do modelo β e ω.

Observamos os seguintes comportamentos:

$\omega < -\frac{3}{2} \rightarrow$ neste caso a temperatura do Universo inicialmente decresce, mas rapidamente passa a aumentar indefinidamente. Este comportamento contradiz as informações observacionais.

$\omega > 0 \rightarrow$ o Universo começa com uma temperatura infinita, e resfria a medida que o mesmo expande. Está caracterizado o cenário big bang.

$-\frac{3}{2} < \omega < 0 \rightarrow$ a temperatura inicial do Universo é zero, e aumenta até atingir um valor máximo, a partir do qual começa a decrescer novamente a zero. Esta temperatura máxima é obtida no momento em que o raio do Universo alcança um valor mínimo diferente de zero. Este é o cenário anti-big bang.

4 Problema do Horizonte

A existência da fase de contração no cenário anti-big bang nos possibilita sugerir uma solução alternativa para o problema do horizonte, visto que, a distância do horizonte própia pode ser uma função crescente do tempo cósmico.

A definição da distância do horizonte própia é dada por:

$$d_H = a(t)\int \frac{dt}{a(t)} = a(\theta)\int a^2(\theta)d\theta \quad . \tag{22}$$

Por simplicidade nos restringiremos ao caso $\omega > -\frac{3}{2}$, $k = 0$ e $p = \rho = 0$, o que nos fornece

$$d_H(\theta) = \sqrt{\frac{3}{2}}\frac{a_o^3}{\sqrt{sin(\sqrt{\beta}\theta)}} tan^{\pm\sqrt{\frac{3}{2\beta}}}(\frac{\sqrt{\beta}\theta}{2}). \tag{23}$$

Ao efetuarmos uma análise assintótica, nós verificaremos que d_H é uma função sempre crescente para $\omega > -\frac{4}{3}$; para $-\frac{3}{2} < \omega < -\frac{4}{3}$, d_H é inicialmente uma funcão decrescente de θ, mas torna-se crescente antes que o fator de escala do Universo atinja seu valor mínimo. Este comportamento sugere uma solução para o problema do horizonte, já que o Universo pode estar completamente envolvido pelo horizonte causal nos primeiros momentos de sua existência.

[1] C. Brans and R.H. Dicke, Phys. Rev. **124**, 925(1961);

[2] D. Dominici, R. Holman and C.W. Kim, Phys. Rev. **D28**, 2983(1983);

[3] F.G. Alvarenga and J.C. Fabris, Astrophysics and Space Science **226/1**, 109-124(1995);

[4] F. G. Alvarenga e J.C. Fabris, Classical and Quantum Gravity **12**, L69-L74(1995);

[5] F.G. Alvarenga and J.C. Fabris, *A Primordial Cosmological Scenario and the Horizon Problem*, a ser puplicado na General Relativity and Gravitation em 5/96.

PPN Constraints in a Naked Singularity Spherical Static Solution

José Pínio Baptista°, Antônio Brasil Batista° e Júlio César Fabris°
and
André Philippe Tourrenc*
°*Departamento de Física*
Universidade Federal do Espírito Santo - UFES, Av. Fernando Ferrari s/n, CEP 29060-900, Vitória - ES, Brazil
**Laboratoire de Gravitation et Cosmologie Relativistes*
Université Pierre Marie Curie, Paris, França

Received March, 1996

In recent paper[1] it was determined cosmological and static spherical symmetric exact solutions for a five dimensional theory with internal timelike dimension. Can this spherical static solution, with its non-standard properties, describes the physics at local scale, for example, at the scale of the solar system? How can we impose observational limits on the strength of the scalar fields (and as a consequence on the introduction of extra time-like dimensions)? These are the questions we want to answer here.

We will consider the three classical tests of General Relativity in the context of the above theory. We will use the Parametrized Post-Newtonian (PPN) approach.

The effective Lagrangian which comes from the dimensional reduction of the Einstein-Maxwell theory in five dimensions can be written as [1],

$$L = \sqrt{-g}\left(\Phi R + \frac{3}{2}\frac{\Psi_{;\rho}\Psi^{;\rho}}{\Phi}\right) \quad , \tag{1}$$

which leads to the following field equations:

$$R_{\mu\nu} - \frac{1}{2}g_{\mu\nu}R = -\frac{3}{2\Phi^2}\left(\Psi_{;\mu}\Psi_{;\nu} - \frac{1}{2}g_{\mu\nu}\Psi_{;\rho}\Psi^{;\rho}\right) + \frac{1}{\Phi}\left(\Phi_{;\mu;\nu} - g_{\mu\nu}\Box\Phi\right) ; \tag{2}$$

$$\Box\Phi - \frac{\Psi_{;\rho}\Psi^{;\rho}}{\Phi} = 0 ; \tag{3}$$

$$\Box\Psi - \frac{\Phi_{;\rho}\Psi^{;\rho}}{\Phi} = 0 . \tag{4}$$

The static spherical symmetric metric has the form,

$$ds^2 = B(r)dt^2 - A(r)dr^2 - r^2(d\theta^2 + sin\theta d\phi^2) \quad . \tag{5}$$

With this choice for the metric, the field equations become

$$\frac{1}{2}\frac{B''}{B} - \frac{1}{4}\frac{B'}{B}\left(\frac{B'}{B} + \frac{A'}{A}\right) - \frac{1}{r}\left(\frac{A'}{A} + 2\frac{\Phi'}{\Phi}\right) = \frac{1}{2}\frac{B'}{B}\frac{\Phi'}{\Phi} ; \tag{6}$$

$$\frac{1}{2}\frac{B''}{B} - \frac{1}{4}\frac{B'}{B}\left(\frac{B'}{B} + \frac{A'}{A}\right) + \frac{1}{r}\frac{B'}{B} = -\frac{1}{2}\left(\frac{\Psi'}{\Phi}\right)^2 - \frac{1}{2}\frac{B'}{B}\frac{\Phi'}{\Phi} ; \tag{7}$$

$$\Phi'' + \left(-\frac{1}{2}\frac{A'}{A} + \frac{1}{2}\frac{B'}{B} + \frac{2}{r}\right)\Phi' = \frac{\Psi'^2}{\Phi} ; \tag{8}$$

$$\Psi'' + (-\frac{1}{2}\frac{A'}{A} + \frac{1}{2}\frac{B'}{B} + \frac{2}{r})\Psi' = \frac{\Phi'}{\Phi}\Psi' \; ; \tag{9}$$

$$1 - \frac{r}{2A}(-\frac{A'}{A} + \frac{B'}{B}) - \frac{1}{A} = \frac{r^2}{2A}(\frac{\Psi'}{\Phi})^2 + \frac{r}{A}\frac{\Phi'}{\Phi} \; . \tag{10}$$

Equation (9) admits the first integral,

$$\Psi' = \Psi_0 u \Phi \quad , \quad u = \left(\frac{A}{B}\right)^{\frac{1}{2}} \frac{1}{r^2} \quad , \Psi_0 = cte \quad . \tag{11}$$

With the aid of (11) we obtain from (8) as

$$\Phi' = \Psi_0 u \Psi + a' \Psi_0 u \quad , \quad a' = cte \quad . \tag{12}$$

If we denote F as a primitive function of u ($F' = u$), we have

$$\Phi = ae^{\Psi_0 F} + be^{-\Psi_0 F} \quad , \tag{13}$$

$$\Psi = ae^{\Psi_0 F} - be^{-\Psi_0 F} - a' \quad . \tag{14}$$

The solution found in [1] corresponds to the case where $a = 0$, $k^2 = \Psi_0$ and $B\Phi = 1$. It leads to the expressions

$$A = \frac{x^2}{1+x^2}(\frac{x}{1+\sqrt{1+x^2}})^{\pm 2} \quad , \tag{15}$$

$$B = (\frac{x}{1+\sqrt{1+x^2}})^{\pm 2} \quad , \tag{16}$$

where $x = \frac{r}{k}$

In general, the PPN parameters are obtained by developing the static spherical symmetric metric in its isotropic form,

$$ds^2 = \bar{B}(r)dt^2 - \bar{A}(r)\left(d\bar{r}^2 + \bar{r}^2 d\theta^2 + \bar{r}^2 sin^2\theta d\phi^2\right) \quad . \tag{17}$$

The central mass field is described, in the post-Newtonian approximation, by means of a development in $\bar{B}$ and $\bar{A}$ [2]:

$$\bar{B} = 1 - 2\alpha\frac{GM}{\bar{r}c^2} + 2\beta\frac{G^2M^2}{\bar{r}^2c^4} + \ldots \; ; \tag{18}$$

$$\bar{A} = 1 + 2\gamma\frac{GM}{\bar{r}c^2} + \ldots \quad . \tag{19}$$

One can also use the standard coordinates,

$$ds^2 = B(r)dt^2 - A(r)dr^2 - r^2(d\theta^2 + r^2 sin^2\theta d\phi^2) \quad . \tag{20}$$

In this case, the PPN development takes the form,

$$B = 1 - 2\alpha\frac{GM}{rc^2} + 2(\beta - \alpha\gamma)\frac{G^2M^2}{r^2c^4} + \ldots \quad , \tag{21}$$

$$A = 1 + 2\gamma\frac{GM}{rc^2} + \ldots \quad . \tag{22}$$

The experimental values are $\alpha = \beta = \gamma \simeq 1$:

- $\alpha = 1$ permits to find the Newtonian theory in the low speed limit;
- $\beta = 1$ leads to acceptable values for the advance of the perihelion of the planets;
- $\gamma = 1$ is compatible with the observed deviations of light rays by the Sun and with the Shapiro's effect.

Among the Eddington and Robertson parameters (α, β and γ), β is experimentally known with the lower accuracy; however, its uncertainty remains smaller than 1%[3]. The General Relativity theory predicts $\alpha = \beta = \gamma = 1$

We develop now the functions B and A given by (16,15). We get,

$$B = 1 - \frac{n}{x} + \frac{n^2}{2}\frac{1}{x^2} + \dots \quad , \tag{23}$$

$$A = 1 - \frac{n}{x} + \dots \quad , \tag{24}$$

where $n = \pm 2$. The condition $\alpha = 1$ leads to $nk = 2\frac{GM}{c^2}$. So,

$$B = 1 - 2\frac{GM}{rc^2} + 2\frac{G^2M^2}{r^2c^4} + \dots \quad , \tag{25}$$

$$A = 1 - 2\frac{GM}{rc^2} + \dots \quad . \tag{26}$$

Identifying this development to (22,21) we obtain $\gamma = -1$ and $\beta = 0$. As consequence, the deviation of light rays $\Delta = 2\frac{GM}{r_0c^2}(1+\gamma)$ and the advance of the perihelion of the planets $\Delta\phi = 6\frac{GM}{L}(\frac{2-\beta+2\gamma}{3})$ are zero.

Remarkably, we have a null result for the gravitational effects of a space-time with spherical symmetry described by (16,15), in spite of the fact that this space-time is strongly curved. This suggests that the considered solutions may not describe the field of a central mass.

The field equations (10,9,8,7,6) admit as a spherical symmetric static solution $\Phi = cte$ and $\Psi = cte$, leading to

$$ds^2 = (1 - 2\frac{GM}{rc^2})dt^2 - (1 - 2\frac{GM}{rc^2})^{-1}dr^2 - r^2(d\theta^2 + sin^2\theta d\phi^2) \quad , \tag{27}$$

that is, the Schwarzschild metric in the standard coordinates. The theory under consideration can describe the field of a central mass. We can ask if this "trivial solution" is unique.

To answer this, we consider the following development for B and A:

$$B = 1 - \frac{\alpha}{x} + \frac{\beta}{x^2} + \dots \quad , \tag{28}$$

$$A = 1 + \frac{\gamma}{x} + \frac{\delta}{x^2} + \dots \quad , \tag{29}$$

where $\frac{1}{x} = 2\frac{GM}{rc^2}$. Using this relation we can rewrite the field equations (10,9,8,7,6) employing the substitutions

$$\frac{d}{dr}() = ()' \quad \rightarrow \quad \frac{d}{dx}() = ()' \quad ; \tag{30}$$

$$r \quad \rightarrow \quad x \quad . \tag{31}$$

Moreover, the substitution $\Psi_0 \rightarrow 2\Psi_0\frac{GM}{c^2}$ implies

$$\frac{d\Psi}{dx} = \Psi' = \Psi_0(\frac{A}{B})^{\frac{1}{2}}\frac{1}{x^2}\Phi \quad . \tag{32}$$

Then, we find the following developments for the terms of interest for us:

$$B = 1 - \frac{\alpha}{x} + \frac{\beta}{x^2} + O_3 \quad , \quad A = 1 + \frac{\gamma}{x} + \frac{\delta}{x^2} + O_3 \quad ; \tag{33}$$

$$\frac{B'}{B} = \frac{\alpha}{x^2} + \frac{\alpha^2 - 2\beta}{x^3} + O_4 \quad , \quad \frac{A'}{A} = -\frac{\gamma}{x^2} + \frac{\gamma^2 - 2\delta}{x^3} + O_4 \quad ; \tag{34}$$

$$\frac{B''}{B} = -2\frac{\alpha}{x^3} + \frac{6\beta - 2\alpha^2}{x^4} + O_5 \quad , \quad (\frac{\Psi'}{\Phi})^2 = \frac{\Psi_0^2}{x^4} + O_5 \quad . \tag{35}$$

Using (6) we calculate $\frac{\Phi'}{\Phi}$:

$$\frac{\Phi'}{\Phi} = \frac{\gamma - \alpha}{2}\frac{1}{x^2} + \frac{\gamma^2 - \alpha^2 + 2\beta - \Psi_0^2}{2}\frac{1}{x^3} + O_4 \quad . \tag{36}$$

Equation (9) leads to

$$(2\beta - \frac{1}{2}\alpha(\alpha - \gamma) + \Psi_0^2)\frac{1}{x^4} + O_5 = 0 \tag{37}$$

implying $2\beta - \frac{1}{2}\alpha(\alpha - \gamma) + \Psi_0^2 = 0$. If we now impose $2b - \frac{1}{2}\alpha(\alpha - \gamma) = 0$ as in General Relativity, we have $\Psi_0 = 0$. So, we find $\Phi' = 0$ and $\Psi' = 0$. We must conclude that the only solution for the theory considered that has the same post-Newtonian limit as General Relativity is the trivial one.

So, this theory can be employed at cosmological level, but it is not valable to represent the local physics, as it is tested today..

References

[1] J.P. Baptista, A.B. Batista and J.C. Fabris, Intern. J. of Mod. Phys. D2, 431(1994);

[2] S. Weinberg,**Gravitation and Cosmology**, Wiley(1972);

[3] C. Will, **Theory and Experiment in Gravitational Physics**, Cambridge University Press(1993).

On the spectrum of γ-fluids

J. A. E. Carrillo[1,*], J. A. S. Lima[2,3,†], A. Maia Jr.[4,‡]

1) Instituto de Física Gleb Wathagin - Unicamp

13.081-970 Campinas - SP - Brasil

2) Department of Physics, Brown University, Box 1843 Providence, RI 02912, USA.

3) Departamento de Física, UFRN, CP 1641, 59072-970, Natal, RN, Brasil.

4) Instituto de Matemática - Unicamp

13.081-970 Campinas - SP - Brasil.

Received March, 1996

The spectrum of massless bosonic and fermionic fluids satisfying the equation of state $p = (\gamma - 1)\rho$ is derived using elementary statistical methods. As a limiting case, the Lorentz invariant spectrum of the vacuum ($\gamma = 0, p = -\rho$) is deduced. These results are in agreement with our earlier derivation for bosons using thermodynamics and semiclassical considerations.

1 Introduction

The class of γ-fluids is the simplest kind of relativistic perfect simple fluids used in the framework of general relativity and cosmology. Such a class is usually defined in terms of so-called "γ-law" equation of state

$$P = (\gamma - 1)\rho \tag{1}$$

where $\gamma \in [0, 2]$. Some special types of media described by the the above relation are: *(i)* vacuum($p = -\rho$, $\gamma = 0$) *(ii)* a random oriented distribution of infinitely thin straight cosmic strings averaged over all directions($p = -\frac{1}{3}\rho$, $\gamma = 2/3$)*(iii)* blackbody radiation ($p = \frac{1}{3}\rho$, $\gamma = 4/3$) and *(iv)* stiff matter ($p = \rho$, $\gamma = 2$). In a series of recent papers (Lima and Santos, 1995; Lima and Maia, 1995a, 1995b), some general properties of this monoparametric family of fluids have been discussed based on thermodynamic and semiclassical considerations. In particular, we have stressed the unusual thermodynamic behavior arising when the γ parameter is smaller than unit.

In the present article, our main goal is to show how the Planckian type distribution for a γ-fluid, which has been discussed there in the framework of the old quantum theory of radiation, can be reproduced in the domain of the statistical mechanics. This allow us to extend the theory for fermions as well. Of course, the third and last step would be to derive the spectrum from a more basic theory as quantum field theory.

2 The Spectrum of γ-Fluids

Now consider the canonical procedure to compute the pressure p and the energy density ρ in elementary statistical mechanics. These quantities are defined by

$$p = kT\left(\frac{\partial \ell nQ}{\partial V}\right)_T, \quad \rho = \frac{kT^2}{V}\left(\frac{\partial \ell nQ}{\partial T}\right)_V \tag{2}$$

where ℓnQ is the grand-canonical thermodynamic potential, which corresponds to a quantum fluid in contact with a thermal reservoir at temperature T. Let us now assume that the γ-fluid behaves like a kind of radiation, which differs from blackbody radiation only due to the equation of state. It thus follows that the chemical potential of

*e-mail:espichan@ifi.unicamp.br

†e-mail:limajas@het.brown.edu

‡e-mail:maia@ime.unicamp.br

any γ-fluid must also be taken identically zero. In this case, by considering a continuous spectrum, we have the well known formula (Itzykson and Zuber, 1980)

$$\ell nQ = -V \int_0^\infty \ell n \left(1 \mp \exp(-\frac{\hbar\omega}{kT})\right) f(\omega) d\omega \tag{3}$$

where the upper and lower sign inside the big parenthesis corresponds to bosons and fermions respectively.

Our aim now is to find the unknown function $f(\omega)$, which is the density of states per energy unit. From equations (1)-(3) we get easily

$$-kT \int_0^\infty \ell n \left(1 \mp \exp(-\frac{\hbar\omega}{kT})\right) f(\omega) d\omega = (\gamma - 1)\hbar \int_0^\infty \frac{\omega f(\omega)}{\exp(\frac{\hbar\omega}{kT}) \mp 1} d\omega \tag{4}$$

The above equation points to a singularity at $\gamma = 1$. This rather pathological case("dust"), describing a zero pressure fluid will not be considered here. A partial integration on the left hand side of (4) furnishes

$$-kT\ell n \left(1 \mp \exp(-\frac{\hbar\omega}{kT})\right) F(\omega)\Big]_0^\infty + \hbar \int_0^\infty \frac{F(\omega)}{\exp(\frac{\hbar\omega}{kT}) \mp 1} d\omega \tag{5}$$

where $F(\omega)$ is a primitive of $f(\omega)$

$$F'(\omega) = f(\omega) \tag{6}$$

Let us now suppose, for a moment, that the first term in (5), which corresponds to a boundary term, vanishes. In what follows, it will become clear under which conditions the function $f(\omega)$ will fullfil such a constraint. Bearing this in mind, we may write from (5) and (6)

$$\int_0^\infty \frac{F(\omega)}{\exp(\frac{\hbar\omega}{kT}) \mp 1} d\omega = (\gamma - 1) \int_0^\infty \frac{\omega f(\omega)}{\exp(\frac{\hbar\omega}{kT}) \mp 1} d\omega \tag{7}$$

The correctness of the above equation will be guaranteed if the functions $f(\omega)$ and $F(\omega)$ obeying (7), satisfy the following relation

$$F(\omega) = (\gamma - 1)\omega f(\omega) \tag{8}$$

In principle, we can not guarantee that equation (8) will furnish all physically meaningful solutions of equations (6) and (7). Our confidence that it is the physical solution is supported by our equivalent earlier result using only thermodynamics and semiclassical considerations(Lima and Maia, 1995b). In addition it is easy to see that Eq. (8) is independent of the statistics of the γ-fluids particles.

From equations (6) and (8) one obtains the differential equation for $f(\omega)$

$$\frac{f'(\omega)}{f(\omega)} = (\frac{2 - \gamma}{\gamma - 1})\frac{1}{\omega} \tag{9}$$

where the prime denotes derivation with respect to w. The solution of above equation is straightforward

$$f(\omega) = A\omega^{\frac{2-\gamma}{\gamma-1}} \tag{10}$$

where A is a γ-dependent integration constant. Now, inserting the above equation into (3) and using (2) we obtain

$$\rho(T) = \int_0^\infty \frac{A\omega^{\frac{1}{\gamma-1}}}{\exp(\frac{\hbar\omega}{kT}) \mp 1} d\omega \tag{11}$$

Therefore, the spectrum of a γ-fluid reads:

$$\rho(\omega, T) = \frac{A\omega^{\frac{1}{\gamma-1}}}{exp(\frac{\hbar\omega}{kT}) \mp 1} \tag{12}$$

For the case of bosons, equations (11) and (12) above are, respectively, (39) and (53) presented by Lima and Maia(1995b). As expected, by introducing a new variable $x = \frac{\hbar\omega}{kT}$, one obtains from (11), the generalized Stefan–Boltzmann law (Lima and Santos, 1995)

$$\rho(T) = \eta T^{\frac{\gamma}{\gamma-1}} \tag{13}$$

where the constant η depends on the γ-parameter as well as of the bosonic(or fermionic) spin degrees of freedom of each field. Note also that the above expression for $\rho(T)$ does not means that the energy density is always finite for any value of γ. In particular, for the vacuum case($\gamma = 0$), ρ effectively does not depends on the temperature, but the constant η is infinite, as it should be from quantum field theory.

3 The Vacuum Infrared Divergence

The validity of equations (12)-(14), is crucially dependent on our earlier hypotheses concerning the boundary term in equation (6). From (8) and (10) it follows that

$$F(\omega) = A(\gamma - 1)\omega^{\frac{1}{\gamma-1}} \quad . \tag{14}$$

Now, inserting the function $F(\omega)$ into (5), we find a divergence in the limit $\omega \to 0$, when $0 \leq \gamma < 1$. In the vacuum case, for instance, equation (12) reduces to

$$\rho_{vac}(\omega, T) = \frac{A\hbar\omega^{-1}}{\exp(\frac{\hbar\omega}{kT}) \mp 1} \quad . \tag{15}$$

As it appears, the spectrum for negative pressures ($0 \leq \gamma < 1$), demands a closer attention due to the inevitable existence of an infrared divergence.

To avoid the infrared catastrophe we proceed in analogy with the Casimir effect, in which the divergent energy density has been regularized by a ultraviolet exponential cut-off $e^{-\alpha\omega}$, with $\alpha > 0$ (Plunien et al, 1986; Ruggiero and Zimmerman, 1977). Accordingly, the infrared exponential cut-off $e^{-\frac{\alpha}{\omega}}$, $\alpha > 0$ will be considered. By introducing the regularized function $F_\alpha(\omega) = F(\omega)e^{-\frac{\alpha}{\omega}}$, it is straighforward to check that $F_\alpha(\omega)$ makes the boundary term in (5) vanishes. Now, returning to equation (6), we may define its regularized counterpart, $f_\alpha(\omega) = F'_\alpha(\omega)$. In this way, as a consequence of (14), the regularized density of states function is given by

$$f_\alpha(\omega) = A(1 + \frac{(\gamma - 1)\alpha}{\omega})\omega^{\frac{2-\gamma}{\gamma-1}} \exp(-\frac{\alpha}{\omega}) \tag{16}$$

which, as should be expected, reduces to $f(\omega)$ in the limit $\alpha \to 0$. Lastly, using (5)-(7) the regularized equation of state reads $P_\alpha = (\gamma - 1)\rho_\alpha$, where the the regularized pressure and energy density are

$$P_\alpha = \int_0^\infty \frac{F_\alpha(\omega)}{\exp(\frac{\hbar\omega}{kT}) \mp 1} d\omega \, , \, \rho_\alpha = \int_0^\infty \frac{\omega f_\alpha(\omega)}{\exp(\frac{\hbar\omega}{kT}) \mp 1} d\omega \quad . \tag{17}$$

Note that the regularized quantities P_α and ρ_α are finite, however, they are cut-off dependent. To eliminate this dependence a renormalization scheme is required. This issue is presently under investigation.

References

[1] J. A. S. Lima and J. Santos(1995). *International Journal of Theorethical Physics*, **34**, 127.

[2] J. A. S. Lima and A. Maia Jr. (1995a). *International Journal of theoretical Physics*, **34**, 1835.

[3] J. A. S. Lima and A. Maia Jr.(1995b). *Physical Review D* , **52**, 5628.

[4] G. Plunien, B. Müller and W. Greiner(1986). *Physics Reports*, **134**, 88.

[5] J. R. Ruggiero, A. H. Zimmerman (1977). *Revista Brasileira de Física*, **7**, 663.

[6] Claude Itzykson and Jean-Bernard Zuber (1980). *Quantum Field Theory*, McGraw-Hill Inc.

Canonical Formulation of Standard Cosmology: Direct Quantum Approach*

M.Novello — J.M.Salim — M.C.Motta da Silva — R.Klippert
LAFEX — Centro Brasileiro de Pesquisas Físicas — Rio de Janeiro

Received March, 1995

In this work we show a procedure to obtain a canonical description of standard cosmology. It is based on the fact that, within the framework of Einstein's General Relativity, the dynamics of spatially homogeneous and isotropic perfect fluid is governed by two equations for a pair of variables (roughly the radius of the Universe and its rate of change). We show that this system admits a Hamiltonian formulation, and we provide its quantum version.

I Introduction

Quantum cosmology has proven itself to constitute a source of arguments about the possibility to present the most favourable states of the universe. Indeed, the most direct and simplest way to analyse the quantum properties of the universe is to consider the "Minisuperspace" [1] approach. This idea was developed to deal with the whole system of Einstein equations of GR in a narrow constrained context, where the majority of degrees of freedom is "frozen". Such a framework has been widely used, although there has been some criticism on this issue [2, 3, 4]. One of the points that have been raised is the necessity to choose a gauge; furthermore, depending on the order that this gauge is chosen — before or after solving Schrödinger equation — a different result is obtained. The procedure basically involves dealing with Wheeler-DeWitt equation, that reduces to the Hamiltonian constraint $\mathcal{H} = 0$. However there is another scheme which, as far as we know, does not seem to have been noticed before as a possible way of dealing with the quantum properties of the universe, which will therefore be presented here.

The basic assumptions of our method are the validity of classical equations of Einstein General Relativity. The method goes back to their reduction to a set of equations that constitute a planar dynamical system[1]. Indeed, Einstein equations for Friedmann universes reduce to a set of equations for ρ (the energy density) and θ (the rate of expansion of the universe) — defined as $\theta \stackrel{\text{def}}{=} 3\dot{A}/A$.

II Friedmann Solution

The Standard Cosmology deals with a spatially homogeneous and isotropic geometry characterized by a single function $A(t)$ — the radius of the universe [2] — and a constant parameter ε — the 3-dimensional (topological) curvature.

Einstein equations for the FRW geometry reduce to the following set[3] of coupled differential equations:

$$G_{00} = -3\left(\frac{\dot{A}}{A}\right)^2 - \frac{3\varepsilon}{A^2} = -\rho + \Lambda$$
$$G_{11} = 2\frac{\ddot{A}}{A} + \left(\frac{\dot{A}}{A}\right)^2 + \frac{3\varepsilon}{A^2} + \frac{2}{A^2}\frac{\ddot{\sigma}}{\sigma} = -p - \Lambda$$
$$G_{22} = 2\frac{\ddot{A}}{A} + \left(\frac{\dot{A}}{A}\right)^2 - \frac{1}{A^2}\frac{\ddot{\sigma}}{\sigma} = -p - \Lambda,$$

*Submitted to Physical Review D.

[1] Recently [5] we have shown that the dynamics of gauge-independent perturbations of FRW universes reduces to a planar autonomous system as well. We have then developed the method of the auxiliary Hamiltonian to analyse it.

[2] We take the geometry of Friedmann-Robertson-Walker (FRW) universes in the form
$ds^2 = dt^2 - A^2(t)\left[d\chi^2 + \sigma^2(\chi)\left(d\vartheta^2 + \sin^2(\vartheta)\,d\phi^2\right)\right]$.

[3] Other components of Einstein equations for this model do not provide any additional information, and will be omitted. Besides, we choose the natural unit system $\hbar = c = 8\pi G = 1$ in order to simplify writings.

where Λ is the cosmological constant, which will be dropped from now on, and a dot means derivative with respect to the parameter in each expression (that is, $\dot{A} \equiv \frac{dA}{dt}$, $\ddot{\sigma} \equiv \frac{d^2\sigma}{d\chi^2}$). Perfect fluid condition implies $G_{11} = G_{22}$, which in turn gives $\frac{\ddot{\sigma}}{\sigma} = -\varepsilon$, where ε classifies the constant topology of the spatial section ($\varepsilon = -1, 0, +1$ for open, plane and closed sections, respectively). Therefore we have

$$\sigma(\chi) = \frac{\sinh\left(\sqrt{-\varepsilon}\,\chi\right)}{\sqrt{-\varepsilon}}.$$

III Basic settings

The first dynamical equation is obtained from the conservation law of the energy momentum tensor of a perfect fluid, as seen from a given comoving observer with normalized 4-velocity $V^\mu = \delta^\mu_0$ and the other one is nothing but Raychaudhuri equation

$$\begin{aligned} \dot{\rho} &= -(1+\lambda)\,\rho\,\theta \\ \dot{\theta} &= -\tfrac{1}{3}\theta^2 - \tfrac{(1+3\lambda)}{2}\rho, \end{aligned} \tag{1}$$

where use has been made of the state equation $p = \lambda\rho$. The constant parameter λ measures the dominant sound velocity in each particular phase of the evolution of the universe, and must be chosen in the interval $\lambda \in [0, 1]$. The value $\lambda = 1/3$ represents the radiation dominant era, which has, as we shall see, a peculiar role in our description of spacetime.

The dynamical system for (ρ, θ), Eqs. (1), has as a first integral the constraint given by $G_{00} = 0$, now written as:

$$\tilde{\Phi} \stackrel{\text{def}}{=} \frac{3\,\varepsilon}{A^2} - \rho + \frac{1}{3}\theta^2 = 0, \tag{2}$$

where the basic variables will be the pair (ρ, θ), and A stands for the time dependent solution for $A(\rho(t))$ of the equation $\rho(t) = \rho_o\, A(t)^{-3(1+\lambda)}$, — for $\lambda \neq -1$, — which is a implicit solution for the first of Eqs. (1) when θ is replaced by the above definition.

IV Canonical Formulation

The recognition of the fact that the above system could have its properties analysed qualitatively seems to have been pointed out at first by [6] (see also [7]). One can thus picture the behaviour of the complete class of the integrals of the dynamical system (1), by depicting the plane (ρ, θ). Such analysis has proved to be extremely worthwhile, yielding some insights concerning the stability of special solutions. However, this formalism does not provide the means for a complete analysis of the system (ρ, θ). The main reason for this is that the dynamical system in this form does not admit a Hamiltonian description. As we shall see shortly, this is just a consequence of an inadequate choice of variables. Indeed, if we choose a new set (q, p) of related variables defined by

$$\begin{aligned} q &\stackrel{\text{def}}{=} \left(\tfrac{3b^2}{2\rho}\right)^{\frac{1}{3(1+\lambda)}} \\ p &\stackrel{\text{def}}{=} \tfrac{1}{3}\theta\left(\tfrac{3b^2}{2\rho}\right)^{\frac{1}{3(1+\lambda)}} = \tfrac{1}{3}\theta\, q, \end{aligned} \tag{3}$$

with b an arbitrary adimensional positive constant[4], then it immediately follows that the corresponding system admits a Hamiltonian description. We note that these new variables are essentially the usual ones:

$$(q, p) \equiv \left(\frac{3b^2}{2\rho_o}\right)^{\frac{1}{3(1+\lambda)}} (A, \dot{A}).$$

Employing these new variables on Eqs. (1), (2) we then get the following constrained canonical Hamiltonian system

$$H(q, p) = \frac{1}{2}p^2 - \frac{b^2}{4}q^{-(1+3\lambda)}, \tag{4}$$

and for convenience we perform a linear transformation on the constraint to get

$$\Phi(q, p) \stackrel{\text{def}}{=} -\frac{q^2}{6}\tilde{\Phi}(\rho(q, p),\, \theta(q, p)) = H(q, p) - H_o \approx 0, \tag{5}$$

[4] Let us remark that we are using geometrical "natural" units $\hbar = c = \kappa = 1$.

where

$$H_o \stackrel{\text{def}}{=} -\frac{\varepsilon}{2}\left(\frac{3\,b^2}{2\,\rho_o}\right)^{\frac{2}{3(1+\lambda)}} \tag{6}$$

is a constant in each stage of the evolution of the FRW universe, and '$\approx$' means *weakly equal*[5]. This shows therefore that the dynamics of such a universe is equivalent to the evolution of a particle acted upon by a potential $V(q) = -\frac{b^2}{4}\,q^{-(1+3\lambda)}$ and subjected to a non holonomic constraint $H(q,\,p) = H_o$.

The above formal mapping between the FRW dynamical system and a single particle acted upon by a potential may be clarified by means of the usual procedure of Newtonian Cosmology: let us supose a massive sphere of radius A and density ρ, and a unit mass test particle on its surface. The total (kinetic $\frac{1}{2}\dot{A}^2$ and potential $-\frac{GM}{A}$) energy of this test particle may be written as[6]

$$\frac{A^2}{6}\left[3\left(\frac{\dot{A}}{A}\right)^2 - \rho\right],$$

which coincides with our former Hamiltonian expression (4). for $\lambda = 1/3$.

The last (strong) equality of Eq. (5) enables us to conclude that the constraint $\Phi(q,\,p) \approx 0$ is dynamically preserved as its Poisson bracket with the Hamiltonian obviously vanishes identically (remember H_o does not depend on canonical variables). This result ensures that no second class constraints arises in this problem. Therefore classical Dirac brackets coincide with the usual Poisson brackets, and the quantization of such a system turns out to be rather simple. We will perform this job in the next section.

The presence of a primary first class constraint means that such constraint is a generator of symmetries of the model, and may in fact be regarded as a Hamiltonian[7] as well. The complete dynamics of the model may be described by the Total Hamiltonian

$$H_T(q,\,p) \stackrel{\text{def}}{=} H(q,\,p) - \mu\,\Phi(q,\,p) = (1-\mu)\,H(q,\,p) + \mu\,H_o \tag{7}$$

where μ plays the role of an arbitrary Lagrange multiplier. The last equality of Eq. (7) shows that the dynamics is formally invariant by such modification, as

$$\frac{d}{dt}\,f(q,\,p) = \{f(q,\,p),\,H_T(q,\,p)\}_{PB} = (1-\mu)\,\{f(q,\,p),\,H(q,\,p)\}_{PB},$$

where $f(q,\,p)$ is an arbitrary function of the canonical variables, provided μ is an arbitrary function of (cosmological) time t. We stress at this point that the canonical Hamiltonian $H(q,\,p)$ yields all physical information we need and, as μ may be chosen arbitrarily, the model turns out to be explicitly invariant under reparametrization of time. For $\mu = const. \neq 1$, which will be assumed from now on, it follows that the total Hamiltonian is constant as well. Renormalizing time by $d\tau \stackrel{\text{def}}{=} (1-\mu)\,dt$ generates a spurious dynamical *cosmological constant* by

$$\tilde{H}_T(q,\,p;\,\tau) \stackrel{\text{def}}{=} \frac{1}{1-\mu}\,H_T(q,\,p) = H(q,\,p) + \frac{\mu}{1-\mu}\,H_o,$$

with all other physical characteristics remaining unchanged. In the above relation the entry τ does not mean explicit dependence, but is merely a label to remember that such Hamiltonian generates translations in time τ. Hamiltonian $\tilde{H}_T(q,\,p;\,\tau)$ will be the main one in order to construct the quantized version of this model, because in its spectrum all references to the arbitrary multiplier μ are left to the specification of the constant shift $\frac{\mu}{1-\mu}\,H_o$.

The Hamiltonian Eq. (4) reduces on-shell to a constant $H(q,\,p) \approx H_o$, yielding the natural result that the energy of a closed system (the *whole* Universe) is a conserved quantity. Similarly $\tilde{H}_T$ is a constant too.

At this point we would like to stress that one of the most striking characteristics of this potential comes from the use of the classical version of Virial Theorem[8]. Indeed this theorem states that, for a potential of the form $V(q) = \alpha\,q^n$ (with finite p, q and constants α, n), the mean values of kinetic and potential energy are related by $\langle T\rangle = \frac{n}{2}\,\langle V\rangle$. In our case $n = -(1+3\lambda)$, which yields, together with Eq. (4), a mean Hamiltonian

$$\langle H\rangle = \langle T\rangle + \langle V\rangle = \frac{(1-3\lambda)}{2}\,\langle V\rangle,$$

which vanishes when $\lambda = 1/3$. This result, together with the on-shell Hamiltonian Eq. (6), suggests the spatial flatness of FRW solutions at the radiation era.

[5] From Dirac's terminology on constrained systems, meaning *equality under constraints*.

[6] Remember that we have set $8\pi G = 1$.

[7] This is the usual procedure when analyzing the problem by means of the Wheeler-De Witt [1] formalism.

[8] In fact the canonical variables above fulfill the conditions of this theorem only for $\varepsilon = 0$, which may be an alternative argument for the following paragraph.

V Quantization

As far as we are able to write a classical Hamiltonian Eq. (4) to describe the standard model, one can consider the canonical quantization of such system. We will limit ourselves here to the particular value $\lambda = 1/3$, because this stage lies in a sufficiently condensed regime in order to justify a quantum description. On the other hand it is appart enough from Planck scales for equilibrium to be achived. Therefore that choice seems to be the best example for the method presented here.

To do that one can then employ the standard quantization procedure to make $(q,\ p)$ into the operators $\left(\hat{q},\ \hat{p} = -i\frac{\partial}{\partial q}\right)$. Denoting the time dependent wave function $\Psi(q,\ \tau) = \mathrm{e}^{-iE\tau}\ \varphi(q)$ we get the stationary Schrödinger equation

$$\ddot{\varphi} + \left(E + \frac{b^2}{4\,q^2}\right)\ \varphi = 0, \tag{8}$$

where $E = (\Psi|\tilde{H}_T|\Psi)$ denotes the shifted energy eigenvalue (of $\tilde{H}_T$) of the state $\Psi(q,\ \tau)$.

The normalized — squared integrable (to unity) — solutions which represent the physical bounded states of such a system, that is, those with negative energy E, are given by

$$\varphi_\nu(q) = N_\nu\ \sqrt{-E\,q}\ K_\nu(\sqrt{-E}\,q), \tag{9}$$

where

$$\begin{aligned} \nu &\stackrel{\text{def}}{=} \tfrac{1}{2}\sqrt{1-b^2} \\ N_\nu &\stackrel{\text{def}}{=} \left[\lim_{x\to\infty}\ \tfrac{x^2}{2}\left\{[K_\nu(x)]^2 - K_{\nu-1}(x)K_{\nu+1}(x)\right\}\right]^{-1/2}, \\ &\equiv \left(\lim_{z\to 0}\left\{\tfrac{z^2}{2}\left[K_{\nu+1}(z) - K_\nu(z)\right] - \nu z\,K_\nu(z)K_{\nu+1}(z)\right\}\right)^{-1/2} \end{aligned} \tag{10}$$

and K_ν are the well known ν-order modified Bessel functions of second type. N_ν is finite due to the strong convergence of $\varphi(x)$ for large x, as one remembers that $\lim_{x\to\infty} K_n(x) = (2\pi\,x)^{-1/2}\mathrm{e}^{-x}$. Negativeness of the energy E means, from Eq. (6), that the spatial 3-sections should be closed ($\varepsilon = +1$).

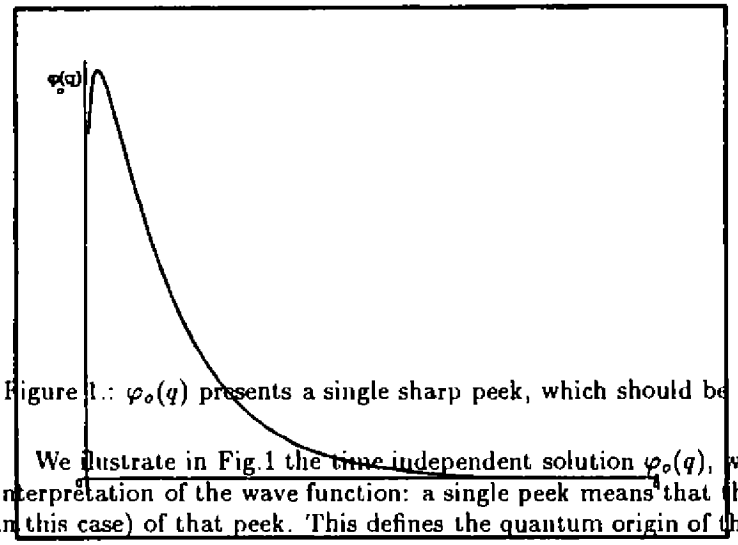

Figure 1.: $\varphi_o(q)$ presents a single sharp peek, which should be interpreted as the classical radius of the Universe.

We illustrate in Fig.1 the time independent solution $\varphi_o(q)$, which is in agreement with the quantum cosmologic interpretation of the wave function: a single peek means that the system presents a definite value (of coordinate q in this case) of that peek. This defines the quantum origin of the classical radius of the Universe.

VI Conclusions

It can easily be verified that the above solution presents a continuum energy spectrum, as ν is independent from E. On the other hand, the solution given by Eq. (9) above presents a critical dependence on the arbitrary parameter b, which seems to restrict it to the range $b \in (0,\ 1]$, in order to preserve ν real. This condition turns out to be the main difference between the quantum and classical descriptions of this system: boundedness quantum condition — that is, the negativeness of the total energy E, which in turn implies $\varepsilon = +1$ from Eq. (6) — translates itself

into a maximum strenght of the potential in Eq. (4). Therefore canonical formalism provides ways to select the topological parameter ϵ for the radiation era in each context, classical (flatness) or quantum (closed topology). We hope similarly conclusions may help the analysis for other stages of the evolution of the Universe.

Acknowledgements
Two of us (MCMS and RK) would like to thank CNPq for grants.

References

[1] J.A.Wheeler, M.C.DeWitt and B.S.DeWitt, *Geometrodynamics and the Issue of the Final State*, (1964).

[2] M.P.Ryan, *Hamiltonian Cosmology*, Springer-Verlag, Heidelberg, (1972).

[3] J.J.Halliwell in *Quantum Cosmology and Baby Universes*. Edited by S.Coleman, J.B.Hartle, T.Piran and S.Weinberg. World Scientific. Singapore, 1991.

[4] N.Pinto-Neto, in *Quantum Cosmology*, proceedings of the VIII Brazilian School of Cosmology and Gravitation. Edited by M.Novello. July, 1995 (to be published).

[5] M.Novello, J.M.Salim, M.C.Motta da Silva, S.E.Jorás and R.Klippert, Phys.Rev.D **51**, 450 (1995); Phys.Rev.D **52**, 730 (1995).

[6] V.A.Belinski and I.M.Khalatnikov, Zh. Eksp. Teor. Fiz. **72**, 3 (1977) [Sov. Phys. JETP **45**, 1 (1977)].

[7] M.Novello and R.A.Araújo, Phys.Rev.D **22**, 260 (1980).

Radiation Waves in Compact Universes: the S^3 and T^3 cases*

Armando Bernui Leo[1]
Centro Brasileiro de Pesquisas Físicas, Rio de Janeiro, BRASIL

Received March, 1996

Estudamos o comportamento de um sistema radiante (composto por um oscilador harmônico acoplado a um campo escalar relativista) em dois espaços-tempo curvos com triespaços compactos (a triesfera S^3 e o tritoro T^3) tanto em condição estática como em expansão monotônica. As equações da evolução temporal do sistema radiante são reduzidas a uma única equação para o oscilador harmônico que contém toda a informação sobre a radiação que ele emitiu e que retorna algum tempo depois – devido a que os triespaços são compactos – entregando-lhe energia. Uma análise numérica dessa equação para cada caso mostra que o fenômeno conhecido como **perda de radiação** (típico no espaço-tempo de Minkowski) se apresenta em todos os casos exceto no espaço-tempo estático onde a parte espacial é a triesfera.

Introduction

A gravitational theory – *e.g.* General Relativity – does not settle the topology of the spacetime manifold which actually is given by hand – coherently with the geometry (*i.e.* with the metric) and probably motivated by observational data – or is infered from sufficient assumptions regarding global properties of the spacetime [1,2]. For instance the commonly accepted – but false – belief that our universe is globally spatial homogeneous fixes almost uniquely the topology of the spacetime. However, present astronomical observations show that the large-scale galaxy distribution is not homogeneous but tends to be clustered in sharp walls separated by vast regions devoid of galaxies [3]. Moreover, recent data show a possible periodic arrangement in the redshift distribution of quasars and cluster of galaxies (as recent deep surveys within small angular regions of the sky has revealed [4]) which favors the idea of universes with **closed** – *i.e.* **compact and without boundary** – spatial sections where periodic distributions can naturally arise [5]. Therefore it results interesting to investigate what could be a plausible (and not only possible) closed topology for our universe.

This work concerns itself with the time-evolution of a radiating system in static and monotonously expanding Friedman-Robertson-Walker (FRW) spacetimes with – topological and geometrically distinct – **compact** three-spaces. The metric of these spacetimes is [6]

$$ds^2 = dt^2 - R^2(t)[\frac{dr^2}{1-kr^2} + r^2(d\theta^2 + \sin^2\theta d\varphi^2)]. \qquad (1)$$

The scale factor $R(t)$ gives the **dynamic** behaviour of the universe and the constant spatial curvature $k(=0,-1,+1)$ specifies the type of **local-geometry** of the three-space (flat, hyperbolic or elliptic, respectively). The compact three-spaces we shall consider are: the **three-sphere** S^3 (simply-connected with elliptic geometry $k=+1$) and the

*work supported by a CLAF-CNPq fellowship
[1]on leave from: Facultad de Ciencias, Universidad Nacional de Ingeniería, Lima, PERU

three-torus T^3 (multi-connected with flat geometry $k = 0$) [1].

The Physical Model and the Evolution Equations

The radiating system is given by an illustrative coupled model [7] composed of a classical harmonic oscillator – representing an **oscillating energy source** – in linear interaction with a relativistic massless scalar field – which will be responsible for the **waves radiation** –. In this model the gravitational field is treated as external, although the conformal coupling with the scalar field is considered. The dynamics of the model is fully described by the action of the system which, in units where $c = 1$, is

$$\begin{aligned} S &= \frac{1}{2}\int_{\mathcal{M}} d^4x\sqrt{-g}\,[g^{\mu\nu}\partial_\mu\phi\partial_\nu\phi - \frac{1}{6}\hat{R}\phi^2] + \frac{1}{2}\int_I dt\,[\dot{Q}^2 - \omega_\epsilon^2 Q^2] \\ &+ \lambda\int_{\mathcal{M}} d^4x\sqrt{-g}\,\rho(t,x)Q(t)\phi(t,x), \end{aligned} \tag{2}$$

where $\mathcal{M} = I \times \mathcal{N}$, $I \equiv [t_0, \infty)$ and $\mathcal{N}$ is the compact three-space; $\hat{R}$ is the scalar curvature of $\mathcal{M}$, $\dot{Q} \equiv dQ/dt$, λ is the coupling constant. Here we consider a point-like coupling between the harmonic oscillator and the scalar field, i.e. $\rho(t,x) = \delta^{(3)}(x)/\sqrt{-g(t,x)}$. The uncoupled frequency ω_ϵ is necessary for a renormalization procedure. From the action (2), variations with respect to Q and ϕ give the coupled evolution equations of the system, namely

$$[\Box + \frac{1}{6}\hat{R}]\phi(t,x) = \lambda\rho(t,x)Q(t), \tag{3}$$

$$\ddot{Q}(t) + \omega_\epsilon^2(t)Q(t) = \lambda\int_{\mathcal{N}} d^3x\sqrt{-g}\,\rho(t,x)\phi(t,x), \tag{4}$$

where $\Box\phi \equiv (\sqrt{-g})^{-1}\,\partial_\mu(\sqrt{-g}\,g^{\mu\nu}\partial_\nu\phi)$. We first solve equation (3) as an initial value problem $\phi = \phi_I + \phi_{II}$, where $\phi_H(t,x)$ satisfies the homogeneous equation of (3) and ϕ_I is given by $\phi_I(t,x) = \int d^4x'\sqrt{-g}G(t',x';t,x)\lambda\rho(t',x')Q(t')$, where the retarded Green function G is a fundamental solution of $\Box + \frac{1}{6}\hat{R}$ [8]. Our initial condition $(\phi(t_0,x), \partial_t\phi(t_0,x)) = (0,0)$ (the scalar field has no initial energy) implies that $\phi_H(t,x) = 0$, therefore $\phi(t,x) = \phi_I(t,x)$.

Profiting the fact that all FRW metrics are local-conformally flat [6], and remembering that the source is point-like and is located at the origin ($x' = 0$), we find [8]

$$G(f(t'),0;f(t),x) = \frac{\delta([f(t) - f(t')]^2 - |x|^2)}{2\pi R(t)R(t')}, \tag{5}$$

piecemeal in conformally Minkowskian regions. The global Green function is found by appropriately matching the local G's. Finally the radiation-reaction equation of the oscillator is found using the relation $\phi = \phi[Q]$ in equation (4).

Radiation-Reaction Eq. in FRW with Compact Three-Spaces

The S^3 case

S^3 is a simply-connected compact three-dimensional manifold with elliptic geometry ($k = +1$). The spacetime metric is obtained from the metric (1) making $k = +1$ and $r = \sin\chi$ where $(\chi,\theta,\varphi) \in S^3$, for $\chi, \theta \in [0,\pi]$, $\varphi \in [0, 2\pi]$.

The spherical symmetry of S^3 implies that $G(f(t'),0;f(t),x) = G(f(t'),0;f(t),\chi)$ [9]. Thus, the Green function for the FRW spacetime with three-space S^3 is

$$G(f(t)-f(t'),\chi) = \frac{1}{4\pi R(t)R(t')\sin\chi}\{\delta(f(t)-f(t')-\chi) + \sum_{n=1}^{\infty}[\Theta_-\delta(f(t)-2\pi n-f(t')-\chi)-\Theta_+\delta(f(t)-2\pi n-f(t')+\chi)]\}, \quad (6)$$

where $\Theta_\pm \equiv \Theta(f(t)-2\pi n\pm\chi)$ and $\Theta(s)=0$ for $s\leq 0$, $\Theta(s)=1$ for $s>0$. Then we find the renormalized (see [9]) radiation-reaction equation of the harmonic oscillator

$$\ddot{Q}_N(t)+2\Gamma\dot{Q}_N(t)+\Omega^2 Q_N(t) = -4\Gamma\sum_{n=1}^{N-1}\Theta(t-t_n)\dot{Q}_{N-n}(g_n(t)), \quad (7)$$

for arbitrary $(Q_0,\dot{Q}_0)\equiv(Q(t_0),\dot{Q}(t_0))$, with $t\in[t_{n-1},t_n]$, $t_n\equiv f^{-1}(2\pi n)$, $2\leq n+1\leq N\equiv[f(t)/2\pi]$ (the symbol $[h]$ means the greatest integer less than $h+1$), and $2\Gamma\equiv\lambda^2/4\pi$. Given t, $N\equiv[f(t)/2\pi]$ defines the interval of solution, afterthat the equation can be solved interval-by-interval $[t_{n-1},t_n]$, starting with $n=1$.
$g_n(t)\equiv f^{-1}(f(t)-2\pi n)$, $n\geq 1$, $g_n:[t_N,t_{N+1}]\to[t_{N-n},t_{N-n+1}]$, for $N\geq n\geq 1$, and with $g_0(t)\equiv t$. It has the following properties: (i) $g_{n+1}(t)<g_n(t)<t$, (ii) $g_n(t_m)=t_{m-n},\forall m\geq n\geq 1; f^{-1}(0)=t_0$, (iii) $\dot{g}_n(t)=R(g_n(t))/R(t)$. Thus, given t, $g_n(t)$ represents a preceding value of t and $\dot{Q}(g_n(t))$ represents the radiation emitted at time $g_n(t)$ that returns – after travel around S^3 – to interact with the source at present time t.

The T^3 case

T^3 is a multi-connected compact flat ($k=0$) three-dimensional manifold obtained identifying the opposite faces of a parallelepiped (here we consider a cube of side a). Its metric tensor is that of the FRW ($k=0$) spacetime. We can express it in cartesian coordinates, $(x,y,z)\in T^3$ and take in mind the topological identification of the point (x,y,z) with $(x+ja,y+la,z+ma),\forall j,l,m$ integers.

A wave emitted from the source (located at $\vec{x}'=\vec{0}$) travels towards the cube faces and – due to the identifications – returns divided in infinite small parts, each one having followed a different path and therefore arriving at a distinct time. The Green function has the same form as (6) with the replacements $\chi\to r\equiv|\vec{x}|$, $2\pi n\to a_n\equiv a\sqrt{j^2+l^2+m^2},\forall j,l,m$ integers and with normalized coefficients c_n/M in the sum terms. It is important to note that due to the discrete analysis we shall perform – where irrational numbers are not considered – M is calculated considering **only** the returning light-rays (that is, those directed towards (j,l,m) all integers); in rigor $c_n/M\to 0$ if we consider "rational" and "irrational" light-rays.
Then, the radiation-reaction equation of the harmonic oscillator is

$$\ddot{Q}_N(t)+2\Gamma\dot{Q}_N(t)+\Omega^2 Q_N(t) = -\frac{4}{M}\Gamma\sum_{n=1}^{N-1}\Theta(t-t_n)c_n\dot{Q}_{N-n}(t-t_n), \quad (8)$$

for arbitrary initial data, with $t\in[t_{n-1},t_n]$, $t_n\equiv f^{-1}(a_n)$, $2\leq n+1\leq N\equiv[f(t)/2\pi]$. These retarded contributions correspond to the light-rays that travel along different paths until they encounter again the oscillator at later times. However light-rays directed toward (p,q,s) where at least one of these numbers is irrational never return to the

origin, therefore do not contribute to the energy of the oscillator.

Numerical Analysis and Conclusions

The numerical solution of the radiation-reaction equations (7) and (8) is used to construct the energy-function of the harmonic oscillator $E(t) = \frac{1}{2}[\dot{Q}^2(t) + \Omega^2 Q^2(t)]$, which is then used for the energy *vs* time plots of Figures 1–4. We assumed $\Gamma = \Omega = 1$ and the initial-data $(Q(t_0), \dot{Q}(t_0)) = (\sqrt{2}, 0)$, which implies that $E(t_0) = 1$. In Fig. 1 we have considered the static $\Re \times S^3$ spacetime (best known as the Einstein universe), with $2\pi R = const. = 1$ and $g_n(t) = t - t_n$, $t_n = n, n \geq 0$. In Fig. 2 the same spacetime with monotonic expansion $R(t) = c(t-1)$, with $c = ln2/2\pi$ is analized, where $\dot{g}_n(t) = (0.5)^n$, $t_n = 2^n, n \geq 0$. Fig. 3 corresponds to the static $\Re \times T^3$ spacetime where $a = const. = 1$ is the side of the cube. In Fig. 4 we consider this spacetime but in monotonic expansion $a = a(t) = \frac{1}{2}t + 1$.

The results show radiation damping in all cases except in the Einstein universe where the time-average of the energy is constant. We can analize these results observing that the absence of radiation damping is due essentially to [9]: a) that every emitted light-ray returns, and b) that they return at a finite time. In fact looking at geodesics in the Einstein universe we observe that conditions a) and b) are satisfied (regarding b) every light-ray emitted at time t returns at $t + 2\pi R$). In the expanding case however – assuming that there is no Future Event Horizon – condition a) is satisfied but b) is not since as the expansion proceeds the time-travel of light-rays is always increasing. In the T^3 static and dynamic cases condition b) is not satisfied since there is no upper limit for the light-rays time-travel.

Acknowledgements

I am grateful to Profs. M. Rebouças and A. Teixeira for initiating me in Cosmic Topology, for helpful discussions and for their kind hospitality at DRP-CBPF, where this work was done thanks to a CLAF-CNPq fellowship.

References

[1] M. Lachiéze-Rey & J.-P. Luminet, Phys. Rep. **254**, 3 (1995)

[2] W. Oliveira, M.J. Rebouças & A.F.F. Teixeira, Phys. Lett. A **188** (1994) 125

[3] M. Geller & J. Huchra, Science **246** (1989) 989

[4] T. Broadhurst *et al*, Nature **343** (1990) 726; L.Fang *et al.*, A&A **106** (1982) 287

[5] H. Fagundes, GRG **24** (1992) 199; P. Budinich *et al*, Found.Phys. **23** (1993) 225

[6] H. Stephani, General Relativity, Cambridge Univ. Press 1993

[7] F. Schwalb & W. Thirring, Ergeb. exak. Natur. **36** (1964) 219; W. Unruh, in Grav. Radiation, Les Houches 1982, eds. DeRuelle & Piran, North-Holland 1983

[8] F. Friedlander, Wave Eq. on a Curved Spacetime, Cambridge Univ. Press 1975

[9] A. Bernui, Appl. Anal. **42** (1991) 157; Ann. Physik **3** (1994) 408

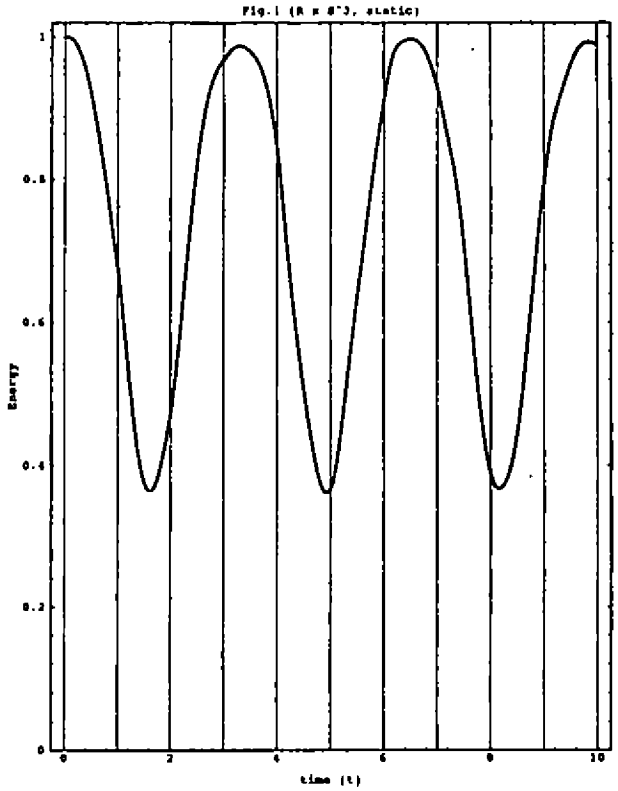
Energy
time (t)

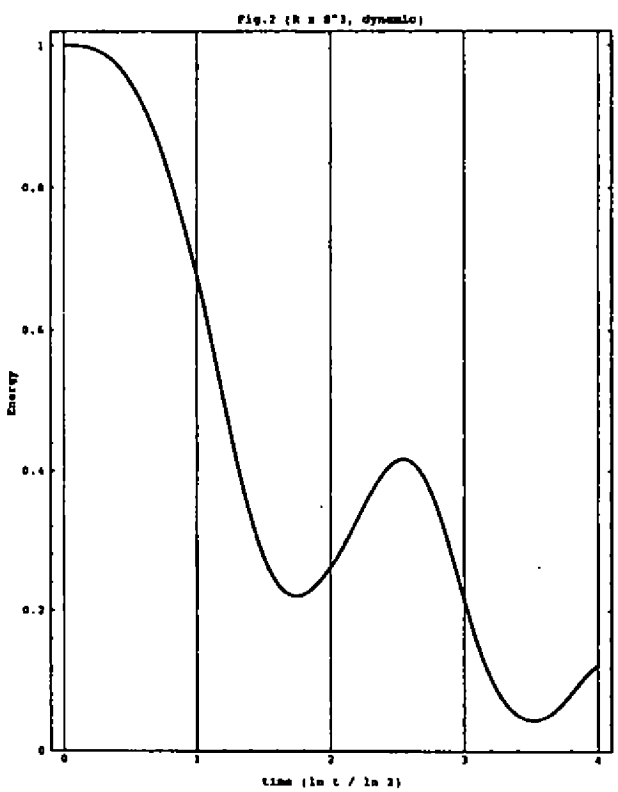
Energy
time (ln t / ln 2)

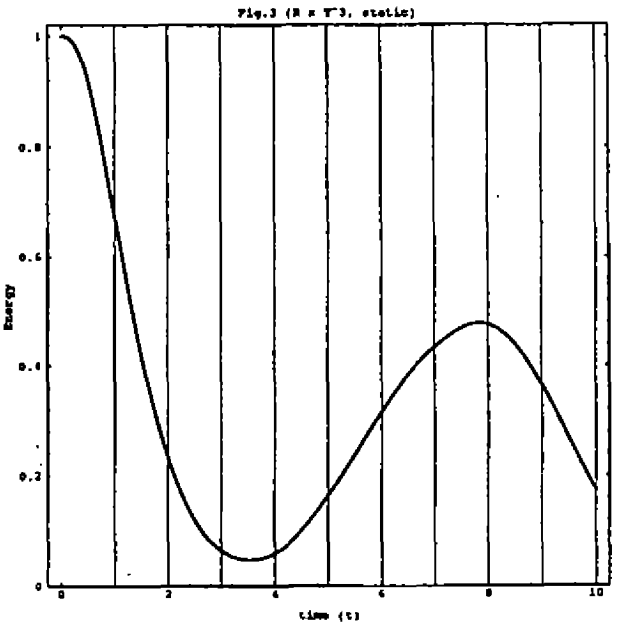
Energy
time (t)

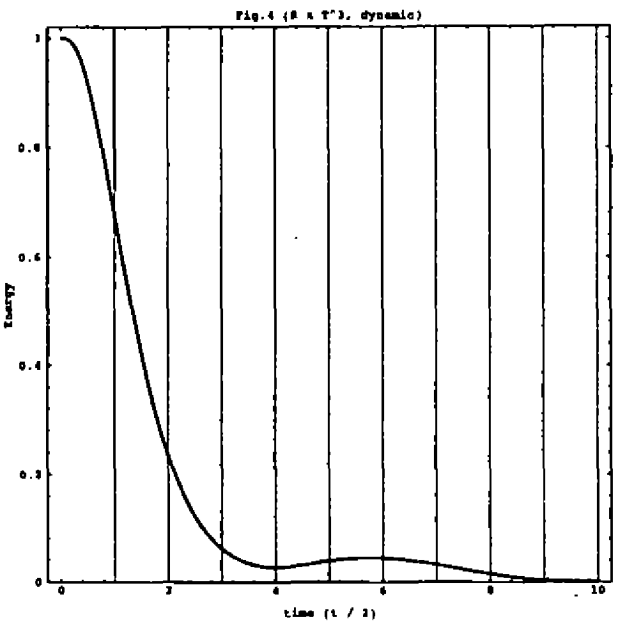
Energy
time (t / 2)

Energia Potencial de Schrödinger e a Eletrodinâmica de Weber

J. J. Caluzi*
Centro de Ciências Exatas - Depto. de Física
Universidade Federal do Espírito Santo - UFES
29060 - 900, Vitória, Espírito Santo

A. K. T. Assis†‡
Instituto de Física 'Gleb Wataghin'
Universidade Estadual de Campinas, UNICAMP
13083 - 970, Campinas, São Paulo

Received March, 1996

Discutimos a abordagem de Schrödinger para interações gravitacionais e a eletrodinâmica de Weber. Então fazemos uso deste modelo para calcularmos a energia de uma carga movendo - se no interior e exterior de um capacitor ideal. Isto resulta em uma velocidade limite, c, e na variação da massa da partícula com o potencial eletrostático e sua velocidade.

I – Interação Gravitacional

Em 1925 Erwin Schördinger propôs uma energia de interação gravitacional entre duas massas pontuais m e m' que é uma função de sua distância r_{ij} e da velocidade radial $\dot{r}_{ij} = dr_{ij}/dt$, [1]. Esta energia W_{ij} é dada por

$$W_{ij} = -\frac{Gmm'}{r_{ij}}\left[3 - \frac{2}{(1-\dot{r}_{ij}^2/c^2)^{3/2}}\right]$$

$$= -\frac{Gmm'}{r_{ij}}\left[3 - 2\left(1 - \frac{1}{c^2}\frac{(\vec{r}_{ij}\cdot\vec{v}_{ij})^2}{r_{ij}^2}\right)^{-3/2}\right]. \qquad (1)$$

Nesta expressão $c = 2.99 \times 10^8\ m/s$ e G é a constante gravitacional ($G = 6.67 \times 10^{-11}\ m^3/s^2kg$). Com $\dot{r}_{ij} = 0$ recuperamos a energia potencial Newtoniana.

Expandindo a eq. (1) até segunda ordem em $\dot{r}_{ij}/c$ obtemos a parte usualmente não explicada do periélio dos planetas e a implementação do princípio de Mach [1, 3].

Schrödinger mostrou que integrando a eq. (1) para uma massa teste m interagindo com um universo homogêneo e isotrópico com uma densidade ρ_0 obtemos

$$W = A\left[\frac{mc^2}{\sqrt{1-v^2/c^2}} - \frac{3mc^2}{c^2}\right]. \qquad (2)$$

Nesta equação $v = |\vec{v}|$ é a velocidade de m relativo a um sistema de referência no qual o universo como um todo é estacionário. A constante A é dada por $4\pi\rho_0 G R_0^2/c^2$, onde R_0 é o raio característico do universo. Se R_0 é estimado como c/H_0, onde H_0 é constante de Hubble, então A pode ser tomado como aproximadamente a unidade, $A = 1$. A partir daqui assumimos $A = 1$. Deve ser resaltado que a eq.(2) é a energia cinética mais a "energia de repouso" da partícula. Assim temos $K_S = W - E_R$, onde K_S é a energia cinética de Schrödinger e E_R a energia de repouso. Fazendo $v/c = 0$ na eq. (2) obtemos $E_R = -mc^2/2$. Com isto K_S é dado por:

$$K_S = \frac{mc^2}{\sqrt{1-v^2/c^2}} - mc^2. \qquad (3)$$

*Internet: CALUZI@CCE.UFES.BR
†Também Professor Colaborador no Departamento de Matemática Aplicada, IMECC,UNICAMP,13081-970, Campinas, SP
‡Internet: ASSIS@IFI.UNICAMP.BR

Vemos que Schrödinger obteve um análogo à energia cinética relativística. Apesar desta similaridade de forma, as duas são conceitualmente bem distintas. A massa que aparece na expressão de Schrödinger é gravitacional, enquanto que na expressão relativística é a massa inercial de repouso. Além disto a expressão de Schrödinger implementa perfeitamente o princípio e Mach por partir de uma expressão completamente relacional que é uma generealização da energia potencial de Weber, como veremos abaixo.

II – Interação Eletromagnética

Estudaremos uma partícula carregada movendo – se ortogonalmente as placas de um capacitor ideal com uma densidade de carga $\pm\sigma$ em suas placas situadas em $\pm x_0$. Para isto vamos utilizar a energia potencial proposta por Weber, [2]. Dada por

$$U_{ij} = \frac{q_i q_j}{4\pi\varepsilon_0}\frac{1}{r_{ij}}\left(1 - \frac{1}{2}\frac{\dot{r}_{ij}^2}{c^2}\right) . \tag{4}$$

Note que expandindo a eq. (1) até segunda ordem em $\dot{r}_{ij}/c$ e substituindo Gmm' por $q_i q_j/4\pi\varepsilon_0$ obtemos a eq. (4), como foi dito acima. Observe também que ao fazermos $\dot{r}_{ij} = 0$ recuperamos o potencial Coulombiano. Ao fazermos isto na eq. (1) obtemos o potencial Newtoniano. Integrando a eq. (4) sobre as duas placas obtemos

$$U_W(\pm x - x_0 > 0) = \pm q\frac{\sigma}{\varepsilon_0}x_0\left(1 + \frac{v^2}{2c^2}\right) , \tag{5}$$

$$U_W(-x_0 \leq x \leq x_0) = q\frac{\sigma}{\varepsilon_0}x\left(1 + \frac{v^2}{2c^2}\right) . \tag{6}$$

III – Energia Total

A energia total da partícula quando consideramos o potencial Weberiano e a energia cinética de Schrödinger é $E = U_W + K_S$ onde E é a energia total, U_W é a energia potencial Weberiana e K_S é a energia cinética de Schrödinger dada pela eq.(3).. Utilizando o princípio de conservação vem: $E(x \leq -x_0) = E(-x_0 \leq x \leq x_0)$. Também utilizando a relação $\sigma = \varepsilon_0\Delta\varphi/2x_0$, onde $\Delta\varphi$ é a diferença de potencial entre as placas ($\Delta\varphi \geq 0$), considerando $x = x_0$, ou seja, a partícula teste saindo pela placa positiva e $q = -e$ (um elétron), teremos

$$\Delta\varphi = \frac{mc^2}{e[1 + \frac{1}{4}\frac{v^2}{c^2}]}\left\{\frac{1}{\sqrt{1 - v^2/c^2}} - 1\right\} . \tag{7}$$

Uma análise numérica da eq. (7) é dada na Figura 1 (curva identificada por $U_W + K_S$).

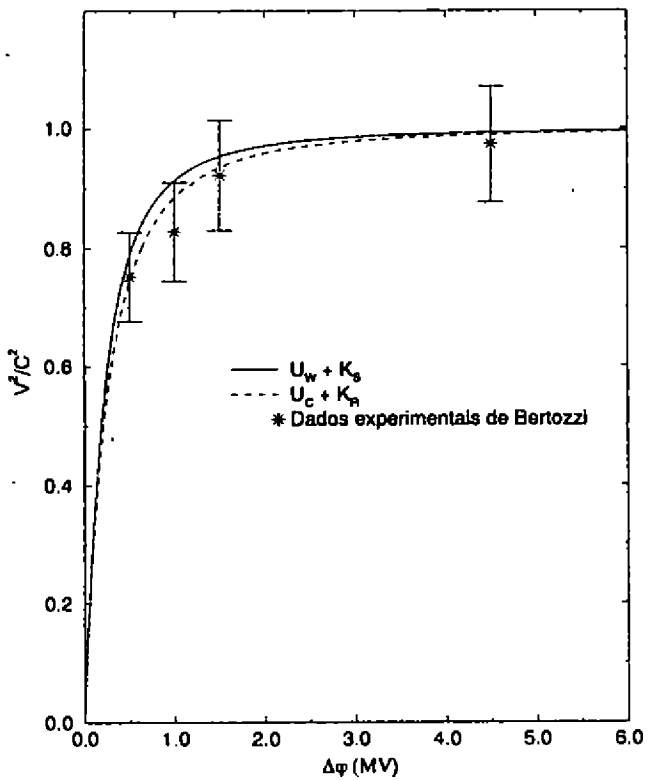

Figura 1. Comparação entre as curvas teóricas para os modelos Weber – Schrödinger e relativístico com os dados experimentais de Bertozzi, com os respectivos erros.

O principal resultado é que a velocidade da partícula acelerada é sempre menor que c e assintótica a c quando $\Delta\varphi \longrightarrow \infty$.

IV – Discussões e Conclusão

Com a finalidade de compararmos os resultados também vamos considerar o tratamento relativístico (energia potencial Coulombiana + energia cinética relativística) e utilizarmos os resultados obtidos na Seção 3. Nos dois modelos utilizamos a conservação de energia na forma $E = K + U$. A energia cinética relativística é dada por $mc^2/\sqrt{1 - v^2/c^2} - mc^2$. Esta expressão é análoga à energia obtida anteriormente. Deve ser novamente resaltado que a massa presente na expressão obtida por Schrödinger tem sua origem na interação gravitacional e a massa presente na energia cinética relativística é a massa inercial da partícula. A energia potencial Coulombiana é obtida das eqs.(5) e (6) fazendo-se $v^2/c^2 = 0$.

No modelo relativístico, $U_C + K_R$, a diferença de potencial em função da velocidade é dada por

$$\Delta\varphi = \frac{mc^2}{e}\left\{\frac{1}{\sqrt{1 - v^2/c^2}} - 1\right\}. \tag{8}$$

A velocidade da partícula, tende a c quando $\Delta\varphi \longrightarrow \infty$, Figura 1 (curva $U_C + K_R$). O modelo Weber-Schrödinger leva ao mesmo resultado, ou seja, a velocidade da partícula tende a c quando $\Delta\varphi \longrightarrow \infty$.

Existe um experimento importante realizado por Bertozzi, [4], onde ele mede o tempo de vôo de um elétron sendo acelerado em um acelerador eletrostático van der Graff e em um acelerador linear, LINAC. Há cinco medidadas em seu experimento nas quais a energia cinética dos elétrons, em MeV, são: 0,5; 1,0; 1,5; 4,5 e 15. A partir da medida

de tempo de vôo dos elétrons em cada medida e da distância viajada pelos elétrons, 8,4 metros, Bertozzi obteve os seguintes valores para v^2/c^2, respectivamente: 0,752; 0,828; 0,922; 0974 e 1,0. Na Figura 1 comparamos os modelos aqui discutidos com os resultados experimentais de Bertozzi. Graficamos v^2/c^2 contra a diferença de potencial que acelera os elétrons. Como podemos ver da Figura 1 o modelo relativístico e o modelo Weber –Schröndiger são compatíveis com os dados experimentais.

Em seu artigo, [4], Bertozzi diz que o erro experimental para todas as medidas é de dez por cento, 10%. Assim também graficamos os dados experimentais de Bertozzi com os respectivos erros. Vemos que as duas curvas teóricas são compatíveis com os dados experimentais dentro da faixa de erro. Como temos somente cinco pontos experimentais e os efeitos de borda devido ao tamanho finito de capacitores reais e a indução de correntes nas placas não foram levados em consideração não podemos decidir entre estas duas últimas curvas teóricas para este experimento.

Maiores estudos são necessários para um melhor entendimento desta situação.

V – Agradecimentos

Os autores desejam agradecer ao CNPq, FAEP e FAPESP pelo suporte financeiro nos últimos anos.

References

[1] SCHRÖDINGER, E. Die Erfüllbarkeit der Relativitätsforderung in der klassischen Mechanik. *Annalen der Physik*, **77**: 325 - 336 (1925).

[2] ASSIS, A. K. T. *Weber's Electrodynamics* (Kluwer Academic Publishers, Dordrecht, 1994).

[3] ASSIS, A. K. T. On Mach's principle. *Foundations of Physics Letters*, **2**: 301 - 318 (1989).

[4] BERTOZZI, W. Speed and kinetic energy of relativistic electrons. *American Journal of Physics*, **32**: 551 - 562 (1962).

Modelo cosmológico multidimensional com viscosidade

Antonio B. Batista, Júlio C. Fabris e Eduardo V. Tonini
CCE, Depart. de Física, UFES, Vitória, ES

June 21, 1996

Introdução

Desenvolveremos uma análise qualitativa das soluções de um modelo cosmológico multidimensional homogêneo e isotrópico onde se considera a presença de um fluido dotado de viscosidade volumétrica. O coeficiente de viscosidade é admitido ser proporcional a uma potência da densidade de energia, como sugerido por Belinskii et al (1977) [1]. As equações de campo são escritas na forma de um sistema dinâmico, e o estudo é desenvolvido usando-se as técnicas conhecidas para esse tipo de problema.

Equações de Campo e Sistema Dinâmico

O elemento de linha para o espaço-tempo $(n+1)$-dimensional [1] é

$$ds^2 = dt^2 - a^2(t)\gamma_{\mu\nu}dx^\mu dx^\nu - b^2(t)\gamma_{ab}dx^a dx^b \quad , \tag{1}$$

onde $\mu,\nu = 0,1,2,3, \quad a,b = 4,5,...,D+3,$ $a(t)$ e $b(t)$ são os fatores de escala dos espaços externo e interno repectivamente, e onde para simplificar, tomamos as curvaturas do espaço interno e externo nulas.

A expressão para o tensor momento-energia para um fluido dotado de viscosidade foi obtida de [2] e é dada por

$$\tilde{T}_{AB} = (\rho + \overline{p})v_A v_B - \overline{p}\tilde{g}_{AB}, \qquad A,B = 0,1,2,...,D+3, \tag{2}$$

com

$$\overline{p} = p' \quad \text{e} \quad \overline{p} = p - \zeta\theta \quad , \theta = v^A{}_{;A} \tag{3}$$

onde ρ é a densidade do fluido, p é a pressão do espaço externo, p' é a pressão do espaço interno, $\zeta > 0$ é a viscosidade volumétrica do espaço externo e de acordo com [1] $\zeta = c_1\rho^\nu$.

As equações de campo são escritas na forma

$$\tilde{R}_{AB} = \tilde{T}_{AB} - \frac{\tilde{g}_{AB}}{(D+2)}\tilde{T} \quad , \tag{4}$$

onde adotamos um sistema de unidades onde $8\pi\tilde{G} = 1$. Usando a métrica de Robertson-Walker, e definindo $H = \frac{\dot{a}}{a}$ e $h = \frac{\dot{b}}{b}$ obtemos

$$\dot{H} = -[H + \frac{(D-1)}{(D+2)}\rho^\nu](3H + Dh) + \beta_4\rho \quad , \tag{5}$$

$$\dot{h} = [-h + \frac{3}{(D+2)}\rho^\nu](3H + Dh) + \beta_7\rho \quad . \tag{6}$$

$$\rho = 3H^2 + 3DHh + \frac{D(D-1)}{2}h^2 \quad . \tag{7}$$

[1] Sendo o espaço interno com dimensão arbitrária D

onde fizemos $c_1 = 1$, sendo $\beta_4 = \frac{1+\alpha(D-1)-D\alpha'}{(D+2)}$ e $\beta_7 = \frac{1-3\alpha+2\alpha'}{(D+2)}$. Desta forma obtemos um sistema bidimensional autônomo.

Pontos Singulares no Infinito

De acordo com [3], as direções dos pontos singulares no infinito são determinadas pela condição

$$-Q(H,h)dH + P(H,h)dh = 0 \quad , \tag{8}$$

onde $P(H,h) = \dot{H}$ e $Q(H,h) = \dot{h}$ são dados pelas equações (5) e (6)respectivamente. Escrevendo as equações de $\dot{H}$ e $\dot{h}$ em termos de coordenadas projetivas, $H = \frac{X}{Z}$ e $h = \frac{Y}{Z}$, substituindo na eq.(8) e usando a condição de ponto singular no infinito, $(X, Y, 0)$, obtemos para análise a expressão:

$$(\frac{3X+(D-1)Y}{D+2})(\rho Z^2)^{\nu}(3X+DY)Z^{1-2\nu} + (\rho Z^2)(X\beta_7 - Y\beta_4) = 0 \quad , \tag{9}$$

onde para qualquer valor de ν temos as direções dos pontos dadas pela expressão

$$\frac{X}{Y} = D\left(-\frac{1}{2} \pm \sqrt{\frac{D+2}{12D}}\right) \quad . \tag{10}$$

Podemos ainda obter

- P/ $\nu < \frac{1}{2}$, $\quad \frac{X}{Y} = \frac{\beta_4}{\beta_7} = \frac{1+\alpha(D-1)-D\alpha'}{1-3\alpha+2\alpha'}$, (11)

- P/ $\nu = \frac{1}{2}$, $\quad (\frac{3X+(D-1)Y}{D+2})(3X+DY) + (3X^2+3DY+\frac{D(D-1)}{2}Y^2)^{\frac{1}{2}}(X\beta_7 - Y\beta_4) = 0$, (12)

- P/ $\nu > \frac{1}{2}$, $\quad \frac{X}{Y} = -\frac{D}{3}$, $\quad \frac{X}{Y} = -\frac{(D-1)}{3}$, (13)

onde no plano X, Y a razão $\frac{X}{Z} = cotg\theta$ fornece a direção dos pontos singulares localizados no infinito. Os pontos cujas direções são determinadas pela eq.(10) estão no limite da região física. Os pontos localizados na direção dada pela eq.(13) estão dentro da região proibida.

Pontos Singulares Finitos

Os pontos singulares finitos são determinados pelas condições $\dot{H} = \dot{h} = 0$. A tabela 1 fornece a localização e a natureza dos pontos singulares, com relação aos valores de ν, α e α'. Devemos ressaltar que quando $\nu = \frac{1}{2}$, para qualquer valor de α e α', temos sempre um ponto singular finito localizado na origem $(H = 0, h = 0)$.

Table 1: Classificação dos Pontos singulares finitos

	$\nu < 0$	$\nu = 0$	$0 < \nu < \frac{1}{2}$	$\frac{1}{2} < \nu < 1$	$\nu \geq 1$
$\alpha' \neq -1$	-	pt de sela (H=0,h=0)	-	-	pt degenerado (H=0,h=0)
$\alpha = \alpha' = -1$	pt de sela (H=0,h)	pts de sela (H=0,h=0) (H=0,h)	pt de sela (H=0,h)	atrator (H=0,h)	atrator (H=0,h) pt degenerado (H=0,h=0)
$\alpha = 0, 1, \frac{1}{3+D}$ $\alpha' = -1$	pt de sela (H=0,h) atrator (H>0,h>0)	pt de sela (H=0,h=0) atrator (H>0,h>0)	pt de sela (H=0,h) atrator (H>0,h>0)	atrator (H=0,h) pt de sela (H>0,h>0)	pt degenerado (H=0,h=0) (atrator (H=0,h) pt de sela (H>0,h>0)

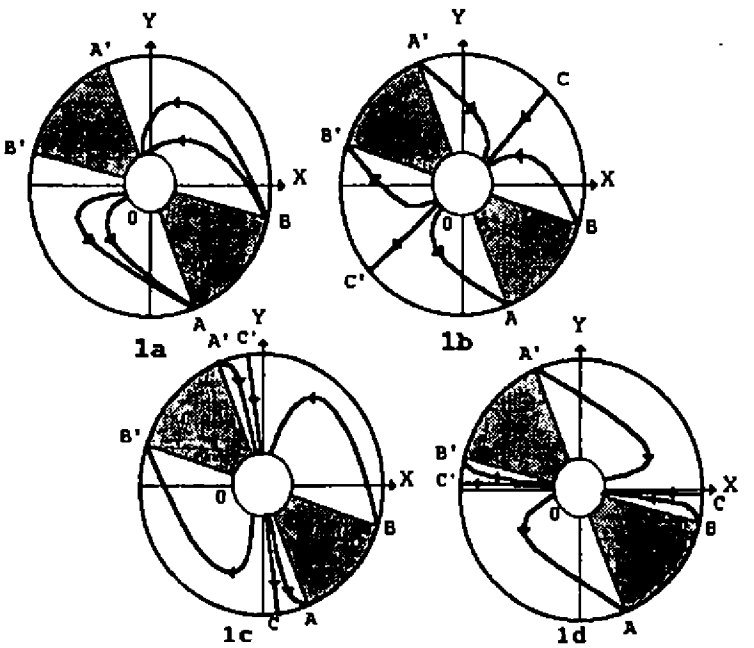

Figura 1. Diagrama de fase evidenciando o comportamento das soluções longe da origem do plano XY.

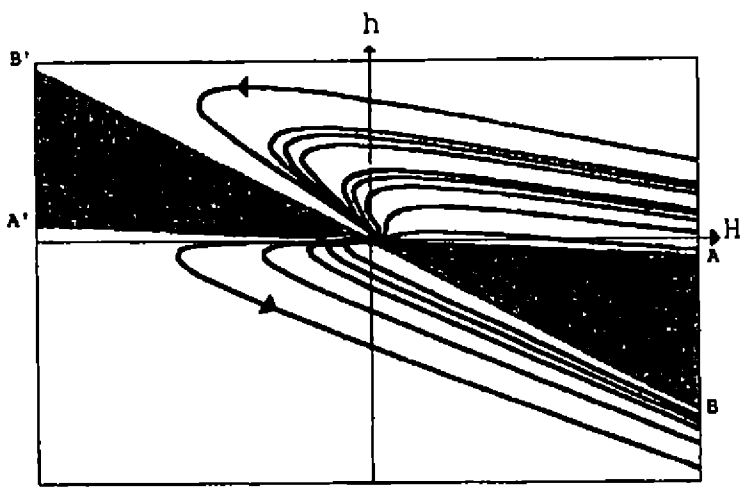

Figura 2. Diagrama de fase para o caso $\nu = \frac{1}{2}$ ou $\nu \geq 1$ e $\alpha' \neq -1$.

Análise dos Diagramas de Fase

Notamos que a influência da viscosidade sobre a estrutura dos diagramas depende do valor de ν. Assim, como podemos observar na eq.(11), para $\nu < \frac{1}{2}$ a estrutura dos diagramas de fase é sensivel aos valores de α e α'. Pela eq.(12), para $\nu = \frac{1}{2}$, vemos que a influência dos parâmetros α e α', já é menor. Para o caso $\nu > \frac{1}{2}$, vemos pela eq.(13) que a estrutura do diagrama de fase, não é influenciada pelas mudanças que ocorrem na equação de estado durante a evolução do Universo.

Na fig.1*a*, no setor BOA' as curvas indicam que o espaço externo se expande, enquanto o espaço interno se contrai. Neste caso o modelo começa a evoluir de um ponto sobre a curva $\rho = 0$. No setor $B'OA$ estão as curvas que terminam sua evolução com o espaço externo expandindo e o espaço interno contraindo tendendo a uma singularidade localizada sobre a curva $\rho = 0$. Na fig.1*b* há o aparecimento de uma solução do tip o Big-Bang começando no ponto C, onde o espaço interno e externo tem o mesmo comportamento inicial(expansão), e uma solução começando no ponto A', onde o espaço externo inicia sua evolução contraindo, com o espaço interno ex pandindo inicialmente. A solução que termina sua evolução no ponto C' é uma solução do tipo Big-Crunch.

Na fig.1*c* aparece uma solução iniciando em C' que representa o Universo com expansão no espaço interno e contração no espaço externo.

Na fig.1*d* o diagrama contém uma solução do tipo Big Bang para o espaço externo enquanto o espaço interno se contrai.

As curvas próximo à origem do plano (H, h), para $\nu \leq 0$, ultrapassam a região proibida ($\rho < 0$). A fig.2 representa o caso $\nu = \frac{1}{2}$ para qualquer valor de α e α' onde o diagrama apresenta um ponto singular na origem. Para o caso $\alpha' \neq -1$ e $0 < \nu < \frac{1}{2}$ ou $\frac{1}{2} < \nu < 1$ não há ponto singular na origem. As soluções assintóticas, próximo à origem, no setor $A0B'$, são as mesmas que no caso sem viscosidade: descrevem uma expansão do espaço externo tendendo ao espaço-tempo de Minkowski.

Na fig.3*a* apresentamos o caso $\nu \geq 1$. Na fig. 3*b* representamos o caso $\nu \geq 1$ e $(\alpha = \alpha' = -1)$, onde temos dois ponto singulares, sendo que para os demais valores de ν, só um ponto singular aparece.

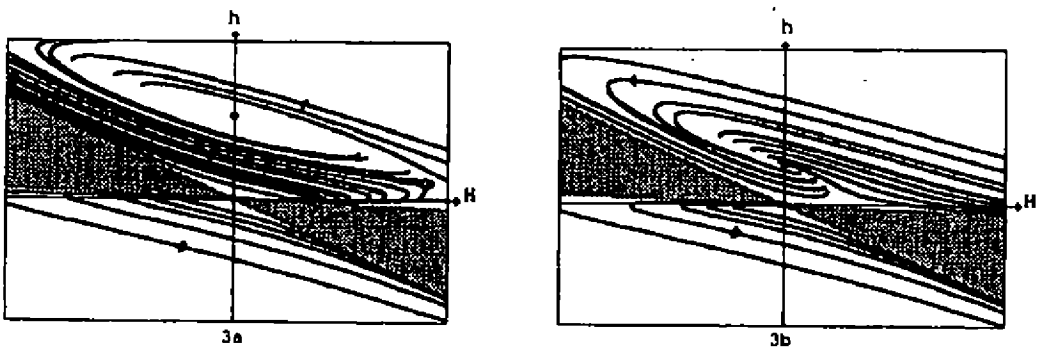

Figura 3. Diagrama de fase para o caso: a) $\nu \geq 1$ e $(\alpha, \alpha') = (0, -1); (1. - 1); (\frac{1}{3+D}, -1)$, b) $\nu \geq 1$ e $\alpha = \alpha' = -1$.

Conclusão

Assim como foi encontrado para os modelos com matéria [6], a maioria das soluções apresentam um estágio inicial onde a influência da matéria pode ser negligenciada e as condições iniciais são determinadadas pelas e quações de Einstein para o vácuo. O modelo apresenta uma propriedade interessante: há soluções onde no início da evolução a densidade de matéria é nula. A seguir aumenta, ao longo da expansão do espaço externo, até um valor máximo, após o qual cai novamente a zero para $t \to \infty$, de acordo com o modelo padrão, no seu estágio final.

References

[1] V. A. Belinskii e I. M. Khalatnikov, *Viscosity and Effcts in Isotropic Cosmologies*, Sov. Phus. JETP, Vol. **45**,$N°$. 1(1977);

[2] S. Chakraborty e G. Nandy, *Viscous Fluid in a Five-Dimensional Cosmological Model*, Astrophys. J., **401**, 437(1992);

[3] G. Sansone e R. Conti, *Non-Linear Differencial Equations*, Pergamon Press, Oxford(1964);

[4] A. B. Batista, J. C. Fabris e E. V. Tonini, *Étude Qualitative des Théories de Kaluza et Klein*, C. R. Acad. Sci. Paris, t.320. sér *II*b, 239(1995);

[5] J.C. Fabris e J. Tossa, *Qualitative Study of Multidimensional Cosmologi- cal Models*, Phys. Lett. **B 296**, 307(1992);

[6] E. V. Tonini, *Estudo Qualitativo de Teorias do Tipo Kaluza-Klein*, Tese de Mestrado(1995), CCE/UFES, Brasil.

A new determination of the galactic rotation curve *

R. Ortiz
Departamento de Física - UFES
Campus Universitário - Vitória - ES - 29060-900
and
L.H. Amaral, J.R.D. Lepine, and W.J. Maciel
Departamento de Astronomia - IAG/USP
Av. Miguel Stéfano, 4200, São Paulo - SP - 04301-904

Received March, 1996

The rotation curve of the Galaxy is obtained from a sample of planetary nebulae and asyntotic giant branch (AGB) stars. The rotation curve exhibits a steep decrease in the solar neighbourhood, and a minimum at about $R = 8.5$ kiloparsecs (adopting $R_\odot = 7.9$ kpc). The curve is fitted with a mass distribution model of the Galaxy, based on the model for star counts in the infrared of Ortiz & Lepine [1] ; the main components are: a spheroid, representing both the bulge and the halo, and two exponential disk components. The surface density of the disk in the solar neighbourhood is $77 M_\odot \mathrm{parsec}^{-2}$, not very different from the value predicted by star counts. This result implies that there is not need for a dark matter component, at least up to a radius of about 12 kpc.

1 Introduction

The internal constitution and dynamics of galaxies are usually studied by means of their rotation curve. Most determinations of the rotation curve are based on observations of young objects, such as young stars, HII regions, and molecular gas data, which are expected to obey the rotation curve more closely. Stellar objects for which individual distances can be obtained, such as open clusters [2], and classical cepheids [3], can be also to be considered as kinematic tracers.

Maciel & Dutra [4] show that more massive, type I planetary nebulae (PNe) follow the galactic rotation curve more closely than type II and III PNe; that means they are young objects and may, in principle, be used as kinematic tracers. A similar behaviour is found among more massive, AGB stars: according to Ortiz & Maciel [5], class I OH/IR stars (oxygen-rich AGB stars, that represent the precursors of type I PNe), may be considered also, kinematic tracers, because of their small deviations from the galactic curve.

In this work we derive the galactic rotation curve, using a mixed population that comprises planetary nebulae, oxygen-rich (OH/IR) and carbon-rich AGB stars as kinematic tracers. Adopting adequate selection criteria in order to select younger objects, a kinematically homogeneous sample is constituted. The curve is fitted by a mass-distribution model that considers several galactic populations, based on a star counts model of Ortiz & Lepine [1]. We discuss the necessity of a dark matter component in this model.

2 The sample

The sample of objects used in this work contains 33 type I planetary nebulae, 80 class I OH/IR stars, and 69 carbon stars that undergo mass loss exceeding a rate of $10^{-6} M_\odot \mathrm{year}^{-1}$. Planetary nebulae were extracted from [4]; OH/IR stars were selected from [6]; and carbon stars were compiled and selected from catalogues [7], and [8].

The distance scales used in this work refer to the original papers: [4] for PNe; [5] and [6] for OH/IR stars; and [9] for carbon-rich stars. The radial velocities of the objects were extracted from the literature (see the papers above for a full reference list).

An additional criterium excluded objects far from the galactic plane ($z > 200$ parsecs), because they may present large deviations of the rotation curve.

*This work was partially supported by FAPESP under grant 91/2315-8, and by CNPq.

3 The model

In this work we compare the results obtained by the sample with a proposed model of distribution of mass which is in turn, derived from the model of Ortiz & Lepine [1] designed for the infrared. The model considers distinct populations for the Galaxy, according to their age, metallicity, and space distribution.

The main components are:

1) a spheroid, represented by the Hernquist's function [10]:

$$\rho(R) = \frac{M_b}{2\pi}\frac{a}{R}\frac{1}{(R+a)^3} \tag{1}$$

where M_b is the total mass of this component and a the scale length.

2) a mixed stellar disk, with surface mass density represented by two exponential laws:

$$\sigma(R) = \sigma_1 e^{-R/\alpha_1} + \sigma_2 e^{-R/\alpha_2} \tag{2}$$

where α_1 and α_2 are the scale lengths of the disk components (thin disk, thick disk), according to the model of Ortiz & Lepine [1]. We use the infinitesimal thin-disk approximation developed by Freeman [11] to obtain the gravitational potential.

3)gas (atomic + molecular), fitted to the CO and HI data [12]. The thin-disk approximation is considered also in this case. The observed gas density can be represented by the following distribution:

$$\sigma(R) = \sigma_o e^{-(\rho R)^2} + \frac{a_1 R^2}{({b_1}^2 + R^2)^{5/2}} + \frac{a_2 R^2}{({b_2}^2 + R^2)^{5/2}} \tag{3}$$

4)a spiral-arm perturbation potential, which considers a two-plus-four component:

$$\begin{aligned}\phi_p(r,\theta) &= ARe^{(-\beta R)}\cos\left(\frac{m\ln(R)}{\tan(i)} - m(\theta-\gamma)\right) + \\ &\quad ARe^{(-\beta R)}\alpha\cos\left(\frac{2m\ln(R)}{\tan(i)} - 2m(\theta-\gamma)\right)\end{aligned} \tag{4}$$

where θ is the galactocentric angle, A is the amplitude of the perturbation, β^{-1} the scale length of the spiral, i the pitch angle, $m = 2$, α is the relative strength of the two-to-four components, and γ a phase angle.

When fitting the model, we consider that the gas distribution is known as well as α_1 and α_2, derived by Ortiz & Lepine [1]. The other parameters are allowed to vary, in order to match the model to the sample.

4 Results

In this work we consider the galactocentric distance of the Sun, $R_\odot = 7.9$ kiloparsecs and the galactic rotation velocity at this point $\Theta_\odot = 184$ km/s ([13] and [1]).

Figure 1 summarizes the fitting of the model to the data. Open circles represent the average value for Θ in the R considered, for the whole sample. The crosses are determinations from the sample of Clemens [14], who used HI and CO data (corrected here for $R_\odot = 7.9$ kpc). Gas data are useful for fitting the mass model in the inner parts of the Galaxy, where PNe and AGB stars were not included in this study. Systematic errors on galactic rotation curve do not compromise the results [15].

A number of interesting features can be observed. The rotation curve presents a broad maximum around $R = 6$ kpc, a sharp minimum at 8.5 kpc, and an enhancement around 10 kpc. The existence of a minimum at 8.5 kpc has been observed by other authors, but its nature has not been fully discussed. It is expected from Oort's constants, which give a negative gradient of rotation velocity near the Sun, while at large distances the rotation curve seems to rise [16]. However, the magnitude of the gradient at the solar neighbourhood obtained in this work is greater than most previous works. Our results indicate also, that the Galaxy possibly presents a flat rotation curve in its external part, like many other spiral galaxies. However, up to $R = 12$ kpc, we do not need a dark matter halo to fit the data; that puts a constraint to the upper limit of density of dark matter.

The local density of matter that fits better the data is $77 M_\odot \text{parsec}^{-2}$, in a good agreement with star counts, since we obtain $51 M_\odot \text{parsec}^{-2}$ from the model of Ortiz & Lepine ($40 M_\odot \text{parsec}^{-2}$ for the stars and $11 M_\odot \text{parsec}^{-2}$ for the gas); the model of Ortiz & Lepine does not take into account white dwarfs which could amount to about 20% of the total mass [17].

References

[1] Ortiz, R., Lepine, J.R.D.: 1993, A&A 279, 90

[2] Hron, J.: 1986, A&A 176, 34

[3] Pont, F., Mayor, M., Burki, G.: 1994, A&A 285, 415

[4] Maciel, W.J., Dutra, C.M.: 1992, A&A 262, 271

[5] Ortiz, R., Maciel, W.J.: 1994, A&A 287, 552

[6] Lepine, J.R.D., Ortiz, R., Epchtein, N.: 1995, A&A 299 453

[7] Loup, C., Forveille, T., Omont, A., Paul, J.F.: 1993, A&AS 99, 291

[8] Kastner, J.H., Forveille, T., Zuckerman, B., Omont, A.: 1993, A&A 275, 163

[9] Guglielmo, F., Epchtein, N., Le Bertre, T., Fouqué, P., Hron, J., Kerschbaum, F., Lepine, J.R.D.: 1993, A&AS 99, 31

[10] Hernquist, L.: 1990, Ap.J. 356, 359

[11] Freeman, K.C.: 1970, Ap.J. 160, 811

[12] Sanders, D.B., Solomon, P.M., Scoville, N.Z.: 1984, Ap.J. 276, 182

[13] Rohlfs, K., Kreitschmann, J.: 1987, A&A 178, 95

[14] Clemens, D.P.: 1985, Ap.J. 295, 422

[15] Amaral, L.H., Ortiz, R., Lepine, J.R.D., Maciel, W.J.: 1996, M.N.R.A.S. in press.

[16] Blitz, L.: 1979, Ap.J. 231, L115

[17] Bahcall, J.N., Soneira, R.M.: 1980, Ap.J.S. 44, 73

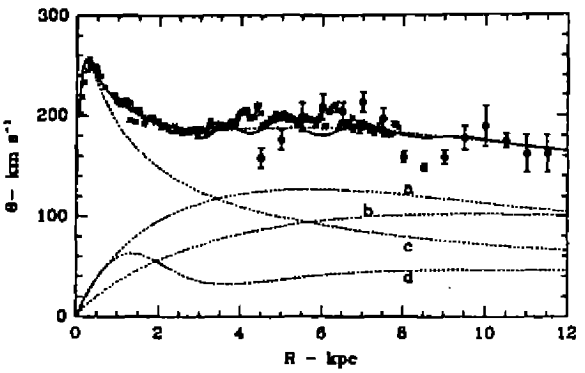

Figure 1. The rotation curve of the Galaxy. Interstellar gas data by Clemens are shown (crosses). The dashed line is the model of mass distribution. The components of the model are also shown: (a) thick disk with 2.6 kpc scale-length; (b) thin disk with 4.5 kpc scale-length; (c) bulge; (d) gas. The solid line represents the mass model plus a model for the spiral arm velocity field.

Determinação dos parâmetros de uma onda gravitacional com uma antena ressonante esférica

Odylio D. Aguiar
Divisão de Astrofísica, INPE, C.P. 515,
S.J. Campos, SP 12201-970, Brazil

Nadja S. Magalhães, Warren W. Johnson and Carlos Frajuca
Phys. & Astron., Louisiana State University
Baton Rouge, LA 70803, USA

Received March, 1996

Mostra-se que a interação de uma onda gravitacional com uma antena ressonante esférica muda a forma da antena para a de um elipsóide. Devido à geometria esférica da antena, estas mudanças ocorrem para qualquer que seja a direção e polarização da onda. Esta propriedade de onidirecionalidade também implica que a antena esférica não possui zonas "cegas" para detecção. Portanto, ao contrário das antenas tipo barra ou interferômetros laser, ela não "perde" nenhum evento. Mostra-se, também, em que condições ela é capaz de determinar a direção e a polarização da onda ou fornecer informações sobre os seis padrões de polarização possíveis para uma onda plana gravitacional fraca em teorias métricas de gravitação.

Introdução

Algumas das vantagens de uma antena de massa ressonante esférica são: ela pode ter uma "visão" espacial sem nenhuma zona cega para detecção, ela pode determinar a direção de uma onda gravitacional confirmada, e ela pode determinar a polarização da onda.

Tanto as barras de Weber como os interferômetros laser têm zonas cegas. Ao contrário disto, esferas de Forward ou buckybolas de Johnson-Merkowitz não tem zonas cegas.

O Elipsóide de Maré

Qual é o formato instantâneo que um conjunto de partículas teste, que formava inicialmente uma superfície esférica, vai assumir sob a presença de uma onda gravitacional monocromática? Na aproximação de campo fraco:
$g_{\mu\nu} = \eta_{\mu\nu} + h_{\mu\nu}, \quad \mu,\nu = 0,1,2,3, \quad |h_{\mu\nu}| \ll 1.$

No referencial do laboratório:

$$\mathbf{h} = [h_{\mu\nu}] = \begin{bmatrix} 0 & 0 & 0 & 0 \\ 0 & h_{xx} & h_{xy} & h_{xz} \\ 0 & h_{yx} & h_{yy} & h_{yz} \\ 0 & h_{zx} & h_{zy} & h_{zz} \end{bmatrix}.$$

sendo $h_{kl} = h_{kl}(\vec{x}, t)$

Para uma onda gravitacional se propagando na direção z' (referencial $x'y'z'$ da onda) e utilizando a gauge TT (Misner, Thorne & Wheeler 1973), a matrix simétrica h tem componentes $h_{xx} = -h_{yy} = h_+$, $h_{xy} = h_{yx} = h_\times$, sendo todos os outros iguais a zero. Se nós escolhermos, agora, a origem do nosso sistema de coordenadas espacial no centro de uma superfície esférica formada por um conjunto de partículas teste, a distância própria destas partículas da origem espaçotempo é dada por:

$$|\vec{\mathbf{v}}|^2 = x_\mu x^\mu = x^\nu g_{\mu\nu} x^\mu. \tag{1}$$

Em um espaçotempo Minkowskiano:

$|\vec{\mathbf{v}}|^2 = -x_0^2 + \vec{\mathbf{x}}^2$ para um instante fixo x_0, definindo a superfície esférica acima mencionada.

Com o objetivo de visualizar o efeito instantâneo de uma onda gravitacional no espaçotempo, nós vamos rodar os eixos x' e y' em relação ao eixo z' de um ângulo λ tal que, para um determinado instante $t = t_0$, $\tan\,\lambda = \sqrt{\frac{h_t - h_+(t_0)}{h_t + h_+(t_0)}}$, onde $h_+(t_0) + h_\times(t_0)$ são as amplitudes de polarização instantâneas no instante $t = t_0$ e

$$h_t \equiv \sqrt{h_+^2(t_0) + h_\times^2(t_0)}. \tag{2}$$

Nós chamamos este referencial de referencial diagonal instantâneo $x''y'z''$. A razão do nome diagonal é simples: após esta rotação $\mathbf{g}$ é diagonal porque os únicos componentes não nulos de $\mathbf{h}$ são $h_{x''x''} = -h_{y''y''} = h_t$.

Neste referencial a equação (1) assume a forma

$$|\mathbf{v}|^2 = -x_0''^2 + (1 + h_t)\,x''^2 + (1 - h_t)\,y''^2 + z''^2. \tag{3}$$

Pelo fato de $h_t \ll 1$ constatamos que para um x_0'' constante a equação acima descreve um elipsóide no espaço $x''y'z''$. Nós chamamos este elipsóide de Elipsóide de Maré, uma vez que ondas gravitacionais produzem acelerações de maré entre partículas. Note que este elipsóide não muda a sua dimensão ao longo da direção z'', a direção de propagação da onda gravitacional; isto é uma conseqüência da transversalidade da gauge TT.

Determinação da Direção da Onda

Assumindo que a Relatividade Geral representa adequadamente a nossa gravitação e retornando à nossa matrix $\mathbf{h}$ no referencial do laboratório, definindo a direção de propagação da onda pelo vetor $\vec{n}$:

$$\vec{n} \equiv \begin{bmatrix} 0 \\ n^x \\ n^y \\ n^z \end{bmatrix}.$$

a direção pode ser encontrada resolvendo uma equação de autovalor (Dhurandhar & Tinto 1988)

$$\mathbf{h}\,\vec{n} = 0\,\vec{n} \tag{4}$$

A solução em coordenadas esféricas no referencial do laboratório é dada por um par de ângulos (θ, ϕ) (pois $\sin\phi) = \pm\sqrt{\ldots}$), correspondendo a direções diametralmente opostas, dadas pelas expressões:

$$\tan\phi = \frac{n^y}{n^x}, \quad \tan\theta = \frac{\sqrt{(n^x)^2 + (n^y)^2}}{n^z} = \frac{n^y}{n^z}\frac{1}{\sin\phi}. \tag{5}$$

Vejamos a seguir um método, que derivamos, e que envolve um cálculo algébrico mais simplificado.

Método Geométrico

Um outro método, de fácil visualização, pode ser encontrado a partir da definição dos vetores:

$\vec{A} \equiv (h_{xx}, h_{xy}, h_{xz}) = h_{xj}\,\hat{\mathbf{e}}^j$, $\vec{B} \equiv (h_{yx}, h_{yy}, h_{yz}) = h_{yj}\,\hat{\mathbf{e}}^j$, $\vec{C} \equiv (h_{zx}, h_{zy}, h_{zz}) = h_{zj}\,\hat{\mathbf{e}}^j$,

onde $\hat{\mathbf{e}}^j$ são os vetores unitários que descrevem o referencial do laboratório quando a onda está presente, as equações (4) podem ser reescritas como

$$\vec{A}\,.\,\vec{n} = \vec{B}\,.\,\vec{n} = \vec{C}\,.\,\vec{n} = 0. \tag{6}$$

Os vetores $\vec{A}$, $\vec{B}$ and $\vec{C}$ são, portanto, coplanares e perpendiculares à direção de propagação da onda gravitacional, que pode, então, ser facilmente determinada se efetuando o produto vetorial entre qualquer dois dos três vetores acima.

Na pratica, $\vec{A}$, $\vec{B}$ and $\vec{C}$ estão relacionados com as diferenças entre os vetores base covariantes do espaço curvo, $\hat{\mathbf{e}}_j$ (os quais descrevem o referencial do laboratório depois da chegada da onda) e os vetores base Cartesianos unitários do espaço Euclideano, $\mathbf{i}_j = \eta_{jk}\,\hat{\mathbf{e}}^k$ (que descrevem o referencial de laboratório antes da onda chegar):

$$\vec{A} = \hat{e}_x - i_x, \qquad \vec{B} = \hat{e}_y - i_y, \qquad \vec{C} = \hat{e}_z - i_z.$$

Vetor Poynting de uma Onda Gravitacional

Para uma onda gravitacional monocromática em um referencial quase inercial da teoria linearizada, a densidade de energia da onda é dada (veja Misner et al. 1973, sect. 35.7; c é a velocidade da luz e G é a constante gravitacional) por $T_{00} = \frac{c^2}{32\pi G} \sum_{i,j=1}^{3} \left\langle \dot{h}^{ij} \dot{h}^{ij} \right\rangle$, onde <> denota uma média sobre vários comprimentos de onda, e o ponto implica uma derivada temporal. Mas, temos que:

$$-h_t^2 = h_{xx}h_{yy} - h_{xy}^2 + h_{xx}h_{zz} - h_{xz}^2 + h_{zz}h_{yy} - h_{zy}^2 = \vec{A} \times \vec{B} \cdot \hat{e}_z + \vec{C} \times \vec{A} \cdot \hat{e}_y + \vec{B} \times \vec{C} \cdot \hat{e}_x. \qquad (7)$$

No referencial diagonal $(\vec{A} \times \vec{B})'' \cdot \hat{e}_z = -h_t^2$ e o vetor Poynting gravitacional fica, portanto, $\vec{S}_g = c T_{00} \vec{n} = \frac{c^3}{16\pi G} \left\langle \dot{h}_0^2 \right\rangle \vec{n} = \frac{c^3}{32\pi G} \left\langle \ddot{\vec{B}}'' \times \ddot{\vec{A}}'' \right\rangle$. Este resultado é análogo a um encontrado na teoria eletromagnética (veja Misner et al. 1973, sect.5.6) com $\ddot{\vec{B}}''$ e $\ddot{\vec{A}}''$ no lugar dos vetores de campo elétrico e magnético.

Antena esferoidal acoplada a transdutores

A matrix **h** no referencial do laboratório tem apenas 5 componentes independentes, pois ela é uma matrix puramente espacial simétrica e sem traço. Portanto, cinco ou mais transdutores (ressonantes ou não) acoplados à superfície de uma antena esferoidal (esfera, buckybola ou outro poliedro simétrico), e que não sejam diametralmente opostos entre si (para não ocorrer redundância), serão suficientes para obter a matrix **h**, que define o estado completo de uma onda gravitacional monocromática – direção de propagação e polarização – a partir dos 5 coeficientes do polinômio, formado pelas 5 funções harmônica esféricas de l=2, que define o estado de oscilação quadripolar da antena.

Caso existam seis ou mais transdutores não ressonantes acoplados, além dos modos quadripolares (l=2) também poderá ser observado o modo monopolar (l=0, m=0). Esta observação adicional permite se determinar os seis padrões de polarização possíveis para uma onda plana gravitacional fraca em teorias métricas de gravitação. Porém, para o caso de transdutores ressonantes, o modo monopolar não ressoa na mesma freqüência que os modos quadripolares para um corpo esferoidal, o que impossibilita que possamos definir aqueles padrões gerais de polarização com apenas uma antena esferoidal. Uma segunda antena será necessária.

Agradecemos Z. Geng, W. O. Hamilton e S. M. Merkowitz por frutíferas discussões, e N. S. M. e C. F. agradecem à CAPES e ao CNPq, respectivamente, pelo suporte.

REFERENCES

Dhurandhar, S.V., & Tinto, M. 1988, MNRAS, 234, 663.
Forward, R.L. 1971, Gen. Relativ. Gravit., 2, 149.
Jonhson, W.W., & Merkowitz, S. 1993, Phys. Rev. Lett., 70, 2367.
Magalhães, N.S., Johnson, W.W., Frajuca, C., & Aguiar, O.D. 1995, MNRAS, 274, 670.
Misner, C.W., Thorne, K.S., & Wheeler, J.A. 1973, Gravitation (W.H. Freeman & Co.).

Model Interacting Boson-Fermion Stars

Cláudio M. G. de Sousa *and J. L. Tomazelli †
International Centre for Theoretical Physics,
P.O. Box 586, 34100, Trieste, Italy

Vanda Silveira
Departamento de Física, Universidade de Brasília, 70910-900, Brasília-DF, Brazil

Received March, 1996

The more accepted cosmological models predict the existence of a hidden matter, the so called Dark Matter, without which the observed luminous mass density does not approximate the expected critical value. Astrophysical observations [1] of gas clouds in spiral galaxies lead one to conclude that the observed luminous mass is not sufficient to explain its orbital velocity: the dark matter should be 3 to 10 times more abundant than the ammount observed for the luminous one.

In spite of the fact they are known for a certain time [2], compact equilibrium configurations of boson fields (boson stars) have recently arouse great interest due to the conjecture that the dark matter may be composed partially by bosonic particles, under the form of compact objects. Since its formation probably occurred in the early universe in the presence of fermions, one may expect that those structures also contain fermions.

This report gives an outline of current-current type interaction between self-gravitating bosons and fermions [3]. Another approach for interaction in a boson-fermion star has been sugested [4] in a different way. In this model one introduces contact interaction for bosons and fermions via

$$\mathcal{L}^{int} = \lambda J_\mu(\Phi) j^\mu(\psi) \ , \tag{1}$$

where

$$J_\mu(\Phi) = i(\Phi^* \partial_\mu \Phi - \Phi \partial_\mu \Phi^*) \ , \tag{2}$$

$$j^\mu(\psi) = \overline{\psi} \gamma^\mu \psi \tag{3}$$

which represent the boson and fermion currents, respectively. The current for the boson fields arises from the usual Lagrangian for boson stars

$$\mathcal{L} = \frac{R}{16\pi G} - \partial_\mu \Phi^* \partial^\mu \Phi - m^2 \Phi^* \Phi \ , \tag{4}$$

where

$$\Phi(r, \tau) = \phi(r) e^{-i\omega\tau} \tag{5}$$

and ω is a frequency which determines the system energy. The cosmological time τ is given by the metric used, which is spherically symmetric chosen in the form

$$ds^2 = -B(r)d\tau^2 + A(r)dr^2 + r^2 d\theta^2 + r^2 \sin^2\theta d\varphi^2 \ . \tag{6}$$

Fermions are introduced as a relativistic perfect fluid in accordance with the prescriptions for pure fermion and boson-fermion stars [4,5]. The total energy-momentum tensor is given by the contribution of boson and fermion matter, and by the interaction term

$$T_{\mu\nu} = T^B_{\mu\nu} + T^F_{\mu\nu} + T^{int}_{\mu\nu} \tag{7}$$

*On leave from Departamento de Física, Universidade de Brasília, 70910-900, Brasília-DF, Brazil *and* International Centre of Condensed Matter Physics, Universidade de Brasília , Caixa Postal 04667, 70919-970, Brasília - DF, Brazil
†On leave from Instituto de Física Teórica–UNESP, Rua Pamplona 145, 01405-900, São Paulo–SP, Brazil

where the labels B, F and 'int' mean boson, fermion and interaction terms, respectively. Due to the metric only two components of the interaction energy-momentum tensor are used to determine the differential equations, namely $T_r^{r\ int}$ and $T_r^{r\ int}$. If one considers $\phi(r)$ as a real scalar field, as usually done for boson stars, $T_r^{r\ int}$ vanishes. This fact is not desirable since this component is representative of the changes in energy corresponding to the interaction. Hence, one is lead to write the scalar field as a sum of real and imaginary parts $\phi(r) = \phi_1(r) + i\phi_2(r)$, with which $|\Phi|^2 = |\phi|^2 = \phi_1^2 + \phi_2^2$.

The mixed configuration considered here takes boson field in its ground-state and the fermion fluid is allowed to display very slow radial velocities. This directly expresses that chemical potential for the Fermi gas is not to high in the kinetic energy scale, and so the Fermi surface allows only very slow velocities at zero temperature.

The interaction introduced by (1) imposes many modifications in the configuration, one of those is a singularity in the evolutional equations. Another interesting feature of this kind of interaction is that the ground-state energy of the configuration increases with λ up to a certain value, where the energy starts decreasing while λ increases. At this point of the system energy the real and imaginary parts of $\phi(r)$ display different behaviours, as shown in the figure.

The approach presented here can give rise to other kind of stellar objects, as stars of WIMP's [6], for which one takes into account interacting boson-fermion stars reinterpreted in the context of minimal supersymmetric standard model. In some sense an enhacement of the emission rate of gravitational waves can be expected due to the interaction within the star body and its neighbourhood.

References

1. E. W. Kolb & M. S. Turner, *The Early Universe* (Addison-Wesley, 1990).
2. R. Ruffini and S. Bonazzola, *Phys. Rev.* **187** (1969) 1767; Ph. Jetzer, *Phys. Rep.* **220**, 4 (1992) 163; A. R. Liddle and M. S. Madsen, *Int. J. Mod. Phys.* **D 1**, 1 (1992) 101.
3. C. M. G. de Sousa, J. L. Tomazelli and V. Silveira, *ICTP preprint* IC/95/187.
4. A. B. Henriques, A. R. Liddle and R. G. Moorhouse, *Phys. Lett.* **B 233** (1989) 99;
   A. B. Henriques, A. R. Liddle and R. G. Moorhouse, *Nucl. Phys.* **B 337** (1990) 737.
5. J. R. Oppenheimer and G. M. Volkoff, *Phys. Rev.* **55** (1939) 374.
6. F. Pisano and J. L. Tomazelli, *Mod. Phys. Lett.* **A** (to appear).

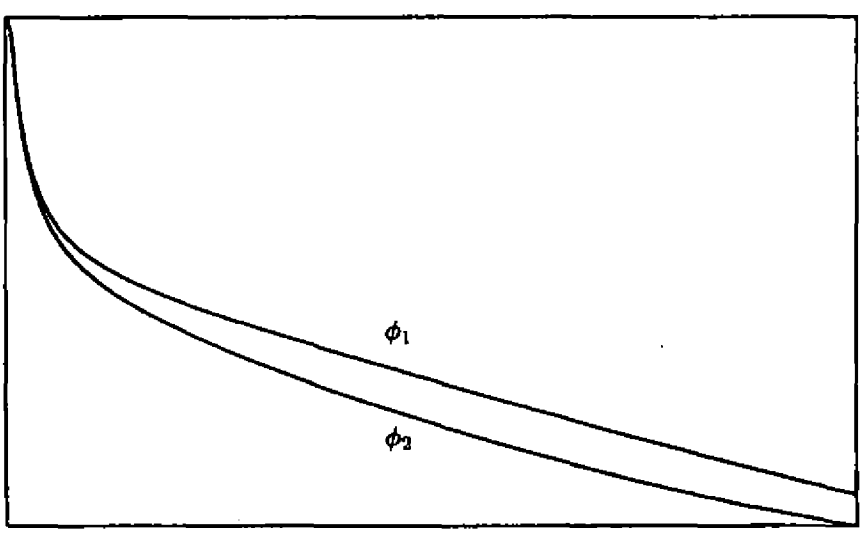

Figura 1. Plotting showing the splitting between ϕ_1 and ϕ_2, respectively the real and imaginary parts of the scalar field $\phi(r)$.

Relatividade geral sem singularidades. Existe buraco negro?

Manoelito M. de Souza, Robson Nascimento Silveira
Universidade Federal do Espírito Santo - Departamento de Física
*29065.900 - Vitória-ES-Brasil**

Received March, 1996

Em um formalismo clássico que incorpora,antecipadamente, o carater discreto e granular da interação quântica, a eletrodinâmica clássica é formulada em termos de fótons clássicos, de um modo consistente e livre de singularidades. Valores médios de fluxos de fótons clássicos é que são singulares e correspondem aos campos do formalismo usual. Assim, as singularidades de campo na Eletrodinâmica Clássica não têm sentido físico, são consequências deste carater de média dos campos.
Aplicamos este formalismo à Teoria da Relatividade Geral. Consideramos o campo gravitacional como sendo descrito pela troca de grávitons clássicos: interações discretas, descritas por um campo tensorial de segunda ordem, simétrico, de massa nula e de natureza granular (localizado). As equações de Einstein geram, então, soluções de simetria esférica, não singulares. O valor médio do fluxo destas soluções é a solução de Schwarzchild.

*e-mail:manoelit@cce.ufes.br

Exact Solutions Related to Nonminimal Gravitational Coupling

C. M. G. de Sousa* and F. E. Mendonça da Silveira
Instituto de Física Teórica-UNESP, Rua Pamplona 145,
01405-900, Bela Vista, São Paulo-SP, Brazil

Received March, 1996

We obtain exact analytic solutions for a typical autonomous dynamical system, related to the problem of a vector field nonminimally coupled to gravity.

Gravity is presently the only interaction that is not inserted in any of the unification schemes. Due to this fact, many toy models have appeared coupling gravity to fields that could have played significant role in the Early Universe, in such wise as to display desirable properties. Special interest has been put in gravity coupled nonminimally to other fields which could generate, among a number of new effects, a non-singular universe.

In this context, dynamical systems techniques have been applied to solve the problem of coupling of gravity to a vector field, whose Lagrangian can be written as [1]

$$\mathcal{L} = \sqrt{-g}\left(\frac{R}{k} - \frac{1}{4}F_{\mu\nu}F^{\mu\nu} + \beta R W_\mu W^\mu\right), \tag{1}$$

where $g = \det g_{\mu\nu}$ ($g_{\mu\nu}$ is the metric tensor), R is the scalar of curvature, $G = k/8\pi$ is the Newtonian gravitational constant in units that $\hbar = c = 1, \mid \beta \mid = 1, W_\mu$ is an arbitrary vector field and $F_{\mu\nu} = W_{[\mu,\nu]}$, where the comma represents ordinary differentiation and the square brackets represent the skew-symmetric part of $W_{\mu,\nu}$.

The Lagrangian (1) leads to a set of equations of motion that can be transformed into an autonomous dynamical system [1]. By choosing the Robertson-Walker metric

$$ds^2 = dt^2 - S^2(t)\left[d\chi^2 + \sigma^2(\chi)(d\theta^2 + sin^2\theta d\phi^2)\right],$$

with the ansatz $W^2 = W^2(t)$, the Lagrangian (1) leads to equations of motion which has a solution given by

$$W^2(t) = \frac{1}{k}\left(1 - \frac{t}{S}\right),$$

$$S(t) = (t^2 + Q^2)^{1/2},$$

where k is the Einstein constant and Q is also a contant. Afterwards one sets $X = 3(\dot{S}/S)$ and $Y = (\dot{\Omega}/\Omega)$, where $\Omega = (1/k) + (\beta W^2)$, to write the equations of motion as

$$\begin{aligned} \dot{X} &= -\frac{1}{3}X^2 + XY, \\ \dot{Y} &= -Y^2 - XY. \end{aligned} \tag{2}$$

Hence, the correct interpretation of functions X and Y is important to the knowledge of the evolution of the model.

*present address: International Centre of Condensed Matter Physics, Universidade de Brasília , Caixa Postal 04667, 70919-900, Brasília - DF, Brazil.

Up to now there was no exact solution for this dynamical system and the analysis was carried out by using qualitative procedure. Here we exhibit the explicit solution in a very simple way.

One can rewrite eqs. (2) in polar coordinates, $\rho = \left(X^2 + Y^2\right)^{1/2}$ and $\theta = \arctan \frac{Y}{X}$, as [2,3]

$$\begin{aligned} \dot{\rho} &= -\rho^2 \left(\frac{1}{3}\cos^3\theta + \sin^3\theta + \cos\theta \sin^2\theta - \cos^2\theta \sin\theta \right), \\ \dot{\theta} &= -2\rho \cos\theta \sin\theta \left(\frac{\cos\theta}{3} + \sin\theta \right). \end{aligned} \tag{3}$$

The phase diagram related to this autonomous dynamical system can be obtained through

$$\frac{\dot{\rho}}{\dot{\theta}} = \frac{d\rho}{d\theta},$$

which leads to

$$\rho = C \exp\left(\frac{1}{2} I\right), \tag{4}$$

where C is an arbitrary positive constant of integration and

$$I = \int \frac{\frac{1}{3}(\cos^3\theta + 3\sin^3\theta) + \cos\theta\sin^2\theta - \cos^2\theta\sin\theta}{\frac{1}{3}\cos^2\theta\sin\theta + \cos\theta\sin^2\theta} d\theta. \tag{5}$$

After a little algebra, involving only basic trigonometric relations, one can show that the solution to integral I readily leads to

$$\rho = C \frac{|\tan\theta|^{1/2}}{|\cos\theta + 3\sin\theta|} \tag{6}$$

We point out that the precise knowledge of the function $\rho(\theta)$ leads to the sketch of the desired phase diagram associate with the autonomous dynamical system without any qualitative analysis about the dynamical system in regions around the origin [1,4].

On the other hand one can choose to study the dynamical system qualitatively by means of the projection on the Poincaré sphere [3,4]. This will provide usefull informations concerning the asymptotic behaviour of the system. As defined in Ref. 3, the Poincaré sphere with unitary radius is placed over the xy-plane, this plane being tangent to the south pole of the sphere. Another frame is in order and it is placed in the centre of the sphere. Projections onto the sphere are taken by joining points of the diagram to the centre of the sphere. This process will gives rise to a drawing on the sphere which is projected orthogonally on the xy-plane. The final portrait of the phase diagram is, then, in a circle with unitary radius where the behaviour at infinity is identified with the border of the circle.

Applying this method [3] to (2) one can obtain the topologies around the singular points at infinity, as in Fig.1. The arrows show the evolution in time. Note that besides the equilibrium points $\tilde{D}(0,0)$, $\tilde{D}'(0,0)$, $\tilde{C}(0,0)$ and $\tilde{C}'(0,0)$, there are the points $\tilde{B}(-1/3,0)$ and $\tilde{B}'(1/3,0)$, the primes indicating antipodes points. The system refuses to give informations on the topology around the origin by the method of linearization. Dulac's test shows there are no limiting cycles. Note that the above mentioned equilibrium points are consistent with eq. (6).

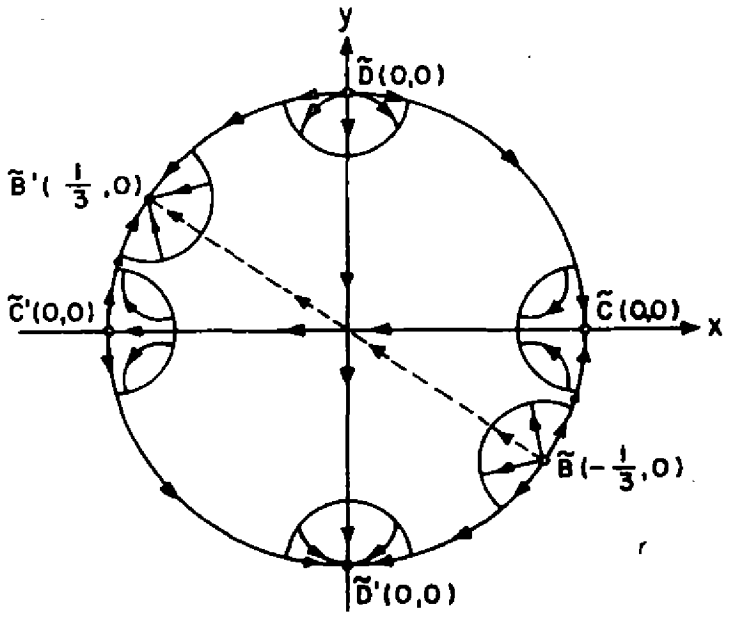

Figura 1. Equilibrium points at infinity and the topology imposed by them. *Empty* balls means unstable points, and full balls stable ones.

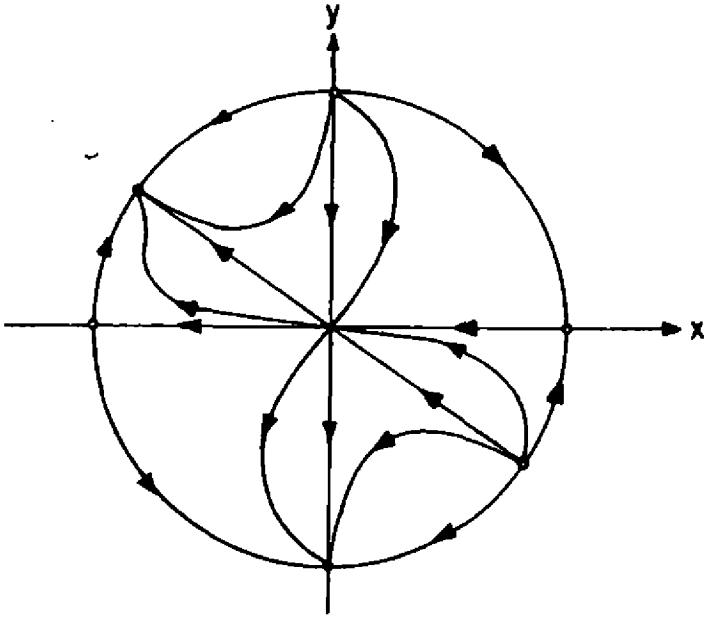

Figura 2. Final aspect of the phase diagram showing the equilibrium points at infinity. Only one integral curve is chosen to each region in the diagram to avoid it to become entangled.

The complete phase diagram which compactifies infinities is shown in Fig.2. Its shape is very close to that in Ref.4; the difference is due to the unusual dimension used. The phase diagram in Ref.1 is obtained in a different way: the projection is taken on the plane which corresponds to $X = 0$ and crosses the poles of the sphere, the xy-plane being tangent to the north pole of the sphere.

Notice that any autonomous planar dynamical system

$$\dot{X} = P(X,Y),$$

$$\dot{Y} = Q(X,Y).$$

allows a similar change of variables, and in polar form the phase diagram arises from

$$\frac{d\rho}{d\theta} = \rho\frac{P(\rho\cos\theta,\rho\sin\theta)+\tan\theta Q(\rho\cos\theta,\rho\sin\theta)}{Q(\rho\cos\theta,\rho\sin\theta)-\tan\theta P(\rho\cos\theta,\rho\sin\theta)} \tag{7}$$

For this reason, exact solutions may be achieved if it is possible to rewrite (7) as

$$\frac{d\rho}{d\theta} = R(\rho)\Theta(\theta)$$

Recently some cosmological models has been investigated in the so-called multidimensional scenario [5], and in a particular case a Maxwell field in higher dimensions is coupled to Einstein-Hilbert Lagrangian. This also leads to a qualitative dynamical system analysis, and, as in eq. (7), the search for exact solutions related to this problem is in progress.

Thanks are due to Professor C. A. P. Galvão for reading the manuscript and for helpful suggestions.

References

1. M. Novello and C. Romero, *Gen. Rel. Grav.*, 19 (1987) 1003–1011 (see also references therein)

2. W. Hurewicz, *Lectures on Ordinary Differential Equations* (Dover, New York, 1990).

3. A. Andronov *et al.*, *Qualitative Theory of Second-Order Dynamic Systems* (John Wiley & Sons, New York, 1973).

4. J. Tossa *et al.*, *C. R. Acad. Sci. Paris*, 314(1992)339–343.

5. J. C. Fabris and J. Tossa, *Phys. Lett.*B 296 (1992) 307–310; J. C. Fabris, *Gen. Rel. Grav.*, 26 (1994) 135–147.

A Computer Algebra Package for Torsion Theories of Gravitation

J.E. Åman*, J.B. Fonseca-Neto†, M.A.H. MacCallum‡
& M.J. Rebouças§

*Institute of Theoretical Physics, University of Stockholm,
Vanadisvägen 9, S-11346 Stockholm, Swenden

†CP 5008 Departamento de Física,
Universidade Federal da Paraíba,
58059-900 João Pessoa-PB, Brazil

§ School of Mathematical Sciences,
Queen Mary & Westfield College, Mile End Road,
London E1 4NS, U.K.

‡ Centro Brasileiro de Pesquisas Físicas,
Rua Dr. Xavier Sigaud, 150,
22290-180 Rio de Janeiro-RJ, Brazil

Received March, 1996

A computer algebra package for tensor and spinor calculations in torsion theories of gravitation (Riemann-Cartan space-time manifolds) is discussed. A set of modules for the classification of the irreducible parts of the curvature tensor of Riemann-Cartan space-time manifolds is presented. The package TCLASSI, which we have developed to decide the local equivalence of Riemann-Cartan space-times manifolds is briefly presented.

The Computer Algebra Package

A great number of relativists seems to spend a large amount of their time in carrying out routine nonnumeric calculations of one sort or another, most of which are algorithmic or semi-algorithmic.

All the main general-purpose computer algebra systems have some sort of facilities for calculation in general relativity (GR). The most extensive set of programs useful in GR are available with REDUCE, MAPLE, MACSYMA, and with MATHEMATICA through the MATHTENSOR package. Nevertheless, there is room for specialized systems like SHEEP/CLASSI. The major reason for this is that they are more efficient for GR calculations than general-purpose systems. For a comparison of CPU times for a specific metric see MacCallum [1].

In GR the underlying manifold M where the calculations are made is that of a four-dimensional Riemannian manifold, i.e., a space-time manifold endowed with a Lorentzian metric and a metric-compatible symmetric connection (Christoffel's symbols $\{{}_b{}^a{}_c\}$). However, it is well known that the metric tensor and the connection can be introduced as independent structures on a given space-time manifold M. In GR there is a unique torsion-free connection on M. In the framework of torsion theories of gravitation (TTG) we have space-time manifolds endowed with Lorentzian metrics and metric-compatible nonsymmetric connections $\Gamma^a{}_{bc}$ (Riemann-Cartan manifolds). Therefore, in TTG the connection has a metric-independent part given by the torsion, and for a characterization of the local gravitational field one has to deal with both metric and connection.

*INTERNET: JA@VANA.PHYSTO.SE
†BITNET: JOEL@DFJP.UFPB.BR
‡INTERNET: M.A.H.MACCALLUM@QMW.AC.UK
§INTERNET: REBOUCAS@CAT.CDPP.BR

As far as we are aware the existing facilities in computer algebra systems for calculations in TTG are quite limited. Actually, we only know of some REDUCE programs for applications to Poincaré gauge field theory [2]. They are written using the REDUCE package EXCALC and basically aim at field equations of TTG [3].

The arbitrariness in the choice of coordinates is a commonly made basic assumption in GR and in TTG. Nevertheless, in these theories it gives rise to the problem of deciding whether or not two apparently different space-time solutions of the field equations are locally the same — the equivalence problem. However, while in GR equivalence means local isometry of two Riemannian space-time manifolds, in TTG besides isometry ($g_{ab} \rightarrow \bar{g}_{ab}$) it means affine collineation (${\Gamma^a}_{bc} \rightarrow {\tilde{\Gamma}^a}_{bc}$) of two Riemann-Cartan space-time manifolds [4].

The LISP-based system SHEEP was partially devised with the equivalence problem for Riemannian manifolds in mind. Frick [5] designed the system and Karlhede [6] and Åman [7] developed the algorithm and the first set of programs required for checking the equivalence of vacuum solutions [8, 9]. Since then, algorithms and programs to extend the treatment to nonvacuum case have been developed by MacCallum, Joly, Åman, Skea and others. They are described in references [1] and [10] - [13], and references therein.

The equivalence problem for Riemann-Cartan space-time manifolds was taken up as part of a collaboration between the group at the School of Mathematical Sciences, QMW, led by Prof. M. A. H. MacCallum, and Prof. M. J. Rebouças's group at the Brazilian Center for Physics Research (CBPF) in Rio. The problem was tackled bearing in mind three basic aspects. First, the mathematical problem of finding the necessary and sufficient conditions for equivalence. Second, the problem of finding practical algorithms for effectively carrying out the calculation. Third, the implementation of the algorithms in the SHEEP/CLASSI computer algebra system.

With the equivalence problem in TTG in view, we have developed working version of the basic modules, which form the package called TCLASSI, extending the facilities of SHEEP/CLASSI to the Riemann-Cartan space-time manifolds of TTG.

Before actually tackling the equivalence problem, we had to implement several mathematical techniques which are used in the algorithm for the resolution of the equivalence problem. First, we have extended the tensor formalism to deal with calculations in coordinates, and noncoordinate frames in which the metric has constant components. Second, we have implemented the spinor formalism for Riemann-Cartan space-time manifolds. Finally, we have considered the Petrov and Segre classifications, and the algebraic classifications of vectors and bivectors.

To close this brief report we mention that a more detailed account of this work can be found, for example, in the references [14, 15] and in the forthcoming article [16].

References

[1] M. A. H. MacCallum, "Computer-aided Classification of Exact Solutions in General Relativity", in *General Relativity and Gravitational Physics (9th Italian Conference)*, edited by R. Cianci, R. de Ritis, M. Francaviglia, G. Marmo, C. Rubano and P. Scudellaro. World Scientific, Singapore (1991).

[2] E. Schrüfer, F. Hehl and J. D. McCrea, "Application of the REDUCE Package EXCALC to Poincaré Gauge Field Theory", *Gen. Rel. Grav.* **19**, 197 (1987).

[3] J. D. McCrea,"REDUCE in General Relativity and Poincaré Gauge Theory", in *Algebraic Computing in General Relativity, Lecture Notes from the First Brazilian School on Computer Algebra*, Vol. II, edited by M. J. Rebouças and W. L. Roque. Oxford U. P., Oxford (1994).

[4] J. B. Fonseca-Neto, M. J. Rebouças and A. F. F. Teixeira, "The Equivalence Problem in Torsion Theories of Gravitation", *J. Math. Phys.* **33**, 2574 (1992).

[5] I. Frick, "SHEEP Manual", University of Stockholm, Institute of Theoretical Physics Tech. Report, 1979. Distributed with the SHEEP sources.

[6] A. Karlhede,"A Review of the Geometrical Equivalence of Metrics in General Relativity" *Gen. Rel. Grav.* **12**, 693 (1980).

[7] J. E. Åman, "Manual for CLASSI: Classification Programs for Geometries in General Relativity", Institute of Theoretical Physics Technical Report, 1987. Third provisional edition. Distributed with the SHEEP sources.

[8] J. E. Åman and A. Karlhede, "A Computer-Aided Complete Classification of Geometries in General Relativity. First Results", *Phys. Lett. A* **80**, 229 (1980).

[9] J. E. Åman and A. Karlhede, "An Algorithmic Classification of Geometries in General Relativity", in *Proceedings of the 1981 ACM symposium on Symbolic and Algebraic Computation* - SYMSAC'81, edited by P. S. Wang. Association of Computing Machinery, New York (1981).

[10] M. A. H. MacCallum, "Classifying Metrics in Theory and Practice", in *Unified Field Theory in More Than 4 Dimensions, Including Exact Solutions*, edited by V. de Sabbata and E. Schmutzer. World Scientific, Singapore (1983).

[11] M. A. H. MacCallum, "Algebraic Computing in General Relativity", in *Classical General Relativity*, edited by W. B. Bonnor, J. N. Islam and M. A. H. MacCallum. Cambridge U. P., Cambridge (1984).

[12] I. Cohen, I. Frick and J. E. Åman, "Algebraic Computing in General Relativity", in *General Relativity and Gravitation*, edited by B. Bertotti, A. Pascolini and F. de Felice. Reidel, Dordrecht (1984)

[13] M. A. H. MacCallum and J. E. F. Skea, " SHEEP: A Computer Algebra System for General Relativity", in *Algebraic Computing in General Relativity, Lecture Notes from the First Brazilian School on Computer Algebra*, Vol. II, edited by M. J. Rebouças and W. L. Roque. Oxford U. P., Oxford (1994).

[14] J. B. Fonseca-Neto, M. J. Rebouças and M. A. H. MacCallum, "Algebraic Computing in Torsion Theories of Gravitation", in *Proceedings of the International IMACS Symposium on Symbolic Computation*, edited by G. Jacob, M. F. Oussous and S. Steinberg. IMACS Press (1993).

[15] J. E. Åman, J. B. Fonseca-Neto, M. A. H. MacCallum and M. J. Rebouças, " TCLASSI: A computer algebra package for torsion theories of gravitation", in *Abstracts of Contributed papers*, 14th International Conference on General Relativity and Gravitation (1995). University of Firenze.

[16] J. E. Åman, J. B. Fonseca-Neto, M. A. H. MacCallum and M. J. Rebouças, "Riemann-Cartan Space-times of Gödel Type", in preparation, to be submitted shortly elsewhere (1996).

Algebraic Classification of the Ricci Tensor in 5-Dimensional Spacetimes

G.S. Hall*, M. J. Rebouças†, J. Santos‡ and A.F.F. Teixeira§

* *Department of Mathematical Sciences*
University of Aberdeen, Aberdeen AB9 2TY, Scotland - U.K.
† § *Centro Brasileiro de Pesquisas Físicas*
Departamento de Relatividade e Partículas
Rua Dr. Xavier Sigaud 150
22290-180 Rio de Janeiro - RJ, Brazil
‡ *Universidade Federal do Rio G. do Norte*
Departamento de Física, Caixa Postal 1641
59072-970 Natal - RN, Brazil

Received March, 1996

A new approach to the algebraic classification of second order symmetric tensors in 5-dimensional space-times is presented. All possible Segre types for a symmetric two-tensor are found and canonical forms for each type are derived.

1 Introduction

In a recent article Santos *et al.* [1] have studied the algebraic classification of second order symmetric tensors defined on 5-dimensional (5-D for short) Lorentzian manifolds M, extending previous results [2, 3, 4]. Their analysis is made without using the previous classifications on lower dimensional space-times. However, as concerns the classification itself, their approach is not straightforward.

In this work we examine the algebraic structure of second order symmetric tensors defined on 5-D space-times under different bases. We shall assume the algebraic classification of the Ricci tensor for 4-D space-times, and then show that the classification recently discussed [1] can be achieved in a considerably simpler way.

2 Basic Theorem

The algebraic classification of the Ricci tensor at a point $p \in M$ can be cast in terms of the eigenvalue problem

$$(R^a{}_b - \lambda\, \delta^a_b)\, V^b = 0, \tag{1}$$

where λ is a scalar, V^b is a vector and the mixed Ricci tensor $R^a{}_b$ may be thought of as a linear operator $R : T_p(M) \longrightarrow T_p(M)$. M is a real 5-dimensional space-time manifold locally endowed with a Lorentzian metric of signature $(-++++)$, $T_p(M)$ denotes the tangent space to M at a point $p \in M$ and latin indices range from 0 to 4.

Our approach to an algebraic classification of $R^a{}_b$ is based upon the following

Theorem: $R^a{}_b$ has at least one real non-null eigenvector with real eigenvalue.

Proof. We initially consider the cases when all eigenvalues of R are real, and make use of a basic result of the theory of Jordan canonical forms [5] for n-square matrices R, which states that there always exist nonsingular

*INTERNET: GSH@MATHS.ABDN.AC.UK
†INTERNET: REBOUCAS@CAT.CBPF.BR
‡INTERNET: JANILO@DFTE-LAB.UFRN.BR
§INTERNET: TEIXEIRA@NOVELL.CAT.CBPF.BR

matrices X such that

$$X^{-1} R X = J \tag{2}$$

where J, the Jordan canonical form of R, is a block diagonal matrix. Suppose first that $R^a{}_b$ has a single eigenvector. In this case it can be brought to a Jordan canonical form $J^a{}_b$ with only one Jordan block, namely

$$J^a{}_b = \begin{bmatrix} \lambda & 1 & 0 & 0 & 0 \\ 0 & \lambda & 1 & 0 & 0 \\ 0 & 0 & \lambda & 1 & 0 \\ 0 & 0 & 0 & \lambda & 1 \\ 0 & 0 & 0 & 0 & \lambda \end{bmatrix}, \tag{3}$$

where $\lambda \in \mathbb{R}$. The matricial equation (2) implies that $RX = JX$. By using this equation and a procedure similar to that of ref. [1], one can rule out this Jordan canonical form (see also ref. [6]). So, at a point $p \in M$ the Ricci tensor R cannot have a single eigenvector.

Suppose now that $R^a{}_b$ has two linearly independent eigenvectors $(\mathbf{k}, \mathbf{n})$ and that they are both null vectors. Let μ and ν be the associated eigenvalues. Then

$$R^a{}_b k^b = \mu k^a , \tag{4}$$
$$R^a{}_b n^b = \nu n^a , \tag{5}$$

where $\mu, \nu \in \mathbb{R}$. Since R_{ab} is symmetric and $(\mathbf{k}, \mathbf{n})$ are linearly independent, eqs. (4) and (5) imply that $\mu = \nu$. Thus, from eqs. (4) and (5) the vector $\mathbf{v} = \mathbf{k} + \mathbf{n}$ is also an eigenvector of R with real eigenvalue μ. Since $\mathbf{k}$ and $\mathbf{n}$ are linearly independent null vectors it follows that $v^a v_a = 2 k^a n_a \neq 0$, so $\mathbf{v}$ is a non-null eigenvector with real eigenvalue.

In the cases where $R^a{}_b$ has more than two linearly independent null eigenvectors one can always use two of them to similarly construct one non-null eigenvector with real eigenvalue. Thus, when all eigenvalues of R are real $R^a{}_b$ has at least one non-null eigenvector with real eigenvalue.

The case when the Ricci tensor has complex eigenvalues can be dealt with as follows [7]. Suppose that $\alpha \pm i\beta$ are complex eigenvalues of $R^a{}_b$ corresponding to the eigenvectors $\mathbf{V}_\pm = \mathbf{Y} \pm i\mathbf{Z}$, where α and $\beta \neq 0$ are real and $\mathbf{Y}, \mathbf{Z}$ are independent vectors defined on $T_p(M)$. Since R_{ab} is symmetric and the eigenvalues are different, the eigenvectors must be orthogonal and hence equation $\mathbf{Y}.\mathbf{Y} + \mathbf{Z}.\mathbf{Z} = 0$ holds. It follows that either one of the vectors $\mathbf{Y}$ or $\mathbf{Z}$ is timelike and the other spacelike or both are null and, since $\beta \neq 0$, not collinear. Regardless of whether $\mathbf{Y}$ and $\mathbf{Z}$ are both null vectors or one timelike and the other spacelike, the real and the imaginary part of (1) give

$$R^a{}_b Y^b = \alpha Y^a - \beta Z^a , \tag{6}$$
$$R^a{}_b Z^b = \beta Y^a + \alpha Z^a . \tag{7}$$

Thus, the vectors $\mathbf{Y}$ and $\mathbf{Z}$ span a timelike 2-dimensional subspace of $T_p(M)$ invariant under $R^a{}_b$. Besides, one can show [1] that the 3-dimensional space orthogonal to this timelike 2-space is spacelike, also invariant under $R^a{}_b$, and contains three orthogonal eigenvectors of $R^a{}_b$ with real eigenvalues. Thus, when $R^a{}_b$ has complex eigenvalues we again have at least one non-null eigenvector with real eigenvalue. This completes the proof of our theorem.

3 Classification

We shall deal with two types of pentad of vectors, namely the semi-null pentad basis $\{\mathbf{l}, \mathbf{m}, \mathbf{x}, \mathbf{y}, \mathbf{z}\}$, whose non-vanishing inner products are

$$l^a m_a = x^a x_a = y^a y_a = z^a z_a = 1 , \tag{1}$$

and the Lorentz pentad basis $\{\mathbf{t}, \mathbf{w}, \mathbf{x}, \mathbf{y}, \mathbf{z}\}$, whose only non-zero inner products are

$$-t^a t_a = w^a w_a = x^a x_a = y^a y_a = z^a z_a = 1 . \tag{2}$$

At a point $p \in M$ the most general decomposition of R_{ab} in terms of a Lorentz basis for symmetric tensors at $p \in M$ is given by

$$\begin{aligned} R_{ab} = {} & \sigma_1 t_a t_b + \sigma_2 w_a w_b + \sigma_3 x_a x_b + \sigma_4 y_a y_b + \sigma_5 z_a z_b + 2\sigma_6 t_{(a} w_{b)} \\ & + 2\sigma_7 t_{(a} x_{b)} + 2\sigma_8 t_{(a} y_{b)} + 2\sigma_9 t_{(a} z_{b)} + 2\sigma_{10} w_{(a} x_{b)} + 2\sigma_{11} w_{(a} y_{b)} \\ & + 2\sigma_{12} w_{(a} z_{b)} + 2\sigma_{13} x_{(a} y_{b)} + 2\sigma_{14} x_{(a} z_{b)} + 2\sigma_{15} y_{(a} z_{b)} , \end{aligned} \tag{3}$$

where the coefficients $\sigma_1, \ldots, \sigma_{15} \in \mathbb{R}$.

We shall now discuss the algebraic classification of the Ricci tensor. Let $\mathbf{v}$ be the real non-null eigenvector referred to in the theorem and let $\eta \in \mathbb{R}$ be the corresponding eigenvalue. Obviously the normalized vector $\mathbf{u}$ defined by

$$u^a = \frac{v^a}{\sqrt{\epsilon\, v^a v_a}} \qquad \text{with} \qquad \epsilon \equiv \text{sign}\,(v^a v_a) = u^a u_a \tag{4}$$

is also an eigenvector of $R^a{}_b$ associated to η.

If the vector $\mathbf{u}$ is timelike ($\epsilon = -1$), one can choose it as the timelike vector $\mathbf{t}$ of a Lorentz pentad $\{\mathbf{t}, \tilde{\mathbf{w}}, \tilde{\mathbf{x}}, \tilde{\mathbf{y}}, \tilde{\mathbf{z}}\}$. The fact that $\mathbf{u} \equiv \mathbf{t}$ is an eigenvector of $R^a{}_b$ can then be used to reduce the general decomposition (3) to

$$\begin{aligned} R_{ab} \;=\; & -\eta\, t_a t_b + \sigma_2\, \tilde{w}_a \tilde{w}_b + \sigma_3\, \tilde{x}_a \tilde{x}_b + \sigma_4\, \tilde{y}_a \tilde{y}_b + \sigma_5\, \tilde{z}_a \tilde{z}_b + 2\,\sigma_{10}\, \tilde{w}_{(a} \tilde{x}_{b)} \\ & + 2\,\sigma_{11}\, \tilde{w}_{(a} \tilde{y}_{b)} + 2\,\sigma_{12}\, \tilde{w}_{(a} \tilde{z}_{b)} + 2\,\sigma_{13}\, \tilde{x}_{(a} \tilde{y}_{b)} + 2\,\sigma_{14}\, \tilde{x}_{(a} \tilde{z}_{b)} \\ & + 2\,\sigma_{15}\, \tilde{y}_{(a} \tilde{z}_{b)}\,, \end{aligned} \tag{5}$$

where $\eta = -\sigma_1$. Using (2) and (5) one finds that the mixed matrix $R^a{}_b$ takes the block diagonal form

$$R^a{}_b = S^a{}_b - \eta\, t^a t_b\,. \tag{6}$$

The first block is a (4×4) symmetric matrix acting on the 4-D spacelike vector space orthogonal to the subspace U of $T_p(M)$ defined by $\mathbf{u}$. Hence it can be diagonalized by spatial rotation of the basis vectors $(\tilde{\mathbf{w}}, \tilde{\mathbf{x}}, \tilde{\mathbf{y}}, \tilde{\mathbf{z}})$. The second block is 1-dimensional and acts on the subspace U. Thus, there exists a Lorentz pentad relative to which $R^a{}_b$ takes a diagonal form with real coefficients.

If $\mathbf{u}$ is spacelike ($\epsilon = 1$) one can choose it as the spacelike vector $\mathbf{z}$ of a Lorentz pentad and using eqs. (2) one similarly finds that $R^a{}_b$ takes the block diagonal form

$$R^a{}_b = S^a{}_b + \eta\, z^a z_b\,, \tag{7}$$

where $\eta = \sigma_5$. But now the 4-D vector space orthogonal to the spacelike subspace of $T_p(M)$ defined by $\mathbf{u}$ is Lorentzian. Then the mixed matrix $S^a{}_b$ effectively acts on a 4-D Lorentzian vector space and is not necessarily symmetric, it is not diagonable in general. As S_{ab} is obviously symmetric, from equation (7) it follows that the algebraic classification of $R^a{}_b$ and a set of canonical forms for R_{ab} can be achieved from the classification of a symmetric two-tensor S on a 4-D space-time.

Thus, using the known classification [7] for 4-D space-times it follows that semi-null pentad bases like (1) can be introduced at $p \in M$ such that the possible Segre types [8] and the corresponding canonical forms for R are given by

Segre type		**Canonical form**	
$[1, 1111]$	$R_{ab} =$	$2\,\rho_1\, l_{(a} m_{b)} + \rho_2\,(l_a l_b + m_a m_b) + \rho_3\, x_a x_b + \rho_4\, y_a y_b$ $+\rho_5\, z_a z_b\,,$	(8)
$[2111]$	$R_{ab} =$	$2\,\rho_1\, l_{(a} m_{b)} \pm l_a l_b + \rho_3\, x_a x_b + \rho_4\, y_a y_b + \rho_5\, z_a z_b\,,$	(9)
$[311]$	$R_{ab} =$	$2\,\rho_1\, l_{(a} m_{b)} + 2\, l_{(a} x_{b)} + \rho_1\, x_a x_b + \rho_4\, y_a y_b + \rho_5\, z_a z_b\,,$	(10)
$[z\,\bar{z}\,111]$	$R_{ab} =$	$2\,\rho_1\, l_{(a} m_{b)} + \rho_2\,(l_a l_b - m_a m_b) + \rho_3\, x_a x_b + \rho_4\, y_a y_b$ $+\rho_5\, z_a z_b\,,$	(11)

and the twenty-two degeneracies thereof, in agreement with Santos *et al.* [1]. Here $\rho_1, \cdots, \rho_5 \in \mathbb{R}$ and $\rho_2 \neq 0$ in (11).

Although the Ricci tensor has been constantly referred to, these results apply to any second order real symmetric tensor defined on 5-D Lorentzian manifolds.

References

[1] J. Santos, M. J. Rebouças and A. F. F. Teixeira, *J. Math. Phys.* **36**, 3074 (1995).

[2] G. S. Hall, *J. Phys. A* **9**, 541 (1976).

[3] G. S. Hall, T. Morgan and Z. Perjés, *Gen. Rel. Grav.* **19**, 1137 (1987).

[4] G. S. Hall, *"Physical and Geometrical Classification in General Relativity"*, Brazilian Center for Physics Research Monograph, CBPF-MO-001/93 (1993).

[5] G. E. Shilov, *Linear Algebra*, (Dover Publications, Inc., New York, 1977).

[6] G. S. Hall, M. J. Rebouças, J. Santos and A. F. F. Teixeira, *"On the algebraic structure of second order symmetric tensors in 5-dimensional space-times"*, submited for publication in *Gen. Rel. Grav.*

[7] G. S. Hall, *Diff. Geom.* **12**, 53 (1984). This reference contains an extensive bibliography on the classification of the Ricci tensor on 4-dimensional space-times.

[8] A detailed, quite good, and useful review of the Segre classification can be found in ref. [7].

Topological Constraints on Maxwell Fields in General Relativity

W. Oliveira,* M.J. Rebouças† and A.F.F. Teixeira ‡

* *Departamento de Física*
Universidade Federal de Juiz de Fora
36036-330 Juiz de Fora - MG, Brazil
† ‡ *Centro Brasileiro de Pesquisas Físicas*
Departamento de Relatividade e Partículas
Rua Dr. Xavier Sigaud 150
22290-180 Rio de Janeiro – RJ, Brazil

Received March, 1996

Two spatially homogeneous solutions of Maxwell's equations in the elliptic Robertson-Walker (RW) space-time geometry are found. It is shown that although both solutions can be accommodated in the RW space-time manifolds whose $t = const$ sections are three-spheres S^3, only one of them is admissible when the sections are quaternionic manifolds Q^3, making explicit the existence of topological constraints on Maxwell fields in Robertson-Walker space-times.

1 Introduction

As general relativity is a purely metrical theory (local) it clearly leaves unsettled the global structure of space-time. The standard local metric approach to space-times has led a number of relativists to implicitly (or explicitly) restrict themselves to purely local geometric features, ignoring the role of topology. However, in cosmology the most important problems are related to the global structure of space-time. The global topology features comes out, for example, in dealing with electric fields produced by bounded sources, when quite often it is chosen as boundary condition that the fields vanish at spatial infinity. This is reasonable if the three-space has the topology of $\mathbb{R}^3$, but it is not that simple if one is concerned with these fields in compact and (or) multiply connected spaces. Although it is sometimes difficult in practice to take into account the global topological features of a manifold, it is important to study this sort of constraints. Moreover, it is significant to underline which (and when) physical results concerning a space-time geometry depend upon the global topology.

In this work we bring forward these matters by discussing two solutions of Maxwell's equations in the elliptic ($\kappa = 1$) Robertson-Walker space-time geometry

$$ds^2 = dt^2 - \left(\frac{A(t)}{1 + \frac{\kappa}{4} r^2} \right)^2 \left[dr^2 + r^2 \left(d\theta^2 + \sin^2 \theta \, d\phi^2 \right) \right], \tag{1.1}$$

with the $t = const$ section endowed with two different compact topologies, namely the three-sphere S^3 and the clockwise quaternionic topology Q^3 [1] - [3]. We show that the elliptic geometry (1.1) can accommodate both solutions of Maxwell's equations if its $t = const$ section is the simply connected compact manifold S^3. However, if its three-space is endowed with the multiply connected compact quaternionic topology Q^3, it can accommodate only one of the two solutions of Maxwell's equations. In other words, this latter topology excludes a solution of Maxwell's differential equations. For a more detailed account of the results we report in this work we refer the reader to ref. [4].

*This work was carried out while he was at Departamento de Física – PUC – Rio, with fellowships from CNPq and FAPERJ.
†INTERNET: REBOUCAS@CAT.CBPF.BR
‡INTERNET: TEIXEIRA@CAT.CBPF.BR

2 Maxwell's Equations and Topological Constraints

The 4-dimensional space-time manifolds, arenas for the Maxwell fields we are concerned with, are endowed with the same elliptic ($\kappa = 1$) Robertson-Walker space-time metric (1.1). They are different in that the $t = const$ sections are two distinct compact, globally homogeneous and locally isotropic manifolds, namely S^3 and Q^3.

The elliptic Robertson-Walker geometry is usually given in the form (1.1). However, we have used cylindrical coordinates relative to which the line element (1.1) takes in the form

$$ds^2 = dt^2 - A^2(t)\left(d\rho^2 + \sin^2\rho\, d\phi^2 + \cos^2\rho\, d\zeta^2\right). \tag{2.1}$$

A set of one-forms ω^A particularly adequate for our purpose is given by [4]

$$\omega^0 = dt, \tag{2.2}$$

$$\omega^1 = A(t)\left[\cos(\zeta-\phi)\,d\rho + \frac{1}{2}\sin 2\rho\,\sin(\zeta-\phi)\,(d\phi + d\zeta)\right], \tag{2.3}$$

$$\omega^2 = A(t)\left[-\sin(\zeta-\phi)\,d\rho + \frac{1}{2}\sin 2\rho\,\cos(\zeta-\phi)\,(d\phi + d\zeta)\right], \tag{2.4}$$

$$\omega^3 = A(t)\left[\cos^2\rho\, d\zeta - \sin^2\rho\, d\phi\right]. \tag{2.5}$$

In a local frame $\{\omega^A\}$ Maxwell's equations take the form

$$F^{AB}{}_{;B} = -J^A \qquad \text{and} \qquad F_{[AB;C]} = 0, \tag{2.6}$$

where F_{AB} is the Maxwell tensor, J^A is the current four-vector and the bracket denotes antisymmetrization.

To reveal our major goal we study two spatially homogeneous magnetic fields F_{AB} and $\bar{F}_{AB}$ in the elliptic RW background (2.1). In the frame (2.2)-(2.5) they are given by

$$F_{12} = -Z(t), \qquad F_{13} = Y(t), \qquad F_{23} = -X(t), \tag{2.7}$$

and

$$\bar{F}_{12} = -H(t)\cos 2\rho, \quad \bar{F}_{13} = H(t)\sin 2\rho\cos(\zeta-\phi), \quad \bar{F}_{23} = -H(t)\sin 2\rho\sin(\zeta-\phi), \tag{2.8}$$

where H, X, Y and Z are arbitrary functions of the time coordinate t. We mention that another pseudo-orthonormal frame exists relative to which the field $\bar{F}_{AB}$ has only one nonvanishing component, i.e. $\bar{F}_{\hat{1}\hat{2}} = -H(t)$.

Using now the package ELDYNF of the suite of algebraic computing programs CLASSI [5], one can easily show that for the electromagnetic field F_{AB} given by (2.7) the Maxwell equations (2.6) for $J^C = -2A^{-1}(0, X, Y, Z)$ are satisfied as long as

$$X(t) = \alpha/A^2, \qquad Y(t) = \beta/A^2, \qquad Z(t) = \gamma/A^2, \tag{2.9}$$

where α, β and γ are arbitrary real constants.

Similarly, for the electromagnetic field $\bar{F}_{AB}$ given by (2.8) one can show using ELDYNF that for

$$\bar{J}^C = 2HA^{-1}[0, \sin 2\rho\sin(\zeta-\phi), \sin 2\rho\cos(\zeta-\phi), \cos 2\rho]$$

Maxwell's equations (2.6) reduce to a single ordinary differential equation, namely

$$\dot{H} + 2H\frac{\dot{A}}{A} = 0, \tag{2.10}$$

which can be easily integrated to give $H = H_0 A^{-2}$, where H_0 is an arbitrary real constant.

The unit three-sphere S^3 is relatively well known to physicists. One can obtain Q^3 by separating from a unit three-sphere S^3 a solid curved cube of height $\pi/2$, and identifying each face with the opposite after a one-quarter clockwise turn [1] - [3].

When the $t = const$ section of the space-time manifold with (1.1) is S^3, and since the three-sphere is the universal covering manifold of the elliptic geometry, there are no topological identifications. Thus, both solutions of Maxwell's equations we have studied in the previous Section can be accommodated in the space-time manifold whose three-space is S^3.

When the $t = const$ section of the space-time manifold is Q^3, however, one has to consider the constraints imposed by the topological identifications. Here, although the congruence of curves defined by the electromagnetic

field (2.7) and (2.9) is compatible with the identifications imposed by the topology of Q^3, the Maxwell field (2.8) (with $H = H_0 A^{-2}$) defines a congruence of curves, which does not couple with the topological identifications imposed by the clockwise quaternionic topology Q^3. Thus, for example, in cylindrical coordinates the events defined by $P = (t, \pi/4, 0, 0)$ and $Q = (t, \pi/4, \pi, 0)$ are the same; however, a straightforward calculation shows that the only nonvanishing component of $\tilde{F}_{AB}$ at P and Q, namely $\tilde{F}_{13}$, is $H(t)$ at P, whereas at Q it is $-H(t)$, making clear that this solution of Maxwell's equations is excluded by the topological constraints imposed by the quaternionic topology Q^3.

Finally we mention that according to King [6] there are two types of spatial homogeneity for tensor fields in the three-sphere S^3, namely left and right homogeneity. This is so because in S^3 one can globally define both left and right invariant vector fields. Using King's definitions of homogeneity the above Maxwell field F_{AB} is right homogeneous, whereas $\tilde{F}_{AB}$ is left homogeneous. We notice that as far as the clockwise quaternionic manifold Q^3 is concerned we can define only one type of homogeneity for tensor fields, namely right homogeneity, since in this manifold only the right invariant vector fields can be globally defined. This fact is in agreement with the exclusion of the left homogeneous Maxwell field $\tilde{F}_{AB}$ by the topology of Q^3.

References

[1] J. R. Weeks, *The Shape of Space*, in the series "Pure and Applied Mathematics," Vol. 96, Marcel Dekker Inc., New York (1985).

[2] W. P. Thurston, *The Geometry and Topology of 3-manifolds*, Princeton University report, unpublished.

[3] P. Scott, *Bull. London Math. Soc.* **15**, 401 (1983).

[4] W. Oliveira, M. J. Rebouças and A. F. F. Teixeira, *Phys. Lett. A* **188**, 125 (1994).

[5] M. A. H. MacCallum and J. E. F. Skea, "SHEEP: A Computer Algebra System for General Relativity," in "Algebraic Computing in General Relativity: Lectures Notes from the First Brazilian School on Computer Algebra," Vol. II, edited by M. J. Rebouças and W. L. Roque, Oxford U. P., Oxford (1994).

[6] D. H. King, *Phys. Rev. D* **44**, 2356 (1991).

The Levi-Civita spacetime

M. F. A. da Silva [1], L. Herrera [2], F. M. Paiva [3] e N. O. Santos [3]

[1] *UNESP-DFQ Campus de Guaratinguetá - Brasil*

[2] *Universidad Central de Venezuela - Venezuela*

[3] *CNPq-Observatório Nacional - Brasil*

Received March, 1996

We consider two exact solutions of Einstein's field equations corresponding to a cylinder of dust with net zero angular momentum. In one of the cases, the dust distribution is homogeneous, whereas in the other, the angular velocity of dust particles is constant [1]. For both solutions we studied the junction conditions to the exterior static vacuum Levi-Civita spacetime. From this study we find an upper limit for the energy density per unit length σ of the source equal $\frac{1}{4}$ for both $\frac{1}{4}$ cases. Thus the homogeneous cluster provides another example [3,4] where the value of σ is less than $\frac{1}{4}$. Using the Cartan Scalars technics we show that the Levi-Civita spacetime gets an extra symmetry for $\sigma = \frac{1}{2}$ or $\frac{1}{4}$. We also find that the cluster of homogeneous dust has a superior limit for its radius, depending on the constant volumetric energy density ρ_0.

1. Introduction

The Levi-Civita metric [5] is the most general cylindrical static vacuum metric. It will be used as the exterior spacetime of static cylindrical sources.

Some non-vacuum exact solutions with cylindrical symmetry may be found in the literature. One very simple solution is the cluster of particles. This source is constituted by a great number of small gravitational particles which move freely under the influence of the field produced by all of them together. A cluster solution was obtained by Teixeira and Som [1], where they suposed a constant angular velocity for the dust particles with an equal number of particles moving in clockwise and anticlockwise directions and found some special cylindrical solutions. From the Teixeira and Som solution, Lathrop and Orsene [4] found an upper limit for the linear mass density of the source. They used a definition for this quantity given by Vishveshwara and Winicour [7].

In 1969 Gautreau and Hoffman [8] demonstrated that there is no timelike circular geodesic in the Levi-Civita metric if $\sigma \geq \frac{1}{4}$. Based on this, Bonnor and Martins [3] conjectured that the Levi-Civita metric does not represent an infinite line mass if $\sigma \geq \frac{1}{4}$. Later, Bonnor and Davidson [2] presented a cylindrical source, filled with perfect fluid, and showed that the matching of this source with the Levi-Civita metric permits values of $\sigma > \frac{1}{4}$, but $< \frac{1}{2}$. In another work, Stela and Kramer [9] found a source with $\sigma \lesssim 0.35$ using a numerical interior solution.

Inspired by the Teixeira and Som solution, and imposing the constance of the energy density of the source, instead of the constance of the angular velocity, we found an exact solution for an homogeneous cylindrical cluster. For both these clusters we studied the junction conditions to the exterior static vacuum Levi-Civita spacetime. We found a superior limit for the linear energy density σ of the source equal $\frac{1}{4}$ for the first case and $\frac{1}{2}$ for the second one. The limit obtained for the Teixeira and Som cluster is in accordance with the limit found by Lathrop and Orsene [4]. The range of σ for the homogeneous cluster solution, extends the range found by Bonnor and Davidson [2], for a perfect fluid. Our solution allows $\sigma = \frac{1}{2}$.

2. The Levi-Civita metric

The general static metric cylindrically symmetric which describes the spacetime (ST) is given by

$$ds^2 = -fdt^2 + e^{\mu}(dr^2 + dz^2) + ld\varphi^2, \tag{1}$$

The exterior vacuum spacetime is described by the Levi-Civita solution

$$f = ar^{4\sigma}, \quad e^{\mu} = r^{4\sigma(2\sigma-1)}, \quad l = \frac{1}{a}r^{2(1-2\sigma)}$$

The non-null Cartan scalars for this metric are

$$\begin{aligned}
\Psi_2 &= -(2\sigma-1)\sigma r^{4\sigma-8\sigma^2-2} \\
\Psi_4 = \Psi_0 &= (4\sigma-1)\Psi_2 \\
\nabla\Psi_{01'} = \nabla\Psi_{50'} &= \sqrt{2}(8\sigma^2-4\sigma+1)(4\sigma-1)(2\sigma-1)\sigma r^{6\sigma-12\sigma^2-3} \\
\nabla\Psi_{10'} = \nabla\Psi_{41'} &= \sqrt{2}(4\sigma-1)(2\sigma-1)\sigma r^{6\sigma-12\sigma^2-3} \\
\nabla\Psi_{21'} = \nabla\Psi_{30'} &= \sqrt{2}(4\sigma^2-2\sigma+1)(2\sigma-1)\sigma r^{6\sigma-12\sigma^2-3}.
\end{aligned} \tag{3}$$

These equations show us that it is a Petrov Type I metric and:

- for $\sigma = 0$ or $\frac{1}{2}$ the metric becomes flat,
- for $\sigma = \frac{1}{4}$ ($\Psi_0 = \Psi_4 = 0$ e $\Psi_2 \neq 0$)$\rightarrow$ Petrov type D,
- for $\sigma = -\frac{1}{2}$ or $1 \rightarrow$ Petrov type D,
- $\sigma = -\frac{1}{2}, 0, \frac{1}{4}, \frac{1}{2}$ and $1 \Rightarrow$ ST acquires isotropies.

The circular geodesics for this metric are

$$(ds/dt)^2 = -\frac{1-4\sigma}{1-2\sigma}ar^{4\sigma},$$

we have that if $\sigma < \frac{1}{4}$, $\sigma = \frac{1}{4}$ or $\sigma > \frac{1}{4}$, the geodesic is timelike, or spacelike, respectively.

A test particle moving in a circular trajectory in this spacetime has angular velocity given by

$$\omega^2 = \frac{2\sigma}{1-2\sigma}a^2r^{2(4\sigma-1)},$$

and three-velocity

$$W^2 = \frac{2\sigma}{1-2\sigma}.$$

So, if $\sigma = \frac{1}{2} \Rightarrow W = \infty$ and $\sigma > \frac{1}{2} \Rightarrow W^2 < 0$ (impossible).

3. Interior spacetime

The interior spacetime is constituted by a dust cluster with rotation around the symmetry axis and null net angular momentum. The energy momentum tensor is

$$T^{\mu}_{\nu} = \frac{1}{2}\rho(u^{\mu}u_{\nu} + v^{\mu}v_{\nu}),$$

with $u^{\mu} = (u^0, 0, 0, \omega)$, $v^{\mu} = (u^0, 0, 0, -\omega)$ and $u^{\mu}u_{\mu} = v^{\mu}v_{\mu} = -1$.

3.1. Homogeneous dust cluster ($\rho = \rho_0$)

The solution of the Einstein's equations which matches with the Levi-Civita metric in the discontinuity surface is given by

$$f = \frac{1}{\sqrt{2}}\left(1-3br^2+\sqrt{(1+br^2)(1-7br^2)}\right)^{\frac{1}{2}} \times \exp\left[\frac{7}{2\sqrt{7}}\left(\arcsin\left[-\frac{(3+7br^2)}{4}\right]-\arcsin\left[-\frac{3}{4}\right]\right)\right], \quad (4)$$

$$e^{\mu} = (1+br^2)^{-2}, \quad (6)$$

with $b \stackrel{\text{def}}{=} k\rho_0/8$ For this cluster the three-velocity becomes

$$W^2 = \frac{\sqrt{1+br^2}-\sqrt{1-7br^2}}{\sqrt{1+br^2}+\sqrt{1-7br^2}}. \quad (7)$$

The junction conditions between the interior spacetime (homogeneous cluster) and exterior spacetime (Levi-Civita) provide

$$\sigma = \frac{1}{4}\left(1-\sqrt{\frac{1-7bR^2}{1+bR^2}}\right), \quad (8)$$

$$a = \frac{b^2R^{4(2\sigma^2-\sigma+1)}}{\sigma^2(2\sigma-1)^2} = (1+bR^2)^2R^{-\frac{4bR^2}{1+bR^2}}. \quad (9)$$

We can conclude that $r^2 \leq \frac{3}{7k\rho_0}$, $0 \leq \sigma \leq \frac{1}{4}$, $0 \leq W \leq 1$ and $1 \leq b \leq \frac{1.3}{R}$

3.2. Dust cluster with constant rotation ($\omega = \omega_0$)

This solution, obtained by Teixeira and Som solution in 1974, is given by

$$f = \frac{1}{2}\left[1+(1+4\omega_0^2r^2)^{\frac{1}{2}}\right],$$

$$e^{\mu} = (1+4\omega_0^2r^2)^{-\frac{1}{4}},$$

$$2\pi\rho = \frac{\omega_0^2}{(1+4\omega_0^2r^2)^{\frac{7}{4}}},$$

with the three-velocity of the dust particles being given by

$$W^2 = \frac{4\omega_0^2r^2}{(1+\sqrt{1+4\omega_0^2r^2})^2}.$$

The junction conditions provide

$$\sigma = \frac{1}{4}\left(1-\frac{1}{\sqrt{1+4\omega_0^2R^2}}\right), \quad (10)$$

$$a = R^{4\sigma(2\sigma-1)}(1+4\omega_0^2R^2)^{\frac{1}{4}}. \quad (11)$$

Thus, $\lim_{R\to\infty}\sigma = \frac{1}{4}$ and $\lim_{r\to\infty}W = 1$. So $\sigma \leq \frac{1}{4}$ in order to generate a Levi-Civita exterior spacetime. There is not any restriction on the radial coordinate of this cluster.

4. Conclusion

We found the exact solutions of Einstein's field equations for an homogeneous cylinder constituted by an equal number of particles of dust moving in clockwise and anticlockwise directions. The matching of this source with the static vacuum of Levi-Civita is allowed only for a specific range of the linear energy density parameter, that is $0 \leq \sigma \leq \frac{1}{4}$. We also found that, for a given volumetric energy density, this source presents an upper limit for its radius. In the literature there is, at least, the van Stockum solution as another cylindrical example in which there

is a limit for the radius of the source depending on its volumetric density [14,15]. In this case, the limitation on the radius comes out in order to avoid a change in the signature of the metric.

Using the solution for a cluster constituted by dust particles with constant angular velocity and zero net angular momentum, obtained firstly by Teixeira and Som [1], and matching it with the Levi-Civita metric, we found that the parameter σ in this case should be smaller or equal than $\frac{1}{4}$. Considering σ as the gravitational mass per unit length this limit is in agreement with the result of Lathrop and Orsene [4]. While for the Teixeira and Som solution the matching does not present a limitation to the radius of the source, for our homogeneous cluster solution the matching imposes a superior limit for its radius, depending on the volumetric energy density ρ_0.

We note from equation (3.4) that circular geodesics in the Levi-Civita spacetime become null when σ is equal $\frac{1}{4}$. Some authors [Gautreau & Hoffmann [3,8] use this fact as a restriction for the linear density of the source. Nevertheless, as pointed out by [6], this result is similar to the Newtonian cylindrical analog case, i. e., for a higher density cylinder, all particles (with speed less than the light) should fall. However this argument is not without problems, since, as showed by Bonnor and Martins [3], in the interval $\frac{1}{4} \leq \sigma \leq \frac{1}{2}$ the gravitational field seems to get weaker as σ increases [16]. Note that $\sigma = \frac{1}{2}$ means that there is no any matter inside the cylinder ($\rho_0 = 0$ and the spacetime is locally flat, in accordance to the Cartan scalars).

The analysis of the Cartan scalars, summarizes the symmetry properties of the Levi-Civita metric. It is in general a Petrov type I metric and becomes a Petrov type D metric when $\sigma = -\frac{1}{2}, 0, \frac{1}{4}, \frac{1}{2}$ and 1. For $\sigma = 0$ or $\frac{1}{2}$ the metric becomes flat, which is in accordance with our cluster solution since when $\sigma = 0$ or $\frac{1}{2}$ the volumetric energy density ρ_0 of the cluster vanishes. For $\sigma = -\frac{1}{2}, \frac{1}{4}, 1$ the metric gets one extra symmetry.

5. References

[1]Teixeira, A. F. F. & Som, M. M. (1974), Il Nuovo Cimento **21 B**, 64.

[2]Bonnor, W. B. & Davidson, W. (1992), *Class. Quant. Grav.* **9**, 2065.

[3]Bonnor, W. B. & Martins, M. A. P. (1991), *Class. Quant. Grav.* **8**, 727.

[4]Lathrop, J. D. & Orsene, M. S. (1980), J. Math. Phys. **27**(1), 152.

[5]Levi-Civita, T. (1917), Rend. Acc. Lincei **26**, 307.

[6]Raychaudhuri, A. K. & Som, M. M. (1962), Proc. Camb. Phyl. Soc. **58**, 338.

[7]Vishveshwara, C. V. & Winicour, J. (1977), J. Math. Phys. **18**, 1280.

[8]Gautreau, R. & Hoffman, R. B. (1969), Nuovo Cimento, **B61**, 411.

[9]Stela, J. & Kramer, D. (1990), Acta Phys. Pol. **B21**, 843.

[10]van Stockum, W. J. (1937), Proc. R. Soc. Edin. **57**, 135.

[11]Tipler, F. J. (1974), Phys. Rev. D, **9**, 2203.

[12]Bonnor, W. B., private communication.

The Finite Temperature Effective Potential of Gauge Theories in the Presence of Magnetic Fields

Rudnei O. Ramos*†
Universidade do Estado do Rio de Janeiro,
Instituto de Física - Departamento de Física Teórica,
20550-013 Rio de Janeiro, RJ

Received March, 1996

We study the effect of intense magnetic fields possible present during cosmological phase transitions. We obtain the phase diagram of an arbitrary phase transition following gauge symmetry breaking as a function of both temperature and magnetic fields. We show that intense magnetic fields during a first order phase transition tend to make the order of the phase transition stronger. We also discuss the relevance of these results for baryogenesis during the electroweak phase transition.

In the hot primordial Universe we expect that a series of cosmological phase transitions may have happened since the Universe started expanding and cooling down. We believe that these cosmological phase transitions (GUT phase transitions and the electroweak phase transitions are typical examples) could possibly be important to answer most of the current questions in cosmology, from the origin of the large-scale structure of the Universe to the excess of baryonic matter [1].

From the quantum field theoretical point of view, phase transitions in gauge theories (or symmetry restoring phase transitions) may be induced not only by high temperatures but also by high densities or by intense magnetic fields [2] (or a combination of these effects[1]. Here, we will be particularly interested in the effect of intense magnetic fields during cosmological phase transitions.

In astrophysics and in cosmology we expect to find sources of intense magnetic fields. For example, magnetic fields of the order of $B \sim 10^{12}G$ may be associated with neutron stars [4], $B \sim 10^{14}G$ with supernovae [5], extragalactic gamma bursts in terms of mergers of massive binary stars may lead to $B \sim 10^{17}G$ [6]. In cosmology we can expect even more intense sources of magnetic fields, like the one associated with superconducting cosmic strings ($B \gtrsim 10^{18}G$). More recently, it has also been suggested by Vachaspati [7] that gradients in the Higgs field during the electroweak phase transition may lead to magnetic fields as strong as $B \sim 10^{23}G$. Vachaspati has shown that these gradients in the Higgs field cannot be compensated by a gauge field transformation, due to the existence of the cosmological boundary condition, where all physical quantities should be uncorrelated over distances larger than the horizon distance (in this case, the horizon distance at the epoch of the electroweak phase transition).

A further indication of the existence of strong magnetic fields in the early Universe may be the existence of the Galactic magnetic field. There are suggestions that the Galactic magnetic field, of order $10^{-6}G$, could come from the amplification, by a dynamo effect, of a weak seed field of order $10^{-18}G$, on a co-moving scale of $100kpc$ [8]. A possible origin of this seed field could be a cosmological one and, therefore, it could be a primordial field. Tracing it back to early times, its magnitude is consistent with the existence of a very intense magnetic field in the early Universe[2].

We are, therefore, lead to ask what could be the consequences of very intense magnetic fields in cosmology and, in particular, during cosmological phase transitions in general. For such study, we take an arbitrary gauge field model, described by a Lagrangian $\mathcal{L}(\phi, \psi, A_\mu)$, composed of (complex) scalar fields ϕ, fermion fields ψ and gauge fields A_μ. Coupling this model with an external magnetic field B (which we are going to take as a constant, in

*E-mail: rudnei@vmesa.uerj.br

†This work has been partially supported by CNPq.

[1] In some extreme situations, coupling the quantum fields to the curvature, we can achieve phase transitions restoring symmetry breaking through a high curvature of the space time [3].

[2] Studies have shown its magnitude is consistent with that value of B as a result of the electroweak phase transition, although are other studies trying to show that it could also come from others cosmological origins, like inflation or string cosmology (see, for instance, [9] and references therein).

a plane, for computational simplicity), we evaluate the effective potential, at 1-loop order, for the model in the presence of temperature T and the magnetic field B, $V_{\rm eff}(\varphi, B, T)$, where $\varphi \equiv \langle\phi\rangle$, is the background scalar (higgs) field.

At 1-loop order, we can write $V_{\rm eff}(\varphi, B, T)$ as

$$V_{\rm eff}(\varphi, B, T) = V_0(\varphi) + \sum_i \frac{n_i}{2} {\rm Tr} \ln \left[\omega_i^2(\varphi, B, T)\right] \ , \tag{1}$$

where $V_0(\varphi)$ is the tree-level potential, n_i denote the field degrees of freedom and ω_i are the field frequencies.

For a constant B field, the ω_i of charged particles are easily written in terms of Landau levels [10] and the above equation can be evaluated, for example, by using zeta-function regularization method, or Schwinger's proper-time integrals. The full evaluation of (1) can be found in [11].

In [11] we have shown that the most important effect of intense magnetic fields during a symmetry restoring phase transition happen when the phase transition is first order. In a first order phase transition, our results show that the presence of strong magnetic fields tend to lead to a stronger first order phase transition, that is, the external magnetic field can raise the potential barrier between a global and a local vacuum, leading to a higher rate of supercooling during the first order phase transition.

This could lead to important effects during, e.g., the electroweak phase transition and in electroweak baryogenesis based scenarios [12]. It has been argued that an electroweak phase transition could satisfy all conditions for generating a baryon asymmetric Universe. Among these conditions, out-of-equilibrium condition is an important ingredient (for a review of electroweak baryogenesis and its challenges see, for instance, [12]). However, recent studies of the electroweak phase transition, in the minimal standard model, have shown that the phase transition is too weak first order, if not second order, and therefore it would not occur in a sufficient out-of-equilibrium state for generating the required matter asymmetry.

If intense magnetic fields are present during the electroweak phase transition, due to, for example, the presence of superconducting cosmic strings formed during some previous phase transition, or due to a backreation effect, since the own phase transition is expected to lead to intense fields, these strong fields could make the phase transition stronger first order and could lead to a favorable scenario of electroweak baryogenesis.

References

[1] E. W. Kolb and M. S. Turner, *The Early Universe* (Addison-Wesley Publ. Co., Redwood City, California, 1990);

[2] D. A. Kirzhnitz and A. D. Linde, *Ann. Phys.* **101**, 195 (1976); A. D. Linde, *Rep. Prog. Phys.* **42**, 389 (1979);

[3] G. M. Shore, *Ann. Phys.* **128**, 376 (1980);

[4] S. L. Shapiro and S. A. Teukolsky, *Black Holes, White Dwarfs and Neutron Stars, The Physics of Compact Objects* (Wiley, New York, 1983);

[5] V. Ginzburg, *High Energy Gamma Ray Astrophysics* (North Holland, Amsterdam, 1991);

[6] R. Narayan, P. Paczyński and T. Piran, *Astrophys. J. Lett.* **395**, L83 (1992);

[7] T. Vachapasti, *Phys. Lett.* **B265**, 258 (1991);

[8] Y. B. Zeldovich, A. A. Ruzmaikin and D. D. Sokoloff, *Magnetic fields in astrophysics* (Gordon and Breach, NY, 1983);

[9] M. Gasperini, M. Giovannini and G. Veneziano, CERN Preprint CERN-TH/95-85 (1995);

[10] A. Salam and J. Strathdee, *Nature* **252**, 569 (1974);ibid, *Nucl. Phys.* **B90**, 203 (1975);

[11] Work in progress.

[12] A. G. Cohen, D. B. Kaplan and A. E. Nelson, *Ann. Rev. Nucl. Part. Sci.* **43**, 27 (1993);

Non-Heisenberg states of the harmonic oscillator

K. Dechoum and H.M. França
Instituto de Física, Universidade de São Paulo
C.P. 66318, 05389-990 São Paulo, SP, Brazil

Received March, 1996

The effects of the vacuum electromagnetic fluctuations and the radiation reaction fields on the time development of a simple microscopic system are identified using a new mathematical method. This is done by studying a charged mechanical oscillator (frequency ω_0) within the realm of stochastic electrodynamics, where the vacuum plays the role of an energy reservoir. According to our approach, which may be regarded as a simple mathematical exercise, we show how the oscillator Liouville equation is transformed into a Schrödinger like *stochastic* equation with a *free* parameter $\hbar'$ with dimensions of action. The role of the physical Planck's constant $\hbar$ is introduced *only* through the zero-point vacuum electromagnetic fields. The perturbative and the exact solutions of the stochastic Schrödinger like equation are presented for $\hbar' > 0$. The exact solutions for which $\hbar' < \hbar$ are called sub-Heisenberg states. These non-perturbative solutions appear in the form of Gaussian, non-Heisenberg states for which the *initial classical uncertainty relation* takes the form $\langle(\Delta x)^2\rangle\langle(\Delta p)^2\rangle = (\hbar'/2)^2$, which includes the limit of zero indeterminacy ($\hbar' \to 0$). We show how the radiation reaction and the vacuum fields govern the evolution of these non-Heisenberg states in phase space guaranteeing their decay to the stationary state with average energy $\hbar\omega_0/2$ and $\langle(\Delta x)^2\rangle\langle(\Delta p)^2\rangle = \hbar^2/4$ at zero temperature. Environmental and thermal effects are briefly discussed and the connection with sirnilar works within the realm of quantum electrodynamics is also presented. We suggest some other applications of the classical non-Heisenberg states introduced in this paper and we also indicate experiments which might give concrete evidence of these states.

In this paper we shall study a charged oscillator by comparing some features of the Quantum Electrodynamics (QED) and the Stochastics Electrodynamics (SED) approaches [1, 2]. Our motivations are inspired in the early attempts of Planck, Einstein and Stern and Nernst to clarify the role of the zero-point energy [3]. Another motivation is the recent tendency to bring classical and quantum theories to a closer (and maybe nonconflicting) relation[1-3].

Within the QED approach, the Heisenberg equation for the unidimensional motion of a charged oscillator (charge e and mass m) is given by

$$m\ddot{x} = -V'(x) + e\,[E_{VF}(t) + E_{RR}(t)] \quad , \tag{1}$$

where $V(x) = \frac{1}{2}\, m\omega_0^2\, x^2$ is the harmonic potential, ω_0 is the oscillator frequency, $x(t)$ is the position operator , $e\,E_{RR}(t)$ $\left(\simeq \frac{2}{3}\frac{e^2}{c^3}\,\dddot{x}\right)$ is the radiation reaction force, and E_{VF} is the electric field associated to the vacuum fluctuations. The total quantized electric field acting on the particle, that is, $E_x(t) \equiv E_{VF} + E_{RR}$ is also an operator, and will be considered only a function of time within the nonrelativistic approximation (the vector potential will be denoted $A_x \equiv A_{VF} + A_{RR}$). An important point to notice is that the quantum equation (1) is identical to the corresponding classical equation of motion. Several authors[2, 3] consider that the quantum fluctuations associated to the electromagnetic fields, namely E_{VF} in (1), are the source of the quantum fluctuations on the position x of the oscillating charge because *only* E_{VF} depends on $\hbar$. In fact, it is not difficult to derive the quantum commutation relation between the position and the canonical momentum of the oscillator. From the *stationary solution* of (1) one can show that:

$$\left[x\,,\, m\dot{x} + \frac{e}{c}\,A_{VF} - \frac{2e^2}{3c^3}\,\ddot{x}\right] = [x\,,\, m\dot{x}] =$$

$$= i\,\frac{8\pi e^2}{3m}\int_0^\infty d\omega\,\frac{\omega\rho_0(\omega)}{(\omega^2-\omega_0^2)^2+(2e^2\omega^3/3mc^3)^2} = i\hbar \quad , \tag{2}$$

follows from the commutation relations associated to the zero-point electromagnetic fields. We observe that the last equality in (2) *is valid only if the radiation reaction force is precisely* $2e^2\,\ddot{x}\,/3c^3$. The validity of (2) within the non-stationary (or transient) regimen, and under special environmental conditions, are discussed in detail in ref. 4. Therefore, we can easily recognize that, as far as the harmonic oscillator is concerned, the QED and the SED descriptions of this system are very similar. As a matter of fact, the Planck's constant $\hbar$ enters in both descriptions *only* through the zero-point fluctuations of the electromagnetic fields . This is the corner-stone of our approach.

According to the classical view, the probability distribution in phase space x and $p \equiv m\dot{x}$ (kinetical momentum) will be denoted by $W(x,p,t)$, and will evolve in time according to the Liouville equation, namely:

$$\frac{\partial W}{\partial t} + \frac{\partial}{\partial x}(\dot{x}\,W) + \frac{\partial}{\partial p}(\dot{p}\,W) = 0 \quad . \tag{3}$$

Since $\dot{p}/m = \ddot{x}$ is related to the stochastic "vacuum" field $E_{VF}(t)$ (see (1)), the above equation (3) can be transformed into a Schrödinger like stochastic equation [4]. Dechoum and França [4] present the Schrödinger like equation in a new form through the introduction of a *free parameter* $\hbar'$ with the dimension of action. They also show how to apply the approximate methods of perturbation theory, in order to make simple calculations. As an example they calculate the rate of exchange of energy of an arbitrary excited state of the oscillator.

A large part of the Dechoum and França paper is devoted to the discussion of exact solutions of the stochastic Schrödinger like equation and to the introduction and interpretation of the **non-Heisenberg states**. The evolution of these states in phase space is also presented in the final part when they discuss the limitations of the approach and suggest some applications of the non-Heisenberg states in more complicated physical systems. They also indicate experiments which may give physical evidence of the non-Heisenberg states.

According to this paper the stochastic Schrödinger like equation, for a charged particle moving in a general potential

$$V(x,t) = a(t)x^2 + b(t)x + c(t) \tag{4}$$

is given by [4]

$$i\hbar'\frac{\partial\psi}{\partial t} = [-\frac{\hbar'^2}{2m}\frac{\partial^2}{\partial x^2} + V(x,t) - ex(E_{VF}+E_{RR})]\psi \tag{5}$$

This equation, and also $|\psi(x,t)|^2$, has a classical stochastic interpretation because it can be derived from (1) and (3).

REFERENCES

[1] T. H. Boyer, Phys.Rev. D **11**, 790 (1975); 809 (1975). See also the remarkable paper by T. W. Marshall, Proc.R.Soc. London Ser.A **273**, 475 (1963).

[2] L. de la Peña and A. M. Cetto in "The Quantum Dice, an Introduction to Stochastic Electrodynamics", Klewer Acad. Publishers, 1996.

[3] P. W. Milonni, in "The Quantum Vacuum: an Introduction to Quantum Electrodynamics" (Academic, Boston, 1994).

[4] K. Dechoum and H. M. França, Found. of Phys. **25**, 11, 1599 (1995).

Fighting Astrophysics Subrahmanyan Chandrasekhar A Life for the Stars*

Herman Julio Mosquera Cuesta
Divisão de Astrofísica, Instituto Nacional de Pesquisas Espaciais - INPE
Avenida dos Astronautas 1758, Caixa Postal 515
CEP 12201-970, São José dos Campos, SP, Brasil
e-mail:herman@das.inpe.br

Received March, 1996

Chandrasekhar's achievements in astrophysics were widespread in many branches. His fruitful work moved from the revolutionary *Theory of White Dwarfs* to *The Mathematical Theory of Black Holes*. From one main stream to the other there were seminal contributions to the stellar structure and evolution, theory of radiative process in astrophysics, hydrodynamics and hydromagnetic stability, galactic morphology and dynamics, black holes physics and gravitational radiation emission from astrophysical sources. Such an intelectual and plentiful scientific heritage deserves on our behalf the most sempiternal acknowledgement and gratitude. So fully convinced that Chandrasekhar's outrageous legacy will keep on guiding our future search for understanding the Universe for decades to come, we devote this brief retrospection to his memory.

There are many fashions to approach this retrospection to the Chandrasekhar scientific legacy. In this article we decided to shortly revise his fundamental contribution to the stellar structure and evolution in his *theory of white dwarfs* to later take a look on other of his personal contributions to the astrophysics fundations.

Adiabatic Index for an Inclosure containing Matter and Radiation

In his first paper [3, 8] Chandrasekhar shows how to obtain the adiabatic index for an admixture of matter and radiation, his approximation to *white dwarf stellar interior*. His procedure will be followed here, not fully detailed, just to rernember his deep thought on what this parameter should be for a massive white dwarf.

A perfect gas is endowed with an equation of state given by [11]:

$$pV^{\frac{4}{3}} = Constant, \tag{1}$$

the well-known polytropic thermodynamic relation.

Curiously, an inclosure of pure radiation behaves exactly like such gas. Perhaps a reminiscence of the *wave-particle duality* of the new quantum theory.

In his approach to study white dwarf thermodynamics he discovered a closed group of thermodynamical parameters; the adiabatic exponents. Chandrasekhar's adiabatic exponents are defined as follows:

$$\Gamma_1 = \beta + \frac{(4-3\beta)^2(\gamma-1)}{\beta + 12(\gamma-1)(1-\beta)} \equiv \gamma_{ad} \tag{2}$$

where $\gamma = \frac{c_p}{c_v}$ the adiabatic index, $\frac{4}{3}$ in eq(1), is a relation of the specific heats of the substance, and $\beta \equiv \frac{p_g}{p}$, with p_g the gas pressure and p, the total pressure. The other indexes are:

$$\Gamma_2 = 1 + \frac{(4-3\beta)^2(\gamma-1)}{\beta^2 + 3(\gamma-1)(1-\beta)(4+\beta)} \tag{3}$$

and,

*Poethic appearance of this subtitle is subtle. It encompasses the fact that main Chandrasekhar motivation to do research in astrophysics was his search for understanding how stars behave, the physics that underlie them with no respect to isolated or clustered stars, galaxies or cosmic black holes.

$$\Gamma_3 = 1 + \frac{(4-3\beta)(\gamma-1)}{\beta + 12(\gamma-1)(1-\beta)(4+\beta)}. \tag{4}$$

These adiabatic exponents obey the relation:

$$\frac{\Gamma_1}{\Gamma_3 - 1} = \frac{\Gamma_2}{\Gamma_2 - 1}. \tag{5}$$

In particluar, from eq(2) is easy to see that: $\Gamma_1 = \gamma$ when $\beta = 1$, and $\Gamma_1 = \frac{4}{3}$, when $\beta = 0$.

These astrophysical quantities are fundamentals for depicting the physical (thermo-hydrodynamics) behavior of main sequence and also evolved stars, and particularly, for the thermodynamical description of life and death of white dwarf stars.

Physics of Extremely Dense Matter

From another point of view, in quantum mechanics is shown that the number of quantum states with momenta between p and $p + dp$ is given by

$$V\frac{8\pi p^2}{h^3}dp \tag{6}$$

Pauli's principle asserts that no two electrons can occupy the same quantum state. So the number of electrons in this interval are

$$N(p)dp \leq V\frac{8\pi p^2}{h^3}dp \tag{7}$$

Now, a completely *degenerate electron gas* is one which all the lowest quantum levels are occupied. This leads to

$$N(p) = V\frac{8\pi p^2}{h^3} \tag{8}$$

and consequently,

$$N = V\frac{8\pi}{h^3}\int_0^{P_0} p^2 dp \tag{9}$$

or

$$N = V\frac{8\pi}{3h^3}P_0^3, \tag{10}$$

where we define the density of quantum states as:

$$n = \frac{N}{V} = \frac{8\pi}{3h^3}P_0^3. \tag{11}$$

The total pressure can be calculated from

$$PV = \frac{1}{3}\int_0^{\infty} N(p)pv_p dp, \tag{12}$$

here v_p is the velocity of the particles with momentum p. So we are left with,

$$P = \frac{8\pi}{3h^3}\int_0^{\infty} p^3\frac{\partial E}{\partial p}dp, \tag{13}$$

where E is the kinetic energy of the electron whose momentum is p.

At this point Chandrasekhar realizes that relativistic effects should be taken into consideration in order to describe correctly white dwarfs's structure. So he used the relativistic relation [1]

[1] The appropriate Newtonian relation is given as: $E = \frac{p^2}{2m}$. This relation, clearly, is not correct for the case of *degenerate matter*. See previous section.

$$E = mc^2\left[\left(1+\frac{p^2}{m^2c^2}\right)^{\frac{1}{2}} - 1\right]; \tag{14}$$

which yields

$$\frac{\partial E}{\partial p} = \frac{1}{m}\left(1+\frac{p^2}{m^2c^2}\right)^{\frac{-1}{2}} p. \tag{15}$$

This leads to

$$P = \frac{8\pi}{3h^3}\int_0^{p_0} \frac{p^4 dp}{\left(1+\frac{p^2}{m^2c^2}\right)^{\frac{1}{2}}}. \tag{16}$$

After some algebraic substitutions (see the book for details) we get:

$$P = \frac{\pi m^4 c^5}{3h^3} f(x) \tag{17}$$

where

$$f(x) = x(2x^3-3)(x^2+1)^{\frac{1}{2}} + sinh^{-1}x. \tag{18}$$

The function f(x) has the assymptotic forms:

$$f(x) \sim \frac{8}{5}x^5 - \frac{4}{7}x^7 + \frac{1}{3}x^9 - \frac{5}{22}x^{11} + \ldots \quad (x \to 0) \tag{19}$$

and

$$f(x) \sim 2x^4 - 3x^2 + \ldots \qquad (x \to \infty) \tag{20}$$

Taking only the first terms in the expansions of $f(x)$ we obtain for the electrons' pressure:

$$P = \left[\frac{1}{20}\left(\frac{3}{\pi}\right)^{\frac{2}{3}}\frac{h^2}{m_e}\right] n^{\frac{5}{3}} \qquad (x \to 0) \tag{21}$$

and

$$P = \left[\frac{1}{8}\left(\frac{3}{\pi}\right)^{\frac{1}{3}} hc\right] n^{\frac{4}{3}} \qquad (x \to \infty). \tag{22}$$

From these equations we can confirm Chandrasekhar's conclusion that the adiabatic index has to be $\frac{4}{3}$ for fully relativistic degenerate white dwarf stars, it reads as a direct confrontation between eq(1) and eq(22), together with eq(11). It is also easy to see, from eq(22), that for non-relativistic degenerate white dwarfs this adiabatic index becomes $\frac{5}{3}$; as found by Chandrasekhar [8, 9].

Chandrasekhar's Theory of Maximum Mass for White Dwarfs.

Describing the mechanical structure of white dwarf encorporates the hydrostatic equilibrium equation and the equation of state for the particles responsible for the pressure that support the star against its gravitational self-attraction. Electron's degree of degeneracy is defined by $x = \frac{p_f}{m_e c}$, where p_f is the Fermi momentum of the electron, which varies as $\rho^{\frac{1}{3}}$.

Equation of state reads:

$$P = C_1 f(x), \qquad \rho = C_2 x^3, \qquad x = \frac{p_f}{m_e c} \tag{23}$$

with

$$p_e = \frac{\pi m_e^4 c^5}{3h^3} f(x) \tag{24}$$

as adapted from eq(17), and

$$f(x) = x(2x^3 - 3)(x^2 + 1)^{\frac{1}{2}} + sinh^{-1}x. \tag{25}$$

as defined in eq(18). Also, the electron density is defined as:

$$n_e = \frac{\rho}{\mu_e m_u} = \frac{8\pi m_e^3 c^3}{3h^3} x^3 \tag{26}$$

is given in eq(11).
Resolution begins with Poison's equation radial component:

$$\frac{1}{r^2}\frac{d}{dr}\left(r^2\frac{d\phi}{dr}\right) = 4\pi G\rho. \tag{27}$$

In this equation $\frac{d\phi}{dr}$ is replaced from the hydrostatic equilibrium equation

$$\frac{dP}{dr} = -\frac{d\phi}{dr}\rho \tag{28}$$

where P and ρ can be substituted from eq(23). Constants C_1 and C_2 are the coeficients of equations(23,24). Thus we get

$$\frac{C_1}{C_2}\frac{1}{r^2}\frac{d}{dr}\left(\frac{r^2}{x^3}\frac{df(x)}{dr}\right) = -4\pi G C_2 x^3. \tag{29}$$

From the quantum mechanical treatment of a completely degenerate electron gas we get for the particles' pressure:

$$P_e = \frac{8\pi c}{3h^3}\int_0^{p_f} p^3 \frac{p/m_e c}{[1 + p^2/(m_e^2c^2)]^{\frac{1}{2}}} dp. \tag{30}$$

By introducing the new variables:

$$\theta \equiv p/m_e c, \qquad x \equiv p_f/m_e c \tag{31}$$

it reads,

$$P_e = \frac{8\pi c^5 m_e^4}{3h^3}\int_0^x \frac{\theta^4 d\theta}{(1+\theta^2)^{\frac{1}{2}}}. \tag{32}$$

The integral can be replaced by

$$\int_0^x \frac{\theta^4 d\theta}{(1+\theta^2)^{\frac{1}{2}}} = \frac{1}{8}\left[x(2x^3 - 3)(x^2 + 1)^{\frac{1}{2}} + sinh^{-1}x\right]. \tag{33}$$

Here, the square bracket corresponds to the $f(x)$ function defined in eq(25).
Differentiating this equation we see that:

$$\frac{1}{x^3}\frac{df(x)}{dr} = 8\frac{d}{dr}\left[(x^2+1)^{\frac{1}{2}}\right] = 8\frac{dz}{dr}, \tag{34}$$

where

$$z^2 \equiv x^2 + 1. \tag{35}$$

With these substitutions in eq(29) we get,

$$\frac{1}{r^2}\frac{d}{dr}\left(r^2\frac{dz}{dr}\right) = \frac{-\pi G C_2^2}{2C_1}(z^2-1)^{\frac{3}{2}}. \tag{36}$$

Replacing r and z for the dimensionless variables ε and ϕ, defined as follows:

$$\varepsilon \equiv \frac{r}{\alpha} \tag{37}$$

$$\varpi \equiv \frac{z}{z_c} \tag{38}$$

where $\alpha = \sqrt{\frac{2C_1}{\pi G}}\frac{1}{C_2 z_c}$, and z_c is density value at the star's center, we obtain through the use of eq(36):

$$\frac{1}{\varepsilon^2}\frac{d}{d\varepsilon}\left(\varepsilon^2\frac{d\varpi}{d\varepsilon}\right) = -\left(\varpi^2 - \frac{1}{z_c^2}\right)^{\frac{3}{2}}. \tag{39}$$

This way we get the *Chandrasekhar's differential equation for the structure of white dwarf stars*[8]. It could be written as

$$\frac{d^2\varpi}{d\varepsilon^2} + \frac{2d\varpi}{\varepsilon d\varepsilon} + \left(\varpi^2 - \frac{1}{z_c^2}\right)^{\frac{3}{2}} = 0. \tag{40}$$

The Chandrasekhar equation looks like an Endem equation for politropes [11], and reduces to this when politropic exponents are n = 3 and n = $\frac{3}{2}$, what corresponds to assymptotic values $z \to \infty$; (i. e. $x \to \infty$), and $z \to 0$; (i .e. $x \to 1$) [12].

Solving it with central conditions

$$\varepsilon = 0, \qquad , \varpi' = 0 \tag{41}$$

we get the density stratification as

$$\rho = C_2 x^3 = C_2(z^2 - 1)^{\frac{3}{2}} = C_2 z_c^3\left(\pi^2 - \frac{1}{z_c^2}\right)^{\frac{3}{2}}. \tag{42}$$

As usual, it surface is found from $\varepsilon = \varepsilon_1$, where ρ becomes zero. It yields,

$$\varepsilon = \varepsilon_1; \qquad , x_1 = 0, \qquad , \varpi_1 = \frac{1}{z_c}. \tag{43}$$

The radius of the star is given by

$$R = \alpha\varepsilon_1 = \sqrt{\frac{2C_1}{\pi G}}\frac{1}{C_2 z_C}\varepsilon_1. \tag{44}$$

Finally, the star mass M is obtained from the functionals of r and z defined in equations(37,38):

$$M = \int_0^R 4\pi r^2 \rho dr \tag{45}$$

Or equivalently,

$$M = 4\pi\alpha^3 C_2 z_c^3 \int_0^{\varpi_1} \varepsilon^2\left(\varpi^2 - \frac{1}{z_c^2}\right)^{\frac{3}{2}} d\varepsilon. \tag{46}$$

In this equation the integrand can be replaced by the left-hand derivative of Chandrasekhar's differential equation(39), thus getting

$$M = 4\pi\alpha^3 C_2 z_c^3\left(-\varepsilon^2\frac{d\varpi}{d\varepsilon}\right)_1. \tag{47}$$

Substituting for α we are left with

$$M = \frac{4\pi}{C_2^2}\left(\frac{2C_1}{\pi G}\right)^{\frac{3}{2}}\left(-\varepsilon^2\frac{d\varpi}{d\varepsilon}\right)_1. \tag{48}$$

This equation runs for the whole range between non-relativistic degenerate to the fully relativistic degenerate white dwarf stars. It requires a numerical solution. Notwithstanding, we are able to derive Chandrasekhar's limiting mass for white dwarfs by restoring the star proper variables (r, z) and their numerical values into it. This follows after forcing the equation to the fully relativistic case; i. e., $x_c = \infty$, to obtain the relation:

$$M_{Ch} = 5.86\mu_e^{-2} M\odot. \tag{49}$$

Since $z_c \rightarrow \infty$ corresponds to a *Lane-Endem functional* of adiabatic index n= 3 [8], as referred to earlier, this equation represents the maximum mass is allowed for any white dwarf star. In other words, no white dwarf star can be heavier than this given limiting maximum mass. [6].

Eddington Confrontation to Chandrasekhar's Relativistic Degeneracy Approach. By the eve of the World war II the energy source of stars on the main sequence on Hertzsprung Russell diagram was pretty well understood as a consequence of Aitkinson, Houtermans, Bethe and Von Weizäcker and their colaborators implementation of Gamow's tunelling mechanism. To astrophysicists the answer to how stars evolve thereafter had been achieved. But a nagging inquiry was bothering around, yet. Knowing that star's light is the by-product of thermonuclear fusion reactions, the point was: what happens when finally their nuclear fuel becomes exhausted? The answer to this puzzle problem had been given in the 1930's. Few people awared of it. A reason for that derives from the fact that the explanation suggested to this key quiry in astrophysics was obscured and ridiculed by the eminent luminarie of the british astronomy, Sir Arthur Stanley Eddington. This episode will be reviewed below.

Meanwhile, in Cambridge Chandrasekhar received his Ph. D. degree in 1933. Since then he was nominated as a fellow of Trinity College, the centre where his well-known astrophysicists Fowler and Eddington were faculty members. He kept this position until 1938 when he moved to University of Chicago as a member of the faculty staff.

With his Ph. D. diploma at hands Chandrasekhar reiniciated a utter study on the limiting mass for white dwarfs. About the end of 1934 ha had gotten demonstrating that for the ten representative white dwarfs he used to check up his theory none of them had a mass heavier than its limiting maximum mass [7]. To obtain this conclusion he ought to solve numerically the differential equation for the stellar structure, eq(39). This way of showing to the astronomical community that his earlier computations were essentially corrects it was suggested to him by the armenian astrophysicist Ambartsumian; some months before [15].

As a magic glove for hands, for January 11^{th} 1935, it was scheduled a Meeting of the Royal Astronomical Society. That was an excelent opportunity to present his revised calculations of the white dwarf stars and their maximum mass. At his turn Chandrasekhar with mastery on the subject did demonstrate that effectively white dwarf stars cannot be heavier than $1.44M\odot$. Otherwise, they should implode under their own gravitational squeeze. An impecable lecture was given. Audithorium responds with a polite aplause.

Eddington's Absurd Behavior of White Dwarfs.

Following Chandrasekhar lecture, another one from Eddington on "Relativistic Degeneracy" was scheduled. After a brief discussion on the Sun destiny and its final quiet death at the white dwarf grave according to Chandrasekhar's analysis, Eddington parted to a description of the sine awaiting for a star as massive as Syrius A, whose mas is $\sim 2.3M\odot$. Rapidly he showed that if Chandrasekhar's theory was right there was no quiet end for this sort of stars and, unavoidably, they must implode. This conclusion shocked Eddington's astrophysical beliefs. How absurd is the white dwarfs' behavior, he reasoned. Why does nature allow for this to happen? Quoting Eddington's words: "Dr. Chandrasekhar had got this result before, but he has rubbed it in in his last paper; and, when discussing it with him, I felt driven to the conclusion that this was a *reductio ad absurdum* of the relativistic degeneracy formula. Various accidents may intervene to save the star, but I want more protection than that. I think there should be a law of nature to prevent a star behaving in this absurd way!". Then Eddington argued against Chandrasekhar mathematical proof saying that people could not trust in it since it was obtain from an inadequate meshing of special relativity and quantum theory. He said: "I do not regard the offspring of such a union as born in lawful wedlock".

A day after the conference Chandrasekhar wrote a letter to Leon Rosenfeld at Copenhagen asking for his opinion, and that one from Bohr's about Eddington's way out for the white dwarf stars' destiny. The response was conclusive. Too much clear for. Both of them could indeed not find any meaning in Eddington's arguments. They concluded Chandrasekhar was right and, therefore, Eddington should find another more physically based escapement. Despite of that, the astronomical community gave no credit to Chandrasekhar's maximum mass limiting. All of them adhered to Eddington's conclusion. They believed, as Eddington, that a *a law of nature to prevent the star from behaving in this absurd way* is to exist, when in fact, there is none. Implosion is compulsory.

Conclusions.

During the intervening years until his departure Chandrasekhar kept eagerly his active pursuit scientific research. All those years did see a number of colleagues and students receiving his advice and friendshipness. Many times

his struggling for unveiling nature's misteries was homaged. On may 27-29; 1975, his colleagues at the University of Chicago, Norman Lebovitz; who joined Chandrasekhar in the sixties' to rediscovering Dirichlet, Dedekind and Riemann works on rotating liquid masses [10], William Reid and Peter Vandervoort of the department of physics organized a Symposium on *Theoretical Principles in Astrophysics and Relativity* to honored him at 65^{th} year. In the papers compilation they wrote as preface: "This book, the proceedings symposium, is likewise dedicated to Chandra. We know that his many friends throughout the world will joint to us in this expression of our admiration and affection"[13]. All of us certainly joined to. Like this one many other meetings around the world were held to tributing to Chandra our gratitude for his fighting.

That year was also the beginning of a definitely new example of his tenacity. During summer, William Press, Saul Teukolsky and a selected team of young physicists held a meeting at Princeton University to put an appropriate epitaph on to the black holes theory. They organized the *Funeral for the Golden Age of Bkack Hole Research*. According to these people there was nothing more interesting at all to be done in this field. They believe the essential aspects of the theory had already been worked out. Particularly, it was guessed that *Teukolsky's equation* encompassed all the things could be said on black holes. Notwithstanding, Chandrasekhar not believed so. So he began for revising the work done thus far. In 1983, at age 73; and after having worked paciently for eight years restudying what people had been done in this field, he gave a surprise to everyone interested in black hole theory. He published his marvelous, deeply elaborate treatise on *The Mathematical Theory of Black Holes* which contains an elegant description of the *perturbation theory technique* to study the black holes' dynamics. One of his last gifts to the relativity community.

The time has come to remember Chandrasekhar's first thought after his discouragement for Eddington attack to his limiting mass achievement: "I felt that astronomers without exception thought that I was wrong. They considered me as sort of *Don Quixote* trying to kill Eddington. As you can imaging, it was a very discouraging experience for me to find myself in a controversy with the leading figure of astronomy and to have my work completely and totally discredited by the astronomical community. I had to make up my mind as to what to do. Should I go on the rest of my life fighting...? It was better for me to change my field of interest and go into something else". So in 1939, after having written his famously quoted book *An Introduction to the Stellar Structure*, Chandrasekhar turned his back to the field that fifty four years later helped him to be honoured with the *Nobel Prize in Physics*, the white dwarfs and the stellar death [15].

To his whole life of science dedication we express our sempiternal admiration [2] [16]. We will endlessly be indebted to Chandra for his also outrageous legacy.

References

[1] Fowler, R. H., Month. Not. Roy. Ast. Soc., **87**, 114, 1926.

[2] Eddington, A. S., *The Internal Constitution of the Stars*, Camb. Univ. Press, 1925.

[3] Chandrasekhar, S., Philosophical Magazine, **II**, 592, 1931.

[4] Chandrasekhar, S., Month. Not. Roy. Ast. Soc., **91**, 446, 1931.

[5] Chandrasekhar, S., Ap. J., **74**, 81, 1931.

[6] Chandrasekhar, S., Month. Not. Roy. Ast. Soc., **95**, 207, 1935.

[7] Chandrasekhar, S., *An Introduction to the Stellar Structure*, Dover Publishers.

[8] Chandrasekhar, S., *Selected Papers of S. Chandrasekhar, Volume I: Stellar Structure and Stellar Atmospheres*, University of Chicago Press, 1989.

[9] Chandrasekhar, S., *The Mathematical Theory of Black Holes*, Oxford Science Publicatios, 1983, Oxf. Univ. Press, 1992.

[10] Chandrasekhar, S., *Ellipsoidal Figures of Equilibrium*, Yale University Press, 1969.

[11] Endem, R., *Gas Spheres (German title:"Gaskugeln)*, Leipzig, 1907.

[12] Kippenhahn, R. and Weigert, A., *Stellar Structure and Evolution*, Springer Verlag, 1990.

[13] Lebovitz, N., Reid, W. and Vandervoort, P., *Theoretical Principles in Astrophysics and Relativity*, University of Chicago Press, 1978.

[14] *Voyage Through the Universe*, Volume VI: Stars, eds. Time-Life Books, 1988.

[15] Thorne, K. S., *Black Holes and Time Warps, The Einstein Outrageous Legacy*, Norton Publishers, 1994.

[16] Astrophysical Journal, Vol. 455, Num. 2, Part 1,407-411, 1995.

[2] Chandrasekhar scientific production was so copious that just in the *Astrophysical Journal*; whose statistics were compiled to celebrate the 100^{th} years of continous issues; published recently in *Ap. J.* Vol. 455, *Number 2, 407-411, 1995*, it is shown that on average Chandrasekhar contributions during his 48 years were 139 papers, the highest mean contribution ever done to the journal.

Produção de Partículas mais pesadas que píons em Interações Hadrônicas

S.L.C. Barroso[1], A.O. de Carvalho[1], M. D.D.O. Marques[1],
R. de Oliveira[1], E.H. Shibuya[1], C.R.A. Augusto[2],
C.E. Navia[2] and F.A. Pinto[2]

1. Instituto de Física 'Gleb Wataghin', UNICAMP

2. Instituto de Física, UFF

Received March, 1996

Utilizando um conjunto de dados obtidos nos detectores de Interações Hadrônicas da Colaboração Brasil-Japão de Raios Cósmicos, mostramos que os secundários destas Interações parecem se dividir em grupos. Esta divisão é tida como consequência da criação de *Estados Intermediários Discretos* entre a colisão hadrônica e a produção dos secundários. Em um cada destes grupos (dois, no caso deste trabalho) foi feita a busca de sinal estatisticamente significante da produção de mésons η. Tal busca indica a produção seletiva de mésons η, já que sinal significativo dos mesmos só foi encontrado em um dos grupos analisados.

I Breve descrição do detector

O detector é constituído essencialmente de material fotossensível acondicionado em envelopes selados. Experimentos específicos adotam geometrias especiais. Detalhes em [0].

II Métodos de análise

O conjunto de fótons provenientes de uma mesma Interação Hadrônica é denominado família. De acordo com a região do detector onde ocorreu a Interação Hadrônica (IH), esta é classificada como A-Jatos (IH na atmosfera sobre o detector), C-Jatos (IH no alvo de carbono) ou Pb-Jatos (IH numa placa de chumbo). A altura do ponto onde ocorreu a IH, ou simplesmente a altura de interação, é também determinada. Verifica-se então se cada uma das famílias identificadas são realmente resultantes de uma única IH com produção isotrópica de secundários usando um algorítimo desenvolvido para tal finalidade. Os dados que atendem tal critério são então submetidos à um segundo algorítimo, chamado de mDW. Nota-se então que o conjunto de dados se divide em grupos. A cada grupo associa-se um Estado Intermediário Discreto diferente, batizados de Mirim, Açú, Guaçú e Centauro. Após isto, busca-se em cada uma das famílias dos grupos Mirim e Açú os pares de fótons provenientes de pions neutros.

Determinados os pares de fótons provenientes de π^0's, os fótons restantes (em cada família) são combinados dois a dois para gerar a distribuição de massas invariantes dos supostos mésons que teriam produzidos estas combinações. Esta distribuição experimental é então comparada com uma distribuição de massas invariantes obtida da mesma maneira de dados simulados sem a produção de η's. Nas IH do tipo A-Jato, foi feita também a busca individual de pares de fótons provenientes de η's. Isto porque notou-se que, entre os fótons não identificados como provenientes de π^0, alguns de energia razoavelmente alta estavam afastados do centro de massa da família. Além disso, verificou-se que a massa invariante da combinação destes fótons era próxima do massa invariante do η. Este tipo de busca não foi feita nos C-Jatos porque, devido a pequena altura de interação dos mesmos, a separação entre os secundários não é suficiente para se usar os critérios citados anteriormente.

III Conclusões

Na figura 1 nota-se como as IH parecem se dividir em alguns tipos diferentes. Na tabela 1 são mostradas algumas grandezas características de cada um destes tipos. A busca estatística de η's nos tipos Mirim e Açú indica a produção seletiva de η's, pois sinal estatisticamente significante da sua produção só foi notado nos Açús (figuras 2).

Na figura 3 vemos a distribuição integral de $\langle P_t \rangle$ para os π^0's e η's identificados nas famílias do tipo Açú - A-Jato, através da busca individual.

A maioria dos componentes da família do tipo Centauro foram identificados como hádrons (nos Açús e Mirins os componentes são, na sua maioria, identificados como fótons). Corrigindo-se então o momento transversal médio de hádrons em forma de fótons $\langle P_{t_h}^{(\gamma)} \rangle$ usando-se uma multiplicidade razoável, obtém-se $\langle P_{t_h} \rangle$ da ordem de 1 GeV/c. Como a família Centauro analizada foi produzida isotropicamente (segundo o algorítimo usado para verificar isotropia, figura 3), podemos descreve-la através de modelos termodinâmicos para IH. Tais modelos mostram que há uma relação entre $\langle P_t \rangle$ do Estado Intermediário e a(s) massa(s) da(s) partícula(s) produzida(s). Então, pode-se associar ao fato de $\langle P_t \rangle$ dos Açús ser maior que o $\langle P_t \rangle$ dos Mirins a produção de uma partícula mais pesada no Açú (no caso o η), como mostram os resultados experimentais. Seguindo esta linha de raciocínio, o valor de 1 GeV/c para o $\langle P_t \rangle$ do Centauro pode ser visto como sinal da produção de partículas mais pesadas que o η nos Centauros. Este valor de $\langle P_t \rangle$, associado a outras características *exóticas* dos Centauros, sugere que os Centauros sejam resultantes não do fenômeno de *Produção Múltipla de Mésons* que ocorre em IH's de alta energia, mas sim duma *Produção Múltipla de Bárions e Anti-Bárions*.

		fótons		π^0		η	
		$\langle N_\gamma \rangle$	$\langle P_t \rangle$ (MeV/c)	$\langle N_{\pi^0} \rangle$	$\langle P_t \rangle$ (MeV/c)	$\langle N_\eta \rangle$	$\langle P_t \rangle$ (MeV/c)
Mirim	A-Jatos	7 ± 0.4	168 ± 13	2.5 ± 0.3	280 ± 17	-	-
	C-Jatos	7 ± 0.5	125 ± 11	2.5 ± 0.4	192 ± 14	-	-
Açú	A-Jatos	15 ± 0.4	385 ± 20	4.6 ± 0.3	547 ± 23	0.6 ± 0.11	1281 ±36
	C-Jatos	17 ± 0.6	258 ± 16	6.4 ± 0.6	387 ± 20	-	-
		hádrons					
		$\langle N_h \rangle$	$\langle P_{t_h}^{(\gamma)} \rangle$ (MeV/c)				
Centauro	A-Jatos	39 ± 4	267 ± 16				

Tabela 1: Resumo dos resultados obtidos. $\langle N_\gamma \rangle$, $\langle N_{\pi^0} \rangle$, $\langle N_\eta \rangle$ e $\langle N_h \rangle$ são, respectivamente, as multiplicidades médias por IH de fótons, π^0's, η's e hádrons.

Referência

1. M.Akashi & outros, Prog. Theor. Phys. Suppl. 32 (1964), 1-2

• Chacaltaya Emulsion Chamber Experiment, Prog. Theor. Phys. Suppl. 47 (1971), 1-125

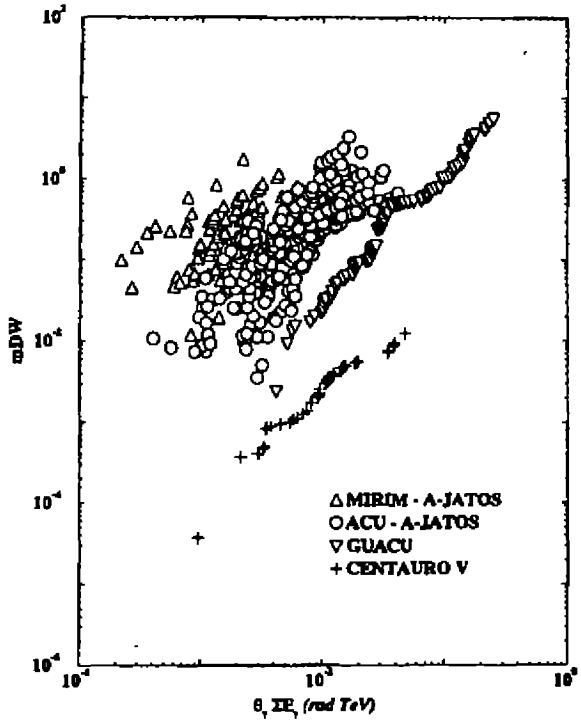

Figura 1: Gráfico do mDW para o Centauro V, Guaçú e as famílias A-Jatos. Notar a separação entre os quatro tipos de Estado Intermediário identificados.

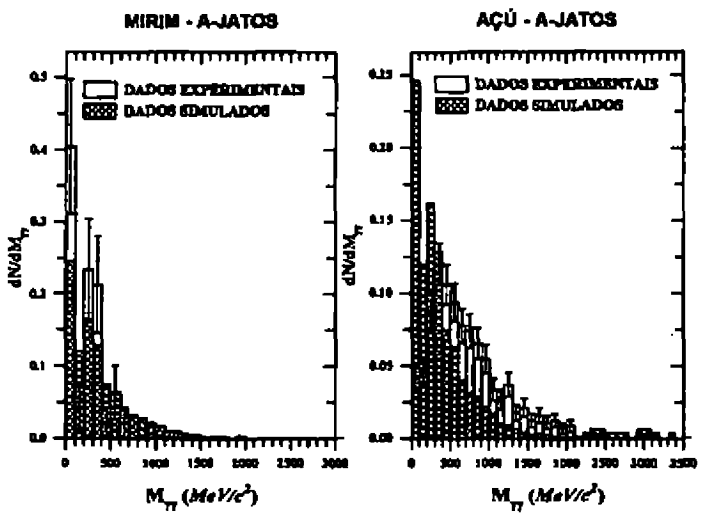

Figura 2: Comparação entre as distribuições de $M_{\gamma\gamma}$ experimental e simulada para famílias do tipo Mirim (esquerda) e Açú (direita). Notar a diferença significativa entre as distribuições para os Açús, principalmente na região de massa invariante do η.

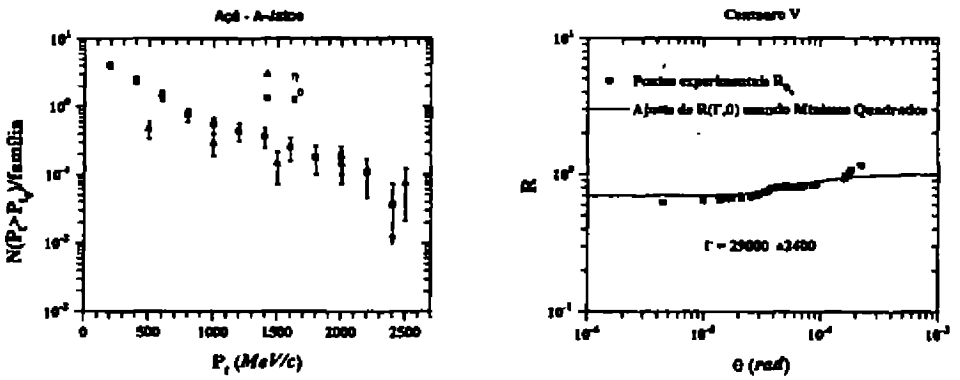

Figura 3: Á esquerda: Distribuição integral de momento transversal de π^0's e η's para A-Jatos do tipo Açú. Á direita: Gráfico do ajuste da função R usada para teste de isotropia. Notar que a qualidade do ajuste é boa, indicando que a família Centauro V atende o critério de isotropia.

Can we measure Charm Hadron Semileptonic Decays in E781 ?

C. O. Escobar, E. Fernandes, F. Garcia, P. Gouffon, N. Kuropatkin *; T.L. Lungov, R.A. de Paula, R. Zukanovich Funchal

Instituto de Física da Universidade de São Paulo

05389-970 C.P. 66318 - São Paulo, SP, Brazil

Received March, 1996

We have used the GE781 Monte Carlo to investigate the E781 trigger and filter efficiencies to several semileptonic decay modes of charm hadrons as well as for simulated FRITIOF/PYTHIA background. A complementary filter, based on the TRD response, was also investigated in order to increase efficiency to semileptonic modes of short living charm hadrons, such as Ξ_c^0.

1 Introduction

The theoretical description of charm hadron decays is, in general, not simple. The models depend on many unknown factors related to our lack of knowledge of the relative importance of exchange and interference diagrams and, specially, of nonperturbative QCD effects.

Semileptonic decays of charm mesons and baryons are nevertheless thought to be particularly simple. The lepton-neutrino system produced by the virtual W boson is well understood and it cannot have strong interactions with the hadronic decay product. The nonperturbative QCD effects on the semileptonic decay amplitudes are parametrized in terms of Lorentz-invariant form factors, which depend only on q^2 , the square of the mass of the virtual W. Morover, in the charm sector, one can use the assumption of CKM matrix unitarity to measure the q^2 dependence of the form factors independently of the determination of CKM elements. This should provide very useful information to improve predictions for b decays [1].

Because they are theoretically more tractable, semileptonic decays represent the best possibility to disentangle weak from nonperturbative QCD effects providing us with a good probe of nonperturbative models. They are probably the best candidates to give us some insight into hadronizatiou phenomena.

Semileptonic decay rates are also reasonably large (a few percent at least) and should be experimentally accessible in E781.

In section 2 we discuss how trigger and filter calculations were made, in section 3 we show our results for some hadronic modes and compare them with previous results [3], in section 4 we show our results for some semileptonic modes, in section 5 background suppression is presented and finally in section 6 we draw our conclusions.

2 Trigger and Filter Calculations

We have used the GE781 [4] Monte Carlo to calculate trigger and filter efficiencies to LUND generated events (signal and background). The trigger response was simulated according to multiplicity matrix proposed in H-643 [2] i.e. three or more positive particles matching the matrix in both hodoscopes.

The filter selection was simulated in the following way. Primary interaction in the target was smeared randomly in z, arround the half thickness of the target. Tracks seen by interaction counter and hodoscope 1 were extrapolated back to the interaction plane and the coordinates of crossing were smeared to simulate track finding resolution. Miss-distance ($m_{\rm dist}$) was calculated considering the primary interaction to have happened in the center of the target. In fact the track finding resolution is not so crucial for miss-distance calculations, the thickness of the target (1.5 mm) being the dominat contribution to the error.

*On leave from Petersburg Nuclear Physics Institut

The TRD (electron transition radiation detector) filter was simulated taking tracks that were seen by both hodoscopes. The coordinates of the hits of these tracks in the TRD chambers were predicted. TRD pulses along a road of ±1 strip around the predicted position were added up to produce the TRD response for this track.

3 Results for some hadronic modes

Before going on to investigate semileptonic modes, we decided to check the results of H-722 [3] for $\Lambda_c^+ \to pK\pi$ with our simulation. We also have simulated $\Lambda_c^+ \to \Lambda^0\pi^+$ because we would like to see how the signal is suppressed in the case of a low multiplicity mode. The Λ_c^+s where generated according to $(1 - x_F)^{4.2}$, so this cross-section behavior is already taken into account in our results.

To do this we have calculated the maximum $m_{\rm dist}$ ($m_{\rm charm}$) for charm decay products seen in the hodoscope 1, for each event.

We will define **reconstructable charm events** [3] as events that have at least one daughter particle from charm decay in hodoscope 1 and with $m_{\rm charm} > 30$. We will calculate ϵ_g global efficiency with respect to the total number of charm events generated. Our results are presented in the following table :

	$\Lambda_c^+ \to pK^-\pi^+$	$\Lambda_c^+ \to \Lambda^0\pi^+$
ϵ_g(trig) (%)	33.9± 1.4	27.5 ± 1.3
ϵ_g(charm + $m_{\rm charm} > 30$) (%)	30.4 ± 1.3	17.9 ± 1.0
ϵ_g(trig + charm + $m_{\rm charm} > 30$) (%)	13 ± 0.9	6.0 ± 0.6

In the case of events $\Lambda_c^+ \to pK^-\pi^+$, we have an approximately equal contribution to the filter from all decay products, in the case of $\Lambda_c^+ \to \Lambda^0\pi^+$, only π^+ contributes.

We observe that our results are compatible with the ones presented in Ref. [3].

4 Results for semileptonic modes

We have generated the following semileptonic decays to study:

- $\Xi_c^0 \to \Xi^- e^+ \nu_e$, with $(1 - x_F)^2$ (Ξ_c^0);
- $\Lambda_c^+ \to \Lambda^0 e^+ \nu_e$, with $(1 - x_F)^{4.2}$ (Λ_c^+);
- $D^0 \to K^- e^+ \nu_e$ (D^0);
- $D_s^+ \to \Phi e^+ \nu_e$ (D_s^+);
- $D^+ \to \bar{K}^0 e^+ \nu_e$ (D^+);

As semileptonic decays are somewhat suppressed by the trigger and the miss-distance cut is bound to diminish the final number of accessible events even more, specially for short living particles, we would like to investigate a complementary filter similar to what was proposed for the RICH [5], but using TRD. The TRD algorithm proposed is much simpler and faster than any possible RICH algorithm and will, most certainly, accept less background.

The TRD detector is very good in separating energetic e^+/e^- from other particles. The efficiency of this selection depends very much on the nature of the background and on the kinematics of the signal one is looking for.

We have investigated the TRD response to signal and background and found that the appropriate cut should be 5-6 TRD pulses.

The TRD filter consists in selecting the events that have at least one positive track coming from one of the targets ($z_v < 0$) with more than 6 TRD pulses (trdsum) along its road and having less than 120 GeV/c. The idea is to **OR** this filter with the miss-distance one.

Our results are presented in the following table:

	Ξ_c^0	Λ_c^+	D^0	D_s^+	D^+
ϵ_g(trig) (%)	23.0	25.4	13.3	17.2	14.6
ϵ_g(charm + $m_{\rm charm} > 30$) (%)	7.9	12.5	38.7	35.8	39.4
ϵ_g(trig + charm + $m_{\rm charm} > 30$) (%)	2.7	4.7	6.2	9.0	7.8
OR (%)	12.6	12.0	8.2	11.1	2.0

Here OR means (trigger + charm+$m_{charm} > 30$)**OR** (trigger+charm+trdsum > 6).
The statistical errors are as follows:

- ϵ_g(trig):3% for D^0 and D^+ modes and 1% for all the others;
- ϵ_g(charm + $m_{charm} > 30$):4% for D^0 and 5% for D^+ modes and 1% for all the others;
- ϵ_g(trig + charm + $m_{charm} > 30$): 1.5% for D^0 and D^+ modes and 0.6% for all the others;
- OR: 2% for D^0 and D^+ modes and 1% for all the others;

Trigger efficiency for D mesons semileptonic decays seem to be about half of the one for charm baryons. This efficiency depends mainly on the x_F distribution for the cross-section, we take here the default distribution given by PYTHIA. In real life, specially with Σ beam, it may be quite different.

Note that the final efficiency (trigger+charm+$m_{charm} >$ cut)) is not a simple product of ϵ_g(trig) * ϵ_g(charm + $m_{charm} >$ cut).

5 Results for background

To study the effect of trigger and filters to background one has to use two types of LUND generated events. FRITIOF events that simulates beam-nucleus interaction, but do not simulate charm production, and PYTHIA events that simulates beam-nucleon interactions.

In the first case one is interested in estimating the real backgroud suppression, as FRITIOF is considered to simulate real backgroup rather well.

In the second case, one is preoccupied to estimate the ratio of signal to background, as signal is also simulated using PYTHIA. On average PYTHIA events have smaller multiplicity than FRITIOF ones but it is supposed to provide the right signal to background ratio.

In the table that follows we present our results:

	FRITIOF	PYTHIA
ϵ_g(trig) (%)	23.5 ± 0.4	9.6 ± 0.8
$\epsilon_g(m_{dist} > 30)$ (%)	4.9 ± 0.2	3.6 ± 0.5
ϵ_g(trig + $m_{dist} > 30$) (%)	1.5 ±0.1	0.7 ± 0.2
OR (%)	4.9 ± 0.2	2.0 ± 0.5

6 Conclusions

Our background investigation confirms the conclusions of Ref. [3]. The trigger efficiency is very sensitive to the background conditions. As these conditions are really not known a priori, our trigger approach should be flexible enough to allow for changes. We have to be able to adapt it to the real experimental conditions.

Trigger on its own almost does not increase signal to background ratio, but reduces rates to a reasonable level so as to make full read-out possible. Trigger combined with miss-distance cut really does a good job suppresing background really increasing the signal to background ratio (five times in the case of $\Lambda_c^+ \rightarrow \Lambda^0 e^+ \nu_e$), but cutting total signal to about 1/3.

Using NA32 data, see Ref [6] one can also estimate the total number of the so-called reconstructable events that we will have on tape for some D meson semileptonic decay modes (1000 h):

- $D_s^+ \rightarrow \Phi e^+ \nu_e$: 9000 events after trigger and miss-distance cut of 30 μm;
- $D^0 \rightarrow K^- e^+ \nu_e$: 32000 events after trigger and miss-distance cut of 30 μm;
- $D^+ \rightarrow \bar{K}^0 e^+ \nu_e$: 14400 events after trigger and miss-distance cut of 30 μm;

The TRD filter in the "OR" scheme improves signal to background ratio to the same level as the "trigger +$m_dist >$ 30 " scheme for hadronic modes. In all our investigations of semileptonic decay modes we found that about 10% of the signal events survive the "OR" scheme. This gives an increase of the total number of events selected, with respect to the "trigger +$m_dist > 30$" scheme, variing from 2 to 5 times, depending on the mode. This will be specially important in the case of short leaving charm hadrons semileptonic decays, that are tremendouosly suppresed without the "OR" scheme. As in semileptonic studies we would like to be able to measure not only

branching ratios but also form factors, the total number of final events in each mode is crucial. If the background level achived with the "OR" scheme is acceptable to the whole experiment we would like to propose to use the TRD filter as a part of the filter program as described here.

These conclusions strictly depend on the TRD algorythm, background conditions and track reconstruction accuracy. We should reserve the possibility to switch some of these options for filter program.

References

[1] J.L. Rosner, "Charm and Beauty in Particle Physics", EFI-95-02, presented at a symposium in honor of A. Martin's retirement in September 1994 at CERN.

[2] The E781 Trigger and DAQ System; J. Engelfried, P. Cooper, and D. Mao. H-643 (1993).

[3] P. Cooper, A. Kulyavtzev and J. Russ, H-722 (1995).

[4] E781 Collaboration, Geant for Experiment 781 User's Guide, v. 2.1 (1995).

[5] J. Engelfried, H-697 (1994).

[6] J. Russ, H-695 (1994).

Note: All H-notes cited here are available through E781 WWW server:

(http://fn781a.fnal.gov/documentation/hnotes_computer_index.html)

Branching ratio for the $\tau \rightarrow \rho\nu_\tau$ decay in DELPHI

J.R.P.Mahon, UERJ; M.E.Pol, CBPF and M. Srivastava, CBPF.

Received March, 1996

1 Introduction

Studing the reaction $e^+e^- \rightarrow Z^0 \rightarrow \tau^+\tau^-$, we determine the branching ratio of the decay $\tau \rightarrow \rho\nu_\tau$ at the DELPHI experiment at LEP, using data taken in 1993.

The good agreement between the DELPHI Monte Carlo and data allows us to estimate efficiencies and the background from τ decays and from other Z^0 decays directly from the Monte Carlo.

2 ρ selection

The DELPHI detector[1] and the $\tau\tau$ selection[2] have already been described.

In order to reconstruct the ρ, we selected τ decays containing one charged particle, $\pi^\pm$ and a π^0 through its decays seen as two (one) photons in the electromagnetic calorimeter. We then required that the angle between the reconstructed track and the π^0 was less than 20^o and that the effective mass of these two particles lies in the interval $0.48 < M_{\pi\pi^o} < 1.2$ GeV/c^2.

2.1 Track selection

The charged $\pi^\pm$ was selected as a single 'good' track in the hemisphere of the decay considered, registered by the tracking detectors within the central region $45^o < \theta < 135^o$, being θ the polar angle with the beam axis, having a momentum greater than 0.5 GeV/c, track length greater than 30 cm, impact parameter consistent with origin at the collision point and vetoed with DELPHI particle identification programs as not being an electron or muon.

2.2 π^o selection

The π^0 reconstruction, which is the most delicate point of the analysis, was done with the following three different criteria:

2.2.1 2 photons

Photons were selected if they were reconstructed in the fiducial region of the barrel electromagnetic calorimeter (HPC), which corresponds to $45^o < \theta < 135^o$. It was also required that their energy was greater than 0.5 GeV and that the longitudinal and transverse profiles of the showers in the calorimeter were compatible with the structure of a photon. Photons that converted in the tracking detectors were also accepted when the effective mass of the e^+e^- pair allowed to reconstruct unambiguously the original photon.

Pairs of photons were combined and considered as a π^o candidate when their effective mass was $0.04 < M_{\gamma\gamma} < 0.3$ Gev/c^2 and the angle between them was less than 10^o. This last cut was done in order to minimise the combinatorial background, as the typical angle between two photons coming from π^o at LEP energies is of the order of 2.5°-3.0°.

2.2.2 1 photon

We also considered the case where only one of the two photons is seen in the detector. This may be due to losses in the cracks of the calorimeter or, in the case of a very energetic π^0, the angle between the photons is so small that the two photons are reconstructed as one.

In order to accept one photon as a 'π^0', we required that its energy was greater than 2.5 GeV.

2.2.3 Merged π^0

This category corresponds to the last case of the previous selection, in the special situation where the profile of the shower in the calorimeter is such that clearly there are indeed two 'merged' photons.

3 Data analysis and results

Background and efficiencies were estimated using simulated events, which were generated with KORALZ[3], fully simulated through the detector with DELSIM[4] and reconstructed with the same algorithm as the real data.

The internal background, coming from other τ decays was determined to be b=15.93±0.16% , the 'external' background from Z^0 decaying into hadrons, electrons and muons was estimated as y=1.30±0.05% for τ identification and x=0.03±0.01% for ρ identification.

The τ selection efficiency, in 4π, is $\varepsilon_{\tau\tau}^{sel}$=49.39±0.11% and the corresponding ρ selection efficiency was found to be ε_{ρ}^{sel}=22.85±0.10%.

The selection performed on the real data amounts to $N_{\tau\tau}^{sel}$=18371±136 $\tau\tau$ pairs and N_{ρ}^{sel}=4933±70 ρ decays.

With these results, we obtained for the Branching Fraction:

$$BR_{93} = \frac{N_{\rho}^{sel}}{2N_{\tau\tau}^{sel}} \frac{(1-b-x)}{(1-y)} \frac{\varepsilon_{\tau\tau}^{sel}}{\varepsilon_{\rho}^{sel}} = (24.71 \pm 0.42)\%$$

3.1 Systematic error

In order to evaluate the systematic error we calculated the Branching Fraction varying the selection cuts one at the time.

For the $\tau\tau$ selection we considered two variations:
a) increase in the number of prongs and tracks in each hemisphere
b) relax the requirement of total reconstructed energy and momentum.

We introduced a bias factor due to KORALZ and the number of generated ρ after the $\tau\tau$ reconstruction.

For the ρ analysis itself, we took the following variations:
1) energy of '1 photon' $\pi^0 > 5.$ GeV.
2) energy of '1 photon' $\pi^0 > 0.$ GeV.
3) energy of photons (for pairs) > 1. GeV
4) π^o mass < 0.5 GeV/c^2
5) $0.3 < M_{\pi\pi^0} < 1.35$ GeV/c^2
6) track momentum > 1.0 GeV/c
7) accept 'standard' identified electron and 'standard' muon
8) just one track in the hemisphere
9) angle between pair of photons < 20°
10) angle between photons and charged track < 60°

Our final result is:

$$BR_{93} = (24.71 \pm 0.42 \pm 0.65)\%$$

The figure shows the effective ρ mass distribution for the three classes of selected π^0 and the total one. Real data is shown as dots, the full histogram corresponds to Monte Carlo and the shaded area to background. The table contains the individual contributions to the systematic error.

Contributions	ΔBR
τ selection a)	0.20
τ selection b)	0.29
KORALZ	0.10
ρ selection 1)	0.09
ρ selection 2)	0.13
ρ selection 3)	0.26
ρ selection 4)	0.13
ρ selection 5)	0.41
ρ selection 6)	0.03
ρ selection 7)	0.03
ρ selection 8)	0.10
ρ selection 9)	0.02
ρ selection 10)	0.00
Total	0.65

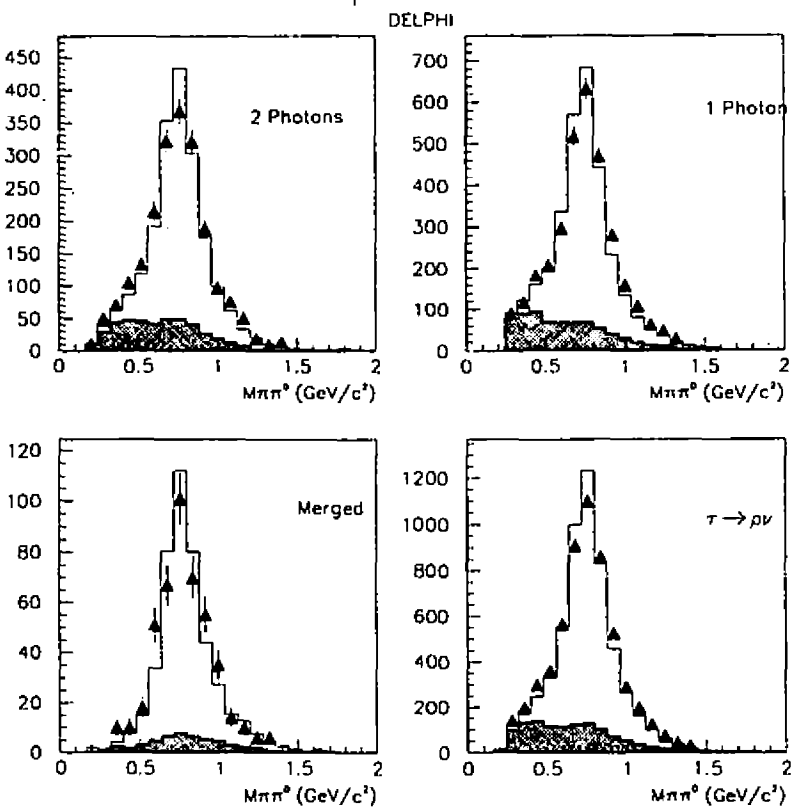

This preliminary result is in agreement with LEP results for τ branching fractions.

4 References

[1] DELPHI Collaboration, Nucl. Instr. and Meth. A303 (1991) 233.
[2] DELPHI Collaboration, Phys. Lett. 357B (1995) 715.
[3] S.Jadach and Z.Was, Comp. Phys. Com. 36 (1985) 191.
[4] DELSIM Reference Manual, DELPHI 89-68 Prog 143, CERN, September 1989.

Abertura e taxa de contagem dos detectores de múons do experimento EASCAMP

E.G.S. Luna, A.C. Fauth, H. Nogima
Instituto de Física 'Gleb Wataghin'
Universidade Estadual de Campinas, Unicamp
13083-970, Campinas, São Paulo, Brasil

Received March, 1996

1 Introdução

Destinado ao estudo da anisotropia da radiação cósmica e procura de fontes pontuais com limiar inferior de energia em torno de 10^{14} eV, o EASCAMP [1], localizado a 22°54'S-47°05'W, em uma profundidade média de 937 g/cm^2 , é um dos poucos experimentos do hemisfério Sul voltado ao estudo dos raios cósmicos. O experimento é constituído por um arranjo de cintiladores plásticos e módulos de reconstrução de trajetórias de partículas compostos de detectores do tipo *streamer* [2]. Tais módulos (telescópios) são utilizados na reconstrução de trajetórias de múons pois, além do estudo da distribuição angular e da anisotropia de eventos muônicos de diferentes multiplicidades, a determinação das trajetórias destas partículas secundárias torna-se um fator importante na melhoria da resolução angular do experimento [3], obtida pela tradicional técnica de tempo de vôo.

O experimento EASCAMP possui três módulos de trajetografia. O maior deles, denominado *detector central* [4], é constituído por quatro planos retangulares horizontais de detecção com áreas iguais de 17,3 m^2, onde cada plano é igualmente separado do outro por uma distância de 1,0 m. O detector central utiliza 1024 canais eletrônicos de detecção para um total de 512 tubos streamer de secção transversal de 29X27 mm^2, semelhantes aos tubos utilizados pelos experimentos MACRO e EASTOP. Os outros dois módulos utilizam tubos streamer com secção transversal de 9X9 mm^2. Um destes telescópios utiliza 800 canais de detecção, com um total de 480 tubos streamer, distribuídos em cinco planos retangulares horizontais de detecção, com áreas de 0,74 m^2, sobrepostos por uma distância de 0,50 m. O outro telescópio utiliza 480 canais eletrônicos para um total de 288 tubos streamer distribuídos em três planos de detecção de área 0,74 m^2, separados por uma distância de 1,0 m.Todos os três telescópios operam com uma mistura ternária de gás à pressão atmosférica.

2 Abertura para partículas individuais

Nos telescópios retangulares a taxa de contagem para partículas individuais é dada por [5]

$$\frac{dN}{dt} = \int_\Omega I(\omega) d\omega \int_S d\sigma.\hat{\mathbf{r}} \tag{1}$$

onde $I(\omega)$ é a distribuição das partículas detectadas (cm^{-2} sr^{-1} s^{-1}), $d\omega = dcos\theta d\varphi$ é o elemento de ângulo sólido (θ: ângulo zenital, φ: ângulo azimutal), $d\sigma.\hat{\mathbf{r}}$ é o elemento de área efetiva na direção de ω, S é a área total e Ω é o ângulo sólido definido pela geometria do telescópio. Assumindo uma intensidade de radiação com distribuição angular zenital da forma $I(\omega) = I_0 cos^n\theta$, a taxa de contagem equivale a

$$\frac{dN}{dt} = I_0 A_n$$

onde

$$A_n = \int_\Omega cos^n\theta d\omega \int_S d\sigma.\hat{\mathbf{r}} \tag{2}$$

é a *abertura* do telescópio. Substituindo as relações

$$d\sigma.\hat{\mathbf{r}} = cos\theta dxdy,$$

$$d\omega = \frac{cos^3\theta}{Z^2} dx'dy'$$

e

$$cos\theta = \frac{Z}{[Z^2 + (x - x')^2 + (y - y')^2]^{1/2}}$$

na equação (2), a abertura de um telescópio retangular de dimensões X, Y e Z, será então

$$A_n = \int_\Omega cos^n\theta d\omega \int_S d\sigma.\hat{\mathbf{r}} = \frac{1}{Z^2} \int_0^X \int_0^X \int_0^Y \int_0^Y cos^{n+4}\theta dxdx'dydy'. \quad (3)$$

Para reduzirmos a equação (3) a uma expressão matemática mais simples, como por exemplo uma integral dupla, devemos utilizar uma função de resposta direcional [6] definida como

$$S(\omega) = \int_S d\sigma.\hat{\mathbf{r}},$$

que representa a área disponível perpendicular à direção de uma partícula na direção $\omega(\theta,\varphi)$. Neste caso a expressão de $S(\omega)$ para um telescópio retangular em função de seus parâmetros geométricos, ou seja, em função de X, Y e Z será

$$S(\omega) = cos\theta[X - |Ztg\theta cos\varphi|][Y - |Ztg\theta sen\varphi|]. \quad (4)$$

Aplicando as transformações

$$\xi = Ztg\theta cos\varphi, (-X \leq \xi \leq X)$$

e

$$\eta = Ztg\theta sen\varphi, (-Y \leq \eta \leq Y),$$

onde agora $cos\theta = Z/[Z^2+\xi^2+\eta^2]^{1/2}$ e $d\omega = (cos^3\theta/Z^2)d\xi d\eta$, encontramos uma expressão para a taxa de contagem de partículas na direção de ω igual a

$$\frac{d^2N}{d\omega dt} = I_0 cos^{n+1}\theta[X - |Ztg\theta cos\varphi|][Y - |Ztg\theta sen\varphi|]. \quad (5)$$

Da mesma forma, a expressão final obtida para a abertura do telescópio é igual a

$$A_n = \int_\Omega cos^n\theta S(\omega)d\omega = \frac{1}{Z^2} \int_{-X}^X \int_{-Y}^Y cos^{n+4}\theta[X - |\xi|][Y - |\eta|]d\xi d\eta$$

$$= \frac{4}{Z^2} \int_0^X \int_0^Y cos^{n+4}\theta(X - \xi)(Y - \eta)d\xi d\eta$$

$$= 4Z^{n+2} \int_0^X \int_0^Y \frac{(X - \xi)(Y - \eta)}{[Z^2 + \xi^2 + \eta^2]^{(n+4)/2}} d\xi d\eta \quad (6)$$

3 Abertura dos detectores de múons do experimento EASCAMP

Em uma intensidade de radiação da forma $I(\omega) = I_0 cos^n\theta$, o valor do expoente n está relacionado ao tipo de radiação e à profundidade em que o detector se encontra. Para múons detectados nas proximidades do nível do mar, $n \approx 2$. Neste caso (em que temos um número n inteiro) podemos calcular uma solução explícita da expressão (6) para o expoente n em questão . Tal solução é representada por

$$A_2 = \frac{1}{2}\{(R_y^2 + Y^2)\frac{X}{R_y} arctg(\frac{X}{R_y}) + (R_x^2 + X^2)\frac{Y}{R_x} arctg(\frac{Y}{R_x}) - \\ -Z[X arctg(\frac{X}{Z}) + Y arctg(\frac{Y}{Z})]\} \quad (7)$$

onde $R_x^2 = X^2 + Z^2$ e $R_y^2 = Y^2 + Z^2$. Para obtermos a estimativa da abertura dos módulos de reconstrução do EASCAMP, basta conhecermos suas dimensões geométricas e substituir seus valores na expressão (7).

As dimensões do módulo central do EASCAMP são X= 404,8 cm, Y= 428,0 cm e Z= 316,0 cm. Substituindo tais valores em (7) encontraremos uma abertura A_c equivalente a

$$A_c = 11,78 m^2 sr. \quad (8)$$

As dimensões dos dois módulos restantes são $X = 0,96cm$, $Y = 0,77cm$ e $Z = 200,0cm$. Neste caso a abertura A_d destes dois telescópios será

$$A_d = 0,23 m^2 sr. \quad (9)$$

4 Conclusão

Neste trabalho encontramos expressões analíticas úteis para a obtenção da abertura e taxa de contagem de telescópios retangulares. Utilizamos os resultados para calcular a abertura dos telescópios de múons do experimento EASCAMP. Os resultados analíticos para a abertura foram possíveis pelo fato de termos utilizado um valor inteiro para o expoente n. Caso contrário seria necessário a utilizacão de métodos numéricos para o cálculo das integrais.

Pretendemos no futuro extender esses cálculos para o caso de eventos de partículas paralelas de multiplicidade $m \geq 2$

References

[1] A. Turtelli Jr., et al, *Proc. 21th Int. Cosmic Ray Conf.*, Adelaide, 3(1990) 184

[2] E. Iarocci, Nucl. Inst. and Meth., 217(1983)30

[3] J. Linsley, *Proc. 20th Int. Cosmic Ray Conf.*, Moscou, 2(1987) 422

[4] A.R.P. Biral, et al, *XVI ENFPC*, Caxambu, a ser apresentando neste encontro

[5] J.D. Sullivan, Nucl. Instr. and Meth., 95(1971)5

[6] J.C. Barton, J. Phys. A Gen. Phys.,4(1971)L 18

Redes neuronais na análise de dados de calorímetros

J.M. Seixas, L.P. Calôba, M.A.P. Vasconcelos e Wan I-Far
COPPE/EE/UFRJ - CP 68504, Rio de Janeiro 21945-970, Brazil
e-mail: seixas@lacc.ufrj.br, seixas@coe.ufrj.br

Received March, 1996

Neste trabalho, apresentamos a aplicação do processamento neuronal na análise de dados de um calorímetro hadrônico de telhas cintilantes. Estão incluídas a compensação de vazamento de energia e a busca da otimização da resolução em energia. Resultados preliminares mostram que, no caso do vazamento de energia, o processamento neuronal é capaz de recuperar inteiramente dados de 100 e 300 GeV. Para os estudos de resolução em energia, o sistema neuronal foi capaz de identificar eventos de 20, 50, 100, 180, 200 e 300 GeV.

1 Introdução

Redes neuronais vêm sendo crescentemente utilizadas em experimentos de física de altas energias, notadamente em problemas de classificadores. Separadores de partículas e sistemas completos de segundo nível de *trigger* para experimentos de grande porte vêm sendo projetados com base em redes neuronais [1]. No caso particular do LHC, novo colisionador de partículas ora em desenvolvimento no CERN (Suiça), os sistemas neuronais de segundo nível de *trigger* com base na calorimetria vêm se mostrando uma opção de projeto, pois tendem a superar os sistemas clássicos em termos de desempenho e possuem um paralelelismo inerente, o que os torna extremamente eficientes em termos do tempo gasto para o processamento [2].

Neste trabalho, apresentamos a aplicação do processamento neuronal na análise *offline* de dados experimentais de um calorímetro hadrônico de telhas cintilantes, ora sendo desenvolvido para uso no LHC [3]. Este calorímetro utiliza telhas de material cintilante como material ativo, sendo que o sinal produzido é transportado até o detector de luz por meio de fibras óticas. O material absorvedor utilizado é o ferro. Um protótipo projetivo com 5 módulos vem sendo testado com sucesso em feixe de partículas no CERN e é deste calorímeto que provêm os dados experimentais utilizados neste artigo. A Figura 1 mostra um módulo deste calorímetro.

O calorímetro de telhas apresenta segmentações longitudinal e radial, visando uma melhor medida das partículas incidentes. Assim sendo, cada módulo está dividido em cinco torres e possui quatro seções de amostragem, sendo que cada uma destas subdivisões apresenta um par de fotomultiplicadoras associado. Isto ocorre, devido ao fato de que para cada telha cintiladora temos o transporte dos sinais por meio de duas fibras óticas, uma para cada lado da telha. Desta forma, se encontram disponíveis 40 sinais para cada módulo, ou seja, um total de 200 sinais para o protótipo em consideração.

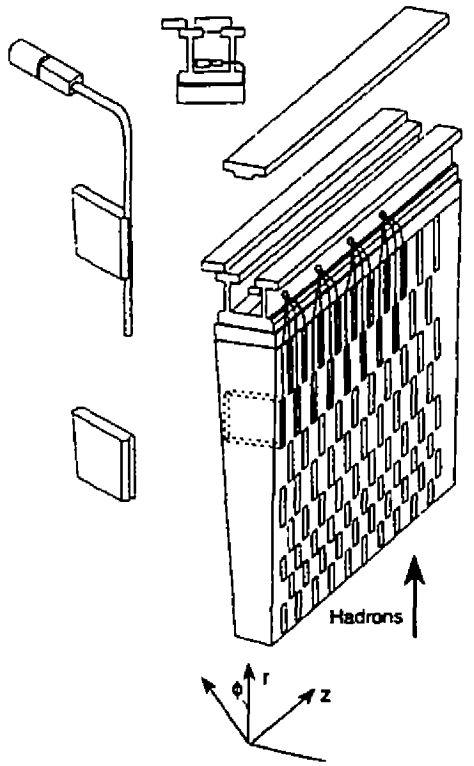

Figura 1. Estrutura dos módulos do calorímetro de telhas. Extraído de [3].

Nas seções seguintes discutimos o uso do processamento neuronal na correção do vazamento de energia para protóticos de dimensões laterais reduzidas, como é o caso do detector por nós utilizado. Além disto, apresentamos um mapeameanto neuronal para a otimização da resolução em energia do calorímetro de Telhas. Os dados experimentais disponíveis foram divididos em dois conjuntos. O primeiro foi utilizado para o treinamento da rede neuronal, enquanto que o segundo conjunto de eventos nao foi usado no procedimento de treinamento da rede e foi utilizado para testar a eficiência da rede.

2 Compensação de Vazamento de Energia

No caso de um protótipo com dimensões laterais restritas, a cascata hadrônica não se encontrará totalmente contida no interior do detector. Desta forma, parte da energia desta cascata não será absorvida pelo calorimetro, caracterizando-se o fenômeno da fuga lateral de energia.

Diversos métodos clásicos têm sido utilizados para compensar tais efeitos [4]. Uma vez que deseja-se identificar a energia de uma dada partícula apesar do vazamento, podemos utilizar o processamento neuronal para mapearmos a energia total medida pelo detector na energia incidente. Para isto, podemos utilizar a informação do perfil de deposição da cascata hadrônica, o qual varia com a energia. Treina-se, portanto, uma rede neuronal para identificar as sútis diferenças presentes na maneira com que partículas de diferentes energias depositam a sua energia no detector.

No caso do calorímetro de telhas, a informação utilizada, inicialmente, é composta de cada célula de leitura do detector, totalizando 200 elementos de energia. Utilizam-se redes do tipo *feedforward* totalmente conectadas, as quais são treinadas pelo método *backpropagation* [6]. Usa-se como função de ativação para os neurônios uma sigmóide, sendo que o neurônio de saída é linear. Com isto buscamos recuperar a escala linear de energia do calorímetro.

A Figura 2 mostra o resultado alcançado para pions de 100 e 300 GeV. A topologia da rede neuronal incluiu 200 nós de entrada, 10 neurônios na camada intermediária e um neurônio de saída. Neste caso, podemos observar que a rede neuronal foi capaz de separar completamente os eventos de cada classe, tendo uma eficiência de 100% na identificação da energia incidente de cada partícula.

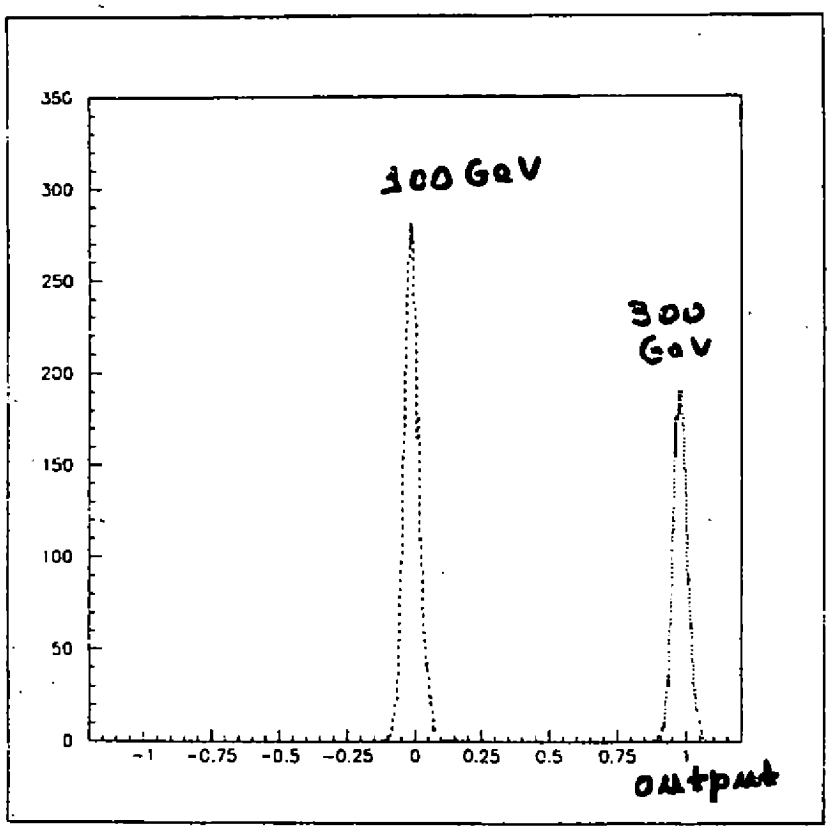

Figura 2. Saída da rede neuronal para pions de 100 e 300 GeV, com vazamento.

Para uma aplicação mais realística desta técnica, teremos que investigar a eficiência da rede neuronal para partículas com valores de energia mais próximos. Estudos neste sentido se encontram em desenvolvimento.

3 Otimização da Resolução em Energia

Para a otimização da medida de energia, é prática comum em calorimetria buscar-se um mapeamento para a medida efetuada das células de detecção que faça com que a resolução em energia seja a mínima possível [5]. Com isto, as células de detecção são ponderadas e consegue-se corrigir alguns efeitos de descompensação do calorímetro. Num tal mapeamento, comumente os seus parâmetros dependem da energia. Para o calorímetro de telhas, tais estudos vêm sendo também efetuados.

Por sua vez, as redes neuronais têm sido usadas com bastante sucesso na realização de mapeamentos multivariáveis [7]. Portanto, podemos utilizar o processamento neuronal para encontrar um mapeamento que permita otimizar a resolução em energia.

Para esta aplicação, a rede neuronal utilizou a mesma topologia da seção anterior. Neste caso, a rede foi treinada para identificar 6 classes de eventos, cobrindo pions de 20,50, 100, 180, 200 e 300 GeV. A Figura 3 mostra a resposta da rede para esta situação, quando pions destas classes são apresentandos à rede após ter-se concluído o treinamento. Da figura, pode-se observar que o sistema neuronal foi capaz de identificar tais eventos.

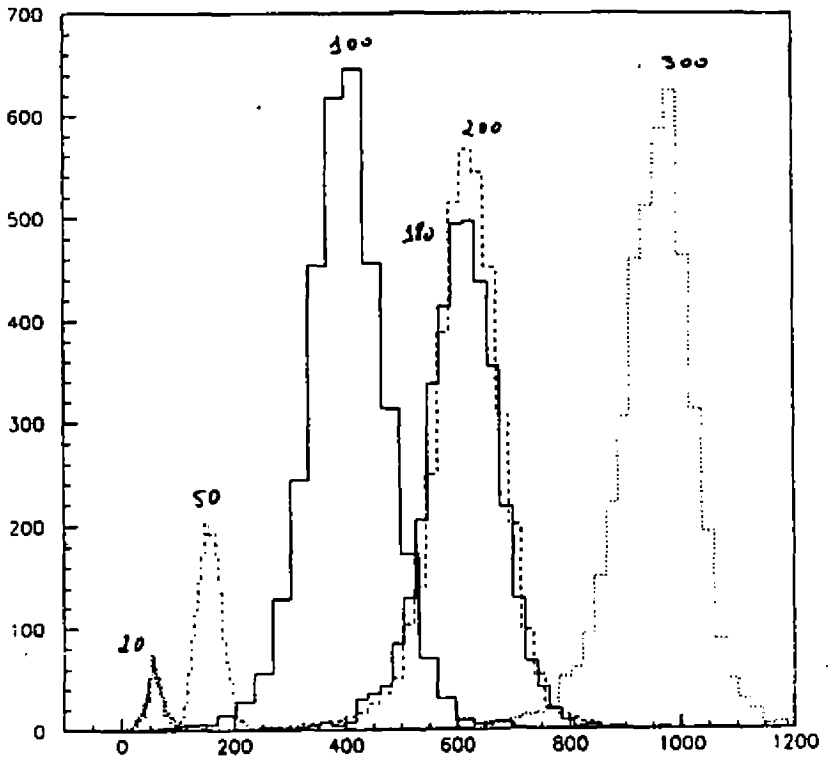

Figura 3. Saída da rede neuronal para pions de 20, 50, 100, 180, 200 e 300 GeV.

Para a aplicação do método proposto, estudos da otimização dos parâmetros da rede para obtermos distribuições Gaussianas para todas as energias e uma resolução em energia que escale com o inverso da raiz quadrada da energia da partícula incidente estão em andamento.

4 Conclusões

O uso de redes neuronais artificiais na análise de dados de um calorímetro hadrônico de telhas cintilantes foi estudado. Duas aplicações foram especialmente exploradas, incluindo a compensação da fuga de energia e a otimização da resolução em energia do detector.

Os resultados até aqui alcançados são encorajadores. Na parte de compensação de energia, o processamento neuronal foi capaz de identificar plenamente pions de 100 e 300 GeV. No que se refere à resolução de energia, o mapeamento neuronal foi capaz de recriar a escala linear de energia para pions de seis energias diferentes.

Estudos utilizando uma maior gama de dados estão sendo realizados no momento, visando estabelecer o alcance de tal técnica enquanto ferramenta de análise em calorimetria.

Agradecimentos

Gostaríamos de expressar nossos agradecimentos ao CNPq pelo apoio a este trabalho e aos nossos colegas da colaboração TILECAL do detector ATLAS, no CERN, pois este trabalho vem sendo realizado no âmbito desta colaboração. Nossos melhores agradecimentos para F. Marroquim pelas valiosas sugestões e discussões frutíferas.

References

[1] Concept for a Second-Level Trigger Using a Neural Network Architecture for the H1-Experiment at Hera. C. Kiesling et al. Proc. Int. Workshop on Software Eng., Artificial Intelligence and Expert Sys. for High-Energy and Nucl. Phys. Oberammergau (Alemanha). World Scientific, pp 411 (1994).

[2] Implementing a Neural Second-Level Trigger System on Digital Signal Processor Technology: The Global Decision Problem. J.M. Seixas, R.W. Santos e L.P. Calôba. Proc. First Workshop on Electronics for LHC Experiments, Lisboa (Portugal). CERN/LHC/95-56, pp 324 (1995).

[3] Construction and Performance of an Iron-Scintillator Hadron Calorimeter with Longitudinal Tile Configuration. F. Ariztizabal et al. **Nuclear Instruments and Methods** A349, pp 384 (1994).

[4] On Muon Production and Other Leakage Aspects of Pion Absorption in a Lead/Scintillating Fiber Calorimeter. D. Acosta et al. **Nuclear Instruments and Methods** A309, pp 143 (1991).

[5] Advances in Hadron Calorimetry. R. Wigmans. **Ann. Rev. Nucl. Part. Sci.** 41 pp 133 (1991).

[6] Neural Networks. A Comprehensive Foundation. S. Haykin. Macmillan (1994).

[7] Introduction to the Theory of Neural Computation. J. Hertz, A. Krogh e R.G. Palmer. Addison-Wesley (1991).

A influência do uso de cintiladores plásticos na caracterização de chuveiros atmosféricos extensos

A.R.P. Biral, J.A. Chinellato, A.C. Fauth, E. Kemp, M.A. Leigui de Oliveira, H. Nogima, M.C. Souza Jr., A. Turtelli Jr.

Instituto de Física Gleb Wataghin

Universidade Estadual de Campinas, Unicamp

Fevereiro de 1996

Utilizando-se de um arranjo experimental onde é acoplado um detector a cintilador plástico com um módulo de tubos "streamer", obtem-se a distribuição de sinais de uma partícula, para o detector a cintilador. Esta distribuição é, então, utilizada para simular os sinais de detectores a cintilador plástico em uma experiência genérica de detecção de chuveiros atmosféricos extensos (CAEs).
É estudada, assim, a influência que os cintiladores exercem na caracterização dos CAE's.

1 Introdução

O grupo de Léptons do Depto. de Raios Cósmicos do IFGW–Unicamp mantém um experimento para a detecção de Chuveiros Atmosféricos Extensos, o EASCAMP [1] [2]. O experimento tem por principais objetivos o estudo da anisotropia da radiação cósmica, a busca no hemisfério sul por fontes pontuais de raios cósmicos de energia superior a $10^{14}eV$ e o estudo da física dos processos que ocorrem na produção de um CAE.

Neste trabalho estudamos a influência que os cintiladores plásticos exercem na determinação dos parâmetros fundamentais dos CAEs. Estamos interessados nas medidas de densidade de partículas realizadas pelos cintiladores. Elas são fundamentais para a determinação da posição do centro dos CAEs e para o conhecimento de parâmetros importantes como a energia do primário, o número total de partículas, a seção de choque de processos hadrônicos, entre outros.

2 Calibração do sinal dos cintiladores

O EASCAMP consiste atualmente de um conjunto de 12 módulos a cintilador plástico e 3 módulos de tubos "streamer". Os detectores a cintilador são formados por uma fotomultiplicadora e um bloco de cintilador plástico acondicionados em uma caixa de madeira no formato de pirâmide de base retangular. O sinal gerado pela fotomultiplicadora é convertido em um número (*canal de ADC*) proporcional à sua carga em um módulo ADC (LeCroy 2249W). Este sinal depende, em última instância, do número de partículas que cruzam o cintilador, da região por onde elas passam e de suas inclinações. A dependência da energia é muito fraca para as partículas relativísticas que excitam o cintilador na região de mínima ionização. Assim, os sinais dos detectores flutuam em torno de um valor médio para um dado número de partículas nas mesmas condições de energia e inclinação. Tais flutuações devem ser levadas em conta na calibração dos sinais pelo número de partículas.

Esta calibração foi obtida por um sistema experimental acoplando um módulo a cintilador plástico sobre um módulo de tubos "streamer". Pelo módulo "streamer " (utilizado como módulo de trajetografia) foram selecionados eventos de uma única partícula cuja projeção do traço incidisse dentro do bloco de cintilador. Na figura 1 aparece a distribuição dos sinais de eventos de uma partícula, normalizados na direção vertical. Note que os sinais se distribuem ao longo do espectro. Como o valor da média desta distribuição é usado como escala na conversão de canal de ADC para número de partículas, a existência da distribuição introduz erros na medida de densidade de partículas.

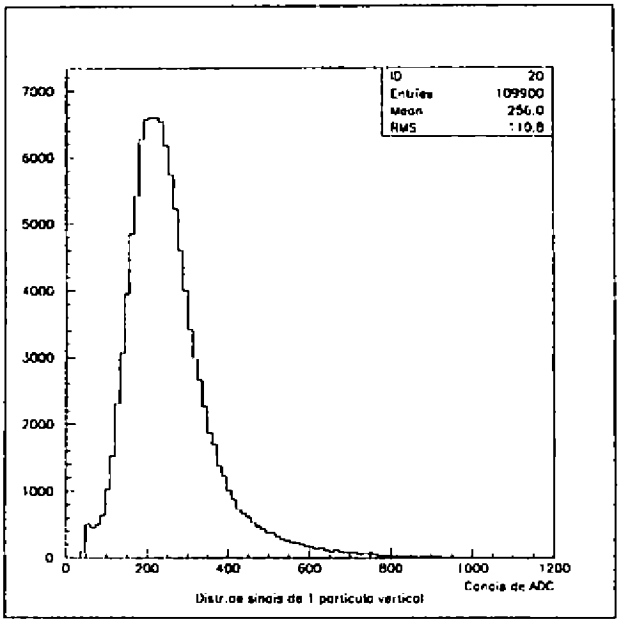

Figura 1. Distribuição de sinais de uma partícula vertical.

3 Simulação e Resultados

Pelo método de Monte Carlo, foi avaliado a influência que as flutuações no sinal dos detectores a cintilador plástico exercem na caracterização de um CAE. A simulação fornece, para cada chuveiro, a densidade de partículas ao nível do mar em função da distância radial do centro. A posição do centro dos CAEs é sorteada com distribuição uniforme na superfície do "array", dentro de um intervalo pré-definido.

As densidades de partículas da simulação dos chuveiros são utilizadas como parâmetros de entrada para o cálculo da posição do centro sem a flutuação do detector (detector ideal) e para simular as densidades com as flutuações dos cintiladores e reaplicadas no cálculo. Para cada CAE, são gerados valores de densidade de partículas ρ_i nos detectores. Supondo que estes são formados por cintiladores de 1 m^2, o número de partículas é dado por $N_i = int(\rho_i)$. Cada partícula produz um sinal cuja distribuição é a da figura 1 e o sinal de mais de uma partícula é a soma dos sinais individuais, o valor do canal de ADC do detector i fica dado por: $ADC_i = \sum_{k=1}^{N_i} sort_k$, onde $sort_k$ é uma variável randômica sorteada da própria distribuição experimental da figura 1. Obtemos, finalmente, um novo conjunto de densidades subtraindo do sinal do ADC o valor do seu pedestal e dividindo pela média da distribuição de uma partícula: $\rho_i' = (ADC_i - ped)/med_1$.

O método de cálculo do centro dos CAEs foi desenvolvido através dos algoritmos do MINUIT. A eficiência do método é medida pela distância do centro simulado até o centro calculado. Na figura 2 estão representados os resultados de um caso estudado: "array" de 25 detectores, com separação de 10 m entre si, chuveiros simulados com os centros distantes do centro do "array" em até $r_{max} = 100\ m$ e iniciados por primários de $10^{15} eV$. Note que os histogramas apresentam uma grande quantidade de eventos com a distância próxima de zero, isto é, com o centro calculado próximo do centro simulado, mostrando a eficiência geral do método. Mas, o mais importante de se notar é o fato de que o caso sem flutuação é mais preciso do que o caso com flutuação: a distribuição sem flutuação se aproxima mais do zero. Este resultado mostra que, devido à existência dos espectros de sinais nos cintiladores, eles exercem uma importante influência na precisão da determinação da posição do centro que deve ser levada em consideração na estimativa da precisão dos experimentos de CAEs. Ainda na figura 2 estão apresentadas as correlações entre as abscissas da posição do centro simuladas (X) e calculadas (XC). O método é tanto mais preciso quanto mais os eventos se localizarem sobre uma reta de inclinação 45°.

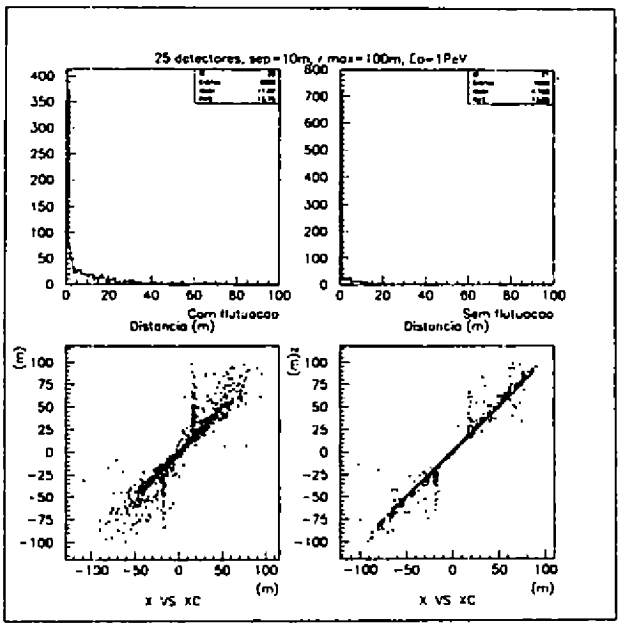

Figura 2. Acima: histogramas das distâncias do centro simulado ao centro calculado. Abaixo: correlação entre as abscissas simuladas e calculadas.

Estudamos, também, a eficiência do método alterando-se os parâmetros da simulação: número de detectores (N° det.), separação entre eles (sep.), raio máximo do sorteio do centro do chuveiro (r_{max}) e energia do primário(E_0). A tabela a seguir resume os resultados obtidos, onde: d distância que contém 90% dos eventos, ou seja, 90% dos eventos neste caso possuem distância entre os centros simulados e calculados menores que $d_{90\%}$ e flut.: flutuação.

Caso	N° det.	sep.(m)	r_{max}(m)	$E_0(eV)$	$d_{90\%}$ s/ flut.(m)	$d_{90\%}$ c/ flut.(m)
1	9	10	100	10^{15}	57.25	64.75
2	25	10	100	10^{15}	13.00	38.00
3	9	20	100	10^{15}	9.25	43.00
4	9	10	20	10^{15}	.026	1.75
5	9	10	100	10^{16}	25.75	52.25

Observamos novamente que a flutuação do detector piora a resolução do método. Além disso temos a comparação entre os desempenhos dos diferentes casos com o caso 1: foi alterado um parâmetro por vez em relação a este caso. Isto fornece informações importantes para o projeto de uma experiência de CAEs.

Além destes estudos, foram obtidos os desempenhos na determinação dos parâmetros do CAE como o número total de elétrons, a idade do chuveiro, a energia do primário e a direção de chegada que são diretamente influenciados pela precisão na determinação do centro, ou seja, quanto melhor se obtem a posição do centro mais precisas são as suas determinações. Estes resultados não serão apresentados neste resumo que podem ser encontrados juntamente com uma descrição detalhada dos procedimentos seguidos neste estudo na referência [3].

References

[1] A. Turtelli et al, *Proc. 21st International Cosmic Ray Conference*, 3 ,*(1990) Adelaide, Australia*

[2] A.R.P.Biral et al, *Proc. XV ENFPC, SBF (1994) pp.161, Cazambu, Brasil*

[3] M.A.Leigui de Oliveira, Tese de Mestrado, IFGW-Unicamp (1995).

Status atual do experimento EASCAMP

A.R. Biral, J.A. Botasso, J.A. Chinellato, A.C. Fauth
E. Kemp, H. Nogima, M.A. Leigui de Oliveira, L.G. dos Santos,
E.L.F. Silva, M.C. Souza Jr., A. Turtelli Jr.
Instituto de Física "Gleb Wataghin"
Universidade Estadual de Campinas (UNICAMP) - SP

Received March, 1996

São mostradas no presente estudo medidas do coeficiente de atenuação atmosférico e mapeamento do céu a partir das direções de chegada dos eventos de chuveiros atmosféricos extensos registrados. Discutir-se-ão também estimativas quanto a resolução angular do experimento, tanto na sua atual configuração como após a sua ampliação.

1 Introdução

O experimento EASCAMP (baseado em Campinas, no departamento de Raios Cósmicos do Instituto de Física "Gleb Wataghin") é constistuido por 4 cintiladores plásticos com 0,7 m^2 de área dispostos em uma configuração quadrada de 14 metros de lado. De valor quase didático, tal experimento vem operando continuamente desde novembro/89, registrando a passagem de frentes de chuveiros atmosféricos através da coincidência quádrupla entre os cintiladores do *array*. Nesse regime de operação estima-se que o experimento apresente um limiar de energia de 10^{14} eV, que se reflete no registro de eventos a uma taxa de 35000 eventos/mês.

Uma vez que se encontra prevista uma ampliação do experimento (que passará a operar com 12 cintiladores dispostos em uma área de 20 X 25 metros quadrados), o presente estudo consiste em uma compilação dos resultados obtidos com os eventos até agora registrados. Embora tal análise não seja sobremaneira conclusiva, tem-se aqui como principal objetivo uma exposição sobre o que pode-se esperar de um experimento de detecção de raios cósmicos, bem como um registro para referências futuras.

2 Detalhes sobre a reconstrução

Através do uso de cintiladores, a direção de chegada de um chuveiro atmosférico extenso é geralmente obtida pelo método do "tempo de vôo" (*time of flight*). Uma suposição básica geralmente aceita é que as partículas carregadas do chuveiro registrado, *a priori*, atingiram cada cintilador a partir de uma frente plana de partículas. Tomando como base essa suposição, a direção de chegada de um plano de partículas pode ser determinada com o tempo de vôo de um conjunto mínimo de 3 cintiladores.

No presente estudo foram selecionados apenas os eventos que apresentassem uma densidade de partículas maior que 9 partículas/m^2 em cada cintilador. Tal seleção teve como objetivo proporcionar uma melhor garantia na precisão temporal dos dados obtidos, além de nos propiciar a reconstrução de eventos cuja frente de partículas mais se aproximasse da configuração de frente plana. Uma vez que a calibração "sinal analógico registrado *versus* número de partículas incidentes" só esteve disponível a partir de junho/94, foram selecionados aproximadamente 75000 eventos, obtidos entre 03/94 e 08/95.

3 Resultados

Como esperado, o fluxo apresenta uma forte atenuação função do ângulo zenital (proporcional a $\cos^{9.7}\theta$), que acaba resultando em um universo de eventos situados em sua maioria com ângulos zenitais não maiores que 25 graus (fig. 1). Tal valor difere do valor usualmente aceito para esse coeficiente (da ordem de 7.5), porém devemos lembrar que a seleção de eventos com densidade que maior que 9 partículas/m^2 nos quatro cintiladores se reflete como uma forte atenuação adicional.

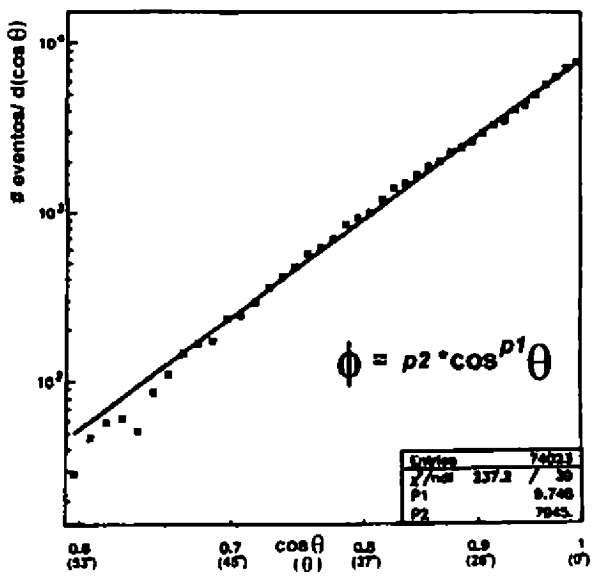

Figure 1.: Atenuação do fluxo de raios cósmicos com cosseno do ângulo zenital, segundo eventos registrados pelo EASCAMP

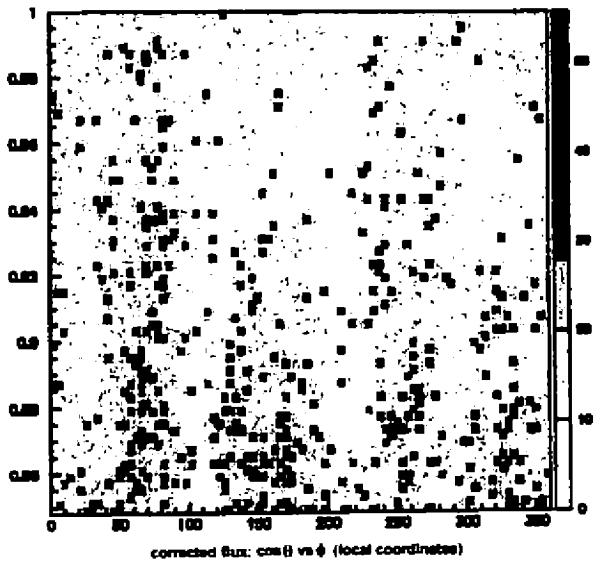

Figure 2.: Reprentação, em coordenadas locais, do fundo uniforme de raios cósmicos através do uso de um fluxo zenital corrigido

A maior parte dos raios cósmicos incidentes é constituida por prótons de alta energia com direções de chegada isotropicamente distribuidas sobre a abóboda celeste, devido as deflexões ocasionadas por campos magnéticos estelares. A obtenção do valor do coeficiente de atenuação do fluxo zenital é um passo delicado no que se refere a obtenção de um "fluxo zenital corrigido", onde o céu se apresente como um fundo uniforme de raios cósmicos. A princípio, esse fundo uniforme e homogênio corrigido seria o ponto de partida no que se refere a procura de fontes pontuais de raios cósmicos, ou a detecção de anisotropias.

O fundo "corrigido" obtido, no sistema de coordenadas locais, se encontra na figura 2. Note que, apesar da aparente existência de acumulos em alguns valores de ângulo azimutal, o que realmente acontece é que o universo de eventos é pequeno no que se refere a flutuação estatística dos dados. Além disso, o coeficiente de atenuação zenital obtido apresenta variações conforme a faixa de ângulos zenitais sob análise, o que nos leva a concluir que a dependência comumente aceita com $\cos^N \theta$ seja de fato aproximada.

4 Estimativas da precisão angular do array

Foram feitos, para a atual configuração de 4 cintiladores e para a futura configuração de 12 cintiladores, estudos da precisão angular do experimento. As estimativas do erro na determinação da direção de chegada dos eventos foi obtida através de simulação.

Basicamente é atribuido a cada cintilador do *array* um tempo de interceptação, supondo a incidência de uma frente plana de partículas carregadas. Posteriormente tais tempos registrados são submetidos a flutuações de ordens varias, e, de posse desses tempos "alterados", a direção do evento é então reconstruido. A diferença entre o ângulo zenital "original" e "reconstruido" é assim avaliada.

Os resultados das configurações horizontais simuladas se encontram na tabela 1 e figura 3. A coluna "Faixa de observação" se refere a faixa de ângulos zenitais onde a distribuição dos valores de ângulo zenital reconstruidos se mostra simetricamente distribuida em torno da direção do eventos incidentes.

Num. det.	Faixa de observação	Dispersão (graus)	Eficiência da reconstrução
4	0 - 35 graus	≈ 3.5	96 %
12	0 - 45 graus	2.5	100 %

Table 1: Características da reconstrução da direção de chegada de eventos através de simulação.

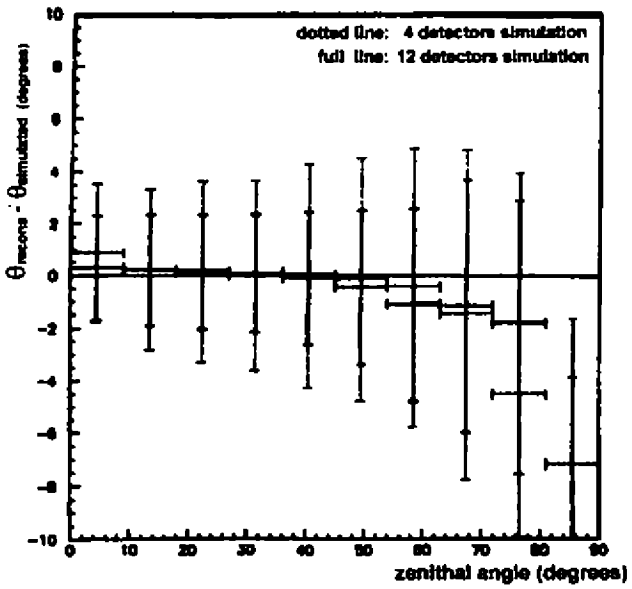

Figure 3.: Diferença entre o ângulo zenital reconstruido (após flutuações nos tempos de chegada) e o ângulo zenital original gerado pela simulação, para faixas de ângulo zenital

5 Conclusão

Apesar da localização geograficamente privilegiada do experimento (observando diretamente o centro galático), o universo de dados de pouco mais de 1 ano de direções de chegada se mostra insuficiente para uma boa caracterização do fluxo de raios cósmicos incidentes sobre o EASCAMP. Faz-se necessário que o experimento seja expandido, de modo que o taxa de eventos registrados aumente, possibilitando assim uma maior estatística e uma maior precisão angular.

Quanto à procura de fontes e anisotropias, está deverá ser realizada através de métodos que não pressuponham correções analíticas pelo uso do coeficiente de atenuação zenital do fluxo de raios cósmicos incidentes. O uso de tais correções, se inevitáveis, deverá ser feito com extremo cuidado.

Detector de cintilação para medidas da componente eletromagnética de chuveiros atmosféricos extensos

A.C.Fauth, E.J.T.Manganote, A.Turtelli Jr.
Instituto de Física 'Gleb Wataghin'
Universidade Estadual de Campinas, Unicamp
13083-970, Campinas, São Paulo, Brasil

Received March, 1996

É apresentado um estudo da performance de um detector modular para a detecção da componente eletromagnética de chuveiros atmosféricos extensos. O detector é composto por uma caixa de forma piramidal contendo uma placa de cintilador plástico e uma fotomultiplicadora. Foram estudadas a resposta temporal e o ganho do detector em função da posição da cintilação e da alta voltagem de operação . Obtivemos uma eficiência de contagem de 85% e uma resolução temporal de 2,0ns.

1 Introdução

O estudo da radiação cósmica de energia superior a 10^{14} eV é realizado através de experimentos localizados na superfície terrestre, devido ao fato do fluxo a partir desta energia ser extremamente reduzido. O que observa-se são os subprodutos da interação das partículas primárias na atmosfera, os chamados chuveiros atmosféricos extensos-CAEs.

A procura por fontes pontuais de raios cósmicos requer que possamos determinar as direções de chegada dessas partículas primárias. Consequentemente estes experimentos devem possuir uma resolução angular da ordem de um grau na determinação da direção de chegada do raio cósmico primário. A medida da direção de chegada da partícula primária é geralmente realizada através do método do tempo de vôo, utilizando-se dezenas de detectores com boa resolução temporal espalhados na superfície terrestre. Devido a processos de espalhamento na atmosfera, principalmente espalhamento múltiplo coulombiano, os elétrons da frente do chuveiro não formam um disco perfeitamente plano, formam uma figura geométrica mais próxima a uma calota esférica, além disso existe a flutuação na densidade de partículas que compõem essa frente de partículas. Os detectores de CAEs geralmente utilizam cintiladores plásticos devido a boa característica temporal deste detector.

A partir de meados dos anos 80, surgiram as primeiras evidências da existência de fontes pontuais na faixa de energia de 10^{15} eV. Novas técnicas estão continuamente sendo propostas para medir a direção de chegada e técnicas de calibração e monitoramento desses experimentos tem sido aprimoradas.

2 Forma geométrica do detector

As principais características que procuramos neste detector são : possuir uma resolução temporal da ordem de poucos nanosegundos e uma resolução de carga da ordem de 100%. Estas características não devem depender fortemente da posição por onde a partícula atravessa a placa de cintilador. Além disso ele deve ser modular e econômico, visto que devemos utilizar muitos desses detectores para medir a componente eletromagnética do CAE.

Para satisfazer as características acima projetamos um detector composto por uma placa de cintilador plástico (100x70x2,5 cm^3) que foi colocada na base de uma caixa de madeira de formato piramidal. No vértice da pirâmide colocamos uma fotomultiplicadora com um fotocátodo de diâmetro igual a 110 mm. Para estudar a uniformidade da resposta do detector em função da posição de passagem da partícula variamos a altura entre a fotomultiplicadora e a placa do cintilador. Procuramos a altura que propicie uma *eficiência* de contagem elevada, um *resolução temporal* da ordem de poucos nanosegundos e uma boa *uniformidade* de resposta do detector, utilizando somente uma fotomultiplicadora.

Para o cintilador e fotomultiplicadora citados acima estudamos qual a melhor distância entre estes. Para uma distância de poucos centímetros a resposta da região central do cintilador é muito mais intensa do que as

regiões das bordas. Aumentando-se a distância cintilador-fotomultiplicadora melhora-se a uniformidade, porém se continuarmos a aumentar a distância a resolução temporal e a eficiência de contagem diminuem. A Figura 1 mostra o comportamento da diferença de tempo entre a borda e a região central do cintilador e a Figura 2 o ângulo sólido para estas regiões . Escolhemos 55cm para a distância considerando que os elétrons que desejamos detectar são relativísticos, que são produzidos em média 100 fótons/100eV [2], que 16,7% da luz produzida emerge por um lado do cintilador [3] e que a eficiência quântica do fotocátodo é 20% [4]

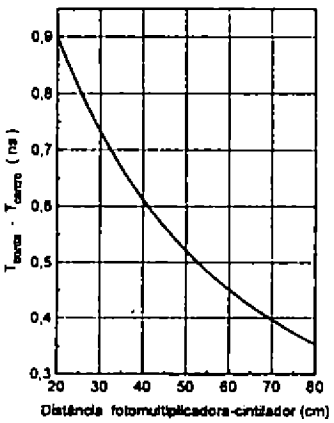

Figura 1. Diferença entre o tempo da luz (direta) emitida na borda e daquela emitida no centro do cintilador em função da distância fotomultiplicadora- cintilador.

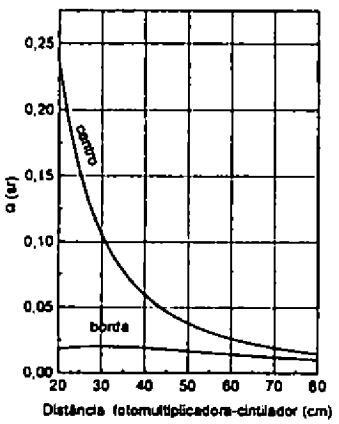

Figura 2. Ângulo sólido da região central e da borda do cintilador em função da distância fotomultiplicadora-cintilador.

3 Montagem experimental

Montamos detectores com a geometria estudada na seção anterior. A parte sensível é uma placa de cintilador plástico NE102A (100x70x2,5 cm^3), a fotomultiplicadora é do modelo Philips XP2040 [4], que foi colocada dentro de um cilindro de mu-metal. A fotomultiplicadora possui um adaptador ótico de forma plano- côncavo de material plástico que permite uma transmissão da luz a partir de 300 nm. Foi realizado o acoplamento ótico entre o fotocátodo e o adaptador ótico com silicone fornecido pelo fabricante.

O espectro da luz emitida pelo cintilador está dentro da região de sensibilidade da fotomultiplicadora e não é afetado pelo adaptador ótico. O divisor de tensão utilizado foi o tipo A indicado pelo fabricante [4]. É importante

notar a necessidade de um cuidadoso ajuste da voltagem entre o fotocátodo e o dinôdo de foco para obter um ganho máximo da fotomultiplicadora.

A caixa de forma piramidal foi construída com placas de madeira de 1cm de espessura e suas paredes internas foram pintadas de branco fosco para difundir a luz de cintilação e assim obtermos um melhor rendimento do detector [1]. Entre os lados da pirâmide e a placa de cintilador existem 6 cm para facilitar a saída da luz de cintilação pelas bordas do cintilador. Aproximadamente 67% da luz produzida no interior do cintilador emerge pelas bordas.

A placa de cintilador plástico foi fixada internamente base da pirâmide por quatro pequenos suportes metálicos, o que possibilita girar o detector mantendo as posições relativas entre o cintilador e a fotomultiplicadora.

Para realização das medidas utilizamos dois outros detectores compostos por uma placa de cintilador plástico NE102A (30x15x2,5 cm^3), um guia de luz de lucite, e uma fotomultiplicadora tipo Philips XP2230. Esses detectores possuem uma resolução temporal de 1,7± 0,2 ns e foram utilizados para disparar a aquisição de múons da radiação cósmica. Realizamos medidas da resposta do detector modular em função da posição de passagem da partícula e da voltagem de trabalho da fotomultiplicadora.

A coincidência temporal (de 50ns) do sinal desses dois detectores determinou a condição de disparo da aquisição de dados. Posicionando adequadamente esses detectores pudemos selecionar a região do detector estudado por onde passaram os múons cósmicos. Assim estudamos quatro regiões do detector modular: centro, borda e vértice da placa, e quando a partícula passa pelo fotocátodo. Para cada evento registramos: a diferença de tempo entre o detector modular e um detector de disparo e a carga do sinal do detector modular. Utilizamos um sistema CAMAC para a aquisição automática de dados e o TDC e ADC utilizados foram da marca LeCroy (11bits, 100ps/canal, 0,25pC/canal).

4 Resultados e discussão

A eficiência de contagem,ε,foi calculada utilizando os dados lidos pelo TDC

$$\varepsilon = 1 - \frac{n.\ \ eventos\ \ \ fundo\ \ \ escala}{n.\ \ total\ \ \ de\ \ \ eventos} \tag{1}$$

O limiar do discriminador foi de -20mV/50Ω. Na Figura 3 mostramos as curvas de eficiência para as regiões estudadas em função da voltagem de trabalho da fotomultiplicadora do detector modular.

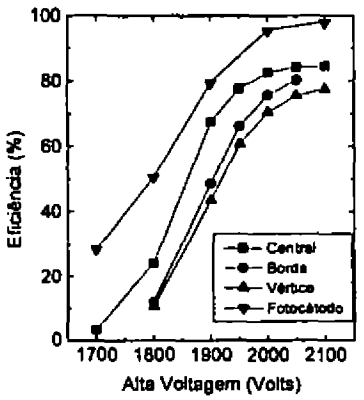

Figura 3. Eficiência de contagem das regiões estudadas do detector modular.

Os histogramas da diferença de tempo entre o detector modular e o cintilador de disparo para a região central são mostrados na Figura 4. Para os menores valores de voltagem a distribuição da esquerda refere-se s partículas

que produziram sinal ao passarem pelo fotocátodo. Para as voltagem mais elevadas esta distribuição é pouco visível devido ao aumento da eficiência de contagem e consequentemente crescimento da relação entre os sinais originados pela luz de cintilação e aqueles gerados no fotocátodo. Para uma partícula vertical a probabilidade dela atingir o fotocátodo é de 1,4%. Notamos também nesta figura o decréscimo do tempo de trânsito da fotomultiplicadora com o aumento a alta voltagem com uma taxa de -2,2ns/100V.

Da análise dos histogramas das diferenças de tempo pudemos calcular a resolução temporal do detector modular em função da alta voltagem. Mostramos estes resultados na Figura 5. Na região do patamar de eficiência a resolução temporal média é 2 ns. Os espectros de carga da região central mostram uma variação da carga de pico de poucos picoCoulomb até valores superiores a uma centena. Pela Figura 3 pode-se ver que o patamar de eficiência ocorre para voltagens superiores a 2000V. A carga média para estas voltagens está entre 50 e 80pC. Logo convém atenuar o sinal na entrada do ADC por cerca de 5X para aumentar o alcance do fundo de escala do ADC (igual a 512pC) para 35 partículas. Isto significa que a resposta do detector saturará para 35partículas/0,7m2. A resolução de carga R=FWHM/Qpico na parte central do cintilador e na região de máxima eficiência é de 100%.

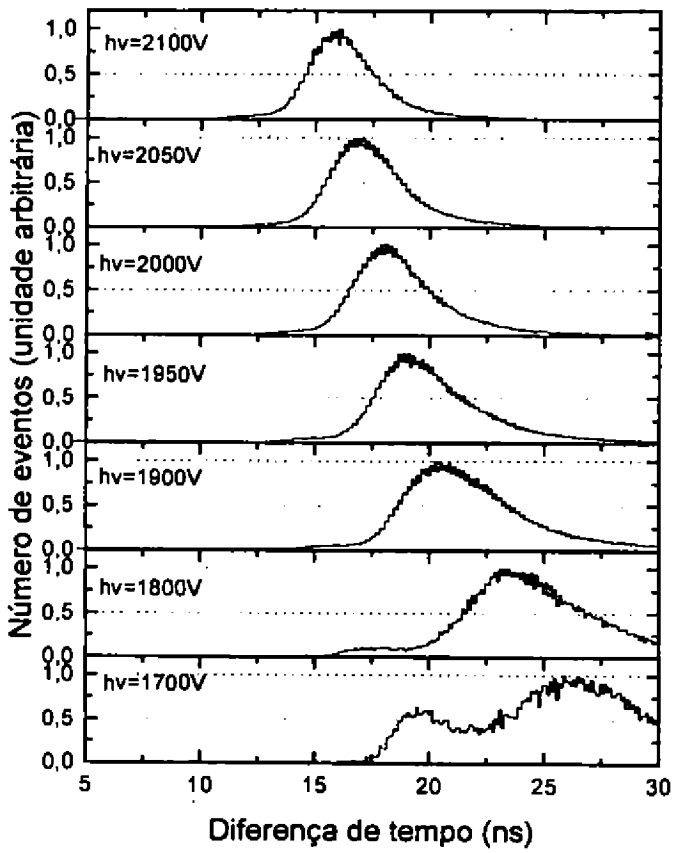

Figura 4. Histogramas das diferenças de tempo entre o detector modular e o detector de disparo em função da voltagem da fotomultiplicadora.

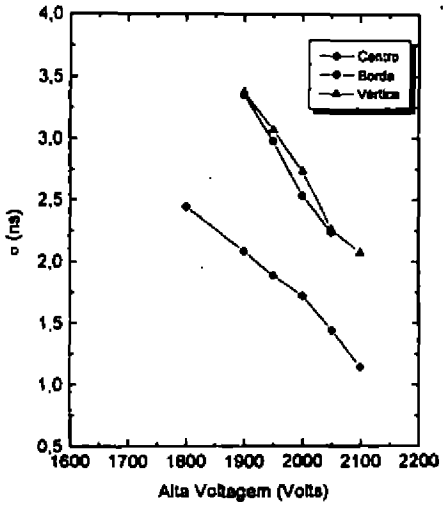

Figura 5. Resolução temporal do detector modular em função da alta voltagem para diferentes regiões do cintilador.

5 Conclusão

Estudamos a performance de um detector modular para ser utilizado na medida da componente eletromagnética de chuveiros atmosféricos extensos. Com uma placa de cintilador e somente uma fotomultiplicadora o detector construído tem uma eficiência de contagem de 85%, uma resolução de carga de 100%, uma resolução temporal de 2ns. A uniformidade da resposta do detector foi estudada e os resultados obtidos foram bons para a utilização pretendida. Obtivemos uma uniformidade na resposta temporal de 1 ns e de 30% na resposta da carga. É bom salientar que estes resultados experimentais foram obtidos com múons relativísticos (partículas na região de mínima ionização), consequentemente a performance do detector para chuveiros atmosféricos extensos será melhor, principalmente quando detectando a parte central do CAE, onde a densidade de partículas é elevada.

Agradecimentos

Agradecemos ao CNPq e FAPESP pelo apoio parcial desta pesquisa e aos técnicos Jair A. Botasso, Edson L. Ferreira da Silva e Haroldo J. Cancio Dias.

References

[1] C.Morello et al, Rap.Int.n.152b/87, Ist.Cosmogeofisica del CNR, Torino, Itália.

[2] R.C.Fernow, Introduction to experimental particle physics, Cambridge

[3] Knoll, Glenn F., Radiation Detection and Measurement, Second Edition, John Wiley&Sons, 1989. University Press (1986).

[4] Philips Data handbook, Electron tubes, Part 9 (1976).

Search for Flavor-Changing Neutral-Currents Decays in the E791 Experiment

Carla Göbel*
Centro Brasileiro de Pesquisas Físicas
Rio de Janeiro, RJ, Brasil

Received March, 1996

We present recent results from Fermilab experiment E791 on the search of the flavor-changing neutral-current decays $D^+ \to \mu^-\mu^+\pi^+$ and $D^+ \to e^-e^+\pi^+$. New upper limits on the branching fractions for these channels are obtained.

1 Introduction

One important feature of the Standard Model (SM) is the diagonality of the neutral currents: flavor-changing neutral-current (FCNC) decays are forbidden at the tree level and can occur only through higher-order loop diagrams, with branching ratios (BR) between 10^{-11} to 10^{-8} [1]. Since the experimental limits are still much higher, e.g. BR($D^+ \to \mu^-\mu^+\pi^+$)$\leq 2 \times 10^{-4}$ [2], finding a BR above 10^{-7} would be strong evidence of a new phenomenon.

To search for rare decays like $D^+ \to \pi^+ l^+ l^-$ ($l = e, \mu$), a high statistics charm sample is needed. Here, we report on the results of a search for the decays $D^+ \to \pi^+\mu^+\mu^-$ and $D^+ \to \pi^+e^+e^{-1}$ in data collected from Fermilab experiment E791.

2 The E791 Experiment

The fixed target experiment E791 [3] recorded over 20 billions events from 500 GeV/c π^- interactions in a segmented target (one platinum, four diamond thin foils). More than 200,000 charm decays were fully reconstructed.

The E791 tracking system consists of Silicon Microstrip Detectors, Wire Chambers and four stations of Drift Chambers. Two dipole magnets are used for momentum analysis. Two Čerenkov counters, hadronic and electromagnetic (EM) calorimeters and muon scintillator counters provide particle identification (ID). In particular, the EM calorimeter is used to identify electrons and muon identification is obtained from a plane of scintillators (muon scintillator wall) located at the end of the spectrometer, after a steel absorber wall which prevents other particles from reaching there.

3 The $D^+ \to \mu^-\mu^+\pi^+$ Search

Charm decays are characterized by the presence of multiple vertices: the primary vertex, where the charm production has ocurred, and secondary vertices, where the charm particles decay. To separate charm candidates from background, events containing a secondary vertex formed by three charged tracks (with total charge ± 1) are selected requiring, among other things, that the secondary vertex be well separated from the primary vertex and located outside the target foils or other solid material and that the momentum vector of the D^+ candidate point back to the primary vertex.

*Representing the E791 Collaboration.
[1] Throughout this text, charge conjugate states are implied.

Aside from non-charm background, which is supressed using the vertex selection criteria described above, when searching for a rare decay like $D^+ \to \mu^-\mu^+\pi^+$ it is very important to take into account backgrounds from other charm decays. The three major contributions to charm background in the $\mu^-\mu^+\pi^+$ mass spectrum from 1.7 to 2.0 GeV/c^2 are $D^+ \to K^-\pi^+\pi^+$, $D^+ \to \pi^-\pi^+\pi^+$ and $D_s^+ \to \pi^-\pi^+\pi^+$. The first one can be eliminated by excluding candidates with a $K^-\pi^+\pi^+$ invariant mass between 1.85 and 1.89 GeV/c^2.[2] In figure 1(a) we show the $\mu^-\mu^+\pi^+$ invariant mass spectrum with no muon ID requirement. The two peaks for $D^+ \to \pi^-\pi^+\pi^+$ (left one) and $D_s^+ \to \pi^-\pi^+\pi^+$ signals can be clearly seen. They are broadened and shifted downward from the true parent masses due to the incorrect assignment of the daughter masses.

To identify muons we require that two oppositely-charged tracks from the decay vertex be identified as muons by separate counters in the muon scintillator wall. The spectrum obtained after muon ID is shown in figure 1(b). The histogram is fitted with four components (solid line): two Gaussians describing the $D^+ \to \pi^-\pi^+\pi^+$ and $D_s^+ \to \pi^-\pi^+\pi^+$ signals, with central value and width taken from the fit to the histogram in figure 1(a), a Gaussian centered at the D^+ mass for $D^+ \to \mu^-\mu^+\pi^+$ and an exponential falling function to describe the remaining background. The fit gives $0.35^{+3.04}_{-2.47}$ events from $D^+ \to \mu^-\mu^+\pi^+$ or 4.4 events at the 90% confidence level (CL) (dashed curve in figure 1(b)).

The 90% CL upper limit on the branching ratio of the decay $D^+ \to \mu^-\mu^+\pi^+$ is calculated using the $D^+ \to K^-\pi^+\pi^+$ channel as normalization and taking into account the relative efficiency of these two channels. The result is [4]:

$$BR(D^+ \to \pi^+\mu^+\mu^-) \leq 1.8 \times 10^{-5} \qquad (90\%\ CL). \tag{1}$$

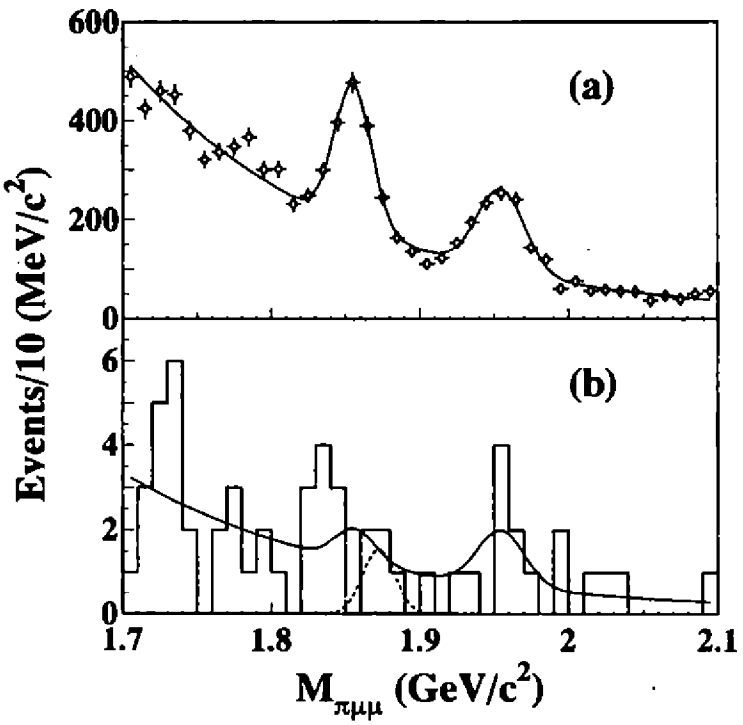

Figure 1. The $\mu^-\mu^+\pi^+$ invariant mass spectrum: (a) with no muon ID requirement. The curve is a fit to the sum of two Gaussians from misidentified $D^+ \to \pi^-\pi^+\pi^+$ and $D_s^+ \to \pi^-\pi^+\pi^+$ and an exponential background; (b) with muon ID. The solid curve is the best fit to a sum of contributions from $D^+ \to \mu^-\mu^+\pi^+$, $D^+ \to \pi^-\pi^+\pi^+$ and $D_s^+ \to \pi^-\pi^+\pi^+$ and an exponential background. The dashed curve shows the size and shape of the $D^+ \to \mu^-\mu^+\pi^+$ contribution ruled out at 90% CL.

[2] This cuts has a negligible effect on $D^+ \to \mu^-\mu^+\pi^+$ efficiency.

4 The $D^+ \to e^-e^+\pi^+$ Search

For $D^+ \to e^-e^+\pi^+$ analysis, the same vertex selection criteria are used and again the $D^+ \to K^-\pi^+\pi^+$ candidate events are excluded with a mass cut. Two oppositely-charged tracks from the secondary vertex must be identified as electrons. The electron ID is based on the deposited energy in the EM calorimeter and the shape of the shower.

The $\pi^+e^+e^-$ mass spectrum after electron ID is shown in figure 2. There are three events from 1.7 to 2.0 GeV/c^2 and only one is inside a search window from 1.83 to 1.89 GeV/c^2. After normalizing the background (diamond points) to two events outside the signal region, the 90% CL upper limit on the number of $D^+ \to e^-e^+\pi^+$ events is 3.6. The size and shape of this contribution is represented by the dashed curve, where the signal is widened to the left due to the loss of energy (bremsstrahlung) suffered by the electrons through the spectrometer.

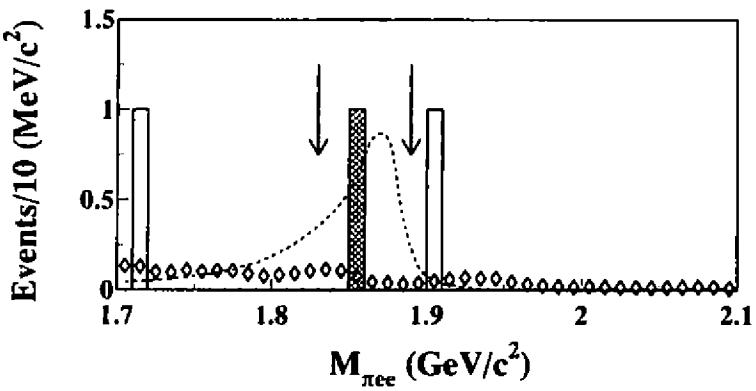

Figure 2. The $\pi^+e^+e^-$ invariant mass spectrum. The estimated background is represented by the diamond points. The dashed curve shows the size and shape of the $D^+ \to e^-e^+\pi^+$ signal excluded at 90% CL.

The 90% CL upper limit on the BR of the $D^+ \to e^-e^+\pi^+$ channel is calculated as for $D^+ \to \mu^-\mu^+\pi^+$ channel. The result [4] is:

$$BR(D^+ \to \pi^+e^+e^-) \leq 6.6 \times 10^{-5} \qquad (90\%\ CL). \tag{2}$$

5 Conclusions

A search for the FCNC decays $D^+ \to \mu^-\mu^+\pi^+$ and $D^+ \to e^-e^+\pi^+$ has been made using the full data set from Fermilab experiment E791. At a 10^{-5} level on the BR, no evidence of flavor-changing neutral-current processes was found. The E791 Collaboration has obtained new upper limits on the BR of these channels, BR($D^+ \to \mu^-\mu^+\pi^+$)$\leq 1.8 \times 10^{-5}$ and BR($D^+ \to e^-e^+\pi^+$)$\leq 6.6 \times 10^{-5}$, which are at least an order of magnitude smaller than those previously published [2,5].

References

1. Schwartz, A.J., *Mod.Phys.Lett.* **A8**, 967 (1993).
2. E653 Collaboration, Kodama, K. *et al.*, *Phys.Lett.* **B345**, 85 (1995).
3. Amato, S., de Mello Neto, J.R.T., de Miranda, J., James, C., Summers, D.J., and Bracker, S.B., *Nucl.Instr.Meth.* **A234**, 535 (1993).
4. E791 Collaboration, Aitala, E.M. *et al.*, "Search for the Flavor-Changing Neutral-Current Decays $D^+ \to \mu^-\mu^+\pi^+$ and $D^+ \to e^-e^+\pi^+$ ", *Phys.Rev.Lett.***76**, 364 (1996).
5. CLEO Collaboration, Hass, P. *et al.*, *Phys.Rev.Lett.* **60**, 1614 (1988); Mark II Collaboration, Weir, A.J. *et al.*, *Phys.Rev.* **D41**,1384 (1990).

Study of the Production of a Single New Charged Heavy Lepton in DELPHI/LEP

M. A. B. do Vale, F. M. L. Almeida and L. de Paula
Instituto de Física - UFRJ

July 2, 1996

Since its discovery in 1975, the tau lepton has been an important laboratory to test the fundamental aspects of the electroweak interactions and confirm many theoretical results predicted by the Standard Model. The discovery of new heavy leptons predicted by extended gauge models would help understanding the problem of the number of quark and lepton generations. Besides that, the large mass of these new leptons allows hadronic decays and so opens the possibility of studying specific strong interaction topics.

In almost all the Standard Model generalizations, new particles are predicted. This is the case of the production of leptonic pairs. This has been intensively studied in LEP until the kinematical limit of $M_Z/2$. Another possibility is the production of a single heavy lepton [1], that up to the moment, has not been detailed studied with high statistics and for different decay channels.

The aim of this work is to investigate the existence of new charged leptons in the $M_Z/2$ and M_Z mass range using the experimental data of DELPHI at LEP/CERN.

The *Instituto de Física* of the UFRJ is in the DELPHI collaboration and has access to the data collected in the period of 1989 until 1995, corresponding to more than 4.0×10^6 Z^o decays. The analysis of these data will be done in the *Instituto de Física* using local and CERN computational resources.

The models studied are: the vector singlet (VSM), the fermion-mirror-fermion (FMF), and the vector doublet (VDM) models. In the VDM model [2], a new neutral lepton and new charged leptons are in doublets with right and left helicities. The FMF model [3] introduces a new right-handed doublet and new left-handed singlets. The VSM [4] includes new left and right-handed leptons in singlets.

Experimentally, a great effort has been done in the case of pair production. For single production, a search [5] has been done in the mass range from 10 GeV up to 225 GeV by the H1 experiment at the electron-proton collider HERA. This work used an integrated luminosity of 528 nb^{-1}.

A fast detector simulation software (SGV) was used to make a preliminary analysis using DELPHI to discriminate the new heavy leptons generated accondingly to the three different models studied (VSM, FMF and VDM). First, we have used only leptonic channels for the heavy lepton decay. In this case, one can see that the DELPHI detector would be able to distinguish clearly not only the existence of a heavy lepton in the mass range from 60 to 80 GeV (figure) , but also, with enough statistics, to discriminate the different models using the angular distribution of the primary lepton.

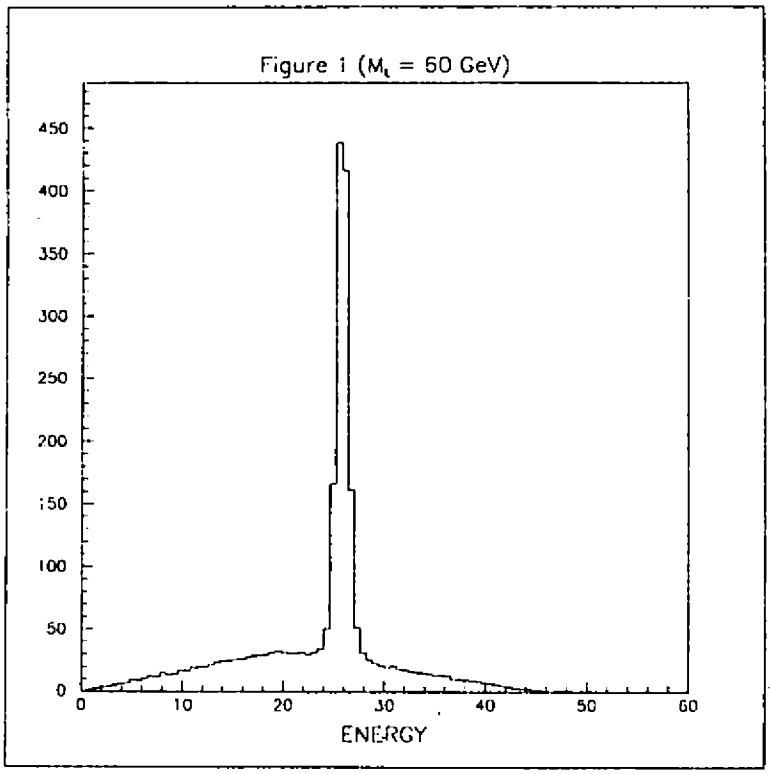

Figure 1. Energy of the particles after the reconstruction.

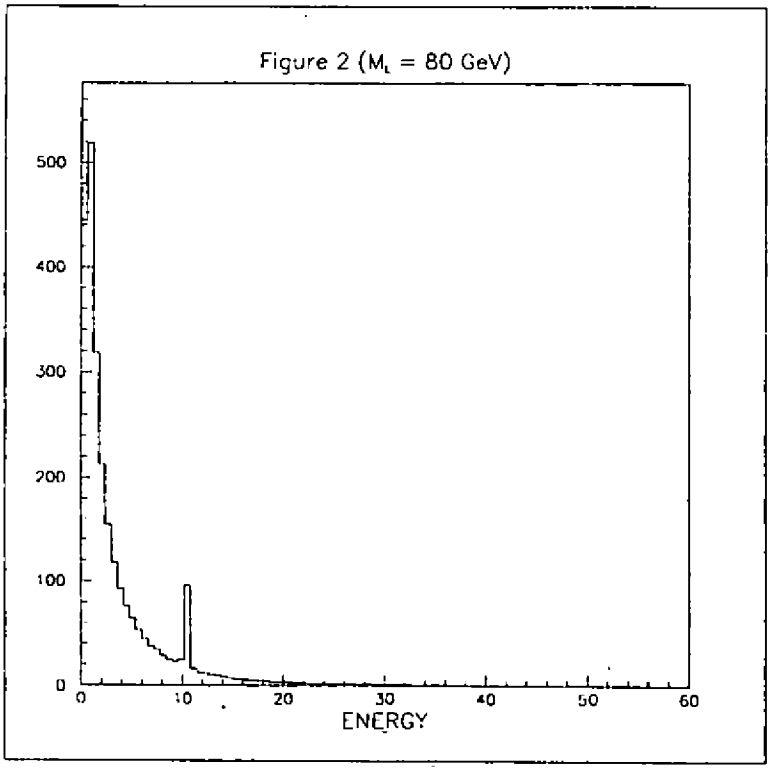

Figure 2.

After the study of the leptonic channels, we have analysed the hadronic channels, that correspond to 70% of the total branching ratio. Here we have also implemented the fragmentation of the quarks into hadrons using the software package JETSET. Figure 2 shows the "seen" primary lepton energy. The primary lepton energy peak at about 10 GeV is related to the heavy lepton mass by the expression $E_e = (s - M_L^2)/2\sqrt{s}$. In despite of a great multiplicity, we can clearly distinguish the existence of a heavy lepton in the hadronic channels. It was shown that the angular distribution of the primary lepton, as in the previous case, can also tag the different models.

References

[1] F. M. L. Almeida, Jr., J. H. Lopes, J. A. Martins Simoes, and C. M. Porto, Phys. Rev. D44, 2836 (1991).

[2] T. Rizzo, Phys. Rev. D34, 2076 (1986).

[3] M. C. Gonzalez-Garcia, A. Santamaria, and J. W. F. Valle, Nucl. Phys. B342, 108 (1990); M. Dittmar, A. Santamaria, M. C. Gonzalez-Garcia, and J. W. F. Valle, Nucl. Phys. B332, 1 (1990).

[4] P. Langacker and D. London, Phys. Rev. D38, 886 (1988); J. Maalampi and M. Roos, Z. Phys. C 44, 319 (1989); E. Nardi and E. Roulet, Phys. Lett. B 248, 139 (1990).

[5] H1 Collab., T. Ahmed et al., Phys. Lett. B340 (1994) 205.

Observation of attenuation behaviour of hadrons in extremly high energy cosmic ray interactions: New hadronic state?

T. Arisawa, Y. Fujimoto, S. Hasegawa, K. Honda,
H. Ito, V.V. Kopenkin, H. Semba
Science and Engineering Research Laboratory,
Waseda University, Tokyo, Japan

M. Tamada
Faculty of Science and Technology,
University, Osaka, Japan

Kinki K. Yokoi
Department of Physics, Aoyama Gakuin University, Tokyo, Japan

G.F. Fedorova, I.P. Ivanenko, A.K. Managadze, I.A. Mikhailova, E.G. Popova,
I.V.Rakobolskaya, T.M. Roganova, L.G. Sveshnikova, O.P. Strogova
Institute of Nuclear Physics,
Moscow State University, Moscow, Russia

Received March, 1996

Experimental results are presented on high energy cosmic-ray hadron interactions recorded in homogenous-type thick lead chambers (total thickness being 60 cm and 110 cm) exposed at the Pamirs (atmospheric depth $596 g/cm^2$. High energy cosmic-ray hadron flux is measured. The attenuation mean free path of the arriving cosmic-ray hadrons of $E_h^7 \geq 6$ TeV measured in the chamber is obtained as $252 \pm 30 g/cm^2$ of lead. However, for the high energy hadrons $E_h^7 > 10 TeV$ constituting cosmi-ray families of the highest energy range, $\Sigma E^\gamma \geq 700$ TeV, which we have been accumulated so far in the series of exposures at the Pamirs and analysed by MSU group, the attenuation mean free path of hadrons in lead has turned out to be as short as $170^{+47}_{-26} g/cm^2$ with 95% CL by the maximum likelihood method. The present experimental result of such a short attenuation length of hadrons in cosmic-ray families is essentially consistent with that obtained fo high energy hadrons $E_\gamma \geq 10$ TeV constituting the "Chiron-type" families of $\Sigma E_\gamma \geq 100$ TeV in the Chacaltaya two-storeyed chamber experiments. The anomalous transition characteristics of high energy hadrons in lead is found and examples are presented. The physical significance of the experimental results on extremely high energy hadron interactions discussed.

Introduction

On the basis of a systematic study of hundreds of cosmic-ray families of visible energy exceeding $100 TeV$ [1] it has been shown that the frequency of exotic cosmic-ray events named "Centauro species" could never be insignificant. The main question is whether the particles produced in the high energy interactiones are already known ordinary hadrons or they are hadrons of novel origin. Existence of new type of interaction might strongly suggest the possibility that secondary particles represent new state of hadrons. Uniform-type lead chambers provide sufficient thickness of traversed material for detailed observation of showers behaviour and give us a clue to clarify the nature of interaction.

Experimental procedure

Our experiment uses a chamber composed of 60 layers of lead plates of 1 cm thickness and the RT6M-type X-ray films that are placed every 1-2 cm of lead (Fig. 1). The chamber is homogeneous in structure and uniform in detection efficiency of showers. The transition of an electron shower in the chamber can be observed at every 1 cm interval through the darkness measurement of photometry. Present paper is based on analysis of $16m^2 \cdot$ year exposure at the Pamirs in 1988-1989. Showers observed in the chamber are classified into "family" which is a bundle of parallel showers with the same arrival direction and "single" which are not accompanied by shower above the detection threshold. Present experiment has $16m^2 \cdot year$ exposure for single showers.

Attenuation of single cosmic ray hadrons in lead

We have selected the deep-starting showers of $\theta < 50$ degrees and $E_\gamma \geq 6$ TeV to make convenient the comparison with the data from [3]. Fig.2 shows the ΔT distribution of all the observed showers. ΔT expresses the shift of depth of the shower maximum from the expected position of pure electro-magnetic cascade of electrin pair origin. The maximum for the $\Delta T < 10 c.u.$ present the contribution of gamma-ray induced showers and exponential decrease demonstrares the hadron attenuation in lead. We obtain $\lambda_{att}^{Pb} = 210 \pm 27 g/cm^2$ within the range $10 \leq \Delta T < 40 c.u.$ This value is consistent with the result [3] $\lambda_{att}^{Pb} = 209 \pm 17 g/cm^2$ obtained in the range $20 \leq \Delta T \leq 78 c.u.$ Vertical flux of hadrons of vissible energy is well reproduced by $I(E_\gamma) = N_0(E_\gamma/10TeV)^{-\beta}/m^2 \cdot year$ with $N_0 = 17 \pm 1$ and $\beta = 3.09 \pm 0.13$. Data [3] give $N_0 - 18 \pm 1$ and $\beta = 3.01 \pm 0.08$. Mututal agreement is beoynd reasonable doubts.

Attenuation mean free path of high energy hadrons

Hitherto 16 superfamilies of total visible energy $\Sigma E_\gamma \geq 700$ TeV have been collected [4] since 1977. The thickness of the chamber varied from exposure to exposure within 40-110 cm Pb. The ΔT distribution of the 143 hadrons of $E_h^\gamma \geq 10$ TeV (closed circles) and 68 hadrons of $E_h^\gamma \geq 20$ TeV (open circles) and $\Delta T \geq 10$ c.u. from families is shown in Fig.3. The attenuation mean free path by least square fitting is given as $\lambda_{att} = 176 \pm 48 g/cm^2$. and $\lambda_{att} = 146 \pm 40 g/cm^2$ respectively. To estimate the attenuation length we also used maximum likelihood method. The normalized distribution $L(\lambda_{att})/\int_0^{infty} L(\lambda_{att}) d\lambda_{att}$ is calculated using the experimental data of each hadron for a finite thickness of the chamber and the observation of the attenuation restricted within a certain interval. Fig.4 gives the normalized distribution for 143 hadrons of $E_h^\gamma \geq 10$ TeV. From the maximum point and width of the distribution we get the value of λ_{att} with 95% confidence level, $\lambda_{att} = 170^{+47}_{-26} g/cm^2$. The same distribution for 68 hadrons of $E_h^{gamma} \geq 20$ TeV is given by $\lambda att = 137^{+57}_{-26} g/cm^2$.

Global relation between attenuation and collision mean free path

The attenuation mean free path depends on the slope of energy spectrum given by formula $\lambda_{att} = \lambda_{coll}/(1 - < (1-K)^\alpha >)$, where K is the inelasticity of the collision and α is the power index of energy spectrum in integral form. Power index α is found to be 2.09 for single arrived hadrons and 1.16 for hadrons in superfamilies. If λ_{coll} is the same for both categories of hadrons, the value of λ_{att} should be larger for hadrons in families by a factor 1.2-1.3. If the hadron interaction is type of ordinary multiple-pion production, the majority of the single hadrons is likely to be nucleons, but most of the hadrons in families will be pions. The collision mean free path λ_{coll} of protons is less than that of pions. So, λ_{att} of hadrons in families should be larger than that of single arrived hadrons, but the experiment shows just the opposite.

Anomalous transition behaviour of high energy cosmic ray hadrons

In the present thick lead chambers we have encountered showers of hadron origin which show anomalous transition behaviour. Fig.5 and Fig.6 show the transition with depth of the shower spot darkness through the whole depth of the chamber without significant attenuation. The event in Fig.6 is composed of two showers of 46 TeV and 73 TeV with the relative distance 1.3 mm. If we assume the vertex point tp be 1 km above the chamber, the relative production p_t of magnitude would be as small as 40 MeV/c. The feature of transition curves seen in the above examples is never rare but was encountered in Chacaltaya experiment too [5] and majority are to be explained as she shower cluster phenomena initiated by particles produced with small p_t in the families which are called "Chiron" [5].

Discussions and summary

The striking fact we found is that the attenuation length of high energy hadrons observed in families originating from extremely high energy cosmic ray interastions over 10^{16} eV is significantly smaller than that of single arrived hadrons. The study of two groups of hadrons, single hadrons and hadrons in families, has been carried out in chambers of the same structure, using the photosensitive materials of the same quality and the same way of shower analysis was applyed. We are led to the conclusion that the observed difference between the two is really significant and indicate the existence of "new hadronic state".

References

[1] *C.M.G. Lattes, Y. Fujimoto and S. Hasegawa* Phys. Rep. 65(1980)151.

[2] *Pamir Collaboration*. Trudy FIAN Vol 154 (in Russian), Nauka, Moscow, 1984.

[3] *I.P.Ivanenko et al.* Proc. Int. Workshop on Super High Energy Hadron Interactions, Tokyo (1991) p.215.

[4] *Pamir Collaboration* Izvestija AN SSSR, ser. fiz., Vol.55(1991)650.

[5] *S. Hasegawa* AIP Conf. Proc. 85(1981)500, ICR report-151-87-5(1987).

Invariant classification of the axially symmetric solutions

Wladimir Seixas
UNESP - Campus de São José do Rio Preto
Departamento de Ciências da Computação e Estatística
Caixa Postal 136
15054-000 - São José do Rio Preto - SP - Brasil
e-mail: seixas@wolverine.ibilce.unesp.br

Received March, 1996

In this work we shall focus on the problem of classifying the axially symmetric solutions following the Cartan-Karlhede procedure. During recent years many works have shown that the stationary axially symmetric solutions admit a specific simple canonical form and when some of its invariant scalars are calculated, factorization properties will occur. Ernst was the first one to recognize the simple canonical form for the Tomimatsu-Sato $\delta = 2$ and 3 solutions. Perjés observed the same form for the Tomimatsu-Sato $\delta = 4$ and 5. The property was confirmed to be valid for all the known stationary axially symmetric metrics by Kerr. In the same way, the factorization properties could be confirmed by calculating the quantities directly via any computer algebra system for most of the known solutions. Hoenselaers and Perjés proved that such a property is general and can be proved by defining a set of polynomials based on the vacuum equations for axially symmetric metrics. This class of metrics can be characterized by searching for solutions to a single complex equation, the Ernst equation. Various combinations of polynomials in the Ernst potential and their derivatives are then factorizable. If it is assumed that the solution is given by $\mathcal{E} = (\alpha - \beta)(\alpha + \beta)^{-1}$, the Weyl spinor components are proportional to $(\alpha + \beta)^{-3}$ and therefore the scalar $B_5 = \Psi_0\Psi_4 - 9\Psi_2{}^2$ is expected to be proportional to $(\alpha + \beta)^{-6}$. In fact, it is proportional to $(\alpha + \beta)^{-5}$, i.e. a factorization in $(\alpha + \beta)$ occurred. This fact should be considered and could give a significant improvement in the study of the classification procedure for this class of solutions since we are seeking for an alternative way of computing the quantities assuming beforehand possible factorizations.

1 The axially symmetric solutions

The axially symmetric stationary metric can be written in the following form (see e.g. [1])

$$ds^2 = f(dt - \omega\, d\phi)^2 - \rho^2 f^{-1} d\phi^2 - e^{\mu}(d\rho^2 + dz^2) \tag{1}$$

where f, ω and μ are functions of ρ and z only. Define the complex function $\mathcal{E} = f + i\,\psi$. The equation $\mathrm{Re}(\mathcal{E})\,\nabla^2\mathcal{E} = \mathcal{E}_z{}^2 + \mathcal{E}_\rho{}^2$ is called the Ernst equation and its solution $\mathcal{E}$, the Ernst potential [2]. Let the following coordinate transformation from (t, ρ, z, ϕ) to the prolate spheroidal coordinates (t, x, y, ϕ) and then to (t, X, Y, ϕ) be given by $x = \cosh X$ e $y = \cos Y$. By defining the operator, $\partial_\pm = \partial_X \pm i\,\partial_Y$, the conditions vacuum conditions can be written as [3]

$$\begin{aligned} \frac{1}{\rho}\left[\partial_\pm(\rho\partial_\mp\mathcal{E}) + \partial_\mp(\rho\partial_\pm\mathcal{E})\right] &= \frac{2}{f}\partial_\pm\mathcal{E}\partial_\mp\mathcal{E} \\ \mp i\rho\partial_\pm\psi &= f^2\partial_\pm\omega \\ \partial_\pm\gamma\partial_\pm\rho &= \frac{1}{2}\partial_\pm{}^2\rho + \frac{\rho}{4f^2}\partial_\pm\mathcal{E}\partial_\pm\mathcal{E}^* \end{aligned} \tag{2}$$

with $\partial_\pm\partial_\mp\rho = 0$ and where $e^{2\gamma} = fe^{\mu}(\cosh^2 X - \cos^2 Y)$.

2 Invariant scalars of the axially symmetric solutions

The factor properties can be directly verified by giving the explicit form of the invariant quantities utilized in the Cartan-Karlhede classification in terms of the Ernst formalism [4]. Initially let us start by considering the following null tetrad [5]

$$\begin{aligned} \mathbf{m} &= \frac{e^{\gamma}}{\sqrt{2f}}\left(\partial_+\rho\, dX + i\,\partial_-\rho\, dY\right) \\ \mathbf{l} &= \frac{\sqrt{2}}{2}\left[\sqrt{f}\,dt - \left(\frac{\rho}{\sqrt{f}} + \sqrt{f}\,\omega\right) d\phi\right] \\ \mathbf{k} &= \frac{\sqrt{2}}{2}\left[\sqrt{f}\,dt + \left(\frac{\rho}{\sqrt{f}} - \sqrt{f}\,\omega\right) d\phi\right] \end{aligned} \tag{3}$$

Since $\mathcal{E} = f + i\,\psi$, in the above null tetrad the Weyl spinor components can be calculated and they are given by [5]

$$\begin{aligned} \Psi_0 &= -\frac{1}{8}e^{-2\gamma}\left[2\partial_-^2\mathcal{E} - 4\partial_-\gamma\partial_-\mathcal{E} + \frac{1}{f}(\partial_-\mathcal{E})^2\right] \\ \Psi_2 &= \frac{1}{8}e^{-2\gamma}\left[2\partial_+\partial_-\mathcal{E} - \partial_+\mathcal{E}\partial_-\mathcal{E}\right] \\ \Psi_4 &= -\frac{1}{8}e^{-2\gamma}\left[2\partial_+^2\mathcal{E} - 4\partial_+\gamma\partial_+\mathcal{E} + \frac{1}{f}(\partial_+\mathcal{E})^2\right] \\ \Psi_1 &= \Psi_3 = 0 \end{aligned}$$

Taking all the possibilities for the Ψ_A's to vanish or not, the following Petrov types can occur:

1. All Ψ_A's equal to zero: Petrov type 0. The solution is a Minkowski spacetime;
2. Only Ψ_0 (or Ψ_4) is different from zero: Petrov type N. This is not an interesting case if we seek solutions which are asymptotically Schwarzschild;
3. Only $\Psi_2 \neq 0$ or Ψ_0, Ψ_2 and Ψ_4 non-vanishing with $B_5 = \Psi_0\Psi_4 - 9{\Psi_2}^2 = 0$: Petrov type D. These solutions are all known [6] and their classification have already been studied in detail by Collins *et. al.* [7];
4. Only Ψ_0 (or Ψ_4) vanishes: Petrov type II. These solutions belong to a class of solutions divided into three distinct cases: the Weyl class, Lewis and van Stockum solutions, the last one admitting at most a group G_3 [1];
5. Only $\Psi_2 = 0$ or all different from zero with $B_5 = \Psi_0\Psi_4 - 9{\Psi_2}^2 \neq 0$: Petrov type I. This is the general case.

As we can verify the Petrov type III does not occur in any of the possibilities listed above. The components of the Weyl spinor can be rewritten as [3]

$$\begin{aligned} \Psi_0 &= \frac{1}{2}\frac{D}{(\alpha+\beta)^3}\frac{T_-}{\partial_-\rho A_+} \\ \Psi_2 &= \frac{1}{2}\frac{D\,M}{(\alpha+\beta)^3} \\ \Psi_4 &= \frac{1}{2}\frac{D}{(\alpha+\beta)^3}\frac{T_+}{\partial_+\rho A_-} \end{aligned} \tag{4}$$

where

$$\begin{aligned} M\,A_\pm &= K_\mp\partial_\pm(\alpha+\beta) - (\alpha+\beta)\partial_\pm K_\mp \\ T_\pm &= (\alpha+\beta)Q_\pm - 3K_\pm\partial_\pm\rho\partial_\pm(\alpha+\beta) \end{aligned} \tag{5}$$

and

$$Q_\pm = \partial_\pm\rho\partial_\pm K_\pm - K_\pm\left(2H_\pm + \partial_\pm^2\rho\right)$$

The Petrov type I is the most interesting case to be considered. Looking at it in details, it follows that in terms of the above relations, that the Petrov type I occurs when (a) $K_\mp\partial_\pm(\alpha+\beta) - (\alpha+\beta)\partial_\pm K_\mp = 0$ and $T_\pm \neq 0$; (b) $B_5 \neq 0$.

The expression for B_5 is given by [3, 4]

$$B_5 = \frac{1}{4}\frac{D^2}{(\alpha+\beta)^5\partial_\pm\rho\partial_\mp\rho\, A}\,B_{\pm 5}$$

where

$$\begin{aligned} B_{\pm 5} &= (\alpha+\beta)\,[Q_{\pm}Q_{\mp} - 9\partial_{\pm}\rho\partial_{\mp}\rho\,\partial_{\pm}K_{\mp}\partial_{\mp}K_{\pm}] - \\ &\quad - 3\,[K_{\pm}\partial_{\pm}\rho\partial_{\pm}(\alpha+\beta)\,Q_{\mp} + K_{\mp}\partial_{\mp}\rho\partial_{\mp}(\alpha+\beta)\,Q_{\pm}] - \\ &\quad - 9\,[K_{\pm}\partial_{\mp}K_{\pm}\partial_{\pm}(\alpha+\beta) + K_{\mp}\partial_{\pm}K_{\mp}\partial_{\mp}(\alpha+\beta)]\,\partial_{\pm}\rho\partial_{\mp}\rho \end{aligned}$$

It is worth noting that the cancellations as well as the factorizations only occur when the right expressions are substituted since the number of definitions and relations (mainly from the field equations) are restricted to a small set. Of course, this fact may bring many difficulties when we are searching for simpler expressions involving the above polynomials.

References

[1] D. Kramer, H. Stephani, M.A.H. MacCallum, and E. Herlt. *Exact solutions of Einstein's field equations*. Deutscher Verlag der Wissenschaften, Berlin, and Cambridge University Press, Cambridge, 1980.

[2] F.J. Ernst. New formulation of the axially symmetric gravitational field problem. *Phys. Rev.*, **167** (5), 1175–1178, 1968.

[3] C. Hoenselaers and Z. Perjés. Factor structure of rational vacuum metrics. *Class. Quant. Grav.*, **7**, 2215–2224, 1990.

[4] W. Seixas. *Computer-aided classification of exact solutions*. PhD thesis, University of London, 1993.

[5] F.J. Ernst. Complex potential formulation of the axially symmetric gravitational field problem. *J. Math. Phys.*, **15** (9), 1409–1412, 1974.

[6] W. Kinnersley. Type D vacuum metrics. *J. Math. Phys.*, **10**, 1195–, 1969.

[7] J.M. Collins, R.A. d'Inverno, and J.A. Vickers. The Karlhede classification of type D vacuum spacetimes. *Class. Quant. Grav.*, **7**, 2005–2015, 1990.

Reconhecimento de eventos simulados na energia do LEP II utilizando redes neuronais

N. Couto[1], Z.D. Thomé[1] e F.M.L. Almeida [2]
1 Programa de Engenharia Nuclear - Coppe/UFRJ
2 Instituto de Física - UFRJ

Received March, 1996

Neste trabalho, apresentamos uma rede neuronal artificial do tipo "feed-forward" com algoritmo de atualização "backpropagation" que é construída e treinada para discriminação de eventos de física de partículas de altas energias do tipo $e^+e^- \to e^+e^- f\bar{f}$, simulados por Monte Carlo via Modelo Padrão (MP) dos eventos de mesmo tipo simulados via mode lo estendido Fermion-Mirror-Fermion (FMF), na energia de 2- GeV (LEP II). Para eventos leptônicos $e^+e^- \to e^+e^- ll$ a rede atinge uma eficiência em torno de 77% enquanto que para os eventos hadrônicos $e^+e^- \to e^+e^-$ hadrons uma eficiência em torno de 98%.

1 Introdução

A física de partículas, especificamente a de altas energias, desempenha um papel de destaque no quadro da física moderna contemporânea. Apesar do sucesso do MP, o qual assenta as bases dessa física, ainda, devido a algumas não evidências experimentais desvios da teoria são permitidos, oportunamente abrindo espaços para quadro teóricos alternativos, como o modelo estendido FMF aqui utilizado.

Neste trabalho, a técnica de processamento neuronal é utilizada para a discriminação entre eventos, provenientes de colisões e^+e^- com energia de 200 GeV no centro de massa, com quatro férmions no estado final, $e^+e^- \to e^+e^- f\bar{f}$ os quais são permitidos pelo MP e pelo FMF.

O trabalho é dividido em duas partes, uma referente a discriminação dos eventos leptônicos provenientes dos dois modelos e a outra referente a discriminação dos eventos hadrônicos. Assim sendo, duas redes são construídas, uma para discriminação leptônica e outra para a hadrônica, uma vez que os vetores de entrada (número de variáveis cinemáticas escolhidas para representar a partícula) das redes tem diferentes dimensões.

2 Simulação e Variáveis de Entrada

Os eventos via MP foram obtidos pelo simulador EXCALIBUR que releva processos físicos nos quais há produção de bósons vetoriais pesados que serão investigados nos colisionadores e^+e^- em um amplo alcance de energia. Na energia do LEP II os processos $e^+e^- \to$ 4fermions são:

$$e^+e \to W^+W^-$$

$$e^+e \to ZZ$$

$$e^+e \to We\nu_e$$

$$e^+e \to Ze^+e^-$$

$$e^+e \to Z\nu_e\bar{\nu}_e$$

Utilizamos o canal $e^+e \to ZZ$

Os eventos via FMF foram obtidos pelo simulador desenvolvido no Instituto de Física/UFRJ dentro do grupo da colaboração Internacional UFRJ/CERN. Para este modelo as partículas do estado final provem do decaimento de um único lépton pesado produzido no estado intermediário do processo e^+e^-.

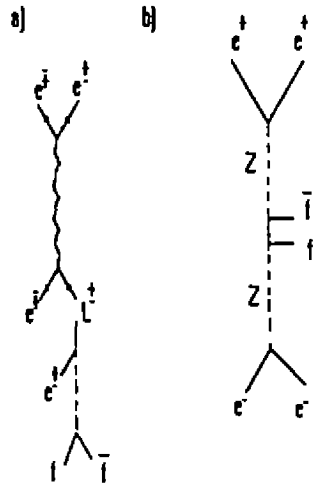

Fig. 2.1 Processos $e^+e \to e^+e^- f\bar{f}$ a) FMF b) MP.

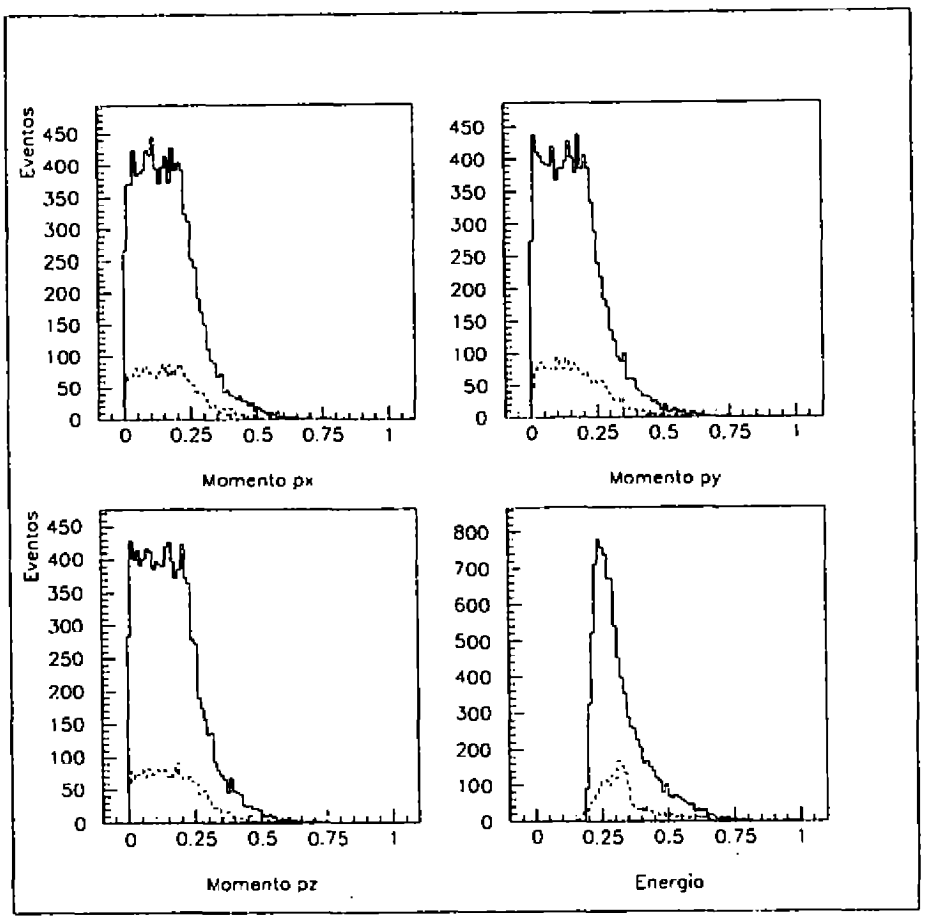

Fig. 3.1. Variáveis normalizadas do elétron para FMF (linha cheia) e MP (linha pontilhada). Canal Leptônico.

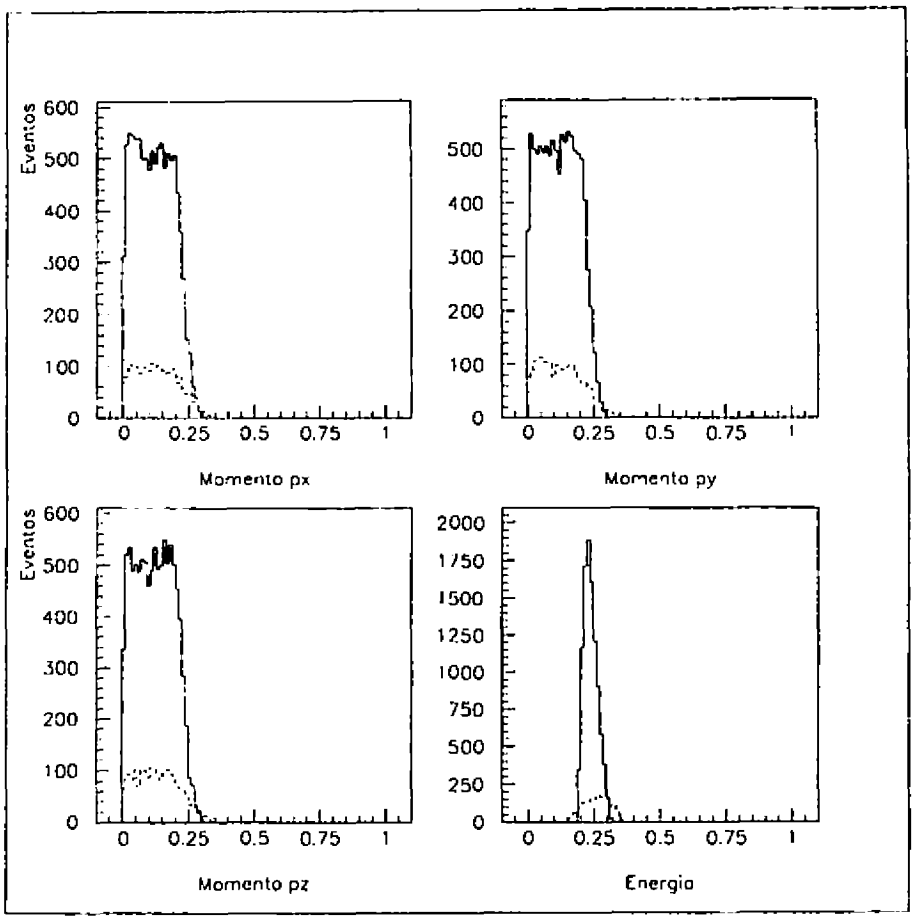

Fig. 3.2. Variáveis normalizadas do elétron para FMF (linha cheia) e MP (linha pontilhada). Canal Hadrônico.

Para os eventos leptônicos o estado final é composto por 4 partículas onde cada uma é representada por seu quadri-momento (E,P_x, P_y, P_z), como variáveis cinemáticas que alimentam o vetor de entrada da rede neuronal, resultando na rede leptônica um vetor de entradde de 16 posições. Enquanto, que para os eventos hadrônicos, o estado final é composto por 14 partículas, já que os quarks e antiquarks sofrem hadronização, onde foram escolhidos os 6 hádrons mais energéticos de cada jato hadrônico, resultando na rede hadrônica um vetor de entrada de 56 posições.

3 Resultados

A região de interesse na qual a rede neuronal deve atuar a fim de discriminar eventos via MP dos eventos FMF, que se superpoem tanto no canal hadrônico quanto leptônico é mostrada nas figuras abaixo, para por exemplo, o elétron que aparece no estado final.

Utilizando uma rede de três camadas configurada com : 16 neurônios na camada de entrada, 10 neurônios na camada oculta e 1 neurônio na camada de saída para o canal leptônico, 10000 eventos ($\simeq$ 50% via MP e $\simeq$ 50 % via FMF) para treinamento da rede e 4000 eventos ($\simeq$ 50% via MP e $\simeq$ 50% via FMF) para teste, foram apresentados fornecendo-nos as seguintes eficiências máximas e parciais por modelo, atingidas pela rede.

Para o canal hadrônico há uma rede de três camadas configurada com 56 neurônios na camada de entrada, 1 neurônio na camada oculta e 1 neurônio na camada de saída, 4000 eventos por treinamento e outros 4000 eventos para teste, foram aleatoriamente apresentados apenas 1000 vezes, fornecendo-nos o seguinte resultado:

Tabela 1 *Eficiência para diferentes números de apresentações.*

Apres.	Efic.	Efic. Modelo	
	Máxima %	MP	FMF
1000	60.57	48.86	100.00
5000	74.27	51.87	100.00
10000	75.92	53.83	100.00
23000	77.90	55.80	100.00

Tabela 2 *Eficiência da rede hadrônica.*

Apres.	Efic.	Efic. Modelo	
	Máxima %	MP	FMF
1000	98.66	99.40	97.93

4 Conclusões e Propostas

Diante dos resultados obtidos, mesmo que preliminares, podemos concluir e propor:

- O uso da técnica em futuros eventos reais torna-se possível, na discriminação de eventos "background" (via MP) dos eventos que representam uma nova física (via FMF);
- A otimização do tempo computacional que foi razoável, em torno de 24 horas para 10000 ciclos de treinamento, uma rede 16:10:16:1, 10000 eventos de treinamento e 4000 de teste, para uma "workstation" SUN 10;
- A melhora da configuração das redes;
- Aplicação de outros algoritmos inteligentes (quando possível !);
- A extensão do estudo para o espalhamento próton-próton na energia do LHC (trabalho em andamento !) e para vários outros canais de decaimento.

References

[1] Halzen, F. e Martin, A.D. - Quarks and Leptons : An Introductory Course in Modern Particle Physics - Jonh Willey (1984)

[2] Berends, F.A et all. - EXCALIBUR - a Monte Carlo program to evaluate all four fermions processes at LEP 200 and Beyound"; INLO-PUB-12/94 (1994)

[3] Almeida, F.M.L. et all. - Phys. Rev. D44; 2836 (1991)

On color transparency

A. Gabriela Grunfeld*, Mario Rocca†
Departamento de Física,
Fac. de Cs. Ex., Universidad Nacional de La Plata,
La Plata, Argentina

Received March, 1996

It has been suggested that a hadron may interact very weakly with nucleons in nuclei when it is forced to adopt a quasipointlike configuration during the lapse it travels through the nucleus. Such configurations have no color charge and a small dipole moment. Therefore they interact only weakly with nuclear matter. This phenomenon has been termed Color Transparency.

Quantum mechanical features of Color Transparency have been studied considering the non-relativistic evolution of a $c\bar{c}$ pair produced, as a small wave packet, inside the nucleus. The soft interaction with nuclear medium has been modeled by dipolar-type interaction.

Our purpose in this work is to study the relativistic evolution of the $c\bar{c}$ system by means of the Klein-Gordon harmonic oscillator Hamiltonian with the inclusion os a homogeneous electric field that accounts for the nuclear medium.

1 Klein-Gordon oscillator

In 1989 Moshinsky and Szczepaniak [1] proposed a new type of interaction in the Dirac equation. This potential is linear in r and the corresponding equation was named Dirac Oscillator because in the non-relativistic limit the harmonic oscillator is obtained.
This kind of interaction was introduced in the Klein-Gordon equation [2][3] trough the minimal coupling replacement:

$$\vec{P} \rightarrow \vec{P} - im\hat{\gamma}\hat{\Omega}\cdot\vec{Q}, \tag{1}$$

where

$$\vec{Q} = \hat{\eta}\vec{q}, \qquad \vec{P} = \hat{\eta}\vec{p}, \qquad \hat{\Omega}_{ij} = \omega_i\delta_{ij} \tag{2}$$

The resulting Klein-Gordon equation is:

$$-\frac{\partial^2}{\partial t^2}\Psi(\vec{q},t) = \left(\vec{p}^{\,2} + m^2\vec{q}\cdot\hat{\Omega}^2\cdot\vec{q} + m\hat{\gamma}\ tr\Omega + m^2\right)\Psi(\vec{q},t), \tag{3}$$

The physical sense of implementing $\hat{\eta}$ and $\hat{\gamma}$ is obscure.
Sakata-Taketani approach is caracterized by:

$$\vec{p} \rightarrow \vec{p} - im\omega\tau_1\vec{r} \tag{4}$$

and

$$i\frac{\partial}{\partial t}\Phi = \left\{\frac{\vec{p}(\tau_3 + i\tau_2)\vec{p}}{2m} + m\tau_3\right\}\Phi, \tag{5}$$

*UNLP
†UNCPBA - Investigador CONICET

with τ_i being the Pauli matrices. $\Phi = column(\phi, \chi)$ is a two-component wave function with the components which could be written as following:

$$\begin{cases} \phi = (\Psi + \frac{i}{m}\partial_t \Psi)/\sqrt{2} \\ \chi = (\Psi - \frac{i}{m}\partial_t \Psi)/\sqrt{2}. \end{cases} \tag{6}$$

Hence, Klein-Gordon equation can be explicitly expressed:

$$\left[\Box + 2m\omega^2 r^2 - 3m\omega + m^2\right]\Psi = 0 \tag{7}$$

We have solved this equation for the isotropic three-dimensional case. The eigenvalues and eigenfunctions are:

$$E^2 = 2(N_1 + N_2 + N_3)\, m\omega + m^2 \tag{8}$$

$N_1, N_2, N_3 = 0, 1 \ldots$

$$\begin{aligned} \Psi_{E\, N_1 N_2 N_3} &= \left[\frac{m\omega}{\pi}\right]^{3/4} \frac{2^{-(N_1+N_2+N_3)/2}}{(N_1!\, N_2!\, N_3!)^{1/2}}\, e^{-i E_{N_1 N_2 N_3} t} \\ &\times\ e^{-(x^2+y^2+z^2)\, m\omega^2/2} \\ &\times\ H_{N_1}(\sqrt{m\omega}\, x)\, H_{N_2}(\sqrt{m\omega}\, y)\, H_{N_3}(\sqrt{m\omega}\, z) \end{aligned} \tag{9}$$

2 Klein-Gordon equation for the charged harmonic oscillator in a uniform electric field

Now we assume that the particle studied previously has a charge q and it is placed in a uniform electric field $\mathcal{E}$ parallel to z axis.
The classical potential energy of a particle placed in a uniform field $\mathcal{E}$ is: $V(\mathcal{E}) = -q\mathcal{E}z$. We introduced this potential energy in the Klein-Gordon equation making the correspondence:

$$-\left(i\frac{\partial}{\partial t}\right)^2 \rightarrow -\left(i\frac{\partial}{\partial t} - q\mathcal{E}z\right)^2 \rightarrow -\left(\frac{\partial}{\partial t}^2 - q^2E^2z^2 - 2iq\mathcal{E}z\frac{\partial}{\partial t}\right) \tag{10}$$

Then, the Klein-Gordon equation reads:

$$(\Box + 2\, i\, q\, \mathcal{E}\, z\frac{\partial}{\partial t} + m\omega^2 r^2 - q^2\mathcal{E}^2z^2 - 3m\omega + m^2)\ \Psi = 0 \tag{11}$$

There exist three cases for $m\omega > q\mathcal{E}$, $m\omega < q\mathcal{E}$ and $m\omega = q\mathcal{E}$ The eigenvalues and eigenvectors are
a) $m\omega > q\mathcal{E}$

$$E^2_{N_1 N_2 N_3} = \left(1 - \frac{q^2\mathcal{E}^2}{m^2\omega^2}\right)\left[(2N_3+1)\sqrt{m^2\omega^2 - q^2\mathcal{E}^2} + 2\left(N_1 + N_2 - \frac{1}{2}\right)m\omega + m^2\right] \tag{12}$$

with N_1, N_2, N_3 natural numbers.

$$\begin{aligned} \phi_{N_1 N_2 N_3} = \left(\frac{m\omega}{\pi}\right)^{3/4} \frac{2^{\frac{N_1+N_2+N_3}{2}}}{(N_1!N_2!N_3!)^{1/2}} e^{-\frac{m\omega}{2}(x^2+y^2)}\, e^{-\frac{\left(\sqrt{m^2\omega^2-q^2\mathcal{E}^2} - \frac{q\mathcal{E}E_{N_1N_2N_3}}{\sqrt{m^2\omega^2-q^2\mathcal{E}^2}}\right)^2}{2\sqrt{m^2\omega^2-q^2\mathcal{E}^2}}} \\ \times H_{N_3}\left(\frac{\sqrt{m^2\omega^2 - q^2\mathcal{E}^2} + \frac{q\mathcal{E}E_{N_1N_2N_3}}{\sqrt{m^2\omega^2-q^2\mathcal{E}^2}}}{(m^2\omega^2 - q^2\mathcal{E}^2)^{1/4}}\right) \end{aligned} \tag{13}$$

This solution corresponds to N_3 even, the other independent solution corresponds to N_3 odd.
b) $m\omega < q\mathcal{E}$

$$E^2_{N_1 N_2 N_3} = \left(\frac{q^2\mathcal{E}^2}{m^2\omega^2} - 1\right)\left[(2N_3+1)\sqrt{-q^2\mathcal{E}^2 - m^2\omega^2} - 2\left(N_1 + N_2 - \frac{1}{2}\right)m\omega + m^2\right] \tag{14}$$

In this case we have two independent solutions:

$$\phi_{N_1 N_2 N_3} = A_{N_1 N_2 N_3} e^{-\frac{m\omega^2}{2}(x^2+y^2+z^2)} H_{N_1}(\sqrt{m\omega}\,x)\, H_{N_2}(\sqrt{m\omega}\,y) e^{-i\frac{\left(\sqrt{q^2\mathcal{E}^2-m^2\omega^2}z-\frac{q\mathcal{E}E_{N_1N_2N_3}}{\sqrt{q^2\mathcal{E}^2-m^2\omega^2}}\right)^2}{2\sqrt{q^2\mathcal{E}^2-m^2\omega^2}}} \times \Phi\left(\frac{1}{4}-\frac{iE_3^2}{2m\omega}, \frac{1}{2}, -i\frac{\left(\sqrt{q^2\mathcal{E}^2-m^2\omega^2}z-\frac{q\mathcal{E}E_{N_1N_2N_3}}{\sqrt{q^2\mathcal{E}^2-m^2\omega^2}}\right)^2}{2\sqrt{q^2\mathcal{E}^2-m^2\omega^2}}\right) \tag{15}$$

$$\phi_{N_1 N_2 N_3} = A_{N_1 N_2 N_3} e^{-\frac{m\omega^2}{2}(x^2+y^2+z^2)} H_{N_1}(\sqrt{m\omega}\,x)\, H_{N_2}(\sqrt{m\omega}\,y) e^{-i\frac{\left(\sqrt{q^2\mathcal{E}^2-m^2\omega^2}z-\frac{q\mathcal{E}E_{N_1N_2N_3}}{\sqrt{q^2\mathcal{E}^2-m^2\omega^2}}\right)^2}{2\sqrt{q^2\mathcal{E}^2-m^2\omega^2}}} \times \Phi\left(\frac{3}{4}-\frac{iE_3^2}{2m\omega}, \frac{3}{2}, -i\frac{\left(\sqrt{q^2\mathcal{E}^2-m^2\omega^2}z-\frac{q\mathcal{E}E_{N_1N_2N_3}}{\sqrt{q^2\mathcal{E}^2-m^2\omega^2}}\right)^2}{2\sqrt{q^2\mathcal{E}^2-m^2\omega^2}}\right) \tag{16}$$

c) $m\omega = q\mathcal{E}$

$$\phi = \left[\frac{-4i}{3}\left(\frac{2|e|\mathcal{E}Ez+E^2-E_1^2-E_2^2+m\omega-\frac{m^2}{3}}{(2|e|\mathcal{E}|E|)^{2/3}}-i0\right)^{3/2}\right]^{1/6} \times W_{0,-\frac{1}{3}}\left(\frac{-4i}{3}\left[\frac{2|e|\mathcal{E}Ez+E^2-E_1^2-E_2^2+m\omega-\frac{m^2}{3}}{(2|e|\mathcal{E}|E|)^{2/3}}-i0\right]^{3/2}\right)^{1/6} \tag{17}$$

When

$$2|e|\mathcal{E}Ez+E^2-E_1^2-E_2^2+m\omega-\frac{m^2}{3}<0 \tag{18}$$

the last solution presents an exponential decay as:

$$e^{\frac{-2}{3}\left(-\frac{2|e|\mathcal{E}Ez+E^2-E_1^2-E_2^2+m\omega-\frac{m^2}{3}}{(2|e|\mathcal{E}|E|)^{2/3}}\right)^{3/2}} \tag{19}$$

(Note that ϕ in all cases is the time-independent solution)

3 Phenomenological model for color transparency

We have the tools to extend the model [4] to a relativistic case.
Specifically: $P(t) = |< f(r,t)|\Psi_0 >|^2$ because if $P(t)/P(0) = 1$ there exist Color Transparency. Up to now we found:

$$f(r,t) = \sum_n C_n e^{-iE_n t}\Psi_n(r) \qquad and \qquad < r^2 >=< f(r,t)|r^2|f(r,t) > \tag{20}$$

We are currently working on this subject, in particular we are implementing the Lorentz transformations in order to express $\mathcal{E}$ in the $c\bar{c}$ center of mass.

References

[1] Moshinsky, A. Szczepaniak, *J. Phys.* A 22, L817 (1989);

[2] S. Bruce, P. Minning *Nuovo Cim.* A 106, 711 (1993).

[3] V.Dvoeglazov, Preprint EFUAZ 94-02.

[4] J.Blaizot et al., *Phys. Rev* D 45, 814 (1992).

Correlation Functions of the Gluon Field and the Observables in Soft High-Energy Scattering

Flávio I. Pereira
Observatório Nacional , CNPq, Rio de Janeiro, Brazil

Erasmo Ferreira
Instituto de Física, Universidade Federal do Rio de Janeiro
P.O.Box 68528, Rio de Janeiro, 21945-970 RJ, Brazil

July 30, 1996

The profile functions of the eikonal formalism, obtained in the model of the stochastic vacuum from combinations of the two kinds of correlation function of the gluon field, are determined and their properties are discussed. The influence of the correlation functions and their characteristic parameter *correlation length* on the observables of soft high-energy scattering are studied. Values are obtained for the gluon condensate and for the correlation length, and the possibility of the description of the experimental data on total and differential elastic cross-sections at high energies for the pp and $\bar{p}p$ systems is investigated.

In the work here described we rebuild the application of the Stochastic Vacuum Model to high energy pp and $p\bar{p}$ elastic scattering developed before (ref.1) , with the purpose of clarifying and improving the determination of the two fundamental QCD parameters that intervene in the evaluation of the observables of total cross-section and forward slope parameter.

Compared to the previous work on the same subject, this paper presents several important changes in methods and results.

1. The correlation functions

Considerations of Lorentz invariance show that there are two independent gluon correlation functions. We call them D and D_1; with same normalization at zero distance $D(0)=D_1(0)=1$. Lattice calculations (ref. 2) have indicated that these two functions have the same exponential decrease at middle and long distances, and that they intervene in gluon correlations in the ratio 3 to 1, namely we may symbolically write that the gluon correlations are of the form $\kappa D + (1-\kappa)D_1$, with $\kappa = 3/4$. In the previous work of ref.1 only the part corresponding to D has been included in the calculations, and now we take into account both D and D_1 contributions.

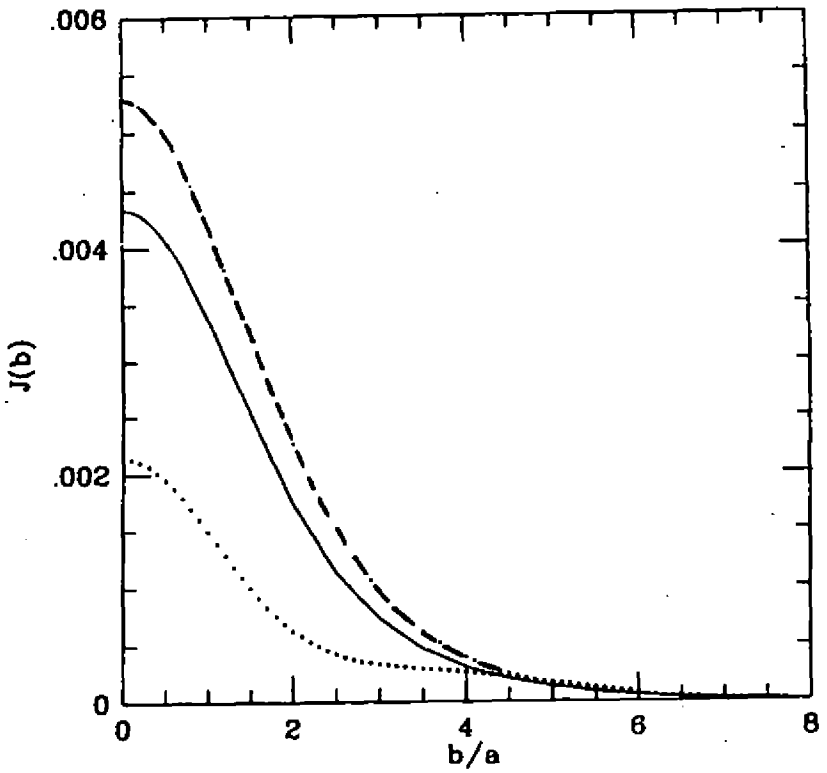

In the impact parameter formalism that we use, the observables are evaluated through the profile functions J(b). In fig.1 we represent the functions J(b) obtained in the cases of pure D (κ=1, in dashed line) , pure D_1 (κ=0, in dotted line) and the mixture with κ=0.75 (solid line). We observe the small magnitude of J(b) for the pure D_1 case, which has justified the neglect of the contributions of this correlation function in previous work.

2. Determination of QCD fundamental quantities

In order to avoid difficulties that may be argued to exist in the interpretation of the value of the gluon condensate which is extracted from lattice calculations, we have now chosen a method that makes use of all existing data on total cross-setions and slope parameters at all energies, showing that the whole collection of these data can be described with a unique choice of values for the QCD parameters of gluon condensate and correlation length.

For a given energy, the fundamental observables are the total cross-section σ_T and the slope parameter B of the differential elastic cross-section. In ref.1 it is shown that the stochastic vacuum model gives expressions for these two quantities in terms of the gluon condensate $\langle g^2\ FF\rangle$, the correlation length a and the hadronic size S (we here consider pp and $\bar{p}p$ scattering only). Using the data for σ_T and B at a given energy, the parameter S can be eliminated from the two expressions, and a curve can be drawn in a figure with a and $\langle g^2\ FF\rangle$ as axes. In fig.2 we draw such curves for the energies 23.5, 62.3, 541 and 1800 GeV. Choosing two energies, and drawing the two corresponding curves, their intersection fixes the values of $\langle g^2\ FF\rangle$ and a. Using all data on pp scattering from CERN ISR (these data range from from $\sqrt{s}$=23.5 to $\sqrt{s}$=62.3 GeV) , and the data on $\bar{p}p$ from CERN SPS (541 GeV) and from the Tevatron ($\sqrt{s}$=1800 GeV), taking all possible pairs of energies, *all* intersections fall in small ranges of values for $\langle g^2\ FF\rangle$ and a : from 2.5 to 4.0 GeV^4 and from 0.28 to 0.34 fermi respectively. These are indeed very reasonable physical ranges for these quantities.

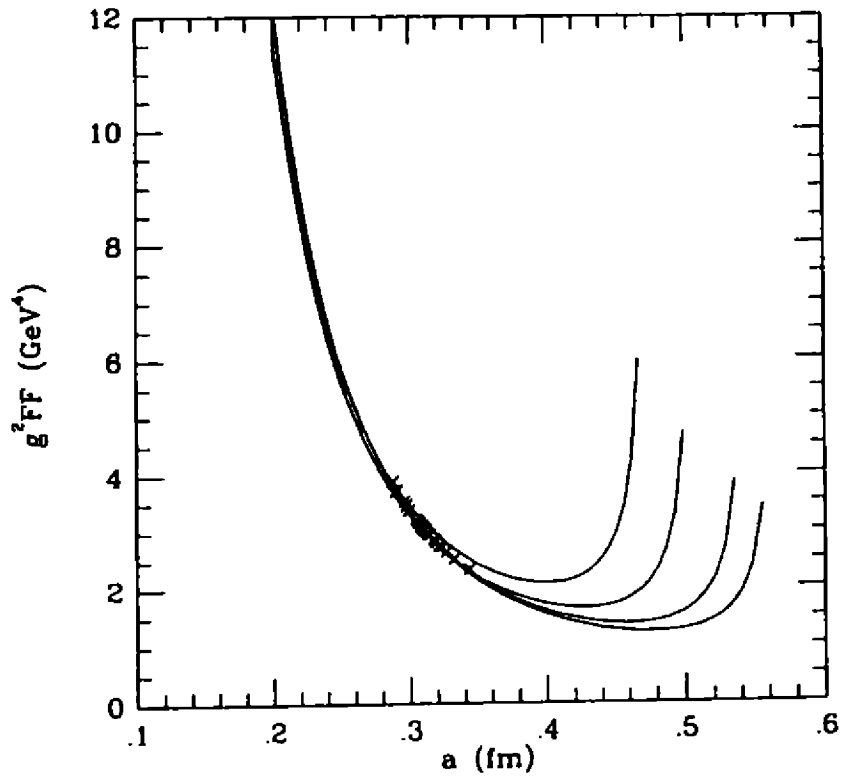

Fig. 2 shows the remarkable clustering of the intersection points along a line. We may be inclined to choose for $\langle g^2\ FF \rangle$ or a an average value taken over the cluster of points. Actually, with some manipulation of the experimental data within their reported error bars we could concentrate the cluster in very small ranges along both axes.

We can easily write an equation for this line of intersection points, which is approximately of the form $\langle g^2 FF \rangle = \text{const}/a^3$. This relation allows us to eliminate one of the two QCD quantities in terms of the other before their final determination is made.

3. Experimental data at high energies

Fig. 3 shows the experimental data for σ_T and B for the pp system at the CERN ISR energies ($\sqrt{s}$ = 23.5, 30.6, 45.0, 52.8, and 62.3 GeV) and for $\bar{p}p$ at 541 GeV (CERN SPS) and 1800 GeV (Fermilab E-710 experiment). At the two lowest energies, instead of the full experimental data, we use the pomeron exchange cross-sections given by the Landshoff-Donnachie parametrization (Ref.3). The line is the result obtained from our model with $a = 0.31$ fm, $\langle g^2 FF \rangle = 3.03$ GeV^4. These values are in the middle of the cluster shown in fig.2, and lead to a good description of the elastic differential cross-sections in the very low t range.

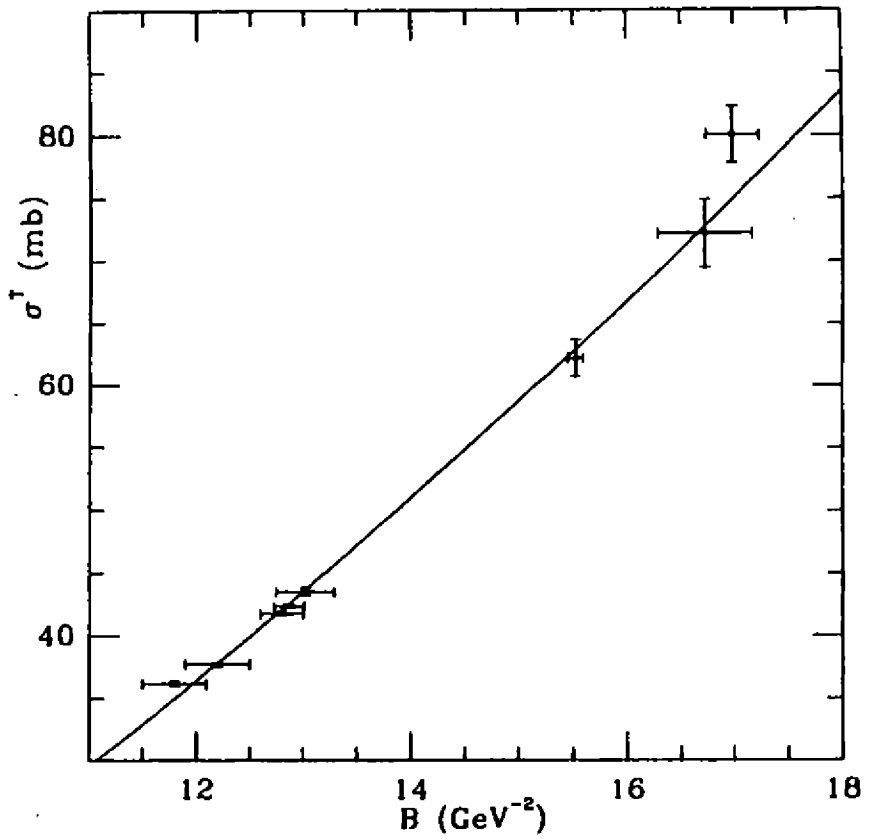

4. Increase of the effective proton radius with the energy

After the QCD parameters are determined, we may return to the original expressions that give the total cross-section in terms of the proton size S, use the experimental values for $\sigma_T(s)$, and determine S as a function of the energy. We find that S increases linearly with log(s).

5. References

Ref. 1 - H.G. Dosch, E. Ferreira and A. Krämer, Phys. Rev. **D50**, 1992-2015 (1994).

Ref. 2 - A.Di Giacomo and H. Panagopoulos, Phys. Lett. **B285**, 133 (1992).

Ref. 3 - A. Donnachie and P.V. Landshoff, Phys. Lett. **B296**, 227 (1992).

Low-Energy Phenomenology in a Class of Calabi-Yau Models

Luis Antonio da Mota*†
Universidade do Estado do Rio de Janeiro,
Instituto de Física - Departamento de Física Teórica,
and
C.B.P.F. - Dr. Xavier Sigaud, URCA, Rio de Janeiro

Received March, 1996

This work presents the last results for the low-energy phenomenology for a class of superstring models, based on Calabi- Yau compactification and with gauge symmetry, at the compactification scale, given by $E_8 x E_6$. Nowadays, there is a fairly precise phenomenology coming out of it. Many phenomenological constraints were imposed in order to determine which of the models was suitable for a description of the "real world".

Introduction

Although the Standard Model has remarkable success when its predictions are compared with experiment, it is thought by many that it corresponds to an effective description of Nature. The reasons for that are now classic and we will not enumerate them. This train of thoughts led to the introduction of many extensions of the Standard Model, namely, Grand Unified Theories (GUTs) and supersymmetric Models (SUSY). One of the criticisms that is made against the Standard Model is that it does not deal with Gravitation. Collecting all these ideas, the motivation for studying the low-energy phenomenology of superstring models is clear, since, besides the fact that they are Supersymmetric-Grand-Unified-Theories (SUSY-GUTs), thus dealing with the main criticisms made to the Standard Model, they also are the only possibly finite and anomaly free quantum description of Gravitation. So, superstring models present themselves as *the* extension to the Standard Model.

One of the major problems in dealing with these models is that nobody knows how to derive the vacuum of the models from the strings. So, one is led to scanning compactified string models looking for consistency with low-energy experiments. Possible candidates are the models resulting from the ten dimensional $E_8 x E_8$ heterotic string compactified on the 3-generation Calabi-Yau manifold of Tian and Yau [1].

Many phenomenological analysis have been performed already on models belonging to this class, we refer the reader to [2] for details and better definition of the class of models. From now on, we are going to concentrate on the most recent results presented in [4]. Of course, these models have, at high energies, a much greater gauge symmetry than the one presented in the Standard Model, so there have to be symmetry-breaking-scales. These are required to: (i) preserve low-energy matt take place along flat directions of the potential; (ii) give heavy masses to all leptoquarks; (iii) keep the standard Higgs and (iv) take place along flat directions of the potential.

The Class of Models

The gauge symmetry of these models is, at high energies, given by E_6 (the other E_8 is the invisible sector relating to the visible one only through gravitational effects). The gauge symmetry is broken (via Wilson-Loops): $E_6 -> SU(3)^3$, after that, we have two intermediate-symmetry-breaking scales: $SU(3)^3 -> SU(3)XSU(2)XSU(2)XU(1) -> S.Model$. The non-sing let matter content of the models is given (at the compactificati by nine families of leptons λ, six families of $\overline{\lambda}$, seven of quarks q and anti-quarks Q and four of $\overline{q}$ $\overline{Q}$. The matter fields are put into **27** of E_6, so

*E-mail: damota@vmesa.uerj.br
†This work was done in collaboration with F. del Aguila e M. Masip, Nuclear Physics B440, pp.3-23 (1995).

$$27- > (1,\overline{3},3) = \lambda + (3,3,1) = q + (\overline{3},1,\overline{3}) = Q$$

The presence of gauge singlet fields was proven to be essential for phenomenological consistency[3]. recently, the couplings were calculated using cohomology techniques of exact spectral sequences[5]. So, with these families of fields, on end up with the Standard Model in the low-energy regime.

Matter-Parity Models

In these string models, one has discrete symmetries constraining the possible couplings appearing in the potential. These symmetries play a very important role. They are part of the matter parity that has to be present. Basically, the models (that already "survived" many phenomenological tests) are divides according to the "kind" of matter parity they show: It has been shown that only two matter parities can be implemented in the class of models that are under investigation here[6]. They correspond to $P_2 = Cg_2$ generating a Z_2 matter parity and $P_3 = Bg_3$, generating a Z_3 discrete group. The B and C appearing above are related to the discrete symmetries[2]. In the case with a discrete symmetry group given by P_3, we find that there are only three patterns of quark mass matrices (consistent with the phenomenological requirements (i)-(iv) above). Unfortunately, none of them can accommodate realistic (observed) quark masses and mixing angles. The problems with these three types of mass matrices are summarized as follows: *type A* - the quark mass matrices are anti-symmetric, due to an exact symmetry, and that would imply that $m_u = 0$ and $m_c = m_t$, thus making these cases unrealistic. *type B* - in this case, the six quark masses can be accommodated but, after a detailed analysis, one can verify that the mixings of the third family are far too small. The relatively large entries with a non-perturbation origin would be in contradiction with our assumptions (phenomenological constraints). *type C* - here the problem is that the u-quark mass is found to be too high. For details (interesting ones) see[4].

In the case with a P_2 matter parity, one can do similar analysis and try to verify if one can find realistic models. For making the analysis simpler, it is more convenient to re-write the potential in terms of C-eigenstates, after doing that, one verifies that we have the following scenario: (i) we can find cases with the same symmetric quark mass matrix problem (patterns A discussed above); (ii) one can find cases where we have massless up-quarks (for absence of the appropriate Yukawa c or we do not have flat directions in the potential. The only interesting case is obtained when the singlet developing VEV has components along the flavour directions (s_1, s_7, s_{13}) (see [4] for the notation). Furthermore, the Higgs responsib intermediate-symmetry-breaking are placed along the flavour directions (λ_1),$(\overline{\lambda}_{1,2})$, (λ_7) and $(\overline{\lambda}_{3,4})$.

So, after careful analysis, this case was singled out as the only one having a realistic phenomenology. In this particular model, the three chiral families of quarks and lepton (after diagonalization of the mass matrices) are found to lie along the following flavour directions:

$$up - quarks : q_3, \alpha_1 q_1 + \alpha_2 q_2 + \alpha_3 q_4, \beta_1 q_6 + \beta_2 q_2 + \beta_3 q_4;$$

$$u^c : u_3^c, \alpha_1 u_1^c + \alpha_2 u_2^c + \alpha_3 u_4^c, \beta_1 u_6^c + \beta_2 u_2^c + \beta_3 u_4^c;$$

$$u^c : d_3^c, \gamma_1 d_1^c + \gamma_2 d_2^c + \gamma_3 d_4^c + \gamma_4 d_6^c, \delta_1 d_5^c + \delta_2 d_2^c + \delta_3 d_4^c + \delta_4 d_6^c;$$

$$lepton - doublets : \epsilon_1 l_1 + \epsilon_2 h_7 + \epsilon_3 h_9, l_6, l_8$$

$$e^c : e_5^c, e_6^c, e_8^c$$

Conclusions

To summarize, we singled out a model as the only one in the whole class being able to provide a realistic low-energy phenomenology. The history of this search is long and we recommend the reader the bibliography in the end of this paper. Basically, the imposition of a set of phenomenological constraints helps us in seeking the "right" vacuum of the string theory. The following set of constraints has to be satisfied

- a model with three-generations
- possibility of intermediate-symmetry-breaking
- no Landau poles
- gauge coupling unification

- correct value for $\sin(\theta)^2$
- light Higgs boson $m_{Higgs} < 1TeV$
- **realistic mass-matrices for the standard fields**
- **realistic CKM-matrix**

The last two constraints (bold) were the strongest ones, eliminating almost all possible cases. They were the last ones to be imposed as well, completing the link from the high energy string theory to the low-energy phenomenology. It is remarkable that such a link could be completed satisfactorily.

References

[1] S.T.Yau, i *Symposium on Anomalies, Geometry and Topology*, ed. W.A.Bardeen and A.R.White (World Scientific,Singapore, 1985).

[2] B.R.Green, K.H.Kirklin, P.Miron and G.G.Ross, **Nuclear Physics, B278** (1986) 667; B.R.Green, K.H.Kirklin, P.Miron and G.G.Ross,**Phys.Lett. B192** (1987) 111; F.del Aguila, G.D.Coughlan and M.Masip, **Phys.lett.B227** (1989) 55; F.del Aguila, G.D.Coughlan and M.Masip,**Nuclear Physics B351** (1991) 90; F.del Aguila, M.Masip and L.A.da Mota, **Phys.lett.B287** (1992) 335;

[3] F.del Aguila, G.D.Coughlan and L.A.da Mota, **Phys.lett.B240** (1990) 389;

[4] F.del Aguila, M.Masip and L.A.da Mota, **Nuclear Physics B440** (1995) 3.

[5] M.G.Eastwood and T.Hubsch, **Commun.Math.Phys. 132** (1992) 57.

[6] G.Lazarides and Q.Shafi,**Nuclear physics, B338** (1990) 442.

A phenomenological model for hadron diffractive dissociation at high energies

R. J. M. Covolan and J. Montanha
Instituto de Física 'Gleb Wataghin', Unicamp
13083-970 Campinas, São Paulo, Brasil

Received March, 1996

A new type of geometrical model is proposed and applied to describe diffractive dissociation processes in soft hadron interactions. Such a model, which is based on a geometric conception of the *Pomeron*-proton cross section and on a set of assumptions derived from the current phenomenology of elastic processes and total cross section, is able to describe a large amount of experimental data of single diffractive processes with just one free parameter. Results for interactions initiated by pp, $\bar{p}p$, $\pi^{\pm}p$ and $K^{\pm}p$ collisions are presented.

In this work we propose a phenomenological model based on the Regge theory [1] that permits an overall description of inelastic diffractive processes initiated by proton-proton and meson-proton collisions. Such an approach is mostly concerned with single diffractive (SD) processes in the soft region ($|t| < 1\ GeV^2$), *i.e.* semihard contributions are beyond the scope of the present work.

The starting point of our analysis is the expression for the double differential cross section for hadron-hadron diffractive dissociation, derived in the context of the Regge theory, which reads

$$\frac{s}{\pi}\frac{d^2\sigma}{dtdM^2} = \frac{[\beta^{\mathbb{P}}_{hh}(t)]^2}{16\pi^2}\left(\frac{s}{M^2}\right)^{2\alpha_{\mathbb{P}}(t)-1}\sigma_{\mathbb{P}h}(M^2,t), \tag{1}$$

where $\beta^{\mathbb{P}}_{hh}(t)$ is the pomeron-hadron coupling factor, $\alpha_{\mathbb{P}}(t)$ is the pomeron trajectory and $\sigma_{\mathbb{P}h}(M^2,t)$ is the pomeron-hadron cross section.

Since the formalism does not provide these three functions, we'll propose here some 'prescriptions' to get them. Such prescriptions should be taken as general statements that should be valid for all hadron-hadron dissociation processes.

1. Analyses of elastic scattering and total cross section data seem to favor a linear trajectory, $\alpha_{\mathbb{P}}(t) = 1+\epsilon+\alpha' t$, with $\epsilon = 0.08$ and $\alpha' = 0.25$.

2. The pomeron-hadron coupling factor, in this approach, depends basically on three quantities, *i.e.* $\beta^{\mathbb{P}}_{hh}(t) = n_h\ \beta_h\ G_h(t)$, where

   n_h — number of valence quarks in a hadron h; β_h — pomeron-hadron coupling constant; $G_h(t)$ — form factor of the interacting hadron.

3. We assume $\sigma_{\mathbb{P}h}$ as proportional to the mean squared radius ($\langle r_h^2 \rangle$) of the interacting hadron as it is 'seen' by elastic scattering or, in other words, as proportional to the slope of the elastic diffraction peak, $\sigma_{\mathbb{P}h} = \delta\ \langle r_h^2 \rangle$, where δ is a normalization parameter.

In order to compare the predictions of the model with experimental data we have to fix the parameters required in each case. As much as possible, we try to do that by taking these parameters as established in other contexts or in independent analyses.

The coupling constant β_h, for instance, is taken from the connection between elastic scattering amplitude and total cross section. By the optical theorem, we have

$$\frac{d\sigma_{el}}{dt}|_{t=0} = \frac{\sigma_{tot}^2}{16\pi}(1+\rho^2) \simeq \frac{\sigma_{tot}^2}{16\pi} \tag{2}$$

Now, using the proton-proton elastic scattering amplitude at the Born level, we can write

$$\frac{d\sigma_{el}}{dt} = \frac{[3\,\beta_p G_p(t)]^4}{16\pi}(\frac{s}{s_0})^{2\alpha_{\mathbb{P}}(t)-2} \tag{3}$$

and

$$\frac{d\sigma_{el}}{dt}|_{t=0} = \frac{(3\,\beta_p)^4}{16\pi}(\frac{s}{s_0})^{2\epsilon}, \tag{4}$$

where s_0 is a scale parameter ($s_0 = 1\ GeV^2$). From (2) and (4), we have

$$\sigma_{tot,\mathbb{P}} \overset{s\to\infty}{\approx} 9\,\beta_h^2\,(\frac{s}{s_0})^{\epsilon}. \tag{5}$$

Some time ago, Donnachie and Landshoff [2] have shown that it is possible to accommodate the behavior of the total cross section data of several hadron-proton processes in a general expression,

$$\sigma_{tot}^{hp} = Ys^{\epsilon} + Zs^{-\nu}, \tag{6}$$

where the first term comes from the pomeron exchange, while the second one represents all secondary reggeon contributions. As we are adopting here the same ϵ (= 0.08) adopted by them [2], by comparison between (5) and (6) we can obtain β_p directly from their fitted parameters, *i.e.* $\beta_p^2 = Y/9$.

For meson-proton elastic scattering, we write

$$\frac{d\sigma_{el}}{dt} = \frac{[2\,\beta_m G_m(t)]^2[3\,\beta_p G_p(t)]^2}{16\pi}(\frac{s}{s_0})^{2\alpha_{\mathbb{P}}(t)-2}, \tag{7}$$

and follow analogous procedure to obtain $\beta_m^2 = Y^2/(36\,\beta_p^2)$.

In so doing, from the Y parameters given in ref.[2] we get $\beta_p^2 = 6.19\ GeV^{-2}$; $\beta_\pi^2 = 5.50\ GeV^{-2}$; $\beta_K^2 = 4.14\ GeV^{-2}$.

For the electric form factor, we have assumed a general dipole formula corresponding to the quasi-elastically scattered particle, that is: $G_h(t) = 1/(1-t/\mu_h^2)^2$, where, for protons (antiprotons), pions, and kaons, we have $\mu_p^2 = 0.71\ GeV^2$; $\mu_\pi^2 = 0.92\ GeV^2$; $\mu_K^2 = 1.45\ GeV^2$.

Now, in order to obtain the pomeron-hadron cross section we must establish the mean squared radius of the hadron interacting at the inelastic vertex. For this purpose, we use two relations found out by Povh and Hüfner [3]:

1. for protons (and antiprotons), we use $\langle r_p^2(s)\rangle = \frac{3}{2}b_{pp}(s)$, where $b_{pp}(s)$ is the slope of the diffractive peak in (anti)proton-proton elastic scattering;

2. for other hadrons (in this paper, π and K), we use $\langle r_h^2(s)\rangle = \langle r_p^2(s)\rangle\ \sigma_{tot,\mathbb{P}}^{hp} / \sigma_{tot,\mathbb{P}}^{pp}$.

For a matter of consistency, we adopt for the slope the following parametrization, $b_{pp}(s) = 11.13 + 0.5\ ln(s/s_0)$, which corresponds to the definition $b \equiv d/dt\ ln[d\sigma/dt]|_{t=0}$ applied to eq.(3).

At this point, the only undefined quantity is the δ parameter. We determine this parameter by fitting the data of pp diffractive invariant cross section at 23.5 GeV measured by the CHLM Collab. at ISR. The value of δ was found to be $\delta = 0.467$.

With this parameter fixed, we are able to describe the invariant cross section data for the entire ISR's energy range, as shown in Fig.1a, together with the Collider results (Fig.1b), in fair way. In order to analize diffractive

dissociation of proton in meson-proton collisions, we use data of the EHS/NA22 Collab. [6], obtained at $\sqrt{s} = 21.5\ GeV$ and $-t = 0.25\ GeV^2$ (Fig. 2), and we find a good agreement between the data and the model. Also in the case where the proton is quasi-elastically scattered and the meson dissociates, our results agree very well with R. L. Cool *et al.* [7] measurements (Fig.3).

References

[1] P. D. B. Collins: *An Introduction to Regge Theory and High Energy Physics*, Cambridge University Press, Cambridge (1977).

[2] A. Donnachie and P. V. Landshoff: Phys. Lett. B **296**, (1992) 227.

[3] B. Povh and J. Hüfner: Phys. Rev. Lett. **58** (1987) 1612; Phys. Rev. D **46** (1992) 990.

[4] M. G. Albrow *et al.*, CHLM Collab.: Nucl. Phys. **B108** (1976) 1.

[5] M. Bozzo *et al.*, UA4 Collab.: Phys. Lett. **136B** (1984) 217, Phys. Lett. **186B** (1987) 227.

[6] M. Adamus *et al.*, EHS/NA22 Collab.: Z. Phys. C **39** (1988) 301.

[7] R. L. Cool *et al.*: Phys. Rev. Lett. **47** (1981) 701.

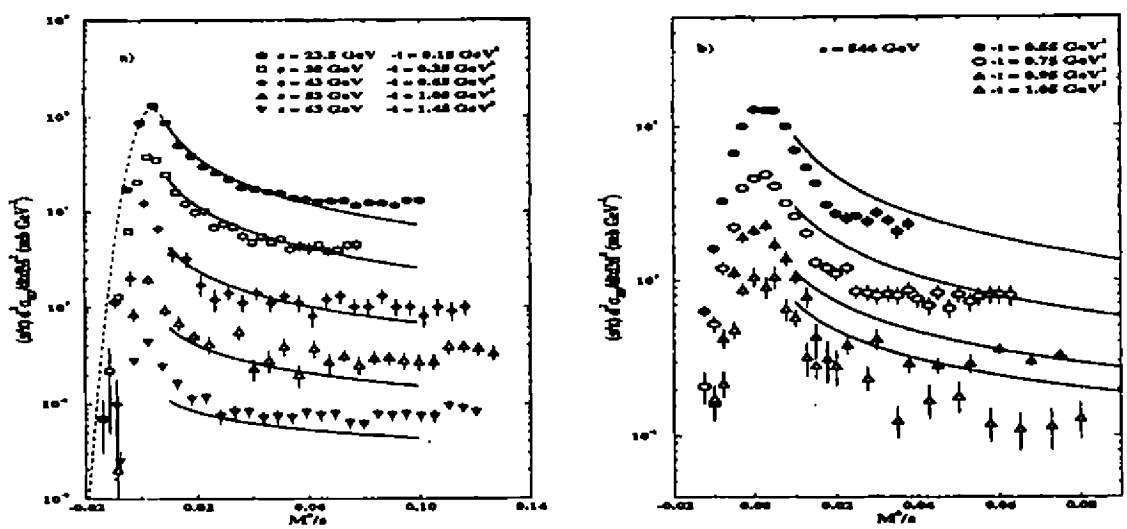

Figure 1:
Results for the invariant cross section distribution $(s/\pi)\, d^2\sigma_{SD}/dtdM^2$ with M^2/s, as given by the model together with some data from: a) ISR [4] and b) Collider [5].

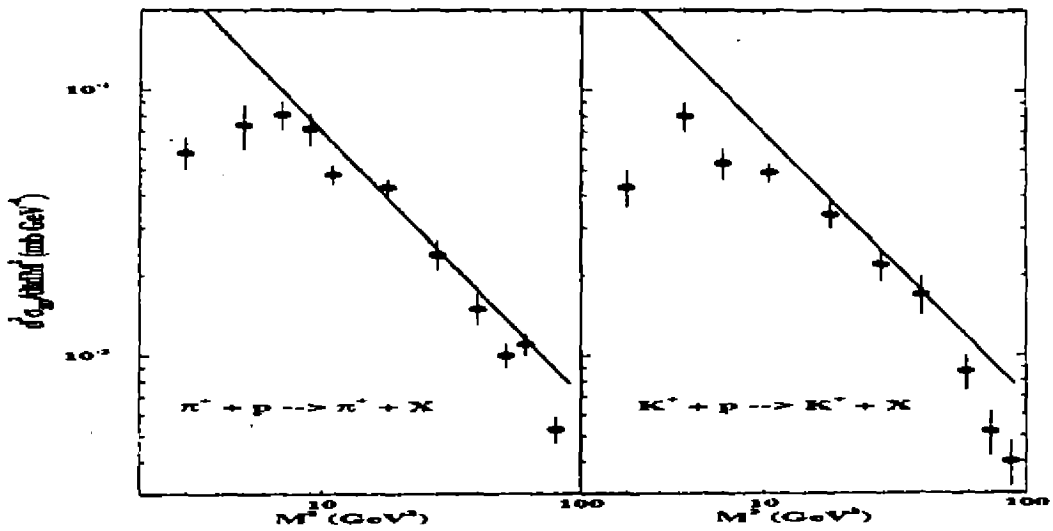

Figure 2:
Results for the non invariant cross section distribution $d^2\sigma_{SD}/dtdM^2$ for $\sqrt{s} = 21.5\ GeV$ and $-t = 0.25\ GeV^2$ as a function of M^2 for the diffraction dissociation of p in π^+p and K^+p reactions as given by the model together with data from NA22 Collaboration.

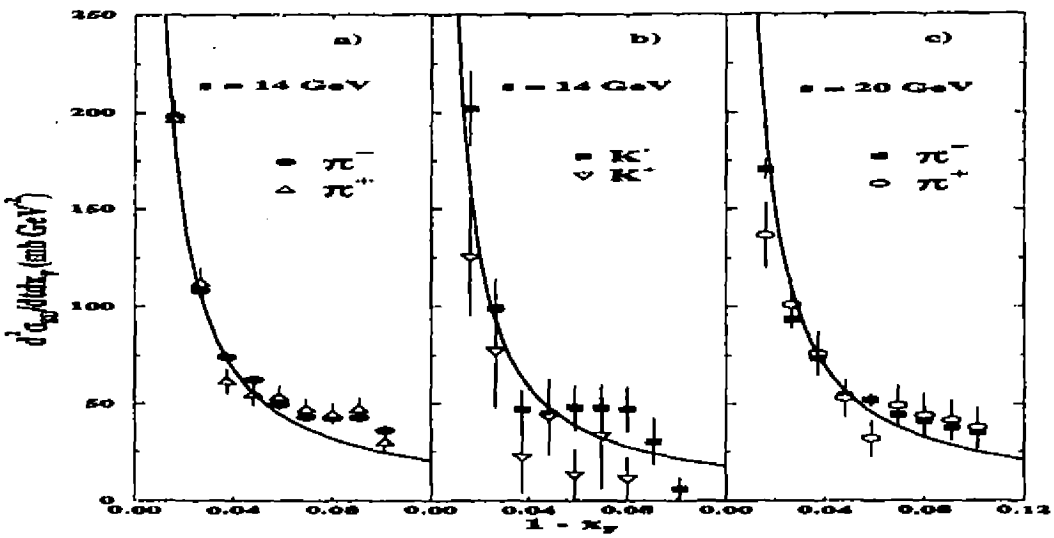

Figure 3:
Results for the invariant cross section distribution $(s/\pi)\, d^2\sigma_{SD}/dtdM^2$ as a function of M^2/s for the diffraction dissociation of π^+, π^-, K^+ and K^- in $\pi^\pm p$ and $K^\pm p$ reactions as given by the model together with data from [7] at $\sqrt{s} = 14\ GeV$ and $\sqrt{s} = 20\ GeV$ and $-t = 0.05\ GeV^2$.

Universality tests for total cross sections

J. Bellandi, A. A. Perez
Instituto de Física Gleb Wataghin-Unicamp,
Cx. Postal 6165, 13083-970, Campinas-SP-Brasil
J. Dias de Deus
Departamento de Física and CENTRA, IST
Av. Rovisco Pais, 1096 Lisboa Codex, Portugal
and
A. B. de Pádua
Departamento de Física, UEL, 86051-970 Londrina-PR-Brasil

Received March, 1996

Starting directly from data we test the universality of the decomposition of total cross section in an asymptotically dominant term, the Pomeron, and a non dominant one, the Reggeon. Without assuming Regge pole model behavior or additive quark model relations we show that data are compatible with both models. Support is not found for models predicting asymptotic equality of total cross sections.

The understanding of the high energy behavior of hadron-hadron collisions remains an open theoretical question of QCD. As the long distance behavior is necessarily present, a pure perturbative treatment, starting from the asymptotic freedom limit, is most certainly not sufficient and non perturbative QCD may have to be included in an essential way. In any case, some universality features, due to the color structure of the theory, must be present in the data.

We do not intend to address here the important and general problem of QCD in soft high energy physics (see [1] for a recent review) but simply to ask, looking directly at data, what conclusions can be drawn concerning universality in high energy elastic scattering data, namely, in total cross sections.

Two very simple models will be taken as reference: the Regge Pole Model (RPM), in the version of Donnachie and Landshoff [2], and the Generalized Additive Quark Model (GAQM), in the version developed in [3]. Both models propose an asymptotically dominating term, the Pomeron, σ^P, and another term decreasing with energy, the Reggeon, σ^R.

In the RPM the emphasis is on the Regge pole behavior of the two components,

$$\sigma^P \sim s^{\alpha_P - 1}, \qquad \sigma^R \sim s^{\alpha_R - 1} \tag{1}$$

α_P and α_R being the intercepts of the Pomeron and Reggeon trajectories, respectively. In the GAQM the emphasis is on relations between total cross sections, for instance [4, 3],

$$\frac{\sigma_{\pi p}}{\sigma_{pp}} = \frac{6}{9} = \frac{2}{3} \tag{2}$$

and

$$(\sigma_{\bar{p}p} - \sigma_{pp}) = 5\,(\sigma_{\pi^- p} - \sigma_{\pi^+ p}) = \frac{5}{2}\,(\sigma_{K^- p} - \sigma_{K^+ p}) = \frac{5}{4}\,(\sigma_{\bar{p}n} - \sigma_{pn})\,. \tag{3}$$

It should be stressed that both models, RPM and GAQM, are at most reasonable approximations as, for instance, multiple scattering absorptive corrections are not included.

We shall write the total cross-section $\sigma(s)$ for a process ab in the form

$$\sigma_{ab}(s) = P_{ab}\sigma^P(s) + R_{ab}\sigma^R(s)\,, \tag{4}$$

where $\sigma^P(s)$ and $\sigma^R(s)$ are, possibly universal, cross sections and the normalization is such that for $\bar{p}p$ we have

$$\sigma_{\bar{p}p}(s) = 9\sigma^P(s) + 5\sigma^R(s)\,. \tag{5}$$

The numbers 9 and 5 are suggested by the GAQM (9 combinations of quark pairs in $\bar{p}p$ and pp, 5 possibilities for quark-antiquark annihilation in $\bar{p}p$).

From the analysis of experimental data made in [2], using Eq.(1), the resulting values for P_{ab} and R_{ab} are the ones presented in Table 1. The values of P_{ab} and R_{ab} of GAQM are also presented in Table 1. Flavor breaking factors in P_{ab} were not included. A parameter u, not fixed by the model, measures the ratio of the forward imaginary parts of the $\bar{q}q$ annihilation amplitudes in the channels u and s, respectively. In general one expects

$$u < 1, \tag{6}$$

the limit $u = 0$ corresponding to strong exchange degeneracy [5]. It should be mentioned that the relations in Eq.(3) are independent of u. Finally, in both models, RPM and GAQM, it is supposed that $P_{ab} = P_{\bar{a}b}$ (Pomeranchuk theorem).

Our strategy here is to go beyond RPM and GAQM and directly test the structure of Eq.(4), with universality of $\sigma^P(s)$ and $\sigma^R(s)$, by looking at data without making use neither of assumption in Eq.(1) nor assumptions in Eq.(2) and Eq.(3).

In order to test the universality of $\sigma^R(s)$ it is enough to consider the positive differences

$$\Delta\sigma_{ab} \equiv \sigma_{\bar{a}b} - \sigma_{ab} > 0. \tag{7}$$

By comparing hadron hp and $\bar{h}p$ processes to pp and $\bar{p}p$ we obtain

$$\Delta\sigma_{pp} = A_h \Delta\sigma_{hp} \tag{8}$$

with

$$A_h \equiv \frac{R_{\bar{p}p} - R_{pp}}{R_{\bar{h}p} - R_{hp}}, \tag{9}$$

A_h being a constant and $A_p = 1$. The parameterization in Eq.(4) thus requires the linear relation in Eq.(8). Plots of $\Delta\sigma_{pp}$ vs. $\Delta\sigma_{\pi p}$, $\Delta\sigma_{Kp}$, $\Delta\sigma_{np}$ are presented in Figs. 1a), 2a) and 3a). The experimental values of A_h and the values from the models RPM and GAQM are given in Table 2.

In order to extract the Pomeron component we shall write

$$\sigma^P_{hp} = \alpha_h \sigma_{hp} - (\alpha_h - 1)\,\sigma_{\bar{h}p} = \sigma_{\bar{h}p} - \alpha_h \Delta\sigma_{hp} \tag{10}$$

with

$$\sigma^P_{hp} = P_{hp}\sigma^P \tag{11}$$

and

$$\alpha_h = \frac{R_{\bar{h}p}}{R_{\bar{h}p} - R_{hp}} \geq 1. \tag{12}$$

By comparing Eq.(10) with the equivalent equation for σ^P_{pp} and introducing the parameter γ_h,

$$\gamma_h = \frac{\sigma^P_{hp}}{\sigma^P_{pp}} \equiv \frac{P_{hp}}{P_{pp}} = const., \tag{13}$$

with $\gamma_p \equiv 1$, one obtains

$$\Delta\sigma_{pp} = \frac{1}{\alpha_p \gamma_h}\left[\alpha_h \Delta\sigma_{hp} + (\gamma_h \sigma_{\bar{p}p} - \sigma_{\bar{h}p})\right]. \tag{14}$$

Consistency of Eq.(14) with Eq.(8) requires

$$\gamma_h \sigma_{pp} - \sigma_{\bar{h}p} = B_h \Delta\sigma_{hp}. \tag{15}$$

In other words, $\gamma_h \sigma_{\bar{p}p} - \sigma_{\bar{h}p}$ must depend linearly on $\Delta\sigma_{hp}$, with

$$B_h = \frac{\gamma_h R_{\bar{p}p} - R_{\bar{h}p}}{R_{\bar{h}p} - R_{hp}} = const., \tag{16}$$

and $B_p = 0$.

In the test of Eq.(15) for various reactions the parameter γ_h was varied and adjusted to reproduce, as best as possible, a linear relations, going through the origin, between $\gamma_h \sigma_{\bar{p}p} - \sigma_{hp}$ and $\Delta\sigma_{hp}$. In Fig. 1b), 2b) and 3b) we present the fits using Eq.(15) and in Table 3 the values of γ_h and B_h experimentally obtained and the ones of RPM and GAQM. One may ask if the tests in Eq.(8) and Eq.(15) or the knowledge of A_h, γ_h and B_h for different reactions, are enough to construct the true "experimental" Pomeron, $\sigma^P(s)$, and Reggeon, $\sigma^R(s)$. Th

In fact, from Eq.(14), Eq.(15) and Eq.(8), we obtain

$$\alpha_h = A_h \alpha_p \gamma_h - B_h. \tag{17}$$

Eq.(17) tells us that α_p and α_h are not determined by knowledge of A_h, γ_h and B_h. The constraints in Eq.(8) and Eq.(15) are *not enough* to fix $\sigma^P(s)$. This can be easily seen in a different way. If one makes the transformation

$$\begin{aligned} \sigma^P &\rightarrow \sigma'^P \equiv \sigma^P + k\sigma^R \\ \sigma^R &\rightarrow \sigma'^R \equiv (1-k)\,\sigma^R \end{aligned} \tag{18}$$

σ_{hp} becomes;

$$\sigma_{hp} = P_{hp}\sigma^P + R_{hp}\sigma^R = P'_{hp}\sigma'^P + R'_{hp}\sigma'^R \tag{19}$$

with

$$\begin{aligned} P'_{hp} &= P_{hp} \\ R'_{hp} &= \frac{R_{hp} - kP_{hp}}{1-k}. \end{aligned} \tag{20}$$

It is straightforward to see that the transformation in Eq.(18), with Eq.(19) and Eq.(20), leaves A_h, γ_h and B_h invariant. For this reason it is not possible to extract unambiguously from data the normalization an the energy dependence of $\sigma^P(s)$ and $\sigma^R(s)$. Eq.(1) is just a possibility.

It is clear that the tests in Eq.(8) and (15) are fairly well satisfied by the data, as can be seen by the quality of our linear fits. So far, we find no indication of deviations from the ansatz Eq.(4). In addition, the quark model relations Eq.(2) and Eq.(3) are approximately satisfied. On the other hand, the results of [2] satisfy reasonably well the universality tests, agreeing with the quark model for relations in Eq.(2) and Eq.(3) giving reasonably values for B_h (the GAQM with $u \sim 0.4$ is also acceptable). Better data - and more data, in particular at higher energy for πp and Kp - are needed in order to have more definitive conclusions. However, the fact that the linear fits with Eq.(8) and Eq.(15) work is in itself highly nontrivial and brings strong support to the universal ansatz Eq.(4).

Another conclusion of this work is that proposed asymptotic equality of total cross sections, $\sigma_{ab}(s) \rightarrow \sigma_{pp}(s)$, [6, 7] does not seem to be favored by data.

An extended version of this work including a discussion on the near forward direction elastic scattering data and on the validity of geometrical models is under preparation.

Acknowledgments

We would like to thank FAPESP and CNPq from Brasil and JNICT from Portugal for financial support.

References

[1] O. Nachtmann, Non perturbative QCD Effects in High Energy Collisions, Heidelberg preprint, HD-THEP-94-42, Talk presented at the 18^{th} Johns Hopkins Workshop, Florence, 1994.

[2] A. Donnachie and P. V. Landshoff, Phys. Lett. **B296** (1992).

[3] J. Dias de Deus, Lett. Nuovo Cimento, **5** (1972) 296

[4] E. M. Levin and L. L. Frankfurt, JETP Lett. **2** (1965) 2; H. J. Lipkin and F. Scheck, Phys. Rev. Lett. **16** (1966) 71.

[5] P. D. B. Collins, An Introduction to Regge Theory, Cambridge University Press, Cambridge, U. K., 1977.

[6] M. Froissart, Phys. Rev. **123** (1961) 1053; A. Martin in 9^{th} Blois Workshop on Elastic and Diffractive Scattering, Brown University, 1993, CERN TH-7093/93.

[7] J. Hüfner and B. Povh, Phys. Rev. **D46** (1992) 990.

[8] M. Kamran, Phys. Rep. **108** (1984) 276.

Table 1

	RPM		GAQM	
Process	P_{ab}	R_{ab}	P_{ab}	R_{ab}
$\bar{p}p$	9	5	9	5
pp	9	2.85	9	$5u$
$\pi^- p$	5.65	1.83	6	$2+u$
$\pi^+ p$	5.65	1.40	6	$1+2u$
$K^- p$	4.90	1.34	6	2
$K^+ p$	4.90	0.41	6	$2u$
$\bar{p}n$	9	4.71	9	4
pn	9	2.78	9	$4u$

Table 2

A_h	EXP.	RPM	GAQM
A_π	6.04 ± 0.24	5.00	5
A_K	2.52 ± 0.05	2.31	2.5
A_n	1.32 ± 0.05	1.11	1.25

Table 3

	EXP		RPM		GAQM	
hp	γ_h	B_h	γ_h	B_h	γ_h	B_h
πp	0.62 ± 0.15	3.27 ± 0.15	0.63	3.04	2/3	$\frac{4/3-u}{1-u}$
Kp	0.53 ± 0.08	1.28 ± 0.03	0.54	1.49	2/3	$\frac{2/3}{1-u}$
np	1.02 ± 0.38	0.38 ± 0.04	1	0.15	1	$\frac{1/4}{1-u}$

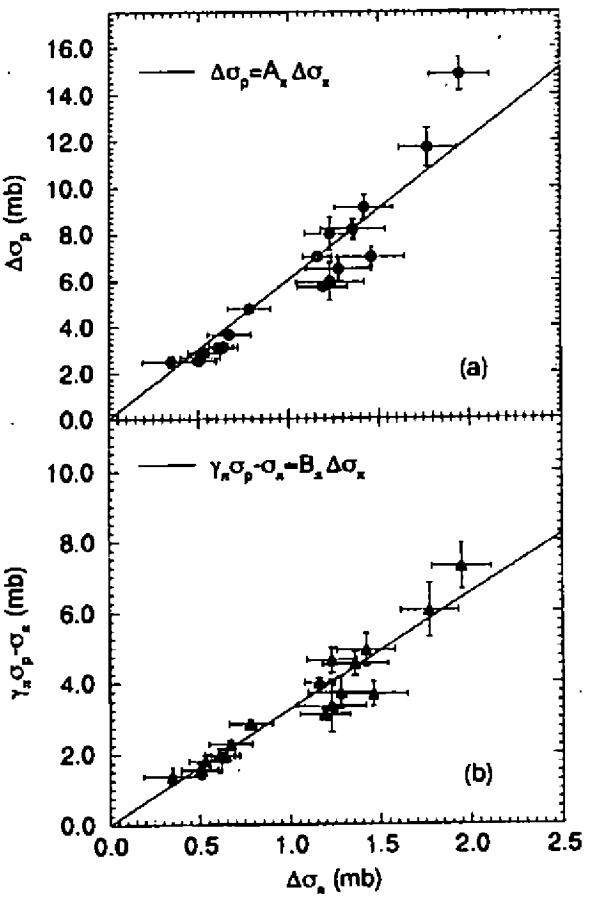

Fig. 1: Universality relations for πp vs. pp, a) Test of Eq.(8): $\Delta\sigma_{pp} = A_\pi \Delta\sigma_{\pi p}$, b) Test of Eq.(15): $\gamma_\pi \sigma_{pp} - \sigma_{\pi^- p} = B_\pi \Delta\sigma_{\pi p}$. The experimental and theoretical values of the parameter, A_π, γ_π and B_π, are given in Table 1 and Table 2. For experimental data see [8].

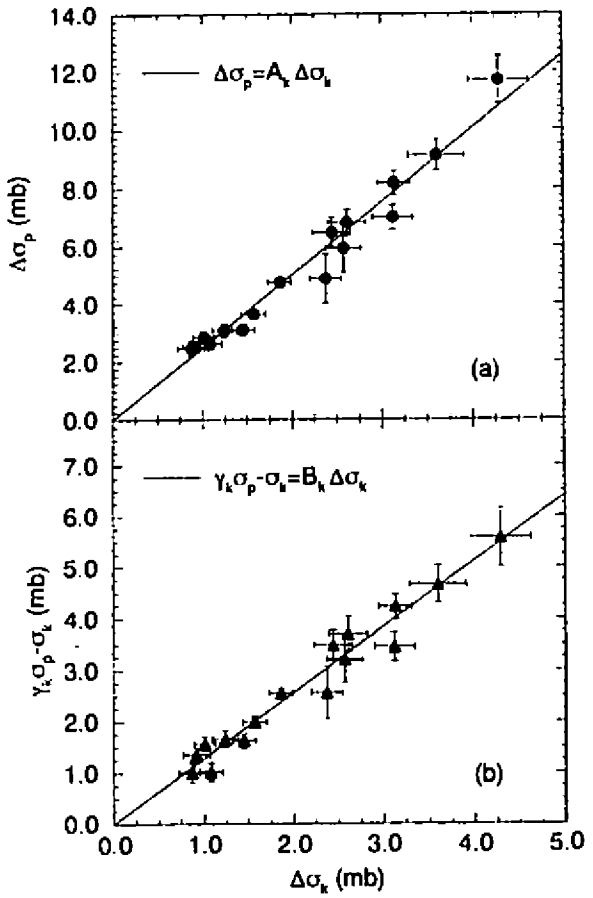

Fig. 2: Universality relations for Kp vs. pp, a) Test of Eq.(8): $\Delta\sigma_{pp} = A_K\Delta\sigma_{Kp}$, b) Test of Eq.(15): $\gamma_K\sigma_{pp} - \sigma_{K^-p} = B_K\Delta\sigma_{Kp}$. The experimental and theoretical values of the parameters, A_K, γ_K and B_K, are given in Table 2 and Table 3. For experimental data see [8].

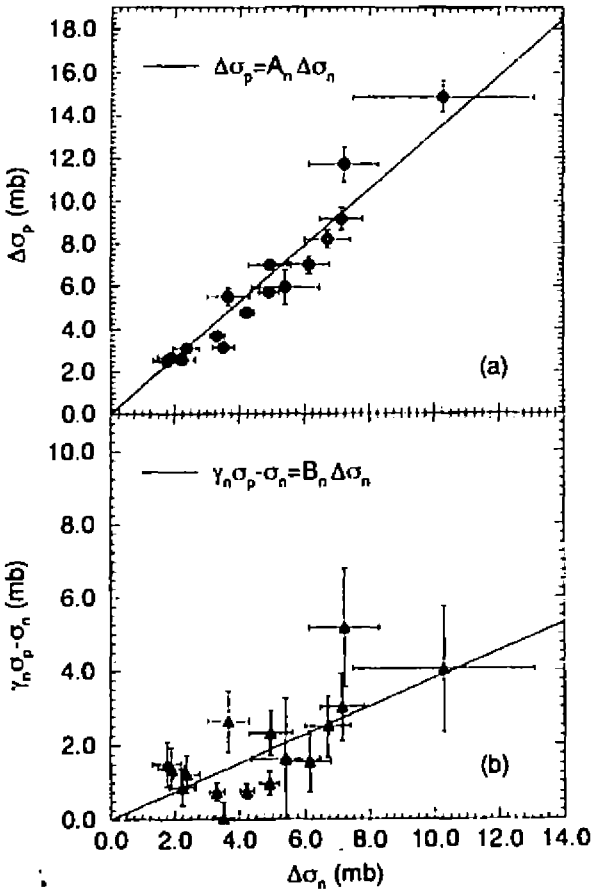

Fig. 3: Universality relations for np vs. pp, a) Test of Eq.(8): $\Delta\sigma_{pp} = A_n\Delta\sigma_{np}$, b) Test of Eq.(15): $\gamma_n\sigma_{pp} - \sigma_{pn} = B_n\Delta\sigma_{np}$. The experimental and theoretical values of the parameters, A_n, γ_n and B_n, are given in Table 2 and Table 3. For experimental data see [8].

Inelastic Overlap Functions in Geometrical Models of Elastic Hadron Scattering *

P.C. Beggio and M.J. Menon
Instituto de Física "Gleb Wataghin"
Universidade Estadual de Campinas (UNICAMP) - SP

Received March, 1996

We present a comparative analysis of the Inelastic Overlap Functions predicted by three geometrical models: Glauber-Velasco, Chou-Yang and Menon-Pimentel. Similarities and differences concerning optical and geometrical aspects are discussed for both pp and $\bar{p}p$ elastic scattering, in the wide range from ISR to Tevatron energies. Comparisons with experimental extraction of the Inelastic Overlap Functions by fit procedures are also presented and discussed.

1 - Introduction

In the Geometrical Approach to high energy hadron scattering, the Inelastic Overlap Function (G_{in}) represents the probability of ocurrence of absorption (inelastic process) as function of the energy and impact parameter [1]

$$\sigma_{in}(s) = \int bdbG_{in}(b,s), \tag{1}$$

where b is the impact parameter, $\sqrt{s}$ the center-of-mass energy, $\sigma_{in}(s)$ the inelastic cross section. The s-channel unitarity connects $G_{in}(b,s)$ with the Profile Function $\Gamma(b)$ (the Fourier transform of the elastic scattering amplitude) through the unitarity condition [1]

$$2Re\Gamma(b,s) = \mid \Gamma(b,s) \mid^2 + G_{in}(b,s) \tag{2}$$

and so with the eikonal, $\Omega(b,s)$, by

$$\Gamma(b,s) = 1 - exp[-\Omega(b,s)]. \tag{3}$$

In the first order Multiple Diffraction Theory (Glauber) the eikonal is expressed by [2]

$$\Omega(b,s) = C \int qdqJ_0(qb)G_AG_Bf, \tag{4}$$

where $G_{A,B}$ are the hadronic form factors, f the elementary (parton-parton) amplitude and C the absorption factor.

Geometrical models are usually distinguished by the phenomenological choices for $G_{A,B}$ and f. Once this is done and the free parameters involved determined by fit to experimental data, (3) and (2) lead to the determination of G_{in} in terms of the eikonal (4):

$$G_{in}(b,s) = 1 - exp[-2Re\Omega(b,s)] = 1 - \mid exp[-\Omega(b,s)] \mid. \tag{5}$$

2 - Predictions from Geometrical Models

Among the various geometrical aprroaches, the Glauber-Velasco (GV), Chou-Yang (CY) and Menon-Pimentel (MP) models are simple and reproduce the general features of data with a reasonably small number of free parameters. Table 1 summarize the choices for $G_{A,B}$ and f in each model.

*Financial Support: CNPq

Model	$G_{A,B}$	f
G-V	eletromagnetic BSWW	$e^{i\phi(q)}[1+aq^2]^{-\frac{1}{2}}$
C-Y	$[1+q^2/m^2(s)]^{-2}$	1
M-P	$[1+q^2/\alpha(s)^2]^{-1}[1+q^2/\beta]^{-1}$	$[1-q^2/a^2][1+q^4/a^4]^{-1}$

Table 1 - Form factors and elementary amplitudes in Glauber-Velasco [3], Chou-Yang [4] and Menon-Pimentel [5] models.

In the GV model the phase $\phi(q)$ is null at collider energies and has the dependence $\phi(q) = (b_1 q^2 + b_2 q^4)$ at ISR. The predictions for G_{in}, scanned from G. Matthiae [1], are presented in Figure 1.a for pp at 52.8 GeV and $\bar{p}p$ at 546 GeV and 1.8 TeV.

For the other two models we performed all the calculation. In the case of MP we made use of the parametrizations for the free parameters from reference [5]. The results for pp at 23.5 GeV and 52.8 GeV and $\bar{p}p$ at 546 GeV and 1.8 TeV are shown in figure 1b. Following Chou and Yang [4], with the values of the free parameters from fits at 23.5 and 546 GeV [4], we carried out linear regressions of the form

$$C(s) = a_1 + a_2 ln(s), \tag{6}$$

$$\frac{1}{m^2} = b_1 + b_2 ln(s), \tag{7}$$

obtaining a_1=2.19, a_2=1.24, b_1=0.837 and b_2=0.072 (all in GeV^{-2}). With this we calculate G_{in} at the same 4 energies referred before. The results are shown in figure 1c.

3 - Experimental Extractions

Through direct fit to experimental data, the G_{in} may be calculated in a model independent way. With suitable parametrizations for the scattering amplitude (sum of exponentials, in general) fits are made to the differential cross section data, so as to furnish the profile function and then G_{in} through eq. (2). In this case the intervals in the transferred momentum with data available play a central role in the accuracy of the result. In this communication we will limit the discussion to pp scattering at 52.8 GeV since it corresponds to the widest range with data available (up to 10 GeV^2).

We shall make use of results from two different fit procedures: Amaldi and Schubert [6] and Carvalho and Menon [7]. The results for G_{in} are shown in part (a) of figure 2. We did not inclued the errors estimated by Amaldi and Schubert which become important above 3.0 fm.

4 - Conclusions

From figure 1 we see that above b$\sim$ 1.5 fm all models predict a dependence on b which is very close to an exponential. However, as the energy increases, the GV results show a uniform shift to large radii and differently, CY and MP predict expanding slopes.

Comparisons with fit results in figure 2 show similar predictions up to b$\sim$ 2.0 fm and at 2.0 $\leq$ b $\leq$ 3.0 fm, the results seems to favour CY and MP models. Above 3.0 fm the errors become important and must be correctly estimated in order to allows quantitative conclusions.

References

1. U. Amaldi, M. Jacob, G. Matthiae, Ann. Rev. Nucl. Sci **26** (1976) 385;G. Matthiae, Rep. Prog. Phys. **57** (1994) 743.
2. R.J. Glauber, in Lectures in Theoretical Phisycs, Vol.I, Ed. W.E. Brittin et al. (interscience, New York, 1959) pp.315-414; M.J. Menon, Phys. Rev. **D48** (1993) 2007.
3. R.J. Glauber, J. Velasco, in Proc 2nd Int. Conf. on Elastic and Diffractive Scattering (editions Frontieres, Gif-sur-Yvette, 1988); Phys. Rev. Lett. **B147** (1984) 380.
4. T.T. Chou, C.N. Yang, Phys. Rev. Lett. **B224** (1990) 113.
5. M.J. Menon and B.M. Pimentel, Hadronic J. **16** (1993) 137; M.J. Menon, Nucl. Phys. B (Proc.Suppl.) **25B** (1992) 94.

6. U. Amaldi and K.R. Schubert, Nucl. Phys. **B166** (1980) 301.

7. P.A.S. Carvalho and M.J. Menon, "Experimental extraction of the proton profile at the highest energies", these proceedings.

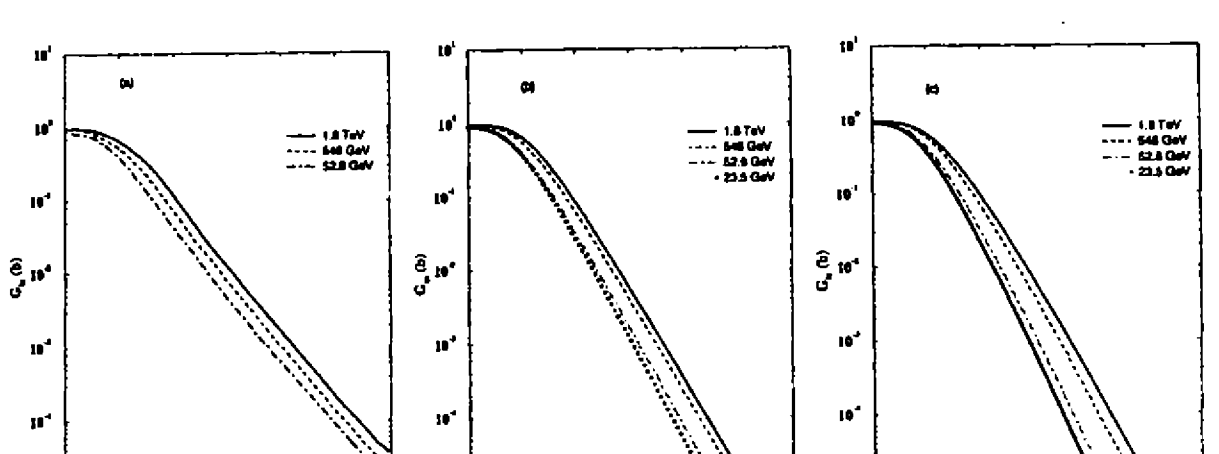

Figure 1 - Predictions for the G_{in}: a) Glauber and Velasco, b) Menon and Pimentel and c) Chou and Yang.

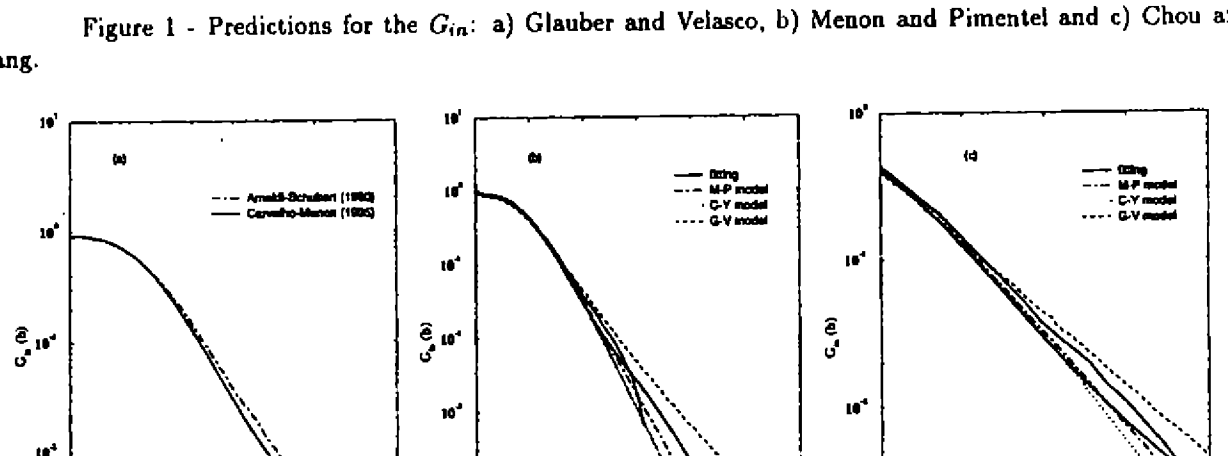

Figure 2 - G_{in} for pp scattering at $\sqrt{s}$=52.8 GeV: a) fit results, b) and c) fit results and model predictions.

Production of Sleptons in the Supersymmetric Standard Model

J. E. Cieza Montalvo*
Instituto de Física, Universidade do Estado do Rio de Janeiro
CEP 20559 – 900 *Rio de Janeiro, Brazil*

Received March, 1996

We study the production of sleptons considering the minimal supersymmetric standard model. We compare the different slepton-pair-production mechanisms, $q\bar{q}$, $gg \to \tilde{l}\bar{l}$, finding that the gg cross section is the largest one due to the fourth-generation heavy quarks.

I Introduction

The Standard $SU(3)_C XSU(2)_L XU(1)_Y$ Model has been very successful in the description of all the present data on the electroweak interactions. However, it leaves many fundamental problems unexplained, such as the magnitudes of particle masses, CP violating mechanisms, charged-current mixing angles, number of generations, etc. To try to solve these problems, one must go beyond the Standard Model and as one extension of it we can take supersymmetry (SUSY).

In this paper, we shall consider the possible existence of sleptons and study the production of this particles in hadronic collisions. Traditionally, the production of sleptons proceeds via the Drell-Yan, i.e. ($q\bar{q} \to \tilde{l}\bar{l}$), the electroweak boson (WW, ...) and the gluon (gg) fusion. O mecanismo de Drell-Yan gives the dominant production [1]. Nevertheless, in high energy hadronic collisions we can take advantage of the high gluon luminosity and a assumption of a four generation of quarks and a squarks [2] to produce sleptons. In this work we shall study the production of sleptons pairs through gluon fusion, assuming the minimal supersymmetric extension of the standard model [3]. We shall demonstrate that when we shall consider the four family of quarks(squarks) the cross section is greatly enhanced, yielding a large number of events which can be extract from the background.

II Subprocess cross section

The conection between the initial gluons and the sleptons occurs, in the MSSM, via loop of quarks and squarks, since these are the only particles with both strong and eletroweak charges. Moreover, since the final state is neutral the S-channel involves only the exchange of the two neutral Higgs bosons, H_1^0 and H_2^0, the Higgs H_3^0 do not contribute why don't exist vertices for $H_3^0\tilde{q}_i\tilde{q}_i$, the Z^0 exchange contribution is proportional to $(M_{\tilde{l}}^2 - M_{\tilde{l}}^2)$, this can be understood due to the $Z^0\tilde{l}\bar{l}$ coupling and to the Z^0 momentum , that gives $(p_{\tilde{l}} - p_{\bar{l}})(p_{\tilde{l}} + p_{\bar{l}}) = M_{\tilde{l}}^2 - M_{\tilde{l}}^2$ and therefore vanishing.

In order to make explicit the direct contributions to the elementary coss-section, we will present them separately

$$\hat{\sigma}^q_{H_1+H_2} = \frac{\alpha^2\alpha_s^2}{64\pi s \sin^4\theta_W}\beta_{\tilde{l}}\left|\sum_{i=1,2}\eta_{\tilde{l}}^{(i)}\chi^{(i)}(\hat{s})\sum_{q=u,d}\eta_q^{(i)}m_q\left[2+(4\lambda_q-1)I_q\right]\right|^2 . \quad (1)$$

*E-mail address: CIEZA@USPIF.IF.USP.BR (internet) or 47602::CIEZA (decnet)

$$\hat{\sigma}^{\tilde{q}}_{H_1+H_2} = \frac{\alpha^2\alpha_s^2}{256\pi s\sin^4\theta_W}\beta_{\tilde{l}}\left|\sum_{i=1,2}\eta_{\tilde{l}}^{(i)}\chi^{(i)}(\hat{s})\right. \\ \left.\times\sum_{\tilde{q}=\tilde{u},\tilde{d}}\sum_{k=L,R}\tilde{\eta}_{\tilde{q}_k}^{(i)}\left(1+2\lambda_{\tilde{q}_k}I_{\tilde{q}_k}\right)\right|^2. \tag{2}$$

Where the summations run over all four generations. $\beta_{\tilde{l}} = \sqrt{1-4M_{\tilde{l}}^2/\hat{s}}$ is the slepton velocity in the C.M. of the subprocess. The loop function $I_{q,\tilde{q}} \equiv I(\lambda_{q,\tilde{q}} = m_{q,\tilde{q}}^2/\hat{s})$ and the coupling constants $\eta_f^{(i)}$, which are functions of the angles α and β, are given in the Appendix. We have also defined:

$$\chi^{(i)}(\hat{s}) = \frac{1}{\hat{s}-M_{H_i}^2+iM_{H_i}\Gamma_{H_i}}$$

with Γ_{H_i} being the Higgs-boson total width.

The interference between the quark and squark-loop contributions is given by

$$\hat{\sigma}^{q-\tilde{q}}_{H_1+H_2} = \frac{\alpha^2\alpha_s^2}{128\pi s\sin^4\theta_W}\beta_{\tilde{l}}\,\Re\left\{\sum_{i=1,2}\eta_{\tilde{l}}^{(i)}\chi^{(i)}(\hat{s})\right. \tag{3}$$
$$\left.\times\sum_{q=u,d}\eta_q^{(i)}m_q\left[2+(4\lambda_q-1)I_q\right]\sum_{j=1,2}\eta_{\tilde{l}}^{(j)}\chi^{*(j)}(\hat{s})\sum_{\tilde{q}=\tilde{u},\tilde{d}}\sum_{k=L,R}\tilde{\eta}_{\tilde{q}_k}^{(j)}\left(1+2\lambda_{\tilde{q}_k}I_{\tilde{q}_k}^*\right)\right\}$$

Where $\Re$ stands for the real part of the expression.

When we assume only light particles running in the loop, the contributions to the cross-section is small, but when we take a heavy generation the cross section is enhanced due to the terms η_q, $\eta_{\tilde{q}}$ which both are proportional to M_q.

Considering the large-λ_i limit and neglecting the resonance effect of the Higgs bosons we have for the quark contribution

$$\hat{\sigma}^{q}_{H_1+H_2} \to \frac{\alpha^2\alpha_s^2}{256\pi s\sin^4\theta_W}\frac{M_q^4}{M_W^4}\beta_{\tilde{l}}\frac{1}{\cos^4\beta}\left(\frac{1}{\sin^4\beta}\right)$$

The squark contribution becomes

$$\hat{\sigma}^{\tilde{q}}_{H_1+H_2} \to \frac{\alpha^2\alpha_s^2}{64\pi\sin^4\theta_W}\left(\frac{M_q^2}{M_W}\right)^4\beta_{\tilde{l}}\,\frac{1}{\hat{s}^3}\frac{1}{\cos^4\beta}\left(\frac{1}{\sin^4\beta}\right)$$

And finaly the interference term

$$\hat{\sigma}^{q-\tilde{q}}_{H_1+H_2} \to \frac{\alpha^2\alpha_s^2}{128\pi\sin^4\theta_W}M_q^2\left(\frac{M_q}{M_W}\right)^4\beta_{\tilde{l}}\,\frac{1}{\hat{s}^2}\frac{1}{\cos^4\beta}\left(\frac{1}{\sin^4\beta}\right)$$

We can see that for large M_q the total cross section for the subprocess $gg \to \tilde{l}\bar{l}$ is enhanced in comparision with the cross section for small M_q, and here state $M_q = M_D \to \frac{1}{\cos^4\beta}$ and $M_q = M_U \to \frac{1}{\sin^4\beta}$.

III Results and Conclusions

The total cross section for the process $pp \to gg \to \tilde{l}\bar{l}$ is related to the subprocess $gg \to \tilde{l}\bar{l}$ total cross section $\hat{\sigma}$ through

$$\sigma = \int_{\tau_{min}}^{1}\int_{\ln\sqrt{\tau_{min}}}^{-\ln\sqrt{\tau_{min}}} d\tau dy G(\sqrt{\tau}e^{y},Q^2)G(\sqrt{\tau}e^{-y},Q^2)\hat{\sigma}(\tau,s) \tag{4}$$

Where $\tau = \frac{i}{s}(\tau_{min} = \frac{4M_f^2}{s})$, with s being the center-of mass energy of the pp system and $G(x,Q^2)$ is the gluon structure function.

In Figure 1 we present the result for the total cross section, for the proton-proton center-of-mass energies of $\sqrt{s} = 14TeV.$, [CERN Large Hadron Collider (LHC)]. Taking into account the expected integrated luminosity for LHC $(10^3 - 10^5 pb^{-1}/yr)$ we can expect a total of the order of $10^2 - 10^4$ sleptons right(left) pairs produced per year.

For this calculation we have used the gluon distribution function given by Duke and Owens [4].

It is to see that the number of events are large and to separate the signal of the backgrounds must be done by a careful Monte Carlo analysis.

Acknowledgments

One of us (J.E.C.M) would like to thank the kind hospitality of the Institute for Physics, University of São Paulo, where this work was done. This work was supported by Conselho Nacional de Desenvolvimento Científico e Tecnológico (CNPq).

IV Appendix

The loop integrals involved in the evaluation of the elementary cross section of Sec. II can be expressed in terms of the function $I_i(\lambda_i)$ which is defined through

$$I_i \equiv I_i(\lambda_i) = \int_0^1 \frac{dx}{x} \ln\left[1 - \frac{(1-x)x}{\lambda_i}\right] = \begin{cases} -2\left[\sin^{-1}\left(\frac{1}{2\sqrt{\lambda_i}}\right)\right]^2 , & \lambda_i > \frac{1}{4} \\ \frac{1}{2}\ln^2\left(\frac{r_+}{r_-}\right) - \frac{\pi^2}{2} + i\pi \ln\left(\frac{r_+}{r_-}\right) , & \lambda_i < \frac{1}{4} \end{cases}$$

with, $r_\pm = 1 \pm (1-4\lambda_i)^{1/2}$ and $\lambda_i = m_i^2/\hat{s}$. Here, $i = q, \tilde{q}$ stands for the particle (quark or squark) running in the loop. Assuming that these particles are heavy, i.e. in the large λ_i limit, we have

$$\lambda_i I_i \to -\frac{1}{2} , \quad \lambda_i[2 + (4\lambda_i - 1)I_i] \to \frac{1}{3}$$

We wrote the couplings of the scalar Higgses $(H_{1,2})$ to the fermions $(f = u, d, \ell)$ as $igm_q\eta_f^{(i)}/2M_Z$. The constants $\eta_f^{(i)}$ are functions of the mixing angles α and β.

$$\begin{aligned} \eta_u^{(1)} &= \frac{\sin\alpha}{\sin\beta} , \quad \eta_d^{(1)} = \frac{\cos\alpha}{\cos\beta} = \eta_\ell^{(1)} \\ \eta_u^{(2)} &= \frac{\cos\alpha}{\sin\beta} , \quad \eta_d^{(2)} = -\frac{\sin\alpha}{\cos\beta} = \eta_\ell^{(2)} \end{aligned}$$

In the case of the pseudo-scalar Higgs (H_3), we wrote the vertex with the fermions as $gm_q\eta_f^{(i)}\gamma_5/2M_Z$, with

$$\eta_u^{(3)} = \frac{\cos\beta}{\sin\beta} , \quad \eta_d^{(3)} = \frac{\sin\beta}{\cos\beta} = \eta_\ell^{(3)} .$$

We also defined the squark-fermions couplings as,

$$\begin{aligned} \tilde{\eta}_{\tilde{u}_L}^{(1)} &= \left(\frac{1}{2} - \frac{2}{3}\sin^2\theta_W\right)\cos(\alpha+\beta) + \left(\frac{m_u}{M_Z}\right)^2 \frac{\sin\alpha}{\sin\beta} \\ \tilde{\eta}_{\tilde{u}_R}^{(1)} &= \frac{2}{3}\sin^2\theta_W\cos(\alpha+\beta) + \left(\frac{m_u}{M_Z}\right)^2 \frac{\sin\alpha}{\sin\beta} \\ \tilde{\eta}_{\tilde{d}_L}^{(1)} &= -\left(\frac{1}{2} - \frac{1}{3}\sin^2\theta_W\right)\cos(\alpha+\beta) + \left(\frac{m_d}{M_Z}\right)^2 \frac{\cos\alpha}{\cos\beta} \\ \tilde{\eta}_{\tilde{d}_R}^{(1)} &= -\frac{1}{3}\sin^2\theta_W\cos(\alpha+\beta) + \left(\frac{m_d}{M_Z}\right)^2 \frac{\cos\alpha}{\cos\beta} \end{aligned}$$

$$
\begin{aligned}
\tilde{\eta}^{(2)}_{\tilde{u}_L} &= -\left(\frac{1}{2} - \frac{2}{3}\sin^2\theta_W\right)\sin(\alpha+\beta) + \left(\frac{m_u}{M_Z}\right)^2 \frac{\cos\alpha}{\sin\beta} \\
\tilde{\eta}^{(2)}_{\tilde{u}_R} &= -\frac{2}{3}\sin^2\theta_W \sin(\alpha+\beta) + \left(\frac{m_u}{M_Z}\right)^2 \frac{\cos\alpha}{\sin\beta} \\
\tilde{\eta}^{(2)}_{\tilde{d}_L} &= \left(\frac{1}{2} - \frac{1}{3}\sin^2\theta_W\right)\sin(\alpha+\beta) - \left(\frac{m_d}{M_Z}\right)^2 \frac{\sin\alpha}{\cos\beta} \\
\tilde{\eta}^{(2)}_{\tilde{d}_R} &= \frac{1}{3}\sin^2\theta_W \sin(\alpha+\beta) - \left(\frac{m_d}{M_Z}\right)^2 \frac{\sin\alpha}{\cos\beta}
\end{aligned}
$$

References

[1] F. del Aguila and M. Ametller, Phys. Lett. **261B**, 326 (1991).

[2] V. A. Novikov, L. B. Okun, A. N. Rozanov, M. I. Vysotsky and V. P. Yurov, Mod. Phys. Lett. **A10**, 1915 (1995).

[3] H. E. Haber and G. L. Kane, Phys. Rep. **117**, 75 (1985).

[4] D. Duke and J. Owens, Phys. Rev. **D30**, 49 (1984).

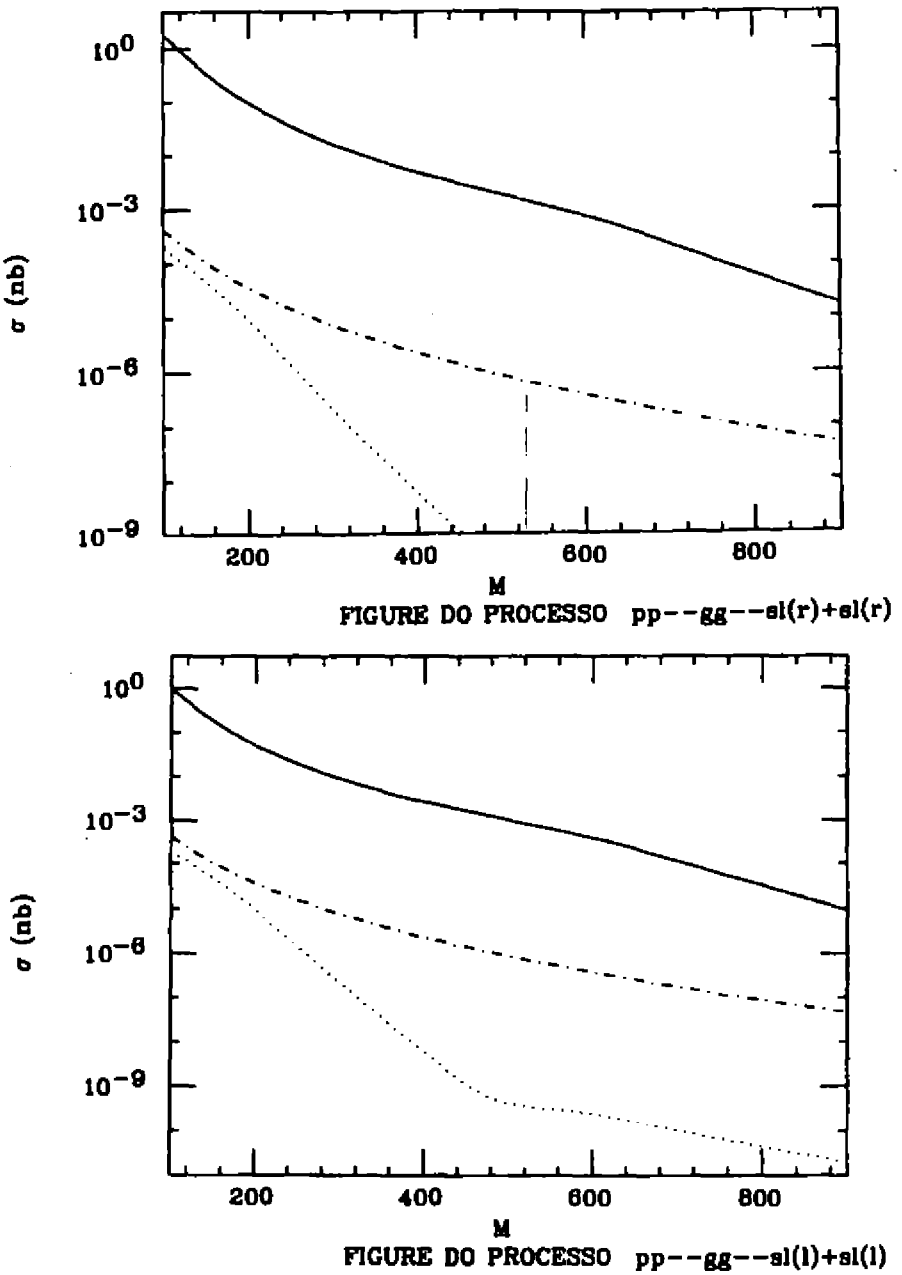

Figure 1. Total cross section for the gluon fusion contribution to slepton production in the MSSM as a function of the slepton mass. For the fourth generation of quarks we assumed $M_D = 600$ GeV and $M_U = 600$ GeV. The curves are for the center of mass energy of (a) $\sqrt{s} = 14$ TeV (LHC) for right-sleptons and (b) $\sqrt{s} = 14$ TeV for left-sleptons. Considering the four generation of quarks and squarks (solid line), the Drell-Yan contribution (dashed line) and the contribution of quark top (dotted line).

Effects of Solar Magnetosonic Waves in Future Solar Neutrino Observations

J.H. Colonia[1], M.M. Guzzo[1] and N. Reggiani[1,2]

[1] *Instituto de Física 'Gleb Wataghin'*
Universidade Estadual de Campinas - UNICAMP
13083-970 Campinas, São Paulo, Brasil

[2] *Laboratório Nacional de Luz Síncroton*
Rua Lauro Vanucci, 1020
13083-970 Campinas, São Paulo, Brasil

Received March, 1996

We assume the existence of solar magnetosonic waves to analyse possible observations of flux fluctuation in experiments which will begin operating in near future. Such predictions include an analysis of the modified solar neutrino spectra which will be detailed observed in these experiments.

Slow magnetosonic waves are produced from solar plasma displacements perturbating the solar magnetic field. As a consequence, when a nonvanishing neutrino magnetic moment is assumed, a fluctuation of the solar neutrino flux anticorrelated with the referred magnetic wave could be observed. This is because the interaction of the solar neutrinos with the solar magnetic field through a nonvanishing neutrino magnetic moment leads to a conversion of an active left-handed neutrino into a nondetectable right-handed one. In a recent paper [1] we solved the Hain-Lüst equation for solar plasma displacements and the evolution equations of neutrinos interacting with the solar magnetic field to conclude that present solar neutrino data can suggest the existence of such solar magnetossonic waves.

Assuming a non-vanishing neutrino magnetic moment, the interaction of neutrinos with a magnetic field will be given by the evolution equations [2]

$$i\frac{d}{dr}\begin{pmatrix}\nu_R(r)\\ \nu_L(r)\end{pmatrix}=\begin{pmatrix}\frac{\sqrt{2}}{2}G_F N_e(r)-\frac{\Delta m}{4E} & \mu_\nu|\vec{B}_\perp(r)|\\ \mu_\nu|\vec{B}_\perp(r)| & -\frac{\sqrt{2}}{2}G_F N_e(r)+\frac{\Delta m}{4E}\end{pmatrix}\begin{pmatrix}\nu_R(r)\\ \nu_L(r)\end{pmatrix} \quad (1)$$

where ν_L (ν_R) is the left (right) handed component of the neutrino field, $\Delta m = |m_L^2 - m_R^2|$ is their squared mass difference, E is the neutrino energy, G_F is the Fermi constant, $N_e(r)$ is the electron number density distribution and $|\vec{B}_\perp(r)|$ is the transverse component of magnetic field.

Solving the equations (1) we can calculate the survival probability of left-handed neutrinos $P(\nu_L \to \nu_L)$ produced in the Sun to arrive at the Earth after interacting with the solar magnetic field $|\vec{B}_\perp(r)|$ periodically perturbated by the magnetosonic waves in the way discussed in the reference [1]. We use the values $5\times10^{-8}\text{eV}^2$ and $3\times10^{-12}\mu_B$ for the mass squared difference Δm and the neutrino magnetic moment μ_ν, respectively, and the standard approximately exponentially decreasing matter density for $N_e(r)$ [3].

New detectors like as SNO [4] and Superkamiokande [5] will be based on ν_e-e^- scattering where the shape of the recoil electron energy spectrum will reflect the solar neutrino spectrum. Only neutrinos coming from one of the rarest nuclear reactions in the Sun, the ^8B decay, which have the widest spectrum ($0-15$ MeV), will produce

neutrinos with sufficient high energy to be observed by the ν_e-e^- scattering detectors. These experiments will permit to observe the suppression in the high energy portion of the ^8B spectrum.

In order to arrive to the expected detection rate in these future experiments we have, first of all, to calculate the survival probability, $P(E,t)$, of a left-handed neutrino created in the central parts of the Sun to achieve the solar surface (beyond this point the magnetic field is negligible and no left-right conversion can occur) after having crossed the fluctuating solar magnetic field. The survival probability will depend on the neutrino energy, therefore, the energy spectrum of the ^8B-neutrinos at the production region has to be taken into account. We considered the spectrum ^8B-neutrino given by the solar standard model in reference [3].

The energy dependence of the survival probability is shown in Fig. 1 for different instants of time when the perturbating magnetosonic wave influence the solar magnetic field with different intensities. We considered the instant $t = 0$, as the moment where the magnetosonic wave is zero and showed how the evolution of this wave alter the survival probability until a period of oscillation is complete. We consider a wave which period is 114 days [1]. After this interval the situation is merely a repetition of what is shown in Fig. 1. Therefore we have the suppression of left-handed neutrinos as they travel from the solar center to the detectors. There is a noticeable energy dependence in the shape of suppression curves. We note marked fluctuations for low energy neutrinos in contrast to the high energy neutrinos where the energy dependence is lower. Note that the time dependence is still appreciable.

In Fig. 2 we show the neutrino spectrum suppression for various instants of time (continuos lines), that is given by the product of the production spectrum [3] (also presented in this figure by the pointed lines) by the survival probability shown in Fig. 1. Note that the spectra shown in this figure are instantaneous spectra, i.e., for each indicated instant of time we show the spectrum of neutrinos arriving at the detectors. We can therefore call these figures as emission spectra.

Finally we have to consider also the energy dependence of the detection process given by the ν_e-e^- cross section. The expected event rate is calculated as $R(E,t) = \Phi^{^8B}_{SSM}(E)\sigma(E)P(E,t)$ where $\Phi^{^8B}_{SSM}(E)$ is the ^8B-neutrino production spectrum given by the Solar Standard Model [3] and $\sigma(E)$ is the cross section ν_e-e^- scattering which increases linearly with energy [6]: $\sigma(E) = 9.2 \times 10^{-45} E$ cm^{2}MeV^{-1}. The energy dependence of the expected event rates is shown in Fig. 3 (continuos lines). These results can be compared with the predicted standard event rates $R_{SSM}(E) = \Phi^{^8B}_{SSM}(E)\sigma(E)$ (pointed lines). The time dependence of this same physical situation is shown in Fig. 4. Due to the fact that future detectors will present accurate measurements and will allow to differentiate neutrinos with different energies, Fig. 4 is depicted for various energy intervals, each one of 1 MeV. This will permit to observe in detail the time dependence for specified energies of the ^8B-neutrinos.

Solar neutrinos are commonly cited as a possible source of informations of the inner part of the Sun. We investigate the effects of the magnetosonic wavés in the solar neutrino detection. We observed that the production spectrum of active solar neutrinos is attenuated by the survival probability of neutrinos which interact, by means of a nonvanishing neutrino magnetic moment, with the solar magnetic field modulated by these magnetosonic waves. We observed that this attenuation is very appreciable in such a way that the accuracy of the future neutrino detectors, from the point of view of both time and energy resolution, will be sufficient to identify the effects of the

magnetosonic waves.

References

[1] M.M. Guzzo, N. Reggiani and P.H. Sakanaka, Phys. Lett. B 357 (1995) 602.

[2] A.Yu. Smirnov, Phys. Lett. B 260 (1991) 161.

[3] J.N. Bahcall and R.K. Ulrich, Rev. Mod. Phys. 60 (1988) 297.

[4] G.T. Ewan, in Frontiers of Neutrino Astrophysics, edited by Y. Suzuki and K. Nakamura, Universal Academy Press, Tokyo (1993) p. 135.

[5] M. Takita, in Frontiers od Neutrino Astrophysics, edited by Y. Suzuki and K. Nakamura, Universal Academy Press, Tokyo (1993) p. 147.

[6] J.N. Bahcall, Neutrino Astrophysics, Cambridge University Press, Cambridge (1989).

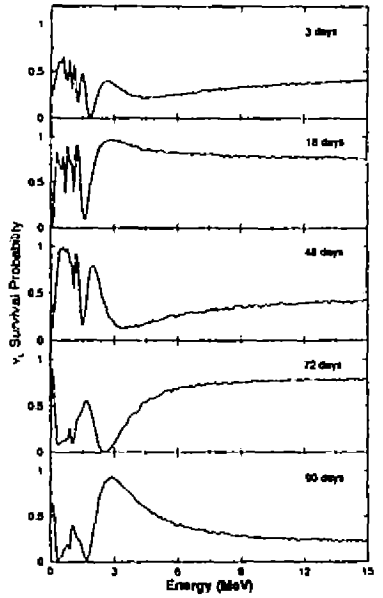

Fig. 1: The survival probability as a function of neutrino energy.

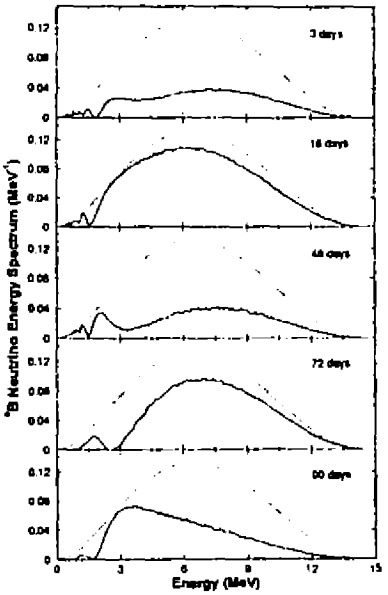

Fig. 2: The emission spectra.

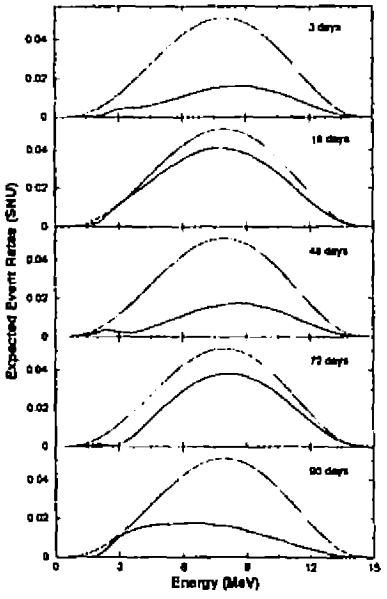

Fig. 3: The detection spectra.

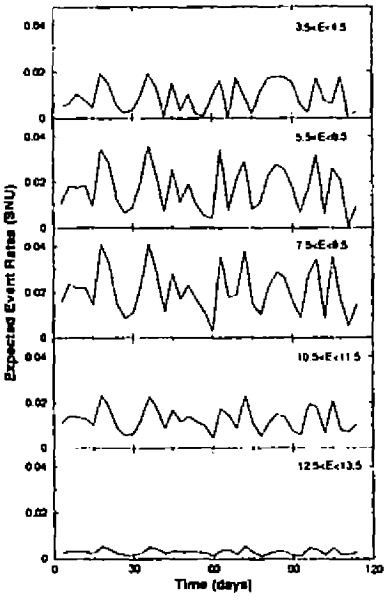

Fig. 4: Time dependence of the detection rate.

The Effect of the Terrestrial Bow Shock in Solar Neutrino Evolution

Marcelo M. Guzzo and Pedro C. de Holanda
Instituto de Física Gleb Wataghin
Universidade Estadual de Campinas, UNICAMP
13083-970 Campinas, SP

Received March, 1996

We analyse the extreme nonadiabatic effects occuring in the terrestrial Bow Shock on left-right solar neutrino conversion, when a nonvanishing neutrino moment is assumed.

In this work, we analyse the consequences on the solar neutrino flux of a narrow region between the Sun and the Earth named Bow Shock, where due to the solar and terrestrial magnetic field interference, the resulting magnetic field is more intense than in its neighbourhood. If we assume that the neutrinos have a nonvanishing magnetic moment μ, the passage through a region like the Bow Shock can result in an helicity change of these neutrinos from left- to right-handed helicity eigenstate $\nu_L \rightarrow \nu_R$. Since right-handed neutrinos do not interact with the detectors, the Bow Shock can be responsible for a decrease in the detection rate of solar neutrinos.

We assumed that the transition felt by the neutrinos passing through the Bow Shock is extremely nonadiabatic, where the magnetic field jumps from 3 to 15×10^{-5} G, falling immediately after to 9×10^{-5} G, where it starts to slowly growing until achieving the value of $O(1)$ G in the Earth proximity. We used the following time evolution equations for a system of a left- and a right-handed neutrinos [1]:

$$i\frac{d}{dt}\begin{pmatrix} \nu_L \\ \nu_R \end{pmatrix} = \begin{pmatrix} \frac{\Delta m}{4p} + \frac{\sqrt{2}}{2}pG_F N_e & \mu B \\ \mu B & -\frac{\Delta m}{4p} \end{pmatrix}\begin{pmatrix} \nu_L \\ \nu_R \end{pmatrix}, \tag{1}$$

where Δm is the neutrino $L - R$ mass squared difference, and $N_e(t)$ and $B(t)$ are the electron density and the magnetic filed intensity felt by the neutrinos at instant t.

The mixing angles that relate left- and right-handed helicity eigenstates to mass eigenstates ν_1 and ν_2, can be written [1]:

$$\tan 2\theta = \frac{4p\mu B}{\Delta m + 2\sqrt{2}pG_F N_e}, \tag{2}$$

and the survival probability of a neutrino created in a left-handed state deep in the Sun to arrive in this same state at the Earth after having crossed a nonadiabatic region is [1]:

$$P_{\nu_L \rightarrow \nu_L} = (1 - X)P^{(ad.)}_{\nu_L \nu_L} + X(1 - P^{(ad.)}_{\nu_L \nu_L}), \tag{3}$$

where X is the transition probability $\nu_1 \nleftrightarrow \nu_2$ in the nonadiabatic region and

$$P^{(ad.)}_{\nu_L \nu_L} = 1/2\{1 + \cos(2\theta_{Sun})\cos(2\theta_{Earth})\}. \tag{4}$$

We will treat the Bow Shock as two extreme nonadiabatic transitions. Therefore we can write X fhe following way:

$$X = Z_1(1 - Z_2) + (1 - Z_2)Z_1,$$

where Z_1 is the $\nu_1 \nleftrightarrow \nu_2$ transition probability in the first Bow Shock boundary and Z_2 is the same probability in the second one. To calculate Z_1 and Z_2, we used the extreme nonadiabatic limit approximation, that consists in considering the nonadiabatic transition as a discontinuos boundary in the neutrino evolution, to obtain:

$$Z_{1(2)} = \sin^2(\theta_2 - \theta_{1(3)})\cos^2\theta_2 \cos^2\theta_{1(3)}, \tag{5}$$

where $\theta_1, \theta_2, \theta_3$ are the mixing angles calculated through Eq. (2) in the region immediately before, during and immediately after the Bow Shock.

In order now to appreciate the validity of our approximations in Eq. (3), we calculate the adiabaticity parameter [1] from the evolution equations (1):

$$\frac{d\theta}{dt} >> \frac{\Delta m + 2\sqrt{2}G_F p N_e}{2p} \frac{1}{\cos 2\theta} . \tag{6}$$

The Bow Shock region can be considered nonadiabatic if

$$10^{18}\mu_B/cv^2 > \frac{\mu}{\Delta m} > 1\mu_B/ev^2 , \tag{7}$$

where we considered the magnetic field difference in the Bow Shock as 10^{-5} G, extending for a region of 10 km and the neutrino energy around 1 MeV.

Using the same parameter in the Sun, we guarantee the adiabaticity in this region if:

$$\mu < 10^{-6}\mu_B , \tag{8}$$

where we replaced $\frac{\sqrt{2}}{2}G_F N_e = 1,25.10^{-11}$eV, the solar radius around 10^6Km, and a magnetic field variation of 10^5 G.

We would like also to obtain a result that, if there was no Bow Shock, all the neutrinos produced in the Sun would stay left-handed. That means to do $P^{(ad.)}_{\nu_L\nu_L} = 1$,which leads to the condition:

$$\mu < 10^{-8}\mu_B . \tag{9}$$

In fig.1, 2 and 3 we show how the Bow Shock can interfere the left-handed neutrino survival probability, for different values of $\mu/\Delta m$. We note that there are regions where an appreciable decrease of this probability occurs. Furthemore the shape of this figure is compatible with a solution to the solar neutrino problem [1], although the size of the probability deflection is not sufficient for this. Nevertheless, an important remark is in order. This effect will not be sensible to solat neutrino detectors on Earth. This is because our results represent the average over several neutrino oscillations. In fact, for values of the magnetic field in the region of the Bow Shock around 10^{-5} G and $\mu_\nu \sim 10^{-11}\mu_B$, we find a neutrino oscillation length around $10^{23}eV^{-1}$, or 10^8 times the distance Earth-Bow Shock. Neutrinos arrive at the Earth in the the same state they arrived at the Bow Shock.

Although our conclusions indicate that the Bow Shock will not significantly alter the solar neutrino flux measured at terrestrial detectors, our calculations can be used to infer that nonadiabatic effects can contribute to left-right neutrino conversion in other physical systems, including conveniently built experiments in accelerators [2].

References

[1] Palash B. Pal, International Journal of Modern Physics A, Vol. 7, No. 22 (1992) 5387-5459

[2] P. C. de Holanda e M. M. Guzzo, in preparation.

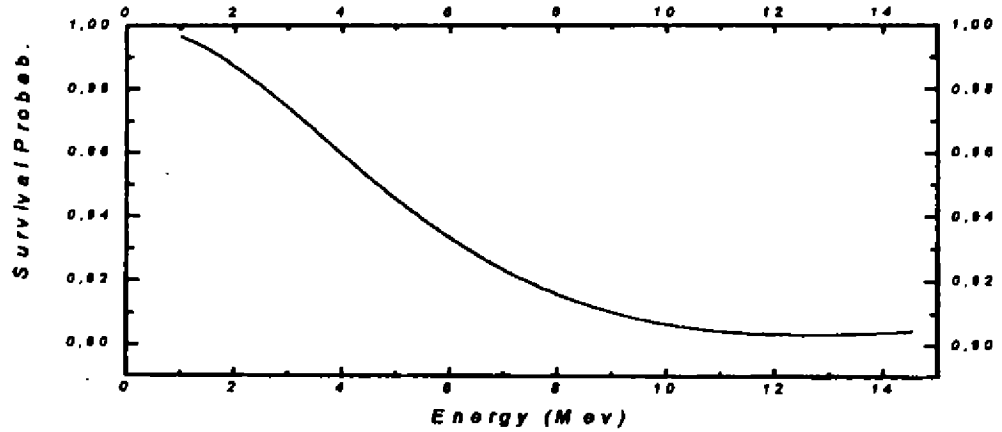

fig. 1 : survival probability for $\mu/\Delta m = 4.10^4\ \mu_B/ev^2$

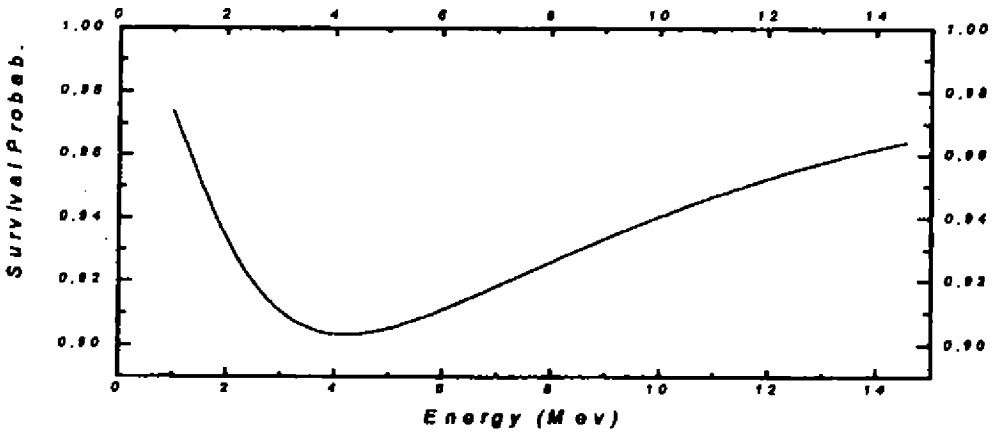

fig. 2 : survival probability for $\mu/\Delta m = 1{,}2.10^5\ \mu_B/ev^2$

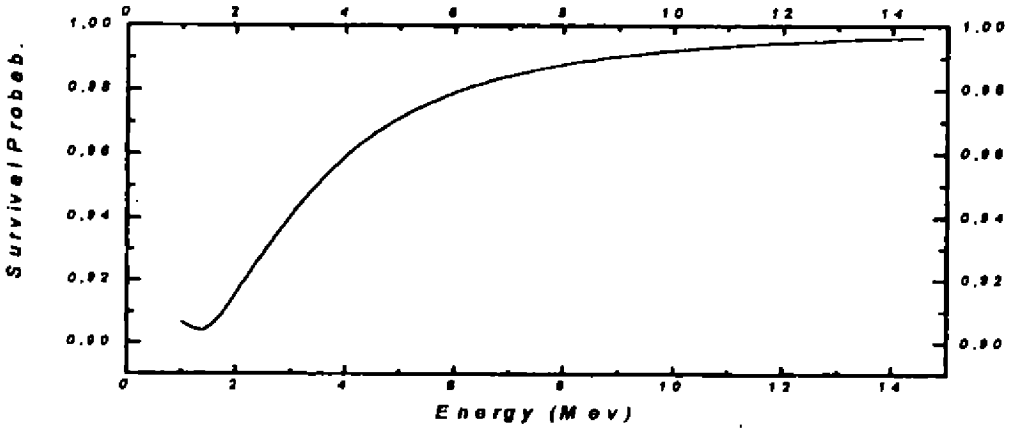

fig. 3 : survival probability for $\mu/\Delta m = 3.10^5\ \mu_B/ev^2$

The Solar Neutrino Propagation and the Slow Solar Magnetosonic Waves

M. M. Guzzo, N. Reggiani and P.H. Sakanaka
Instituto de Física Gleb Wataghin
Universidade Estadual de Campinas, UNICAMP
13083-970 Campinas, SP

Received March, 1996

We analyse the different behaviour of Homestake and ^{71}Ga experiments and Kamiokande data as a consequence of the interaction of neutrinos produced in the Sun with a fluctuating solar magnetic filed by means of a nonvasnihing neutrino magnetic moment. The fluctuations of the solar magnetic filed are calculated solving the Hain-Lüst equation. The appearence of slow magnetosonic waves simulate the time behaviour of solar neutrino data.

Time variation of the solar neutrino flux has been an interesting discussion in the context of the solar neutrino problem. Analyzing individually each experimental point obtained from solar neutrino detectors, we see that they are widely dispersed in Homestake [1] and ^{71}Ga experiments [2][3] results, presenting values that vary from approximately 0 to 1 times the standard solar model theoretical predictions [4]. Furthermore, observing their experimental errors we can conclude that these experimental points are not compatible (at 1 σ-level) between them. Kamiokande data [5], on the contrary, do not present this dispersion since their experimental points are statistically compatible (at 1 σ-level) with a certain mean value. This apparently different behavior of Homestake and ^{71}Ga experiments and Kamiokande data could suggest that the former have observed a certain time variation in solar neutrino flux while the last ones show no compelling evidence for this variation.

In this paper we analyze the possibility of such data behavior being a consequence of the interaction of neutrinos produced in the Sun with a fluctuating solar magnetic field by means of a nonvanishing neutrino magnetic moment [6]. Using a numerical procedure that calculates the fluctuations of the solar magnetic field as a consequence of the solar plasma motion [7], we show that the so called slow magnetosonic waves appear in the solar magnetic field and present typical period of order of one hundred days. Interesting enough we show that these slow magnetosonic waves are sufficient to understand the refered apparently different behavior of the experimental data [8].

The magnetic waves are calculated considering that they can be generated by small displacements of the solar plasma, $\vec{\xi}$, from an equilibrium configuration. The time evolution of these displacements is described by the linearized equation of motion [9]

$$\rho\frac{\partial^2\vec{\xi}}{\partial t^2} = \vec{F}(\vec{\xi}) = \vec{\nabla}(\gamma p\vec{\nabla}.\vec{\xi}) - \vec{b}\times(\vec{\nabla}\times\vec{B}_0) - \vec{B}_0\times(\vec{\nabla}\times\vec{b}), \tag{1}$$

where ρ is the density, p is the pressure, $\gamma = 1.0$, $\vec{B}_0$ is the equilibrium magnetic field and $\vec{b}$ is the magnetic perturbation generated by the displacement $\vec{\xi}$ given by $\vec{b} = \vec{\nabla}\times(\vec{\xi}\times\vec{B}_0)$. Considering an exponential time dependence for the displacement $\vec{\xi}$,
$\vec{\xi}(r,\theta,z,t) = e^{-iwt}\vec{\xi}(r,\theta,z)$, the frequency of the wave w and the displacement $\vec{\xi}$ can be found solving the eigenvalue equations $-\rho w^2\vec{\xi} = \vec{F}(\vec{\xi})$.

We are interested in the behavior of the magnetic field inside the Sun along the trajectory of the neutrinos that reach the Earth. This trajectory is localized around the plane of the solar equator. We can use therefore cylindrical coordinates to solve the eigenvalue equations to obtain the magnetic perturbations in this region. We

consider the plane of the equator coincident with one of the planes of the cylinder perpendicular to the z axis. In cylindrical coordinates the linearized equations of motion present a very useful feature: for each Fourier component (m, k) they separate out into a second-order differential equation for ξ_r and two relations expressing ξ_θ and ξ_z in terms of ξ_r and $\frac{d\xi_r}{dr}$ [7]. This property permits us to obtain all the components of the displacement $\vec{\xi}$, and, consequently, all the components of the fluctuation of the magnetic field solving just the differential equation for ξ_r. This differential equation was first obtained by Hain and Lüst [10] and is solved numerically imposing appropriate boundary conditions.

We take for the equilibrium profile for the magnetic field the model proposed by Akhmedov and Bychuk in the Ref. [11]:

$$B_0(r) = \begin{cases} a_1 \left(\frac{0.2}{r+0.2}\right)^2 \mathrm{G} & \text{for } 0 \le r \le 0.7 \\ a_2 \left[1 - \left(\frac{r-0.7}{0.3}\right)^2\right] \mathrm{G} & \text{for } 0.7 < r \le 1\,, \end{cases} \tag{2}$$

where $a_1 \approx 10^5 - 10^7$ and $a_2 \approx 10^4 - 10^5$ in such a way that the continuity of the magnetic field at the point $r = 0.7$ is satisfied (r is the radial distance from the center of the Sun normalized by the solar radius 6.96×10^5 km). The equilibrium magnetic field $\vec{B}_0$ is chosen in the z direction. We assume the matter density distribution, ρ, usually accepted to fit the predictions of the standard solar model [4], i.e., an approximately monotocally decreasing exponential function in the radial direction from the center to the surface of the Sun [4]. We consider the pressure proportional to the density.

The results of our calculations indicate that a known kind of stable fluctuations are found in the region of squared frequencies of order $w^2 \approx 10^{-15}$ sec^{-2}, corresponding to a period around 100 days. These fluctuations, localized out of the Alfvén and slow continua and characterized by $\vec{\nabla}.\vec{\xi} \neq 0$, are usually refered to as slow magnetosonic waves.

Since we are assuming a non-vanishing neutrino magnetic moment, the interaction of neutrinos with a magnetic field will be given by the evolution equations [12]

$$i\frac{d}{dr}\begin{pmatrix} \nu_R(r) \\ \nu_L(r) \end{pmatrix} = \begin{pmatrix} \frac{\sqrt{2}}{2}G_F N_e(r) - \frac{\Delta m}{4E} & \mu_\nu |\vec{B}_\perp(r)| \\ \mu_\nu |\vec{B}_\perp(r)| & -\frac{\sqrt{2}}{2}G_F N_e(r) + \frac{\Delta m}{4E} \end{pmatrix} \begin{pmatrix} \nu_R(r) \\ \nu_L(r) \end{pmatrix} \tag{3}$$

where ν_L (ν_R) is the left (right) handed component of the neutrino field, $\Delta m = |m_L^2 - m_R^2|$ is their squared mass difference, E is the neutrino energy, G_F is the Fermi constant, $N_e(r)$ is the electron number density distribution and $|\vec{B}_\perp(r)|$ is the transverse component of magnetic field given by $\vec{B}_\perp^2 = (B_0 + b_z)^2 + b_\theta^2$. Solving the equations (3) we can calculate the survival probability of left-handed neutrinos $P(\nu_L \to \nu_L)$ produced in the Sun to arrive at the Earth after interacting with the solar magnetic field $|\vec{B}_\perp(r)|$ perturbated by the fluctuations calculated in this paper. We can therefore compare this survival probability with experimental data.

We can now compare the experimental panorama of the Homestake and Kamiokande experiments with our calculations. To solve Equation (3) we use the values 10^{-7} eV^2 and $3 \times 10^{-12}\mu_B$ for the mass squared difference Δm and the neutrino magnetic moment μ_ν. In our calculations the perturbation of the magnetic field is obtained using the displacement $\vec{\xi}$, characterized by $m = 2$, $k = 10^{-7}$, and $w^2 = 9.41 \times 10^{-15}$. We observe [8] that some general features of the refered experimental data can be found also in the calculated survival probability. In particular we observe that this survival probability varies from 0.15 to 0.65 for Homestake while its amplitude is much smaller for Kamiokande.

Neutrinos have been indicated as a possible source of experimental informations of the inner part of stars and supernovae, which are in general very difficult to obtain through other observational methods. The solar magnetic field behavior in the very interior of the Sun has no direct experimental evidence other than the solar neutrino flux observations (if we assume a nonvanishing neutrino magnetic moment). In this paper we analyze the possibility of interpretating these observations as an evidence of the existence of slow magnetosonic waves in the Sun.

Although statistical fluctuations can not, in the light of the present data, be discarded to explain the behavior of the solar neutrino data, it is not possible also to discard the time behavior of these experimental observations as a consequence of a physical effect in the Sun.

Finally we say that an analysis of short period (around 10 - 100 days) time variations in Kamiokande data could be interesting to add new informations on the possible existence of solar slow magnetic waves. Nevertheless a conclusive analysis of the consequences of the slow magnetic waves will have to wait for more precise experimental data to be obtained in future solar neutrino experiments (see [13] and references therein). Experiments like Superkamiokande [14] and SNO [15] will measure the spectrum of high energy neutrinos in a quite accurate way. Time variation of neutrino flux presenting a period of approximately 100 days could be interpreted as the effetc of slow solar magnetosonic waves. This effect can be distinguished from flux modulation due to seasonal variation of Sun-Earth distance and vacuum oscillations. This is because it will be possible to investigate flux variation of neutrinos with a fixed energy. Such time variations will be different if neutrinos have evolution equations like (3) or evolve as in MSW [16] or vacuum oscillation phenomenon. Note, for instance, that the two free parameters μ_ν and Δm appear in different elements of the evolution matrix (3). Therefore, differently from what happens in pure oscillation phenomenon, where the corresponding free parameters vacuum mixing angle and squared mass difference appear in the same elements in the evolution matrix, fitting future experimental data using the expected theoretical probability equations will allow precise determination of Δm and the value of the average of the product $\mu_\nu|\vec{B}_\perp|$. Together with other possible model independent analysis we will be able to use solar neutrino data as a source of informations about the physics of neutrinos as well as the inner part of the Sun.

Acknolegedments

The authors would like to thank Fundação de Amparo à Pesquisa do Estado de São Paulo (FAPESP) and Conselho Nacional de Desenvolvimento Científico e Tecnológico (CNPq) for several financial supports.

References

[1] R. Davis et al., Proc. of the XXI Int. Cosmic Ray Conference, Adelaide, Australia, vol. 7 (1990) p. 155.

[2] P. Anselmann et al., Phys. Lett. B 285 (1992) 390.

[3] A.I. Abazov et al., Phys. Rev. Lett. 67 (1991) 3332.

[4] J. Bahcall and R.K. Ulrich, Rev. Mod. Phys. 60 (1988) 298.

[5] K.S. Hirata et al., Phys. Rev D44 (1991) 2241.

[6] M. Voloshin, M.I. Vysotsky and L. Okun, Yad. Fiz. 44 (1986) 677 [Sov. J. Nucl. Phys. 44 (1986) 440].

[7] J. P. Gloedbloed and P. H. Sakanaka *The Physics of Fluids* 17 (1974) 908.

[8] M.M. Guzzo, N. Reggiani and P.H. Sakanaka, Phys. Lett. B 357 (1995) 602.

[9] I. B. Bernstein, E. A. Frieman, M. D. Kruskal and R. M. Kulsrud *Proc. Roy. Soc.* A224 (1958) 1.

[10] K. Hain and R. Lüst *Z. Naturforsh* 13a (1958) 936.

[11] E. Kh. Akhmedov and O.V. Bychuk, Sov. Phys. JETP 68 (1989) 250.

[12] A. Yu. Smirnov, Phys. Lett. B 260 (1991) 161.

[13] Future Solar Neutrino Experiments, in Nucl. Phys. B (Proc. Suppl.) 38 (1995) 90-95.

[14] Y. Tatsuka, Superkamiokande, ICCR-Report 227-90-20 (1990).

[15] H. Chen, Phys. Rev. Lett. 55 (1985) 1534.

[16] S.P. Mikheyev and A.Yu. Smirnorv, Nuovo Cimento C 9 (1986) 17; Yad. Fiz. 42 (1985) [Sov. J. Nucl. Phys. 42 (1985) 913]; L. Wolfenstein, Phys. Rev. D 17 (1978) 2369; 20 (1979) 2634.

Soluções não adiabáticas para a oscilação entre neutrinos

J. Bellandi, J. R. Fleitas
Instituto de Física 'Gleb Wataghin'
Universidade Estadual de Campinas, Unicamp
13083-970, Campinas, São Paulo, Brasil

Received March, 1996

Recentemente [1], obtivemos a representação matricial para o operador exponencial $\exp[\Gamma_n]$, onde Γ_n é uma matriz $n \times n$. Discutiu-se também a representação para a função de Green associada a equação de evolução temporal de um sistema de dois níveis. Utilizamos esses resultados neste trabalho para reanalisar as transições ressonantes entre neutrinos propagando na matéria.

A equação de evolução de um sistema de dois neutrinos de sabores é dada por

$$i\frac{d}{dt}\phi = H\phi \tag{1}$$

onde ϕ é um spinor a 2 componentes,

$$\phi = \begin{pmatrix} \nu_e \\ \nu_\mu \end{pmatrix} \tag{2}$$

e H é tal que

$$H_1 = \begin{pmatrix} 0 & \frac{\Delta}{4E}\sin 2\theta \\ \frac{\Delta}{4E}\sin 2\theta & \frac{\Delta}{2E}\cos 2\theta \end{pmatrix} \tag{3}$$

para a hamiltoniana no vácuo e

$$H_2 = \begin{pmatrix} 0 & \frac{\Delta}{4E}\sin 2\theta \\ \frac{\Delta}{4E}\sin 2\theta & \frac{\Delta}{2E}\cos 2\theta - 2A \end{pmatrix} \tag{4}$$

para a hamiltoniana na matéria, onde $\Delta = m_1^2 - m_2^2$, E é a energia, θ o ângulo de mixing no vácuo e A o campo de interação do neutrino com a matéria

$$A = \alpha e^{-\beta t} \tag{5}$$

com $\alpha = 1.25 \times 10^{-11}\ eV$ e $\beta = 3.13 \times 10^{-15}\ eV$.

Em [1] obtemos, sem ambiguidade, a expressão para o ângulo de mixing, que no contexto da hamiltoniana dada por (4), é escrita como

$$\sin^2 2\theta_m = \frac{\sin^2 2\theta}{\left[4A(t)\frac{E}{\Delta} - \cos 2\theta\right]^2 + \sin^2 2\theta} \tag{6}$$

para o ângulo de mixing na matéria.

A solução da equação (1) via função de Green é

$$\phi(t) = G(t, t_0)\phi(t_0) \tag{7}$$

onde

$$G(t, t_0) = G_2(t, t_c) \cdot G_1(t_c, t_0) \tag{8}$$

$$[G_1(t, t_0)] = \exp[i\theta_m\sigma_2] \cdot M_1 \cdot \exp[-i\theta_m\sigma_2] \tag{9}$$

$$[G_2(t_c, t_0)] = \exp[i\theta\sigma_2] \cdot M_2 \cdot \exp[-i\theta\sigma_2] \tag{10}$$

onde $[M_l(t, t_0)]_{jk} = \exp\left[-i\lambda_j^l(t - t_0)\right]\delta_{jk}$ e λ_j^l são os autovalores de H_1 e H_2 respectivamente.

Considerando-se a situação dinâmica tal que no domínio de H existe um único ponto de fase estacionária [4], ou seja, existe um único ponto de ressonância, escrevemos a função de Green como

$$G(t,t_0) = G_2(t,t_{R+}) \cdot G_R(t_{R+},t_{R-}) \cdot G_1(t_{R-},t_0) \tag{11}$$

onde t_{R+} e t_{R-} representam os limites a direita e a esquerda do ponto de ressonância respectivamente. Como calculado por Bellandi *et al* [3], escrevemos a matriz de ressonância como

$$G(t_{R+},t_{R-}) = \begin{pmatrix} \frac{1-\xi^2}{1+\xi^2} & -\frac{2i\xi}{1+\xi^2}e^{-i\theta} \\ -\frac{2i\xi}{1+\xi^2}e^{i\theta} & \frac{1-\xi^2}{1+\xi^2} \end{pmatrix}$$

onde $\xi^2 \leq 1$, e

$$\xi = \sqrt{\frac{\pi}{2}}\frac{\Delta}{4E}\frac{\sin 2\theta}{\sqrt{|\frac{d^2}{dt^2}\rho(t)\,|_{t=t_R}}}$$

$$\rho(t) = \int^{t_R}[\frac{\Delta}{4E}\sin 2\theta + 2A(\lambda)]d\lambda$$

Desprezando-se os termos oscilante, escrevemos a probabilidade de permanência e troca adiabática como

$$\begin{aligned} P_P^{adiab} &= \cos^2(\theta_m-\theta)\left[\cos^2\theta\cos^2\theta_m + \sin^2\theta\sin^2\theta_m\right] \\ &\quad + \sin^2(\theta_m-\theta)\left[\cos^2\theta\sin^2\theta_m + \sin^2\theta\cos^2\theta_m\right] \end{aligned} \tag{12}$$

$$\begin{aligned} P_T^{adiab} &= \sin^2(\theta_m-\theta)\left[\cos^2\theta\cos^2\theta_m + \sin^2\theta\sin^2\theta_m\right] \\ &\quad + \cos^2(\theta_m-\theta)\left[\cos^2\theta\sin^2\theta_m + \sin^2\theta\cos^2\theta_m\right] \end{aligned} \tag{13}$$

e a probabilidade de permanência não adiabática como

$$P_P = (1-X)P_P^{adiab} + XP_T^{adiab} \tag{14}$$

onde X é a probabilidade de level crossing ([3]),

$$X = \left(\frac{1-\xi^2}{1+\xi^2}\right)^2\sin^2(\theta_m-\theta) + \frac{2\xi^2}{(1+\xi^2)^2}\left[\cos^2(\theta_m-\theta) + \cos^2(\theta_m+\theta)\right] \tag{15}$$

Na *Figura* 1 mostramos o comportamento de P_P com E/Δ, reproduzindo os resultados de P. Pal [5] e S. Petcov [6].

Trabalho financiado pelo CNPq.

References

[1] J. Bellandi, M. M. Guzzo. J. R. Fleitas, V. M. de Aquino , *On the Matricial Representation of Exponential Operators* , Submetido ao **International Journal of Mathematical Education in Science and Technology**, agosto, 1995;

[2] J. Bellandi, *Funções de Green*, Notas de Física 1, Unicamp, 1992;

[3] M.M.Guzzo, J.Bellandi and V.M.de Aquino; Phys.Rev. **D49** (1994), 1404;

[4] A. Erdélyi, *Asymptotic Expansions*, Dover, NY, 1956;

[5] P. Pal, International Journal of Modern Physics **A**, No. 22 (1992), 5387-5459;

[6] S. T. Petcov, Phys. Lett. **B 200**, 373, (1988).

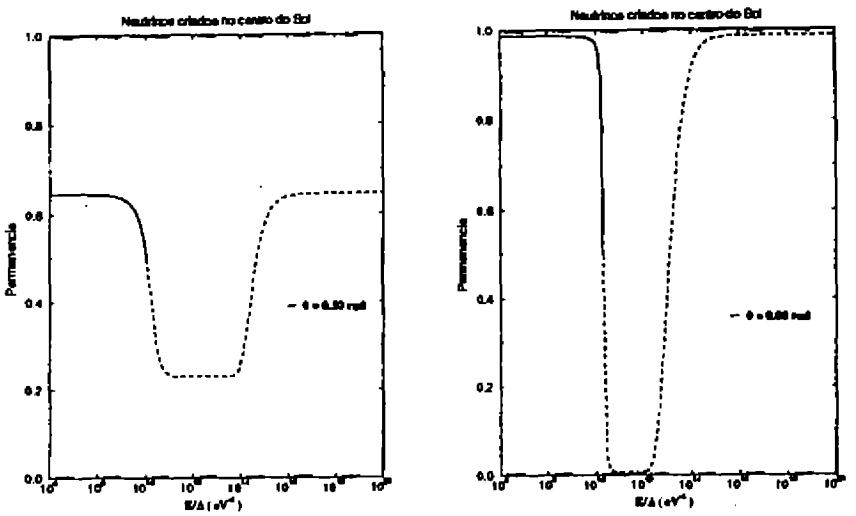

Figura 1: Probabilidade de Permanência para neutrinos criados no centro do Sol.

Experimental Extraction of the Proton Profile at the Highest Energies*

P. A. S. Carvalho and M. J. Menon
Instituto de Física 'Gleb Wataghin'
Universidade Estadual de Campinas - Unicamp
13083-970 Campinas, São Paulo, Brasil.

Received March, 1996

We introduce a novel complex analytic parametrization for the elastic hadronic scattering amplitude at high energy. Through the CERN-minuit routine we fit all proton-proton differential cross sections data above $\sqrt{s} = 10$ GeV. The Profile Function and the Inelastic Overlap Function are then extracted from this model-independent approach. Our preliminary results show characteristic blackening and expasion effects, which are presented and discussed.

1 - Introduction

In the impact parameter representation the elastic scattering amplitude F is given by the Fourier-Bessel transform of the Profile Function [1],

$$F(q,s) = i \int bdbJ_o(qb)\Gamma(b,s), \tag{1}$$

where b is the impact parameter, q the transferred momentum, $\sqrt{s}$ the center-of-mass energy, J_o the Bessel Function and $\Gamma(b,s)$ the Profile Function (PF). The s-channel unitarity in the impact parameter space connects the PF with the Inelastic Overlap Function (IOF) $G_{in}(b,s)$ by [1],

$$2Re\Gamma(b,s) = \mid \Gamma(b,s) \mid^2 + G_{in}(b,s). \tag{2}$$

In the optical analogy (Fraunhofer diffraction of light), Re $\Gamma(b,s)$ represents the degree of absortion of an incident wave caused by the obstacle and so, may be seen as describing the hadronic opacity as function of b and s. The IOF represents the absorption into open inelastic channels and its integration over the impact parameter plane leads to the total inelastic cross section:

$$\sigma_{in}(s) = 2\pi \int bdbG_{in}(b,s). \tag{3}$$

Extraction of the PF and IOF from experimental data is usually performed by suitable parametrizations for the scattering amplitude F(q,s) and fits to experimental differential cross section and ρ-parameter data:

$$\frac{d\sigma}{dq^2} = \pi \mid F(q,s) \mid^2, \qquad \rho(s) = \frac{ReF(0,s)}{ImF(0,s)}. \tag{4}$$

This is our goal in this work: in section 2 we present the fit method and in section 3 the results for Re $\Gamma(b,s)$ and $G_{in}(b,s)$. Conclusions and final remarks are the content of section 4.

2 - Fit Procedure and Results

We introduce the following parametrization for the scattering amplitude

$$F(q,s) = i\sum_{j=1}^{2} \alpha_j(1+i\lambda)e^{-\beta_j q^2} + i\sum_{j=3}^{5} \alpha_j e^{-\beta_j q^2}, \tag{5}$$

*Financial Support: CNPq

with the constraint

$$\lambda(s) = -\rho(s)\frac{\sum_{j=1}^{5}\alpha_j}{\alpha_1+\alpha_2}, \tag{6}$$

where α_i, β_i, i=1,2,...,5 are real free parameters and $\rho(s)$ is the experimental ρ-value at each energy.

Making use of the CERN-minuit routine we fit seven sets of pp differential cross section data above $\sqrt{s}$ = 10 GeV. These sets may be classifyied into two groups: G1: $\sqrt{s}$=13.8 and 19.4 GeV, G2: $\sqrt{s}$=23.5, 30.7, 44.7, 52.8 and 62.5 GeV. The group G2 was critically analysed by Amaldi and Schubert [2,3] and corresponds to a coherently normalized data set. This is not true for the group G1.

The results of our fits are show in figure 1 and table 1 (numerical values of the free parameters are available from the authors) and will be discussed in section 4.

$\sqrt{s}(GeV)$	N	$\chi^2/d.f.$
13.8	100	1.87
19.4	124	2.64
23.5	134	0.95
30.7	173	1.47
44.7	207	2.14
52.8	206	1.65
62.5	124	1.11

Table 1. Number of experimental data points and chi square per degree of fredom at each energy.

3 - Profile and Inelastic Overlap Functions

Substitution of parametrization (5)-(6) into equation (1) and then into equation (2) gives the Re $\Gamma(b,s)$ and $G_{in}(b,s)$. The results at 23.5 and 62.5 GeV as function of the impact parameter are displayed in figure 3. Conversely, for G_{in}, figure 3 shows the dependence with the energy at two different values of the impact parameter.

4 - Conclusions and Final Remarks

From table 1 (and figure 1) our fits present χ^2/d.f.=1$\sim$2 for group G2 and χ^2/d.f.=2$\sim$3 for group G1, which is statistically satisfactory. In figure 1c we observe that the real part of the scattering amplitude changes sign at high energies, as predicted from dispersion relations analysis [4].

Figure 2 shows that hadrons become blacker and larger (section 1) as the energy increases in the ISR region (group G2) and that at fixed energies, $G_{in}(b)$ is nearly exponential above b$\sim$1.0 fm.

From figure 3 the central opacity, $G_{in}(0,s)$, decreases with the energy in the region 13-19 GeV and is nearly constant at 23-62 GeV. However in the peripheral region (b$\sim$1.0 fm) it increases at 23-62 GeV.

Similar results were obtained by Amaldi and Schubert with a parametrization that obey geometrical scaling [2,5]. However our novel parametrization (5)-(6) does not assume this hipothesis and so is more general (less restrictive).

In spite of all these features our final results for the IOF and PF are somewhat qualitatives since the propagation of errors from the fit parameters was not taken into account. We are currently investigating this subject.

References

1. - U. Amaldi, M. Jacob, G. Matthiae, Ann. Rev. Nucl. Sci 26 (1976) 385.

2. - U. Amaldi and K.R. Schubert, Nucl. Phys. **B166** (1980) 301.

3. - K. R. Schubert, Tables on Nucleon-Nucleon scattering, in Landolf-Bornstein, Numerical Data and Functional Relationships in Science and Tecnology, New Series, vol. 1/9a (1979).

4. - W. Grein; R. Guigas and P. Kroll, Nucl. Phys. B89 (1975) 93.

5. - C. Furget, M. Buenerd, P. Valin, Z. Phys. C47 (1990) 377.

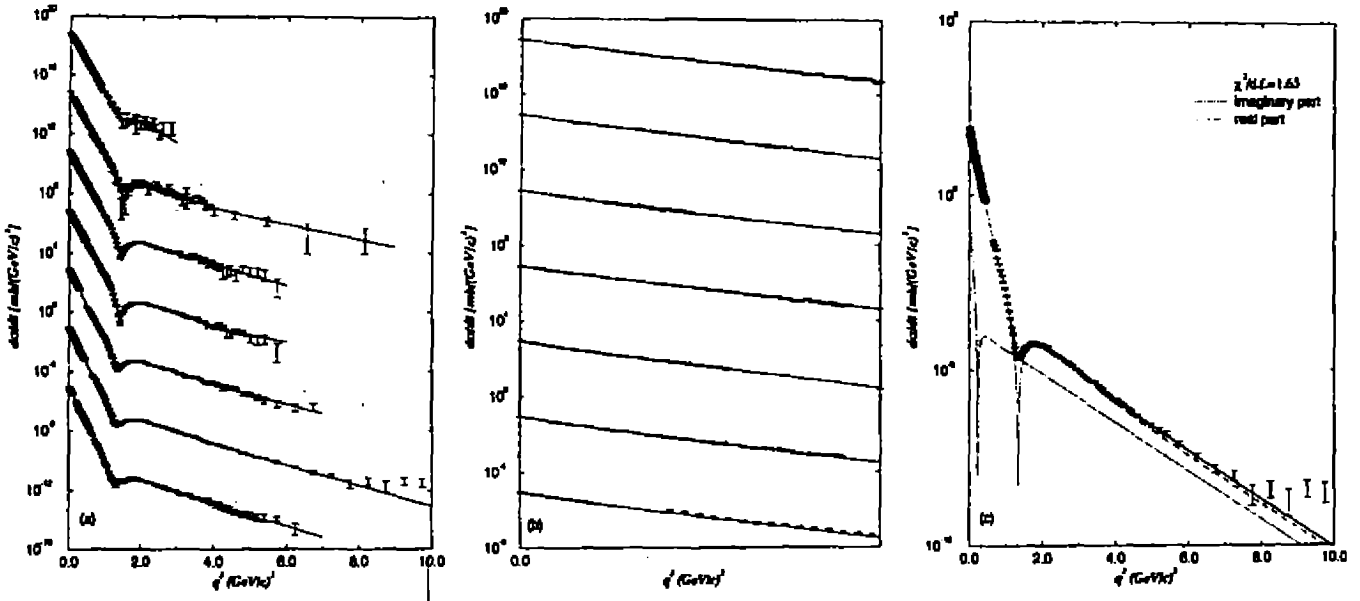

Figure 1: Fit to pp differential cross section data: (a) complet region in transferred momentum; (b) diffraction peak; (c) contribution of the real and imaginary part of the scattering amplitude at the energy of 52.8 GeV. Experimental data are from reference [2,3].

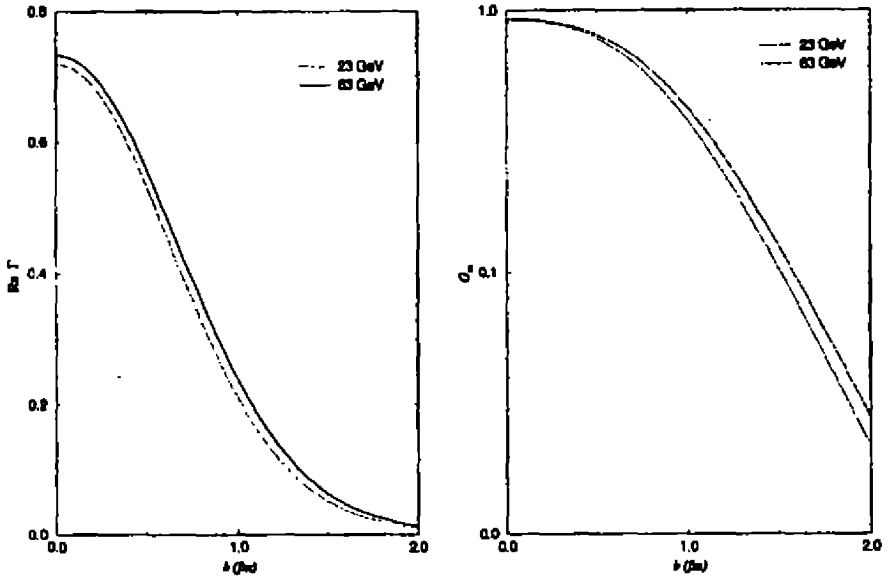

Figure 2: Real part of PF and the IOF as function of the impact parameter at ISR energy region.

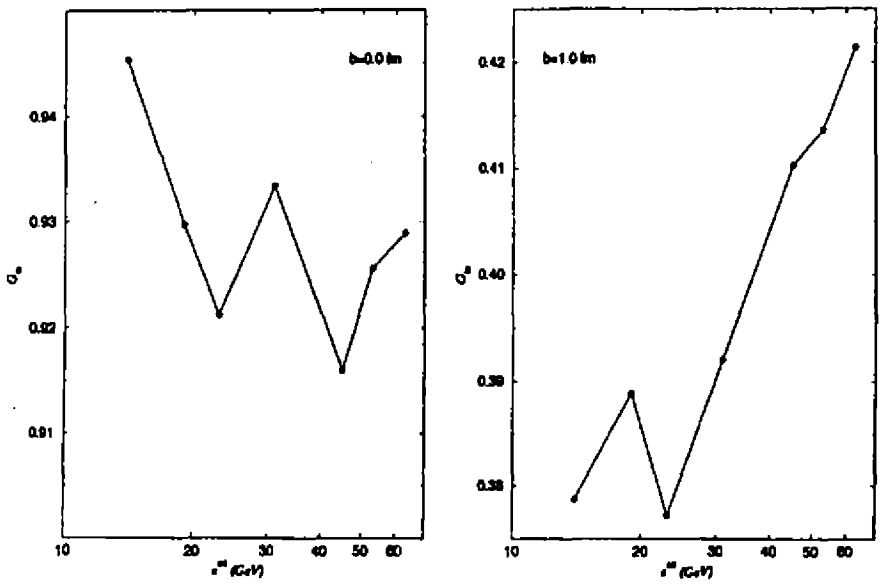

Figure 3: Extracted values of the IOF as function of the energy at two fixed parameters.

Phenomenological approach to elastic proton-proton scattering above 10 GeV*

A.F. Martini and M.J. Menon
Instituto de Física 'Gleb Wataghin', Unicamp
13083-970 Campinas, São Paulo, Brasil

Received March, 1996

Elastic pp scattering above $\sqrt{s} = 10$ GeV is investigated in a Multiple Diffraction Model, with complex averaged elementary (parton-parton) amplitude. The model predictions describe the general features of experimental data on differential cross section, total cross section and the ρ-parameter (ratio of the real to the imaginary part of the forward amplitude). Extrapolations to Cosmic-Ray energies predict total cross sections above the (model dependent) results from the Akeno Collaboration and are in agreement with the reanalysis performed by N.N. Nikolaev.

1 Multiple Diffraction Model

In high energy elastic hadron scattering the Eikonal Approach and the Multiple Diffraction Theory (Glauber) connect hadronic form factors, G_A, G_B, averaged elementary (parton-parton) amplitude, f, with the hadronic amplitude, F_{AB}, through the well known formulas [1]

$$F_{AB}(q,s) = i\int bdbJ_0(qb)[1-e^{-\Omega_c(b,s)}] \equiv i < 1-e^{-\Omega_c(b,s)} >,$$

$$\Omega_c(b,s) = -iC\int qdqJ_0(qb)G_A(q,s)G_B(q,s)f(q,s) = -iC < G_A G_B f >$$

where q^2 denotes the momentum transfer squared, b the impact parameter, $\sqrt{s}$ the center-of-mass energy, C the absorption factor and $\Omega_c(b,s)$ the complex eikonal.

In a Multiple Diffraction Model recently developed the following parametrizations have been used [2]

$$G_j = [(1+q^2/\alpha_j^2)(1+q^2/\beta_j^2)]^{-1}, \quad j = A, B$$

$$Im\{f(q,s)\} = \frac{1-q^2/a^2}{1+q^4/a^4}, \qquad Re\{f(q,s)\} = \lambda(s) Im\{f(q,s)\}.$$

For pp elastic scattering the complex hadronic amplitude reads,

$$ReF_{pp}(q,s) =< e^{-\Omega_{pp}}\sin(\lambda\Omega_{pp}) >,$$
$$ImF_{pp}(q,s) =< 1-e^{-\Omega_{pp}}\cos(\lambda\Omega_{pp}) >$$

where

$$\Omega_{pp} = C < \frac{1}{[(1+q^2/\alpha^2)(1+q^2/\beta^2)]^2}\frac{1-q^2/a^2}{1+q^4/a^4} >$$

and

$$\Omega_c = (1-i\lambda)\Omega_{pp}.$$

With this formalism we have only five free parameters, $C, \alpha^2, \beta^2, a^2$ and λ, which may be determined through fits to the experimental data on differential cross section and the ρ-parameter.

*Financial support: Capes and CNPq

$$\frac{d\sigma}{dq^2} = \pi |F_{pp}(q,s)|^2, \quad \rho = \frac{Re\{F_{pp}(0,s)\}}{Im\{F_{pp}(0,s)\}}.$$

Previous analysis limited to ISR energies (23.5 - 62.5 GeV) led to a satisfactory description of the experimental data [2, 3]. In this communication we extend the analysis to lower energies (but above 10 GeV) and present extrapolations to cosmic ray energies ($\sqrt{s} \geq 10$ TeV).

2 Fits and Results

Investigation of pp experimental data on differential cross section and ρ-parameter (7 sets of data between 13.8 and 62.5 GeV; see figure 1 led to the following results for the behaviour of the free parameters in terms of the energy:

- Constant free parameters:

$$a^2 = 8.2\, GeV^2, \qquad \beta^2 = 1.80\, GeV^2$$

- Free parameters depending on energy:

$$C(s) = 14.26 - 1.65[\ln(s)] + 0.159[\ln(s)]^2 \quad (GeV^{-2}),$$

$$\frac{1}{\alpha^2} = 2.57 - 0.217[\ln(s)] + 0.0243[\ln(s)]^2 \quad (GeV^{-2}),$$

$$\lambda(s) = \frac{0.0695[\ln(s/s_0)]}{1 + 0.118[\ln(s/s_0)] + 0.015[\ln(s/s_0)]^2}, \qquad s_0 = 400\, GeV^2.$$

We observe that this procedure does not correspond to solve an "inverse problem" only: we were able to extract the energy dependence of the free parameters (and this is not so usual in multiple diffraction models). Predictions for the differential cross sections, ρ-parameter and total cross sections are shown in figures 1 and 2. We observe that with the exception of the dip region at the ISR energies all predictions are in full agreement with the experimental data.

3 Extrapolations to Cosmic Ray Energies

At present, for pp scattering, experimental data from acelerator experiments are available only up to $\sqrt{s} = 62.5\, GeV$, the top ISR energy (figures 1 and 2). Extensive air shower data from the Akeno Cosmic Ray Observatory allows the determination of the proton-air cross section in the interval $\sqrt{s} : 6 \sim 25\, TeV$. For these data σ_{tot}^{pp} may be derived using a nuclear model. Two distinct results come from this kind of analysis: the results from the Akeno Collaboration [4] and a reanalysis performed by N.N. Nikolaev [5]. The differences in total cross section evaluation are about 30 mb. Both results are shown in figure 2 (right).

Assuming that our parametrization may be valid at this so high energy region we performed extrapolation for the total cross section. As we see in figure 3 our result is in agreement with the reanalysis by Nikolaev.

References

[1] R.J. Glauber, in Lectures in Theoretical Physics, vol. I, ed. W.E. Britten et al. (Interscience, New York, 1959) pp. 315-414; M.J. Menon, Phys. Rev. D48 (1993) 2007.

[2] A.F. Martini and M.J. Menon, XV Brazilian National Meeting on Particle and Fields (Sociedade Brasileira de Física, São Paulo, 1995) p 208; A.F. Martini, Master Thesis, IFGW-UNICAMP (1995).

[3] A.F. Martini and M.J. Menon, "Multiple Diffraction Approach to Proton- Proton Scattering at ISR Energies", submited to Brazilian Journal of Physics.

[4] M. Honda et al., Phys. Rev. Lett. 70 (1993) 525.

[5] N.N. Nikolaev, Phys. Rev. D48 (1993) R1904.

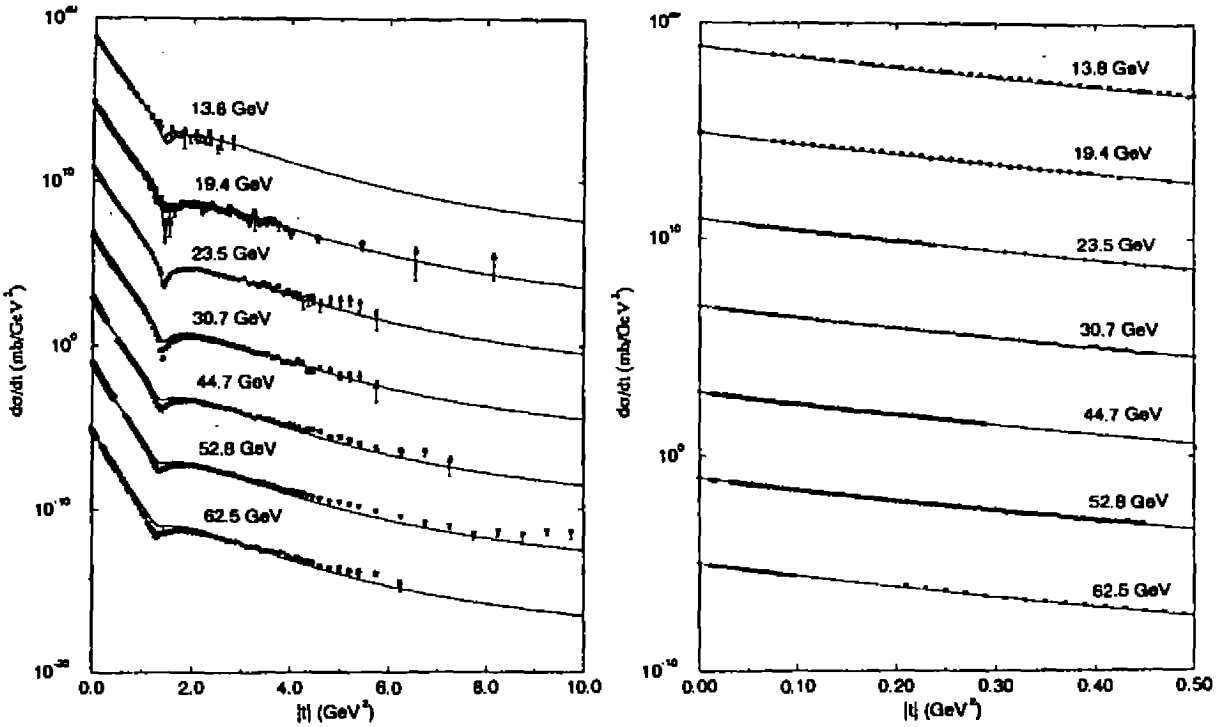

Figure 1: Model predictions and experimental data on pp differential cross section: large transferred momentum (left) and peak region (right). Curves and data were multiplied by powers of 10.

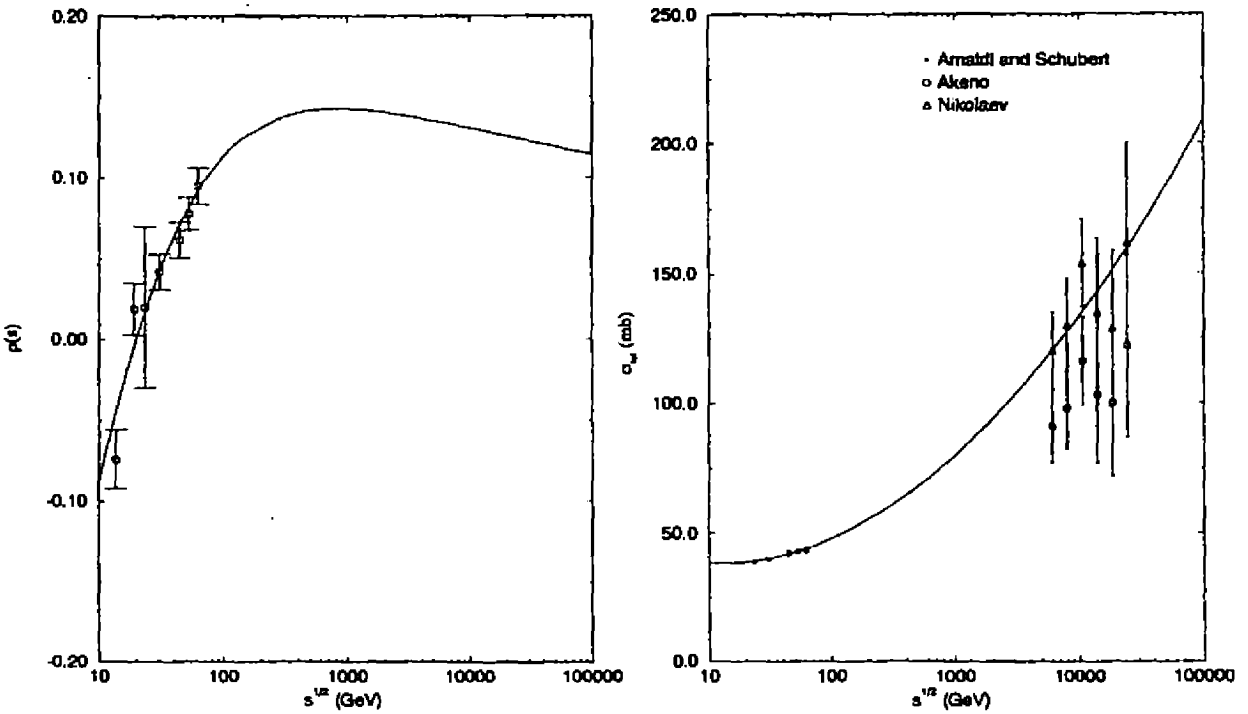

Figure 2: Model prediction and experimental data on the ρ-parameter (left) and total cross section (right). The data for the total cross section are from ISR (blacksquare) and model dependent results by Akeno Collaboration (circle) and the reanalysis by Nikolaev (triangle).

Preliminary Results on $\pi^- p$ Scattering in a Multiple Diffraction Approach*

M.J. Menon[1] and J.T.S. Paes[2]

[1] *Instituto de Física 'Gleb Wataghin', Unicamp*

13083-970 Campinas, SP, Brasil

[2] *Departamento de Física, Universidade Federal do Pará*

66075-900 Belém, PA, Brasil

Received March, 1996

We analyse $\pi^- p$ elastic scattering at $\sqrt{s} = 19.4\ GeV$ ($P_{lab} = 200\ GeV/c$) in the framework of a Multiple Diffraction Model recently developed for pp scattering. Hadronic form factor for the proton and pion are parametrized by double and simple poles, respectively. Taking account of flavour contents we assume similar *complex* averaged elementary (parton-parton) amplitude as in the pp case. With three free parameters our results reproduce quite well the $\pi^- p$ differential cross section data. Profile functions for $\pi^- p$ and pp scattering are also presented and discussed.

1 Introduction

Through a Multiple Diffraction Model for pp elastic scattering recently developed, a satisfactory description of the experimental data above $\sqrt{s} = 10\ GeV$ was achieved [1]. Two novel aspects of this model are the introduction of a complex elementary parton-parton amplitude and the following prediction for the proton hadronic form factor as function of energy and transferred momentum:

$$G_p(q,s) = \frac{1}{(1+q^2/\alpha^2)(1+q^2/\beta^2)}, \tag{1}$$

where $\beta^2 = 1.80\ GeV^2$ and

$$\frac{1}{\alpha^2} = 2.57 - 0.217[lns] + 0.0243[lns]^2\ (GeV^{-2}). \tag{2}$$

In this communication we extend the analysis to $\pi^- p$ elastic scattering at $\sqrt{s}$=19.4 GeV. To this end we make use of the above prediction for the proton and introduce a *complex* elementary amplitude associated to the $\pi^- p$ scattering. We shall use here the notation axplained by Martini and Menon in these proceedings [1].

2 Formulation

For pion-proton scattering the complex-eikonal is expressed by:

$$\Omega_C = -iC_{\pi p} \int_0^\infty q dq J_0(qb) G_p G_\pi f_{\pi p} \equiv -iC_{\pi p} < G_p G_\pi f_{\pi p} >, \tag{3}$$

where $G_p(q,s)$ is calculated from (1) and (2) at each energy. Our formulation is based on two essential assumptions:

a) We use a simple pole parametrization for the (unknow) pion hadronic form factor

$$G_\pi = \frac{1}{1+q^2/\gamma^2}, \tag{4}$$

*Financial Support:CNPq and Capes-PICD

with γ^2 free parameter;

b)Taking account of the u and d flavour contents in both pion and proton we assume, as first approximation, an averaged elementary amplitude with the same transferred momentum dependence as in the pp case, but with the ratio between real and imaginary parts as free parameter:

$$Imf_{\pi p} = \frac{1 - q^2/a^2}{1 + q^4/a^4}, \tag{5}$$

$$Ref_{\pi p} = \lambda_{\pi p}(s) Imf_{\pi p}, \tag{6}$$

with $\lambda_{\pi p}(s)$ free parameter. For the same reason we assume the same value of the (constant) a^2-parameter obtained in the pp analysis : $a^2 = 8.20\ GeV^2$. Through (3) to (5) and according to the notation in reference [1], we have

$$\Omega_C = (1 - i\lambda_{\pi p})\Omega_{\pi p}, \tag{7}$$

with

$$\Omega_{\pi p} = C_{\pi p} < \frac{1 - q^2/a^2}{(1 + q^2/\alpha^2)(1 + q^2/\beta^2)(1 + q^2/\gamma^2)(1 + q^4/a^4)} >, \tag{8}$$

analytically integrable:

$$\Omega_{\pi p}(b, s) = C_{\pi p}[A_1 k_0(\alpha b) + A_2 k_0(\beta b) + A_3 k_0(\gamma b) + A_4 kei_0(ab) + A_5 ker_0(ab)], \tag{9}$$

where $A_i, i = 1, ...5$ are algebraic functions of α^2, β^2, γ^2 and a^2 and kei, ker are Thompson functions. The connection with the differential cross section $d\sigma/dq^2$ and the ρ-parameter is obtained through the hadronic scattering amplitude:

$$ReF_{\pi p}(q, s) =< e^{-\Omega_{\pi p}(b,s)} sin[\lambda_{\pi p}(s)\Omega_{\pi p}(b, s)] >, \tag{10}$$

$$ImF_{\pi p}(q, s) =< 1 - e^{-\Omega_{\pi p}(b,s)} cos[\lambda_{\pi p}(s)\Omega_{\pi p}(b, s)] >, \tag{11}$$

$$\frac{d\sigma}{dq^2} = \pi |F_{\pi p}(q, s)|^2, \tag{12}$$

$$\rho(s) = \frac{ReF_{\pi p}(0, s)}{ImF_{\pi p}(0, s)}. \tag{13}$$

3 Fit and Results

With this formalism we have for πp scattering only three free parameter: $C_{\pi p}$, γ^2 and $\lambda_{\pi p}$. The former two are obtained by fit to the differential cross section data and then the later is determined so as to reproduce the experimental ρ-value. The results obtained for $\pi^- p$ elastic scattering at $\sqrt{s} = 19.4\ GeV$ are shown in figure 1. This description of the experimental data was obtained with the following values of the free parameters:

$$C_{\pi p} = 6.20\ GeV^2,\ \gamma^2 = 0.42\ GeV^2,\ \lambda_{\pi p} = 0.0756. \tag{14}$$

We observe that the real part of the scattering amplitude changes sign as predicted by dispersion relations [3]. We have also calculated the Profile Functions,

$$\Gamma(b, s) = -i < F(q, s) >,$$

for both reactions, $\pi^- p$ and pp, at $\sqrt{s} = 19.4\ GeV$. The results for the real part are presented in figure 2.

In optical grounds we may interpret this behaviour as meaning that the proton is blaker and larger than the pion at the same energy. Our preliminary results show good agreement with experimental data. A complete analysis for $\pi^+ p$ and $\pi^- p$ scattering at different energies is being carried out and results will be presented elsewhere.

References

1. A.F. Martini and M.J. Menon, " Phenomenological Approach to Elastic Proton-Proton Scattering above 10 GeV ", these proceedings.

2. Z. Asa'd et al., Nucl. Phys. B255 (1985) 273 ; R. Rubinstein et al., Phys. Rev. D30 (1984)1413; A. Schiz et al., Phys. Rev. D24 (1981) 26; D.S. Ayres et al., Phys. Rev. D15 (1977) 2105; C.W. Akerlof et al., Phys. Rev. D14 (1976) 2864; A.S. Carroll et al., Phys. Lett. 80B (1979) 423; A.S. Carroll et al., Phys. Lett. 61B (1976) 303.

3. J.B. Bronzan,G.L. Kane and U.P. Sukhatme, Phys. Lett. B49 (1974) 272.

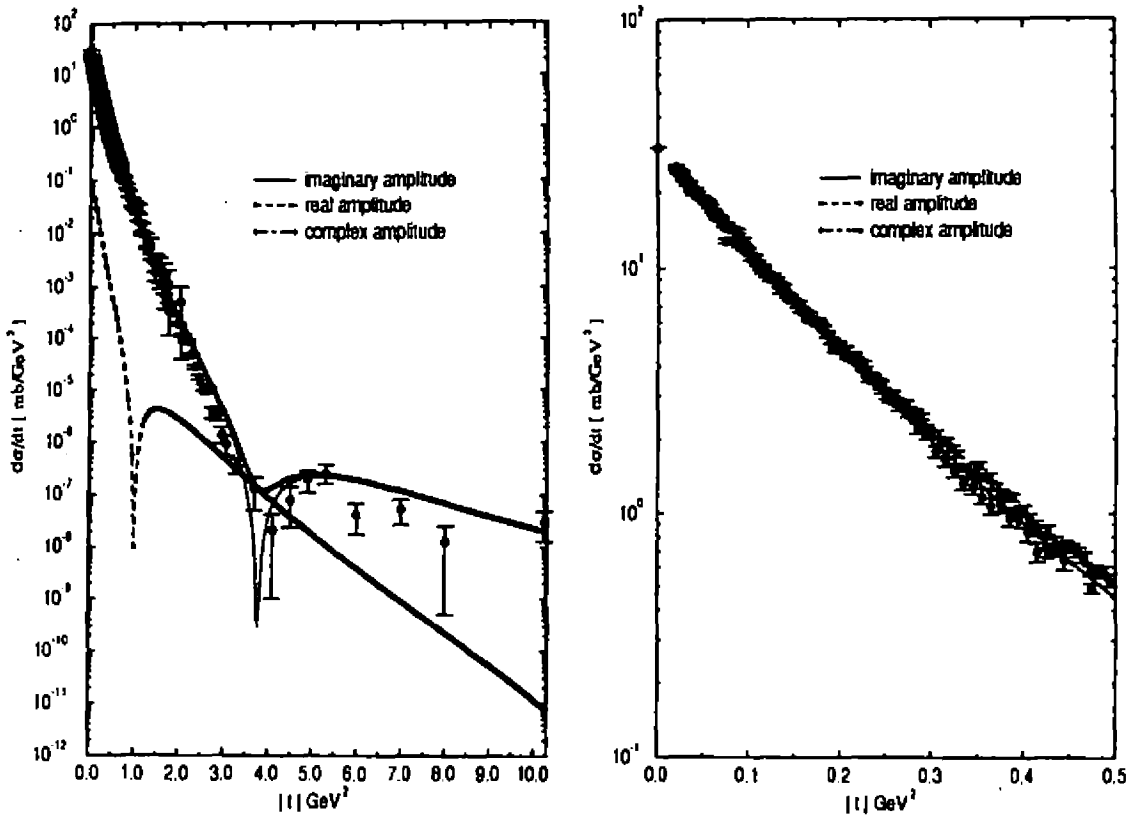

Figure 1: Results for $\pi^- p$ elastic scattering and experimental data [2].

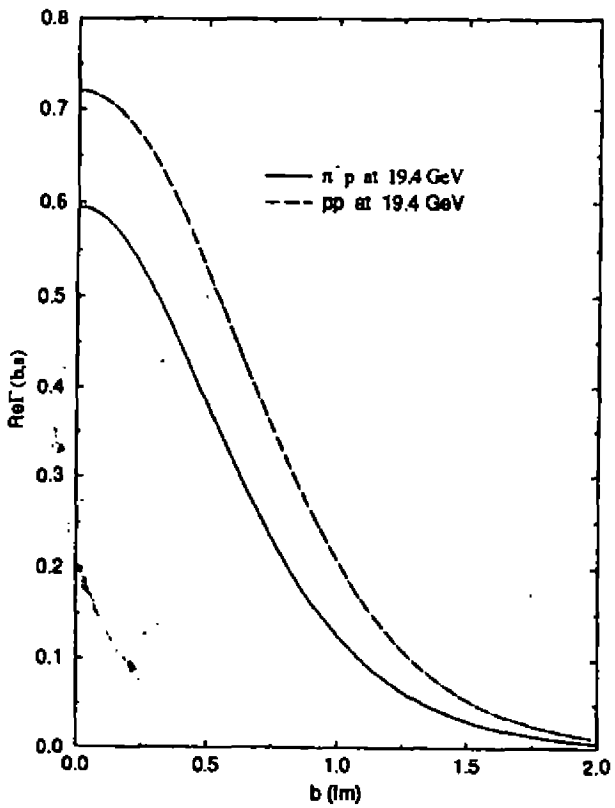

Figure 2: Predictions for the real part of the Profile Function.

Dynamical generation of supersymmetry

Ashok Das (University of Rochester)
Marcelo Hott (UNESP - Guaratinguetá)

Received March, 1996

Conventionally, in the study of supersymmetric theories, one starts with a free theory which is invariant under supersymmetry transformations (transformations which take bosons into fermions and vice versa). This requires bosons and fermions (the superpartners) of the theory to have equal masses (or frequencies if one is dealing with quantum mechanical oscillators). Interactions are then introduced so as to maintain the tree level supersymmetry or build on it.

We will show within the context of a quantum mechanical model how a theory can develop supersymmetry dynamically in the presence of interactions. More specifically, we will start with a free theory of a bosonic and a fermionic oscillator of unequal frequencies which is not supersymmetric and show that in the presence of interactions this theory can become supersymmetric. This is what we call dynamical generation of supersymmetry and it does not require the boson and the fermion to have equal frequencies (masses) at the perturbative level (although the nonperturbative masses will be degenerate).

Let us start with a quantum mechanical theory of a free bosonic and fermionic oscillator described by the Hamiltonian,

$$H_0 = \omega a^\dagger a + \epsilon c^\dagger c \tag{1}$$

where a and c stand for the bosonic and the fermionic annihilation operator respectively with ω and ϵ representing their respective frequencies. The creation and the annihilation operators for the bosons (fermions) satisfy the standard (anti) commutation relations[1]. As is well known, when $\omega = \epsilon$, this defines the supersymmetric oscillator [1-3] which is invariant under the supersymmetric transformations generated by the supercharges [1]

$$Q = a^\dagger c \quad \text{and} \quad \bar{Q} = c^\dagger a \tag{2}$$

In our entire discussion, however, we will assume that $\omega \neq \epsilon$. Our starting theory is, therefore, not supersymmetric since the bosonic and the fermionic frequencies (masses) are not equal. However, let us now look at the following interacting Hamiltonian [4-5],

$$H = \omega a^\dagger a + \epsilon c^\dagger c + g(a^\dagger + a)c^\dagger c \tag{3}$$

where g represents the strength of the interaction. We will now show that for the specific value of the coupling parameter (We assume $\epsilon > \omega$.)

$$\epsilon - \omega = \frac{g^2}{\omega} \tag{4}$$

the Hamiltonian in Eq.(3) becomes supersymmetric.

To show this, let us consider the fermionic charges

$$\begin{aligned} Q &= a^\dagger c \exp\left(\frac{g}{\omega}(a^\dagger - a)\right) \\ \bar{Q} &= \exp\left(-\frac{g}{\omega}(a^\dagger - a)\right) c^\dagger a \end{aligned} \tag{5}$$

With the standard (anti) commutation relations of the theory, it is straightforward to show that

$$\begin{aligned} [Q, H] &= (\epsilon - \omega - \frac{g^2}{\omega})Q \\ [\bar{Q}, H] &= -(\epsilon - \omega - \frac{g^2}{\omega})\bar{Q} \end{aligned} \tag{6}$$

It is clear now that when the condition in Eq.(4) holds, these fermionic charges are conserved and define supersymmetric transformations under which the interacting Hamiltonian in Eq.(3) is invariant. It is also straightforward to show that

$$[Q, \bar{Q}]_+ = \frac{1}{\omega}[H - (\epsilon - \omega - \frac{g^2}{\omega})c^\dagger c] \tag{7}$$

This shows that the conserved charges Q and $\bar{Q}$ satisfy the conventional supersymmetry algebra when Eq.(4) holds. The Hamiltonian H of Eq.(3) can be easily checked (with the condition in Eq.(4)) to be invariant under the supersymmetry transformations

$$\begin{aligned} \delta a &= -\lambda(1 + \frac{g}{\omega}a^\dagger)\exp(\frac{g}{\omega}(a^\dagger - a))c \\ \delta a^\dagger &= -\frac{g}{\omega}\lambda a^\dagger c \exp(\frac{g}{\omega}(a^\dagger - a)) \\ \delta c &= 0 \\ \delta c^\dagger &= \lambda a^\dagger \exp(\frac{g}{\omega}(a^\dagger - a)) \end{aligned} \tag{8}$$

and

$$\begin{aligned} \bar{\delta} a &= \frac{g}{\omega}\bar{\lambda}\exp(-\frac{g}{\omega}(a^\dagger - a))c^\dagger a \\ \bar{\delta} a^\dagger &= \bar{\lambda}\exp(-\frac{g}{\omega}(a^\dagger - a))c^\dagger(1 + \frac{g}{\omega}a) \\ \bar{\delta} c &= \bar{\lambda}\exp(-\frac{g}{\omega}(a^\dagger - a))a \\ \bar{\delta} c^\dagger &= 0 \end{aligned} \tag{9}$$

Here λ and $\bar{\lambda}$ are the two constant Grassmann parameters of the supersymmetry transformations.

Thus, we see that even though the starting theory is not supersymmetric and the bosonic and the fermionic oscillators have different frequencies (masses), for a particular value of the interaction strength, the interacting Hamiltonian has become supersymmetric. The theory has generated supersymmetry dynamically. Since the bosons and the fermions correspond to different frequencies, it is worth investigating the structure of the supersymmetric spectrum of states in this theory. It can be easily checked that the superpartner states now involve coherent states in a nontrivial way (Eq.(4) is assumed.).

$$\begin{aligned} Q|n_a, n_c = 1\rangle &= \frac{1}{\sqrt{n_a!}}a^\dagger(a^\dagger - \frac{g}{\omega})^{n_a}|\frac{g}{\omega}, n_c = 0\rangle \\ \bar{Q}|n_a + 1, n_c = 0\rangle &= \sqrt{\frac{n_a + 1}{n_a!}}(a^\dagger + \frac{g}{\omega})^{n_a}|-\frac{g}{\omega}, n_c = 1\rangle \end{aligned} \tag{10}$$

Here we have introduced the coherent states defined by [6]

$$|\alpha, n_c\rangle = \exp(\alpha(a^\dagger - a))|n_a = 0, n_c\rangle \tag{11}$$

Thus, we see that the relation between the perturbative supersymmetric partner states, in this case, are not as simple as in the conventional supersymmetric theories.

Finally, let us note here that this theory can be exactly solved and all of the above features can be seen in a simpler way as follows. Let us define a generalized Bogoliubov transformation defined by the operator

$$U = \exp(-\frac{g}{\omega}(a^\dagger - a)c^\dagger c) \tag{12}$$

This defines a unitary transformation leading to

$$\begin{aligned} b &= UaU^\dagger = (a + \frac{g}{\omega}c^\dagger c) \\ b^\dagger &= Ua^\dagger U^\dagger = (a^\dagger + \frac{g}{\omega}c^\dagger c) \\ f &= UcU^\dagger = \exp(\frac{g}{\omega}(a^\dagger - a))c \\ f^\dagger &= c^\dagger \exp(-\frac{g}{\omega}(a^\dagger - a)) \end{aligned} \tag{13}$$

These new variables satisfy the canonical (anti) commutation relations like the original fields since the transformation is unitary. It is now straightforward to check that the interacting Hamiltonian of Eq.(3) can be rewritten in terms of these new variables as

$$H = \omega b^\dagger b + (\epsilon - \frac{g^2}{\omega}) f^\dagger f \tag{14}$$

The energy eigenstates and the eigenvalues in terms of these variables are quite simple, namely,

$$H|n_b, n_f\rangle = E_{n_b,n_f}|n_b, n_f\rangle \tag{15}$$

with

$$E_{n_b,n_f} = \omega n_b + (\epsilon - \frac{g^2}{\omega}) n_f \tag{16}$$

with $n_f = 0, 1$ and $n_b = 0, 1, 2, \cdots$. It is clear now that when Eq.(4) is satisfied the theory is nothing other than the supersymmetric oscillator in terms of these new variables. The supersymmetric partner states are the conventional ones in the quanta of the redefined variables. We also note that when $\epsilon - \frac{g^2}{\omega} < 0$, the ground state of the theory becomes fermionic [4] whereas if $\epsilon - \frac{g^2}{\omega} = 0$, the fermions completely drop out of the theory. Simple as the Hamiltonian in Eq.(3) may appear to be, it really has a rich structure. It is clear now (see, e.g., [1-3]) from the form of the Hamiltonian in Eq.(14) and the unitary transformation in Eq.(12) that one could also have started with a more complicated interacting Hamiltonian in Eq.(3) which would have resulted in a supersymmetric, interacting Hamiltonian in terms of the variables b and f.

To conclude, we have shown in a simple quantum mechanical model how supersymmetry can be dynamically generated in the presence of interactions even when the free theory may not be supersymmetric. It remains to be seen if and how this idea can be generalized to relativistic quantum field theories. The properties of such theories would be quite interesting to investigate.

References

1. A. Das, " Field Theory: A Path Integral Approach ", World Scientific, Singapore 1994.
2. E. Witten, Nucl. Phys. **B188** (1981) 513.
3. P. Salomonson and J.W. van Holten, Nucl. Phys. **196** (1982) 509.
4. This model was used earlier as a toy model in the study of bound states in quantum field theories in S.P. Misra, Indian J. Phys. **61B** (1987) 287.
5. See also, A. Das in " A Gift for Prophecy ", ed. E.C.G. Sudarshan, World Scientific, Singapore 1995.
6. R.J. Glauber, Phys. Rev. Lett. **10** (1963) 84; E.C.G. Sudarshan, Phys. Rev. Lett. **10** (1963) 277.

Cheshire Cat Scenario in a $3+1$ dimensional Hybrid Chiral Bag*

M. De Francia[†] H. Falomir[‡] E. M. Santangelo[§]

Departamento de Física

Facultad de Ciencias Exactas

Universidad Nacional de La Plata

C.C. 67 (1900) La Plata - Argentina

Received March, 1996

The hybrid chiral bag [1, 2] is an effective model to describe the behavior of strongly interacting baryons. In this model, color degrees of freedom are confined to a bounded region and coupled to a bosonic external field (skyrmion) through boundary conditions.

These two phase models (TPM) are intermediate between two successful descriptions of baryons: bag models [3, 4] - with QCD degrees of freedom at short distances - and Skyrme model [5, 6, 7], an effective (non renormalizable) nonlinear sigma model, useful when the low energy properties of baryons are considered.

An interesting feature of Chiral Bag Models (CBM) is the appearance of the so called Cheshire Cat Principle (CCP) [1, 8], according to which fermionic degrees of freedom can be replaced by bosonic ones in certain regions of space, the resulting position of the limit of separation between the two phases having no physical consequences.

In $1+1$-dimensions, the Cheshire Cat behavior follows from the bosonization of fermionic fields [1]. In the $3+1$ case, topological quantities, such as the baryonic number, have a similar behavior [9] but, for non topological ones, the CCP is expected to be only approximately valid.

We study the energy of a four-dimensional hybrid model consisting of quarks and gluons confined to a spherical bag plus a truncated exterior Skyrme field in a hedgehog configuration. It is our aim to study the dependence of the total energy on the size of the bag, thus testing the Cheshire Cat hypothesis.

The Casimir energy of quarks under chiral boundary conditions and that corresponding to gluons inside the bag are obtained, by making use of functional techniques introduced in previous studies of the subject [10, 11].

The contributions due to the valence quarks in the interior region and to the external Skyrme field are then added, so as to complete the total energy in the two phase model. To construct the Skyrme field in the hedgehog configuration, the Atiyah-Manton profile [12] is used.

Imposing the validity of the TPM, even in the $R \to 0$ limit, the renormalization constants are determined. Moreover, the continuity of the axial flux in the interface between the bag and the skyrmion helps us to analize the parameters of the model F_π and $c(R)$.

The total energy is obtained, showing (Figure) a good agreement with the Cheshire Cat hypotesis in the range of $0 < R < 1$fm.

The study of CBM at finite temperature [13, 14] is an interesting effective approach to the analysis of deconfinement transitions. In those references, successive approximations to the problem, based on the validity of the Cheshire Cat hypothesis at $T = 0$ have been made. The present results give a ground to such hypothesis, thus making it sensible to look for the presence of deconfinement transitions only in the temperature-dependent contributions to the free energy of the bag.

*This work was partially supported by CONICET and Fundación Antorchas, Argentina

[†]e-mail: defranci@dartagnan.fisica.unlp.edu.ar

[‡]e-mail: falomir@dartagnan.fisica.unlp.edu.ar

[§]email: mariel@dartagnan.fisica.unlp.edu.ar

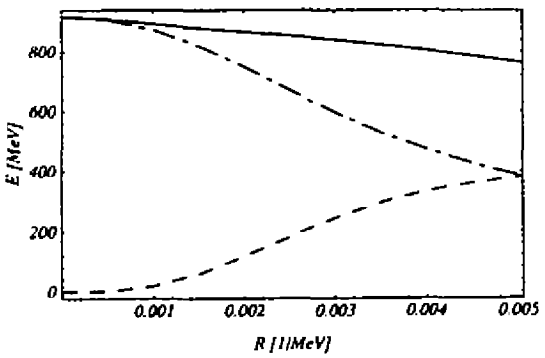

Figure 1: Two Phase model energy; — : Complete model ; - - - : Skyrmion's sector ; - · - : Bag's sector

References

[1] M. Rho. Cheshire Cat Hadrons. *Physics Reports*, 240(1,2):1–142, 1994.

[2] G. E. Brown, A. D. Jackson, M. Rho, and V. Vento. The nucleon as a topological chiral soliton. *Physics Letters*, 140B(5,6):285–289, 1984.

[3] A. Chodos, R. L. Jaffe, C. B. Thorn, and V. Weisskopf. New extended model of hadrons. *Physical Review*, 9D(12):3471–3495, 1974.

[4] fA. Chodos and C. B. Thorn. Chiral invariance in a bag theory. *Physical Review*, 12D(9):2733–2743, 1975.

[5] T. H. R. Skyrme. A unified field theory of mesons and baryons. *Nuclear Physics*, 31:556–569, 1962.

[6] E. Witten. Current Algebra, Baryons and Quark confinement. *Nuclear Physics*, 223B:433–444, 1983.

[7] G. S. Adkins, C. R. Nappi, and E. Witten. Static properties of nucleons in the Skyrme model. *Nuclear Physics*, 228B:552–566, 1983.

[8] S. Nadkarni, H. B. Nielsen, and I. Zahed. Bosonization relations as Bag Boundary Conditions. *Nuclear Physics*, B253:308–322, 1985.

[9] J. Goldstone and R. L. Jaffe. Baryon number in Chiral Bag Models. *Physical Review Letters*, 51(17):1518–1521, 1983.

[10] M. De Francia. Free energy for massless confined fields. *Physical Review*, 50D:2908–2919, 1994.

[11] M. De Francia, H. Falomir, and E. M. Santangelo. Free energy of a four dimensional chiral bag. *Physical Review*, 45D(6):2129–2139, 1992.

[12] M. F. Atiyah and N. S. Manton. Skyrmions from instantons. *Physics Letters*, 222(3,4):438–442, 1989.

[13] H. Falomir, M. Loewe, and J. C. Rojas. Hybrid models at finite temperature and deconfinement. *Physics Letters*, 300(3):278–282, 1993.

[14] M. Loewe and S. Perez-Oyarzún. On the Finite Size of the Bag and the Critical Deconfining Temperature in Hybrid models. *Physics Letters*, 322B:413–418, 1994.

Solução de Buraco Negro para a Gravitação Topológica

M. M. Leite e V. O. Rivelles
Instituto de Física , Universidade de São Paulo
Cx. Postal 66318, CEP 05389-970, São Paulo, SP, Brasil

Received March, 1996

A teoria da gravitação em duas dimensões pode ser formulada como uma teoria de calibre do grupo de Poincaré estendido [1] ,cujas relações de comutação são :

$$[\mathrm{P}_a, \mathrm{P}_b] = \epsilon_{ab}\mathrm{Z}$$

$$[\mathrm{P}_a, \mathrm{J}] = -\epsilon_a^b \mathrm{P}_b$$

sendo que as outras relações de comutação são nulas. Para construir uma ação invariante de calibre,precisamos de um multipleto de campos de calibre e um de multiplicadores de Lagrange dados em termos dos geradores por:

$$A = A_\mu d\xi^\mu = (e_\mu^a P_a + w_\mu J + a_\mu Z)d\xi^\mu, \tag{1}$$

$$\eta = \eta^a P_a + \eta^2 J + \eta^3 Z, \tag{2}$$

onde ξ^μ são coordenadas do espaço-tempo e a curvatura de calibre é dada em termos do potencial de calibre através de:

$$F_{\mu\nu} = \partial_\mu A_\nu - \partial_\nu A_\mu + [A_\mu, A_\nu]. \tag{3}$$

Ao longo deste trabalho usamos as seguintes convenções :

$$\epsilon^{01} = 1; h_{ab} = diag(-1, 1) \tag{4}$$

enquanto que a métrica de Killing tem as seguintes componentes:

$$h_{ab}\ , h_{a2} = h_{a3} = 0\ , h_{23} = 1 \tag{5}$$

obtidas do operador de Casimir da álgebra de Poincaré estendida,sendo usada para levantar e baixar índices do grupo que são aqueles associados aos geradores P_a,ao gerador J e ao gerador Z.
Na ausência de matéria a ação de gravidade pura é dada por um invariante topológico(índice de Pontriagin) que é invariante de calibre

$$S' = \int_{M^2} \mathrm{Tr}(\eta F), \tag{6}$$

onde o traço é tomado sobre os índices do grupo. Quando acoplamos fontes não-abelianas a esta teoria livre da gravidade,i.e.,acoplamos partículas pontuais sem massa com simetria interna que descrevem uma linha de universo W^1,parametrizada pela curva $x(\tau)$, a ação torna-se [2] :

$$S = \int_{M^2} \mathrm{Tr}(\eta F) + e_1 \int_{M^2}\int_{W^1} d\tau \mathrm{Tr}(QA_\mu)\dot{x}^\mu(\tau)\delta^2(\xi - x(\tau)) + e_1 \int_{W^1} \mathrm{Tr}(Kg^{-1}\dot{g})d\tau + \tag{7}$$

$$e_2 \int_{M^2}\int_{W^1} d\tau \mathrm{Tr}(Q\eta)\delta^2(\xi - x(\tau))$$

onde as fontes não-abelianas são descritas em termos do elemento do grupo g, e_1 e e_2 são as constantes de acoplamento do campo de calibre e dos multiplicadores de Lagrange,respectivamente,com as fontes. O elemento do grupo g é parametrizado em termos dos geradores

$$g = exp(\theta^a P_a) exp(\theta^2 J) exp(\theta^3 Z) \tag{8}$$

enquanto que as fontes têm a seguinte expressão em termos de g

$$Q(\tau) = g(\tau) K g^{-1}(\tau), \tag{9}$$

onde K assume valores constantes na álgebra de Poincaré estendida. As equações de movimento para as fontes são obtidas através da variação da ação em relação aos elementos do grupo g,ou seja

$$e_1 \frac{dQ^a}{d\tau} - e_1 \dot{x}^\mu (e^b_\mu \epsilon^a_b Q^2 - w_\mu \epsilon^a_b Q^b) - e_2 \epsilon^a_b (\eta^b Q^2 - \eta^2 Q^b) = 0 \tag{10}$$

$$e_1 \frac{dQ^2}{d\tau} = 0 \tag{11}$$

$$e_1 \frac{dQ^3}{d\tau} + (e_1 \dot{x}^\mu e^a_\mu Q^b - e_2 \eta^a Q^b) \epsilon_{ab} = 0. \tag{12}$$

Quando a ação é variada em relação aos multiplicadores de Lagrange , obtemos as equações de campo para o setor gravitacional

$$\epsilon^{\mu\nu} (\partial_\mu e^a_\nu + w_\mu e^b_\nu \epsilon^a_b) + e_2 \int_{W^1} d\tau \delta^2(\xi - x(\tau)) Q^a(\tau) = 0, \tag{13}$$

$$\epsilon^{\mu\nu} \partial_\mu w_\nu + e_2 \int_{W^1} d\tau \delta^2(\xi - x(\tau)) Q^2 = 0, \tag{14}$$

$$\epsilon^{\mu\nu} (\partial_\mu a_\nu + \frac{1}{2} e^a_\mu e^b_\nu \epsilon_{ab}) + e_2 \int_{W^1} d\tau \delta^2(\xi - x(\tau)) Q^3 = 0. \tag{15}$$

Finalmente, tomando a variação da ação com respeito aos campos de calibre,obtemos as equações de campo para os multiplicadores de Lagrange (setor do dilaton) :

$$\epsilon^{\mu\nu} (\partial_\nu \eta_2 + e^a_\nu \epsilon^b_a \eta_b) + e_1 \int_{W^1} d\tau Q_2(\tau) \delta^2(\xi - x(\tau)) \dot{x}^\mu = 0 \tag{16}$$

$$\epsilon^{\mu\nu} (\partial_\nu \eta_a - w_\nu \epsilon^b_a \eta_b + \eta_3 \epsilon_{ab} e^b_\nu) + e_1 \int_{W^1} d\tau Q^a \delta^2(\xi - x(\tau)) \dot{x}^\mu = 0 \tag{17}$$

$$\epsilon^{\mu\nu} \partial_\nu \eta_3 + e_1 \int_{W^1} d\tau Q_3 \delta^2(\xi - x(\tau)) \dot{x}^\mu = 0. \tag{18}$$

Para resolvermos tais equações,fazemos escolhas de calibre consistentes com o número de parâmetros de calibre da teoria. Em particular quando o espaço-tempo apresenta topologia trivial as soluções não representam buracos negros,enquanto que no caso de topologia não-trivial existem horizontes de eventos que caracterizam os buracos negros.

Em se tratando de topologia trivial do espaço-tempo,há dois sistemas de coordenadas diferentes que fornecem fixações de calibre consistentes, que são as coordenadas de Schwarzschild e coordenadas do cone de luz. Em tais sistemas de coordenadas é possível (em particular nas coordenadas de Schwarzschild) perceber que uma transformação de coordenadas torna o espaço-tempo Minkowskiano localmente,equivalente a um observador acelerado em movimento hiperbólico em coordenadas de Rindler[3]. Portanto não há incompleteza geodésica implicando que este tipo de solução não corresponde de fato a buracos negros.

No caso de topologia não-trivial há dois sistemas de coordenadas diferentes que fornecem fixações de calibre consistentes: as coordenadas de Schwarzschild e as coordenadas conformes.

Em coordenadas de Schwarzschild, fazemos a seguinte escolha de calibre ($(\xi^0, \xi^1) = (t, x)$)

$$e^0_0 = e^0_0(x) \quad e^1_1 = (e^0_0)^{-1} \quad e^0_1 = e^1_0 = 0 \tag{19}$$

$$Q^0 = Q^1 = 0 \, , w_0 = -ac(x) \, , w_1 = 0 \tag{20}$$

sendo que a = *constante*. Para a linha de universo das fontes , escolhemos $x^0 = \tau$ e $x^1 = 0$. A solução para as fontes são :

$$Q^3 = A = constante\ , Q^2 = -\frac{a}{e_2} = constante. \tag{21}$$

Para o setor gravitacional , temos

$$e_0^0 = (b + 2a|x|)^{\frac{1}{2}} \tag{22}$$

$$a_0 = -x + e_2 A\epsilon(x) + B \tag{23}$$

enquanto que para o setor do dilaton, obtemos as seguintes soluções (com o calibre fixo de forma que o dilaton é independente do tempo) :

$$\eta_3 = \Lambda \tag{24}$$

$$\eta_0 = \frac{\Lambda}{a}\epsilon(x)(b + 2a|x|)^{\frac{1}{2}} \tag{25}$$

$$\eta_1 = 0 \tag{26}$$

$$\eta_2 = \frac{\Lambda}{a}|x| + C. \tag{27}$$

O elemento de linha é

$$ds^2 = -(b + 2a|x|)dx^2 + (b + 2a|x|)^{-1}dt^2 \tag{28}$$

análogo ao elemento de linha de Schwarzschild em quatro dimensões. A curvatura escalar neste caso,

$$R = 4a\delta(x), \tag{29}$$

exibe uma singularidade na origem que não pode ser removida por transformações de coordenadas por ser uma singularidade física. Portanto, existe incompleteza geodésica uma vez que a região $x < 0$ é proibida e é impossível mapear o plano (x,t) completamente,pois aquelas transformações de coordenadas descritas no caso trivial "param" literalmente na hipérbole que caracteriza a singularidade. Por outro lado, um buraco negro é caracterizado por um horizonte de eventos, que é uma superfície tipo-luz,i.e., o vetor normal a esta superfície tem norma nula. Com esta prescrição o horizonte de eventos do elemento de linha anterior é obtido

$$|x| = -\frac{b}{2a}, \tag{30}$$

implicando que b e a têm sinais contrários. Esta solução corresponde àquela obtida por Mann e colaboradores [4] , partindo do comportamento tipo delta de Dirac no escalar de curvatura. Em coordenadas conformes a escolha de calibre é

$$e_0^0 = e_0^0(x); e_0^0 = e_1^1; e_1^0 = e_0^1 = 0; a_1 = 0 \tag{31}$$

$$Q^0 = Q^1 = 0; w_0 = a\epsilon(x); w_1 = 0 \tag{32}$$

e para a linha de universo das fontes a escolha é a mesma daquela feita em coordenadas de Schwarzschild. A solução para as fontes é

$$Q^3 = A' = constante; Q^2 = \frac{a}{e_2} = constante. \tag{33}$$

Para o setor gravitacional obtemos :

$$e_0^0 = e^{-a|x|} \tag{34}$$

$$a_0 = \frac{1}{2a}\epsilon(x)e^{-2a|x|} + e_2 A'\epsilon(x) + B' \tag{35}$$

e para o setor do dilaton (o calibre é fixo de forma que o dilaton é independente do tempo) temos que

$$\eta_3 = \Lambda \tag{36}$$

$$\eta_0 = -\frac{\Lambda}{a}c(x)e^{-a|x|} \tag{37}$$

$$\eta_1 = 0 \tag{38}$$

$$\eta_2 = \frac{\Lambda}{2a^2}e^{-2a|x|} + C'. \tag{39}$$

O elemento de linha do espaço-tempo é dado por

$$ds^2 = e^{-2a|x|}(-dt^2 + dx^2) \tag{40}$$

sendo que a curvatura escalar também diverge em $x = 0$ de acordo com uma função delta de Dirac, de forma análoga ao caso anterior . No cálculo do horizonte de eventos a prescrição é a mesma do caso anterior , com a diferença que definimos a componente contravariante do vetor normal e usamos a métrica covariante para calcular a norma do vetor normal. Novamente , como o vetor normal tem norma zero obtemos o horizonte em $|x| = \infty$. Note que este sistema de coordenadas é incompleto,pois só descreve o interior (ou exterior) do buraco negro sendo insuficiente para descrever todas as regiões do espaço-tempo. Esta solução corresponde àquela encontrada no trabalho de Brown e colaboradores [5], no contexto do modelo de Jackiw-Teitelboim.
É interessante enfatizar que o buraco negro em coordenadas conformes é equivalente ao buraco negro em coordenadas de Schwarzschild [4] , pois têm a mesma topologia e estão relacionados por uma transformação de coordenadas.
Pretendemos estudar o caso supersimétrico[6] a fim de entender como a não localidade no setor fermiônico infuencia na solução para o espinor de Killing covariantemente conservado, e como este altera as soluções acima descritas. Um outro ponto que pode ser investigado é a termodinâmica destes buracos negros bem como a quantização das soluções .

Referências

[1] - D.Cangemi, R.Jackiw , Phys. Rev. Lett, 69, 233 (1992).
[2] - A.P.Balachandran, S.Borchardt, A.Stern , Phys.Rev.D 17, 3247 (1978).
[3] - W. Rindler , Essential Relativity (Springer-Verlag , New York (1969).
[4] - R.B.Mann, A.Shiekh, I.Tarasov, Nucl.Phys.B **341**,134 (1990).
[5] - J.D.Brown, M.Henneaux, C.Teitelboim , Phys.Rev.D **33**,319 (1986).
[6] - V.O.Rivelles, Phys.Lett.B **321**,189 (1994); M.M.Leite, V.O.Rivelles, Class.Quantum Grav.**12**,627 (1995).

Geometry of Quantum Group Twists

A. P. Demichev*
Centro Brasileiro de Pesquisas Físicas - CBPF/CNPq,
Rua Dr. Xavier Sigaud, 150, 22290-180, Rio de Janeiro, RJ Brasil

Received March, 1996

We show that R-matrices of all simple quantum groups have the properties which permit to present quantum group twists as transitions to other coordinate frames on quantum spaces.

1.Introduction.

Quantum spaces which appear in the frame of quantum group theory [1] have many unusual properties, in particular, q-deformed differential calculi [2] and, in general, non-commuting coordinates. In one-dimensional space q-derivative can be represented by Jackson difference operator. This, in turn, provides description of a quantum mechanical particle on a one-dimensional lattice [3]. Thus a q-deformation of a differential calculus apparently leads to space discretization. The relation of the non-commutativity of coordinates to space discretization is not so straightforward and causes problems in construction of field theories on q-spaces. Indeed, it means that operators of coordinates can not be diagonalized simultaneously and have not common eigenvalues. On the other hand, asymptotic (free) states of a particle scattering process are well described by usual non-deformed Minkowski geometry and Poincaré group representations.

A natural preliminary step to understand a relation of low energy particle phenomenology to physics in q-deformed space-time can be a reduction of a number of non-commuting coordinates, retaining q-deformed differential calculus and q-symmetry. This work is devoted to the study of such possibility.

As is well known, quantum spaces, related to each other by twists [4] of corresponding q-groups, have different commutation relations for coordinates [5]. The key idea of our approach is to present a group twist as a kind of q-deformed transition to another frames. As was shown in [6], q-deformed Minkowski space-time with non-commuting coordinates which corresponds to pure twisted Poincaré group (i.e. to the q-group obtained from the classical one by a twist) can be constructed from a usual Minkowski space with help of appropriate coordinate transformation and q-generalization of 4-beins.

In the present paper we generalize this partial result to twists of non-trivially deformed all simple groups. More precisely, we will show that known R-matrices for all simple q-groups have the property which permits to describe the twist procedure as a transformation of q-space coordinates. It seems natural to require that reasonable theory must be physically equivalent in different coordinate frames. So one can choose a most suitable frame, in particular, with most simple commutation relations.

2.Quantum group twists and quantum coordinates.

As is shown in [4], multiparametric quantum groups can be obtained from a one-parametric q-group via so called twists of a quasi-triangular Hopf algebra. Consider at first the case of q-deformations of $GL(N)$ groups. In this case a twist of R-matrix in fundamental representation R is described with help of diagonal matrix $F = diag(f_{11}, f_{12}, \dots, f_{nn})$ with $f_{ij}f_{ji} = 1$ so that R-matrix $R^{(F)}$ of the twisted group $GL_{r,\tilde{q}_{ij}}(N)$ has a form $R^{(F)} = F^{-1}RF^{-1}$. Here R is (in general, also multiparametric) R-matrix of the initial group $GL_{r,q_{ij}}(N)$ and

$$\tilde{q}_{ij} = q_{ij}f_{ij}^2 \ . \tag{1}$$

Coordinates of the initial quantum space $C_q^N[x^i]$ satisfy the commutation relations (CR) [1, 5]

$$x^i x^j = q_{ij}x^j x^i \tag{2}$$

and coordinates of the twisted space $C_q^{(F)N}[\tilde{x}^i]$ have the CR

$$\tilde{x}^i \tilde{x}^j = \tilde{q}_{ij}\tilde{x}^j \tilde{x}^i \ . \tag{3}$$

*on leave of absence from Moscow State University, Russia

Now we introduce the algebra $E_q^N[e^i, g_j]$ with the generators $\{e^i, g_i\}_{i=1}^N$ which commute with coordinates and put

$$\tilde{x}^i = e^i x^i \qquad \text{(no summation)} . \tag{4}$$

The elements e^i play the role of components of a q-deformed (diagonal) N-bein. CR for them follows from (1)-(4)

$$e^i e^j = f_{ij}^2 e^j e^i , \tag{5}$$

and g_i are inverse elements

$$g_i e^i = 1 . \tag{6}$$

The coordinates $\tilde{x}^i$ are transformed by a q-matrix $\tilde{T}$

$$\tilde{x}'^i = \sum_{j=1}^N \tilde{T}^i{}_j \tilde{x}^j . \tag{7}$$

Then using (4),(6) one obtains from (7) transformations of the coordinates x^i

$$x'^i = \sum_{j=1}^N g_i \otimes \tilde{T}^i{}_j \otimes e^j \otimes x^j . \tag{8}$$

We used in (8) a cross-product sign to stress that the elements from the different sets commute with each other (the elements g_i in (8) must be considered as the inverse elements to generators e^i of another copy of an algebra E_q^N with respect to the elements e^i entering the same formula). The relation (8) means that the coordinates x^i are transformed by the matrix T with the entries

$$T^i{}_j = g_i \otimes \tilde{T}^i{}_j \otimes e^j \qquad \text{(no summation)} . \tag{9}$$

Using (6) one can express the matrix $\tilde{T}$ through T

$$\tilde{T}^i{}_j = e^i \otimes T^i{}_j \otimes g_j \qquad \text{(no summation)} . \tag{10}$$

One can check straightforwardly that x'^i defined by (8) satisfy the correct CR

$$x'^i x'^j = q_{ij} x'^j x'^i .$$

The general reason for this is the following property of the R-matrices: if a q-matrix T satisfies TT-relation defined by the corresponding R-matrix, then the $\tilde{T}$-matrix defined by (9) or (10) satisfies the relation with twisted R-matrix $R^{(F)}$.

To prove this statement let us write TT-relation (CR for entries of a matrix T) in explicit form

$$\sum_{p,s} R^{mn}_{ps} T^p{}_u T^s{}_v = \sum_{s,r} T^m{}_s T^n{}_r R^{rs}_{uv}$$

and substitute $T^i{}_j$ by their expressions (9) in terms of $\tilde{T}^i{}_j$. This gives the relation for the latter

$$\sum_{p,s} R^{mn}_{ps} g_p g_s e^u e^v \tilde{T}^p{}_u \tilde{T}^s{}_v = \sum_{s,r} \tilde{T}^n{}_s \tilde{T}^m{}_r g_n g_m e^s e^r R^{rs}_{uv} . \tag{11}$$

Remind that in this relation the elements g_i must be considered as inverse elements for the generators e^i of another copy of an algebra E_q^N and so they commute with the elements e^i entering the same relation.

Using explicit form of multiparametric R-matrix for $GL_{r,q_{ij}}(N)$ group [1, 5] one can show that

$$R^{mn}_{ps} g_p g_s e^u e^v = g_n g_m e^u e^v R^{(F)mn}_{ps} ,$$

where $R^{(F)}$ is the twisted matrix of the same form but with the twisted parameters $\tilde{q}_{ij} = q_{ij} f_{ij}^2$. Analogous consideration for the RHS of (11) shows that this relation can be rewritten in the form

$$\sum_{p,s} R^{(F)mn}_{ps} \tilde{T}^p{}_u \tilde{T}^s{}_v = \sum_{s,r} \tilde{T}^n{}_s \tilde{T}^m{}_r R^{(F)rs}_{uv} . \tag{12}$$

Thus twisted q-matrices can be constructed with the help of q-deformed N-beins (5),(6) and the formula (9) which is direct generalization (q-deformation) of a relation between matrices of transformations in different coordinate frames.

In the case of q-deformation of simple groups of the series B_N, C_N, D_N there is one more structure, namely an invariant length [1] $L_q = \sum_{i,j} x^i C_{ij} x^j = \sum_i l_i x^{i'} x^i$, where $i' = N + 1 - i$. Values of the coefficients l_i can be found in [1] and are not essential for our consideration. To preserve L_q, components of a q-bein must satisfy the additional constraints $e^i e^{i'} = e^{i'} e^i = 1$, $i = 1, ..., N/2$ for C_N, D_N series; $i = 1, ..., (N+1)/2$ for B_N series. In particular, for the series B_N: $e^{(N+1)/2} = 1$. These constraints reduce number of twist parameters, which from the geometrical point of view define CR for the components of the q-beins, so that the number is equal to $k(k-1)/2$, where k is rank of a group.

Explicit form of R-matrices [1, 5] again gives that the R-matrices have the property analogous to that of the A_N groups and the matrices $\hat{T}$ defined by (9),(10) satisfy the CR (12) for twisted quantum groups.

The interpretation of twists as transitions to other q-coordinate frames is extended to differential calculi on q-spaces. Indeed, using the CR which define a q-deformed differential calculus in multiparametric case [5], one can straightforwardly check that the relations

$$d\tilde{x}^i = e^i dx^i \ , \qquad \tilde{\partial}_i = g_i \partial_i \ ,$$

convert differential calculus on a q-space to the one on a twisted q-space.

Acknowledgement

This work was supported by Brazilian Research Council (Conselho Nacional de Desenvolvimento Cientifico e Tecnológico) and partially by INTAS-93-1630 project.

References

[1] L.D.Faddeev, N.Yu.Reshetikhin and L.A.Takhtadjan, Algebra i Analis, 1 (1989) 178 (Transl.: Leningrad Math. Jour., 1 (1990) 193).

[2] J.Wess and B.Zumino, Nucl.Phys.Suppl., 18B (1990) 302.

[3] A.Dimakis and F.Müller-Hoissen, Phys.Lett., B295 (1992) 242.

[4] V.G.Drinfel'd, Leningrad Math.Jour., 1 (1989) 1419.
N.Yu.Reshetikhin, Lett.Math,Phys., 20 (1990) 331.

[5] A.Schirrmacher, Z.Phys., C50 (1991) 321.
A.Schirrmacher, Jour. of Phys., A24 (1991) L1249.

[6] M.Chaichian and A.Demichev, Jour.Math.Phys., 36 (1995) 398.

On the effect of fermion quartic self-interactions over the photon masses in (1+1)D

A. de Souza Dutra e C. P. Natividade
UNESP/Campus de Guaratinguetá-DFQ

H. Boschi Filho
UFRJ/IF - Depto. Física Teórica

Received March, 1996

In this work we discuss the effect of quartic self-interacting terms on the dynamically generated mass for the photons. This effect should be expected due to the fact that, in (1+1)D, the dynamically generated mass has its origin in the fermion loop diagram. Here we will solve the vector and chiral gauge models with fermion self-interacting terms.

For the vector case we have the Lagrangian density in the topologically trivial sector given by

$$L = \bar{\Psi}(i\gamma_\mu\partial^\mu - e\gamma_\mu A^\mu)\Psi - \frac{1}{4}F^{\mu\nu}F_{\mu\nu} - \frac{g^2}{2}\left(\bar{\Psi}\gamma_\mu\Psi\right)^2 + J_\mu A^\mu + \bar{\theta}\Psi + \bar{\Psi}\theta, \tag{1}$$

which after using the identity

$$\exp\left\{\frac{g^2}{2}\int d^2x\left(\bar{\Psi}\gamma_\mu\Psi\right)^2\right\} = \frac{1}{N}\int \mathcal{D}B_\mu \exp\left\{\frac{e^2}{2}B_\mu B^\mu - eg\bar{\Psi}\gamma_\mu B^\mu\Psi\right\}, \tag{2}$$

looks like

$$L = \bar{\Psi}(i\gamma_\mu\partial^\mu - e\gamma_\mu(A^\mu + gB^\mu)\Psi - \frac{1}{4}F^{\mu\nu}F_{\mu\nu} + \frac{e^2}{2}B_\mu B^\mu - \frac{1}{2\alpha}(\partial_\mu A^\mu)^2 + sources. \tag{3}$$

Now, doing the transformation $A_\mu \equiv \bar{A}_\mu - g\bar{B}_\mu$, ($\bar{B}_\mu \equiv gB_\mu$), the Lagrangian density becomes:

$$L = \bar{\Psi}(i\gamma_\mu\partial^\mu - e\gamma_\mu\bar{A}^\mu)\Psi - \frac{1}{4}\bar{F}^{\mu\nu}\bar{F}_{\mu\nu} - \frac{1}{4}\bar{B}^{\mu\nu}\bar{B}_{\mu\nu} + \frac{1}{2}\bar{F}^{\mu\nu}\bar{B}_{\mu\nu} - \frac{1}{2\alpha}\left(\partial_\mu\bar{A}^\mu\right)^2 +$$

$$- \frac{1}{2\alpha}\left(\partial_\mu\bar{B}^\mu\right)^2 + \frac{1}{2\alpha}\left(\partial_\mu\bar{A}^\mu\right)\left(\partial_\mu\bar{B}^\mu\right) + J_\mu(\bar{A}^\mu - \bar{B}^\mu) + \bar{\theta}\Psi + \bar{\Psi}\theta. \tag{4}$$

In order to decouple this Lagrangian density, we decompose the vector fields $\bar{A}^\mu$ and $\bar{B}^\mu$ into their transverse and longitudinal components through,

$$e\bar{A}^\mu = \partial_\mu\eta_A + \epsilon_{\mu\sigma}\,\partial^\sigma\chi_A; e\bar{B}^\mu = \partial_\mu\eta_B + \epsilon_{\mu\sigma}\,\partial^\sigma\chi_B, \tag{5}$$

and perform the transformation

$$\Psi(x) = U_5(x)\psi(x); \bar{\Psi}(x) = \bar{\psi}(x)\bar{U}_5(x), \tag{6}$$

where $U_5 \equiv \exp(-i\eta_A + \gamma_5\chi_A)$ and $\bar{U}_5 \equiv \exp(i\eta_A + \gamma_5\chi_A)$, whose non-trivial jacobian in the trivial topological sector is given by

$$J_F = \exp\left\{-\frac{\lambda}{2\pi}\int d^2x\left[\chi_A\Box\chi_A\right]\right\}, \tag{7}$$

where λ is the arbitrary regularization parameter. So, we get the following effective Lagrangian density:

$$L = \bar{\psi}(i\gamma_\mu\partial^\mu)\psi + \frac{1}{2e^2}\left[(\Box\chi_A)^2 + (\Box\chi_B)^2\right] + \frac{1}{2g^2}\left[(\partial_\mu\eta_B)^2 + (\partial_\mu\chi_B)^2\right] +$$

$$-\frac{1}{e^2}\Box\chi_A\Box\chi_B + \frac{\lambda}{2\pi}(\partial_\mu\chi_A)^2 - \frac{1}{2\alpha e^2}(\Box\eta_A)^2 - \frac{1}{2\alpha e^2}(\Box\eta_B)^2 + \frac{1}{\alpha e^2}\Box\eta_A\Box\eta_B +$$

$$+\frac{1}{e}J_\mu\left[\partial^\mu(\eta_A - \eta_B) + \epsilon^{\mu\sigma}\,\partial_\sigma(\chi_A - \chi_B)\right] + \bar{\theta}U_5\psi + \bar{\psi}\bar{U}_5\theta. \tag{8}$$

Now, in order to decouple the above Lagrangian density we do a further transformation:

$$\begin{pmatrix}\chi_A\\ \chi_B\end{pmatrix} = \begin{pmatrix} a\cos(\phi) & a\sin(\phi)\\ -\sin(\phi) & \cos(\phi)\end{pmatrix}\begin{pmatrix}\hat{\chi}_A\\ \hat{\chi}_B\end{pmatrix},$$

$$\begin{pmatrix}\eta_A\\ \eta_B\end{pmatrix} = \begin{pmatrix} 1 & 1\\ 0 & 1\end{pmatrix}\begin{pmatrix}\hat{\eta}_A\\ \hat{\eta}_B\end{pmatrix}, \tag{9}$$

where $a \equiv (\pi/\lambda g^2)^{\frac{1}{2}}$, $\tan(2\phi) = \gamma/(\beta - \alpha)$, and $\alpha \equiv a^2/2e^2, \beta \equiv 1/2e^2, \gamma \equiv -a/2e^2$. From which we obtain the decoupled Lagrangian density,

$$L = \bar{\psi}(i\gamma_\mu\partial^\mu)\psi + \frac{1}{2g^2}\left[(\partial_\mu\hat{\eta}_B)^2 + (\partial_\mu\hat{\chi}_B)^2 + (\partial_\mu\hat{\chi}_A)^2\right] - \frac{(a^2+1)}{2e^2}(\Box\hat{\chi}_A)^2 +$$

$$-\frac{1}{2\alpha e^2}(\Box\hat{\eta}_A)^2 + \frac{J^\mu}{e}\left(\partial_\mu\hat{\eta}_A + (a^2+1)^{\frac{1}{2}}\,\epsilon_{\mu\sigma}\,\partial^\sigma\hat{\chi}_A\right) + fermionicsources. \tag{10}$$

Now, remembering that

$$D_{\mu\nu}(k) = \frac{\delta^2 Z}{\delta J_\mu \delta J_\nu}|_{J=0} = -\frac{1}{e^2}\left[k_\mu k_\nu D_{\hat{\eta}_A} + (a^2+1)\,\epsilon_{\mu\sigma}\epsilon_{\nu\rho}\,k^\sigma k^\rho D_{\hat{\chi}_A}\right], \tag{11}$$

and $\epsilon_{\mu\sigma}\epsilon_{\nu\rho} = g_{\mu\nu}g_{\sigma\rho} - g_{\mu\rho}g_{\sigma\nu}$, we obtain the photon propagator:

$$D_{\mu\nu}(k) = -\frac{i}{(k^2 - m^2)}\left\{g_{\mu\nu} - \left[1 - \frac{\alpha(k^2 - m^2)}{k^2}\right]\frac{k_\mu k_\nu}{k^2}\right\}, \tag{12}$$

with

$$m^2 = \frac{\lambda e^2}{(\pi + \lambda g^2)}, \tag{13}$$

where we see the effect of the self-interactions through its coupling constant g. So, for a vanishing g one recovers the usual Schwinger mass (in this case $\lambda = 1$ due to the gauge invariance), and for a very large g one have $m^2 \cong \left(\frac{e}{g}\right)^2$. Showing a kind of *screening* coming from the fermionic self-interaction. Furthermore it is remarkable that the arbitrariness due to the regularization parameter disappears in this limit.

A similar analysis can be done in the case of the chiral interaction. In this case after similar calculations as above, one gets the following dynamical mass:

$$m_{ch}^2 = \frac{a^2e^2}{[2(a-1)\pi + a^2g^2]}, \tag{14}$$

which also has the correct limit when $g \longrightarrow 0$, and for large values of g has the same form of the previous case.

Finally we show that, for example, in the case of the vector model, this self-interaction is in some way equivalent to the model with Wess- Zumino term. In this case one has

$$L = \bar{\Psi}(i\gamma_\mu\partial^\mu - e\gamma_\mu A^\mu)\Psi - \frac{1}{4}F^{\mu\nu}F_{\mu\nu} + \frac{ae^2}{2}A_\mu A^\mu + L_{WZ} \tag{15}$$

with

$$L_{WZ} = \frac{a}{2}\partial_\mu\theta\partial^\mu\theta + ae\partial_\mu\theta A^\mu. \tag{16}$$

Now, performing the transformation $A_\mu = \tilde{A}_\mu - \frac{1}{e}\partial_\mu\theta$, and integrating over the Wess-Zumino field, one obtains the effective Lagrangian density:

$$L_{eff} = \bar{\Psi}(i\gamma_\mu\partial^\mu - e\gamma_\mu\tilde{A}^\mu)\Psi - \frac{1}{4}\tilde{F}^{\mu\nu}\tilde{F}_{\mu\nu} - \frac{1}{4a}\left(\bar{\Psi}\Psi\right)^2, \tag{17}$$

which is a Schwinger model with a Thirring-like self- coupling term, and where the regularization parameter a is related to the coupling constant.

Supersymmetric Quantum Mechanics and the Hulthén Potential

Elso Drigo Filho
Instituto de Biociências, Letras e Ciências Exatas-UNESP
Departamento de Física,
Rua Cristovão Colombo, 2265
15055 São José do Rio Preto, SP, Brazil

Regina Maria Ricotta
Faculdade de Tecnologia de São Paulo, CEETPS-UNESP
Praça Fernando Prestes, 30
01121-060 São Paulo, SP, Brazil

Received March, 1996

Supersymmetric Quantum Mechanics (SQM) has been used to solve Schroedinger equation of solvable potentials, [1], partially solvable ones, [2], in the WKB-approximation, [3], and it has also been applied in variational method, as recently suggested,[4], [5], [6].

1 Introduction

The supersymmetric formalism has already been used to study some aspects of the Hulthén potential, [7], [8]. Here, the exact analytical solution for this potential is reobtained, for $l = 0$, showing the consistency of the method. When $l \neq 0$ we interpret that the supersymmetry is "broken" by the potential barrier terms. Nonetheless, the supersymmetry gives us eigenfunctions that allow us to compute the eigenvalues of the variational method, [6]. The eigenfunctions for $2p$ and $3d$ states are evaluated for some values of the parameter delta. Our results are compared with direct numerical integration data, [9].

2 The Hulthén Potential with $l = 0$

The Hamiltonian for the Hulthén potential ($l = 0$) can be written as:

$$H_1 = -\frac{1}{2}\frac{d^2}{dr^2} - \frac{\delta e^{-\delta r}}{1 - e^{-\delta r}}. \tag{1}$$

From the Hamiltonian hierarchy we can obtain its eigenfunctions and eigenvalues for the n-th ground state Hamiltonian, [10], [11]. The hierarchy is given by

$$H_n - E_0^{(n)} = a_n^+ a_n^- \tag{2}$$

with creation and anihilation operators defined in terms of the superpotential

$$a_n^\pm = \frac{1}{\sqrt{2}}(\mp\frac{d}{dr} + W_n(r)). \tag{3}$$

The n-th superpotential is given by

$$W_n(r) = -\frac{n\delta e^{-\delta r}}{1 - e^{-\delta r}} + \frac{1}{n} - \frac{n}{2}\delta \tag{4}$$

that corresponds to the n-th member of the Hamiltonian hierarchy:

$$V_n(r) = W_n^2(r) - \frac{d}{dr}W_n(r) = \frac{n(n-1)\delta^2 e^{-2\delta r}}{2(1 - e^{-\delta r})^2} - \frac{[n(1-n)\delta + 2]\delta e^{-\delta r}}{2(1 - e^{-\delta r})}. \tag{5}$$

The superalgebra allows us to relate these results with the original Hamiltonian by the relations:

$$E_n^{(1)} = E_0^{(n+1)}, \quad \Psi_n^{(1)}(r) = a_1^+ a_2^+ ... a_n^+ \Psi_0^{(n+1)}(r). \tag{6}$$

The energy-eigenvalue and eigenfunction, eq.(6), are

$$E_n^{(1)} = \frac{1}{2}(-\frac{n}{2}\delta + \frac{1}{n})^2 \tag{7}$$

$$\Psi_0^{(n)}(r) = (1 - e^{-\delta r})^n e^{-[\frac{1}{n} - \frac{n}{2}\delta]r}. \tag{8}$$

We can verify that the energy-eigenvalues(7) are in fact the ones given in reference [12].

3 The Hulthén Potential with $l \neq 0$

The Hamiltonian for the Hulthén potential when $l \neq 0$ is written as:

$$H = -\frac{1}{2}\frac{d^2}{dr^2} - \frac{\delta e^{-\delta r}}{1 - e^{-\delta r}} + \frac{l(l+1)}{2r^2}. \tag{9}$$

The potential barrier term prevent us to build the superfamily as in the $l = 0$ case, since the potential is not exactly solvable. But based in our results for the case $l = 0$, we introduce a new effective potential whose functional form is suggested by eq.(5),

$$V_{eff}(r) = -\frac{\delta e^{-\delta r}}{1 - e^{-\delta r}} + \frac{l(l+1)}{2}\frac{\delta^2 e^{-2\delta r}}{(1 - e^{-\delta r})^2}. \tag{10}$$

We note that, for small values of δ, the second term of (10) gives us a potential barrier term of (9) in first approximation. As the effective potential given by (10) has the same functional form as (5), we can solve the Schroedinger problem by the factorisation method of SQM and find the whole super family. The superpotential of the n-th member of the family is given by

$$W_n(r) = B_n \frac{e^{-\delta r}}{1 - e^{-\delta r}} + C_n \tag{11}$$

where

$$B_n = -\frac{1}{2}(\delta + \sqrt{\delta^2 + 4B_{n-1}(B_{n-1} - \delta)}), \quad C_n = -\frac{B_{n-1}(\delta - 2C_{n-1}) - B_n\delta}{2B_n}, \tag{12}$$

and the energy and wave functions are given by (6), where

$$B_1 = -\frac{\delta}{2}(1 + \sqrt{1 + 4l(l+1)}), \quad C_1 = -\frac{\delta}{2}\frac{B_1 + 2}{B_1}, \quad B_0 = 0. \tag{13}$$

The energy eigenvalues and wave functions given by (6) are

$$E_0^{(n+1)} = \frac{1}{2}C_{n+1}^2 \tag{14}$$

$$\Psi_0^{(1)} = (1 - e^{-\delta r})^{-\frac{B_1}{\delta}} e^{-C_1 r}. \tag{15}$$

Notice that B's and C's depend on l. Fixing $l = 0$ we recover the original Hulthén potential, as expected.

We now look at the Hulthén potential (9) and solve the Schroedinger problem by the variational method. We start from V_{eff} given by (10) whose eigenfunctions are given by (6) and (15). For the state $2p$ we use the first member of the superfamily ($l = 1$) as our trial wave function, changing δ by the variational parameter μ, i.e.,

$$\Psi_\mu = \Psi_0^{(1)}(r, \mu) = (1 - e^{-\mu r})^{-\frac{B_1}{\mu}} e^{-C_1 r}. \tag{16}$$

The energy is obtained by minimisation with respect to μ. Thus, the equation to be minimised is

$$E_\mu = \frac{\int_0^\infty \Psi_\mu(r)[-\frac{1}{2}\frac{d^2}{dr^2} - \frac{\delta e^{-\delta r}}{1 - e^{-\delta r}} + \frac{l(l+1)}{2r^2}]\Psi_\mu(r)dr}{\int_0^\infty \Psi_\mu(r)^2 dr}. \tag{17}$$

The integration has to be carried out numerically. Our explicit values for the $2p$, $(l = 1)$ and $3d$, $(l = 2)$ energy states for some values of the parameter δ are listed bellow in Table 1. They are shown together with direct numerical integration data.

Table 1. Energy eigenvalues as a function of the screening parameter for the states $2p$ and $3d$, [eq.(17)]. Comparison is made with numerical data of Ref.[9].

State	Delta	Variational result	Numerical Integration
2p	0.025	-0.112760	-0.1127605
	0.050	-0.101042	-0.1010425
	0.075	-0.089845	-0.0898478
	0.100	-0.079170	-0.0791794
	0.150	-0.059495	-0.0594415
	0.200	-0.041792	-0.0418860
3p	0.025	-0.043601	-0.0437069
	0.050	-0.032748	-0.0331645
	0.075	-0.023010	-0.0239397
	0.100	-0.014433	-0.0160537

4 Conclusions

We have obtained from the formalism of SQM the exact analytical eigenfunction and energy eigenvalue for the Hulthén potential for $l = 0$. When $l \neq 0$, we used an effective potential suggested by the case $l = 0$, to give us a variational trial wave function. The energies for the $2p$ and $3d$ states were obtained for some values of the parameter δ.

We note that better results have been obtained for the $2p$ state, for small values of δ. This is expected since for small values of δ the effective potential (10) becomes closer to the original Hulthén potential (9), and for l small the contribution of this angular moment term in the potential is also small. The advantage of using the effective potential (10) is the fact that we can vary its parameters without changing its functional form. This is reinforced by the constructive method of determining wave functions based on supersymmetry. We stress, however that this is a variation of the so called shape invariant potential, since it does not change its functional form in the hierarchy but does not follow the usual definition of shape invariance, [13].

References

[1] G. Lévai, Lect. Notes in Phys. **427** (1993) 427, Ed. H. V. von Geramb, Springer-Verlag

[2] E. Drigo Filho, Mod. Phys. Rev. **A9** (1994) 411

[3] R. Dutt, A. Khare and U. P. Sukhatme, Am. J. Phys. **59** (1991) 723

[4] E. Drigo Filho, "XII Encontro Nacional de Física de Partículas e Campos, Brasil", Abstract Book, p.40 (1992) (Brazilian Society of Physics)

[5] E. Gozzi, M. Reuter and W. D. Thacker, Phys. Lett. **A183** (1993) 29; F. Cooper, J. Dawson and H. Shepard, Phys. Lett. **A187** (1994) 140

[6] E. Drigo Filho and R. M. Ricotta, Mod. Phys. Lett. **A10** (1995) 1613

[7] U. Laha, C. Bhattacharyya, K. Roy and B. Talukdar, Phys. Rev. **C38** (1988) 558

[8] B. Talukdar, U. Das, C. Bhattacharyya and P. K. Bera, J. Phys. A: Math. Gen. **25** (1992) 4073

[9] Y. P. Varshni, Phys. Rev. **A41** (1990) 4682

[10] C. V. Sukumar, J. Phys. A: Math. Gen. **18** (1985) L57

[11] E. Drigo Filho and R. M. Ricotta, Mod. Phys. Lett. **A4** (1989) 2283

[12] C. S. Lan and Y. P. Varshni, Phys. Rev. **A4** (1971) 1875

[13] L. Gedenshtein, JETP Lett. **38** (1983) 356

New mathematical objects in String Theory

Leonidas Sandoval Junior

Instituto de Física - Universidade de São Paulo

Cx. Postal 66318 - 05389-970, São Paulo, SP, Brasil

Received March, 1996

It is shown how to obtain objects called *Eichler integrals* in the mathematical literature that can be used for calculating scattering amplitudes in String Theory. These Eichler integrals are also new examples of Eichler integrals with poles.

I. Introduction

The concept of an Eichler integral is closely related to the concept of automorphic forms. Although automorphic forms have a large range of applications in Physics and in particular in String Theory, Eichler integrals remain relatively unknown objects to both mathematicians and physicists. One can picture Eichler integrals as a generalization of the concept of automorphic forms, and they are related to the better known *Beltrami differentials* that are used in String Theory in the calculation of multiloop scattering amplitudes of strings.

We begin with a description of the main properties of automorphic forms with one example that will be useful when we describe one of the new Eichler intregrals. The definition of Eichler integrals is given next, with one example that can be used in String Theory[1].

II. Automorphic forms

An automorphic form of weight q is a function[2] $\phi(z)$ that transforms in the following way under a projective transformation P_a:

$$\phi\left(P_a(z)\right) = \left[\frac{\partial P_a(z)}{\partial z}\right]^q \phi(z) \ .$$

Automorphic forms with just one pole will be more of our interest since the order of the pole is limited in a simple way by the Riemann-Roch theorem[3]. We now give one example of these functions that will be useful for our calculation of an Eichler integral that can be used in String Theory.

A. Example

In the multiloop case of String Theory, let us consider only projective transformations P_a with finite fixed points α_a and β_a acting on a Riemann sphere with genus g. We then consider the following series:

$$P_w(z) = \sum_b \frac{(z-\alpha_b)(z-\beta_b)}{w_b(\alpha_b-\beta_b)} \frac{\delta w_b}{\epsilon} \ . \tag{1}$$

where the sum is over all the elements of the Schottky group formed by these transformations and δw_b and ϵ are infinitesimals. Performing a projective transformation $z \to T_a(z)$, $a = 1, \ldots, g$, and after a change of variables, we obtain

$$P_w(T_a(z)) = T_a'(z) \sum_c \frac{(z-\alpha_c)(z-\beta_c)}{w_c(\alpha_c-\beta_c)} \frac{\delta w_c}{\epsilon}$$

Since we are summing over all elements of the Schottky group (with the condition that the fixed points are finite) we then see that the expression on the right hand side is equivalent to the series we started with so that

$$P_w(T_a(z)) = T_a'(z) P_w(z) \ ,$$

i.e. $P_w(z)$ is an automorphic form with weight one.

III. Eichler integrals

An Eichler integral of order q is defined in the following way[4,5]: it is a function $f(z)$ that transforms like

$$f(T_a(z)) = \left[\frac{\partial T_a(z)}{\partial z}\right]^q [f(z) + P^{q+1}(z)]$$

where $P^{q+1}(z)$ is a polynomial at most of order $q+1$. It can be pictured as a generalization of the concept of automorphic form. Eichler integrals are related to automorphic forms in the following way[4]: given an Eichler integral of order q, we then have

$$\phi(z) = \left(\frac{\partial}{\partial z}\right)^{2q+1} f(z) \tag{2}$$

where $\phi(z)$ is an automorphic form of weight $q+1$, i.e.

$$\phi(T_a(z)) = \left[\frac{\partial T_a(z)}{\partial z}\right]^{q+1} \phi(z) .$$

Here is an example of an Eichler integral that is used in the calculation of the multiloop amplitudes of bosonic strings.

A. Example

We want a function that transforms like

$$f_w(T_a(z)) = T_a'(z) f_w(z) - \frac{\partial T_a(z)}{\partial w_a}\frac{\delta w_a}{\epsilon} \tag{3}$$

where

$$T_a(z) = \frac{\alpha_a(z-\beta_a) - w_a\beta_a(z-\alpha_a)}{(z-\beta_a) - w_a(z-\alpha_a)}$$

for every $a = 1, \ldots, g$, i.e. the action of $T_a(z)$ on this function causes an infinitesimal change in the multipliers w_a. So, this function must transform like

$$f_w(T_a(z)) = T_a'(z)\left[f_w(z) + \frac{(z-\alpha_a)(z-\beta_a)}{w_a(\alpha_a-\beta_a)}\frac{\delta w_a}{\epsilon}\right] . \tag{4}$$

In addition to this, we also demand that

$$f_a(S_a(z)) = f_a(z) \tag{5}$$

where $z \to S_a(z)$ is the transformation that takes z once around the a_a-loop for $a = 1, \ldots, g$.

In order to find the Eichler integral that transforms like this, we shall make analogies between the Eichler integral obtained for one loop[6] and the function that we must have for the multiloop case. First we notice that the series $P_w(z)$ defined in (1),

$$P_w(z) = \sum_b \frac{(z-\alpha_b)(z-\beta_b)}{w_b(\alpha_b-\beta_b)}\frac{\delta w_b}{\epsilon} ,$$

transforms like

$$P_w(T_a(z)) = T_a'(z) P_w(z)$$

so that it is the generalization for the multiloop case of the polynomial $(z-\alpha)$ for the one loop case.

Now we must try to find an analogue of the Weierstraß ζ-function suitable to the multiloop case. This can be obtained by first generalizing the concept of a θ function and of the Weierstraß ζ-function. This function is given by the hyperelliptic ζ function[8,9] or best, the $\bar{\zeta}$ function[1]. In our first attempt we attach a $\bar{\zeta}_b(v)$ function to every element of the series $P_w(z)$ so that we have

$$f_{1w}(z) = \sum_b \frac{\delta w_b}{\epsilon}\frac{(z-\alpha_b)(z-\beta_b)}{w_b(\alpha_b-\beta_b)}\bar{\zeta}_b(v) .$$

This function will not transform the way we want, since the term $\frac{(z-\alpha_b)(z-\beta_b)}{\alpha_b-\beta_b}$ and the first abelian integrals $v_b(z)$ do not transform in the same way. We then go to the next step which is making $\bar{\zeta}$ a function not of the first abelian integrals $v_b(z)$, but of variables $u_b(z)$ (such a change of variables can be justified, as in Baker[8], §192) such that

$$u_b(z) = \ln\left(\frac{z-\alpha_b}{z-\beta_b}\right) - \ln\left(\frac{\alpha_a}{\beta_a}\right) .$$

Under a change $z \rightarrow T_a(z)$, and after a change of variables, these variables will change like

$$u_b(T_a(z)) = \ln w_{ca} + u_c(z) ,$$

where the coefficient w_{ca} is given by

$$w_{ca} = \frac{(1-w_a)\beta_c - (\beta_a - w_a\alpha_a)}{(1-w_a)\alpha_c - (\beta_a - w_a\alpha_a)} .$$

We then redefine the generalized θ function $\theta(v)$ in the following way:

$$\theta(u) = \sum_{n=-\infty}^{\infty} \exp\left[\sum_{c,d=1}^{g}(n_c+\delta_c)\frac{1}{2}\ln w_{cd}(n_d+\delta_d) + \sum_{c=1}^{g} 2\pi i\gamma_c(n_c+\delta_c) + \sum_{c=1}^{g} u_c(n_c+\delta_c)\right] . \tag{6}$$

Defining now

$$\bar{\zeta}_b(u) = \frac{\partial}{\partial u_b}\ln\theta(u) \tag{7}$$

we have

$$\bar{\zeta}_b\left(u(T_a(z))\right) = \bar{\zeta}_b(u) - \delta_{ab}$$

and

$$\bar{\zeta}_b\left(u(S_a(z))\right) = \bar{\zeta}_b(u) .$$

We then define the following function:

$$f(z) = \sum_b \frac{\delta w_b}{\epsilon}\frac{(z-\alpha_b)(z-\beta_b)}{w_b(\alpha_b-\beta_b)}\bar{\zeta}_b\left(u(z)\right) . \tag{8}$$

This function transforms like

$$\begin{aligned} f_w(T_a(z)) &= T_a'(z)\sum_c \frac{\delta w_c}{\epsilon}\frac{(z-\alpha_c)(z-\beta_c)}{w_c(\alpha_c-\beta_c)}\left[\bar{\zeta}_c\left(u(z)\right) - \delta_{ac}\right] \\ &= T_a'(z)\left[\sum_c \frac{\delta w_c}{\epsilon}\frac{(z-\alpha_c)(z-\beta_c)}{w_c(\alpha_c-\beta_c)}\bar{\zeta}_c\left(u(z)\right) - \frac{\delta w_a}{\epsilon}\frac{(z-\alpha_a)(z-\beta_a)}{w_a(\alpha_a-\beta_a)}\right] \end{aligned}$$

and

$$f_w(S_a(z)) = f_w(z) .$$

Since we are summing over all the elements of the Schottky group, we then have:

$$\begin{aligned} f_w(T_a(z)) &= T_a'(z)\left[f_w(z) - \frac{\delta w_a}{\epsilon}\frac{(z-\alpha_a)(z-\beta_a)}{w_a(\alpha_a-\beta_a)}\right] , \\ f_w(S_a(z)) &= f_w(z) \end{aligned}$$

which are the transformation properties we wanted. So we have obtained the Eichler integral that has the effect of changing infinitesimally the variables w_a of a Riemann surface of genus g. This function can be used in order to calculate the measure for the multiloop scattering amplitudes of bosonic strings using the Group Theoretic approach[6].

References

[1] L.Sandoval Jr., *Eichler integrals and String Theory*, J.Math.Phys. 37 (1996) 2510
[2] L.R.Ford, Automorphic Functions (1951) Chelsea, NY
[3] M.Schlichenmaier, An introduction to Riemann surfaces, algebraic curves and moduli spaces (1989) Springer-Verlag
[4] L.V.Ahlfors, Finitely generated Kleininan groups, Amer.J.Math. 86 (1964) 413, Amer.J.Math. 87 (1965) 759
[5] L.V.Ahlfors, The structure of a finitely generated Kleininan group, Acta Math. 122 (1969) 1
I.Kra, On cohomology of Kleininan groups: II, Ann.Math. 90 (1969) 576
L.Bers, Eichler integrals with singularities, Acta Math. 127 (1971) 11
I.Kra, On cohomology of Kleinian groups III. Singular Eichler integrals, Acta Math. 127 (1971) 23
I.Kra, On the vanishing of and spanning sets for Poincaré series for cusp forms, Acta Math. 153 (1984) 47
I.Kra, Eichler cohomology and the structure of finitely generated Kleinian froups, in Advances in the Theory of Riemann Surfaces - *Proceedings of the 1969 Stony Brook Conference*, Edited by L.V.Ahlfors, L.Bers, H.M.Farkas, R.Gunning, I.Kra, and H.E.Rauch (1971) Princeton Univ. Press
[6] P.C.West, A brief review of the Group Theoretic approach to string theory, in *Conformal Field Theories and related topics*, Proceedings of the Third Annecy Meeting on Theoretical Physics, LAPP, Annecy le Vieux, France, Nucl.Phys. B (Proc.Suppl.) 5B (1988) 217, edited by P.Bin/'etruy, P.Sorba and R.Stora (1988), North Holland;
in *Ninth Workshop on Grand Unification*, edited by R.Bartoutaud (1988) World Scientific;
and in *1988 Electroweak Interactions and Unified Theories*, Proceedings of the XXIIIrd Rencontre de Moriond, edited by J.Tran Thanh Van (1988) Edition Frontiéres
[7] A.Neveu and P.C.West, Group Theoretic approach to the perturbative string S-matrix, Phys.Lett. 193B (1987) 187
[8] H.F.Baker, Abel's Theorem and Allied Theory Including the theory of theta functions (1987) Cambridge University Press
[9] D.Munford, Tata lectures on theta, vol. II, in Progress in Mathematics 28 (1984) Boston, Birkhauser

The Causal Phase in (2+1)-dimensional QED

J. L. Boldo*, B. M. Pimentel† and J. L. Tomazelli‡

Instituto de Física Teórica

Universidade Estadual Paulista

Rua Pamplona, 145

01405-900 - São Paulo, SP - Brazil

Received March, 1996

The scattering operator S in Fock space for quantum electrodynamics in an external time-dependent electromagnetic field $A_\mu(x)$ is uniquely determined up to a phase[1]. This phase is related to vacuum fluctuations due to the presence of the external potential A and, therefore, must depend on it. We can determine the phase $\lambda[A]$ in QED_3 in lowest order of perturbation theory, by imposing Bogoliubov's local causality condition[2] on S, and show that the vacuum-vacuum amplitude is ultraviolet finite.

The S-matrix S in Fock space exists, if and only if P_+SP_- is a Hilbert-Schmidt operator. In this case it is given by

$$\mathbf{S} = C\, e^{S_{+-}S_{--}^{-1}b^\dagger d^\dagger} : e^{(S_{++}^{\dagger -1}-1)b^\dagger b} :: e^{(1-S_{--}^{-1})dd^\dagger} : e^{S_{--}^{-1}S_{-+}db} , \tag{1}$$

where

$$S_{ij} = P_i S P_j , \quad i,j = +,- \tag{2}$$

and

$$|C|^2 = \det(1 - S_{+-}S_{-+}^\dagger) . \tag{3}$$

The first factor in (1) describes electron-positron pair creation, the second one electron scattering, the third one positron scattering and the last one pair annihilation.

The differential causality condition for the Fock space S-operator is

$$\frac{\delta}{\delta A_\mu(y)}\left(\Omega, \mathbf{S}^\dagger \frac{\delta \mathbf{S}}{\delta A_\nu(x)}\Omega\right) = 0, \text{ for } x^0 < y^0 . \tag{4}$$

As we have said, the S-matrix in Fock space can be uniquely determined up to a phase,

$$\mathbf{S} = e^{i\varphi}\tilde{\mathbf{S}} , \tag{5}$$

where $\tilde{\mathbf{S}}$ is unitary, and given by expression (1). Inserting (5) into (4) we obtain

$$\frac{\delta}{\delta A_\mu(y)}\left(\mathbf{S}\Omega, \frac{\delta \mathbf{S}}{\delta A_\nu(x)}\Omega\right) = i\frac{\delta^2\varphi}{\delta A_\mu(y)\delta A_\nu(x)} + \frac{\delta}{\delta A_\mu(y)}\left(\tilde{\mathbf{S}}\Omega, \frac{\delta \tilde{\mathbf{S}}}{\delta A_\nu(x)}\Omega\right) . \tag{6}$$

It can be shown from the unitarity of $\tilde{\mathbf{S}}$ that the last term in (6) is purely imaginary. Consequently, the real part of the causality condition (4) is automatically satisfied while for the imaginary part we may choose φ conveniently such that (4) holds.

We now turn to the determination of the causal phase in lowest order of perturbation theory. We have

$$\tilde{\mathbf{S}}\Omega = C(\Omega + \sum_{mn}(S_{+-})_{mn} b_m^\dagger d_n^\dagger \Omega + \ldots) , \tag{7}$$

*Supported by CAPES

†Partially supported by CNPq

‡Supported by CAPES

where we have put S_{--}^{-1} equal to the unity in lowest order. Taking the functional derivative of (7) with respect to $A_\nu(x)$ and keeping only terms of order $O(A)$ in the resulting expression, we arrive at

$$\left(\tilde{\mathbf{S}}\Omega, \frac{\delta\tilde{\mathbf{S}}}{\delta A_\nu(x)}\Omega\right) = iC^2\,\Im m\mathrm{Tr}\left(S_{-+}^{\dagger}\frac{\delta S_{+-}}{\delta A_\nu(x)}\right) . \tag{8}$$

In lowest order we may set $C^2 = 1$.

The local causality condition (4) together with expressions (6) and (8) yield

$$F(x,y) \stackrel{def}{=} \frac{\delta^2\varphi}{\delta A_\mu(y)\delta A_\nu(x)} + \Im m\frac{\delta}{\delta A_\mu(y)}\mathrm{Tr}\left((S_{+-})^{\dagger}\frac{\delta S_{+-}}{\delta A_\nu(x)}\right) = 0 \tag{9}$$

for $x^0 < y^0$.

Next we calculate the second term in (9). In lowest order of perturbation theory, we have

$$S_{+-}^{(1)} = -i(2\pi)^{-1}P_+(\mathbf{p})\gamma^0 e\not{A}(p+q)P_-(-\mathbf{q}) . \tag{10}$$

As in reference [3] we use the following representation for the Dirac matrices in (2+1) dimensions:

$$\gamma^0 = \sigma_3 , \quad \gamma^1 = i\sigma_1 , \quad \gamma^2 = i\sigma_2 \tag{11}$$

where σ_j are the Pauli matrices.

From (10) we obtain

$$\mathrm{Tr}\frac{\delta}{\delta A_\mu(y)}(S_{+-})^{\dagger}\frac{\delta S_{+-}}{\delta A_\nu(x)} = e^2(2\pi)^{-5}\int d^2p\int d^2q\, e^{i(p+q)(x-y)}\mathrm{tr}[P_-(-\mathbf{q})\gamma^0\gamma^\mu P_+(\mathbf{p})\gamma^0\gamma^\nu P_-(-\mathbf{q})]$$
$$= -\int d^3k\, e^{ik(x-y)}\hat{P}^{\mu\nu}(k) , \tag{12}$$

$\hat{P}^{\mu\nu}(k)$ is not but the tensor of pair creation in (2+1) dimensions, which is given by[3]

$$\hat{P}^{\mu\nu}(k) = -e^2(2\pi)^{-3}T^{\nu\mu}(k) , \tag{13}$$

where

$$T^{\nu\mu}(k) = \int d^3p\,\delta(p^2-m^2)\Theta(p^0)\delta[(k-p)^2-m^2]\Theta(k^0-p^0)\,t^{\nu\mu}(k,p) \tag{14}$$

with

$$t^{\nu\mu}(k,p) = \mathrm{tr}[\gamma^\mu(\not{p}+m)\gamma^\nu(\not{k}-\not{p}-m)] . \tag{15}$$

It follows from the gauge invariance of (13) that

$$\hat{P}^{\mu\nu}(k) = \hat{P}_S^{\mu\nu}(k) + \hat{P}_A^{\mu\nu}(k) \tag{16}$$

with

$$\hat{P}_S^{\mu\nu}(k) = (k^\mu k^\nu - k^2 g^{\mu\nu})\tilde{B}(k^2) , \quad \hat{P}_A^{\mu\nu}(k) = im\varepsilon^{\mu\nu\alpha}k_\alpha\tilde{\Pi}^{(2)}(k^2) . \tag{17}$$

Performing the trace in (15) and the resulting momentum integral in (14) we find that[3]

$$\tilde{B}(k^2) = \frac{-e^2}{2(4\pi)^2}\frac{k^2+4m^2}{k^2}\Theta(k^2-4m^2)\frac{\Theta(k_0)}{\sqrt{k^2}} , \tag{18}$$

$$\tilde{\Pi}^{(2)}(k^2) = \frac{-e^2}{2(2\pi)^2}\Theta(k^2-4m^2)\frac{\Theta(k_0)}{\sqrt{k^2}} . \tag{19}$$

Substituting (12) and (13) in (9), we rewrite the causal function $F(x,y)$ as

$$F(x,y) = \frac{\delta^2\varphi}{\delta A_\mu(y)\delta A_\nu(x)} + \frac{e^2}{(2\pi)^5}\Im m\int d^3k\, e^{ik(x-y)}T^{\nu\mu}(k) . \tag{20}$$

We can evaluate the imaginary part of the last term in the above equation taking into account (13) and (16)-(19). Thus, we have

$$T^{\nu\mu}(k) = T_S^{\nu\mu}(k) + T_A^{\nu\mu}(k) , \tag{21}$$

where $T_S^{\nu\mu}(k)$ is real and even in k while $T_A^{\nu\mu}(k)$ is imaginary and odd in k. Hence,

$$F(x,y) = \frac{\delta^2\varphi}{\delta A_\mu(y)\delta A_\nu(x)} + \frac{e^2}{(2\pi)^5}\left[\int_{k_0>0} d^3k\, \sin k(x-y) T_S^{\nu\mu}(k) - i\int_{k_0>0} d^3k\, \cos k(x-y) T_A^{\nu\mu}(k)\right] . \tag{22}$$

In order to write the last term in (22) as a complex Fourier transform we must continue $T^{\nu\mu}(k)$ antisymmetrically to $k_0 < 0$

$$F(x,y) = \frac{\delta^2\varphi}{\delta A_\mu(y)\delta A_\nu(x)} + \frac{i}{2}\int d^3k\, e^{-ik(x-y)}[d_S^{\mu\nu}(k) - d_A^{\mu\nu}(k)] , \tag{23}$$

where

$$d_S^{\mu\nu}(k) = (k^\mu k^\nu - k^2 g^{\mu\nu})B(k^2) \ , \ d_A^{\mu\nu}(k) = im\varepsilon^{\mu\nu\alpha}k_\alpha \Pi^{(2)}(k^2) . \tag{24}$$

and

$$B(k^2) = \frac{-e^2}{2(4\pi)^2}\frac{k^2+4m^2}{k^2}\Theta(k^2-4m^2)\frac{\mathrm{sgn}(k_0)}{\sqrt{k^2}} , \tag{25}$$

$$\Pi^{(2)}(k^2) = \frac{-e^2}{2(2\pi)^2}\Theta(k^2-4m^2)\frac{\mathrm{sgn}(k_0)}{\sqrt{k^2}} . \tag{26}$$

The Fourier transform of a causal function vanishing for $x^0 - y^0 = t < 0$ satisfies a dispersion relation. Since $d_S^{\mu\nu}(k)$ and $d_A^{\mu\nu}(k)$ are real and purely imaginary, respectively, they cannot be the Fourier transform of a causal function. The lacking imaginary part of $d_S^{\mu\nu}(k)$ and the lacking real part of $d_A^{\mu\nu}(k)$ must de supplied by the first term containing the phase $\varphi[A]$,

$$\frac{\delta^2\varphi}{\delta A_\mu(y)\delta A_\nu(x)} = \frac{i}{2}\int d^3k\, e^{-ik(x-y)}[ir_S^{\mu\nu}(k) - r_A^{\mu\nu}(k)] , \tag{27}$$

where

$$r_S^{\mu\nu}(k) = \frac{1}{\pi}\int_{-\infty}^{+\infty} dl \frac{d_S^{\mu\nu}(kl)}{(l-i0)^2(1-l+i0)}$$

$$= \frac{\beta}{\pi}(k^\mu k^\nu - k^2 g^{\mu\nu})\left[\frac{1}{\sqrt{k^2}}\left(1+\frac{4m^2}{k^2}\right)\log\left(\frac{1-\sqrt{\frac{k^2}{4m^2}}}{1+\sqrt{\frac{k^2}{4m^2}}}\right) + \frac{4m}{k^2}\right] , \tag{28}$$

and

$$r_A^{\mu\nu}(k) = \frac{i}{\pi}\int_{-\infty}^{+\infty} dl \frac{d_A^{\mu\nu}(kl)}{(l-i0)(1-l+i0)} = \frac{i\beta}{\pi}4im\varepsilon^{\mu\nu\alpha}\frac{k_\alpha}{\sqrt{k^2}}\log\left(\frac{1-\sqrt{\frac{k^2}{4m^2}}}{1+\sqrt{\frac{k^2}{4m^2}}}\right) , \tag{29}$$

with $\beta \equiv -e^2/[2(4\pi)^2]$.

The causal phase is obtained by two integrations

$$\varphi[A] = \frac{1}{2}\int d^3x \int d^3y \frac{\delta^2\varphi}{\delta A_\mu(y)\delta A_\nu(x)} A_\mu(y)A_\nu(x) + O(A^4)$$

$$= \frac{\pi}{2}\int d^3k \left[\left(\frac{k^\mu k^\nu}{k^2} - g^{\mu\nu}\right)\Pi_1^{(1)}(k) + im\varepsilon^{\mu\nu\alpha}k_\alpha \Pi_1^{(2)}(k)\right] A_\mu(k)A_\nu^*(k) , \tag{30}$$

where

$$\Pi_1^{(1)}(k) = \beta\left[\sqrt{k^2}\left(1+\frac{4m^2}{k^2}\right)\log\left(\frac{1-\sqrt{\frac{k^2}{4m^2}}}{1-\sqrt{\frac{k^2}{4m^2}}}\right) + 4m\right] , \tag{31}$$

$$\Pi_1^{(2)}(k) = -\frac{4\beta}{\pi\sqrt{k^2}}\log\left(\frac{1-\sqrt{\frac{k^2}{4m^2}}}{1+\sqrt{\frac{k^2}{4m^2}}}\right) . \tag{32}$$

If we decompose the electromagnetic fields which appear in the integrand of (30) into the respective real and imaginary parts we see that $\varphi[A]$ is indeed real. The S-operator in Fock space $\mathbf{S}[A]$ is then completely determined.

By means of (1) and (5) we obtain the vacuum-vacuum amplitude

$$(\Omega, \mathbf{S}\Omega) = Ce^{i\varphi}(\Omega, e^{S_+ - S_-^{-1}b^\dagger d^\dagger}\Omega) = Ce^{i\varphi} \ . \tag{33}$$

The absolute square

$$|(\Omega, \mathbf{S}\Omega)|^2 = C^2 = 1 - P \tag{34}$$

must be equal to one minus the total probability P of pair creation,

$$P = -2\pi \int d^3k \, \hat{P}^{\mu\nu}(k) A_\mu(k) A_\nu^*(k) \ , \tag{35}$$

since the external field can change the vaccum state only into pair states. In order to combine the normalization constant C with $e^{i\varphi}$ we write the former in the exponential form

$$C = \exp\left[\pi \int d^3k \ldots + O[A^4]\right] \ .$$

Hence, from (16)-(19) we get

$$C = \exp\{\frac{\pi}{2} \int d^3k \left[\left(\frac{k^\mu k^\nu}{k^2} - g^{\mu\nu}\right) \Pi_2^{(1)}(k^2) + im\varepsilon^{\mu\nu\alpha} k_\alpha \Pi_2^{(2)}(k^2)\right] A_\mu(k) A_\nu^*(k)\} \ , \tag{36}$$

where

$$\Pi_2^{(1)}(k^2) = \beta\sqrt{k^2}\left(1 + \frac{4m^2}{k^2}\right)\Theta(k^2 - 4m^2) \ , \ \Pi_2^{(2)}(k^2) = \frac{4\beta\Theta(k^2 - 4m^2)}{\sqrt{k^2}} \ . \tag{37}$$

Finally, taking into account (30)-(33), (36) and (37), we obtain the vacuum-vacuum amplitude

$$(\Omega, \mathbf{S}\Omega) = \exp\{i\frac{\pi}{2} \int d^3k \left[\left(\frac{k^\mu k^\nu}{k^2} - g^{\mu\nu}\right) \Pi^{(1)}(k^2) + im\varepsilon^{\mu\nu\alpha} k_\alpha \Pi^{(2)}(k^2)\right] A_\mu(k) A_\nu^*(k)\} \ , \tag{38}$$

where

$$\Pi^{(1)}(k^2) = \Pi_1^{(1)}(k^2) - i\Pi_2^{(1)}(k^2) \ , \ \Pi^{(2)}(k^2) = \Pi_1^{(2)}(k^2) - i\Pi_2^{(2)}(k^2) \ . \tag{39}$$

In contrast with the four-dimensional case, the vacuum-vacuum amplitude is ultraviolet finite and exhibits an additional contribution from the antisymmetric part of the vacuum polarization tensor in (2+1)-dimensional space-time[3], which emerges from the topological structure of the theory.

References

[1] G. Scharf, Finite Quantum Electrodynamics, Springer Verlag, Berlin (1989);

[2] N. N. Bogoliubov, D. V. Shirkov, Introduction to the Theory of Quantized Fields, John Wiley, New York (1980);

[3] G. Scharf, W. F. Wreszinski, B. M. Pimentel and J. L. Tomazelli, Ann. of Phys. **231** (1994), 185.

Hamilton-Jacobi formulation and singular systems

B. M. Pimentel*and R. G. Teixeira†
Instituto de Física Teórica - Universidade Estadual Paulista
Rua Pamplona 145 - 01405-900 - São Paulo, S.P.Brazil

Received March, 1996

Recently the Hamilton-Jacobi formulation for first order constrained systems has been developed. In such formalism the equations of motion are written as total differential equations in many variables. We generalize the Hamilton-Jacobi formulation for singular systems with second order Lagrangians and apply this new formulation to Podolsky electrodynamics, comparing with the results obtained through Dirac's method.

1 Introduction

Systems with higher order Lagrangians have been studied with increasing interest because they appear in many relevant physical problems. As examples we have the consistent regularization of ultraviolet divergences in gauge-invariant supersymmetric theories [1] or effective Lagrangians in gauge theories [2]. Besides this, the fact that gauge theories have singular Lagrangians is in itself a motivation to the study of the formalism for second order singular Lagrangians.

The Lagrangian formulation for constrained systems can be found in references [3] and [4] while the Hamiltonian formulation of singular systems is usually made through a formalism developed by Dirac [5]. In this formalism the constraints caused by the Hessian matrix singularity are added to the canonical Hamiltonian and then the consistency conditions are worked out, being possible to eliminate some degrees of freedom of the system. Dirac also showed that the gauge freedom is caused by the presence of first class constraints.

The study of new formalisms for singular systems may provide new tools to investigate these systems. In classical dynamics, different formalisms (Lagrangian, Hamiltonian, Hamilton-Jacobi) provide different approaches to the problems, each formalism having advantages and disadvantages in the study of some features of the systems and being equivalent among themselves. In the same way, different formalisms provide different views of the features of singular systems, which justify the interest in their study.

Here we generalize the Hamilton-Jacobi formalism that was recently developed [6] to include singular second order Lagrangians. In Sect. 2 we develop the Hamilton-Jacobi formulation for a general second order system and apply this formalism to the case of a singular second order system in Sect. 3. An example is solved using Hamilton-Jacobi formalism in Sect. 4 and compared with Dirac's approach used in ref.[9]. Finally, Sect. 5 is devoted to the conclusions.

2 Hamilton-Jacobi formalism for second order Lagrangians

Recently a new formalism for singular first order systems was developed by Güler [6] who obtained a set of Hamilton-Jacobi partial differential equations for such systems using Carathéodory's equivalent Lagrangians method and wrote the equations of motion as total differential equations.

In this section we will use Carathéodory's method to develop the Hamilton-Jacobi formalism to a general second order Lagrangian. This formalism can be applied to any second order Lagrangian and is not limited to singular ones. The singular case will be considered in the next section.

*Partially supported by CNPq
†Supported by CAPES

Carathéodory's equivalent Lagrangians method to second order Lagrangians says that, given a Lagrangian $L(q_i, \dot{q}_i, \ddot{q}_i, t)$, we can obtain a completely equivalent one by:

$$L' = L\left(q_i, \dot{q}_i, \ddot{q}_i, t\right) - \frac{dS\left(q_i, \dot{q}_i, t\right)}{dt} \tag{1}$$

These Lagrangians are equivalent because the action integral given by them have simultaneous extremes. So we can choose the function $S(q_i, \dot{q}_i, t)$ in such a way that L' becomes an extreme and then we reduce the variational problem of finding extreme for the Lagrangian L to a problem of differential calculus. To do this we must find a set of functions $\varphi_i(q_i, \dot{q}_i, t)$, $\beta_i(q_i, t)$ and $S(q_i, \dot{q}_i, t)$ such that

$$L'(q_i, \beta_i, \varphi_i, t) = 0 \tag{2}$$

and for all neighborhood of $\dot{q}_i = \beta_i(q_i, t)$ and $\ddot{q}_i = \varphi_i(q_i, \dot{q}_i, t)$:

$$L'\left(q_i, \dot{q}_i, \ddot{q}_i, t\right) > 0 \tag{3}$$

With these conditions satisfied the Lagrangian L' will have a minimum in $\dot{q}_i = \beta_i\left(q_i, t\right)$ and $\ddot{q}_i = \varphi_i\left(q_i, \dot{q}_i, t\right)$ and consequently the action integral will have a minimum. So, the solutions of the differential equations will correspond to extremes of the action integral.

Using condition (2) we have:

$$\left.\frac{\partial S}{\partial t}\right|_{\substack{\dot{q}_i=\beta_i \\ \ddot{q}_i=\varphi_i}} = \left[L\left(q_i, \dot{q}_i, \ddot{q}_i, t\right) - \frac{\partial S\left(q_i, \dot{q}_i, t\right)}{\partial q_i}\dot{q}_i - \frac{\partial S\left(q_i, \dot{q}_i, t\right)}{\partial \dot{q}_i}\ddot{q}_i\right]\Bigg|_{\substack{\dot{q}_i=\beta_i \\ \ddot{q}_i=\varphi_i}} \tag{4}$$

Since $\dot{q}_i = \beta_i$ and $\ddot{q}_i = \varphi_i$ are minimum points of L' we must have

$$\left.\frac{\partial L'}{\partial \ddot{q}_i}\right|_{\substack{\dot{q}_i=\beta_i \\ \ddot{q}_i=\varphi_i}} = 0 \Rightarrow \left.\frac{\partial S}{\partial \ddot{q}_i}\right|_{\dot{q}_i=\beta_i} = \left.\frac{\partial L}{\partial \ddot{q}_i}\right|_{\substack{\dot{q}_i=\beta_i \\ \ddot{q}_i=\varphi_i}} \tag{5}$$

Analogously:

$$\left.\frac{\partial L'}{\partial \dot{q}_i}\right|_{\substack{\dot{q}_i=\beta_i \\ \ddot{q}_i=\varphi_i}} = 0 \Rightarrow \left.\frac{\partial S}{\partial q_i}\right|_{\dot{q}_i=\beta_i} = \left[\frac{\partial L}{\partial \dot{q}_i} - \frac{d}{dt}\frac{\partial S}{\partial \dot{q}_i}\right]\Bigg|_{\substack{\dot{q}_i=\beta_i \\ \ddot{q}_i=\varphi_i}}, \tag{6}$$

From these results, using the definitions for the conjugated momenta for second order Lagrangians (see ref.[7] and ref.[8]) and writing $\dot{q}_i = \bar{q}_i$, we have from equation (4) that, to obtain an extreme of the action, we must get a function $S(q_i, \dot{q}_i, t)$ such that:

$$\frac{\partial S}{\partial t} = -H_0 \tag{7}$$

$$H_0 = p_i\,\bar{q}_i + \pi_i\,\dot{\bar{q}}_i - L \tag{8}$$

$$p_i = \frac{\partial S}{\partial q_i}; \pi_i = \frac{\partial S}{\partial \bar{q}_i} \tag{9}$$

These are the fundamental equations of the equivalent Lagrangian method, equation (7) being called the Hamilton-Jacobi partial differential equation (HJPDE).

3 Formulation for singular second order Lagrangians

We consider now the application of the formalism developed in the previous section to a system with a singular second order Lagrangian. When the Hessian matrix has a rank $n - R$, $R < n$, the momenta variables will not be independent among themselves. In this case we can choose the order of accelerations $\dot{\bar{q}}_i = \ddot{q}_i$ in such a way that the minor of rank $n - R$ in the bottom right corner has nonvanishing determinant:

$$\det\left\|\frac{\partial^2 L}{\partial \dot{\bar{q}}_a\, \partial \dot{\bar{q}}_b}\right\| = \det\left\|\frac{\partial \pi_b}{\partial \dot{\bar{q}}_a}\right\| \neq 0; a, b = R+1, \ldots, n \tag{10}$$

Therefore we can solve the $n-R$ accelerations $\dot{\bar{q}}_a$ in terms of the coordinates $(q,\bar{q})$, the momenta π_a and the unsolved accelerations $\dot{\bar{q}}_\alpha$ $(\alpha=1,...,R)$ as follows:

$$\dot{\bar{q}}_a = f_a\left(q_i,\bar{q}_i,\pi_b,\dot{\bar{q}}_\alpha\right) \tag{11}$$

Besides this, we can write for the momenta π_a and p_a:

$$\pi_a = -H_a^\pi\left(q_i,\bar{q}_i,p_a,\pi_a\right) \tag{12}$$

$$p_a = -H_a^p\left(q_i,\bar{q}_i,p_a,\pi_a\right) \tag{13}$$

Anyway, from a general constraint given by any expression like $\Phi_\alpha\left(p,q,\pi,\bar{q}\right)=0$ we can always obtain expressions like equations (12) and (13) (see ref.[8]).

The Hamiltonian H_0, given by equation (8), becomes

$$H_0 = p_a\,\dot{\bar{q}}_a + \dot{\bar{q}}_\alpha\; p_\alpha|_{p_\beta=-H_\beta^p} + \pi_a f_a + \dot{\bar{q}}_\alpha\;\pi_\alpha|_{\pi_\beta=-H_\beta^\pi} - L\left(q_i,\bar{q}_i,\dot{\bar{q}}_\alpha,\dot{\bar{q}}_a=f_a\right) \tag{14}$$

where $\alpha,\beta=1,...,R$; $a=R+1,...,n$, and will not depend explicitly upon the accelerations $\dot{\bar{q}}_a$.

From this point we will adopt the following notation: the coordinates t and q_α will be called t_0 and t_α, respectively, and $\bar{q}_\alpha$ will be called $\bar{t}_\alpha$. The momenta p_a and π_a will be called P_a^p and P_a^π, respectively, and the momentum P_0 will be defined as:

$$P_0 = \frac{\partial S}{\partial t} \tag{15}$$

Then, to obtain an extreme of the action integral, we must find a function $S\left(q_i,\bar{q}_i,t\right)$ that satisfies the following set of HJPDE

$$H_0' = P_0 + H_0 = 0;\; H_\alpha'^p = P_\alpha^p + H_\alpha^p = 0;\; H_\alpha'^\pi = P_\alpha^\pi + H_\alpha^\pi = 0 \tag{16}$$

were we use $p_a=\frac{\partial S}{\partial q_a}$; $\pi_a=\frac{\partial S}{\partial \bar{q}_a}$ in the expressions above.

From the definition above and equation (14) we have

$$\frac{\partial H_0'}{\partial \pi_b} = \dot{\bar{q}}_b - \dot{\bar{q}}_\alpha\frac{\partial H_\alpha^\pi}{\partial \pi_b} - \bar{q}_\alpha\frac{\partial H_\alpha^p}{\partial \pi_b} \tag{17}$$

$$\frac{\partial H_0'}{\partial p_b} = -\dot{\bar{q}}_\alpha\frac{\partial H_\alpha^\pi}{\partial p_b} - \bar{q}_\alpha\frac{\partial H_\alpha^p}{\partial p_b} + \bar{q}_b = \bar{q}_b - \dot{\bar{q}}_\alpha\frac{\partial H_\alpha^\pi}{\partial p_b} - \bar{q}_\alpha\frac{\partial H_\alpha^p}{\partial p_b} \tag{18}$$

where $\alpha=1,...,R$; $a,b=R+1,...,n$.

Remembering that $\dot{q}_i=\dot{\bar{q}}_i$ and multiplying by $dt=dt_0$ we have from equations (17) and (18)

$$d\,\bar{q}_i = \frac{\partial H_0'}{\partial \pi_i}dt_0 + \frac{\partial H_\alpha'^p}{\partial \pi_i}dt_\alpha + \frac{\partial H_\alpha'^\pi}{\partial \pi_i}d\,\bar{t}_\alpha;\; i=1,...,n \tag{19}$$

$$dq_i = \frac{\partial H_0'}{\partial p_i}dt_0 + \frac{\partial H_\alpha'^p}{\partial p_i}dt_\alpha + \frac{\partial H_\alpha'^\pi}{\partial p_i}d\,\bar{t}_\alpha;\; i=1,...,n \tag{20}$$

$$dq_0 = dt = \frac{\partial H_0'}{\partial P_0}dt_0 + \frac{\partial H_\alpha'^p}{\partial P_0}dt_\alpha + \frac{\partial H_\alpha'^\pi}{\partial P_0}d\,\bar{t}_\alpha = \frac{\partial H_0'}{\partial P_0}dt_0 = dt_0 \tag{21}$$

noticing that for $i=\beta=1,...,R$ we have an obvious identity.

Considering that we have a solution $S\left(q_i,\dot{q}_i,t\right)$ of the set of HJPDE given by equations (16) and using equations (19) and (20), we can obtain total diferential equations for the momenta:

$$d\pi_i = -\frac{\partial H_0'}{\partial\,\bar{q}_i}dt_0 - \frac{\partial H_\alpha'^p}{\partial\,\bar{q}_i}dt_\alpha - \frac{\partial H_\alpha'^\pi}{\partial\,\bar{q}_i}d\,\bar{t}_\alpha \tag{22}$$

$$dP_0 = -\frac{\partial H_0'}{\partial t_0}dt_0 - \frac{\partial H_\alpha'^p}{\partial t_0}dt_\alpha - \frac{\partial H_\alpha'^\pi}{\partial t_0}d\,\bar{t}_\alpha \tag{23}$$

$$dp_i = -\frac{\partial H_0'}{\partial q_i}dt_0 - \frac{\partial H_\alpha'^p}{\partial q_i}dt_\alpha - \frac{\partial H_\alpha'^\pi}{\partial q_i}d\,\bar{t}_\alpha \tag{24}$$

These equations together with equations (19), (20), (21) and

$$dZ = \left(-H_0 + p_a \frac{\partial H_0'}{\partial p_a} + \pi_a \frac{\partial H_0'}{\partial \pi_a}\right) dt_0 + \left(-H_\alpha^p + p_a \frac{\partial H_\alpha'^p}{\partial p_a} + \pi_a \frac{\partial H_\alpha'^p}{\partial \pi_a}\right) dt_\alpha + \left(-H_\alpha^\pi + p_a \frac{\partial H_\alpha'^\pi}{\partial p_a} + \pi_a + \frac{\partial H_\alpha'^\pi}{\partial \pi_a}\right) d\bar{t}_\alpha \tag{25}$$

where $Z = S\left(q_i, \dot{q}_i, t\right)$, are the total differential equations for the characteristics curves and, if they form a completely integrable set, their simultaneous solutions determine $S\left(q_i, \bar{q}_i, t_0\right)$ uniquely by the initial conditions.

4 Example: Podolsky generalized electrodynamics

In this section we will consider a continuous system with Lagrangian density dependent on the dynamical field variables and its derivatives upon second order: $\mathcal{L} = \mathcal{L}\left(\psi, \partial\psi, \partial^2\psi\right)$. We adopt the metric $\eta_{\mu\nu} = diag(+1,-1,-1,-1)$ with Greek indices running from 0 to 3 while Latin indices run from 1 to 3. As stated previously, the generalization of the formalism presented in Sections 2 and 3 is straightforward, being necessary only to consider that the momenta, conjugated respectively to $\dot{\psi}^a$ and $\ddot{\psi}^a$, are now given by:

$$p_a = \frac{\partial \mathcal{L}}{\partial \dot{\psi}^a} - 2\partial_k \left(\frac{\partial \mathcal{L}}{\partial\left(\partial_k \dot{\psi}^a\right)}\right) - \partial_0 \left(\frac{\partial \mathcal{L}}{\partial \ddot{\psi}^a}\right) \tag{26}$$

$$\pi_a = \frac{\partial \mathcal{L}}{\partial \ddot{\psi}^a} \tag{27}$$

With this modification we consider the case of Podolsky electrodynamics which is based on the following Lagrangian

$$\mathcal{L} = -\frac{1}{4} F_{\mu\nu} F^{\mu\nu} + a^2 \partial_\lambda F^{\alpha\lambda} \partial_\rho F_\alpha{}^\rho \tag{28}$$

were $F_{\mu\nu} = \partial_\mu A_\nu - \partial_\nu A_\mu$.

An analysis of the Hamiltonian formalism for this theory was carried out in ref.[9] and we compare some of the results presented there with the formalism developed here. With our dynamical variables chosen as A^μ and $\bar{A}^\mu = \dot{A}^\mu$ the conjugated momenta, as given by definitions (26) and (27), are:

$$p_\mu = -F_{0\mu} - 2a^2 \left(\partial_k \partial_\lambda F^{0\lambda} \delta^k{}_\mu - \partial_0 \partial_\lambda F_\mu{}^\lambda\right) \tag{29}$$

$$\pi_\mu = 2a^2 \left(\partial_\lambda F^{0\lambda} \delta^0{}_\mu - \partial_\lambda F_\mu{}^\lambda\right) \tag{30}$$

The canonical Hamiltonian is:

$$H_c = \int d^3x \left[\bar{A}^0 \partial^i \pi_i + p_i \bar{A}^i + \frac{1}{4a^2} \pi_i \pi^i + \pi_i \partial_k F^{ik} + \pi_i \partial^i \bar{A}_0 + \frac{1}{4} F_{\mu\nu} F^{\mu\nu} + \frac{1}{2}\left(\bar{A}_i - \partial_i A_0\right)\left(\bar{A}^i - \partial^i A_0\right) - a^2 \left(\partial_k \bar{A}^k - \partial_k \partial^k A_0\right)\left(\partial_i \bar{A}^i - \partial_i \partial^i A_0\right)\right] \tag{31}$$

Using Hamilton-Jacobi formalism we have:

$$H_0' = H_C + P_0;\ P_0 = \frac{\partial S}{\partial t} \tag{32}$$

$$H_1' = \pi_0;\ H_2' = p_0 - \partial^k \pi_k \tag{33}$$

The total differential equation for A^i is

$$dA^i = \frac{\partial H_0'}{\partial p_i} dt + \frac{\partial H_1'}{\partial p_i} d\bar{A}_0 + \frac{\partial H_2'}{\partial p_i} dA_0 \tag{34}$$

$$dA^i = \frac{\partial H_0'}{\partial p_i}dt = \frac{\partial H_C}{\partial p_i}dt \Rightarrow dA^i = \bar{A}^i\, dt \tag{35}$$

and simply gives us the definition of $\bar{A}^i$.

For $\bar{A}^i$ we have:

$$d\,\bar{A}^i = \frac{\partial H_0'}{\partial \pi_i}dt + \frac{\partial H_1'}{\partial \pi_i}d\,\bar{A}_0 + \frac{\partial H_2'}{\partial \pi_i}dA_0 = \left(\frac{1}{2a^2}\pi^i + \partial_k F'^{ik} + \partial^i\,\bar{A}_C\right)dt \tag{36}$$

For the momenta p_i and p_0 we have

$$dp^i = -\frac{\partial H_0'}{\partial A_i}dt - \frac{\partial H_1'}{\partial A_i}d\,\bar{A}_0 - \frac{\partial H_2'}{\partial A_i}dA_0 = \left[-\partial^i\partial^k\pi_k + \partial_k\partial^k\pi^i - \partial_k F^{ki}\right]dt \tag{37}$$

and

$$dp^0 = -\frac{\partial H_0'}{\partial A_0}dt - \frac{\partial H_1'}{\partial A_0}d\,\bar{A}_0 - \frac{\partial H_2'}{\partial A_0}dA_0 = \left[-\partial_i\left(\bar{A}^i - \partial^i A_0\right) - 2a^2\partial^k\partial^k\left(\partial_i\,\bar{A}^i - \partial_i\partial^i A_0\right)\right]dt \tag{38}$$

Finally for π^i we have:

$$d\pi^i = -\frac{\partial H_0'}{\partial\,\bar{A}_i}dt - \frac{\partial H_1'}{\partial\,\bar{A}_i}d\,\bar{A}_0 - \frac{\partial H_2'}{\partial\,\bar{A}_i}dA_0 = \left[-p^i - F'^{0i} - 2a^2\partial^i\partial_k F'^{0k}\right]dt \tag{39}$$

Equations (37), (38) and (39) are completely equivalent to the results obtained in ref.[9]. Especifically, equations (38) and (39) give us the secondary constraint obtained in ref.[9] that isn't present in the total differential equations.

5 Conclusions

We obtained a generalization of Hamilton-Jacobi formalism whose results agree with those obtained using Dirac's formalism. In this formalism those coordinates whose correspondent accelerations can't be solved in function of the momenta are arbitrary variables of the theory. We obtained a set of Hamilton-Jacobi partial differential equations in terms of these variables and from this set we obtained the equations of motion of the system as the total differential equations for the characteristics. These total differential equations so obtained must satisfy integrability conditions and for these conditions to be satisfied the nature of the constraints (first class or second class) will play an essential role. The study of these integrability conditions is in progress as well as the generalization of the present formalism for Lagrangians of order higher than two.

References

[1] K. S. Stelle: *Phys. Rev. D*, **16**, 953 (1977). P. West: *Nucl. Phys. B*, **268**, 113 (1986).

[2] A. I. Alekseev, B. A. Arbuzov and V. A. Baikov: *Theor. Math. Phys.* (Engl. Transl.), **52**, 739 (1982); **59**, 372 (1983).

[3] K. Sundermeyer: *Lecture Notes in Physics*, 169 (1982)

[4] E. C. G. Sudarshan and N. Mukunda: *Classical Dynamics: A Modern Perspective* (John Wiley & Sons Inc., New York, 1974).

[5] P. A. M. Dirac: *Can. J. Math.*, **2**, 129 (1950); *Can. J. Math.*, **3**, 1 (1951); *Lectures on Quantum Mechanics* (Belfer Graduate School of Science, Yeshiva University, New York, N.Y., 1964)

[6] Y.Güler: *Nuovo Cimento B*, **107**, 1389 (1992); *Nuovo Cimento B*, **107**, 1143 (1992)

[7] M. Ostrogradski: *Mem. Ac. St. Petersbourg*, **1** (1850) 385

[8] D. M. Gitman and I. V. Tyutin: *Quantization of Fields with Constraints* (Springer-Verlag, 1990)

[9] Carlos A. P. Galvão and B. M. Pimentel: *Can. J. Phys.*, **66**, 460 (1988)

The Supersymmetric Two Boson Hierarchy*

J. C. Brunelli†
Universidade de São Paulo, Instituto de Física - DFMA
CP 66318 - CEP 05389-970, São Paulo - SP, Brasil
and
Ashok Das
Department of Physics and Astronomy
University of Rochester
Rochester, NY 14627, USA

Received March, 1996

We summarize some properties of the supersymmetric integrable Two Boson equation (sTB). We present its nonstandard Lax formulation and tri-Hamiltonian structure, its reduction to the supersymmetric nonlinear Schrödinger equation (sNLS) and the local as well as nonlocal conserved charges. We discuss the graded cubic algebra of the nonlocal conserved charges. We point out that the sTB and sNLS equations can be viewed as a constrained nonstandard supersymmetric Kadomtsev-Petviashvili system (sKP). Finally, we identify the second Hamiltonian structure of the sTB equation with the twisted $N = 2$ superconformal algebra.

The study of integrable models has provided for a long time a crossover arena between mathematical and theoretical physics [1]. Recently, these models have found a relevant role in the study of strings through the matrix models [2]. So, its is natural to study supersymmetric integrable models since they are likely to play an important role in the superstrings [3]. The most widely studied supersymmetric integrable system is the supersymmetric KdV (sKdV) equation [4]. But, there are other integrable systems, which can be obtained by supersymmetrization of other well known bosonic ones and may have an important role in physical applications in the study of the super matrix models. We give a description of some of our recent results [5-9] on the supersymmetric Two Boson equation [6]. A detailed review of this system and other results can be found in our review paper [10].

The Two Boson system (TB) is a dispersive generalization of the long water wave equation [11] and has appeared in the literature in the study of bosonic matrix models [12]. The equations for this $1+1$ dimensional integrable system are

$$\begin{aligned} \frac{\partial J_0}{\partial t} &= (2J_1 + J_0^2 - J_0')' \\ \frac{\partial J_1}{\partial t} &= (2J_0 J_1 + J_1')' \end{aligned} \tag{1}$$

The TB equation has a tri-Hamiltonian structure [11] which can be obtained from modified Gelfand-Dikii brackets [13]. The second Hamiltonian structure is related to a Virasoro-Kac-Moody algebra for a $U(1)$ current (an affine algebra) [13].

A supersymmetric generalization of (1) can be constructed [6] if we introduce the fermionic superfields $\Phi_0 = \psi_0 + \theta J_0$, $\Phi_1 = \psi_1 + \theta J_1$ and the supercovariant derivative $D = \frac{\partial}{\partial\theta} + \theta\frac{\partial}{\partial x}$. The most general, local, dynamical

*This work was supported in part by CNPq (J.C.B.) and the U.S. Department of Energy Grant No. DE-FG-02-91ER40685 (A.D.).
†Permanent address: Universidade Federal de Santa Catarina, Depto. de Física - CFM - Campus Universitário - Trindade - CP 476 - CEP 88040-900 - Florianópolis - SC, Brazil

equations in the superspace which are consistent with all the canonical dimensions and which reduce to (1) in the bosonic limit are

$$\begin{aligned}
\frac{\partial\Phi_0}{\partial t} &= -(D^4\Phi_0) + 2(D\Phi_0)(D^2\Phi_0) + 2(D^2\Phi_1) \\
&+ a_1 D(\Phi_0(D^2\Phi_0)) + a_2 D(\Phi_0\Phi_1) \\
\frac{\partial\Phi_1}{\partial t} &= (D^4\Phi_1) + b_1 D((D^2\Phi_1)\Phi_0) + 2(D^2\Phi_1)(D\Phi_0) - b_2 D(\Phi_1(D^2\Phi_0)) \\
&+ 2(D\Phi_1)(D^2\Phi_0) + b_3\Phi_1\Phi_0(D^2\Phi_0) + b_4 D(\Phi_1\Phi_0)(D\Phi_0) \\
&+ b_5 D(\Phi_0(D^4\Phi_0)) + b_6 D(\Phi_0(D^2\Phi_0))(D\Phi_0)
\end{aligned} \tag{2}$$

where a_i and b_i are arbitrary parameters. However, equations (2) are integrable only for specific choices of a_i and b_i. In fact, a consistent Lax representation can be obtained for the system (2) with the Lax operator

$$L = D^2 - (D\Phi_0) + D^{-1}\Phi_1 \tag{3}$$

and the nonstandard Lax equation

$$\frac{\partial L}{\partial t} = [L, (L^2)_{\geq 1}] \tag{4}$$

where $D^{-1} = \partial^{-1}D$. So, the most general supersymmetric extension of the dynamical equations (1) which is integrable is given by

$$\begin{aligned}
\frac{\partial\Phi_0}{\partial t} &= -(D^4\Phi_0) + (D(D\Phi_0)^2) + 2(D^2\Phi_1) \\
\frac{\partial\Phi_1}{\partial t} &= (D^4\Phi_1) + 2(D^2((D\Phi_0)\Phi_1))
\end{aligned} \tag{5}$$

These are the supersymmetric Two Boson equations (sTB) [6]. It is straightforward to check that these equations are invariant under the $N = 1$ supersymmetry transformation $\theta \to \theta + \epsilon$ and $x \to x + \theta\epsilon$.

Since equations (5) are integrable we have an infinite number of local conserved charges in involution which can be obtained from

$$Q_n = \mathrm{sTr}\, L^n = \int dz\, \mathrm{sRes}\, L^n \qquad n = 1, 2, 3, \ldots \tag{6}$$

They are bosonic and are invariant under the supersymmetry transformation.

Defining the Hamiltonians of the sTB system as $H_n = \frac{(-1)^{n+1}}{n} Q_n$ we can write the sTB equations (5) as a Hamiltonian system [6]

$$\partial_t \begin{pmatrix} \Phi_0 \\ \Phi_1 \end{pmatrix} = \mathcal{D}_1 \begin{pmatrix} \frac{\delta H_2}{\delta\Phi_0} \\ \frac{\delta H_2}{\delta\Phi_1} \end{pmatrix} = \mathcal{D}_2 \begin{pmatrix} \frac{\delta H_1}{\delta\Phi_0} \\ \frac{\delta H_1}{\delta\Phi_1} \end{pmatrix} = \mathcal{D}_3 \begin{pmatrix} \frac{\delta H_1}{\delta\Phi_0} \\ \frac{\delta H_1}{\delta\Phi_1} \end{pmatrix} \tag{7}$$

where the first structure has the local form

$$\mathcal{D}_1 = \begin{pmatrix} 0 & -D \\ -D & 0 \end{pmatrix} \tag{8}$$

and the second has the nonlocal form [8]

$$\mathcal{D}_2 = \begin{pmatrix} -2D - 2D^{-1}\Phi_1 D^{-1} + D^{-1}(D^2\Phi_0)D^{-1} & D^3 - D(D\Phi_0) + D^{-1}\Phi_1 D \\ -D^3 - (D\Phi_0)D - D\Phi_1 D^{-1} & -\Phi_1 D^2 - D^2\Phi_1 \end{pmatrix} \tag{9}$$

The third structure, which is highly nonlocal, can be written as $\mathcal{D}_3 = \mathcal{R}\mathcal{D}_2 = \mathcal{R}^2\mathcal{D}_1$ where $\mathcal{R} = \mathcal{D}_2\mathcal{D}_1^{-1}$.

The s'TB equation reduces to many other supersymmetric integrable models such as the sKdV and mKdV [6,9,10]. Let us show how the supersymmetric nonlinear Schrödinger equation (sNLS) [14,5] can be obtained from the s'TB system [6,9]. Defining the fermionic superfields $Q = \psi + \theta q$ and $\overline{Q} = \overline{\psi} + \theta\overline{q}$, the invertible transformation

$$\begin{aligned} \Phi_0 &= -(D\ln(DQ)) + (D^{-1}(\overline{Q}Q)) \\ \Phi_1 &= -\overline{Q}(DQ) \end{aligned} \tag{10}$$

yields, after a slightly involved derivation [6], the following equations from (5)

$$\begin{aligned} \frac{\partial Q}{\partial t} &= -(D^4Q) + 2\left(D((DQ)\overline{Q})\right)Q \\ \frac{\partial \overline{Q}}{\partial t} &= (D^4\overline{Q}) - 2\left(D((D\overline{Q})Q)\right)\overline{Q} \end{aligned} \tag{11}$$

These are the sNLS equations without free parameters obtained in [10] and shown to satisfy various tests of integrability [5]. In [7] we have shown that (11) has a nonstandard Lax representation with Lax operator given by

$$\mathcal{L} = -\left(D^2 + \overline{Q}Q - \overline{Q}D^{-1}(DQ)\right) \tag{12}$$

The bi-Hamiltonian structure for the sNLS system was derived from the s'TB ones, through the field redefinition in (10). This can be found in reference [9].

If we rewrite the operator $\mathcal{L}$ using the supersymmetric Leibnitz rule we get

$$\mathcal{L} = -\left(D^2 + \sum_{n=-1}^{\infty} \Psi_n D^{-n}\right) \tag{13}$$

where $\Psi_{-1} = 0$ and $\Psi_n = (-1)^{[\frac{n+1}{2}]}\overline{Q}(D^nQ)$, $(n \geq 0)$. Here, Ψ_{2n} (Ψ_{2n+1}) are bosonic (fermionic) superfields. In this way $\mathcal{L}$ has the form of the Lax operator for the sKP hierarchy and, therefore, we can think of the sNLS system as a constrained supersymmetric Kadomtsev-Petviashvili system (sKP) but of the nonstandard kind (even the s'TB can be viewed as a constrained sKP system). However, the Lax operator $\mathcal{L}$ in this case is an even parity operator and not of the usual Manin-Radul form [4]. This is a new system, namely, a nonstandard supersymmetric KP hierarchy, and was studied in [7]. It gives a new supersymmetric KP equation and unifies all the KP and mKP flows.

As we have already pointed out the s'TB equation, given by the Lax operator (3), has conserved local charges Q_n obtained from the integer powers of the Lax operator as in (6). Also, the sTB has a supersymmetric charge Q which is local and conserved and implements the supersymmetric transformation. For the sTB equation we also have the presence of nonlocal charges [8] and they can be obtained from

$$F_{\frac{2n-1}{2}} = \mathrm{sTr}\, L^{\frac{2n-1}{2}} \qquad n = 1, 2, 3, \ldots \tag{14}$$

These nonlocal charges are conserved and are fermionic. The nonlocal charges $F_{\frac{2n-1}{2}}$ as well as Q are not supersymmetric.

We can now ask about the algebra of these charges Q_n, Q and $F_{\frac{2n-1}{2}}$ [8]. First, we obtain

$$\{Q_n, Q_m\}_1 = \{Q_n, F_{\frac{2m-1}{2}}\}_1 = \{Q_n, Q\}_1 = 0 \tag{15}$$

which simply implies that these charges are conserved under any flow of the hierarchy. The fact that Q and $F_{\frac{2n-1}{2}}$ are not supersymmetric is expressed by

$$\begin{aligned}
\{Q, Q\}_1 &= -Q_2 \\
\{Q, F_{1/2}\}_1 &= Q_1 \\
\{Q, F_{3/2}\}_1 &= \frac{1}{2}Q_2 \\
\{Q, F_{5/2}\}_1 &= \frac{1}{3}Q_3 + \frac{1}{24}Q_1^3
\end{aligned} \tag{16}$$

And the algebra for the lowest order nonlocal charges is

$$\begin{aligned}
\{F_{1/2}, F_{1/2}\}_1 &= 0 \\
\{F_{1/2}, F_{3/2}\}_1 &= Q_1 \\
\{F_{1/2}, F_{5/2}\}_1 &= Q_2 \\
\{F_{3/2}, F_{3/2}\}_1 &= 2Q_2 \\
\{F_{3/2}, F_{5/2}\}_1 &= \frac{7}{3}Q_3 + \frac{7}{24}Q_1^3 \\
\{F_{5/2}, F_{5/2}\}_1 &= 3Q_4 - \frac{5}{8}Q_1^2 Q_2
\end{aligned} \tag{17}$$

So, the algebra of the conserved charges of the sTB system closes as a graded nonlinear algebra. The cubic terms in the algebra above arise from boundary contributions when nonlocal terms are involved. In fact, algebras of nonlocal charges showing nonlinearity of the cubic kind are present in various other systems and are related with Yangian structures [15,16]. The nonlinearity in (16) and (17) appear to be redefineable to cubic terms [8]. This is well known for the nonlinear sigma model [16].

From (16) and (17) we see that $F_{3/2}$ has the same algebra, with the other generators of the algebra, as the supersymmetry charge Q. Thus, this can be identified with a second supersymmetry charge and this shows that the sTB equation has in fact an $N = 2$ extended supersymmetry [17].

Finally, with the linear change of variables $\bar{\xi} = -\frac{1}{2}(\psi_0' - \psi_1)$ and $\xi = \frac{1}{2}\psi_1$ the second Hamiltonian structure (9), in terms of components, gives the following nonvaninshing Poisson brackets [10]

$$\begin{aligned}
\{J_0(x), J_0(y)\}_2 &= 2\delta'(x-y) \\
\{J_0(x), J_1(y)\}_2 &= (J_0\delta(x-y))' - \delta''(x-y) \\
\{J_0(x), \bar{\xi}(y)\}_2 &= -\bar{\xi}\delta(x-y) \\
\{J_0(x), \xi(y)\}_2 &= \xi\delta(x-y) \\
\{J_1(x), J_1(y)\}_2 &= J_1'\delta(x-y) + 2J_1\delta'(x-y) \\
\{J_1(x), \bar{\xi}(y)\}_2 &= \bar{\xi}\delta'(x-y) \\
\{J_1(x), \xi(y)\}_2 &= \xi'\delta(x-y) + 2\xi\delta'(x-y) \\
\{\bar{\xi}(x), \xi(y)\}_2 &= -\frac{1}{4}J_1\delta(x-y) + \frac{1}{4}(J_0\delta(x-y))' - \frac{1}{4}\delta''(x-y)
\end{aligned} \tag{18}$$

This local algebra is nothing other than the twisted $N = 2$ superconformal algebra [18] whose bosonic limit is the Virasoro-Kac-Moody algebra for the sTB system [10].

References

1. L.D. Faddeev and L.A. Takhtajan, "Hamiltonian Methods in the Theory of Solitons" (Springer, Berlin, 1987); A. Das, "Integrable Models" (World Scientific, Singapore, 1989); L. A. Dickey, "Soliton Equations and Hamiltonian Systems" (World Scientific, Singapore, 1991).
2. D. J. Gross and A. A. Midgal, Phys. Rev. Lett. **64**, 127 (1990); E. Brézin and V. A. Kazakov, Phys. Lett. 236B, 144 (1990); M. Douglas and S. H. Shenker, Nucl. Phys. **B335**, 635 (1990).
3. L. Alvarez-Gaumé, H. Itoyama, J. Manês and A. Zadra, Int. J. Mod. Phys. **A7**, 5337 (1992).
4. Y. I. Manin and A. O. Radul, Commun. Math. Phys. **98**, 65 (1985); P. Mathieu, J. Math. Phys. **29**, 2499 (1988).
5. J. C. Brunelli and A. Das, J. Math. Phys. **36**, 268 (1995).
6. J. C. Brunelli and A. Das, Phys. Lett. **B337**, 303 (1994).
7. J. C. Brunelli and A. Das, Rev. Math. Phys. **7**, 1181 (1995).
8. J. C. Brunelli and A. Das, Phys. Lett. **B354**, 307 (1995).
9. J. C. Brunelli and A. Das, Mod. Phys. Lett. **A10**, 2019 (1995).
10. J. C. Brunelli and A. Das, Int. J. Mod. Phys. **A10**, 4563 (1995).
11. B.A. Kupershmidt, Commun. Math. Phys. **99**, 51 (1985).
12. H. Aratyn, L.A. Ferreira, J.F. Gomes and A.H. Zimerman, Nucl. Phys. **B402**, 85 (1993); L. Bonora and C.S. Xiong, Int. J. Mod. Phys. **A8**, 2973 (1993).
13. J. C. Brunelli, A. Das and W.-J. Huang, Mod. Phys. Lett. **9A**, 2147 (1994).
14. G.H.M. Roelofs and P.H.M. Kersten, J. Math. Phys. **33**, 2185 (1992).
15. D. Bernard, "An Introduction to Yangian Symmetries", in Integrable Quantum Field Theories, ed. L. Bonora et al., NATO ASI Series B: Physics vol. 310 (Plenum Press, New York, 1993).
16. E. Abdalla, M. C. B. Abdalla, J. C. Brunelli and A. Zadra, Commun. Math. Phys. **166**, 379 (1994).
17. S. Krivonos and A. Sorin, Phys. Lett. **B357**, 94 (1995); S. Krivonos, A. Sorin and F. Toppan, Phys Lett. **A206**, 146 (1995).
18. E. Witten, Commun. Math. Phys. **117**, 353 (1988); **118**, 411 (1988); Nucl. Phys. **B340** 281 (1990); T. Eguchi and S. Yang, Mod. Phys. Lett. **A4**, 1693 (1990).

Sugawara Construction of the q-Deformed Energy-Momentum Tensor

E. Batista*, J. F. Gomes†, I. J. Lautenschlegner‡
Instituto de Física Teórica, UNESP

Received March, 1996

We present a constructionn of the q-Deformed Energy-Momentum tensor in terms of $U_q(\widehat{su}(2))$ currents. We also find a q-analogue of the classical equivalence theorem, which states that for simply laced level one affine Lie algebras, the total Energy-Momentum tensor is proportional only to the Cartan Sub-Algebra part.

1 Introduction

In the last decade, it has become well known that conformal symmetries play an important role in a broad class of two dimensional models in field theory and statistical mechanics. The Physical content of these models may be extracted by use of representation theory of the Virasoro algebra [1], generated by the Energy-Momentum tensor. In special, there are models in two dimensions, such as WZNW models, in which the Energy-Momentum tensor may be written quadratically in terms of currents of an affine Lie algebra [8], the so called Sugawara construction.

Quantum groups also appeared as underlying symmetry in many physical systems such as integrable models, lattice statistical models with anisotropy, quantum Hall effect and conformal field theories. The algebraic structure is characterized by the so called Hopf algebras dependent on a deformation parameter $q = e^{\epsilon}$ [4]. When the classical limit ($q \to 1$) is taken, the features of these symmetries disappear leaving only the usual symmetries. As an example, a q-deformed version of Fubini-Veneziano model was proposed by replacing the ordinary oscillators by q-deformed ones in the operator formalism, it was shown that this new model lead to non-linear Regge trajectories [3].

Many efforts have been made in order to find a q-deformed version of Virasoro algebra [9] [10] [5]. The principal motivation is to construct new field theoretical models in two dimensions which posses this q-deformed conformal symmetry. This work consists in a construction of the Energy-Momentum tensor in terms of currents of $U_q(\widehat{su}(2))$ q-deformed Kac-Moody algebra, this is a q-analogue of Sugawara construction. We also show that the constituent parts of this Energy-Momentum tensor satisfy a closed quadratic algebra.

2 The Classical Case

The $\widehat{su}(2)$ current algebra is defined by three currents

$$E^{\pm}(z) = \sum_{n=-\infty}^{\infty} E_n^{\pm} z^{-n-1} \quad ; \quad H(z) = \sum_{n=-\infty}^{\infty} H_n z^{-n-1} \quad . \tag{1}$$

They satisfy the OPE relations (for k=1)

$$\begin{aligned} H(z)E^{\pm}(w) &\sim \frac{\pm\sqrt{2}E^{\pm}(w)}{(z-w)} \quad |z| > |w|, \\ H(z)H(w) &\sim \frac{1}{(z-w)^2} \quad |z| > |w|, \\ E^{+}(z)E^{-}(w) &\sim \frac{1}{(z-w)^2} + \frac{\sqrt{2}H(w)}{(z-w)} \quad |z| > |w|, \end{aligned} \tag{2}$$

*Supported by FAPESP
†Partially supported by CNPq
‡Supported by CNPq

where the symbol $\sim$ means equality up to regular terms.

It is possible to construct a vertex operator realization for this Kac-Moody algebra at level one [7]. Define the Fubini-Veneziano field to be

$$\xi(z) = Q - iP\ln z + i\sum_{n\neq 0}\frac{\alpha_n}{n}z^{-n} \quad , \tag{3}$$

where the oscillators α_n and modes P and Q satisfy

$$[\alpha_n, \alpha_m] = n\delta_{m+n,0} \quad ; \quad [Q, P] = i \quad .$$

The currents (1) are defined in terms of (3) as

$$E^{\pm}(z) = :e^{\pm i\sqrt{2}\xi(z)}: \quad ; \quad H(z) = i\partial_z\xi(z) \quad ,$$

where the dots denote the normal ordering among oscillators α_n and $H_0 = P$.

The classical Energy-Momentum tensor is defined in terms of $\widehat{su}(2)$ currents as

$$T(z) = \frac{1}{6}\left({}^{\times}_{\times}H^2(z){}^{\times}_{\times} + {}^{\times}_{\times}E^+(z)E^-(z){}^{\times}_{\times} + {}^{\times}_{\times}E^+(z)E^-(z){}^{\times}_{\times}\right) \quad , \tag{4}$$

here, the crosses denote normal ordering among the modes defined by expressions (1), this is equivalent to find the regular part of the OPE after taking the equal point limit. The classical equivalence theorem states that the Energy-Momentum tensor (4), when currents are written in vertex operator realization, is equivalent to

$$T(z) = \frac{1}{2}{}^{\times}_{\times}H^2(z){}^{\times}_{\times} \quad . \tag{5}$$

3 The q-Deformed Case

In order to obtain a q-deformed version of the Energy-Momentum tensor, we take as starting point the quantum affine Lie algebra $U_q(\widehat{su}(2))$ at level k=1, we shall be assuming the deformation parameter to be a pure phase, i.e. $q = e^{i\epsilon}$ for ϵ real. Defining new currents

$$\begin{aligned}
\Psi(z) &= \sum_{n\geq 0}\Psi_n z^{-n} = q^{\sqrt{2}H_0}\exp\left\{\sqrt{2}(q-q^{-1})\sum_{n>0}H_n z^{-n}\right\} \quad , \\
\Phi(z) &= \sum_{n\leq 0}\Phi_n z^{-n} = q^{-\sqrt{2}H_0}\exp\left\{-\sqrt{2}(q-q^{-1})\sum_{n<0}H_n z^{-n}\right\} \quad .
\end{aligned} \tag{6}$$

Here, the expression $(\Psi(z) - \Phi(z))/(\sqrt{2}z(q-q^{-1}))$ is the q-deformed generalization of the classical $H(z)$ current. The OPE relations of this algebra are [2]

$$\begin{aligned}
\Psi(z)\Phi(w) &= \frac{(z-wq^3)(z-wq^{-3})}{(z-wq)(z-wq^{-1})}\Phi(w)\Psi(z) \quad , \\
\Psi(z)E^{\pm}(w) &= q^{\pm 2}\frac{(z-wq^{\mp\frac{5}{2}})}{(z-wq^{\pm\frac{3}{2}})}E^{\pm}(w)\Psi(z) \quad , \\
E^{\pm}(z)\Phi(w) &= q^{\pm 2}\frac{(z-wq^{\mp\frac{5}{2}})}{(z-wq^{\pm\frac{3}{2}})}\Phi(w)E^{\pm}(z) \quad , \\
E^+(z)E^-(w) &\sim \frac{1}{w(q-q^{-1})}\left\{\frac{\Psi(wq^{\frac{1}{2}})}{z-wq} - \frac{\Phi(wq^{-\frac{1}{2}})}{z-wq^{-1}}\right\} \quad , \\
E^{\pm}(z)E^{\pm}(w) &= \frac{(zq^{\pm 2}-w)}{(z-wq^{\pm 2})}E^{\pm}(w)E^{\pm}(z) \quad |z| > |w|.
\end{aligned} \tag{7}$$

The vertex operator realization for these operators [6] using the q-deformed oscillators

$$[\alpha_n, \alpha_m] = \frac{[2n][n]}{2n}\delta_{m+n,0} \quad ; \quad [Q, P] = i \quad . \tag{8}$$

Define a Fubini-Veneziano field

$$\xi^{\pm}(z) = Q - iP\ln z + i\sum_{n<0}\frac{\alpha_n}{[n]}(zq^{\mp\frac{1}{2}})^{-n} + i\sum_{n>0}\frac{\alpha_n}{[n]}(zq^{\pm\frac{1}{2}})^{-n} \quad . \tag{9}$$

and the step operators for $U_q(\widehat{su}(2))$

$$E^{\pm}(z) = :\exp\left\{\pm\sqrt{2}\xi^{\pm}(z)\right\}: \quad , \tag{10}$$

and the modes $H_n = \alpha_n$, $H_0 = P$. Using the Baker-Campbell-Haussdorff formula we find the expression for the OPE $E^{+}(z)E^{-}(w)$, and so, expanding the numerator in q-Taylor series, we determine the pole structure in (7) and the regular terms which the first order term is given by

$$\overset{\times}{\times} E^{+}(w)E^{-}(w)\overset{\times}{\times} = \frac{1}{2[2]w^2(q-q^{-1})^2}\left\{[q^{-3}(A^1(wq^2)-1)+(q-q^{-1})]\Psi(wq^{\frac{1}{2}}) + \right.$$

$$\left. + \Phi(wq^{-\frac{1}{2}})[q^3(B^1(wq^{-2})-1)-(q-q^{-1})]\right\} + \mathcal{O}(q-q^{-1}) \quad . \tag{11}$$

where the composite fields A^{α} and B^{α} are defined as

$$A^{\alpha}(w) = \Phi^{-1}(wq^{-\frac{\alpha}{2}})\Psi(wq^{\frac{\alpha}{2}}) \quad ; \quad B^{\alpha}(w) = \Phi(wq^{-\frac{\alpha}{2}})\Psi^{-1}(wq^{\frac{\alpha}{2}}) \quad . \tag{12}$$

Note that the regular part depends only on currents related to Cartan Sub-Algebra, this enables one to write the general expression of the q-deformed Energy-Momentum tensor as a family of operators labeled by two indices

$$T^{\alpha;\beta}(z) = \frac{1}{2[2]z^2(q-q^{-1})^2}\left\{A^{\alpha}(zq^{\beta}) + B^{\alpha}(zq^{\beta}) - 2\right\} \quad , \tag{13}$$

with A^{α} and B^{α} defined by expressions in (12). The algebra of the q-deformed Energy-Momentum tensor (13) do not close, however its components A^{α} and B^{α} define a quadratic algebra, namely

$$\begin{aligned}
A^{\alpha}(z)A^{\beta}(w) &= f(zq^{\frac{\alpha}{2}};wq^{-\frac{\beta}{2}}) : A^{\alpha}(z)A^{\beta}(w) : \quad , \\
B^{\alpha}(z)B^{\beta}(w) &= f(zq^{\frac{\alpha}{2}};wq^{-\frac{\beta}{2}}) : B^{\alpha}(z)B^{\beta}(w) : \quad , \\
A^{\alpha}(z)B^{\beta}(w) &= f^{-1}(zq^{\frac{\alpha}{2}};wq^{-\frac{\beta}{2}}) : A^{\alpha}(z)B^{\beta}(w) : \quad , \\
B^{\alpha}(z)A^{\beta}(w) &= f^{-1}(zq^{\frac{\alpha}{2}};wq^{-\frac{\beta}{2}}) : B^{\alpha}(z)A^{\beta}(w) : \quad ,
\end{aligned} \tag{14}$$

where the analytic structure is given by: $f(z;w) = \frac{(z-wq)(z-wq^{-1})}{(z-wq^3)(z-wq^{-3})}$. The higher order terms in the q-Taylor expansion of the OPE $E^{+}(z)E^{-}(w)$ lead us to a more general class of q-deformed Energy-Momentum tensors in Sugawara form which generalizes the expression (13).

References

[1] A.A. Belavin, A.M. Polyakov and A.B. Zamolodchikov: Nucl. Phys. B241 (1984) 333-380.

[2] A. H. Bougourzi and L. Vinet: preprint CRM-2181 (1994).

[3] M. Chaichian, J.F. Gomes and P. Kulish: Phys. Lett. B311 (1993) 93. M. Chaichian, J.F. Gomes and R. Gonzalez-Felipe: Phys. Lett. B341 (1994) 147-152.

[4] V.G. Drinfel'd: Proceedings of the International Congress of Mathematicians, Berkeley (1986) 798-820.

[5] E. Frenkel and N. Reshetikhin: preprint q-alg/9505025.

[6] I. B. Frenkel and N. H. Jing: Proc. Nat'l. Acad. Sci. (USA) 85(1988) 9373.

[7] P. Goddard and D. Olive: Int. J. Mod. Phys. A1 (1986) 303-414.

[8] V.G. Knizhnik and A.B. Zamolodchikov: Nucl. Phys. B247 (1984) 83-103

[9] C.H. Oh and K. Singh: preprint hep-th/9407001.

[10] H. Sato: Nucl. Phys. B393 (1993) 412-458.

Primary fields in a q-deformed conformal field theory

E. Batista*, J. F. Gomes† and I. J. Lautenschleguer‡
Instituto de Física Teórica UNESP, Rua Pamplona 145
01405-900 São Paulo Brazil

February 1996

Primary fields in the framework of a q-deformed conformal field theory are defined. Some realizations of q-deformations of the Virasoro algebra and a q-deformed version of the $N = 1$ superconformal algebra are also discussed.

A primary field $\phi(w)$ of conformal weight h is defined by its OPE with the energy momentum tensor $T(z)$(where w e z denote complex variables)

$$T(z)\phi(w) = \frac{h\phi(w)}{(z-w)^2} + \frac{\partial\phi(w)}{(z-w)} + \text{regular terms.} \tag{1}$$

A q-deformation of the theory is achieved by replacing (1) by the corresponding q-analogue

$$(T(z)\phi(w))_q = \frac{1}{w(q-q^{-1})}\left\{\frac{\phi(wq)}{z-wq^h} - \frac{\phi(wq^{-1})}{z-wq^{-h}}\right\} + \text{regular terms.} \tag{2}$$

An abelian field $H(z)$ can be Laurent expanded in terms of a q-deformed infinite Heisenberg algebra $H_q(\infty)$

$$H(z) = \sum_{n=-\infty}^{\infty} a_n z^{-n-1}, \tag{3}$$

where the oscillators a_n obey the following commutation relation

$$[a_n, a_m] = [n]\delta_{m+n,0}, \tag{4}$$

with $[n] = q^n - q^{-n}/q - q^{-1}$.

Its OPE is given by

$$H(z)H(w) =: H(z)H(w) : + \frac{1}{(z-wq)(z-wq^{-1})}, \tag{5}$$

where we choose $|q| = 1$ and the dots denote normal ordering in the sense that the positive oscillator modes are moved to the right of those with negative.

We now evaluate the OPE of $T(z) = \frac{1}{2} : H^2(z) :$ with $H(w)$

$$T(z)H(w) = \frac{1}{w(q-q^{-1})}\left(\frac{H(wq)}{z-wq} - \frac{H(wq^{-1})}{z-wq^{-1}}\right) + \text{regular terms } |z| > |w|. \tag{6}$$

Therefore one can infer that $H(z)$ is a spin 1 primary field and that $T(z)$ can be considered as the energy momentum tensor. The shifts in the arguments of $H(w)$ in the r.h.s. require an extra index for the closure of the algebra of the energy moment

Generalizing we are able to define a family of operators

$$T^{\alpha}(z) = \frac{1}{2} : H(zq^{\frac{\alpha}{2}})H(zq^{-\frac{\alpha}{2}}) : \quad (\alpha \in Z), \tag{7}$$

*Supported by FAPESP
†Supported in part by CNPq
‡Supported by CNPq

which possesses an OPE algebra

$$
\begin{aligned}
T^{\alpha}(z)T^{\beta}(w) &= \frac{1}{wq^{\frac{\beta+\alpha}{2}}(q-q^{-1})}\left(\frac{T^{\beta-\alpha+1}(wq^{\frac{-\alpha+1}{2}})}{z-wq^{\frac{\beta-\alpha}{2}+1}} - \frac{T^{\beta-\alpha-1}(wq^{\frac{-\alpha-1}{2}})}{z-wq^{\frac{\beta-\alpha}{2}-1}}\right) + \\
&+ \frac{1}{wq^{\frac{-\beta+\alpha}{2}}(q-q^{-1})}\left(\frac{T^{-\beta-\alpha+1}(wq^{\frac{-\alpha+1}{2}})}{z-wq^{\frac{-\beta-\alpha}{2}+1}} - \frac{T^{-\beta-\alpha-1}(wq^{\frac{-\alpha-1}{2}})}{z-wq^{\frac{-\beta-\alpha}{2}-1}}\right) + \\
&+ \frac{1}{wq^{\frac{\beta-\alpha}{2}}(q-q^{-1})}\left(\frac{T^{\beta+\alpha+1}(wq^{\frac{\alpha+1}{2}})}{z-wq^{\frac{\beta+\alpha}{2}+1}} - \frac{T^{\beta+\alpha-1}(wq^{\frac{\alpha-1}{2}})}{z-wq^{\frac{\beta+\alpha}{2}-1}}\right) + \\
&+ \frac{1}{wq^{\frac{-\beta-\alpha}{2}}(q-q^{-1})}\left(\frac{T^{-\beta+\alpha+1}(wq^{\frac{\alpha+1}{2}})}{z-wq^{\frac{-\beta+\alpha}{2}+1}} - \frac{T^{-\beta+\alpha-1}(wq^{\frac{\alpha-1}{2}})}{z-wq^{\frac{-\beta+\alpha}{2}-1}}\right) + \\
&+ \frac{1}{4(z-wq^{\frac{\beta-\alpha}{2}+1})(z-wq^{\frac{\beta-\alpha}{2}-1})(z-wq^{\frac{-\beta+\alpha}{2}+1})(z-wq^{\frac{-\beta+\alpha}{2}-1})} + \\
&+ \frac{1}{4(z-wq^{\frac{-\beta-\alpha}{2}+1})(z-wq^{\frac{-\beta-\alpha}{2}-1})(z-wq^{\frac{\beta+\alpha}{2}+1})(z-wq^{\frac{\beta+\alpha}{2}-1})} \quad |z|>|w|. \qquad (8)
\end{aligned}
$$

In the limit $q \to 1$, we have $[a_n, a_m] = n\delta_{n+m,0}$ and the $T^{\alpha}(z)$ become $T(z) = \frac{1}{2} : H^2(z) :$, which satisfies the Virasoro algebra with central charge $c = 1$. Hence the algebra (8) represents a bosonic realization of the q-Virasoro algebra.

Other realization can be achieved by means of free fermions. Let $\psi(z)$ be a fermionic field with OPE

$$\psi(z)\psi(w) = :\psi(z)\psi(w): + \frac{1}{(z-w)} \quad |z|>|w|. \qquad (9)$$

A family of operators can be defined

$$L^{\alpha}(z) = \frac{1}{[\alpha](q-q^{-1})} : \psi(zq^{\frac{\alpha}{2}})\psi(zq^{-\frac{\alpha}{2}}) : \qquad (10)$$

satisfying the algebra

$$
\begin{aligned}
L^{\alpha}(z)L^{\beta}(w) &= \frac{1}{[\alpha][\beta]w(q-q^{-1})}\left(\frac{[\alpha+\beta]L^{\alpha+\beta}(wq^{\frac{\alpha}{2}})}{q^{\frac{\beta-\alpha}{2}}(z-wq^{\frac{\beta+\alpha}{2}})} + \right. \\
&+ \frac{[-\alpha-\beta]L^{-\alpha-\beta}(wq^{-\frac{\alpha}{2}})}{q^{\frac{-\beta+\alpha}{2}}(z-wq^{\frac{-\beta-\alpha}{2}})} - \frac{[\alpha-\beta]L^{\alpha-\beta}(wq^{\frac{\alpha}{2}})}{q^{\frac{-\beta-\alpha}{2}}(z-wq^{\frac{-\beta+\alpha}{2}})} + \\
&- \frac{[-\alpha+\beta]L^{-\alpha+\beta}(wq^{\frac{-\alpha}{2}})}{q^{\frac{\beta+\alpha}{2}}(z-wq^{\frac{\beta-\alpha}{2}})} + \frac{1}{(z-wq^{\frac{-\beta-\alpha}{2}})(z-wq^{\frac{\beta+\alpha}{2}})} + \\
&- \left.\frac{1}{(z-wq^{\frac{-\beta+\alpha}{2}})(z-wq^{\frac{\beta-\alpha}{2}})}\right) \quad |z|>|w|. \qquad (11)
\end{aligned}
$$

In the limit $q \to 1$ these $L^{\alpha}(z)$ become

$$L(z) = \frac{1}{2} : \partial\psi(z)\psi(z) :, \qquad (12)$$

which satisfies the Virasoro algebra with central charge $c = \frac{1}{2}$. Hence the algebra (11) represents a fermionic realization of the q-Virasoro algebra.

We also note that $\psi(w)$ is a spin $\frac{1}{2}$ primary field since its OPE with the energy momentum tensor $L^2(z)$ is given by

$$L^2(z)\psi(w) = \frac{1}{(q-q^{-1})w}\left(\frac{\psi(wq)}{z-wq^{\frac{1}{2}}} - \left(\frac{\psi(wq^{-1})}{z-wq^{-\frac{1}{2}}}\right) + \text{regular terms.} \qquad (13)\right.$$

One can also define a family of operators

$$G^{\alpha}(z) = H(zq^{\frac{\alpha}{2}})\psi(zq^{-\frac{\alpha}{2}}), \qquad (14)$$

where $H(z)$ is given by (3) and $\psi(z)$ is a free fermion. These operators represent a q-deformed version of the operator $G(z) = H(z)\psi(z)$.

The $OPE's$ referring to a q-deformed version of the $N = 1$ superconformal algebra are

$$\begin{aligned} G^\alpha(z)G^\beta(w) &= \frac{2q^{\frac{\alpha}{2}}T^{\beta+\alpha}(wq^{\frac{\alpha}{2}})}{z - wq^{\frac{-\beta+\alpha}{2}}} + \\ &+ \frac{[\beta-\alpha+1]L^{\beta-\alpha+1}(wq^{\frac{-\alpha+1}{2}})}{q^{\frac{\beta-1}{2}+\alpha}(z - wq^{\frac{\beta-\alpha}{2}+1})} + \\ &- \frac{[\beta-\alpha-1]L^{\beta-\alpha-1}(wq^{\frac{-\alpha-1}{2}})}{q^{\frac{\beta+1}{2}+\alpha}(z - wq^{\frac{\beta-\alpha}{2}-1})} + \\ &+ \frac{q^{-\frac{\alpha}{2}}}{(z - wq^{\frac{-\beta+\alpha}{2}})(z - wq^{\frac{\beta-\alpha}{2}+1})(z - wq^{\frac{\beta-\alpha}{2}+1})} \quad |z| > |w|, \end{aligned} \tag{15}$$

$$\begin{aligned} T^\alpha(z)G^\beta(w) &= \frac{1}{2wq^{\frac{\beta}{2}}(q - q^{-1})}\left(\frac{q^{-\frac{\alpha}{2}}G^{\beta-\alpha+1}(wq^{\frac{-\alpha+1}{2}})}{z - wq^{\frac{\beta-\alpha}{2}+1}} + \right. \\ &- \frac{q^{-\frac{\alpha}{2}}G^{\beta-\alpha-1}(wq^{\frac{-\alpha-1}{2}})}{z - wq^{\frac{\beta-\alpha}{2}-1}} + \frac{q^{\frac{\alpha}{2}}G^{\beta+\alpha+1}(wq^{\frac{\alpha+1}{2}})}{z - wq^{\frac{\beta+\alpha}{2}+1}} + \\ &- \left.\frac{q^{\frac{\alpha}{2}}G^{\beta+\alpha-1}(wq^{\frac{\alpha-1}{2}})}{z - wq^{\frac{\beta+\alpha}{2}-1}}\right) \quad |z| > |w|, \end{aligned} \tag{16}$$

$$L^\alpha(z)G^\beta(w) = \frac{1}{[\alpha]wq^{-\frac{\beta}{2}}(q - q^{-1})}\left(\frac{G^{\beta-\alpha}(wq^{\frac{\alpha}{2}})}{z - wq^{\frac{-\beta+\alpha}{2}}} - \frac{G^{\beta+\alpha}(wq^{\frac{-\alpha}{2}})}{z - wq^{\frac{-\beta-\alpha}{2}}}\right) \quad |z| > |w|. \tag{17}$$

In the limit $q \to 1$ we recover the usual undeformed $N = 1$ superconformal algebra. Details about the construction of a q-deformed $N = 2$ superconformal algebra (making use of the vertex operators) may be seen in [7].

Bibliography

[1] C.H.Oh and K. Singh, *J. Phys. A: Math. Gen.* **27** (1994), 3439.

[2] H. Sato, *Nucl. Phys.* **B 393** (1993), 442.

[3] A.H. Bougourzi and L. Vinet, *A Quantum Analogue of the Boson-Fermion Correspondence* - CRM-2181 preprint (1994).

[4] P. Goddard and D. Olive, *Int. J. Mod. Phys.* **A 1** (1986), 303.

[5] H. Sato, *OPE Formulae for Deformed Super-Virasoro Algebras* - NBI-HE-95-34 preprint (1995).

[6] M. Chaichian, P. Presnajder, *Phys. Lett.* **B 277** (1992), 109.

[7] E. Batista, J.F. Gomes and I.J. Lautenschleguer, *Non Abelian Sugawara Construction and the q-Deformed $N = 2$ Superconformal Algebra* - IFT preprint (1996).

Sphalerons in the presence of a finite density of fermions

D.G. Barci[a)], E.S. Fraga[b)] and C.A.A. de Carvalho[c)]
Instituto de Física, Universidade Federal do Rio de Janeiro
C.P. 68528, CEP 21945-970, Rio de Janeiro, RJ, Brasil

Received March, 1996

In a previous work [2], we have studied a one-dimensional system of interacting fermions and bosons that starts in a metastable vacuum and gradually decays to the true one. The process considered was the nucleation of bubbles of true vacuum inside the false one via thermal activation. Our main purpose was the analysis of the stability of these bubbles and the calculation of the decay rate as a function of time, in the presence of a finite density of fermions at finite temperature. The inclusion of fermions proved to be remarkable as it has changed qualitative features of the physics of metastability.

The fact that we were working with a one-dimensional system allowed us to solve the problem exactly by means of inverse scattering methods. However, as we climb up to higher dimensions, this mathematical tool is no more available. Thus, for higher dimensions, we are compelled to make some kind of approximation for the evaluation of the fermionic determinant that encodes the fermion effects on the system. This may be accomplished by the use of a funcional gradient expansion for the determinant.

The model Lagrangian has the following form

$$\mathcal{L} = \frac{1}{2}(\partial_\mu\phi)(\partial^\mu\phi) - [V(\phi) - V(\phi_2)] + \bar{\psi}_a(i\gamma^\mu\partial_\mu - \mu - g\phi)\,\psi_a \tag{1}$$

where μ is the bare mass of the fermions, g is the coupling constant, $\psi_a(x)$ is the fermion field, a denotes fermion species, $\phi(x)$ is a scalar field and ϕ_2 is a local minimum of the potential $V(\phi) = \frac{g^2}{2}(\phi - \phi_0)^2\left(\phi + \phi_0 + \frac{2\mu}{g}\right)^2 + j\phi$, where ϕ_0 is a constant and j is an external current, responsible for the asymmetry of the potential even in the purely bosonic case.

Throughout this work, we will be interested on the effects of fermions on the bosonic field. Thus, in order to construct an effective theory for the bosons, we must integrate over the fermions to obtain an effective action. However, integrating over the fermions means calculating the determinant $S_F = -ln[det(i\gamma^\mu\partial_\mu - \mu - g\phi)] = -tr[ln(i\gamma^\mu\partial_\mu - \mu - g\phi)]$. In one spatial dimension it is possible to perform an exact calculation making use of inverse scattering methods [5, 6, 2]. For three spatial dimensions, however, we must make some kind of approximation.

After the fermionic integration, we may rewrite the effective action as

$$S_{eff}[\phi] = \int d^\nu x \left\{\frac{1}{2}(\partial_\mu\phi)(\partial^\mu\phi) - [V(\phi) - V(\phi_2)]\right\} - tr[ln(i\gamma^\mu\partial_\mu - \mu - g\phi)] \tag{2}$$

where $\int d^\nu x \equiv \int_0^T dt \int d^D x$. The field configuration that extremizes (2) must satisfy the Euler-Lagrange equation

$$\Box\phi = -\frac{\partial V}{\partial\phi} - Sp < x|\frac{1}{i\gamma^\mu\partial_\mu - \mu - g\phi}|x > \tag{3}$$

where Sp means trace over the spin degrees of freedom.

We may calculate this Green function using a functional gradient expansion. This means that we will focus on the long distace (small momentum) properties of the theory. For such purpose, we use the identity [9, 10]

$$< x|\frac{1}{i\gamma^\mu\partial_\mu + M(x)}|x >= \int \frac{d^\nu p}{(2\pi\hbar)^\nu}\frac{1}{\gamma^\mu p_\mu + M(x)}\sum_{n=0}^{\infty}\left(\Delta M(\frac{\hbar}{i}\frac{\partial}{\partial p}, x)\frac{1}{\gamma^\mu p_\mu + M(x)}\right)^n \tag{4}$$

where

$$\Delta M(\frac{\hbar}{i}\frac{\partial}{\partial p}, x) = \partial_\mu M(x)\frac{\hbar}{i}\frac{\partial}{\partial p_\mu} + \frac{1}{2}\partial_\mu\partial_\nu M(x)(\frac{\hbar}{i})^2\frac{\partial^2}{\partial p_\mu\partial p_\nu} + \ldots \tag{5}$$

Expanding this identity up to second order in the derivatives and explicitly performing the integrals, we obtain the equations of motion (after suitable redefinitions of the free parameters) $\Box\phi = -\frac{\partial V}{\partial \phi}\left[\frac{(\mu+g\phi)^2}{(\mu+g\phi)^2+\frac{g^2}{6\pi}}\right]$, for $\nu = 2$, and $\Box\phi = -\frac{\partial V}{\partial \phi}$, for $\nu = 4$.

We shall note that, in the case of $\nu = 4$, the only effect of the fermions is (to this order of approximation) to renormalize the free parameters of the theory. We will see later that this situation is completely changed if we include a gap and bound states in the fermionic spectrum.

Based on the results of our previous work, we shall seek for *sphaleron*-like solutions for the equations of motion obtained [1, 2, 4, 7].

Defining $\varphi \equiv \phi + \mu/g$, we have, in the thin-wall approximation [1], for $\nu = 2$,

$$\varphi_{sph} = \varphi_2 + \varphi_P[tanh(\xi - \xi_0) - tanh(\xi + \xi_0)] \tag{6}$$

where $\varphi_P \equiv \frac{1}{2}\left[2(3\varphi_2^2 - \varphi_0^2) + \frac{1}{\pi} - \frac{2\varphi_0^2}{3\pi\varphi_2^2}\right]^{1/2}$, $\xi \equiv g\varphi_P(x - x_{c.m.})$ and ξ_0 may be written in terms of the parameters. The parameter $x_{c.m.}$ reflects the translational invariance of the equation of motion and ξ_0 is related to what is usually called the radius of the sphaleron, beeing extremely important in the analysis of stability.

Through the calculations above, we have imposed a bubble-like profile [2] and assumed that $\mu/g >> 1$, consistent with the conditions for the validity of the gradient expansion, in order to obtain a closed form for the function that represents the sphaleron.

For the $\nu = 4$ case, with $\phi = \phi(\vec{r})$ and assuming a solution with radial symmetry, we have, in the thin-wall approximation,

$$\phi_{sph}(r) = \phi_2 - \tilde{\phi}_P[tanh(g\tilde{\phi}_P r + \tilde{\xi}_0)] \tag{7}$$

where $\tilde{\phi}_P \equiv \left(\frac{3\phi_2^2 - \phi_0^2}{2}\right)^{1/2}$ and $\tilde{\xi}_0 \equiv \frac{1}{2}cosh^{-1}\left(\frac{2\phi_2}{\sqrt{2(\phi_0^2 - \phi_2^2)}}\right)$.

Therefore, we have a true vacuum bubble, of radius $\tilde{\xi}_0$, centered at the origin. The situation is the same we would encounter in a purely bosonic system.

The last results show us that the calculation of the fermionic determinant performed before does not generate the complete effective action. In fact, in order to avoid a naive calculation of this determinant, we must take into account the influences of a bubble-like background on the fermionic spectrum. Instead of a simple continuum, we have the presence of a gap together with pairs of symmetric bound states [2, 5] (We will consider, for simplicity, just one couple). Thus, we have a richer spectum and we must incorporate its effects in the definition of our trace.

Therefore, the complete effective action has the following form

$$\begin{aligned} S_{eff}[\phi] &= \int d^\nu x \frac{1}{2}(\partial_\mu\phi)(\partial^\mu\phi) - [V(\phi) - V(\phi_2)] + \\ &+ \frac{g}{2}\int [D\phi]\int d^\nu x < x|\frac{1}{i\gamma^\mu\partial_\mu + M(x)}|x > + \\ &+ n_+ g\int [D\phi]\int d^\nu x d^\nu y \psi_B^*(x,[\phi]) < x|\frac{1}{i\gamma^\mu\partial_\mu + M(x)}|y > \psi_B(y,[\phi]) \end{aligned} \tag{8}$$

where the first term is the bosonic contribution, the second term represents the "Dirac sea" and the last one is due to the bound states. ψ_B is the wavefunction of a bound state and $n_\pm$ are their occupation numbers ("doping").

The only term that remains to be calculated is the last one. The difficulty of the calculation resides on the form of $\psi_B(x,[\phi])$. However, it is already known [3] that the charge associated with a bubble tends to concentrate on its surface in a gaussian-like way. For our purposes, we suppose that a delta-like distribution will be a reasonable approximation.(We are implicitly assuming that the occupation of the bound states will not affect in an appreciable way the form of the bubble. In the one-dimensional case, it is an exact result [2, 5]). Thus, we will assume, for the wavefunctions, the form $\psi_B(\vec{x},t) = [\delta(|\vec{x}| - \xi_0)e^{i\omega t}$. Then, the complete effective action, for the $\nu = 2$ case, is given by

$$\begin{aligned} \frac{S_{eff}^{(2)}}{T} &= -\int dx\left\{\frac{1}{2}\left(\frac{d\phi}{dx}\right)^2 - [V(\phi) - V(\phi_2)]\right\} - \\ &- \frac{g}{24\pi}\int dx\frac{\nabla^2\phi}{(\mu + g\phi)} + n_+ g\alpha_2\phi_p tanh(2\xi_0) \end{aligned} \tag{9}$$

The form of the contribution due to the presence of fermions is in complete agreement with the results previously obtained [2], providing a positive check of our method of approximation. The results for the $\nu = 4$ case together with graphics of the energy as a function of the sphaleron's radius for both cases will appear soon in a detailed paper.

Acknowledgements

The authors acknowledge CNPq and FUJB for finantial support.

References

[a)] e-mail: dbarci@if.ufrj.br

[b)] e-mail: fraga@if.ufrj.br

[c)] e-mail: aragao@if.ufrj.br

[1] D. Boyanovsky and C.A.A. de Carvalho, Phys. Rev. **D48**, 5850 (1993).

[2] E.S. Fraga and C.A.A. de Carvalho, to appear in Phys. Rev. **B52**, 7448 (1995).

[3] Yu-Lu, "Solitons and Polarons in Conducting Polymers" (World Scientific), 1988 (and references therein).

[4] D. Boyanovsky, C.A.A. de Carvalho and E.S. Fraga, Phys. Rev. **B50**, 2889 (1994).

[5] C.A.A. de Carvalho, Nucl. Phys. **B324**, 729 (1989).

[6] S. Novikov, S.V. Manakov, L.P. Pitaevskii and V.E. Zakharov, "Theory of Solitons" (Consultants Bureau), 1984.

[7] C.A.A. de Carvalho, C.A. Bonato and G.B. Costamilan, J. Phys. **A**: Math. Gen. L1153–L1157 (1989).

[8] Luiz Davidovich in *Multiphoton Processes, Proceedings of the* 5^{th} *International Conference on Multiphoton Processes*, Paris, France, September, 1990. (Edited by G. Mainfray and P. Agostini).

[9] Zhao-bin Su and B. Sakita, Phys. Rev. **B38**, 7421 (1988). Prasanta K. Panigrahi, Rashmi Ray and B. Sakita, Phys. Rev. **B42** 4036 (1990).

[10] C.A.A. de Carvalho, D.G. Barci and L. Moriconi, Phys. Rev. **B50**, 4648 (1994).

On bosonization in 3 dimensions

D. G. Barci*
Instituto de Física, Universidade Federal do Rio de Janeiro
C.P. 68528, Rio de Janeiro, RJ, 21945-970, Brasil

C. D. Fosco†
High Energy Group, International Centre for Theoretical Physics
P.O. Box 586, 34100 Trieste, Italy
and
L. E. Oxman‡
Departamento de Física, Facultad de Ciencias Exactas y Naturales,
Universidad de Buenos Aires, Ciudad Universitaria, 1428, Buenos Aires, Argentina

Received March, 1996

During the last few years many different proposals have been considered to bosonize fermionic theories in 3 dimensions [1, 2, 3, 4, 5]. In Ref. [2], order-disorder field operators related to a free massless Dirac field were defined. Applying canonical quantization methods, a bosonic, non-local and gauge-invariant action for an Abelian vector field was constructed, the approximate bosonization rules (in Euclidean spacetime) being

$$\begin{aligned} \bar{\psi}\,\partial\!\!\!/\psi &\rightarrow \frac{1}{4}F_{\mu\nu}(-\partial^2)^{-1/2}F_{\mu\nu} + \frac{i}{2}\theta\,\epsilon_{\mu\nu\lambda}A_\mu\partial_\nu A_\lambda + nqt \\ \bar{\psi}\gamma_\mu\psi &\rightarrow \beta\,\epsilon_{\mu\nu\lambda}\partial_\nu A_\lambda - \beta\theta\,(-\partial^2)^{-1/2}\partial_\nu F_{\mu\nu} + nqt \end{aligned} \tag{1}$$

where ψ is a two-component Dirac spinor, A_μ is a $U(1)$ gauge field, and nqt means non-quadratic terms in A_μ (the neglecting of non-quadratic terms is what makes this bosonization approximate).

In Ref. [4], functional methods were applied to derive bosonization formulae for the free massive Thirring model, and in [5], the Abelian and non-Abelian cases in any dimension $d \geq 2$ were considered. These 'long distance' bosonization rules are reliable for the description of phenomena where the fermionic current is not a strongly varying field, with a typical scale of variation much bigger that the inverse of the fermion mass. In this regime, either the free massive Dirac field or the Thirring model (in 3 dimensions) can be mapped to Chern-Simons theories by using the approximate bosonization rules

$$\begin{aligned} \bar{\psi}(\partial\!\!\!/ + m)\psi &\rightarrow \pm\frac{i}{2}\epsilon_{\mu\nu\lambda}A_\mu\partial_\nu A_\lambda \\ \bar{\psi}\gamma_\mu\psi &\rightarrow \pm i\sqrt{\frac{1}{4\pi}}\,\epsilon_{\mu\nu\lambda}\partial_\nu A_\lambda \end{aligned} \tag{2}$$

This is valid to leading order in $\frac{1}{m}$, while the inclusion of the next-to-leading order term would lead to a Maxwell-Chern-Simons theory instead.

As it was stressed in [4, 5], the possibility of finding exact bosonization rules (in this functional approach), depends on our ability to compute the fermionic determinant in the presence of a background field exactly. Thus

*Present Address: Instituto de Física, Universidade do Estado do Rio de Janeiro, Rio de Janeiro, RJ 20550, Brasil
†Present Address: Centro Atómico Bariloche, Bariloche, Argentina
‡Present Address: Instituto de Física, Universidade Federal do Rio de Janeiro, C.P. 68528, Rio de Janeiro, RJ, 21945-970, Brasil

in 3 dimensions we must use an approximation scheme. The one presented in [4, 5] amounts to expanding the corresponding effective action in powers of $\frac{\partial}{m}$.

The question presents itself about how to extend this approximation in order to include cases where the derivative expansion is no longer valid, as it is indeed the case for massless fermions.

In this letter we attempt to overcome this kind of limitation by including the full momentum dependence in the one-loop quadratic part of the effective action. Whence the results will also be valid for the massless case, without spoiling the proper low-momentum features. As no momentum expansion is performed, there is no instability problem. Keeping the full momentum dependence one introduces a non-locality in the bosonized action, a property shared with the approach of [2]. This non-locality is unavoidable as soon as the derivative expansion, which always produces local terms, is discarded. For massless fermions in particular, one cannot escape the non-locality, since there is a branch cut at zero momentum so the one-loop vacuum-polarization tensor cannot be analytic there.

We start by constructing a bosonized version of the generating functional of current correlation functions in the case of a free fermionic field in three dimensions, reviewing the procedure followed in [5]. This method allows us to demonstrate the equivalence between

$$Z(s) = \int [d\psi][d\bar{\psi}] \exp\left[-\int d^3x\, \bar{\psi}(\not{\partial} + i \not{s} + m)\, \psi\right] \tag{3}$$

and

$$Z(s) = \int [dA]\,[db] \exp\left[-T(b) - i \int d^3x\, A_\mu(\epsilon_{\mu\nu\lambda}\partial_\nu b_\lambda - \epsilon_{\mu\nu\lambda}\partial_\nu s_\lambda)\right] \tag{4}$$

where $T(b)$ denotes the fermionic effective action in the presence of an external vector field

$$T(b) = -\log\det(\not{\partial} + i \not{b} + m)\,. \tag{5}$$

We now make the approximation of retaining up to quadratic terms in b_μ in (5). This is consistent with the approaches of ref.'s [2] and [5] [1]. The quadratic part of $T(b)$ may be split as

$$\begin{aligned} T(b) &= T_{PC}(b) + T_{PV}(b) \\ T_{PC}(b) &= \int d^3x\, \frac{1}{4} F_{\mu\nu}(b)\, F(-\partial^2)\, F_{\mu\nu}(b) \\ T_{PV}(b) &= \int d^3x\, \frac{i}{2} b_\mu\, G(-\partial^2)\, \epsilon_{\mu\nu\lambda}\partial_\nu b_\lambda \end{aligned} \tag{6}$$

where T_{PC} and T_{PV} come from the parity-conserving and parity-violating pieces of the vacuum-polarization tensor, respectively [6]. The function F in (6) is regularization-independent, and a standard one-loop calculation yields

$$\tilde{F}(k^2) = \frac{|\,m\,|}{4\pi k^2}\left[1 - \frac{1 - \frac{k^2}{4m^2}}{(\frac{k^2}{4m^2})^{\frac{1}{2}}} \arcsin(1 + \frac{4m^2}{k^2})^{-\frac{1}{2}}\right], \tag{7}$$

where here and in what follows we shall always denote momentum-space representation by putting a tilde over the corresponding coordinate-space representation quantity. The function $\tilde{G}$ in (6) is regularization *dependent*, and can be written as

$$\tilde{G}(k^2) = \frac{q}{4\pi} + \frac{m}{2\pi\,|\,k\,|} \arcsin(1 + \frac{4m^2}{k^2})^{-\frac{1}{2}}, \tag{8}$$

where q can assume any integer value [7, 8], and may be thought of as the effective number of Pauli-Villars regulators, namely, the number of regulators with positive mass minus the number of negative mass ones.

Now, we can integrate out the b_μ field obtaining:

[1] This is equivalent to introducing a 'coupling constant' e by means of the redefinition $b_\mu \to e b_\mu$, and working up to order in e^2.

$$Z(s) = \int [dA] \exp - \int d^3x [\frac{1}{4} F_{\mu\nu} C_1 F_{\mu\nu} - \frac{i}{2} A_\mu C_2 \epsilon_{\mu\nu\lambda} \partial_\nu A_\lambda + i(\frac{u_+ - u_-}{2}) s_\mu \frac{1}{\sqrt{-\partial^2}} \partial_\nu F_{\nu\mu} - i(\frac{u_+ + u_-}{2}) s_\mu \epsilon_{\mu\nu\lambda} \partial_\nu A_\lambda] \quad (9)$$

where

$$C_1 = \frac{1}{2} \frac{|u_+|^2(F - iG) + |u_-|^2(F + iG)}{-\partial^2 F^2 + G^2}$$
$$C_2 = \frac{i}{2} \frac{|u_+|^2(F - iG) - |u_-|^2(F + iG)}{-\partial^2 F^2 + G^2} \quad (10)$$

Let us discuss now the explicit form adopted by (10) for the cases $m \to \infty$ and $m \to 0$, to make contact with the results of reference [5] (particularized to the Abelian $d = 3$ case) and reference [2], respectively. This is achieved by evaluating C_1 and C_2 in the corresponding limits, and this is in turn determined by the values of F and G. When $m \to \infty$, C_1 tends to a constant which multiplies the Maxwell term. This is neglected to leading order in a derivative expansion, since there is also a Chern-Simons term, multiplied by the constant factor C_2:

$$C_2 \to 4\pi |u|^2 \times (q + \frac{m}{|m|}) . \quad (11)$$

C_2 is regularization-dependent, and its ambiguity is reflected here by the undefined constant q. To compare with [5], we partially fix q by the condition $q + \mathrm{sgn}(m) = \pm 1$, and chosing $u_+ = u_- = u = \frac{1}{2\pi}$, we see that the bosonized action (denoted S_{bos}), in the partition function (9) reduces to

$$S_{bos} = \int d^3x \left(\pm \frac{i}{2} A_\mu \epsilon_{\mu\nu\lambda} \partial_\nu A_\lambda - \frac{i}{\sqrt{4\pi}} s_\mu \epsilon_{\mu\nu\lambda} \partial_\nu A_\lambda \right) , \quad (12)$$

which agrees with the result of [5].

Now we discuss the limit $m \to 0$. In this case we have for F and G the behaviours

$$F(k^2) \to \frac{e^2}{16} |k|^{-1} \quad , \quad G(k^2) \to \frac{q}{4\pi} \quad (13)$$

which imply for C_1 and C_2

$$C_1 \to \frac{16|u|^2}{|k|} \quad C_2 \to \frac{4\pi |u|^2}{q} . \quad (14)$$

By taking then

$$\tilde{u}_+ = \tilde{u}_- = \frac{1}{4} e^{i\alpha} , \quad (15)$$

the bosonized action in coordinate space assumes the form

$$S_{bos} = \int d^3x (\frac{1}{4} F_{\mu\nu} \frac{1}{\sqrt{-\partial^2}} F_{\mu\nu} - \frac{i}{2} \frac{\pi}{4q} \epsilon_{\mu\nu\lambda} A_\mu \partial_\nu A_\lambda - \frac{\sin\alpha}{4} s_\mu \frac{\partial_\nu F_{\nu\mu}}{\sqrt{-\partial^2}} - i \frac{\cos\alpha}{4} \epsilon_{\mu\nu\lambda} \partial_\nu A_\lambda) , \quad (16)$$

thus with the identifications

$$\theta = \frac{\pi}{4q} , \quad \alpha = \arctan \frac{\pi}{4q} , \quad \beta = \frac{\cos\alpha}{4} , \quad (17)$$

the bosonized action becomes identical with the one of Equation (1), which is the Euclidean version of the one of Ref. [2].

Acknowledgements

D. G. B. was supported by CNPq and FUJB, Brasil, L. O. by CONICET , Argentina, and C. D. F. by the ICTP, Italy.

References

[1] F. D. Haldane, Helv. Phys. Acta **65** (1992) 52.

[2] E. C. Marino, Phys. Lett. **B 263** (1991) 63.

[3] A. Kovner and P. S. Kurzepa, Phys. Lett. **B 321** (1994) 129.

[4] E. Fradkin and F. A. Schaposnik, Phys. Lett. **B 338** (1994) 253.

[5] F. A. Schaposnik, 'A comment on bosonization in $d \geq 1$ dimensions', F. A. Schaposnik, hep-th/9505049.

[6] R. Jackiw and S. Templeton, Phys. Rev. **D 23** (1981) 2291; S. Deser, R. Jackiw and S. Templeton, Phys. Rev. Lett. **48** (1982) 975;

[7] J. Fröhlich and T. Kerler, Nucl. Phys. **B 354** (1991) 369;

[8] 'The ζ-function answer to parity violation in three dimensional gauge theories', R. E. Gamboa Saravi, G. L. Rossini and F. A. Schaposnik, hep-th/9411238.

[9] 'Canonical quantization of non-local field equations', D. G. Barci, L. E. Oxman and M. Roca, hep-th/9503101.

[10] I. J. R. Aitchison, C. D. Fosco and J. A. Zuk, Phys. Rev. **D 48** (1993) 5895.

Higher-derivative Massive Schwinger Model

C. G. Carvalhaes, L. V. Belvedere, R. L. P. G. Amaral and N. A. Lemos
Instituto de Física, Universidade Federal Fluminense
Av. Litorânea, s/n, Boa Viagem, Niterói, CEP 24210-340, R J, Brasil.

Received March, 1996

A natural extension for the free higher-derivative model studied in Ref. [1] is the introduction of a higher-derivative mass term in the Lagrangean density - which now reads

$$\mathcal{L}(x) = i\bar{\psi}(x)(\partial\partial^{\dagger})^{N}\partial\psi(x) - m\bar{\psi}(x)\,(\partial\partial)^{N}\,\psi(x). \tag{1}$$

The chiral symmetry is broken by the mass term and the model exhibts only global gauge symmetry. We consider in details the canonical quantization of the third-order generalization ($N = 1$). Using the light-cone variables, the Lagrangian density can be w

$$\mathcal{L} = i\psi^{*}_{(1)}\partial_{-}^{3}\psi_{(1)} + i\psi^{*}_{(2)}\partial_{+}^{3}\psi_{(2)} - m\psi^{*}_{(1)}\Box\psi_{(2)} - \psi^{*}_{(2)}\Box\psi_{(1)}. \tag{2}$$

We take the basic variables as being $v_1 = \psi_{(1)}, v_2 = \partial_{-}\psi_{(1)}, v_3 = \partial_{-}^{2}\psi_{(1)} + im\partial_{+}\psi_{(2)}$. The nonvanishing equal-time anticommutation relations, obtained through the Dirac brackets, are

$$\{\psi_{(1)}, \partial_{-}^{2}\psi^{*}_{(1)}\} = -\{\partial_{-}\psi_{(1)}, \partial_{-}\psi^{*}_{(1)}\} = \frac{i}{m}\{\partial_{-}\psi_{(1)}, \partial_{+}^{2}\psi^{*}_{(2)}\} = -\frac{1}{m^{2}}\{\partial_{-}^{2}\psi_{(1)}, \partial_{-}^{2}\psi^{*}_{(1)}\} = \delta. \tag{3}$$

Introducing the Fourier decomposition for the fields, we obtain, from the equations of motion in momenta space, the quantum solution

$$\tilde{\psi}_{(1)}(k) = a(k)\delta(k^{2} - m^{2}) + b_{(2)}(k_{-})\delta(k_{+}) + c_{(1)}(k_{+})\,\delta(k_{-}) - \frac{k_{+}^{2}}{m}b_{(1)}(k_{+})\,\frac{d}{dk_{-}}\delta(k_{-}) \tag{4}$$

The effect of the mass term is the introduction of a massive mode in the mode expansion. Tachyon excitations do not appear. In a more general case, taking a nth-order derivative into account, this decomposition will generate one massive mode and $n - 1$ mas

Introducing the fields

$$\begin{aligned}
\psi^{(m)}_{(1,2)}(x) &= -i\int d^{2}k\, a(k)k_{\mp}\delta(k^{2} - m^{2})e^{-ikx}, \\
\frac{1}{\partial_{+}}\xi_{(1)}(x^{+}) &= \int_{-\infty}^{\infty} dk_{+}c_{(1)}(k_{+})e^{-ik_{+}x^{+}}, \\
\frac{1}{\partial_{+}}\eta_{(1)}(x^{+}) &= \int_{-\infty}^{\infty} dk_{+}b_{(1)}(k_{+})\,e^{-ik_{+}x^{+}},
\end{aligned} \tag{5}$$

and defining the operator

$$\frac{1}{\partial_{-}}\psi^{(m)}_{(1)}(x) = -\frac{1}{m^{2}}\partial_{+}\psi^{(m)}_{(1)}(x), \tag{6}$$

the original field turns out to be

$$\psi_{(1)}(x) = \frac{1}{\partial_{-}}\psi^{(m)}_{(1)}(x) + \frac{1}{\partial_{+}}\xi_{(1)}(x^{+}) + \frac{1}{\partial_{-}}\eta_{(2)}(x^{-}) + \frac{ix^{-}}{m}\partial_{+}\eta_{(1)}(x^{+}), \tag{7}$$

where the operators $1/\partial_\pm$ acting on the massless modes follow the prescriptions:

$$\partial_\pm \left\{ \frac{1}{\partial_\pm} \eta_{(1,2)}(x^\pm) \right\} = \eta_{(1,2)}(x^\pm). \tag{8}$$

From the equations of motion we can verify that the field $\psi^{(m)} = (\psi^{(m)}_{(1)}, \psi^{(m)}_{(2)})^T$ obeys

$$(i\partial\!\!\!/ - m)\,\psi^{(m)}(x) = 0. \tag{9}$$

Using the anticommutation laws (3)

$$\{\ \psi^{(m)}_{(1)}(x), \psi^{(m)*}_{(1)}(y)\} = -\delta(x^1 - y^1), \quad \{\eta_{(1)}(x), \eta^*_{(1)}(y)\} = 0 \tag{10}$$

$$\{\ \eta_{(1)}(x), \xi^*_{(1)}(y)\} = \frac{2i}{m}\frac{\partial}{\partial x^1}\delta(x^1 - y^1), \ \{\xi_{(1)}(x), \xi^*_{(1)}(y)\} = \frac{16}{m^4}\frac{\partial^4}{\partial (x^1)^4}\delta(x^1 - y^1). \tag{11}$$

Since the field $\psi^{(m)}$ is a solution of (9), we conclude, considering the relations above and its dimension and Lorentz properties (which can be found from (7)), that $\psi^{(m)}$ is a Dirac field quantized with negative

We can diagonalize the structure of anticommutation by introducing two usual massless fermions φ^1 and φ^2, satisfying

$$\left\{\varphi^1_{(1)}(x^+), \varphi^{1\,*}_{(1)}(y^+)\right\} = -\left\{\varphi^2_{(1)}(x^+), \varphi^{2\,*}_{(1)}(y^+)\right\} = \delta(x^1 - y^1). \tag{12}$$

In terms of these fields, for an arbitrary integer p, we have

$$\eta_{(1)} = i(-1)^{p+1}\frac{M}{m}\partial_+^{-p}\left(\varphi^1_{(1)} - \varphi^2_{(1)}\right), \tag{13}$$

$$\xi_{(1)} = \frac{1}{2M}\partial_+^{p+1}\left(\varphi^1_{(1)} + \varphi^2_{(1)}\right) + (-1)^{p+1}\frac{M}{2m^4}\partial_+^{3-p}\left(\varphi^1_{(1)} - \varphi^2_{(1)}\right), \tag{14}$$

$$\begin{aligned}\psi_{(1)} &= \frac{1}{\partial_-}\psi^{(m)}_{(1)} + \frac{1}{2M}\partial_+^{p}\left(\varphi^1_{(1)} + \varphi^2_{(1)}\right) + (-1)^{p+1}\frac{M}{m}\left[\left(\frac{1}{2m^3}\partial_+^{2-p} - \frac{x^-}{m}\partial_+^{1-p}\right)\left(\varphi^1_{(1)} - \varphi^2_{(1)}\right)\right. \\ &+ \left. i\partial_-^{-p-1}\left(\varphi^1_{(2)} - \varphi^2_{(2)}\right)\right].\end{aligned} \tag{15}$$

Here M is an external parameter of dimension $dimM = dim(m^{p+1})$. Under Lorentz transformations, $M \to \lambda^{-p+1}M$. In spite of being p an arbitrary parameter, it is impossible to describe the original fields locally in terms of free

The conserved current is given by a product between fields and associated momenta. In terms of the diagonal fields we have

$$j^\mu(x) = -\overline{\psi}^{(m)}(x)\gamma^\mu\psi^{(m)}(x) + \overline{\varphi}^1(x)\gamma^\mu\varphi^1(x) - \overline{\varphi}^2(x)\gamma^\mu\varphi^2(x). \tag{16}$$

Now, we shall discuss the third-order derivative massive Schwinger model, defined by the Lagrangian density

$$\mathcal{L} = -\frac{1}{4}(F_{\mu\nu})^2 + i\overline{\Psi}\left(\not{D}\not{D}^\dagger + im\not{D}\right)\not{D}\Psi. \tag{17}$$

$$F_{\mu\nu} = \partial_\mu A_\nu - \partial_\nu A_\mu, \ \not{D} = \gamma^\mu(\partial_\mu - ieA_\mu), \ \not{D}^\dagger = \gamma^0\not{D}\gamma^0. \tag{18}$$

Following Ref. [2], we go first to the interaction picture, where the fields are free. By a Legendre transformation in (17) we obtain

$$H = H_0 + H_I, \tag{19}$$

where H_I comes from the mass term:

$$H_I = -m\left[(D_-\Psi_{(1)})^*(D_+\Psi_{(2)}) + (D_+\psi_{(2)})^*(D_-\Psi_{(1)})\right]. \tag{20}$$

The operator solution in the interaction picture is

$$\Psi(x) =: e^{i\gamma^5[\lambda\tilde{\Sigma}(x) + \delta\tilde{\eta}(x)]} : \Xi(x) \tag{21}$$

Here, Ξ is a third-order free massless fermion field:

$$\Xi_{(1)}(x) = \frac{1}{\sqrt{2}}\left[\frac{1}{m'} + \frac{m'}{2}\left(\frac{x^-}{2}\right)^2\right]\chi^1_{(1)}(x^+) + \frac{1}{\sqrt{2}}\left[\frac{1}{m'} - \frac{m'}{2}\left(\frac{x^-}{2}\right)^2\right]\chi^3_{(1)}(x^+) + x^-\chi^2_{(1)}(x^+). \qquad (22)$$

The mass parameter m' is Lorentz variant and χ^j are free and canonicaal Dirac field operators.

The contribution of hamiltonian H_I is evaluated by the point-splitting limit prescription

$$H_I(x) = \lim_{\epsilon\to 0}\left\{(\partial_-\chi_{(1)}(x+\epsilon)^* : e^{-i[\lambda\hat{\Sigma}(x+\epsilon)+\delta\hat{\eta}(x+\epsilon)]} :: e^{-i[\lambda\hat{\Sigma}(x)+\delta\hat{\eta}(x)]} : \partial_+\chi_{(2)}(x) + h.c.\right\} \qquad (23)$$

By computing (23), the operator solution Ψ in the Heisenberg picture is immediatly found. The rule of the hamiltonian (23) is to modify the dynamics of the scalar fields. So we can get the solution just examining the evolution of the scal

References

[1.] R. L. P. G. Amaral, L. V. Belvedere, and N. A. Lemos, Phys. Rev. **D8**, 3443 (1993).

[2.] M. B. Halpern, Phys. Rev. **D12**, 1684 (1975).

Relativistic Temperature

Costa, S. S.; Matsas, G. E. A.
Instituto de Física Teórica - UNESP
R. Pamplona, 145 - CEP 01405-900 - São Paulo - SP

Received March, 1996

1 Introduction

There is an ancient controversy about how temperature transforms under boosts. Traditionally this issue has been discussed in the context of thermodynamics, which seemed to be the proper framework to deal with these questions. However, thermodynamical variables are not naturally related with space and time coordinates. Consequently, in order to use the Lorentz transformations to determine how temperature transforms under boosts, one should introduce extra hypothesis. Unhappily, different hypothesis have lead distinct researchers to reach opposite conclusions (see, for example, Ref.[1]).

Here, we analyze this problem from a completely different point of view. Rather than using thermodynamical hypothesis we define explicitly a mathematical model of a thermometer in the context of quantum field theory and study directly its behavior when it is moving in a background thermal bath.

2 Detectors as thermometers

An Unruh-DeWitt detector is a two-level monopole with a very definite energy gap, ω, between its fundamental and excited levels, respectively, in the proper frame of the detector. Such a detector will be supposed to interact, for sake of simplicity, with a thermal bath of scalar particles. The excitation rate of this detector can be associated with the number of particles present in the bath. The particle spectrum as measured by an inertial detector moving with velocity v with respect to the rest frame of the bath is

$$n(\omega) = \frac{1}{2\pi\gamma v\beta_0} \ln\left[\frac{1 - e^{\gamma(1+v)\beta_0\omega}}{1 - e^{\gamma(1-v)\beta_0\omega}}\right] \tag{1}$$

where $T_0 \equiv \beta_0^{-1}$ is the temperature of the bath as measured in its rest frame, and $\gamma \equiv (1 - v^2)^{-\frac{1}{2}}$ is the usual Lorentz factor. Notice that in the limit $v \to 0$ this expression reduces to the usual Planckian form

$$n_0(\omega) = \frac{1}{e^{\beta_0\omega} - 1} \tag{2}$$

while in the limit $v \to 1$ we obtain $n(\omega) \to 0$. The main difficulty in giving a natural prescription to define how temperature transforms under boosts is directly connected with the fact that (1) does not have the Planckian form for some effective temperature $T_{eff} = T_{eff}(T_0, v)$.

3 Different procedures, different temperatures

Next we show that different thermometers measure different temperatures.

Let us consider first a thermometer modeled by a slow moving detector with a small energy gap, that is, with $\omega\beta_0 \ll 1$ and $v \ll 1$, what transforms the detector in a counter of particles with low frequencies. The particle spectrum in this regime can be obtained from (1):

$$n(\omega\beta_0 \ll 1) \approx \frac{1}{\omega\beta_0}\left(1 - \frac{v^2}{6}\right)$$

This result must be compared with the case in which the detector is at rest ($v = 0$):

$$n_0(\omega\beta_0 \ll 1) \approx \frac{1}{\omega\beta_0}$$

Hence, it is natural to define in this case the following effective temperature

$$T_{(-)} \approx T_0\left(1 - \frac{v^2}{6}\right) \tag{3}$$

Now, let us consider another thermometer modeled by a detector prepared to count all the particles, giving the total density of particles associated with the distribution $n(\omega)$

$$\overline{n} = \int n(\omega)\frac{\omega^2}{2\pi^2}d\omega$$

where $\frac{\omega^2}{2\pi^2}$ is a normalization factor. By using equation (1) we obtain

$$\overline{n} = \frac{\gamma\zeta(3)}{\pi^2\beta_0^3}$$

while by using the Planckian spectrum (2) for detectors at rest we obtain

$$\overline{n}_0 = \frac{\zeta(3)}{\pi^2\beta_0^3}$$

where $\zeta(x)$ is the zeta function. Thus, in this case it is natural to define another effective temperature

$$T_{(+)} = T_0\left(1 - v^2\right)^{-\frac{1}{6}}$$

In the slow moving regime ($v \ll 1$) we obtain

$$T_{(+)} \approx T_0\left(1 + \frac{v^2}{6}\right) \tag{4}$$

Notice that $T_{(+)} \neq T_{(-)}$ as anticipated in the very beginning of this section.

4 Conclusion

Briefly, there is not a natural way to define how temperature transforms under boosts. In particular, different thermometers measure different temperatures as can be explicitly seen by comparing (3) against (4). However, this must not be seen as a theoretical challenge, since the whole physics associated with moving observers in a background thermal bath is contained in the particle spectrum (1).

It is important to reafirm that this result suggests that the question of how to transform temperature under Lorentz transformations is not a simple one, not making sense unless one defines carefully what the considered thermometer is.

References

[1] R. Aldrovandi and J. Gariel, Phys. Lett. A **170**, 5 (1992).

[2] S.S. Costa and G.E.A. Matsas, Phys. Lett. A **209**, 155 (1995).

Grassmann Algebra and the High Temperature Expansion for Fermions

I.C. Charret and M.T. Thomaz,
Instituto de Física - Universidade Federal Fluminense
R. Gal. Milton Tavares de Souza s/nº,
Campus da Praia Vermelha, Niterói, R.J., 24210-340, Brazil.
E.V. Corrêa Silva
Centro Brasileiro de Pesquisas Físicas
R. Dr. Xavier Sigaud nº 150, Rio de Janeiro, R.J., 22290-180, Brazil
S.M. de Souza
Instituto de Física - Universidade Federal do Rio de Janeiro
P. Box: 68528, Rio de Janeiro, R.J., 21945-970, Brazil.

Received March, 1996

We calculated previously the grand-canonical partition function of the Hubbard model in d=2(1+1) up to first order in β. Now we make an extension of this calculation to include the term of order β^2. We obtained the exact coefficient of order β^2 for the grand-canonical partition function of the model.

1 A Survey on Grassmann's Algebra

Due to anticommutative nature of the fermions, the Grassmann's algebra is suitable for dealing with these problems. For a Grassmann's algebra of dimension 2^{2N}, we have $2N$ generators, that are representated by: $\bar{\eta} = (\bar{\eta}_1, \bar{\eta}_2, ..., \bar{\eta}_N)$ and $\eta = (\eta_1, \eta_2, ..., \eta_N)$. They obey the algebra:

$$\{\eta_i, \eta_j\} = \{\bar{\eta}_i, \bar{\eta}_j\} = \{\bar{\eta}_i, \eta_j\} = 0. \tag{1}$$

It's a known result that [1]:

$$\int \prod_{i=1}^{N} d\bar{\eta}_I d\eta_I \; exp\left[\sum_{I,J=1}^{N} \bar{\eta}_I A_{I,J} \eta_J\right] = det\mathbf{A}, \tag{2}$$

where the entries of matrix **A** are commuting quantities. Recently, we showed that gaussian integrals multiplied by products of pairs of generators of the form $\bar{\eta}_i \eta_j$, can be exactly calculated [2]. These integrals are equal to the determinants of a new matrix **B**, obtained from **A** by cutting rows and columns. For example:

$$\int \prod_{i=1}^{N} d\bar{\eta}_I d\eta_I \; \bar{\eta}_l \eta_k \; \exp\left[\sum_{I,J=1}^{N} \bar{\eta}_I A_{I,J} \eta_J\right] = \det \mathbf{B}(l,k), \tag{3}$$

where,

$$\mathbf{B}_{i,j}(l,k) = \begin{cases} \mathbf{A}_{i,j} & \text{if } i \neq l \text{ and } j \neq k, \\ \delta_{i,j}\delta_{j,k} & \text{if } i = l \text{ or } j = k \end{cases} \tag{4}$$

and $\det \mathbf{B}(l,k)$ is the cofactor of matrix **A** when the line l and column k are deleted. In general, for N pairs of the form $\bar{\eta}_i \eta_j$, we have

$$\int \prod_{i=1}^{N} d\bar{\eta}_I d\eta_I \; \bar{\eta}_{I_1}\eta_{J_1}\bar{\eta}_{I_2}\eta_{J_2}\cdots\bar{\eta}_{I_N}\eta_{J_N} \; exp\left[\sum_{I,J=1}^{N} \bar{\eta}_I A_{I,J} \eta_J\right] = \det \mathbf{B}, \tag{5}$$

where $\det \mathbf{B}$ is cofactor of matrix **A** [2].

2 High Temperature Expansion

The grand-canonical partition function is defined as:

$$\mathcal{Z} = Tr[exp(-\beta \mathbf{K})], \tag{6}$$

where $\beta = 1/kT$ and $\mathbf{K} = \mathbf{H} - \mu\mathbf{N}$. $\mathbf{H}$ is the hamiltonian of the system, $\mathbf{N}$ is the total number of particles and μ is the chemical potential.

The high temperature expansion of the grand-canonical partition function is:

$$\mathcal{Z} = Tr[1 - (\beta\mathbf{K})] + \frac{1}{2!}(\beta)^2 Tr[\mathbf{K}]^2 - \frac{1}{3!}(\beta)^3 Tr[\mathbf{K}]^3 + O(\beta)^4. \tag{7}$$

In order to calculate the terms in Z, we need to obtain the trace of the various powers of $\mathbf{K}$. In the context of the Grassmann algebra, the trace of the power of an operator $(\mathbf{K})^n$ is given by

$$Tr[\mathbf{K}]^n = \int \prod_{l=1}^{N} \prod_{i=0}^{n-1} d\bar{\eta}_{l_i} d\eta_{l_i} \quad exp\left[\sum_{l=1}^{N} \sum_{i=0}^{n-1} \bar{\eta}_{l_i}(\eta_{l_i} - \eta_{l_{i+1}})\right] \times$$
$$\times \quad \mathbf{K}^N(\bar{\eta}_{l_0}, \eta_{l_0}) \ldots \mathbf{K}^N(\bar{\eta}_{l_{n-1}}, \eta_{l_{n-1}}), \tag{8}$$

where l represents the space site and spin index, and, i is the temperature index. $\mathbf{K}^N(\bar{\eta}_{l_i}, \eta_{l_i})$ means that $\mathbf{K}$ is in the normal ordered form.

Using all the above results, we calculate analyticaly the grand canonical partition function of Hubbard model in d=2(1+1) up to order β^2.

3 Hubbard Model d=2(1+1)

The Hubbard model is used in solid state physics to describe the behaviour of itinerant electrons in narrow energy bands in metals [4]...

The Hubbard hamiltonian is:

$$\mathcal{H} = \sum_{i,j=1}^{N} t_{i,j} a^{\dagger}_{i,\sigma} a_{j,\sigma} + U \sum_{i=1}^{N} a^{\dagger}_{i,\uparrow} a_{i,\uparrow} a^{\dagger}_{i,\downarrow} a_{i,\downarrow} - \frac{1}{2} g \mu_B B \sum_{i=1}^{N} \sigma a^{\dagger}_{i,\sigma} a_{i,\sigma}, \tag{9}$$

where N is the number of space sites. The first term in H is the hopping term. The second one represents the intra-atomic interaction between electrons of opposite spins. The last one is the interaction between the total magnetization and an external magnetic field B.

We consider the case of a linear chain obeying periodic boundary conditions.

Generators of the associated Grassmann algebra is: $\eta_\sigma(x_i, \tau_j)$, where σ is the spin index, x is the site and τ is the temperature index.

The functions $\mathbf{K}^N(\bar{\eta}, \eta)$ given by (8) are combinations of multivariable Grassmann integrals [5].

4 Results

We showed previously [3, 5] that the grand partition function up to order β is:

$$\mathcal{Z}^1_N = 2^{2N}\left[1 + N\beta(\mu - E_0 - \frac{U}{4})\right], \tag{10}$$

where the coeficient of β in the above expression is proportional to N. Therefore, we take the thermodynamic limit of $\mathcal{Z}_N$, and obtained well defined results that agree with known results in the literature [6].

The β^2 term of Z, in eq.(7),written in terms of the Grassmann algebra generators is:

$$Tr[\mathbf{K}]^2 = \int \prod_{I=1}^{4N} d\bar{\eta}_I d\eta_I \quad exp\left[\sum_{I,J=1}^{N} \bar{\eta}_I A_{IJ} \eta_J\right] \times$$
$$\times \mathbf{K}^N(\bar{\eta}, \eta; i = 0)\mathbf{K}^N(\bar{\eta}, \eta; i = 1). \tag{11}$$

The matrix **A** has a block structure, where the up and down spin sectors decouple [5].

$$\begin{bmatrix} \mathbf{A}^{\uparrow\uparrow} & \mathbf{0} \\ \mathbf{0} & \mathbf{A}^{\downarrow\downarrow} \end{bmatrix}, \tag{12}$$

where we have

$$\begin{bmatrix} \mathbf{1}_{N\times N} & -\mathbf{1}_{N\times N} \\ \mathbf{1}_{N\times N} & \mathbf{1}_{N\times N} \end{bmatrix}. \tag{13}$$

Using the result (3), the multivariable Grassmann integrals are calcutated for any positive integer value of N, and we obtained,

$$\begin{aligned} Tr[\mathbf{K}^2] &= \frac{N}{2}2^{2N}\left\{N\left(2(E_0-\mu)^2+U(E_0-\mu)+\frac{U^2}{8}\right)+(E_0-\mu)^2+\right. \\ &+ \left.\lambda_B^2+U(E_0-\mu)+\frac{3U^2}{8}+2t^2\right\}, \end{aligned} \tag{14}$$

where $\lambda_B = g\mu_B B$.

Using the above result, we obtained the grand-canonical partition function to order β^2. The generating functional of the connected Green's functions is given by:

$$\begin{aligned} \frac{1}{N}ln\mathcal{Z}_N^2 &= \left\{2ln2-\beta(E_0-\mu+\frac{U}{4})+\right. \\ &+ \left.\frac{\beta^2}{4}\left[(E_0-\mu)^2+U(E_0-\mu)+\lambda_B^2+2t^2+\frac{3U^2}{8}\right]\right\}. \end{aligned} \tag{15}$$

It's important to point out that the terms of $\mathcal{Z}$ up tp order β^2 are exact. The result is valid for any value of constants that caracterize the model.

5 Acknowledgement

I.C.C., E.V.C.S and S.M.S. thank CNPq for financial support, and, M.T.T thanks CNPq and FINEP for partial financial suport.

References

[1] C. Itzykson and J.B. Zuber, *Quantum Field Theory*, (McGraw-Hill, 1980), page 442.

[2] I.C. Charret, S.M. de Souza and M.T. Thomaz, *A Note on Moments of Gaussian Grassmann Multivariable Integrals*, to be submitted.

[3] I.C. Charret, E.V. Corrêa Silva, S.M. de Souza and M.T. Thomaz, Proceedings of XV Brazilian National Meeting on Particles and Fields,1994, Angra dos Reis, Brazil, page 238.

[4] J.Hubbard, Proc. Roy. Soc. **A277** (1963) 237; **A281** (1964) 401.

[5] I.C. Charret, E.V. Corrêa Silva, S.M. de Souza and M.T. Thomaz, J.Math.Phys. **36** (1995) 4100.

[6] M. Takahashi, Prog.Theo.Phys. **47** (1972) 69.

Fermi edge restoration in the Tomonaga-Luttinger model with impurities

C.M.Naón, M.C.von Reichenbach and M.L.Trobo
Depto. de Física. Universidad Nacional de La Plata.
CC 67, 1900 La Plata, Argentina.
Consejo Nacional de Investigaciones Científicas y Técnicas, Argentina

Received March, 1996

We study the Tomonaga-Luttinger model in the presence of magnetic impurities. By using a recently proposed field-theoretical approach to non-local bosonization we obtain the effective action describing the low-energy charge and spin density fluctuations. From this action the dispersion relations of the collective modes are readily found. We also compute the momentum distribution and show that the electron-impurity scattering allows to have restoration of the Fermi liquid behavior.(Contact naon@venus.fisica.unlp.edu.ar).

Recent advances in the field of nanofabrication have allowed to build ultranarrow semiconductor structures in which the motion of the electrons is confined to one dimension [1] . These developments have triggered an intense experimental [2] and theoretical [3] activity in the last few years. Edge states in quantum Hall effect devices [4] constitute another interesting example of an essentially 1D system that can be understood in terms of a chiral Luttinger liquid picture.

One of the main tools for the theoretical study of the one-dimensional (1D) electron system is the Tomonaga-Luttinger model (TL) [5]-[6] which describes a non-relativistic gas of massless particles with linearized free dispersion relation and two-body interactions. This model displays the so called Luttinger liquid (LL) behavior [7] : the jump discontinuity in the electron momentum distribution is washed out as soon as the interaction is switched on, even at $T = 0$. Therefore, based on this model one would expect that the experimental results should indicate a clear deviation from the normal Fermi liquid behavior (FL). However, the available experimental data are consistent with the existence of the edge singularity in the momentum distribution [8] .This fact raises an interesting question concerning the validity of the TL model as a description of real 1D systems.

The main purpose of this letter is to show how the TL model can be easily modified in order to have a restoration of the Fermi edge singularity. To this end we shall use a recently proposed path-integral approach to non-local bosonization [9]. In this framework the usual TL action can be expressed as certain limit of a non-local QFT in which non-locality allows one to consider general potentials responsible for the two-body interactions. What we do here is to add a Kondo-like term to the usual electron-electron scattering term of the TL model and show under which conditions the presence of a magnetic impurity can lead to normal FL behavior. The role of impurities in 1D systems has been intensively explored recently, in connection with a variety of problems ranging from Anderson localization [10] to the Kondo problem in the Luttinger liquid [11] [12] [13].

On the other hand, it has been shown that the presence of impurities can lead to the reappearence of the Fermi surface [14]. But this result was obtained for a model with quadratic free dispersion relation, including non-magnetic impurities and using the random phase approximation. In most of these works local electron-electron (e-e) and electron-impurity (e-i) interactions were considered, and the attention was paid mainly to the changes in the impurity features.

In the present letter we use the impurity representation introduced by Andrei [15] in order to study a finite density of impurities interacting non-locally with electrons through both spin-density and spin-current coupling terms. Indeed, as will be shown later, it is the existence of non-zero spin-current fluctuations which opens up the

possibility of recovering a Fermi edge in the momentum distribution.

Following the lines of Ref [9] we consider the action

$$\begin{aligned} S &= \int d^2x\,[\bar{\Psi} i\partial\!\!\!/ \Psi - \int d^2y\; J^a_\mu(x) V^{ab}_{(\mu)}(x,y) J^b_\mu(y) - \\ &- \int d^2y\; J^a_\mu(x) U^{ab}_{(\mu)}(x,y) S^b_\mu(y) + d^\dagger i\partial_t d], \end{aligned} \tag{1}$$

where Ψ and d are the electron and impurity fields with up and down components corresponding to right and left movers respectively. Let us recall that according to Andrei's approach [15] the impurities are allowed to move with the constraint that they carry zero kinetic energy. (this is reflected in the absence of a $d^\dagger\partial_x d$ in (1)). We have defined $J^a_\mu = \bar{\Psi}\gamma_\mu\lambda^a\Psi$, $S^a_\mu = \bar{d}\gamma_\mu\lambda^a d$, with $\lambda^a (a = 0,1,2,3)$ the U(2) generators related to charge and spin conservation. As shown in [9], the action (1) with $U_{(\mu)} = 0$, describes the zero-temperature TL model when only forward scattering diagrams are taken into account. (For simplicity we set $v_F = 1$ and $p_F = 0$. The dependence on the Fermi momentum p_F will be considered later. See eq.(9)). If we disregard spin-flipping processes we can restrict our analysis to the maximal Abelian subgroup of U(2), generated by λ^0 and λ^1. The two-body potential matrices are diagonal whose elements can be written in terms of the g-functions defined by Sólyom [18] as

$$\begin{aligned} V^{00}_{(0)} &= \frac{1}{4}(g_{4\parallel} + g_{4\perp} + g_{2\parallel} + g_{2\perp}), \\ V^{11}_{(0)} &= \frac{1}{4}(g_{4\parallel} - g_{4\perp} + g_{2\parallel} - g_{2\perp}), \\ V^{00}_{(1)} &= \frac{1}{4}(-g_{4\parallel} - g_{4\perp} + g_{2\parallel} + g_{2\perp}), \\ V^{11}_{(1)} &= \frac{1}{4}(-g_{4\parallel} + g_{4\perp} + g_{2\parallel} - g_{2\perp}). \end{aligned}$$

The TL model, with charge-density fluctuations only, corresponds to $V^{00}_{(1)} = V^{11}_{(1)} = 0$. In a completely analogous way we introduce the potentials that couple electron and impurity currents: one has just to replace V by U and g by h in the above expressions. The magnetic interaction, i.e. the coupling betwen spin densities and currents only, corresponds to the case $U^{00}_{(0)} = U^{00}_{(1)} = 0$ ($h_{4\parallel} = -h_{4\perp}, h_{2\parallel} = -h_{2\perp}, U^{11}_{(0,1)} = (h_{2\parallel} \pm h_{4\parallel})/2$). Let us now consider the partition function of the system

$$Z = \int D\bar{\Psi} D\Psi D\bar{d} D d Da\; exp - [S + \int d^2x\; a(d^\dagger d - n)], \tag{2}$$

where S is given by (1) and a is a Lagrange multiplier that fixes the impurity number to be n. (Please see [16] for details concerning the treatment of the impurity). Exactly as we did in [9] for the "clean" system ($U_{(\mu)} = 0$), we express (2) in terms of fermionic determinants. This can be achieved by introducing auxiliary vector fields A_μ, B_μ. After some standard manipulations we get

$$Z = \int DADB e^{-S'[A,B]} det(i\partial\!\!\!/ - \sqrt{2}\,A\!\!\!/) det(i\gamma_0\partial_t - B\!\!\!/),$$

with

$$\begin{aligned} S' \quad [A,B] &= \int d^2x\; d^2y [\sqrt{2} B^a_\mu(x) a^{ab}_{(\mu)}(x,y) A^b_\mu(y) - \\ &- B^a_\mu(x) \int d^2u\; d^2v\; a^{ac}_{(\mu)}(x,u)(b^{-1}_{(\mu)})^{cd}(u,v) a^{db}_{(\mu)}(v,y) B^b_\mu(y)], \end{aligned}$$

where we have defined the inverse potentials $a_{(\mu)}$ and $b_{(\mu)}$ through the identities

$$\int d^2u V^{ac}_{(\mu)}(x,u) b^{cd}_{(\mu)}(u,y) = \delta^{ad}\delta^2(x-y),$$
$$\int d^2u U^{ac}_{(\mu)}(x,u) a^{cd}_{(\mu)}(u,y) = \delta^{ad}\delta^2(x-y). \quad (3)$$

The fermionic determinant involving the field A_μ can be readily computed by well-known path-integral techniques [19] based on the change

$$\Psi = e^{-\sqrt{2}(\gamma_5\Phi+i\eta)}\chi,$$
$$\bar{\Psi} = \bar{\chi}e^{-\sqrt{2}(\gamma_5\Phi-i\eta)},$$
$$A_\mu = \epsilon_{\mu\nu}\partial_\nu\Phi + \partial_\mu\eta, \quad (4)$$

with $\Phi = \Phi^a\lambda^a, \eta = \eta^a\lambda^a$.

The result is

$$det(i\not{\partial} - \sqrt{2}\not{A}) = (deti\not{\partial})exp\frac{1}{\pi}\int d^2x\ \Phi\Box\Phi.$$

Concerning the determinant associated with the impurity, its evaluation is more subtle. However, we were able to extend the standard technique [19] to solve this particular problem. (The details of this calculation will be reported elsewhere. An alternative treatment can be found in [16]). We thus get

$$det(i\gamma_0\partial_t - \not{B}) = det(i\gamma_0\partial_t)exp\frac{-1}{4\pi}\int d^2x\{B_0^2 - B_1^2 +$$
$$+ \int d^2y\Theta(x_0-y_0)\partial_x\delta(x_1-y_1)\times$$
$$[\ B_0(x)B_1(y) + B_1(x)B_0(y)]\}.$$

Putting all this together and going to momentum space one gets a bosonic action depending on Φ and η (the collective modes) and the impurity variables B_0 and B_1. These last fields, in turn, can be easily integrated out. Thus, we finally obtain

$$Z = \int D\Phi D\eta\ exp - \{S^{00}_{eff} + S^{11}_{eff}\}, \quad (5)$$

with

$$S^{ii}_{eff} = \frac{1}{(2\pi)^2}\int d^2p[\Phi^i(p)A^{ii}(p)\Phi^i(-p) +$$
$$+ \eta^i(p)B^{ii}(p)\eta^i(-p) + \Phi^i(p)\frac{C^{ii}(p)}{2}\eta^i(-p) +$$
$$+ \eta^i(p)\frac{C^{ii}(p)}{2}\Phi^i(-p)], \quad (6)$$

where A^{ii}, B^{ii} and C^{ii} depend on the Fourier transforms of the inverse potentials defined in (3). Eqs (5) and (6) are our first non-trivial results. Indeed, we have obtained a completely bosonized action describing the dynamics of charge density (CDW) and spin density (SDW) excitations (associated with the fields Φ^0, η^0 and Φ^1, η^1 respectively). As we can see from (5), these modes remain decoupled as in the impurity free case. Moreover, due to the absence of backscattering and spin-flipping the effective action is quadratic and consequently the potentials do not get renormalized. The dispersion relations of the collective modes are given by

$$\omega^2(q) = q^2\frac{1 + \frac{2}{\pi}V_{(0)} + \frac{1}{2\pi^2}(U^2_{(0)} - 2U_{(0)}U_{(1)})}{1 + \frac{2}{\pi}V_{(1)} - \frac{1}{2\pi^2}U^2_{(1)}}, \quad (7)$$

where we have omitted 00 (11) superindices in the potentials, corresponding to CDW's (SDW's). We have also gone back to real frequencies: $p_0 = i\omega$, $p_1 = q$. The usual forward Kondo interaction corresponds to $V_{(1)}^{11} = U_{(1)}^{11} = 0, U_{(0)}^{11} = J_{ZF}$. In this case Eq.(7) shows that the impurities tend to increase the phase velocity of the SDW's (u_σ) irrespectively of the interaction being ferro or antiferromagnetic. On the other hand, if one includes spin-current fluctuations ($U_{(1)}^{11} \neq 0$) the behavior of u_σ depends on the relative sign between $U_{(0)}^{11}$ and $U_{(1)}^{11}$. For instance, for fixed J_{ZF} and $U_{(1)}^{11} \gg J_{ZF}$, $V_{(0)}^{11}$ one has $u_\sigma^2 \propto 2J_{ZF}/U_{(1)}$ and one sees that large spin-current fluctuations tend to reduce u_σ.

From now on we shall specialize the discussion to the TL model with both spin-density (Kondo-like) and spin-current electron-impurity interactions. Thus, we set

$$\begin{aligned} V_{(1)}^{00} &= V_{(1)}^{11} = 0 = U_{(0)}^{00} = U_{(1)}^{00}, \\ \frac{2}{\pi} V_{(0)}^{00} &= r, \\ \frac{2}{\pi} V_{(0)}^{11} &= s, \\ (U_{(0)}^{11})^2 &= (U_{(1)}^{11})^2 = 2\pi^2 t. \end{aligned}$$

where, for simplicity, we have chosen $U_{(0)}^{11} = U_{(1)}^{11}$. In this way we reduce the parameter space from 4 to 3 dimensions, keeping thus our analysis as simple as possible.

For repulsive electron-electron interaction one has $r > 0$ and $s > 0$, whereas $t > 0$ for both ferromagnetic and antiferromagnetic Kondo coupling. In order to study the momentum distribution we compute the fermionic 2-point function. To be specific we consider $G_{1\uparrow}$ (similar expressions are obtained for $G_{2\uparrow}$, $G_{1\downarrow}$ and $G_{2\downarrow}$),

$$\begin{aligned} G_{1\uparrow}(x,y) &= < \Psi_{1\uparrow}(x)\Psi_{1\uparrow}^{\dagger}(y) > \\ &= G_{1\uparrow}^{(0)}(x,y) < e^{\sqrt{2}\{[\Phi^0(y)-\Phi^0(x)]+i[\eta^0(y)-\eta^0(x)]\}} >_{00} \times \\ &\times < e^{\sqrt{2}\{[\Phi^1(y)-\Phi^1(x)]+i[\eta^1(y)-\eta^1(x)]\}} >_{11}, \end{aligned} \tag{8}$$

where we have used (4) to relate $G_{1\uparrow}$ with the free propagator $G_{1\uparrow}^{(0)}$, in which the Fermi momentum p_F is easily incorporated [9]. The symbol $<>_{ii}$ means vacuum expectation value with respect to the action (6). Taking the limit $z_0 \to 0$ ($z = x - y$) in (8) and inserting the result in the definition of the momentum distribution $N_{1\uparrow}(q)$, one gets

$$N_{1\uparrow}(q) = C(\Lambda) \int dz_1 \frac{e^{-i(q-p_F)z_1}}{z_1} e^{-\int dp_1 \frac{1-\cos p_1 z_1}{p_1} \Gamma(p_1)}, \tag{9}$$

where $C(\Lambda)$ is a normalization constant depending on an ultraviolet cutoff Λ, and $\Gamma(p_1)$ depends on p_1 through the potentials in the form

$$\Gamma(r,s,t) = f(r,0) + f(s,t) - h(s,t). \tag{10}$$

In the above equation we have defined the functions

$$f(s,t) = \frac{(\mid 1+s-t \mid^{1/2} - \mid 1-t \mid^{1/2})^2}{\mid 1+s-t \mid^{1/2} \mid 1-t \mid^{1/2}}, \tag{11}$$

$$h(s,t) = \frac{2t(t-t_c)}{\mid 1+s-t \mid^{3/2} \mid 1-t \mid^{1/2}}, \tag{12}$$

with $t_c = 9/8 - 1/2(s-1/2)^2$.

We have now reached the main point of our discussion. We want to determine under which conditions it is possible to have $\Gamma(r,s,t) = 0$, since in this case one immediately has $N_{1\uparrow}(q) \propto \Theta(q - p_F)$, i.e. normal FL behavior. First of all we note that for $t = 0$ (impurity free case) $\Gamma(r,s,0)$ cannot vanish for any value of r and s other than $r = s = 0$, which corresponds to the non-interacting Fermi gas. On the other hand, the first two terms in (10) are positive definite. This means that the only chance to obtain $\Gamma = 0$, in a non-trivial (interacting) situation, is to

have $t > t_c$. This necessary condition determines a "critical" parabola in the space of potentials, $t(s) = t_c$, below which FL behavior is forbidden. Enforcing also the condition $\omega^2 > 0$ in (7), in order to have normal modes with real frequencies, one finds two disjoint regions where the FL edge could be, in principle, restored: $t > 1 + s$ and $t < 1, t > t_c$. However, one also has to satisfy $f(r, 0) > 0$, which for $\Gamma = 0$ yields

$$F(s,t) = h(s,t) - f(s,t) > 0. \tag{13}$$

A simple numerical analysis of $F(s,t)$ shows that the above inequality is not fulfilled for $0 < t < 1$. The electron-impurity coupling is not strong enough in this region as to eliminate the LL behavior. On the contrary, for $t > 1+s$ equation (13) can be always satisfied. Moreover, in this region, for $\Gamma = 0$ we obtain the following analytical solution for r in terms of $F(s,t)$:

$$r = F^2/2 + 2F + (1 + F/2)(F^2 + 4F)^{1/2}. \tag{14}$$

To illustrate this result it is useful to consider the local case, corresponding to contact interactions (r, s and t are constants). From the precedent discussion we conclude that for $0 < t < 1$ (region I) one necesarilly has LL behavior, whereas for $t > s + 1$ (region III) FL behavior is admitted. Note that for $1 < t < s + 1$ (region II) the frequency of the SDW's becomes imaginary. Let us stress that, for $t > s + 1$, Eq(14) defines a surface in the space of potentials on which FL behavior takes place. This is our main result. One particular solution belonging to this "FL surface" is obtained by choosing $s = 0$ in (14), which yields

$$r(t) = \frac{2t(3t-2) + 2(2t-1)\sqrt{3t^2 - 2t}}{(t-1)^2}.$$

This curve corresponds to the case in which the SDW's dispersion relation is given by $\omega^2 = q^2$. For t large r approaches a minimum value $r_{min} = 6 + 4\sqrt{3}$, a feature that is shared with each curve $s = constant$ on the FL surface.

Let us stress that the extension of our analysis to the case $U^{11}_{(0)} \neq U^{11}_{(1)}$ is straightforward. In this case one gets an expression for $r(s, t_1, t_2)$ (with $t_1^{1/2} \propto U^{11}_{(0)}$ and $t_2^{1/2} \propto U^{11}_{(1)}$), similar to (14), that defines a 3D manifold of the 4D parameter space. What is crucial in our approach is the contribution of the spin-current e-i interactions, which has not been considered in recent studies, mainly concerned with the thermodynamical and transport properties of the 1D Kondo problem [11] [12] [13]. Indeed, for $t_2 = 0$ it can be easily shown that the system behaves as LL in the whole parameter space.

We should also emphasize that we have considered the simplest possible version of the TL model with magnetic impurities, in the sense that, having neglected backscattering and spin-flipping processes, no renormalization of the couplings takes place. Our result shows how to tune up the initial parameters of the model in order to have a Fermi edge in $N(q)$. Qualitatively one sees that the weaker is the e-i interaction strength the stronger must be the repulsive e-e interaction, and this behavior is independent of the magnetic couplings being ferromagnetic or antiferromagnetic. This result seems to contradict the results of ref.[12] in which two different strong-coupling stable fixed points, corresponding to ferromagnetic and antiferromagnetic couplings respectively, are found. However one should bear in mind that in contrast to these authors we have neglected backward scattering and at the same time we have considered spin-currents e-i interactions. Another interesting aspect of this "tuning" mechanism is that, eventhough our FL surface involves large couplings, for t sufficiently large, r becomes stable, i.e. almost independent of t and close to its minimum value given above. This behavior resembles the situation encountered in the 3D Kondo problem which exhibits a strong coupling fixed point for $g_k \to \infty$ [16],[17]. In summary, we have studied a simple modification of the TL model that describes the interaction of electrons with localized magnetic impurities at zero temperature. One of the advantages of our technique is that it permits to handle non-local interactions in a very practical way. In particular it enabled us to obtain the exact dispersion relations of the collective modes in terms of general (momentum-dependent) potentials Eq.(7). We have also computed the electron momentum distribution (Eq.(9)). Finally, by analyzing this result we have found one region in the space of potentials in which the FL

behavior can be recovered as an effect of the interaction between the electrons and the magnetic impurities. Our result suggests that spin-currents interactions could play a central role in edge restoring mechanisms.

Acknowledgements

The authors are partially supported by Fundación Antorchas (Buenos Aires, Argentina) under grant A-13218/1-000069.

References

[1] Solid State Physics: Semiconductor Heterostructures and Nanostructures, C.W.J. Beenakker and H.van Houten,(Academic, Boston, 1991) and references therein.

[2] W.Hansen et al, Phys. Rev. Lett. **38** 2586 (1987);
T.Deniel et al, Phys. Rev. B **38** 12732 (1988);
C.H.Siroski and U.Merkt, Phys. Rev. Lett **62** 2164 (1989);
T. Egeler et al, Phys. Rev. Lett. **65** 1804 (1990);
T.Deniel et al, Phys.Rev.Lett **66** 2657 (1991).

[3] S.Das Sarma and W.Y.Lai, Phys. Rev. B **32**, 140 (1985);
W.Y.Lai and S.Das Sarma, ibid **33**, 8874 (1986);
W.Y.Lai, A.Kobayashi and S.Das Sarma, ibid **34**, 7380 (1986);
W.M.Que and G.Kirczenow, ibid **37**, 7153 (1988);
Q.Li and S.Das Sarma, ibid **40**, 5860 (1989);
Q.Li, S.Das Sarma and R.Joynt, ibid **45** 13713 (1992);
T.Ogawa, A.Furusaki and N.Nagaosa, Phys. Rev. Lett **68**, 3638 (1992);
D.K.K.Lee and Y.Chen, ibid 69, 1399 (1992).

[4] X.G.Wen Phys. Rev. B **41**, 12838 (1990), ibid **43** 11025 (1991);
M.Stone Ann. Phys. (N.Y.) **207** 38 (1991), Int. J. Mod. Phys. B **5** 509 (1991).

[5] S.Tomonaga, Prog. Theor. Phys. **5**, 544 (1950);
J.Luttinger, J. Math. Phys. **4**, 1154 (1963).

[6] D.Mattis and E.Lieb, J. Math. Phys. **6**, 304 (1965).

[7] F.Haldane, J.Phys.C:Solid State Phys **14**, 2585 (1981).

[8] A.Plaut et al. Phys. Rev.Lett.**67**,1642 (1991);
A.Goñi et al. Phys. Rev. Lett.**67**, 3298 (1991);
J.Calleja et al., Solid State Commun. **79**, 911 (1991).

[9] C.M.Naón, M.C.von Reichenbach and M.L.Trobo, Nucl.Phys.B **435** [FS], 567 (1995).

[10] T.Giamarchi and H.J.Schulz, Phys. Rev. B **37** 325 (1988).

[11] D.H. Lee and J. Toner, Phys. Rev. Lett. **69** 3378 (1992).

[12] A.Furusaki and N.Nagaosa, Phys. Rev. Lett. **72** 892 (1994).

[13] P.Frojdh and H.Johannesson, Phys. Rev. Lett. Phys. Rev. Lett. **75** 300 (1995).

[14] B.Hu and S.Das Sarma, Phys. Rev. B **48**, 5469 (1993).

[15] N.Andrei, Phys. Rev. Lett. **45** 379 (1980).

[16] E.Fradkin, F.Schaposnik and M.C. von Reichenbach, Nucl. Phys. **B [FS] 316**, 710 (1989).

[17] I.Affleck and A.W.W. Ludwig, Nucl.Phys.B **360**, 641,(1991).

[18] J.Sólyom, Adv.in Phys. **28**, 201 (1979).

[19] K.Furuya, R. Gamboa-Saraví and F.Schaposnik, Nucl. Phys.B **208**, 159 (1982).

Integrable Multiparametric $SU(N)$ Chain

Angela Foerster[1], Itzhak Roditi[2] and L.M.C.S. Rodrigues[2]
[1] *Instituto de Física da UFRGS*
Av. Bento Gonçalves, 9500
91501-970 - Porto Alegre, RS - Brazil
[2] *Centro Brasileiro de Pesquisas Físicas - CBPF*
Rua Dr. Xavier Sigaud, 150
22290-180 - Rio de Janeiro, RJ - Brazil
[a] *ANGELA@IF1.UFRGS.BR*
[b] *RODITI@.CBPFSU1.CAT.CBPF.BR*
[c] *LIGIA@CBPFSU1.CAT.CBPF.BR*

Received March, 1996

In this work we obtain the Hamiltonian for an $SU(N)$ chain with twisted boundary conditions and find that the underlying algebraic structure is the multiparametric deformation of $SU(N)$ enlarged by the introduction of a central element.

We start with the following multiparametric generalization of the $SU(N)$ R-matrix, first introduced by Perk and Schultz [1],

$$\begin{aligned} R(x,q,\{p\}) &= a(x,q)\sum_{\alpha}^{N} e^{\alpha\alpha}\otimes e^{\alpha\alpha} + b(x)\sum_{\alpha\neq\beta}^{N} p_{\alpha\beta}e^{\alpha\alpha}\otimes e^{\beta\beta} \\ &+ c_{-}(x,q)\sum_{\alpha<\beta}^{N} e^{\alpha\beta}\otimes e^{\beta\alpha} + c_{+}(x,q)\sum_{\alpha\beta}^{N} e^{\alpha\beta}\otimes e^{\beta\alpha}\ , \end{aligned} \tag{1}$$

where x is the spectral parameter and

$$a(x,q) = xq - \frac{1}{xq}\ ,\ b(x) = x - \frac{1}{x}\ ,\ c_{-}(x,q) = \frac{1}{x}\,(q-\frac{1}{q})\ ,\ c_{+}(x,q) = x(q-\frac{1}{q})\ . \tag{2}$$

q and $p_{\alpha\beta}$ are $1+\frac{N(N-1)}{2}$ independent parameters with $p_{\alpha\beta},\alpha,\beta = 1,\cdots N(\alpha<\beta)$, $p_{\beta\alpha} = (p_{\alpha\beta})^{-1}$. The $N\times N$ matrices $e^{\alpha\beta}$ have elements $(e^{\alpha\beta})^{\gamma\rho} = \delta^{\alpha\gamma}\delta^{\beta\rho}$.

It is easy to check that the R-matrix (1) satisfies the Yang-Baxter equation

$$R_{12}(x_{12},q,\{p\})R_{13}(x_{13},q,\{p\})R_{23}(x_{23},q,\{p\}) = R_{23}(x_{23},q,\{p\})R_{13}(x_{13},q,\{p\})R_{12}(x_{12},q,\{p\})\ . \tag{3}$$

The Lax operator associated to (1) is

$$\begin{aligned} L(x,q,\{p\}) &= x\sum_{\alpha}^{N} q^{W_\alpha}\prod_{\beta\neq\alpha}(p_{\alpha\beta})^{W_\beta}e^{\alpha\alpha} - \frac{1}{x}\sum_{\alpha}^{N} q^{-W_\alpha}\prod_{\beta\neq\alpha}(p_{\alpha\beta})^{W_\beta}e^{\alpha\alpha} + \\ &+ c_{+}(x,q)\sum_{\alpha\beta} X^{+}_{\beta\alpha}e^{\alpha\beta} + c_{-}(x,q)\sum_{\alpha<\beta} X^{-}_{\beta\alpha}e^{\alpha\beta}\ , \end{aligned} \tag{4}$$

where in the fundamental representation $W_\alpha = e^{\alpha\alpha}$ and $X_{\alpha\beta} = e^{\alpha\beta}(\alpha\neq\beta)$; $X^{+}_{\alpha\beta}(X^{-}_{\alpha\beta})$ has non-zero elements above (below) the diagonal.

The R matrix (1) and the Lax operator (4) obey the Fundamental Commutation Relation (FCR)

$$R_{12}(x_{12},q,\{p\})L^{1}_{n}(x_1,q,\{p\})L^{2}_{n}(x_2,q,\{p\}) = L^{2}_{n}(x_2,q,\{p\})L^{1}_{n}(x_1,q,\{p\})R_{12}(x_{12},q,\{p\})\ . \tag{5}$$

Following the general procedure of Faddeev et al [2], we construct an integrable multiparametric version of a quantum Hamiltonian for a n_0 length $SU(N)$ chain

$$\mathcal{H} = \sum_{i=1}^{n_0} h_{i,i+1} \quad (n_0 + 1 \equiv 1) \,, \tag{6}$$

where

$$h_{i,i+1} = \frac{q+q^{-1}}{2} - \frac{q+q^{-1}}{2} \sum_{\alpha=1}^{N} e_i^{\alpha\alpha} e_{i+1}^{\alpha\alpha} - \frac{q-q^{-1}}{2} \sum_{\alpha\neq\beta}^{N} sign(\alpha-\beta) e_i^{\alpha\alpha} e_{i+1}^{\beta\beta} - \sum_{\alpha\neq\beta}^{N} p_{\alpha\beta} e_i^{\alpha\beta} e_{i+1}^{\beta\alpha} \,. \tag{7}$$

This model is exactly solved by the Algebraic Nested Bethe Ansatz method. This procedure is carried out in $(N-1)$ steps and the Bethe Ansatz equations for the level "l" ($l = 1, \cdots N-1$) are given by

$$\prod_{r\neq l+1}^{N} p_{rl+1}^{N_r} \prod_{s\neq l}^{N} p_{ls}^{N_s} \prod_{i=1}^{n_{l-1}} \frac{a(x_k^{(l)}/x_i^{(l-1)})}{b(x_k^{(l)}/x_i^{(l-1)})} \prod_{i'=1}^{n_l} \left(\frac{a(x_{i'}^{(l)}/x_k^{(l)})}{b(x_{i'}^{(l)}/x_k^{(l)})} \frac{b(x_k^{(l)}/x_{i'}^{(l)})}{a(x_k^{(l)}/x_{i'}^{(l)})} \right) \prod_{i''=1}^{n_{l+1}} \frac{b(x_{i''}^{(l+1)}/x_k^{(l)})}{a(x_{i''}^{(l+1)}/x_k^{(l)})} = -1 \,,$$

$$k = 1, \cdots, n_l \,. \tag{8}$$

Here $n_N = 0, x^{(0)} = 0, N_i = n_{i-1} - n_i$ and $\prod_{i=1}^{0}$ is assumed to be one. Therefore, the diagonalization of the Hamiltonian (6) is reduced to a system of coupled algebraic equations for the Bethe Ansatz parameters $x_k^{(l)}, (l = 1, \cdots N-1; k = 1, \cdots n_l)$. We observe that each parameter $x^{(l)}$ couples just with its neighbour-level parameter $x^{(l\pm1)}$ (except $x^{(1)}(x^{(N-1)})$, which couples only with $x^{(2)}(x^{(N-2)})$).

Now we show that the general Hamiltonian (6) describes a $SU(N)$ chain with twisted periodic boundary conditions. For that sake we perform the similarity transformations generated by

$$U = c^{-\frac{1}{2}\sum_{i=1}^{n_0}(i-1)\sum_{\alpha=1}^{N-1}\xi^\alpha H_\alpha^i} \,. \tag{9}$$

The coefficients ξ^α are fixed when we impose the conditions

$$p_{\alpha\beta} U e_i^{\alpha\beta} e_{i+1}^{\beta\alpha} U^{-1} = e_i^{\alpha\beta} e_{i+1}^{\beta\alpha} \;;\; \alpha = 1, \cdots N-1 \,, \tag{10}$$

under which (6) particularizes to the Hamiltonian for the $SU(N)$ spin chain with twisted periodic boundary conditions

$$\begin{aligned} \mathcal{H} \;=\; & \sum_{i=1}^{n_0-1} \left\{ \frac{q+q^{-1}}{2} - \frac{q+q^{-1}}{2} \sum_{\alpha=1}^{N} e_i^{\alpha\alpha} e_{i+1}^{\alpha\alpha} - \frac{q-q^{-1}}{2} \sum_{\alpha\neq\beta}^{N} sign(\alpha-\beta) e_i^{\alpha\alpha} e_{i+1}^{\beta\beta} \right\} + \\ & - \sum_{i=1}^{n_0-1} \sum_{\alpha\neq\beta}^{N} e_i^{\alpha\beta} e_{i+1}^{\beta\alpha} - \sum_{\beta\neq\alpha}^{N} (p_{\alpha\beta}^{n_0} e_{n_0}^{\alpha\beta} e_1^{\beta\alpha} + p_{\alpha\beta}^{-n_0} e_1^{\alpha\beta} e_{n_0}^{\beta\alpha}) \end{aligned} \tag{11}$$

The case $N = 2$ was previously discussed in the literature [3].

The multiparametric Hamiltonian (6) is not quantum group invariant. Nevertheless, the quantum group structure also appears in this context. The underlying algebraic structure is obtained directly from the FCR (7) noting that now W_i and $X_{\alpha\beta}$ are considered as abstracts elements of the algebra. Besides, the W_α are now combinations of a central element Z and operators $\hat{H}_\alpha$,

$$W_\alpha = \frac{1}{N} \sum_{\alpha=1}^{N} w_{\alpha\rho} \hat{H}_{\rho-1} \quad , \quad \hat{H}_0 \equiv Z \,, \tag{12}$$

that respectively concide with I and H_α in the fundamental representation.

The coproduct is obtained by considering the product of two $L's$ acting on two internal spaces; we find

$$\Delta Z = Z \otimes \mathbf{1} + \mathbf{1} \otimes Z \tag{13}$$

$$\Delta \hat{H}_\alpha = \hat{H}_\alpha \otimes \mathbf{1} + \mathbf{1} \otimes \hat{H}_\alpha \tag{14}$$

$$(\Delta X_{\nu\mu}^{+}) = q^{W_\nu} \prod_{\beta\neq\mu} p_{\mu\beta}^{W_\beta} \otimes X_{\nu\mu}^{+} + X_{\nu\mu}^{+} \otimes q^{W_\nu} \prod_{\beta\neq\nu} p_{\nu\beta}^{W_\beta}$$

$$+\Omega \sum_{\beta<\mu} X^{+}_{\beta\mu} \otimes X^{+}_{\nu\beta} \tag{15}$$

$$(\Delta X^{-}_{\nu\mu}) = q^{-W_\mu} \prod_{\beta\neq\mu} p^{-W_\beta}_{\mu\beta} \otimes X^{-}_{\nu\mu} + X^{-}_{\nu\mu} \otimes q^{-W_\nu} \prod_{\beta\neq\nu} p^{-W_\beta}_{\nu\beta}$$

$$+\Omega \sum_{\beta\mu} X^{-}_{\beta\mu} \otimes X^{-}_{\nu\beta} \tag{16}$$

Thus, the introduction of a central element has allowed us to construct a coherent co-product which makes appear the underlying algebraic structure of the $SU(N)$ chain with twisted boundary conditions.

References

[1] J.H.H. Perk and C.L. Schultz, Phys. Lett. **A84**, 407 (1981); C.L. Schultz, Physica **A112**, 71 (1983).

[2] E. Sklyanin, L. Takhtajan and L. Faddeev, Teor. Matem. Fiz. **40**, 194 (1979).

[3] M. Monteiro, I. Roditi, L. Rodrigues and S. Sciuto, Mod. Phys. Lett. A **10**, 419 (1995); F.C. Alcaraz et al, Annals of Phys. **182** 280, (1988).

Estudo Numérico da Estabilidade do Vácuo Simétrico para Campos Escalares em Cosmologias Anisotrópicas

H. Fleming†, R.M. Teixeira Filho† e M.D.R. Sampaio‡
†*Departamento de Física Matemática, IFUSP*
‡*Department of Physics, University of Durham, England*

July 31, 1996

Um campo escalar acoplado conformemente à gravitação possui na lagrangeana um termo proporcional à curvatura escalar que pode funcionar como um "termo de massa de sinal trocado". Se o Universo é o de Friedmann aberto, um valor esperado não nulo, variável no tempo, é possível e motivou um modelo de violação espontânea de CP que resiste aos efeitos térmicos do universo primordial. Neste trabalho mostramos, numericamente, que esse mecanismo não depende do alto grau de simetria dos modelos de Friedmann, podendo ocorrer em várias cosmologias anisotrópicas.

1 Introdução

O mecanismo de quebra espontânea de simetria (QES) tem-se mostrado muito importante na construção de modelos em teoria de campos. A maioria dos modelos com QES são baseados no modelo de Goldstone que considera na Lagrangeana o termo de massa satisfazendo $m^2 < 0$. Existem outros modelos que prescindem desta hipótese. É o caso do modelo de Coleman-Weinberg [1], em que a QES ocorre quando consideramos as correções radiativas da teoria.

O estudo da teoria de campos em espaços curvos tem mostrado que o acoplamento conforme à gravitação pode conduzir a modelos com quebra espontânea de simetria sem a necessidade da hipótese $m^2 < 0$. Em particular, a teoria $\lambda(\phi^*\phi)^2$ no modelo de Friedmann-Robertson-Walker (FRW) aberto apresenta quebra espontânea da simetria de gauge [2] [3]. Também, mecanismos de violação CP de origem cosmológica sem restauração da simetria a altas temperaturas tem sido proposto [4] [5]. No entanto, seria desconfortável se esta quebra de simetria dependesse do alto grau de simetria do modelo de FRW. Neste trabalho mostramos que a QES não está restrita a este modelo. Analisando a teoria $\lambda(\phi^*\phi)^2$ com acoplamento conforme à gravitação em diversos modelos cosmológicos homogêneos (espacialmente) e anisotrópicos, mostramos que a QES se dá para diversos destes modelos. A análise da teoria quântica do campo ϕ é feita na aproximação de árvore e a temperatura zero.

2 Teoria $\lambda(\phi^*\phi)^2$ com Acoplamento Conforme à Gravitação

A extensão de uma teoria de campos formulada no espaço de Minkowski para espaços curvos não é unívoca. Assim, teorias distintas em espaços curvos podem conduzir à mesma teoria no espaço de Minkowski. Neste contexto, a escolha de um modelo em espaços curvos deve levar em conta outras considerações. A preservação das simetrias da teoria é um destes fatores. A teoria $\lambda(\phi^*\phi)^2$ com massa nula é invariante em relação ao grupo conforme de quinze parâmetros. Mostra-se que a Lagrangeana para esta teoria em espaços curvos que preserva a invariância conforme

é dada por:

$$\mathcal{L} = \frac{1}{2}g^{\mu\nu}(\partial_\mu\phi^*\partial_\nu\phi + \partial_\nu\phi^*\partial_\mu\phi) + \frac{R}{6}(\phi^*\phi) - \frac{\lambda}{6}(\phi^*\phi)^2 \tag{1}$$

onde $g^{\mu\nu}$ é o tensor métrico do espaço-tempo e R a sua curvatura escalar de Ricci.

Sendo a ação, S, dada por

$$S = \int d^4x\sqrt{-g}\mathcal{L}\left(\phi, \frac{\partial\phi}{\partial x^\mu}\right),$$

onde $g = det[g_{\mu\nu}]$, a equação de movimento para ϕ, $\frac{\delta S}{\delta\phi} = 0$, resulta:

$$\Box\phi(x) - \frac{R}{6}\phi(x) + \frac{\lambda}{3}\phi(x)^*\phi^2(x) = 0, \tag{2}$$

onde

$$\Box \equiv \frac{1}{\sqrt{-g}}\partial_\mu(\sqrt{-g}g^{\mu\nu}\partial_\nu).$$

Considerando a temperatura zero e numa aproximação de árvore, o valor esperado no vácuo (VEV) do campo $\phi, < \phi >= v(x)$, satisfaz à equação (2), isto é,

$$\Box v(x) - \frac{R}{6}v(x) + \frac{\lambda}{3}v(x)^*v^2(x) = 0. \tag{3}$$

Estaremos restritos a espaços homogêneos. Assim, supomos v(x) translacionalmente invariante ($\partial_i v(x) = 0, i = 1, 2, 3$).

O tensor energia-momento do campo ϕ é dado por:

$$T^\mu_\nu = \partial^\mu\phi^*\partial_\nu\phi + \partial_\nu\phi^*\partial^\mu\phi - \delta^\mu_\nu\mathcal{L} + \frac{1}{3}\{R^\mu_\nu - \nabla^\mu\nabla_\nu + \delta^\mu_\nu\Box\}\phi^*\phi, \tag{4}$$

A densidade de energia $\epsilon(t) =< 0|T^0_0|0 >$ na aproximação em árvore resulta

$$\epsilon(t) = g^{00}|\partial_0 v|^2 + \frac{1}{3}\left[R^0_0 - \frac{R}{2} + \Box - \nabla^0\nabla_0\right]|v|^2 + \frac{\lambda}{6}|v|^4 \tag{5}$$

onde $|...|$ indica módulo da função.

Por conveniência de cálculo, reescrevemos as equações (3) e (5) em termos da função $u(x) = \sqrt{\frac{\lambda}{3}}v(x)$.

$$\Box u(x) - \frac{R}{6}u(x) + u(x)^*u^2(x) = 0 \tag{6}$$

e

$$\begin{aligned}\epsilon'(t) &\equiv \frac{\lambda}{3}\epsilon(t) \\ &= g^{00}|\partial_0 u|^2 + \frac{1}{3}\left[R^0_0 - \frac{R}{2} + \Box - \nabla^0\nabla_0\right]|u|^2 + \frac{1}{2}|u|^4.\end{aligned} \tag{7}$$

3 Modelos Cosmológicos Homogêneos e Anisotrópicos

Utilizando o "pacote" MATHTENSOR para o programa MATHEMATICA, obtivemos as equações (6) e (7) para alguns modelos cosmológicos homogêneos e anisotrópicos cujos elementos de linha são dados a seguir.

A) Bianchi Tipo I - Vácuo (Kasner)

$$ds^2 = dt^2 - t^{2p_1}dx^2 - t^{2p_2}dy^2 - t^{2p_3}dz^2 \tag{8}$$

onde,

$$p_1 + p_2 + p_3 = 1; p_1^2 + p_2^2 + p_3^2 = 1; p_1 \neq p_2 \neq p_3$$

B)Bianchi Tipo VI - Poeira (p=0) (Dun - Tupper [6])

$$ds^2 = dt^2 - 4t^2dx^2 - te^{-2x}dy^2 - te^{2x}dz^2 \tag{9}$$

C)Bianchi Tipo VI - Vácuo (Ellis - MacCallum) [6])

$$ds^2 = t^{-1/2}e^{t^2}(dt^2 - dx^2) - 2te^{-2x}dy^2 - 2te^{2x}dz^2 \tag{10}$$

D)Bianchi Tipo IV - Vácuo (Harvey e Tsoubelis [7])

$$\begin{aligned} ds^2 &= dt^2 - t'^2dx^2 - t'^{8/5}e^{-2x}dy^2 \\ &- t'^{8/5}e^{-2x}(\ln t'^{4/5} - x)(dydz + dzdy) \\ &- t'^{8/5}e^{-2x}\left[1 + \left(\ln t'^{4/5}\right)^2 - 2x\ln t'^{4/5} + x^2\right]dz^2 \end{aligned} \tag{11}$$

onde $t' = \frac{5}{4}t$

E)Bianchi Tipo III - $p = \rho$ (Wainwright et al) [8])

$$ds^2 = (\sinh(2t))^2(dt^2 - dx^2) - e^{-4x}(\sinh(2t))^2dy^2 - dz^2 \tag{12}$$

F)Bianchi Tipo V - $p = \rho$ (Wainwright et al) [8])

$$ds^2 = \sinh(2t)(dt^2 - dx^2) - e^{-2x}\sinh(2t)(dy^2 + dz^2) \tag{13}$$

Nossa análise está restrita apenas às soluções complexas da equação (6) da forma $u(t)e^{i\theta}$ (u(t) é real e θ= const.). Assim, podemos considerar u(t) real na equação (6).

4 Resultados e Conclusões

Resolvemos numericamente as equações para u(t) nos modelos considerados usando um algorítmo tipo Runge-Kutta[9] para diversas condições iniciais.

A análise de estabilidade da solução simétrica u(t) = 0 é feita no sentido do menor valor de densidade de energia, isto é, se o cálculo numérico indica soluções com $\epsilon(t) < 0$ para algum intervalo de t ($t > 0$), a solução u(t) = 0 é considerada instável. Nos modelos **A**, **B** e **D**, onde uma mudança de variáveis elimina a dependência na variável temporal dos coeficientes da equação (6), fizemos também a análise da estabilidade local da solução simétrica, linearizando as equações do sistema dinâmico equivalente.

Nos modelos **A**, **B** e **D**, a linearização das equações do sistema dinâmico equivalente em torno da solução simétrica mostrou que esta é instável. A análise numérica confirmou estes resultados. Também, a análise numérica mostrou que a solução simétrica nos modelos **E** e **F** é instável, isto é, existem soluções com densidade de energia negativa ($\epsilon(t) < 0$).

Como podemos ver, a quebra espontânea de simetria numa teoria $\lambda(\phi^*\phi)^2$ acoplada conformemente à gravitação não depende do alto grau de simetria do modelo de FRW. A análise numérica em diversas cosmologias homogêneas e anisotrópicas mostrou que a QES ocorre em diversos destes modelos.

References

[1] S.Coleman, E.Weinberg; Phys.Rev D, vol 7, 6 (1973)

[2] A.A.Grib, V.M.Mostepanenko; JETP Lett. **25**, 277 (1977)

[3] H.Fleming, J.L.Lyra, C.P.C.Prado e V.L.Silveira; Lett. Nuovo Cimento **27**, 261 (1980)

[4] H.Fleming; Phys. Lett. **146B**, 191 (1984)

[5] H.Fleming, W.L.Truppel; Il Nuovo Cimento **105A**, n.2 (1992)

[6] K.A.Dunn, B.O.J.Tupper; The *Astroph. Journal*, **204**, 322 (1976)

[7] A.Harvey, D.Tsoubelis; Phys.Rev. D, **15**, n.10 (1977)

[8] J.Wainwright et al, GRG **10**, n.3, 259 (1979)

[9] W.H.Press et al, "Numerical Recipes", Cambridge, 1992

The bosonic and fermionic partition functions on S^3

A.C. V. V. de Siqueira, E.R. Bezerra de Mello and V. B. Bezerra

Departamento de Física, Universidade Federal da Paraíba

58059-970 João Pessoa, Pb-Brazil

July 31, 1996

In this paper we calculate regularized expressions for the bosonic and fermionic partition functions for a field theory defined on a hyper-sphere S^3. We also analyze their behavior with the radius r_o of this manifold, and see that for specific values of the field's masses, closed expressions can be obtained, which present a completly different behavior as we take $r_o \to \infty$, indicating isolated discontinuities of these partition functions with the masses of the matter fields.

1 Introduction

The path-integral quantization[1] is a very powerful technique to quantize a physical system. By this elegant formalism it is possible to investigate several physical phenomena in gauge theories[2], like, for example, quantum anomalies[3].

The study of a quantum field theory, defined by a matter field ϕ living on a given manifold with a defined metric tensor $g_{\mu\nu}(x)$, is conveniently made by the use of the path integral functional

$$Z[g] = \int [d\phi] e^{iS[\phi,g]},$$

where $S[\phi, g]$ is the classical action for the matter field defined on the manifold. The Euclidean version of this expression can be obtained for a static space-time by the changing $t \to it$. In this case the functional $Z[g]$, is related with the Euclidean "partition function" which given by the following expression

$$Z_E[g] = \int [d\phi] e^{-S_E[\phi,g]},$$

where we have used, in both case, $\hbar = 1$.

In this paper we follow the second approach, in order to study the behavior of a matter field in a finite geometry S^3. Specifically, we study the bosonic and fermionic matter fields, on this manifold, and by the explicity calculation of the eigenvalues for the Klein-Gordon and Dirac operators defined in this geometry, we calculate their respective determinants, and consequently their partition functions.

The Euclidean action for the matter field in a given compact geometry is given by

$$S_E[\phi, g] = \int d^D x \sqrt{g} \phi K \phi,$$

where K is a non-negative self-adjoint operator, which in our case, represents the Klein-Gordon or Dirac one.

The partition function is then expressed by the following identity

$$Z_E[g] = [\prod_n \lambda_n]^{-\mu} = [\det K]^{-\mu}$$

where $\mu = 1/2$ or -1 for a neutral scalar or fermionic matter field, respectively, and $\{\lambda_n\}$ is the real positive eigenvalues of K.

As we shall see by direct computation, this finite geometry, provide us a discrete set of the eigenvalues for these operators, but the product of them is formally infinite. So, in order to obtain a finite result for $D = \prod_n \lambda_n$ we shall use the well defined ζ-function regularization procedure.

Our motivation to determine and study the partition functions for bosonic and fermionic matter fields on S^3, is to investigate how this particular finite geometry can produces a well defined and finite theory, and how the partition function depends on the radius of the hyper-sphere and also on the mass of the matter field.

This paper is organized as follows. In section 2, we analyze the Klein-Gordon operator for a massive scalar field on S^3, and show explicitly its eigenvalues. We also calculate a finite and well defined expression for its determinant, and consequently the partition function for this spin 0-particle. Also in this section we complete the analysis considering the massless case. In section 3, we compute the Dirac operator determinant, in an indirect way, using the relation betwen this operator and the square root of the bosonic one[4], which fortunately, for this geometry reduces to our previous analysis as we shall see. In section 4, we give our conclusion and remarks about this paper.

2 The Scalar Partition Function on S^3

The Klein-Gordon operator for a scalar massive field in a positive defined metric space is given by

$$K_{(S)} = -\nabla^2 + M^2, \tag{1}$$

where ∇^2 is the Laplace-Beltrami differential operator, which in a generic metric space is writen as

$$\nabla^2 = g^{ij}(\partial_i\partial_j - \Gamma^l_{ij}\partial_l).$$

For our specific case the manifold is the hyper-sphere S^3 and the bosonic partition function is given by

$$Z_E^{(B)} = [\det(K_{(S)})]^{-1/2} = (\prod_n \lambda_n)^{-1/2}, \tag{2}$$

where λ_n is the positive eigenvalue of the Klein-Gordon operator defined in this geometry.

The product above is formally divergent. In order to obtain a finite result for it, and then to extract physical information about our system, we shall use the well defined ζ-function regularization procedure for this calculation, and get, consequently a trustworthy expression to $Z_E^{(B)}$.

The eigenvalues for this operator defined on S^3, an hyper-sphere of radius r_o, is given by[5]

$$\lambda_n = n(n+2)r_o^{-2} + M^2, \tag{3}$$

which appear with multiplicity

$$\delta(n) = (n+1)^2 .$$

The partition function must be calculated taking into account this fact. The regularized expression for the Klein-Gordon determinant is given by

$$\det(K_{(S)}) = \exp[-\frac{d}{dz}\zeta_{r_o,M}(0)], \tag{4}$$

where we define the $\zeta_{r_o,M}(z)$-function by

$$\zeta_{r_o,M}(z) = \sum_{s=1}^{\infty} \frac{s^2}{[s^2+x]^z}, \tag{5}$$

with $x = M^2r_o^2 - 1$.

Bellow we present our calculation for $\det(K_{(S)})$ in the following cases:

a) Explicit expression for $\mid x \mid < 1$.

b) Formal expression for any value of x.

c)The massless case will be studied at the end of this section, in a separated analysis.

Now, let us present only our results concerning the product of the eigevalues for the mentioned cases:

a) For the case of $\mid x \mid < 1$, we can obtain an explicit expression for $D = \Pi_n\lambda_n$, which is given by

$$D = \exp[\frac{1}{2\pi^2}\zeta_R(3) - \frac{1}{2}\sum_{p=0}^{\infty}\frac{x^{p+1}}{p+1}\frac{(2\pi)^{2p}}{(2p)!}B_{2p}], \tag{6}$$

where B_n are the Bernoulli numbers and $\zeta_R(z)$,the Riemann zeta-function.

b) A formal expression for D is presented below, however it cannot be expressed as a finite combination of elementary functions. It is given by

$$D = \exp[\frac{1}{2\pi^2}\zeta_R(3) - \pi\int_0^{\sqrt{x}} dz z^2 \coth(\pi z)]. \tag{7}$$

(One can see that the expression above reproduces (2.6) for the case $\mid x \mid < 1$[6].)

Although, for this case, we cannot obtain an explicit expression for D, we can analyze the behavior of $Z_E^{(B)}$ with r_o, in the limit as r_o is much bigger than M^{-1}. For this limit, $x >> 1$, and after some steps we get:

$$D = \exp[\frac{1}{2\pi^2}\zeta_R(3) - \frac{\pi M^3 r_o^3}{3} + \frac{e^{-2\pi M r_o}}{2\pi^2}(1 + 2\pi M r_o + 2\pi^2 M^2 r_o^2) + O(e^{-4\pi M r_o}) + C], \tag{8}$$

where 'C ' is a finite numerical constant.

The partition function is given, in this approximation, by

$$Z_E^{(B)} \simeq C' \exp[\frac{\pi M^3 r_o^3}{6} - \frac{e^{-2\pi M r_o}}{4\pi^2}(1 + 2\pi M r_o + 2\pi^2 M^2 r_o^2) + ...], \tag{9}$$

where, again, C' is a numerical constant.

As we can see, $Z_E^{(B)}$ presents a divergent behavior as the radius of S^3 goes to infinite, and this divergence, given by the exponential of a term proportional to the volume Ω of this manifold, reproduce a non-null thermodynamics limit.

c)For the case where the bosonic field presents no mass, the calculation of the Klein-Gordon determinant is a little bit different. For this case we have to consider only non-zero eigenvalues, in order to obtain an explicit and well defined expression for the partition function. So, we easily can show that

$$\det(K_{(S)}) = \exp[-\frac{d}{dz}\zeta(0)], \tag{10}$$

where the zeta function for this determinant is,

$$\zeta(z) = r_o^{2z}\sum_{s=2}^{\infty}\frac{s^2}{(s^2-1)^z} \tag{11}$$

It is worthy to mention that in the zeta function above the summation starts at $s = 2$. This apparent irrelevant shift in the infinite spectrum of the operator is responsible for a completely different behavior of the partition function compared with the previous one, the massive case. The explicit expression for $Z_E^{(B)}$ can be obtanied in a closed form after some calculations, and using properties of the Riemann $\zeta-$function. The results is

$$Z_E^{(B)} = \pi^{-1/2} r_o^{-1} \exp[-\frac{1}{4\pi^2}\zeta_R(3)], \tag{12}$$

which evidently goes to zero as r_o tends to infinite.

3 The Fermionic Partition Function

The Dirac operator for a massive fermionic field in a positive defined metric space, can be written as

$$K_{(F)} = i\gamma^\mu\nabla_\mu - m, \tag{13}$$

where $\nabla_\mu = \partial_\mu + \Gamma_\mu$, being Γ_μ the spin connection, and $\gamma^\mu(x) = e^\mu_{(a)}(x)\gamma^{(a)}$,where $e^\mu_{(a)}(x)$ are the tetradic basis vectors. The indices $\mu, a = 1, 2, 3$. Because of the positive-definite signature for the metric tensor $g_{\mu\nu}$ we shall use for the constant 2×2 matrices $\gamma^{(a)}$ a representation which obey the algebra $\{\gamma^{(a)}, \gamma^{(b)}\} = -2\delta^{(a)(b)}$ with $\delta^{(a)(b)} = diag(+,+,+)$.

In a three dimensional space it is possible to define two inequivalent Dirac operators $K_{(F)} = i\gamma^\mu\nabla_\mu - m$ and $K'_{(F)} = i\gamma^\mu\nabla_\mu + m$ which can be related by a parity transformation P, that for the Euclidean case can be defined as a reflexion in all axes: $x^\mu \rightarrow -x^\mu$. It can be shown that these two operators present symetric spectra. Given their eigenvalues equations

$$K_{(F)}\Psi_\lambda = \lambda\Psi_\lambda,$$

and

$$K'_{(F)}\Psi'_\lambda = \lambda'\Psi'_\lambda$$

under P transformation, we get $\lambda \rightarrow \lambda' = -\lambda$, as demonstrated in [7]

Because the fermionic determinants are also formally the product of their respective eigenvalues λ and λ', we see that they may differ for, at most, a sign. Admiting that for this geometry both determinants coincides [8], we can develop an indirect method to obtain them. Instead of calculating explicitly the spectra of these operators, we shall adopt another procedure, which as we shall see, for this geometry, reduces to the determination of the spectrum for a Klein-Gordon operator, already calculated by us in the previous section. Let us take the product of the Dirac operators $K_{(F)}$ and $K'_{(F)}$. Then, we get[4]

$$K_{(F)}K'_{(F)} = -(-\nabla^2 - \frac{R}{4} + m^2), \tag{14}$$

where$R = R^{\mu}_{\mu}$ is the curvature scalar, which for this manifold is equal to $6r_o^{-2}$.

The Dirac operator determinant is then expressed, up to sign, by the square root of the Klein-Gordon one, where the mass term is modifield by the presence of the curvature scalar. So, the fermionic partition function is expressed by

$$Z_E^{(F)} = \pm[\det(-\nabla^2 + m^2 - \frac{3r_o^{-2}}{2})]^{1/2}. \tag{15}$$

As we also can see $Z_E^{(F)}$ does not present singularity, however if the bosonic operator present null eigenvalues, we get a trivial fermionic partition function: $Z_E^{(F)} = 0$. This situation may happen if, for example, the parameter $M^2 = m^2 - \frac{3r_o^{-2}}{2}$ is zero . In order to avoid this problem, and get a non-zero value for (15), we have to reduce the spectrum of the bosonic operator extracting from the original Hilbert space for the Dirac operator the corresponding eigenfunction. In other words, what we are saying is that the fermionic spectrum is related with the bosonic one identifying an effective mass for the latter by: $m^2_{(f)} = M^2 = m^2 - \frac{3r_o^{-2}}{2}$, and in the case of $M^2 = 0$, an explit calculation to the fermionic determinant, gets zero as result. Now defining a new partition function $Z_E^{(F)}$, for this special situation, we get

$$Z_E^{(F)} = \exp[-\frac{1}{2}\frac{d}{dz}\zeta(0)], \tag{16}$$

where the zeta-function above was defined in Eq.(11), giving the following result for $Z_E^{(F)}$:

$$Z_E^{(F)} = \pi^{1/2} r_o \exp[\frac{1}{4\pi^2}\zeta(3)], \tag{17}$$

which is proportional to r_o.

For the positive parameter M^2, the bosonic eigenvalues are all positives, consequently the fermionic partition function cannot vanishes.Using previous results we can write

$$Z_E^{(F)} = \exp\left[\frac{1}{4\pi^2}\zeta_R(3) - \frac{\pi}{2}\int_o^{\sqrt{x}} dz z^2 \coth(\pi z)\right], \tag{18}$$

with $x = M^2 r_o^2 - 1$.

4 Concluding Remarks

In this paper we have analized the model composed by a bosonic matter field on the sphere S^3. For this system we have shown the complete set of discrete eigenvalues, and using the ζ-function regularization procedure, we calculated the bosonic partition function $Z_E^{(B)}$. Although for the massive bosonic case we could not give a closed expression to it, we could analyse the behavior of this partition function as r_o, the radius of the sphere, goes to infinite. For the massless case, on the other hand, we could obtain an explicit expression for $Z_E^{(B)}$, and also could see the difference between the behavior of both partition functions as r_o tends to infinite. This fact can be explained by the spectrum of the bosonic operator taking into account in the calculation of the partition function. What we conclude from this analysis is that the main difference between these two partition functions is not only due to the presence of the mass itself. The most important fact lies in the number of eigenstates considered in the functional integration.

In this paper we also have analysed, indirectly, the model composed by a fermionic matter field on S^3. Although we have not found explicitly the spectrum of the Dirac operator in this manifold, we could obtain the Dirac operator

determinant and the respective partition function, by the bosonic one, with the mass term modified by the presence of the scalar curvature. The analysis for this model could then be developed by previous results.

Acknowledgment
We would like to thank Prof. Ramón Mendoza for stimulating and helpful discussions during the course of this work. This work was partially supported by Conselho Nacional de Desenvolvimento Científico e Tecnológico (CNPq).

References

[1] R.P. Feynman and A.R. Hibbs, "Quantum Mechanics and Path Integrals ". Mc. Graw-Hill, New York (1965)

[2] L.D. Faddeev and V.N. Popov, Phys. Rev. Lett **25**, 30 (1967)

[3] F. Fujikawa, Phys. Rev. Lett. **44**, 1733 (1980)

[4] A. Lichnerowicz, Atti. Accad. Naz. dei Lincei, Rendiconti **33** (1962), 187; and Jean Pierre Bourguignon, Rend. Sen. Mat. Univers. Politecn. Torino, **44** (1986), 3.

[5] "The Bosonic and Fermionic Partition Function os S^3", by A. C. V. V. de Siqueira, E. R. Bezerra de Mello and V. B. Bezerra. Depto. de Física (UFPB) preprint.

[6] I. S. Gradshteyn and I.M. Ryzhik "Table of Integrals, Series and Products": Academic Press, Inc. 4th edition (1980).

[7] A.J. Niemi and G.W. Semenoff Nucl. Phys. **B 276**, 173 (1986)

[8] A.J. Niemi and G.W. Semenoff Nucl Phys. **B 269**, 131 (1986)

New applications in negative dimensional integration method

A. T. Suzuki*,*and R. M. Ricotta**
* Instituto de Física Teórica - UNESP
** Faculdade de Tecnologia de São Paulo - CEETPS - UNESP

July 31, 1996

Strictu sensu negative dimensions are neither real nor realizable to us who live this side of the D^+-dimensional universe; they belong to the realm of the immaginary, maybe even ficcional world that is allowed for theoreticians to play with. Nonetheless, the concept of negative dimensions can be introduced in a very simple way, and its uses and consequences can be pursued in a methodical manner. As one of the examples of such application is its usefulness as a powerful tool to evaluate D^+-dimensional integrals, whose typical example in Quantum Field Theory is the Feynman integral. As toy examples, we consider a few of the one-loop integrals in the special case of a non-covariant gauge, namely, the light-cone gauge and show how the results in the principal value (PV) and Mandelstam-Leibbrandt (ML) prescriptions can be obtained. We present also an altogether different application such as proving fundamental relations among different hypergeometric functions of unity argument and some constrained parameters.

1 INTRODUCTION

The D^--dimensional integration method, or Negative Dimensional Integration Method (NDIM) to evaluate Feynman diagrams was first devised and considered by Halliday and Ricotta [1] back in the 80's and some sample calculations were performed. They have pointed out that the technique can be viewed from several perspectives [1, 2]. We shall here adopt the NDIM as defined from the result for the familiar D^+-dimensional Gaussian integral, i.e.,

$$\int d^D q\, e^{-\lambda q^2} = \left(\frac{\pi}{\lambda}\right)^{D/2} \tag{1}$$

which is notably an analytic function of the dimension D. Projecting out the powers of the exponential function in the integrand, we have

$$\sum_{n=0}^{\infty} \frac{(-\lambda)^n}{n!} \int d^D q\, (q^2)^n = \left(\frac{\pi}{\lambda}\right)^{D/2} \tag{2}$$

which can be satisfied if and only if

$$\int d^D q\, (q^2)^n = (-1)^n \pi^{D/2} \Gamma(n+1) \delta_{n+D/2,0} \tag{3}$$

Since by assumption $n \geq 0$, necessarily $D \leq 0$. In other words, the usual D^+-dimensional Gaussian integral itself is a projection for D^-. This fact leads us to the realization that we are in fact dealing with a fermionic object. Indeed, Dunne and Halliday [3] have shown the amazing property that the above q-(bosonic)-integral in D^- dimensions corresponds to a θ-(fermionic)-integral in D^+ dimensions. This correspondence between the Grassmannian D^+-dimensional integral and the bosonic D^--dimensional integral guarantees the property of translation invariance of the latter. Of course, direct proof of this translational invariance is possible and proven in D^- dimensions, though somewhat tedious to do [1,2].

*e-mail: suzuki@axp.ift.unesp.br

The last equation enables us to define what we call the negative dimensional integral representation for the discrete Kronecker's delta,

$$\delta_{\alpha+\beta,0} = \frac{(-1)^{-\alpha}}{\pi^{-\beta}\Gamma(\alpha+1)} \int d^{2\beta}q\,(q^2)^{\alpha} \tag{4}$$

in analogy to the well-known result from the theory of distributions that defines the continuous Dirac delta "function" in terms of an integral representation of the type

$$\delta(r-r') = \frac{1}{(2\pi)^D} \int d^D k\, e^{ik\cdot(r-r')} \tag{5}$$

where k and r are (positive) D-dimensional vectorial objects.

2 SUM THEOREMS AND OTHER APLICATIONS

An interesting application can be thought of for NDIM, and this has to do with an original way of proving sum theorems for hypergeometric series. Consider for instance the following hypergeometric function

$${}_2F_1(-m,b;c;1) = \sum_{n=0}^{\infty} \frac{(-m)_n (b)_n}{(c)_n\, n!} \tag{6}$$

where m is a positive integer. Note that since $(-m)_n \equiv 0$ for $n > m$, the sum is in fact a truncated sum.

Using the negative dimensional representation for the Kronecker's delta the above sum can be readily performed, yielding [4]

$${}_2F_1(-m,b;c;1) = \frac{(c-b)_m}{(c)_m} \tag{7}$$

which is the standard result for the Vandermonde's theorem. [5][1]

In a similar manner, we can get the Saalschutz [6] theorem for the sum of truncated Saalschutzian hypergeometric series ${}_3F_2(a,b,c;d,e;1)$[2]. As before, being truncated, means that at least one of the numerator parameters (a,b,c) is negative. In order to get this theorem, we restrict ourselves to the case where two of these are negative, so that we introduce two negative dimensional integral counterpart for the two Kronecker deltas. Then, supposing $a < 0$, $c > b$, we have [4]

$${}_3F_2(-m,a,b;c,1+a+b-c-m;1) = \frac{(c-a)_n\,(c-b)_n}{(c)_n\,(c-a-b)_n} \tag{8}$$

A further novel application in this line has to do with the proof for the fundamental relations among the ${}_3F_2$'s. As an example, let us consider the following ${}_3F_2(a,b,c;d,e;1)$, with b and c negative integers and $b < c$. As before, for each of the negative integer parameters we associate a negative dimensional integral representation for the Kronecker's delta together with two constrained summations and after some algebraic manipulations, we arrive at

$$\begin{aligned} {}_3F_2(a,b,c;d,e;1) \;=\; & \frac{\Gamma(b-c)\Gamma(d)\Gamma(e)\Gamma(1-a)}{\Gamma(b)\Gamma(d-c)\Gamma(e-c)\Gamma(1+c-a)} \\ & {}_3F_2(c,1+c-d,1+c-e;1+c-a,1+c-b;1) \end{aligned}$$

which is one of the fundamental relations among ${}_3F_2$ with special value for the argument, namely, $z = 1$. One notes that the usual relation has in it two similar terms with b and c interchanged. However, since in our case these parameters are constrained, the second term vanishes and we are left with only one non-vanishing term.

3 ONE-LOOP LIGHT-CONE INTEGRALS

In the covariant case, the basic one-loop integral structure is given by

$$I_{SE}(i,j;p^2) = \int d^D q\,(q^2)^i\,[(q-p)^2]^j \tag{9}$$

[1] A special case for the Gauss summation formula.

[2] A Saalschutzian hypergeometric function is the one in which the paramenters obey the following constraint: d+e = a+b+c+1.

which in NDIM yields

$$I_{SE}(i,j;p^2) = (-\pi)^{D/2}(p^2)^{\sigma}\frac{(1+\sigma)_{-2\sigma-D/2}}{(1+i)_{-\sigma}(1+j)_{-\sigma}} \tag{10}$$

where we have defined the caracteristic power $\sigma \equiv i+j+D/2$ and the Pochhammer's symbols

$$(a)_n \equiv \frac{\Gamma(a+n)}{\Gamma(a)} \tag{11}$$

One notes that the usual Feynman integral ensues from the above integral when we analytic continue it to positive D and negative values of i and j.

However, for the light-cone gauge, it is well-known that Feynman integrals in such a gauge are notoriously more complex to evaluate than in the covariant case. We shall explore two different approaches: (i) In the first case, we shall consider a theory where we have a one-degree violation of covariance (one external light-like vector, $n^2 = 0$); (ii) whereas in the second case, we introduce a two-degree violation of covariance (two light-like vectors, $n^2 = n^{*2} = 0$).

For the former case, the typical one-loop structure is given by

$$I_1(i,j,\mu;p,n) = \int d^Dq\,(q^2)^i\,[(q-p)^2]^j\,(q\cdot n)^{\mu} \tag{12}$$

which yields in NDIM,

$$I_1(i,j,\mu;p,n) = (-\pi)^{D/2}(p^2)^{\sigma}(p\cdot n)^{\mu}\frac{(1-i-\mu-D/2)_{-j-D/2}}{(1+i)_{j+D/2}(1+j)_{-2j-D/2}} \tag{13}$$

In analytic continuing this result, we have two cases to consider, namely, the cases $\mu > 0$ and $\mu < 0$. In both cases, analytic continuation yields the usual PV results.

For the latter case, we consider only the tadpole-like integral

$$I_2(i,\mu,\nu;p,n,n^*) = \int d^Dq\,[(q-p)^2]^j\,(q\cdot n)^{\mu}\,(q\cdot n^*)^{\nu} \tag{14}$$

which yields in NDIM,

$$I_2(j,\mu,\nu;p,n,n^*) = \pi^{D/2}\left(\frac{-2p\cdot np\cdot n^*}{n\cdot n^*}\right)^{j+D/2}\Omega(j,\mu,\nu;p,n,n^*) \tag{15}$$

where we have defined

$$\Omega(j,\mu,\nu;p,n,n^*) \equiv \frac{(p\cdot n)^{\mu}(p\cdot n^*)^{\nu}}{(1+j)_{-2j-D/2}(1+\mu)_{j+D/2}(1+\nu)_{j+D/2}} \tag{16}$$

Here, one peculiarity is that the exponent $\nu \geq 0$ *always*. This means that the Pochhammer's symbol containing it, i.e., $(1+\nu)_{j+D/2}$ must *never* be analytic continued. The other Pocchhammer's symbol, namely $(1+\mu)_{j+D/2}$, is to be analytic continued or not according to whether $\mu < 0$ or $\mu > 0$ respectively. Bearing in mind these restrictions, analytic continuation of the above result yields the causal results from the ML prescription in the light-cone gauge [7]. This is really quite an amazing result, since no prescription has been called upon to deal with the so-called "unphysical" singularities characteristic of the algebraic gauges. The only outstanding property of translational invariance displayed by the negative dimensional integrals seems to take care of the causality principle required by the *ad hoc* prescriptions devised to treat positive dimensional light-cone integrals.

4 REFERENCES:

[1] I.G.Halliday, and R.M.Ricotta, *Phys. Lett. B193* (1987) 241

[2] R.M.Ricotta, *J.J.Giambiagi Festschrift*, ed. by H.Falomir et al., World Scientific, Singapura, 1990

[3] G.V.Dunne, and I.G.Halliday, *Phys. Lett.* **B193** (1987) 247
[4] "Uma Prova Original para os Teoremas de Vandermonde e de Saalchutz", in the Proceedings of the XV Encontro Nacional de Física de Partículas e Campos, Caxambu, MG (1994) 276
[5] C.F.Gauss, *Ges. Werke* **3** (1866) 123, 207
[6] L.Saalschutz, *Zeitschrift fur Math. u. Phys.* **35** (1890) 186
[7] A.T.Suzuki, *Modern Phys. Lett. A* **8** (1993) 2365

O formalismo Batalin-Tyutin na quantização dos Skyrmions

Jorge Ananias Neto*e Wilson Oliveira†
Departamento de Física, ICE
Universidade Federal de Juiz de Fora, 36036-330
Juiz de Fora, MG, Brazil

Received March, 1996

Aplicamos o formalismo Batalin-Tyutin, que converte os vínculos de segunda classe em primeira, na quantização dos modos rotacionais dos Skyrmions. Calculamos o Hamiltoniano estendido e o gerador funcional no gauge unitário onde reobtemos o Lagrangiano original. Discutimos o espectro da teoria estendida, onde observamos um termo extra no Hamiltoniano quântico usual.

Devido ao vínculo ser do tipo tri-esfera, a quantização dos Skyrmions apresenta relações não triviais nos parenteses de Dirac que levam a problemas de ordenamento na definição do operador momento[1]. Neste trabalho vamos aplicar o formalismo Batalin-Tyutin[2] com o objetivo de contornar esta ambiguidade. O método consiste em transformar os vínculos de segunda classe em primeira através da extensão do espaço de fase com novas variáveis.

A expanção do Lagrangiano do modelo de Skyrme em coordenadas coletivas[1] é dada por

$$L = -M + \lambda Tr[\partial_0 A \partial_0 A^{-1}] = -M + 2\lambda \dot{a}^i \dot{a}^i, \quad i = 0, 1, 2, 3\,, \tag{1}$$

onde as expressões de M e λ podem ser encontradas na referência[1]. A é uma matriz SU(2) a qual pode ser expandida como $A = a^0 + a.\tau$. O vínculo primário é

$$T_1 = a^i a^i - 1 \approx 0. \tag{2}$$

Introduzindo o momento conjugado

$$\pi^i = \frac{\partial L}{\partial \dot{a}_i} = 4\lambda \dot{a}^i, \tag{3}$$

podemos reescrever Hamiltoniano na forma

$$H_c = \pi^i \dot{a}^i - L = 4\lambda \dot{a}^i \dot{a}^i - L = M + 2\lambda \dot{a}^i \dot{a}^i = M + \frac{1}{8\lambda} \sum_i \pi^{i\,2}. \tag{4}$$

Então, a quantização usual é feita substituindo π^i por $-i\partial/\partial a_i$ em (4), com os autovalores dado por

$$E = M + \frac{1}{8\lambda} l(l+2), \quad l = 1, 2, \ldots\,. \tag{5}$$

Usando o procedimento usual de Dirac, achamos o vínculo de segunda classe

$$T_2 = a^i \pi_i \approx 0, \tag{6}$$

obtido pela conservação com o Hamiltoniano total

$$H_T = H_c + \lambda_c T_1, \tag{7}$$

onde λ_c é o multiplicador de Lagrange. Nenhum vínculo adicional é gerado pelo procedimento iterativo. Os vínculos T_1 and T_2 são de segunda classes, satisfazendo a algebra de Poisson

*e-mail:jorge@fisica.ufjf.br
†e-mail:wilson@fisica.ufjf.br

$$\Delta_{\alpha\beta} = \{T_\alpha, T_\beta\} = -2\epsilon_{\alpha\beta}a^i a^i,\ \alpha,\beta = 1,2 \tag{8}$$

onde $\epsilon_{\alpha\beta}$ é o tensor antisimétrico. Aplicando o formalismo BT[2], vamos introduzir novas coordenadas b^i para converter os vínculos de segunda classe, T_α, em primeira, com a algebra de Poisson dessas novas coordenadas dada por

$$\{b^\alpha, b^\beta\} = \omega^{\alpha\beta}, \tag{9}$$

onde $\omega^{\alpha,\beta}$ é uma matriz antisimétrica. É possível mostrar que os vínculos de primeira classe, $\tilde{T}_\alpha$, são dados pela relação

$$\tilde{T}\alpha = X_{\alpha\beta}b^\beta, \tag{10}$$

satisfazendo à condição

$$X_{\alpha\mu}\omega^{\mu\nu}X_{\beta\nu} = -\Delta_{\alpha\beta}. \tag{11}$$

Então, os novos vínculos de primeira classe são escritos como

$$\begin{aligned}\tilde{T}_1 &= T_1 + b^1,\\ \tilde{T}_2 &= T_2 - a^i a^i b^2,\end{aligned} \tag{12}$$

na qual são fortemente involutivos, isto é, $\{\tilde{T}_\alpha, \tilde{T}_\beta\} = 0$.

O Hamiltoniano involutivo no espaço de fase estendido é dado por uma série infinita

$$\tilde{H} = H_c + \sum_{n=1}^{\infty} H^{(n)}, \tag{13}$$

onde $H^{(n)}$ é escrito como

$$\tilde{H}^{(n)} = -\frac{1}{n}b^\mu\omega_{\mu\nu}X^{\nu\rho}G_\rho^{(n-1)},\ (n \geq 1). \tag{14}$$

A expressão de $G_\rho^{(n)}$ pode ser obtida na referência [5]. Desenvolvendo a expressão (13) o Hamiltoniano estendido pode ser somado numa forma fechada

$$\tilde{H} = M + \frac{1}{8\lambda}\frac{(a^i a^i)}{a^i a^i + b^1}\pi_j\pi_j - \frac{1}{4\lambda}\frac{(a^i a^i)b^2}{a^i a^i + b^1}a^j\pi_j + \frac{1}{8\lambda}\frac{(a^i a^i)^2(b^2)^2}{a^i a^i + b^1}. \tag{15}$$

Vamos agora calcular o funcional gerador Z, usando o formalismo de Faddeev-Senjanovic[3]. As novas variáveis, b^μ, são identificadas como um par canonicamente conjugado no formalismo Hamiltoniano, $b^1 \to 2\phi, b^2 \to \pi_\phi$. Então a expressão geral do funcional gerador é

$$Z = N\int [d\mu]\exp\{i\int dt(\dot{a}^i\pi_i + \dot{\phi}\pi_\phi - \tilde{H})\}, \tag{16}$$

com a medida $[d\mu]$ dada por

$$[d\mu] = [da^i][d\pi_i][d\phi][d\pi_\phi]\prod_{\alpha,\beta=1}^{2}\delta(\tilde{T}_\alpha)\delta(\chi_\beta)|det\{\tilde{T}_\alpha, \chi_\beta\}|. \tag{17}$$

A condição de fixação de gauge χ_β é escolhida de tal forma que o determinante na medida não se anule. Escolhendo o gauge unitário, $\chi_1 = a^i a^i - 1, \chi_2 = a^i\pi_i$, é possível mostrar[5] que o funcional gerador Z reproduz o Lagrangiano original

$$Z = N\int [da^i]\,\delta(a^i a^i - 1)\exp\{i\int dt(-M + 2\lambda\dot{a}^i a^i)\}. \tag{18}$$

Este resultado indica, sem dúvida nenhuma, a consistência da teoria.

Para obter o espectro da teoria, os vínculos (12) vão ser considerados como equações fortes. Podemos então substituir o par (b^1, b^2) pelas coordenadas coletivas (a_i, π_i) no Hamiltoniano (15). Se π_j descreve o momento de uma particula livre, $\pi_j = -i\frac{\partial}{\partial x^j}$, os autovalores da Energia são dados por

$$E = M + \frac{1}{8\lambda}[I(I+2) - 2I] \tag{19}$$

Comparando a expressão (19) com (5), vemos que um termo extra aparece na ultima equação. Cabe aqui ressaltar que resultados semelhantes foram obtidos por outros autores[4], usando procedimentos diferentes. Mais detalhes do formalismo Batalin-Tyutin aplicado aos Skyrmions podem ser encontrados na referência[5].

Referências

1.Jorge Ananias Neto, J.Phys.G21 (1995) 695.
2.N.Banerjee, S.Ghosh and R.Banerjee, Nucl.Phys.B417 (1994) 257.
R.Amorim and J.Barcelos-Neto, BFT Quantization of chiral- boson theories, Preprint UFRJ-IF-FPL-013/95.
3.L.D.Faddeev, Theor.Math.Phys.1 (1970) 1.
P.Senjanovich, Ann.Phys.(N.Y.) 100 (1976) 277.
4.K.Fujii, K.I.Sato, N.Toyota and A.P.Kobushkin,
Phys.Rev.Lett. 58,7 (1987) 651. H. Verschelde, Phys.Lett.B215 (1988) 444.
5.The Batalin-Tyutin Formalism on the Collective Coordinates Quantization of the SU(2) Skyrme Model, Wilson Oliveira and Jorge Ananias Neto, Preprint UFJF 1995.

Geometrização da Teoria de Gauge Clássica

Marcos Jardim*
Universidade Estadual de Campinas
Inst. de Matemática, Estatística e Ciência da Computação
*Departamento de Matemática, e-mail:*jardim@ime.unicamp.br

Received March, 1996

Introdução. Nos últimos vinte anos um grande número de trabalhos surgiu explorando a interação entre geometria e topologia e teoria de campos clássica e quântica, impulsionando avanços tanto em física como em matemática. O presente trabalho preocupa-se com os aspectos clássicos desta interação.

Começamos por apresentar o cenário matemático em que teorias de campo de *gauge* são bem definidas, assim como os objetos matemáticos apropriados. Mostramos como expressar lagrangeanas geometricamente e obter as respectivas equações de movimento via método variacional.

Focamos em especial as equações de campo de Yang-Mills e suas versões acopladas com a matéria (Yang-Mills-Higgs e Yang-Mills Dirac) e com o campo gravitacional (Einstein-Yang-Mills). Soluções para estas equações possuem uma estrutura geométrica e topológica bastante rica e fornecem subsídios para o entendimento de certos fenômenos físicos interessantes.

Cenário Matemático. Para modelar o espaço-tempo, usamos uma variedade diferenciável **M** compacta, conexa, orientável de dimensão 4, provido de uma métrica g. Seja P um fibrado principal sobre **M** com grupo estrutural SU(n).

Uma conexão ω é interpretada como sendo o *potencial de gauge* e a respectiva curvatura $\Omega = d\omega + \omega \wedge \omega$ é interpretada como sendo o *campo de gauge*. Uma mudança de *gauge* corresponde a uma mudança de parametrização de **M**. Semi-classicamente, F representa o bóson vetorial responsável por intermediar a interação (fótons, glúons, $W^{+,-}$ e Z^0). Campos de matéria (elétrons, quarks) são representados por secções do fibrado vetorial associado a P:

$$\begin{array}{cc} \text{campo escalar (Higgs)} & \phi : M \to \mathbf{C} \\ \text{campo spinorial (Dirac)} & \psi : M \to \mathbf{C}^4 \end{array}$$

A conexão neste fibrado vetorial representa a interação do campo de *gauge* com a matéria. Note ainda que todos os campos (de calibre e de matéria) encontram-se acoplados com o campo gravitacional representado pela métrica g na variedade base; este acoplamento pode ou não ser levado em conta, dependendo-se de se desejar ou não considerar a gravidade.

Sobre o cenário matemático apresentado acima, veja [3] e [4].

Yang-Mills. A ação da teoria de Yang-Mills descrevendo um bóson vetorial propagando livremente no espaço-tempo **M** é dada por:

$$\mathcal{L}_{YM}[\omega] = \int_M \Omega \wedge *\Omega$$

Tomando uma variação sobre a conexão $\omega_t = \omega + t\alpha$ obtem-se as equações de campo de Yang-Mills:

$$\frac{d}{dt}\mathcal{L}_{YM}[\omega_t]\Big|_{t=0} = 0 \Rightarrow D^*\Omega = 0 \qquad (1)$$

O acoplamento com o campo gravitacional está embutido no operador estrela de Hodge $*$ e não foi levado em consideração.

*Mantido por uma bolsa do CNPQ

Atiyah [1] e outros mostraram que todas as soluções desta equação módulo invariância de *gauge*, chamadas *instantons*, são auto-duais ($\Omega = *\Omega$) e formam uma variedade diferenciável cuja dimensão depende do grupo estrutural e da topologia da base; trabalhando sobre este espaço de configuração dos campos de *gauge*, Donaldson [7] demonstrou um resultado de classificação de 4-variedades (modelos do espaço-tempo).

Yang-Mills-Higgs. A ação agora é dada por:

$$\mathcal{L}_{YMH}[\omega,\phi] = \int_M \Omega \wedge *\Omega + (\nabla\phi, \nabla\phi) - m^2 (\phi,\phi)$$

representando o acoplamento do campo de calibre com um campo escalar ϕ; a métrica está escondida no produto interno hermitiano $<,>$. Um termo de auto-acoplamento do campo escalar $\lambda(\phi,\phi)$ também pode ser adicionado, inserindo uma não-linearidade na propagação do campo de Higgs.

Variações na conexão $\omega_t = \omega + t\alpha$ e $\nabla_t = \nabla + t\eta$ e no campo escalar $\phi_t = \phi + s\psi$ levam às equações de movimento

$$\begin{array}{l} \frac{d}{dt}\mathcal{L}_{YM}[\omega_t,\phi_s]\Big|_{t=0} = 0 \quad \Rightarrow \quad D^*\Omega = J \\ \frac{d}{dt}\mathcal{L}_{YM}[\omega_t,\phi_s]\Big|_{s=0} = 0 \quad \Rightarrow \quad \nabla^*\nabla\phi - m^2\phi = 0 \end{array} \tag{2}$$

onde J é a corrente associada ao campo escalar e $\nabla^*\nabla$ é o análogo do laplaciano neste contexto. Propriedades das soluções destas equações são discutidas em [5] e [6].

Yang-Mills-Dirac. Vamos agora acoplar o campo de Yang-Mills com um campo spinorial; a ação deste modelo é:

$$\mathcal{L}_{YMH}[\omega,\psi] = \int_M \Omega \wedge *\Omega + (\psi, \delta\psi) - m(\psi,\psi)$$

onde δ denote o operador de Dirac do fibrado spinorial, responsável pelo acoplamento do campo spinorial com a conexão. Novamente a métrica está inserida no produto interno $<,>$.

Tomando variações na conexão $\omega_t = \omega + t\alpha$ e δ

$$\begin{array}{l} \frac{d}{dt}\mathcal{L}_{YM}[\omega_t,\phi_s]\Big|_{t=0} = 0 \quad \Rightarrow \quad D^*\Omega = J \\ \frac{d}{dt}\mathcal{L}_{YM}[\omega_t,\phi_s]\Big|_{s=0} = 0 \quad \Rightarrow \quad \delta\psi - m\psi = 0 \end{array} \tag{3}$$

onde J é a corrente associada ao campo spinorial. Propriedades das soluções destas equações são discutidas em [6].

Einstein-Yang-Mills. Lembremos primeiramente que a equação de Einstein para o campo gravitacional pode ser obtida por princípio variacional a partir da lagrangeana:

$$\mathcal{L}_E[g] = \int_M k\sqrt{-\det g}\, d^4x$$

onde k é a curvatura escalar associada à métrica g, tomando-se uma variação sobre a métrica $g_t = g + th$:

$$\frac{d}{dt}\mathcal{L}_E[g_t,\phi_s]\Big|_{t=0} = 0 \Rightarrow R_{\mu\nu} - \frac{1}{2}kg_{\mu\nu} = 0$$

Somando-se a lagrangeana de Yang-Mills $\mathcal{L}_{YM}$ com a lagrangeana de Einstein $\mathcal{L}_E$ e tomando-se variações tanto na métrica (levando em conta o acoplamento campo gravitacional-campo de *gauge*) obtemos um par de equações acopladas não-lineares, as equações de Einstein-Yang-Mills:

$$\begin{array}{l} \frac{d}{dt}\mathcal{L}_{EYM}[\omega_t,g_s]\Big|_{t=0} = 0 \quad \Rightarrow \quad D^*\Omega = 0 \\ \frac{d}{dt}\mathcal{L}_{EYM}[\omega_t,g_s]\Big|_{s=0} = 0 \quad \Rightarrow \quad R_{\mu\nu} - \frac{1}{2}kg_{\mu\nu} = T_{\mu\nu} \end{array} \tag{4}$$

onde $T_{\mu\nu} = \Omega_{\mu\alpha}\Omega^{\alpha}_{\mu} + \frac{1}{4}g_{\mu\nu}\Omega_{\alpha\beta}\Omega^{\alpha\beta}$ é o tensor de energia-momento associado ao campo de calibre $\Omega_{\mu\nu}$.

Nem a equação de Einstein nem a equação de Yang-Mills possuem soluções estáticas não-singulares e com simetria esférica em suas versões desacopladas. As equações de Einstein-Maxwell (caso abeliano das equações de Einstein-Yang-Mills) também não possuem este tipo de solução. Entretanto, a não-comutatividade do campo de calibre mais geral faz com que existam soluções deste tipo para o grupo estrutural SU(2) (veja [2]). Tais soluções possuem uma estrutura física bastante rica.

Acoplamento com a matéria. O procedimento para se obter equações de movimento de campos de matéria acoplados à gravidade é análogo ao que utilizamos para obter as equações de Einstein-Yang-Mills.

Tomamos uma lagrangeana que é a soma da lageangeana de Einstein com a lagrangeana do campo de matéria (Higgs ou Dirac). Fazendo variar o campo de matéria, obtemos simplemente a respectiva equação de movimento livre (sem fontes). Mas a variação da métrica resulta na equação de Einstein para o campo gravitacional com um tensor de energia-momento do lado direito; desta maneira, o campo de matéria age como fonte para o campo gravitacional. Como exemplo, tomamos as equações de Einstein-Higgs para o acoplamento da gravidade com um campo escalar, com lagrangeana dada por:

$$\mathcal{L}_{EH}[g,\phi] = \int_M \left(k\sqrt{-\det g} + \langle \nabla\phi, \nabla\phi \rangle - m^2 \langle \phi, \phi \rangle \right) d^4x$$

obtendo as equações :

$$\begin{array}{lll} \frac{d}{dt}\mathcal{L}_{EH}[g_t,\phi_s]\Big|_{t=0} = 0 & \Rightarrow & R_{\mu\nu} - \frac{1}{2}k g_{\mu\nu} = T_{\mu\nu} \\ \frac{d}{dt}\mathcal{L}_{EH}[g_t,\phi_s]\Big|_{s=0} = 0 & \Rightarrow & \nabla^*\nabla\phi - m^2\phi = 0 \end{array} \qquad (5)$$

onde $T_{\mu\nu}$ é o tensor de energia-momento associado ao campo escalar ϕ. Claramente, o procedimento é essencialmente o mesmo para se obter um par de equações para o acoplamento da gravidade com um campo spinorial; seria ainda possível escrever três equações acopladas para o campo gravitacional interagindo com um campo de calibre e um campo de matéria, os dois últimos também interagentes.

References

[1] M. Atiyah. *Geometry of Yang-Mills fields.* Lezione Fermiane. Pisa: Accademia Nazionali dei Lincei, Scuola Normale Superiore (1979).

[2] Bartnik & McKinnon. Particle-like solutions to the Einstein- Yang-Mills equations. *Phys. Rev Lett.* 61(2) p.141 (1988).

[3] D. Bleecker. *Gauge theory and variational principle.* Reading: Addison-Wesley (1981).

[4] A. Derdzinski. *Geometry of the Standard Model of particles.* New York: Springer-Verlag (1992).

[5] A. Jaffe & C. Taubes. *Vortices and Monopoles.* Boston: Birkhäuser (1980).

[6] T. Parker. Gauge theories in four dimensional riemannian manifolds. *Commun. Math. Phys.* 85(4) p.563-602 (1982).

[7] S. Donaldson & P. Kronheimer, *Geometry of four manifolds.* Oxford: University Press (1990).

Geração Dinâmica de Massa no Modelo Gross-Neveu

V. S. Alves†, M. Gomes†, A. J. da Silva† e L. C. Malacarne‡
†*Universidade de São Paulo, Dep. de Física-Matemática, Instituto de Física*
Caixa Postal 20516 - CEP 01452-900 São Paulo-SP, Brasil
‡*Universidade Estadual de Maringá, Paraná - PR, Brasil*

July 31, 1996

O trabalho consiste no estudo sobre a possibilidade de geração dinâmica de massa no modelo de Gross-Neveu na expansão $1/N$ em $(2+1)D$, através da análise das equações de Schwinger-Dyson (SD). Analisamos as equações de SD para o propagador completo do férmion, e estudamos dois regimes distintos: para $\underline{N}$ grande, obtivemos uma solução de massa constante, gerada dinamicamente, que quebra a simetria de paridade quando usamos férmions de duas componentes, já encontrada na literatura [1]; por outro lado, para $\underline{N}$ pequeno, a única possibilidade compatível com as equações de SD corresponde a situação onde metade dos férmions adquirem uma massa positiva e outra metade uma massa igual e negativa sem quebra de paridade. Foi encontrada uma solução a qual todavia, somente seria realizável para $N < 1.5$, o que não é fisicamente aceitável. A conclusão é portanto que no modelo Gross-Neveu a geração dinâmica de massa só é possível com a quebra de paridade, para N grande.

1 Apresentação do Modelo

O modelo Gross-Neveu massivo, com N campos fermiônicos é dado pela seguinte densidade de Lagrangiana,

$$\mathcal{L} = \bar{\psi}(i\gamma^\mu \partial_\mu - M)\psi - \frac{1}{2N} g(\bar{\psi}\psi)^2 \quad . \tag{1}$$

O campo fermiônico ψ (e também $\bar{\psi}$) carrega dois índices: ψ^a_α, $\underline{a}$ é o índice de simetria interna ($U(N)$, $a = 1, 2, ..., N$) e $\underline{\alpha}$ é o índice de Lorentz.

Podemos reescrever (1), equivalentemente, da seguinte forma,

$$\mathcal{L} = \bar{\psi}(i\partial\!\!\!/ - M - \frac{\sigma}{\sqrt{N}})\psi + \frac{1}{2g}\sigma^2 \quad . \tag{2}$$

onde $\sigma = \frac{g}{\sqrt{N}}\bar{\psi}\psi$, é um campo auxiliar.

2 Quebra de Paridade

As equações de SD são dadas pela figura 1. Os propagadores representados por linhas simples, contínua e tracejada, são os propagadores do férmion e do campo σ, respectivamente. Os propagadores representados por linhas cheias são os propagadores completos, com as inserções de auto-energia, como mostrado na figura 2.

Na ordem dominante em $1/N$, a função de vértice é dada pela contribuição trivial $(\frac{-i}{\sqrt{N}})_{\alpha\beta}\delta_{ab}$. Desta forma as equações de SD relevantes se reduzem as parcelas de auto-energia do férmion e do campo σ, como mostradas na figura 3.

As expressões analíticas das figuras 3 são ,

$$(-i\Xi(p))_{\alpha\beta}\delta_{ad} = -\frac{1}{N}\int \frac{d^3k}{(2\pi)^3}\Delta_\sigma(p-k)\,(S(k))_{\alpha\beta}\delta_{ad} +$$

$$+ (1)_{\alpha\beta}\delta_{ad}\Delta_\sigma(q=0)tr\int\frac{d^3k}{(2\pi)^3}S(k) \ , \tag{3}$$

e

$$i\Pi(p) = tr\int\frac{d^3k}{(2\pi)^3}(S(p+k)\,S(k) \ , \tag{4}$$

onde a operação de traço nas expressões acima são sobre os índices de Lorentz e S representa o propagador completo do férmion.

Usando as propriedades da operação de traço das matrizes de Dirac e alguns truques, encontra-se que $\Pi(p) = -\frac{D}{2\pi}G(p,M)$, com $G(p,M) = \frac{|M|}{2} + \frac{(4M^2-p^2)}{4\sqrt{p^2}}ArcSinh(\frac{\sqrt{p^2}}{\sqrt{4M^2-p^2}})$.

Deste modo, o propagador completo do campo σ se escreve como,

$$\Delta_\sigma = \frac{i}{1/g + \Pi(p)} = \frac{2i\pi/D}{\frac{2\pi}{Dg} - G(p,0)} = \frac{16i/D}{i|p| + \frac{16}{Dg}} \ , \tag{5}$$

onde D é a dimensionalidade das matrizes de Dirac.

Escrevemos a auto-energia do férmion como $\Xi(p) = -\not{p}A(p) + \Sigma(p)$, onde $A(p)$ é a renormalização da função de onda dos férmions e $\Sigma(p)$ a função de massa que queremos encontrar. Como o propagador cheio do férmion pode ser escrito como $S^{-1}(p) = S_0^{-1}(p) + i\Sigma(p)$, temos que $S(p) = i\frac{\not{p}(1+A(p))+\Sigma(p)}{p^2(1+A(p))^2-\Sigma^2(p)}$, e após alguns cálculos chega-se a,

$$\Sigma(p) = \frac{1}{N}\int\frac{d^3k}{(2\pi)^3}\frac{\Delta_\sigma(p-k)\Sigma(k)}{k^2(1+A(k))^2-\Sigma^2(k)} - D\Delta_\sigma(q=0)\int\frac{d^3k}{(2\pi)^3}\frac{\Sigma(k)}{k^2(1+A(k))^2-\Sigma^2(k)} \ . \tag{6}$$

Para o regime de N grande, vemos de (6), que em termos de potências de $\frac{1}{N}$, a primeira parcela da expressão é sub-dominante em relação à segunda. Podemos então desprezá-la em relação à segunda. Se considerarmos ainda uma situação onde $A(k) = 0$ e $\Sigma(p) = M = cte$, então $M = -D\Delta_\sigma(q=0)\int\frac{d^3k}{(2\pi)^3}\frac{M}{k^2-M^2}$, que é a mesma expressão obtida por M. Gomes, V. O. Rivelles e A. J. da Silva [1], para a equação de "gap" do modelo Gross-Neveu em $3D$ (na expansão $1/N$). Tal como discutido pelos autores acima, a expressão acima fixa g como uma função da massa gerada. Conclui-se portanto que no regime de N grande há geração dinâmica de massa para o campo ψ e por consequência disto há uma quebra de paridade para a representação de férmions de duas componentes.

Para o regime de N pequeno, vamos buscar soluções para a massa gerada dinamicamente com as seguintes condições : $A(k) = 0$ e $\Sigma_i(p) = \Sigma(p)$, para $i = 1, 2, ..., L$ e $\Sigma_i(p) = -\Sigma(p)$, para $i = L+1, L+2, ..., N$. Utilizando (6) encontramos as seguintes expressões para $i = 1, 2, ..., L$ e $i = L+1, L+2, ..., N$, respectivamente

$$\Sigma(p) = \frac{1}{N}\int\frac{d^3k}{(2\pi)^3}\frac{\Delta_\sigma(p-k)\Sigma(k)}{k^2-\Sigma^2(k)} - \frac{D}{N}(2L-N)\Delta_\sigma(q=0)\int\frac{d^3k}{(2\pi)^3}\frac{\Sigma(k)}{k^2-\Sigma^2(k)} \ , \tag{7}$$

e

$$\Sigma(p) = \frac{1}{N}\int\frac{d^3k}{(2\pi)^3}\frac{\Delta_\sigma(p-k)\Sigma(k)}{k^2-\Sigma^2(k)} + \frac{D}{N}(2L-N)\Delta_\sigma(q=0)\int\frac{d^3k}{(2\pi)^3}\frac{\Sigma(k)}{k^2-\Sigma^2(k)} \ . \tag{8}$$

Observando as duas equações acima notamos que elas são inconsistentes, a não ser no caso em que $L = \frac{N}{2}$, ou seja, metade dos férmions adquirem uma massa positiva e a outra metade uma massa igual e negativa. Com isto em mente, vamos dar prosseguimento à análise da equação (8) (ou (9)), sobre a possibilidade de geração de massa. Vamos, por comodidade, trabalhar com a expressão (8) no espaço euclidiano. Deste modo,

$$\Sigma(p) = \frac{16}{DN}\int\frac{d^3k}{(2\pi)^3}\frac{\Sigma(k)}{k^2+\Sigma^2(k)}\frac{1}{|p-k|+\frac{16}{Dg}} \ . \tag{9}$$

A equação integral acima não é fácil de ser tratada. Devemos tentar fazer uma simplificação . Introduzimos inicialmente um parâmetro de escala[1] $\alpha = \frac{16}{Dg}$, e consideramos apenas a região onde $p << \alpha$ (qualquer massa não nula que poderá ser gerada será muito menor que esse "cut-off". Assim, a geração dinâmica de massa nessa situação , se ocorrer, será um fenômeno de pequenos momentos). O estudo analítico da equação acima é facilitada se separarmos a integração em k em duas regiões, e o resultado fornece, após fazermos a integração nos angulos,

[1] Este "cut-off",é um parâmetro de massa natural da teoria.

$$\Sigma(p) = \frac{8}{DN\pi^2}\left\{\int_0^p dk\,\frac{k^2\Sigma(k)}{k^2+\Sigma^2(k)}\,\frac{1}{p+\alpha} + \int_p^\alpha dk\,\frac{k^2\Sigma(k)}{k^2+\Sigma^2(k)}\,\frac{1}{k+\alpha}\right\}\ , \tag{10}$$

com $2\alpha\frac{d\Sigma(p)}{dp}\Big|_{p=\alpha} + \Sigma(p)|_{p=\alpha} = 0$, e $0 < \Sigma(p)|_{p=0} < \infty$, que representam as condições de contorno ultra-violeta (U.V) e infra-vermelha (I.V), respectivamente, a qual $\Sigma(p)$ deve satisfazer. Se impusermos que $\alpha >> \Sigma(p)$, haverá uma região $p >> \Sigma(p)$ pertencente ao intervalo $0 \leq p < \alpha$ na qual (10) poderá ser linearizada, ou seja,

$$\frac{d}{dp}\left[(p+\alpha)^2\frac{d\Sigma(p)}{dp}\right] = -\frac{8}{DN\pi^2}\Sigma(p)\ . \tag{11}$$

Nesse regime linear, a equação acima é uma equação diferencial que admite a seguinte solução , $\Sigma(p) = A_1(p+\alpha)^{a_+} + A_2(p+\alpha)^{a_-}$, onde $a_\pm = -\frac{1}{2} \pm \frac{1}{2}\sqrt{1-\frac{N}{N_c}}$, com $N_c = \frac{32}{D\pi^2}$.

Devemos analisar duas situações distintas. Para $N > N_c$, a é real, o que implica em termos a seguinte solução $\Sigma(p) \sim \frac{1}{\sqrt{p+\alpha}}\,(p+\alpha)^{\pm\frac{1}{2}(1-\frac{N}{N_c})^{\frac{1}{2}}} = (p+\alpha)^{\frac{\pm\lambda-1}{2}}$, com $0 < \lambda < 1$. A solução para a potência negativa em λ não satisfaz a condição de contorno I.V, enquanto que para a potência positiva esse comportamento não é compatível com a condição de contorno U.V, e portanto apenas $\Sigma(p) = 0$ é solução . Por outro lado, para $N < N_c$, a é complexo e admite a seguinte solução oscilatória,

$$\Sigma(p) = \frac{1}{\sqrt{p+\alpha}}Sen\left(\frac{1}{2}\sqrt{\frac{32}{DN\pi^2}-1}\;Ln\left[\frac{p+\alpha}{\Sigma(0)}\right]+\delta\right)\ , \tag{12}$$

onde δ é uma fase e $\Sigma(0)$ é um fator de escala logaritimico. Vemos da expressão acima que no caso de N ser menor que o valor crítico (< 1.5) haverá geração de massa para os férmions, sem no entanto haver quebra de paridade neste caso.

Entretanto, esta solução não reflete uma situação física aceitável pois N (ou L) deve ser um número inteiro[2], e a solução encontrada nos leva a termos $L = \frac{1}{2}$. Podemos dizer então que o modelo Gross-Neveu no regime de N pequeno, com a hipótese de que metade dos férmions adquirem uma massa positiva e a outra metade uma massa igual e negativa, não gera dinamicamente massa para o campo fermiônico.

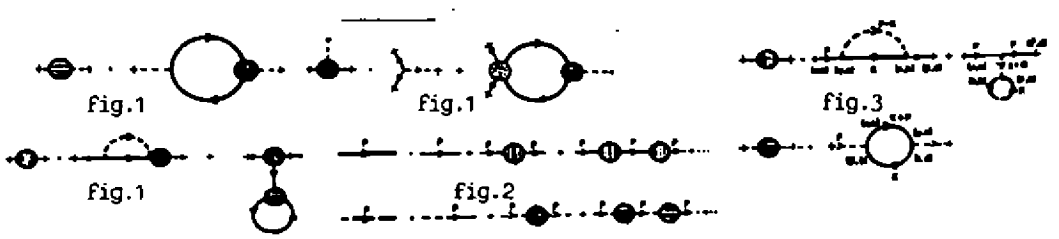

References

[1] Dynamical parity violation and the Chern-Simons term - M. Gomes, V. O. Rivelles, and A. J. da Silva; Phys. Rev.**D41**, 1363, (1990);

[2] Spontaneous breaking of parity in $(2+1)$- dimensional QED - Thomas Appelquist, Mark J. Bowick, Dimitra Konabali, and L. C. R. Wije - wardhana; Phys. Rev. **D33**, 3774, (1986);

[3] Quebra dinâmica de paridade e anomalia de spin em $(2+1)$ dimensões - M. Gomes, V. O. Rivelles, and A. J. da Silva; Preprint do Instituto de Física da USP - Departamento de Física-Matemá tica;

[4] Gauge structure, anomalies, and mass generation in a three-dimensional Thirring model - M. Gomes, R. S. Mendes, R. F. Ribeiro, and A. J. da Silva; Phys. Rev.**D43**, (1991);

[5] M. O. C. Gomes, *Apostila do Curso de Introdução à Teoria Quântica de Campos I e II*, IFUSP, (1993);

[6] On Quantum Field Theorie in Odd Dimensional Spaces - M. Gomes; Preprint do Instituto de Física da USP - Departamento de Física-Matemática.

[2] N representa o número de campos de Dirac.

Explicit connection between conformal field theory and 2+1 Chern-Simons theory

D. C. Cabra* and G. L. Rossini*
Departamento de Física, Universidad Nacional de La Plata
C.C. 67, (1900) La Plata, Argentina

Received March, 1996

We give explicit field theoretical representations for the observables in the transverse lattice version of 2+1 dimensional Chern-Simons theory in terms of gauge invariant composites of 2D WZW fields. Wilson loop correlators are evaluated in the path integral framework using decoupling techniques, thus confirming previous results.

Since the pionnering work of Witten [1], the connection between 1+1 conformal field theory and 2+1 Chern-Simons (CS) theory has been extensively studied [2]. In a recent work [3] a new version of this connection has been presented. In fact, using the so-called transverse lattice construction [4] it was shown that the use of left-right asymmetric G_k gauged Wess-Zumino-Witten (WZW) action for the link fields leads to a group G pure CS theory in the continuum limit. Using this approach, Wilson loop correlators were evaluated in the lattice version by using representation theory of chiral algebras.

Following this route we give in the present note explicit operator realizations of the Wilson loop operators in terms of gauge invariant composites of two dimensional gauged WZW fields. Using decoupling techniques in the path integral framework, we show how to factorize both the partition function of the system and the observables. To test our construction we evaluate Wilson loop correlators. Our results are in agreement with those presented in ref.[1] (and reobtained in ref.[3]).

For the sake of clarity we first review the transverse lattice construction [3] and then present our approach. The transverse lattice geometry consists of a 2D manifold, which is taken as a Minkowski space M_2, and a transverse discrete dimension, which is taken as a periodic chain of N sites (S_1 topology). One introduces a link field [1] $g_n(x^+, x^-)$ governed by a level k WZW action [5]

$$kW[g_n] = \frac{k}{8\pi}\int_{M_2} d^2x Tr(\partial_\mu g_n \partial^\mu g_n^{-1}) + k\Gamma[g_n] \tag{1}$$

where g_n takes values in a simple Lie group G and $\Gamma[g_n]$ is the Wess-Zumino term

$$\Gamma[g] = \frac{1}{12\pi}\int_Y d^3y \epsilon^{ijk} Tr(g^{-1}\partial_i g g^{-1}\partial_j g g^{-1}\partial_k g) \tag{2}$$

with $\partial Y = M_2$. The coupling between two-dimensional layers is accomplished through gauge fields $A_{\mu,n}$; g_n is left-coupled to $A_{\pm,n}$ and right-coupled to $A_{\pm,n+1}$. The corresponding interaction term in the action is given by [6]

$$I[g_n, A_{\pm,n}, A_{\pm,n+1}] = \frac{k}{2\pi}\int_{M_2} d^2x Tr[A_{-,n+1}g_n^{-1}\partial_+ g_n - A_{+,n}\partial_- g_n g_n^{-1}$$
$$+A_{+,n}g_n A_{-,n+1}g_n^{-1} - \frac{1}{2}(A_{-,n}A_{+,n} + A_{+,n+1}A_{-,n+1})]. \tag{3}$$

The action $S_n = kW[g_n] + I[g_n, A_{\pm,n}, A_{\pm,n+1}]$ is not invariant under gauge transformations. Indeed, the change in the action S_n reads

$$\delta S_n = \frac{k}{2\pi}\int_{M_2} d^2x Tr[\Omega_n \epsilon^{\mu\nu}\partial_\mu A_{\nu,n} - \Omega_{n+1}\epsilon^{\mu\nu}\partial_\mu A_{\nu,n+1}] \tag{4}$$

*CONICET, Argentina

[1] Our conventions for light cone coordinates are $x^\pm = \frac{1}{\sqrt{2}}(x^0 \pm x^1)$.

which is related to the non-Abelian anomaly in two dimensions [7]. Note that in case the coupling was left-right symmetric ($A_{\pm,n} = A_{\pm,n+1}$) the variation would vanish; this would be equivalent to gauging the anomaly free vector subgroup of the left and right global quiral symmetry of the WZW model.

As we explained above, the entire system consists of a periodic chain of 2D layers. Its action is simply given by

$$S = \sum_{n=1}^{N} S_n. \tag{5}$$

This system is gauge invariant because of the cancellation of the second term in (4) with the first term coming from the variation corresponding to the following site. We will refer to this interplay as gauge invariance of the junctions.

In order to make contact with the 2+1 CS theory, we follow ref. [3] and represent the link field g_n as a function on the transverse lattice,

$$g_n = \exp(-\int_{x^3}^{x^3+a} A_3(x^+, x^-, x^3)dx^3). \tag{6}$$

Here a is the spacing of the lattice and $x^3 = na$ will become a continuous coordinate as $a \to 0$, $N \to \infty$, while $Na = L$ remains constant. In this limit the phase exponent in (6) can be written as $-aA_3$, with A_3 evaluated in $x^3 = (n + 1/2)a$. Using this parametrization in eq.(5) one obtains

$$\lim_{\substack{a \to 0 \\ N \to \infty}} S = \frac{k}{2\pi} \int_{M_2 \times S_1} d^3x \epsilon^{ijk} Tr[A_i \partial_j A_k - \frac{2}{3} A_i A_j A_k] \equiv S_{CS}, \tag{7}$$

which corresponds to the level k CS action for the gauge group G.

Once the connection (7) between classical actions is established, one is naturally led to study the quantization of both theories and the relation between their observables. This study has been performed in ref.[3] in the framework of canonical quantization, using the representation theory of the Virasoro algebra for the 1+1-dimensional layers and then solving the constraints arising from gauge invariance of S in eq.(5). In this way, the correspondence between the physical states of the lattice CS theory and some Wilson loops of the continuum CS theory has been proved. In our investigation, we shall instead work in the path-integral approach using decoupling techniques [6, 8]. This will allow us to construct explicit operator expressions for Wilson loops in the lattice CS theory.

We start from the partition function of the lattice CS theory

$$\mathcal{Z} = \int \prod_{n=1}^{N} \mathcal{D}A_{\mu,n} \mathcal{D}g_n e^{iS} \tag{8}$$

with S given by eq.(5) and perform the (decoupling) change of variables

$$\begin{aligned} A_{+,n} &= f_n^{-1} \partial_+ f_n, \\ A_{-,n} &= h_n^{-1} \partial_- h_n, \\ g_n &= f_n^{-1} g_n^{(0)} h_{n+1}. \end{aligned} \tag{9}$$

After this change the action S takes the form

$$S = \sum_{n=1}^{N} (kW[g_n^{(0)}] - kW[f_n h_n^{-1}]), \tag{10}$$

where the Polyakov-Wiegmann identity has been used [9].

Taking into account the Jacobians and fixing the gauge, (we also change $f_n \to \tilde{f}_n = f_n h_n^{-1}$ (with unit Jacobian)), we obtain the decoupled partition function

$$\mathcal{Z} = \mathcal{Z}_{gh} \int \prod_{n=1}^{N} \mathcal{D}g_n^{(0)} e^{ikW[g_n^{(0)}]} \int \prod_{n=1}^{N} \mathcal{D}\tilde{f}_n e^{-i(2C_v+k)W[\tilde{f}_n]}. \tag{11}$$

For each site n one has a conformal field theory with vanishing total central charge, built up from the different sectors: a ghost sector, a level k WZW sector and a negative level WZW sector. Notice that, although the partition

function of the theory is completely decoupled, BRST quantization condition connects the different sectors in order to ensure unitarity [8, 10].

We will now show that the lattice version observables naturally lead to Wilson loop operators in the continuum CS limit.

The observables in the lattice are constructed from gauge invariant composites of WZW fields, which in turn belong to integrable representations of the group G. In order to keep a simple notation we will discuss the specific example of $SU(2)_k$, although the extension to $SU(N)_k$ and more general groups is straightforward. The integrable representations of $SU(2)_k$ are characterized by the spin $j = 0, 1/2, \ldots, k/2$ [11].

We consider

$$R_j(x^+, x^-) = Tr_j \prod_{n=1}^{N} g_n^{(j)}(x^+, x^-) \tag{12}$$

where Tr_j means matrix trace in the representation of spin j.

To see the connection of these fields with Wilson loop operators one has to use eq.(6) (now in the representation j) obtaining

$$R_j(x^+, x^-) = Tr_j \prod_{n=1}^{N} e^{-aA_3(x^+, x^-, na+a/2)} \tag{13}$$

which in the continuum limit gives

$$R_j(x^+, x^-) \longrightarrow_{a\to 0} Tr_j P(e^{-\int_C dx^\mu A_\mu}). \tag{14}$$

This is the expression for Wilson loop operators winding once around a circle C passing through (x^+, x^-) in each layer and carrying flux in the representation j.

The identification (14) is also valid at the quantum level. We checked this statement by evaluating up to three point correlators using the decoupled picture (11). In this picture the fields in eq.(12) can be written in terms of the decoupled variables $g_n^{(0)}$, $\tilde{f}_n$ as

$$R_j(x^+, x^-) = Tr_j \prod_{n=1}^{N} (\tilde{f}_n^{(j)})^{-1}(x^+, x^-) g_n^{(0)(j)}(x^+, x^-). \tag{15}$$

Thus, correlators involving R_j's factorize in the level k and level $-(k+4)$ WZW sectors.

The conformal dimensions of the primary fields in a level K $SU(2)$ WZW theory are given by $C_j/(K + C_v)$, where $C_j = j(j+1)$ is the Casimir in the spin j representation and the adjoint Casimir is $C_v = 2$. For the fields $g_n^{(0)(j)}$ and $\tilde{f}_n^{(j)}$ we have

$$\begin{aligned} h[g_n^{(0)(j)}] &= \frac{j(j+1)}{k+2} \\ h[\tilde{f}_n^{(j)}] &= -\frac{j(j+1)}{k+2} \end{aligned} \tag{16}$$

and hence the conformal dimension of R_j vanishes. This implies that the correlators are independent of the coordinates [2] (x^+, x^-), this being in correspondence with the topological nature of Wilson loop operators.

The one point correlator vanishes except for the trivial $j = 0$ representation, in which the fields correspond to the identity operator, giving

$$\langle R_j \rangle = \delta_{j0}. \tag{17}$$

For the two point correlator one obtains

$$\langle R_{j_1}(x_1) R_{j_2}(x_2) \rangle = \delta_{j_1 j_2} \tag{18}$$

Finally, for the three point correlator one has

$$\langle R_{j_1}(x_1) R_{j_2}(x_2) R_{j_3}(x_3) \rangle = \delta(j_1, j_2, j_3) \tag{19}$$

where $\delta(j_1, j_2, j_3)$ means 1 in case that j_1, j_2 and j_3 satisfy a triangular condition and 0 otherwise.

[2] This fact is a direct consequence of conformal symmetry for the two and three point correlators. In the four point case the analysis is more involved but coordinate independence can be proved following ref.[12] (see section 3.2).

Our results (17), (18) and (19) coincide with the expectation value of one, two and three unknotted Wilson loops given by Witten [1] in terms of the fusion rules of the symmetry group thus confirming our Ansätze. In summary, we have given an explicit operator realization of the Wilson loop operators (winding once around S_1 and carrying flux in the representation j) in terms of gauge invariant products of WZW fields in the transverse lattice formulation. We have also shown how to decouple the lattice partition function and within this scheme we have explicitly evaluated correlators of up to three unknotted Wilson loops. The results we have obtained are in agreement with those found by Witten in [1].

References

[1] E.Witten, Comm.Math.Phys. **121** (1989) 351.

[2] G.Moore and N.Seiberg, Phys.Lett. **B220** (1989) 422; S.Elitzur, G.Moore, A.Schwimmer and N.Seiberg, Nucl.Phys. **B326** (1989) 108; L.Alvarez-Gaumé, J.M.Labastida and V.Ramallo, talk at the Annecy Meeting commemorating R.Stora's 60th birthday, CERN preprint TH 5799/90; L.F.Cugliandolo, G.L.Rossini and F.A.Schaposnik, Phys.Lett. **B267** (1991) 200.

[3] P.Griffin, Mod.Phys.Lett.**A7** (1992) 601.

[4] W.Bardeen and R.Pearson, Phys.Rev.**D14** (1976) 547; W.Bardeen, R.Pearson and E.Rabinovici, Phys.Rev.**D21** (1980) 1037.

[5] E.Witten, Comm.Math.Phys. **92** (1984) 455.

[6] K.Gawedzki and A.Kupiainen, Nucl.Phys.**B320** (1989) 625; P.Bowcock, Nucl.Phys.**B316** (1989) 80.

[7] A.Polyakov and P.Wiegmann, Phys.Lett.**B131** (1983) 121; R.E.Gamboa Saraví, F.A.Schaposnik and J.E.Solomin, Nucl.Phys.**B185** (1981) 238.

[8] D.Karabali, Q.Park H.Schnitzer and Z.Yang, Phys.Lett.**B216** (1989) 307.

[9] A.Polyakov and P.Wiegmann, Phys.Lett.**B141** (1984) 223.

[10] T.Kugo and I.Ojima, Progr.Theor.Phys **66** (1979) 1.

[11] D.Gepner and E.Witten, Nucl.Phys.**B278** (1986) 493.

[12] S.Naculich and H.J.Schnitzer, Nucl.Phys.**B347** (1990) 687.

[13] V.Knizhnik and A.B.Zamolodchikov, Nucl.Phys.**B247** (1984) 83.

[14] A.B.Zamolodchikov and V.A.Fateev, Sov.Phys.JEPT**62** (1985) 215

[15] E.Verlinde, Nucl.Phys.**B300** (1988) 360.

[16] F.D.Haldane, Z.N.C.Ha, J.C.Talstra, D.Bernard and V.Pasquier, Phys.Rev.Lett**69** (1992) 2021.

[17] D.Bernard, V.Pasquier and D.Serban, Nucl.Phys. **B428** (1994) 612, hept-th/9404050; P.Bouwknegt, A.Ludwig and K.Schoutens, Phys.Lett.**B338** (1994) 448; hep-th/9412108.

Método de Schwinger para o efeito Casimir fermiônico

M. V. Cougo-Pinto, C. Farina e A. Tort
Instituto de Física, Universidade Federal do Rio de Janeiro
CP 68528, Rio de Janeiro, RJ 21945-970, Brasil

Received March, 1996

O efeito Casimir de um campo de Dirac massivo confinado entre duas placas infinitas e paralelas é calculado usando-se um método proposto por Schwinger. A condição de contorno usada é a de corrente nula através das placas, inspirada no confinamento de quarks do modêlo de sacola MIT para hádrons. Usamos o método de regularização de Schwinger, de truncamento no tempo próprio seguido do uso da fórmula de soma de Poisson.

Embora tenha sido originalmente predito[1] e observado[2] no campo eletromagnético, o efeito Casimir é uma propriedade de qualquer campo quântico relativístico. Sua relevância no caso de campos de Dirac é óbvia em qualquer problema envolvendo os campos de matéria, como ocorre, por exemplo, no modelo de sacola MIT para hádrons[3]. Inspirados no confinamento de *quarks* deste modelo usamos a condição de contorno de uma fronteira impermeável aos férmions, aplicada entretanto à geometria mais simples de duas placas paralelas infinitas ladeando o campo. Para um campo, como o de Dirac, que obedece equações diferenciais de primeira ordem, não podemos usar condições de contorno de Dirichlet ou de Neumann, que são as adotadas comumente para o campo eletromagnético e demais campos bosônicos; adotamos então uma que não somente é compatível com a equação de Dirac como também descreve de modo bastante natural a impermeabilidade das placas, qual seja, de corrente de férmions nula através das placas. Se j é a corrente do campo de Dirac e n a normal na fronteira, a restrição descreve-se pela equação: $n_\mu j^\mu = 0$. Esta condição , conhecida como condição de contorno MIT, é implementada impondo-se ao campo de Dirac ψ, na fronteira, a seguinte equação linear: $in_\mu \gamma^\mu \psi = \psi$ [3].

Aqui apresentamos o cálculo da energia de Casimir do campo de Dirac usando o método de Schwinger [4], que é baseado em uma fórmula originalmente proposta para calcular ações efetivas em eletrodinâmica quântica [5]. O poder do método de Schwinger já foi verificado para campos bosônicos nos casos sem massa [4,6] e com massa [7], tanto em temperatura nula quanto em temperatura finita [8], estando já estabelecida sua conexão [9] com o método de soma dos modos de energia do ponto zero. Também no caso em consideração mostramos que o método de Schwinger leva-nos rápida e diretamente à resposta final, o que o torna especialmente útil para investigações teóricas e construções de modelos.

Começamos então pela fórmula de Schwinger para a ação efetiva [4]:

$$W^{(1)}(s_o) = \frac{i}{2}\int_{s_o}^{\infty} \frac{ds}{s}\, Tr\, e^{-isH} \,, \tag{1}$$

na qual H é o hamiltoniano do tempo-próprio s, s_o é o truncamento no tempo-próprio, e Tr é o traço total, funcional e matricial (para o campo de Dirac a falta de um fator 4 será sentida se este último for esquecido). Para obtermos a energia de Casimir $\mathcal{E}$ tomamos a variação da energia do vácuo do estado $|0-\rangle$, anterior à introdução das placas,

para o estado $|0+\rangle$, posterior à introdução das mesmas. Uma vez que ambos os estados são estacionários temos que $\langle 0+|0-\rangle = \exp(-i\mathcal{E}T)$, onde T é o tempo gasto na medição de $\mathcal{E}$. Usando então a equação $\langle 0+|0-\rangle = \exp(i\mathcal{W}^{(1)})$ [4], que define a ação efetiva, obtemos:

$$\mathcal{E} = -\frac{\mathcal{W}^{(1)}}{T} . \tag{2}$$

Consideremos pois o campo massivo livre de Dirac confinado entre duas placas infinitas e perpendiculares ao eixo OZ, uma em $z = 0$ e a outra em $z = a$. Podemos considerar inicialmente que as placas são quadrados grandes, de lado L e depois de calcular a pressão de Casimir tomar o limite $L \to \infty$. Aplicando a condição de contorno MIT a uma solução da equação de Dirac do tipo onda plana de momento p, obtemos para a componente z: $p_z = n\pi/2a$, onde $n \in 2\mathbb{N} - 1$ e $\mathbb{N}$ é o conjunto dos inteiros positivos. Para o caso em consideração $H = (-\partial^2 + m^2)\mathbb{1}$ [5], onde m é a massa do campo de Dirac e $\mathbb{1}$ é a matriz unidade 4 x 4. Com estes dados é fácil obter para o traço:

$$Tr\, e^{-isH} = 4\,\frac{L^2 T}{\sqrt{i(4\pi s)^3}} e^{-ism^2} \sum_{n\in 2\mathbb{N}-1} e^{-is(n\pi/2a)^2} .$$

Este traço pode ser modificado por meio da fórmula de soma de Poisson [10],

$$\sum_{n\in\mathbb{N}} e^{-n^2\pi\tau} = \frac{1}{\sqrt{\tau}} \sum_{n\in\mathbb{N}} e^{-n^2\pi/\tau} + \frac{1}{2\sqrt{\tau}} - \frac{1}{2} ,$$

e ser substituído em (1) para se obter a seguinte expressão para a ação efetiva:

$$\begin{aligned} \mathcal{W}^{(1)}(s_o) &= -T(L^2 a)\frac{m^4}{8\pi^2}\int_{im^2 s_o}^{\infty} ds\, s^{-3} e^{-s} - TL^2 \frac{(m/2\pi)^2}{a\,(am)^2} \times \\ &\times \sum_{n\in\mathbb{N}} \left[2\int_0^{a^2/is_o} ds\, s\, e^{(am)^2 s^{-1} - (2n)^2 s} - \int_0^{a^2/is_o} ds\, s\, e^{(am)^2 s^{-1} - n^2 s} \right] , \end{aligned} \tag{3}$$

onde na primeira integral a variável de integração foi mudada de acordo com $s \mapsto im^2 s$ e na segunda, de acordo com $s \mapsto a^2/is$. O primeiro termo no lado direito desta equação é proporcional ao volume contido entre as placas e representa pois uma densidade de energia uniforme espalhada em todo o espaço. Tal densidade independe da presença ou não das placas e é portanto espúria em nossos cálculos; no limite em que o truncamento no tempo próprio desaparece, $s_o \to 0$, ela diverge para a seguinte expressão: $-TL^2 am^4 \Gamma(-2)/8\pi^2$, na qual Γ é a função gama de Euler. Os outros termos no lado direito da equação (3) dão a dependência da ação efetiva em relação à separação a entre as placas; tomando o limite $s_o \to 0$ desta parte obtemos a parte fisicamente significante $\mathcal{W}^{(1)}$. Substituindo $\mathcal{W}^{(1)}$ em (2) obtemos [11] a seguinte expressão para a energia de Casimir:

$$\mathcal{E} = -L^2 \frac{(m/2\pi)^2}{a} \sum_{n\in\mathbb{N}} \frac{1}{n^2} [2K_2(2amn) - K_2(4amn)] , \tag{4}$$

onde K_2 é a função de Bessel modificada. No limite de massa nula a expressão (4) reduz-se a (cf. fórmula **9.6.9** em [12]):

$$\mathcal{E} = -L^2 \frac{7\pi^2}{2880a^3} ,$$

que é o mesmo resultado obtido com outros métodos [13] e que leva à seguinte expressão para a pressão de Casimir: $p_C = -7\pi^2/960a^4$. Como no caso do campo eletromagnético, a pressão tende a juntar as placas, mas neste caso de campo fermiônico sem massa ela é maior pelo fator 7/4.

No limite de massa grande a energia de Casimir é dada por (cf. fórmula **9.7.2** em [12]):

$$\mathcal{E} \sim -L^2 \frac{m^2}{4\pi^2 a} \sqrt{\frac{\pi}{ma}}\, e^{-2am} ,$$

que é igual ao limite de massa grande para bósons [14] multiplicado pelo fator 4 proveniente do traço espinorial. Este é um resultado a ser esperado uma vez que $m \to \infty$ corresponde ao limite clássico no qual bósons e férmions tornam-se indistinguíveis.

É interessante notar que neste caso de campo fermiônico a auto-energia de cada placa não aparece no formalismo. A causa desta ausência pode ser facilmente rastreada no formalismo e é dada pelo fato de que no caso fermiônico os modos discretos do momento p_z são numerados por $2\mathbb{N} - 1$ e não por $\mathbb{N}$, como no caso bosônico. Observemos finalmente que os mesmos resultados aqui apresentados são obtidos [15] usando-se a regularização por continuação analítica que foi proposta na referência [6].

Agradecimentos. Agradecemos Arvind N. Vaidya, M. Asorey and A. J. Ségui-Santonja por discussões proveitosas neste assunto e ao CNPq pelo auxílio financeiro.

Referências

[1] Casimir, H. B. G.: *Proc. Kon. Nederl. Akad. Wetensch.* **51** (1948),793.

[2] Sparnay, M. J.: *Physica* **24** (1958), 751.

[3] Chodos, A., Jaffe, R. L., Johnson, K., Thorn, C. B., and Weisskopf, V. F.: *Phys. Rev.* **D9** (1974), 3471.

[4] Schwinger, J.: *Lett. Math. Phys.* **24** (1992), 59.

[5] Schwinger, J.: *Phys. Rev.* **82** (1951), 664.

[6] Cougo-Pinto, M. V., Farina, C., and Ségui-Santonja, A. J.: *Lett. Math. Phys.* **30** (1994), 169.

[7] Cougo-Pinto, M. V., Farina, C., and Ségui-Santonja, A. J.: *Lett. Math. Phys.* **31**, (1994), 309.

[8] Cougo-Pinto, M. V., Farina, C. and Tort, A.: *Schwinger's method for the Casimir effect at finite temperature, Lett. Math. Phys.*, **34** (1995), 373.

[9] Albuquerque, L. C., Farina, C., Rabello, S. and Vaidya, A.: aceito para publicação em *Lett. Math. Phys.*

[10] Poisson, S. D.: *Journal de l'Ecole Polytechnique* **XII**, (cahier XIX) (1823), 420.

[11] Gradshteijn, I. S. and Ryzhik, I. M.: *Tables of Integrals, Series, and Products*, Academic Press, New York, London, 1965. Formula **3.471**,9.

[12] *Handbook of Mathematical Functions*, Eds.: Abramovitz, M. and Stegun, I., Dover Publications, Inc., New York, 1965.

[13] Johnson, K.: *Acta Physica Polonica* **86** (1975), 865.

[14] Plunien, G., Muller, B., and Greiner, W.: *Physica* **145A** (1987), 202.

[15] Cougo-Pinto, M. V., Farina, C. and Tort, A.: *Schwinger's method for the fermionic Casimir effect*, aceito para publicação em *Lett. Math. Phys.*.

Tunelamentos: Catástrofes Quânticas

C. A. A. de Carvalho[*]
Instituto de Física, Universidade Federal do Rio de Janeiro,
Cx. Postal 68528, CEP 21945-970, Rio de Janeiro, RJ, Brasil

R. M. Cavalcanti[†]
Departamento de Física, Pontifícia Universidade Católica do Rio de Janeiro,
Cx. Postal 38071, CEP 22452-970, Rio de Janeiro, RJ, Brasil

Received March, 1996

A função de partição, $Z(\beta)$, de um sistema quântico unidimensional pode ser expressa em termos de uma integral de caminho:

$$Z(\beta) = \int_{-\infty}^{\infty} dx_0 \int_{x(0)=x_0}^{x(\beta\hbar)=x_0} [Dx(\tau)]\, e^{-S/\hbar} , \tag{1}$$

$$S = \int_0^{\beta\hbar} d\tau \left[\frac{1}{2}M\dot{x}^2 + V(x)\right] . \tag{2}$$

Dado um potencial arbitrário, $V(x)$, não é possível, em geral, calcular essa integral de forma exata. Resultados aproximados podem ser obtidos utilizando-se métodos perturbativos[1, 2], variacionais[1, 2] ou numéricos[3]. Outro método, muito popular, é a aproximação semi-clássica[4, 5]. O objetivo do presente trabalho é: i) apresentar uma fórmula geral para $Z_{sc}(\beta)$ que não requer um conhecimento detalhado do movimento clássico,[1] ii) mostrar como o tunelamento pode ser relacionado com a ocorrência de certas singularidades nessa fórmula, e iii) fazer um estudo dessas singularidades usando os métodos da Teoria da Catástrofe.

A aproximação semi-clássica de (1) fornece

$$Z_{sc}(\beta) = \int_{-\infty}^{\infty} dx_0 \sum_{j=1}^{N(x_0,\beta)} e^{-S_j(x_0,\beta)/\hbar} \Delta_j^{-1/2}(x_0,\beta) , \tag{3}$$

onde $S_j(x_0,\beta)$ é a ação da j-ésima trajetória clássica, $x_j(\tau)$, satisfazendo as condições de contorno $x_j(0) = x_j(\beta\hbar) = x_0$, $\Delta_j(x_0,\beta)$ é o determinante do operador de flutuações em torno de $x_j(\tau)$,

$$\Delta_j(x_0,\beta) = \mathrm{Det}\left(-M\frac{d^2}{d\tau^2} + V''[x_j(\tau)]\right) , \tag{4}$$

e $N(x_0,\beta)$ é o número de trajetórias clássicas que minimizam a ação.

Em termos dos pontos de retorno do movimento clássico, a ação tem a seguinte expressão:

$$\begin{aligned} S_j(x_0,\beta) &= \beta\hbar V(x_\pm^j) \pm 2\int_{x_0}^{x_\pm^j} dx\, M v(x, x_\pm^j) \\ &\quad + 2n\int_{x_-^j}^{x_+^j} dx\, M v(x, x_\pm^j) , \end{aligned} \tag{5}$$

onde $v(x,y) \equiv \sqrt{(2/M)[V(x) - V(y)]}$ e x_+^j (x_-^j) são os pontos de retorno à direita (esquerda) de x_0. O primeiro termo em (5) corresponde ao limite de alta temperatura de $Z(\beta)$, no qual as trajetórias clássicas colapsam num

[1] Por movimento clássico queremos dizer movimento satisfazendo a equação de Euler-Lagrange $M\ddot{x} - V'(x) = 0$, que é a equação de movimento para uma partícula movendo-se no potencial *menos* V.

ponto[1, 2] e, portanto, $x_+^j\,(x_-^j) \to x_0$. No caso de movimento em regiões em que o potencial invertido (isto é, $-V$) é ilimitado (daqui pra frente chamado de movimento ilimitado), $n = 0$. No caso de movimento periódico, n é igual ao número de períodos e o segundo termo está ausente. Finalmente, no caso de movimento limitado aperiódico, todos os termos estão presentes.

Para trajetórias com um único ponto de retorno ($n = 0$), $x_\pm^j$ são dados implicitamente por

$$\tau(x_0, x_\pm^j) \equiv 2\int_{x_0}^{x_\pm^j} \frac{dx}{v(x, x_\pm^j)} = \pm\beta\hbar\,, \tag{6}$$

e o determinante de flutuações por

$$\Delta_j(x_0,\beta) = \pm\frac{4\pi\hbar[V(x_\pm^j) - V(x_0)]}{MV'(x_\pm^j)}\left[\frac{\partial\tau(x_0,y)}{\partial y}\right]_{y=x_\pm^j}. \tag{7}$$

A fórmula acima somente é válida para trajetórias com um único ponto de retorno. No entanto, como mostraremos mais adiante, trajetórias com dois ou mais pontos de retorno são pontos de sela da ação, e, portanto, não contribuem para a aproximação semi-clássica de (1).

A única informação requerida pelas fórmulas (5) e (7) sobre as trajetórias clássicas são seus pontos de retorno. Para mostrar a simplificação que isso acarreta no cálculo de $Z_{sc}(\beta)$, tomemos como exemplo o oscilador harmônico, $V(x) = \frac{1}{2}M\omega^2x^2$. Nesse caso, dados x_0 e β, existe apenas uma trajetória clássica, cujo (único) ponto de retorno é dado por $x_+(x_-) = x_0/\cosh(\beta\hbar\omega/2)$ para $x_0 < 0\,(> 0)$. S_1 e Δ_1 também podem ser facilmente calculados, o resultado final (nesse caso, exato) sendo

$$\begin{aligned} Z_{sc}(\beta) &= \int_{-\infty}^{\infty} dx_0\, e^{-(M\omega x_0^2/\hbar)\tanh(\beta\hbar\omega/2)} \\ &\quad\times\sqrt{\frac{M\omega}{2\pi\hbar\sinh(\beta\hbar\omega)}}\,. \end{aligned} \tag{8}$$

Um exemplo menos trivial é dado pelo potencial $V(x) = \lambda x^4$. Nesse caso, o uso das fórmulas (5)-(7) fornece como resultado[2]

$$\begin{aligned} Z_{sc}(\beta) &= \int_0^K du\sqrt{\frac{2M^2u^2}{\pi\lambda\beta^3\hbar^4}\left[1 + \frac{\mathrm{cn}(u,k)}{u\,\mathrm{sn}(u,k)\,\mathrm{dn}(u,k)}\right]} \\ &\quad\times\ \exp\left\{-\frac{M^2u^3}{3\lambda\beta^3\hbar^4}\left[\frac{4\,\mathrm{sn}(u,k)\,\mathrm{dn}(u,k)}{\mathrm{cn}^3(u,k)} - u\right]\right\}, \end{aligned} \tag{9}$$

com $k = 1/\sqrt{2}$ e $K = \int_0^{\pi/2} d\varphi\,(1 - \frac{1}{2}\sin^2\varphi)^{-1/2} = 1{,}85407\ldots$, e onde $\mathrm{cn}(u,k)$, $\mathrm{sn}(u,k)$ e $\mathrm{dn}(u,k)$ são funções elípticas de Jacobi[6].

Uma situação mais interessante ocorre no caso do oscilador anarmônico, $V(x) = \lambda(x^2 - a^2)^2$. Para $x^2 > a^2$, só há trajetórias com um único ponto de retorno. Contudo, na região $x^2 < a^2$, onde o movimento clássico é limitado, pode haver mais de uma trajetória clássica para valores dados de x_0 e β.

Numa região de movimento clássico limitado (um poço em $-V$), tal como $x^2 < a^2$ no caso do oscilador anarmônico, o número de trajetórias clássicas varia com a temperatura. Se $0 \le \beta < \pi/\hbar\omega_m$ (onde $\omega_m = \sqrt{-V''(x_m)/M}$ é a freqüência das pequenas oscilações em torno x_m, mínimo local de $-V$), para cada x_0 nessa região existe uma única trajetória clássica. Se $x_0 < x_m\,(> x_m)$ essa trajetória vai para a esquerda (direita) e retorna para x_0. Se $x_0 = x_m$, a partícula fica em repouso no fundo do poço. É este regime de trajetória única que corresponde ao limite de alta temperatura.

Quando $\beta = \pi/\hbar\omega_m$, a solução $x(\tau) = x_m$ torna-se instável. Seu operador de flutuações é o de um oscilador harmônico com $\omega^2 = \omega_m^2$, cujo determinante é $\Delta(x_m,\beta) = 2\pi\hbar\sin(\beta\hbar\omega_m)/M\omega_m$. Ele se anula quando $\beta = \pi/\hbar\omega_m$ e torna-se negativo quando $\beta > \pi/\hbar\omega_m$. Ao mesmo tempo, surgem duas novas trajetórias clássicas, simétricas em relação a x_m, como mostra a Fig. 1. Assim, em $x_0 = x_m$ nós vamos de um regime de trajetória única para um regime de três trajetórias quando passamos por $\beta = \pi/\hbar\omega_m$. As duas novas trajetórias são mínimos degenerados, ao passo que x_m torna-se um ponto de sela da ação, apresentando um único modo negativo.

[2] Detalhes sobre a obtenção deste resultado, bem como outros exemplos e a dedução da Eq. (7), serão apresentados num trabalho futuro.

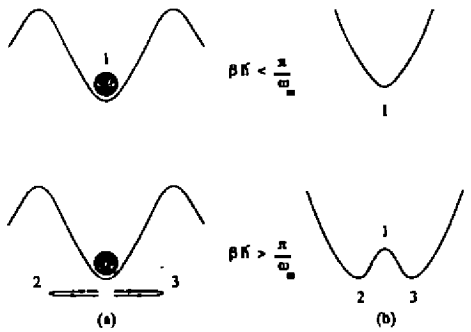

Figure 1.: (a) Trajetórias clássicas com $x_0 = x_m$ para $\beta < \pi/\hbar\omega_m$ (1) e $\beta > \pi/\hbar\omega_m$ (2 and 3); (b) Esboço de como os extremos mudam ao longo da direção instável no espaço de funções.

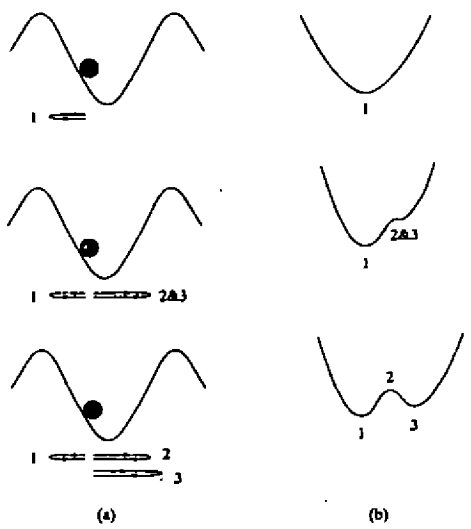

Figure 2.: (a) Trajetórias clássicas com $x_0 \neq x_m$ para $\beta < \beta_c$ (1), $\beta = \beta_c$ (1 and 2&3) e $\beta > \beta_c$ (1,2 and 3), $\pi/\hbar\omega_m < \beta_c < 2\pi/\hbar\omega_m$; (b) Esboço de como os extremos mudam ao longo da direção instável no espaço de funções.

Quando β cresce além de $\pi/\hbar\omega_m$, uma situação análoga ocorre para outros valores de x_0 dentro do poço. Quando o determinante de flutuações em torno da trajetória clássica correspondente a um dado x_0 se anula, surge uma nova trajetória clássica. Seu (único) ponto de retorno se encontra do lado oposto, com relação a x_m, de x_0. A nova trajetória pode, portanto, ser interpretada como uma trajetória tunelante, já que ela atravessa uma região classicamente proibida de V. Se β cresce ainda mais, essa trajetória tunelante desdobra-se em duas, uma das quais é um mínimo local da ação, enquanto a outra é um ponto de sela, com um único modo negativo. A Fig. 2 ilustra essa transição de um regime de trajetória única para um regime de três trajetórias. Conforme β cresce, aumenta a região na qual existem três trajetórias clássicas com o mesmo valor de x_0. As fronteiras dessa região são definidas pelos pontos x_0 nos quais $[\partial\tau(x_0, y)/\partial y]_{y=x_\pm^j} = 0$.

O fenômeno descrito nos dois parágrafos anteriores é análogo à ocorrência de cáusticas em Ótica[7], onde o papel de trajetórias clássicas é desempenhado pelos raios de luz, extremos da distância ótica. As cáusticas ocorrem nos pontos onde a densidade de raios, e portanto a intensidade luminosa, diverge (daí seu nome). No nosso caso, isso se reflete na divergência do integrando de (3) nas fronteiras que separam as regiões de uma trajetória das regiões de três trajetórias clássicas, já que $\Delta(x_0, \beta)$ se anula nesses pontos.

Ambos os fenômenos são exemplos de catástrofes. Elas ocorrem quando dois ou mais extremos de uma função (no nosso caso, um funcional) coalescem, ou então quando extremos surgem onde não havia nenhum. A Teoria da Catástrofe[7, 8, 9] classifica tais singularidades de acordo com a sua codimensão no espaço de controle, formado pelos parâmetros "externos" do sistema. No nosso caso, esse espaço é bidimensional (x_0 e β), e portanto só podem ocorrer catástrofes de codimensão 1 (dobra) ou 2 (cúspide). A situação que estudamos corresponde a uma cúspide.

Uma seqüência de cúspides ocorre quando baixamos a temperatura. Toda vez que β passa por um valor igual

a um múltiplo inteiro de $\pi/\hbar\omega_m$, surgem duas novas soluções com valores de x_0 nas vizinhanças de x_m. No entanto, apesar do número cada vez maior de extremos, correspondendo a trajetórias com um número crescente de tunelamentos, apenas dois deles minimizam a ação. Numa aproximação semi-clássica com tempo imaginário, apenas esses dois extremos devem ser somados. Com efeito, a aproximação semi-clássica consiste em expandir a ação em torno de um extremo e integrar sobre as flutuações quadráticas em torno do mesmo. Para que tal integral convirja (após uma eventual regularização) é necessário que todos os modos sejam positivos.[3] (O mesmo argumento não se aplica quando o tempo é real, pois nesse caso as flutuações quadráticas dão origem a integrais de Fresnel, para as quais esse problema de convergência não ocorre.)

Dos dois mínimos da ação, um deles só existe para $\beta < \pi/\hbar\omega_m$, e somente para certos valores de x_0. A transição de uma região de um mínimo para uma região de dois mínimos ocorre nos pontos em que o determinante de flutuações se anula devido ao surgimento de uma cáustica, levando ao surgimento de uma singularidade no integrando da Eq. (3). Tal singularidade é um artefato da aproximação semi-clássica. Ela desaparece quando se faz uma aproximação mais refinada[7, 10, 11], na qual se incluem flutuações cúbicas e quárticas na direção do espaço de funções na qual a instabilidade se desenvolve. De qualquer forma, a presença dessa singularidade não é desastrosa, já que ela é integrável.

Nós gostaríamos de agradecer Roberto Iengo, por conversas proveitosas, Ildeu de Castro Moreira, por indicar a Ref. [9], e Flavia Maximo, por ajudar com as figuras. Parte deste trabalho foi desenvolvido no ICTP, e teve suporte financeiro do CNPq.

References

[*] e-mail: aragao@if.ufrj.br

[†] e-mail: rmc@fis.puc-rio.br

[1] R. P. Feynman and A. R. Hibbs, *Quantum Mechanics and Path Integrals* (McGraw-Hill, New York, 1965).

[2] R. P. Feynman, *Statistical Mechanics* (Benjamin, Reading, Mass., 1972).

[3] M. Creutz and B. Freedman, Ann. Phys. (NY) **132** (1981), 427.

[4] H. M. Nussenzveig, *Integrais de Trajetória*, Escola de Verão Jorge André Swieca, Vol. I (1981).

[5] R. Rajaraman, *Solitons and Instantons* (North-Holland, Amsterdam, 1987).

[6] I. S. Gradshteyn and I. M. Ryzhik, *Table of Integrals, Series and Products*, Academic Press, New York (1965).

[7] M. Berry, in *Physics of Defects*, Les Houches Session XXXV (1980), eds R. Balian et al. (North-Holland, Amsterdam, 1981).

[8] R. Thom, *Structural Stability and Morphogenesis* (Benjamin, Reading, MA, 1975); T. Poston and I. N. Stewart, *Catastrophe Theory and its Applications* (Pitman, London, 1978); E. C. Zeeman, *Catastrophe Theory: Selected Papers 1972-1977* (Addison-Wesley, Reading, MA, 1977).

[9] P. T. Saunders, *An Introduction to Catastrophe Theory* (Cambridge University Press, Cambridge, 1980).

[10] G. Dangelmayr and W. Veit, Ann. Phys. (NY) **118** (1979), 108.

[11] U. Weiss, *Quantum Dissipative Systems* (World Scientific, Singapore, 1993).

[3] Há uma técnica muito popular no estudo de sistemas metaestáveis em que modos negativos são continuados analiticamente e os resultados são interpretados como taxas de decaimento[11]. Tal procedimento, contudo, não é aplicável ao problema que estamos estudando.

A Symbolic Computing Environment for Doing Calculations in Quantum Field Theory

E.S. Cheb-Terrab*, E.V Corrêa-Silva†and L.A. da Mota‡
Symbolic Computing Group
Theoretical Physics Department — UERJ

Received March, 1996

A computational environment, as a set of MapleV R.3 routines for doing symbolic calculations in Quantum Field Theory, is presented. The *QFT* package's routines extend the standard MapleV computational domain by introducing representations for anticommutative and noncommutative objects, tensors, spinors and gauge fields, as well as related objects and procedures (Dirac matrices, differential operators, functional differentiation w.r.t indexed fields, sum rule for repeated indices, etc.). Furthermore, the *QFT* routines permit the user-definition of algebra rules for the commutation/anticommutation of operators, to be taken into account during the calculations.

1 Introduction

Physics researchers often experience the sensation that performing calculations by hand is still more comfortable and simpler than carrying them out in any symbolic computation system. This is due to the lack of computational facilities that would allow the user to work with his computer as naturally as he would with paper and pencil. The existing packages, having been designed to attain specific purposes, fail to provide the desired flexibility.

In this work we present our efforts to implement a computational environment for doing calculations in Field Theory research, being currently materialized as a package named *QFT*, written using the MapleV symbolic computation language. This release includes:

- routines implementing all the basic operations for the required new symbolic objects, such as &* (noncommutative product), **inv**(erse w.r.t &*), **Tr**(ace), **gdiff**(erentiation w.r.t Grassmann parameters) etc.;
- background checkup of the user's input concerning tensor, spinor or gauge indices for consistency;
- the possibility of introducing algebra rules for quantum operators of any type;
- most of the basic simplifications and normal forms for algebraic expressions containing the new objects, in order to take the most advantage of the standard MapleV Library as a whole.

In many aspects, the *QFT* package synthesizes and extends the *partials*[1] and *Grassmann*[2] packages[1], which already implemented functional differentiation w.r.t tensor fields and the basic commands for working with anticommutative and noncommutative objects.

We shall not detail here language and programming issues, but restrict ourselves to outlining the main ideas of our project.

2 A Computational Environment

The construction of a computational environment can be pictured as the mirroring of the "paper and pencil world" into the "keyboard and screen world". Calculations in the "paper and pencil" sense involve a number of objects with definite properties, among which operations of various degrees of complexity are performed. Hence two steps are essential for the solid founding of a computational environment:

*terrab@vmesa.uerj.br
†ecorrea@vmesa.uerj.br
‡damota@vmesa.uerj.br

[1] These packages can be found at http://dft.if.uerj.br/symbcomp.htm

1. The definition of a computational domain, i.e., the representation of all objects that may possibly enter the input or output of calculations, together with the characterization of their properties.

2. The implementation of the basic operations among the elements of the computational domain.

A careful construction of these elements sets up the base for the future implementation of more complex and powerful operations.

2.1 Defining the *extended* computational domain

When doing calculations by hand, an object is usually characterized by the following:

- Every object has a name of its own.
- An object may have indices of various natures, such as tensor, spinor or internal (gauge) type. The name of an index consists of a root (initial string with purely alphabetical characters) eventually followed by a suffix of purely numerical characters; the root identifies its nature.
- There may exist symmetry properties among the indices of an object. An object may be totally symmetric (or antisymmetric) in its indices of one or another type, or it may be symmetric in some of its indices and antisymmetric in some others.
- Objects may be subject to commutation and anticommutation relations.

Concerning these points, we define as *extended* computational domain the computational objects representing tensors, spinors, and objects containing internal group indices; including their symmetry properties and any special algebra rules.

To define an object as belonging to the *extended* computational domain (a QFT object), a special routine, **Define** was prepared.

Once an object is defined as a QFT object, each time a command of the package finds such an object, the command will operate taking into account all the mathematical properties of these extended objects and of the basic operations defined for them (see subsection 2.2).

An object may also be included in the computational domain through background definition, which consists in the automatic application of **Define** to objects matching a pre-defined pattern, as the package's commands processes a mathematical expression.

Some default QFT objects, automatically loaded with the package are: the Pauli and Dirac matrices, the metric and the Levi-Civitta tensors, and differential operators such as $\partial\mu$, the Laplacian and the d'Alembertian.

2.2 Setting up the basic operations for the *extended* computational domain

By setting up the basic operations we mean: the setting of the algebra and differentiation rules for the new objects; the, say, first level operations, as the inverse and trace of an object etc.; and the definition of *canonical forms* and simplifications to be applied by default to the returned results.

The basic algebraic operations and differential operators implemented with the QFT package are:

- Summation, represented by the operator '+'.
- The sum rule for repeated indices. In other words, the recognition of dummy indices of any type as such.
- The noncommutative product, represented by the '&*' operator, according to Maple standard convention (see [2]).
- Differentiation. Both ordinary (**gdiff**) and functional (**fdiff**) differentiation must take into account the particular properties of anti/noncommutative objects (see [1] and [2]), as well as the sum rule for repeated indices.

As first level operations we introduced command representations for:

- the trace of an object, represented by the function **Tr**;
- the inverse of an object, represented by the function **inv**.

Default simplifications and canonical forms

We take as a general rule that good mathematical expressions are the "simplest ones", though there is a great deal of scope in defining "simplest" from the computational point of view. The manipulations performed by default by the package commands were classified into three categories:

Simplifications related to the & product*

- the application of the distributive property of noncommutative product with respect to summation;
- the identity element as the result of the product of an object and its inverse;
- the vanishing of any product containing 0 as an operand.

Simplifications with respect to dummy indices

- recognition of dummy indices as dummy indeed:
- reduction of expressions involving the metric and Levi-Civitta tensor to expressions that do not involve these objects, whenever possible;
- vanishing of products containing objects symmetric and antisymmetric with respect to the same pair of indices.

Rewriting of an expression into its "canonical form"

It often occurs that mathematical expressions with different syntaxes have the same meaning. From the computational point of view it is highly advantageous that all those expressions be translated into a unique, simple, and equivalent form - which we shall call their "canonical form".

The careful design of a canonical form for a given class of expressions takes into account not only purely mathematical aspects, but also computational efficiency and speed.

3 Background checking and internal representation

Extensive and repetitive calculations, even the simplest ones, are quite often plagued by mistakes when performed by hand. Sometimes tracing those mistakes itself is such an awkward task that it seems preferable either to start everything over again - hoping our attention will not betray us this time - or to find a more pleasant thing to dedicate our attention to. For that reason, we took as a principle that a background checking of arguments should be performed by every command of the *QFT* package. In other words, calculations are continuously being monitored for inconsistencies; for instance, all the operands in a summation should have the same set of free indices (the same applies to both sides of an equation), and repeated indices should not appear more than twice.

Great care has been employed in writing up clear and specific error messages for the user, to be displayed whenever an inconsistency is detected, thus interrupting the calculation.

The objects belonging to the *extended* computational domain (see subsection 2.1), have two different representations: the "external" and "internal" one. The former intends to be as similar as possible to the "paper and pencil" way of writing, and is used in every input (by the user) and output (by the *QFT* commands); the latter is suitable for more efficient and quick processing, and is used by the *QFT* commands in all intermediate calculations. Hence, when processing algebraic expressions, the package's commands first convert all the *extended* objects in a given input expression into their internal representations; only then calculations are actually performed and, finally, the result is converted back into a user-readable form, and displayed on the screen.

4 Conclusion

The *QFT* package is being designed as a basic calculating tool for physics researchers in Quantum Field Theory[2]. It is divided into five modules, each of them performing different tasks:

a. *QFT*- Define, concerned with the definition of the computational domain.

[2]This work was supported by Universidade do Estado do Rio de Janeiro (UERJ), and the "Conselho Nacional de Desenvolvimento Científico e Tecnológico" (CNPq).

b. *QFT*-general, which deals with the inverse and trace of objects, as well as with noncommutative product manipulation.

c. *QFT*-representation, related to the translation of objects into their internal representation.

d. *QFT*-simplify, where simplification due to dummy indices and rewriting of expressions into their canonical form is handled.

e. *QFT*-differentiation, which implements Grassmann and functional derivatives for the objects of the computational domain.

The implementation of the first three modules has been completed. The remaining modules are still in preparation.

This package was designed as a basis for future packages related to more complex tasks (functional integration, dimensional regularization, building of perturbative series, etc.). We are now designing some of these complex-task packages and expect to report related work in the near future.

References

[1] E.S. Cheb-Terrab, "Maple procedures for partial and functional derivatives", Computer Physics Communications, 79 409 (1994).

[2] E.S. Cheb-Terrab, "Symbolic Computing with Grassmann variables", submitted to Journal of Symbolic Computation, (October/1995).

On The Generalization of Proper Time

Marcelo de O. Terra-Cunha
Physics Department, IFGW-Unicamp
Campinas, 13081-970, S.P., Brazil
e-mail: tcunha@ifi.unicamp.br
and
Márcio A. F. Rosa
Mathematics Department, IMECC-Unicamp
Campinas, 13081-970, S.P., Brazil

July 31, 1996

In this work we present three possibilities for the generalization of proper time. Experimental tests can distinguish among them and this is a possible test for the reality of Kaluza-Klein extra dimensions.

1 Introduction

One of the first experimental tests of the Theory of Special Relativity was the life time dilatation of high velocity muons. Nowadays this is still an exercise or example in many text books.

The General Relativity proper time is given by

$$d\tau^2 = g_{\mu\nu}dx^\mu dx^\nu \tag{1}$$

which sometimes can be written in an appropriated frame as

$$d\tau^2 = dt^2 - (dx^1)^2 - (dx^2)^2 - (dx^3)^2 \tag{2}$$

where we put $c = 1$. If the world-line of a particle is parameterized by t, and putting $v^i = \frac{dx^i}{dt}$, we have

$$d\tau^2 = (1 - v^2)dt^2 \tag{3}$$

where $v^2 = (v^1)^2 + (v^2)^2 + (v^3)^2$.

The Lorentz factor is then defined by

$$dt = \gamma d\tau \quad \text{or} \quad \gamma = (1 - v^2)^{\frac{-1}{2}} \tag{4}$$

Since $d\tau$ is an invariant the life time of unstable particles depends linearly on γ, what is verified experimentally. We observe however that this is valid only for free particles, in the absence of fields different from the gravitational one.

Now we outline three possible ways of generalizing the concept of proper time when the particle is under the action of other fields. We trust that experimental measures of life time could distinguish among them. For the sake of simplicity (both, theoretical and experimental) we consider only electromagnetic fields in a gravitational background, but generalizations to include other interactions can be done.

2 The Possibilities

2.1 General Relativity

The proper time should be given by eq. (1) but with $g_{\mu\nu}$ determined by Einstein equation

$$G_{\mu\nu} = 8\pi T_{\mu\nu} \tag{5}$$

where the R.H.S. must include the electromagnetic stress-energy tensor [M-T-W]

$$T_{\mu\nu} = \frac{1}{4\pi}(F^\alpha_\mu F_{\nu\alpha} - \frac{1}{4}F^{\alpha\beta}F_{\alpha\beta}) \tag{6}$$

2.2 Apsel's Propose

D. Apsel [A] started from the Einstein-Maxwell action density and added an extra term to proper time, defined by him as

$$d\tau = (g_{\mu\nu}dx^\mu dx^\nu)^{\frac{1}{2}} + \frac{q}{m}A_\mu dx^\mu \tag{7}$$

in order to explain a supposed discrepancy between positive and negative muons life time which he trusts J. Bailey et all [B] had measured. Besides the theoretical problems of this approach, we point that Apsel has made use of averaged values obtained from different experiments in which muons were under different electromagnetic field conditions.

2.3 Kaluza-Klein Theory

It is well known that, in Kaluza-Klein context, a "five-dimensional Einstein-Hilbert Lagrangian" ([T], [A-C-F]) leads to field equations which decouple in Einstein equation (with the electromagnetic $T_{\mu\nu}$) and Maxwell equations.

Also five-dimensional geodesics project on known four-dimensional particle trajectories, being the momentum canonically associated to the fifth coordinate the electric charge q of the particle.

Then, it sounds natural to give direct physical meaning to the five-dimensional arc length (instead of the four-dimensional one) and work with[1]

$$d\tau^2 = \gamma_{MN}dx^M dx^N \tag{8}$$

The fifth dimension is usually considered periodic with length of some hundred times Planck length ([K]), and although we have no direct access to it, we note that the fifth velocity can be obtained from the cylindrical condition assumed ([T]) and from the four-dimensional projection of the trajectory.

3 Experimental Possibilities

We trust that particle accelerators working nowadays are able to test if any among these three possibilities is better than the others. It is even possible that experimental data already stored be enough, and the only need would be to work them out.

4 Discussion

Certainly General Relativity is not a complete theory (the last 35 years of Einstein's work show this). Kaluza-Klein theories are truth possibilities and hopes toward a unified field theory. In E. Witten's words ([W] ,p.415)

> "This theory [Kaluza-Klein] is surely one of the most remarkable ideas ever advanced for unification of electromagnetism and gravitation."

The experimental test suggested here can show if the extra dimension has physical reality or if it is just a good mathematical tool (or toy).

References

[A-C-F] Appelquist, T.; Chodos, A. & Freund, P.G.O. **Modern Kaluza-Klein Theories**, Frontiers in Physics - Lecture Note Series, Addison Wesley (1987).

[A] Apsel, D. Gravitation and Electromagnetism **General Relativity and Gravitation 10**(4), p.297 (1979).

[B] Bailey, J. et all Measurement of Relativistic Time Dilatation for Positive and Negative Muons in a Circular Orbit **Nature 268**(28), p.301 (1977).

[K] Klein, O. The Atomicity of Electricity as a Quantum Theory Law **Nature 118**, p.516 (1926). Reprinted in [A-C-F].

[M-T-W] Misner, C.W.; Thorne, K.S. & Wheeler, J.A. **Gravitation**, W.H. Freeman and Company (1973).

[T] Tonnelat, M.A. **Les Théories Unitaires de l'Électromagnetisme et de la Gravitation - Livre II**, Gauthier-Villars (1965).

[W] Witten, E. Search for a Realistic Kaluza-Klein Theory **Nuclear Physics B186** p.412 (1981).

[1] Notation: Capital latin indexes take values 0,1,2,3,5; greek indexes take values 0,1,2,3.

A Superspace Formulation for the Master Equation

Everton M. C. Abreu[1,2] and Nelson R. F. Braga[1]

[1] *Instituto de Física, Universidade Federal do Rio de Janeiro, Caixa Postal 68528, 21945 Rio de Janeiro, RJ, Brazil*

[2] *Instituto de Física, Universidade do Estado do Rio de Janeiro, Rua São Francisco Xavier 524, CEP 20550 Rio de Janeiro, RJ, Brazil*

Received March, 1996

The Batalin Vilkovisky (BV) formalism[1, 2, 3], also called field antifield quantization, is a Lagrangian BRST procedure that generalizes the Faddeev Poppov mechanism.

It is known that superspace formulations for gauge field theories can be build up in such a way that the BRST transformations are realized as translations in a Grasmannian coordinate[5].

In the present article we will investigate a superspace version of the field antifield formalism at higher order in $\hbar$.

Considering a gauge field theory characterized by a classical action $S_0[\phi^i]$ we introduce ghosts, antighosts and auxiliary fields associated to the original gauge invariance of S_0 in the usual way.

$$\delta_0 \phi^A = R^A[\phi] \tag{1}$$

Following [6] let us define the enlarged BRST algebra as :

$$\delta\phi^A = \pi^A; \delta\tilde{\phi}^A = \pi^A - R^A[\phi - \tilde{\phi}]; \delta\pi^A = 0; \delta\phi^{*A} = B^A; \delta B^A = 0 \tag{2}$$

And the total action as:

$$S = S_0[\phi^i - \tilde{\phi}^i] - \delta(\phi^{*A}\tilde{\phi}^A) + \delta\psi[\phi^A] \tag{3}$$

where $\psi[\phi^A]$ is a fermionic functional representing the gauge fixing of the original symmetries (1). Now, the BRST superspace formulation is obtained introducing superfields of the general form:

$$\Phi(x,\theta) = \phi(x) + \theta\delta\phi(x). \tag{4}$$

We can define a superfield action as:

$$\underline{S} = S_0[\Phi^i - \tilde{\Phi}^i] - \frac{\partial}{\partial\theta}\{\Phi^{*A}\tilde{\Phi}^A + \psi[\Phi^a]\} \tag{5}$$

This object actually has a trivial superspace structure as it's θ component is zero ($\underline{S} = S$).

We remark that the superspace action (5) is physically equivalent to the BV action at classical level.

The quantum action can be expanded in a power series in $\hbar$ as:

$$W(\phi^A, \phi^{*A}) = S(\phi^A, \phi^{*A}) + \sum_{p=1}^{\infty} \hbar^p M_p(\phi^A, \phi^{*A}) \tag{6}$$

The BRST transformation for some quantity X in the BV language [7] is:

$$\delta X = (X, W) - i\hbar\Delta X \tag{7}$$

if we choose $X = W$

$$\delta W = i\hbar\Delta W \tag{8}$$

So, the action has the following superspace structure:

$$\underline{W} = W + \theta i\hbar\Delta W \tag{9}$$

Actually the general form for the superfield $\underline{W}$ of eq. (9) is just formal, in the same way as the master equation itself.

Let us now define the operator

$$\underline{\Delta} \equiv \int dx \int d\theta \int d\theta' \frac{\delta_r}{\delta\Phi^A(x,\theta)} \frac{\delta_l}{\delta\Phi^{*A}(x,\theta')} \tag{10}$$

The Pauli Villars regularization procedure is the most suitable for the BV formalism at one loop order[3, 4, 8, 9]. We will build up a Pauli Villars superfield action corresponding to a collective field version of the standard PV action:

$$\begin{aligned} \underline{S}_{PV} &= \frac{1}{2}(\underline{\chi}^A - \underline{\tilde{\chi}}^A)(TO)_{AB}(\underline{\chi}^B - \underline{\tilde{\chi}}^B) \\ &- \frac{1}{2}M(\underline{\chi}^A - \underline{\tilde{\chi}}^A)T_{AB}(\underline{\chi}^B - \underline{\tilde{\chi}}^B) - \frac{\partial}{\partial\theta}(\underline{\chi}^{*A}\underline{\tilde{\chi}}^A) \end{aligned} \tag{11}$$

The non extended (without collective fields) BRST algebra for the PV fields reads:

$$\delta_0\chi^A = K_{AB}\chi^B \tag{12}$$

Let us assume that a regularized form of the BRST change in the total action $(\delta S_T)_{Reg.}$ was calculated, such that the desired regularized ΔS:

$$i\hbar\left(\Delta S\right)_{Reg} = \left(\delta S_T\right)_{Reg} \tag{13}$$

The violation of the master equation is of the form:

$$\Delta W + \frac{i}{2\hbar}(W, W) = \mathbf{A} = c^\alpha A_\alpha$$

The symmetries associated to the ghosts c^α are said to be broken.

In the present one loop level superspace formalism this, so called Wess Zumino mechanism, corresponds to finding out a superfield:

$$\underline{M}_1 = M_1 + \theta\left(i\Delta S\right)_{Reg} \tag{14}$$

one says that the anomalies have been canceled.

Let us consider W2 gravity theory as an interesting example:

$$S_0 = \frac{1}{2\pi}\int d^2x\,[\partial\phi\bar{\partial}\phi - h(\partial\phi)^2]$$

The BRST algebra associated to this theory is:

$$\delta_0\phi = c\partial\phi\,;\ \delta_0 h = \bar{\partial}c - h\partial c + \partial h c\,;\ \delta_0 c = (\partial c)c \tag{15}$$

The corresponding superfield action at classical level is:

$$\underline{S} = \underline{S}_0 + \underline{S}_1 + \underline{S}_2 \tag{16}$$

To realize the Wess Zumino mechanism one includes an extra field ρ and an additional shift symmetry associated to an extra ghost d:

$$\delta_0\,\rho = \partial c + c\,\partial\rho + d$$

We build up the superfields:

$$\Omega(x,\theta) = \rho(x) + \theta\pi^{[\rho]}(x) \tag{17}$$

We define the PV superfield action:

$$\underline{S}_{PV} = \underline{S}_{PV\,0} + \underline{S}_{PV\,1} + \underline{S}_{M} \tag{18}$$

Defining now the total action as

$$\underline{S}_T = \underline{S} + \underline{S}_{PV} = S_T + \theta\delta S_T \tag{19}$$

The superfield action at one loop order is:

$$\underline{M}_1(\alpha) = M_1(\alpha) + \theta\Big(i(\Delta S)_{Reg}(\alpha) + \mathbf{A}(\alpha)\Big) \tag{20}$$

where $M_1(\alpha)$ is the Wess Zumino term. For the $\alpha = 0$ case:

$$\begin{aligned}\underline{M}_1(\alpha=0) &= \frac{1}{12\pi}\{\frac{1}{2}\partial(\Omega-\tilde{\Omega})\overline{\partial}(\Omega-\tilde{\Omega}) - \frac{1}{2}(H-\tilde{H})(\partial(\Omega-\tilde{\Omega}))^2 \\ &+ (H-\tilde{H})\partial^2(\Omega-\tilde{\Omega})\}\end{aligned} \tag{21}$$

and

$$\overline{A} = \frac{1}{12\pi}(\partial^2 h - \partial\overline{\partial}\rho + \partial h\partial\rho + h\partial^2\rho)$$

We have shown that the (formal) master equation of the BV formalism can be represented as the requirement of a (formal) superspace structure for the quantum action. At one loop order, using the collective field approach to BV, we have shown that the Pauli Villars regularization procedure can be translated to superspace and that the superfied associated to the one loop order term of the action involves the anomalies and Wess Zumino terms.

The authors would like to thank Ashok Das for very important discussions. This work is supported in part by CNPq, FINEP, FAPERJ, FUJB and CAPES (Brazilian Research Agencies).

References

[1] I. A. Batalin and G. A. Vilkovisky, Phys. Lett. B102 (1981) 27, Phys. Rev. D28 (1983) 2567.

[2] M.Henneaux and C.Teitelboim, Quantization of Gauge Systems, Princeton University Press 1992, Princeton, New Jersey.

[3] J. Gomis, J. Paris and S. Samuel, Phys. Rep. 259 (1995) 1.

[4] W.Troost, P.van Nieuwenhuizen and A. Van Proeyen, Nucl. Phys. B333 (1990) 727.

[5] S. Ferrara, O. Piguet and M. Schweda, Nucl. Phys. B119 (1977) 493; K. Fujikawa, Progr. Theor. Phys. 59 (1978) 2045.

[6] J. Alfaro and P. H. Damgaard, Nucl. Phys. B404 (1993) 751.

[7] M. Henneaux, "Lectures on the Antifield-BRST Formalism for gauge Theories", Nucl. Phys. B - Proc. Suppl. 18A (1990) 47.

[8] W. Troost and A.Van Proeyen, Regularization and the BV formalism, presented at "Strings 93", Berkeley, May 1993.

[9] F.De Jonghe, The Batalin-Vilkovisky Lagrangian Quantization scheme with applications to the study of anomalies in gauge theories, PH.D. thesis K.U. Leuven, HEP-TH 9403143.

On the Nonrelativistic Limit of the φ^4 Theory in 2+1 Dimensions

M. Gomes, J. M. C. Malbouisson[**], and A. J. da Silva

Instituto de Física, Universidade de São Paulo,

Caixa Postal 66318, 05389-950, São Paulo, SP, Brazil.

July 31, 1996

It is generally believed that nonrelativistic field theories can be obtained from corresponding relativistic ones as appropriated limits for low momenta. Nonrelativistic approximations can be constructed by making canonical transformations over the Lagrangians[1] or by amending the nonrelativistic theories with other interaction terms, representing the effect of the integration of the relativistic degrees of freedom, inspired in the renormalization group spirit[2]. Also, nonrelativistic field theories in (2 + 1) dimensions have been obtained by transforming the matter field to eliminate from the Lagrangian rapidly oscillating terms as the mass m of the basic field increases indefinitely [3][4].

We study the nonrelativistic limit of the theory of a real self-interacting scalar field whose Lagrangian density is given by

$$\mathcal{L} = \frac{1}{2}\partial_\mu\phi\partial^\mu\phi - \frac{1}{2}m^2\phi^2 - \frac{\lambda}{4!}\phi^4 + \mathcal{L}_{c.t.}, \tag{1}$$

where ϕ, m and λ are renormalized quantities. In (2 + 1) dimensions, this theory is super-renormalizable and the only divergences are those arising from the two loop self-energy diagram. We calculate the 1PI four-point function to one loop order in an approximation for low external momenta such that it is possible to know from what part of the Hilbert space each contribution comes.

The approximation procedure consists of the following steps. Firstly, we use the Feynman identity

$$\frac{1}{ab^n} = \int_0^1 dx \frac{nx^{n-1}}{[(b-a)x + a]^{n+1}} \tag{2}$$

and make the necessary change of variables, to put the integrand in a symmetric form. We then integrate over k^0, over the angular part of the $\vec{k}$ and perform the parametric integral. The remaining integration over $|\vec{k}|$ is then divided into two parts, corresponding to the low (L) and high (H) energy contributions of the loop integration, by introducing an intermediate cutoff Λ such that $|\vec{p}| << \Lambda << m$ and $\frac{|\vec{p}|}{\Lambda} \simeq \frac{\Lambda}{m}$. In the low energy sector, $0 \leq |\vec{k}| < \Lambda$, we approximate the integrand by expanding it in powers of $\frac{|\vec{p}|}{m}$ and $\frac{|\vec{k}|}{m}$. In the high energy part, $\Lambda < |\vec{k}| < \Lambda_0(\to \infty)$, relativistic virtual modes are involved and only $\frac{|\vec{p}|}{m}$ can be considered a small quantity. Keeping all contributions up to order η^2 , where $\eta \simeq \frac{|\vec{p}|}{m}$ ($\simeq \frac{|\vec{p}|^2}{\Lambda^2} \simeq \frac{\Lambda^2}{m^2}$), we are able to evaluate the amplitude up to order $\frac{|\vec{p}|^2}{m^2}$, separating the contributions that comes from low and high loop momenta. Notice that, since in our prescription the integration over k^0 is unrestricted, locality in time is guaranteed.

The contributions of each channel (s, t and u) to the 1-loop scattering amplitude are calculated separating the low and high parts and one finds the t and u contribution comes entirely from the high-energy states in the Hilbert space and are of subleading order. This is natural since these processes involve virtual pair creation and annihilation not allowed in any nonrelativistic theory where propagation is only forward in time [4]. Adding, separately, all the low and high energy contributions, one obtains, in an arbitrary reference frame but for external nonrelativistic particles on the mass shell and up to order $\frac{|\vec{p}|^2}{m^2}$,

$$\begin{aligned} A^{NR}_{(1)L} &= \lambda + \frac{\lambda^2}{32\pi m}\left\{-\left(1 - \frac{(\vec{p}_1 - \vec{p}_2)^2}{8m^2}\right)\left[\ln\left(\frac{4\Lambda^2}{(\vec{p}_1 - \vec{p}_2)^2}\right) + i\pi\right]\right. \\ &\left. + \frac{(\vec{p}_1 - \vec{p}_2)^2}{4\Lambda^2} + \frac{(\vec{p}_1 - \vec{p}_2)^4}{8\Lambda^4} - \frac{3\Lambda^2}{2m^2} + \frac{21\Lambda^4}{16m^4}\right\} \end{aligned} \tag{3}$$

and

$$A^{NR}_{(1)H} = \frac{\lambda^2}{32\pi m}\left\{\left(1-\frac{(\vec{p}_1-\vec{p}_2)^2}{8m^2}\right)\ln\left(\frac{\Lambda^2}{4m^2}\right)-\frac{(\vec{p}_1-\vec{p}_2)^2}{4\Lambda^2} -\frac{(\vec{p}_1-\vec{p}_2)^4}{8\Lambda^4}+\frac{3\Lambda^2}{2m^2}-\frac{21\Lambda^4}{16m^4}-4+\frac{(\vec{p}_1-\vec{p}_2)^2}{24m^2}\right\}. \tag{4}$$

The nonrelativistic approximation of the 1-loop scattering amplitude obtained, $A^{NR}_{(1)} = A^{NR}_{(1)L}+A^{NR}_{(1)H}$, is independent of the auxiliary cutoff Λ, as it should, and coincides with the small momentum expansion of the exact relativistic amplitude up to order $\vec{p}^2/m^2$. This indicates that our approximation procedure can be applied with confidence in others theories where, eventually, exact analytical calculations can not be done.

The procedure of symmetrizing the integrand, using (2) and making convenient changes of variables, which is independent of space-time dimension, can be used to symplify the calculation of the two-point function. It disentangles the loop variables, allows the (k^0, l^0) integration to be donne exactly and then leads to a much easier computation of the "sunset" graph. Introducing the same intermediate cutoff Λ for both loop variables, one sees that both divergent and finite parts of the self-energy come entirely from the high, relativistic, virtual states, as it is expected (the L-L part of $\hat{\Sigma}_{(2)}$ is of order η^2). Using dimensional regularization, one gets

$$\hat{\Sigma}^{(\dim)}_{(2)}(p,m,\lambda,d) = \frac{i\lambda^2}{192\pi^2}\left[\frac{1}{3-d}+(\ln 2-\gamma)-E\left(\frac{p^2}{m^2}\right)\right], \tag{5}$$

where the function $E(z)$ is defined by

$$E(z) = \frac{1}{2\pi}\int_0^1 dx\int_0^1 dy\frac{y\ln\left(2\left[1-zD(x,y)\right]\right)}{\left[yC(x,y)\right]^{3/2}} \tag{6}$$

with $C(x,y) = yx(1-x)+(1-y)$ and $D(x,y) = (1-y)(1-(1-y)/C(x,y))$. With this result, the mass and wave function renormalization program can be implemented .

The approximation we have introduced not only permits the identification of the origin (in the Hilbert space) of each contribution, but it also allows the construction of a nonrelativistic reduction scheme at the level of the Green's functions.Notice that, for the purpose of comparison with amplitudes calculated from a nonrelativistic theory (with usual normalization), we need to multiply (3) and (4) by

$$(16w_{p1}w_{p2}w_{p1'}w_{p2'})^{-1/2} \simeq \frac{1}{4m^2}\left(1-\frac{\vec{p}_1^2+\vec{p}_2^2}{2m^2}+\ldots\right) \tag{7}$$

Let us initially analyze the above expressions for the NR amplitude up to the dominant order of the 1-loop correction, that is, let us consider

$$A_L = \frac{A^{NR}_{(1)L}}{4m^2} = \frac{\lambda}{4m^2}-\frac{\lambda^2}{128\pi m^3}\left[\ln\left(\frac{4\Lambda^2}{(\vec{p}_1-\vec{p}_2)^2}\right)+i\pi\right] \tag{8}$$

and

$$A_H = \frac{A^{NR}_{(1)H}}{4m^2} = \frac{\lambda^2}{128\pi m^3}\ln\left(\frac{\Lambda^2}{4m^2}\right). \tag{9}$$

One can see that equation (8) coincides with the result from the nonrelativistic theory specified by the Lagrangian density

$$\mathcal{L}_{NR} = \phi^\dagger\left(i\partial_t+\frac{\nabla^2}{2m}\right)\phi-\frac{v_0}{4}(\phi^\dagger\phi)^2, \tag{10}$$

with $v_o = \lambda/4m^2$ (compare with equation (2.13) of ref. [4]), if Λ is reinterpreted as a genuine (nonrelativistic) ultraviolet cutoff. Such an interpretation, however, can only be sustained after performing a nonrelativistic reduction procedure as follows. First, notice that, neglecting terms of order η or higher the low energy contribution for $\hat{\Sigma}^{NR}_{(2)}$ vanishes identically. This agrees with the nonrelativistic result where there is no correction at all to the propagator. We then fix the large parameter m and promote Λ to be the ultraviolet cutoff of the reduced nonrelativistic theory. This last step is the fundamental reinterpretation required for our reduction process.

The above nonrelativistic reduction of the leading term of the L-contribution to the two particle scattering amplitude is equivalent to the $m \to \infty$ limit effectuated on the classical Lagrangian [3][4] and it is also reproduced by making a Foldy-Wouthuysen transformation in the free part of the Lagrangian (1) [5]. An interesting aspect of this reduction procedure is that the contribution of high energy states appears providing the necessary counter-term to make the amplitude finite instead of logarithmic divergent. One can, in this way, better understand the renormalization of the nonrelativistic model of ref. [4].

Let us now examine the sub-dominant order. Disregarding constant terms which can be absorbed into a coupling constant renormalization, the low energy part is

$$A_L = \frac{\lambda}{4m^2} - \frac{\lambda}{4m^2}\frac{(\vec{p}_1+\vec{p}_2)^2+(\vec{p}_1-\vec{p}_2)^2}{4m^2} - \frac{\lambda^2}{128\pi m^3}\left[1-\frac{2(\vec{p}_1+\vec{p}_2)^2+3(\vec{p}_1-\vec{p}_2)^2}{8m^2}\right]\left[\ln\left(\frac{4\Lambda^2}{(\vec{p}_1-\vec{p}_2)^2}\right)+i\pi\right]. \quad (11)$$

To reproduce the new terms appearing in this expression, we add to (10) the effective interaction Lagrangian

$$\mathcal{L}_{int} = \frac{v_1}{4}\left(\phi^\dagger\frac{\nabla^2}{m^2}\phi^\dagger\phi^2 + \frac{(\vec{\nabla}\phi^\dagger)^2}{m^2}\phi^2\right) + \frac{v_2}{4}\left(\phi^\dagger\frac{\nabla^2}{m^2}\phi^\dagger\phi^2 - \frac{(\vec{\nabla}\phi^\dagger)^2}{m^2}\phi^2\right) \quad (12)$$

which is the more general, dimension 6, quadrilinear local nonrelativistic interaction. For the calculation of the contributions arising from these new vertices we will have to introduce ultraviolet cutoffs. It is easily verified that the polynomial part of the result is cutoff dependent and this freedom can be used to adjust it to match the polynomial part of (11). For that reason, we restrict the discussion to the non-polynomial part of the additional contribution which, in one loop order and up to $\mathcal{O}(\vec{p}^2/m^2)$, is (again, disregarding constant terms)

$$-\frac{m}{8\pi}v_0\left(v_1\frac{(\vec{p}_1+\vec{p}_2)^2}{m^2}+v_2\frac{(\vec{p}_1-\vec{p}_2)^2}{m^2}\right)\left[\ln\left(\frac{4\Lambda^2}{(\vec{p}_1-\vec{p}_2)^2}\right)+i\pi\right]. \quad (13)$$

Comparing with (11) we find $v_1 = -\lambda/16m^2$ and $v_2 = -3\lambda/32m^2$, which fixes the effective nonrelativistic Lagrangian up to the order $\vec{p}^2/m^2$.

The method we have used provides a systematic way of extracting different orders in $|\vec{p}|/m$ in the nonrelativistic approximation. The effective Lagrangian obtained is equivalent, in the leading order, to the quantum mechanical delta function potential. The new terms arising in the subleading order, however, can not be interpreted in terms of a two body potential.

References

[*] Supported in part by Conselho Nacional de Desenvolvimento Científico e Tecnológico (CNPq) e Fundação de Amparo à Pesquisa do Estado de São Paulo (FAPESP).

[**] On leave of absence from Instituto de Física, Universidade Federal da Bahia, Salvador, 40210-340, Brazil.

[1] L. L. Foldy and S. A. Wouthuysen, Phys. Rev. **78**, 29 (1950); K. M.Case, Phys. Rev. **95**, 1323 (1954).

[2] K. G. Wilson, Phys. Rev. **B4**, 3174 (1971); G. P. Lepage, proceedings of TASI-89, 1989; T. Kinoshita and G . Lepage in "Quantum Electrodynamics", T. Kinoshita ed, World Scientific, Singapore, 1990.

[3] R. Jackiw and S. Y. Pi, Phys. Rev. **D42**, 3500 (1990). The $m \to \infty$ limit of ϕ^4 theory in four dimensions was introduced by M. A. B. Bég and R. C. Furlong, Phys. Rev. **D31**,1370 (1985).

[4] O. Bergman, Phys. Rev. **D46**, 5474 (1992); T. Haugset and F. Ravndal, Phys. Rev. **D49**, 4299 (1994).

[5] J. D. Bjorken and S. D. Drell, "Relativistic Quantum Mechanics", McGraw-Hill, New York, (1964).

A Topological Bound for Electroweak Vortices from Supersymmetry

José D. Edelstein* and Carlos Núñez
Departamento de Física, Universidad Nacional de La Plata
C.C. 67, (1900) La Plata, Argentina
hep-th/9507102

Received March, 1996

We study the connection between $N = 2$ supersymmetry and a topological bound in a two-Higgs-doublet system having an $SU(2) \times U(1)_Y \times U(1)_{Y'}$ gauge group. We derive Bogomol'nyi equations from supersymmetry considerations showing that they hold provided certain conditions on the coupling constants, which are a consequence of the huge symmetry of the theory, are satisfied.

Supersymmetric Grand Unified Theories (SUSY GUTs) have attracted much attention in connection with the hierarchy problem in possible unified theories of strong and electroweak interactions [1, 2]. In view of the requirement of electroweak symmetry breaking, these models necessitate an enrichment of the Higgs sector [3], posing many interesting questions both from the classical and quantum point of view. In fact, many authors have explored the existence of stable vortex solutions in a variety of multi-Higgs systems [4, 5] which mimic the bosonic sector of SUSY GUTs, as it happens in the abelian Higgs model [6].

Vortices emerging as finite energy solutions of gauge theories can be usually shown to satisfy a topological bound for the energy, the so-called Bogomol'nyi bound [7]. Bogomol'nyi bounds were shown to reflect the presence of an extended supersymmetric structure [8]-[11] - this requiring certain conditions on coupling constants - where the central charge coincides with the topological charge. Being originated in the supercharge algebra, the bound is expected to be exact quantum mechanically.

Since multi-Higgs models can be understood to be motivated by SUSY GUTs, Supersymmetry is a natural framework to investigate Bogomol'nyi bounds. We shall study, then, the supersymmetric generalization of the $SU(2) \times U(1)_Y \times U(1)_{Y'}$ model with two-Higgs first introduced in Ref.[5]. The theory has the same gauge group structure as that of supersymmetric extensions of the Weinberg-Salam Model that arise as low energy limits of E_6 based Grand Unified or superstring theories. In spite of being a simplified model (in the sense that its Higgs structure is not so rich as that of Grand Unified theories), it can be seen as the minimal extension of the Standard Model necessary for having Bogomol'nyi equations. We show that the Bogomol'nyi bound of the model, as well as the Bogomol'nyi equations, are straight consequences of the requirement of $N = 2$ supersymmetry imposed on the theory. We also show explicitely that a necessary condition to achieve the $N = 2$ model implies certain relations between coupling constants that equal those found in [5] for the existence of a Bogomol'nyi bound.

The $SU(2) \times U(1)_Y \times U(1)_{Y'}$ gauge theory in $2+1$, introduced in Ref.[5], is described by the action

$$S = \int d^3x \left[-\frac{1}{4}\vec{W}_{\mu\nu} \cdot \vec{W}^{\mu\nu} - \frac{1}{4}F_{\mu\nu}F^{\mu\nu} - \frac{1}{4}G_{\mu\nu}G^{\mu\nu} + \frac{1}{2}\sum_{q=1}^{2} |\mathcal{D}_\mu^{(q)}\Phi_{(q)}|^2 - V(\Phi_{(1)}, \Phi_{(2)}) \right] \tag{1}$$

where $\Phi_{(1)}$ and $\Phi_{(2)}$ are a couple of Higgs doublets under the $SU(2)$ factor of the gauge group, A and B are real scalar fields and $\vec{W} = W^a\tau^a$ is a real scalar in the adjoint representation of $SU(2)$. The specific form of the potential will be determined below. The strength fields can be written in terms of the gauge fields A_μ, B_μ and $\vec{W}_\mu$. The covariant derivative is defined as:

$$\mathcal{D}_\mu^{(q)}\Phi_{(q)} = \left(\partial_\mu + \frac{i}{2}gW_\mu^a\tau^a + \frac{i}{2}\alpha_{(q)}A_\mu + \frac{i}{2}\beta_{(q)}B_\mu \right) \Phi_{(q)}, \qquad q=1,2 \tag{2}$$

*Consejo Nacional de Investigaciones Científicas y Técnicas.

where g is the $SU(2)$ coupling constant while $\alpha_{(q)}$ and $\beta_{(q)}$ represents the different couplings of $\Phi_{(q)}$ with A_μ and B_μ. A minimal $N = 1$ supersymmetric extension of this model is given by an action which in superspace reads:

$$\begin{aligned} S_{N=1} &= \frac{1}{2}\int d^3x d^2\theta \left[\overline{\Omega}_A\Omega_A + \overline{\Omega}_B\Omega_B + \overline{\Omega}^a_{\vec{W}}\Omega^a_{\vec{W}} - \overline{\mathcal{D}\mathcal{A}}\mathcal{D}\mathcal{A} - \overline{\mathcal{D}\mathcal{B}}\mathcal{D}\mathcal{B} - \overline{\mathcal{D}\mathcal{W}^a}\mathcal{D}\mathcal{W}^a + \xi_1\mathcal{A} + \xi_2\mathcal{B}\right. \\ &+ \left.\frac{1}{2}\sum_{q=1}^{2}\left[(\overline{\nabla^{(q)}\Upsilon_{(q)}})^a(\nabla^{(q)}\Upsilon_{(q)})^a + i\Upsilon^\dagger_{(q)}\left(\sqrt{2\lambda_1^{(q)}}\mathcal{A} + \sqrt{2\lambda_2^{(q)}}\mathcal{B} + \sqrt{2\lambda_3}\mathcal{W}^a\tau^a\right)\Upsilon_{(q)}\right]\right] \end{aligned} \tag{3}$$

where

$$\nabla^{(q)}\Upsilon_{(q)} = \left(\mathcal{D} + \frac{i}{2}g[\Gamma_{\vec{W}},] - \frac{i}{2}\alpha_{(q)}[\Gamma_A,] + \frac{i}{2}\beta_{(q)}[\Gamma_B,]\right)\Upsilon_{(q)}. \tag{4}$$

$\Upsilon_{(q)} \equiv (\Phi_{(q)}, \Psi_{(q)})$ are a couple of complex doublet superfields, $\mathcal{A} \equiv (A, \chi_A)$, $\mathcal{B} \equiv (B, \chi_B)$ and $\mathcal{W} \equiv (W^a, \chi^a_{\vec{W}})\tau^a$ are real scalar superfields and $\Gamma_A \equiv (A_\mu, \rho_A)$, $\Gamma_B \equiv (B_\mu, \rho_B)$ and $\Gamma_{\vec{W}} \equiv \Gamma^a_{\vec{W}}\tau^a = (W^a_\mu, \lambda^a)\tau^a$ are three spinor gauge superfields in the Wess-Zumino gauge. Ω_A, Ω_B and $\Omega^a_{\vec{W}}$, are the corresponding superfield strengths. Concerning $\lambda_1^{(q)}$, $\lambda_2^{(q)}$, λ_3, ξ_1 and ξ_2, they are real constants whose significance will be clear below. Finally, $\mathcal{D}$ is the usual supercovariant derivative, $\mathcal{D} = \partial_{\overline{\theta}} + i\overline{\theta}\not{\partial}$, while the γ-matrices are represented by $\gamma^0 = \tau^3$, $\gamma^1 = i\tau^1$ and $\gamma^2 = -i\tau^2$. In the sake of simplicity, we shall consider configurations with vanishing A, B and $\vec{W}$[1]. Then, the Higgs potential in (3) takes the form:

$$V(\Phi_{(1)}, \Phi_{(2)}) = \left(\sum_{q=1}^{2}\sqrt{\lambda_1^{(q)}}\Phi^\dagger_{(q)}\Phi_{(q)} - \frac{\xi_1}{\sqrt{2}}\right)^2 + \left(\sum_{q=1}^{2}\sqrt{\lambda_2^{(q)}}\Phi^\dagger_{(q)}\Phi_{(q)} - \frac{\xi_2}{\sqrt{2}}\right)^2 + \lambda_3\left(\sum_{q=1}^{2}\Phi^\dagger_{(q)}\tau^a\Phi_{(q)}\right)^2. \tag{5}$$

In order to extend the supersymmetric invariance of the theory to $N = 2$, we consider transformations with a complex parameter [9, 11]. We first combine all the spinors into Dirac fermions as:

$$\Sigma_A \equiv \chi_A - i\rho_A \quad , \quad \Sigma_B \equiv \chi_B - i\rho_B \quad \text{and} \quad \Xi^a \equiv \chi^a_{\vec{W}} - i\Lambda^a. \tag{6}$$

The fermionic contribution to the (non-minimal part of the) interaction lagrangian can be written as

$$\begin{aligned} L_{Fer,int} &= \sum_{q=1}^{2}\left[\frac{\alpha_{(q)} + \sqrt{8\lambda_1^{(q)}}}{4}\overline{\Psi}_{(q)}\Sigma_A\Phi_{(q)} + \frac{\beta_{(q)} + \sqrt{8\lambda_2^{(q)}}}{4}\overline{\Psi}_{(q)}\Sigma_B\Phi_{(q)} + \frac{g + \sqrt{8\lambda_3}}{4}\overline{\Psi}_{(q)}\Xi^a\tau^a\Phi_{(q)}\right. \\ &- \left.\frac{\alpha_{(q)} - \sqrt{8\lambda_1^{(q)}}}{4}\overline{\Psi}_{(q)}\tilde{\Sigma}_A\Phi_{(q)} - \frac{\beta_{(q)} - \sqrt{8\lambda_2^{(q)}}}{4}\overline{\Psi}_{(q)}\tilde{\Sigma}_B\Phi_{(q)} - \frac{g - \sqrt{8\lambda_3}}{4}\overline{\Psi}_{(q)}\tilde{\Xi}^a\tau^a\Phi_{(q)}\right], \end{aligned} \tag{7}$$

where $\tilde{\Xi}^a$, $\tilde{\Sigma}_A$ and $\tilde{\Sigma}_B$ are the charge conjugates of Ξ^a, Σ_A and Σ_B respectively. Now, transformations with complex parameter η are equivalent to transformations with a real parameter followed by a phase transformation for fermions, $\{\Xi^a, \Sigma_A, \Sigma_B, \Psi_{(q)}\} \longrightarrow e^{i\alpha}\{\Xi^a, \Sigma_A, \Sigma_B, \Psi_{(q)}\}$. Then, $N = 2$ supersymmetry requires invariance under this fermion rotation. One can easily see from (7) that fermion phase rotation invariance is achieved if and only if:

$$\lambda_3 = \frac{g^2}{8} \quad , \quad \lambda_1^{(q)} = \frac{\alpha^2_{(q)}}{8} \quad \text{and} \quad \lambda_2^{(q)} = \frac{\beta^2_{(q)}}{8}. \tag{8}$$

These conditions, imposed by the requirement of extended supersymmetry, fix the coupling constants exactly as they appear in [5]. Thus, we have shown that the potential and the coupling constants of the $SU(2) \times U(1)_Y \times U(1)_{Y'}$ model are simply dictated by $N = 2$ supersymmetry. This result is analogous to that recently found in the Abelian Higgs model [11].

We shall now analyse the $N = 2$ algebra of supercharges for our model. To construct the conserved charges we follow the Noether method and obtain $Q[\eta] \equiv \overline{\eta}Q + \overline{Q}\eta$, with

$$\begin{aligned} \overline{Q} &= -\frac{i}{2}\int d^2x\left\{\Sigma^\dagger_A\left[\frac{1}{2}\epsilon^{\mu\nu\lambda}F_{\mu\nu}\gamma_\lambda + \sum_{q=1}^{2}\frac{\alpha_{(q)}}{2}\Phi^\dagger_{(q)}\Phi_{(q)} - \xi_1\right] + \Sigma^\dagger_B\left[\frac{1}{2}\epsilon^{\mu\nu\lambda}G_{\mu\nu}\gamma_\lambda + \sum_{q=1}^{2}\frac{\beta_{(q)}}{2}\Phi^\dagger_{(q)}\Phi_{(q)}\right.\right. \\ &- \left.\left.\xi_2\right] + \Xi^{\dagger a}\left[\frac{1}{2}\epsilon^{\mu\nu\lambda}W^a_{\mu\nu}\gamma_\lambda + \frac{g}{2}\sum_{q=1}^{2}\Phi^\dagger_{(q)}\tau^a\Phi_{(q)}\right] - i\sum_{q=1}^{2}\Psi^\dagger_{(q)}\gamma^\mu\mathcal{D}^{(q)}_\mu\Phi_{(q)}\right\} \end{aligned} \tag{9}$$

[1] The $SU(2) \times U(1)_Y \times U(1)_{Y'}$ theory with its full field content is considered in Ref.[12].

Since we are interested in connecting the $N = 2$ supercharge algebra with Bogomol'nyi equations and bound, we impose static configurations with $A_0 = B_0 = W_0^a = 0$, and we restrict ourselves to the bosonic sector of the theory after computing the algebra. We obtain, after some calculations

$$\{\tilde{Q}, Q\} = 2\overline{\eta}\gamma_0\eta P^0 + \overline{\eta}\eta Z \tag{10}$$

where

$$P^0 = E = \frac{1}{2}\int d^2x \left[\frac{1}{2}(W_{ij}^a)^2 + \frac{1}{2}(F_{ij})^2 + \frac{1}{2}G_{ij}^2 + \sum_{q=1}^{2}|\mathcal{D}_i^{(q)}\Phi_{(q)}|^2 + V(\Phi_{(1)}, \Phi_{(2)})\right] \tag{11}$$

while the central charge is given by:

$$\begin{aligned} Z &= -\int d^2x \left[\frac{1}{2}\epsilon^{ij}F_{ij}\left(\sum_{q=1}^{2}\frac{\alpha_{(q)}}{2}\Phi_{(q)}^\dagger\Phi_{(q)} - \xi_1\right) + \frac{1}{2}\epsilon^{ij}G_{ij}\left(\sum_{q=1}^{2}\frac{\beta_{(q)}}{2}\Phi_{(q)}^\dagger\Phi_{(q)} - \xi_2\right)\right. \\ &+ \left.\frac{g}{4}\epsilon^{ij}W_{ij}^a\sum_{q=1}^{2}\Phi_{(q)}^\dagger\Phi_{(q)} + i\epsilon^{ij}\sum_{q=1}^{2}(\mathcal{D}_i^{(q)}\Phi_{(q)})(\mathcal{D}_j^{(q)}\Phi_{(q)})^*\right] = \frac{1}{2}\oint \mathcal{V}_i dx^i, \end{aligned} \tag{12}$$

where $\mathcal{V}^i$ is given by

$$\mathcal{V}^i = \left(\xi_1 A_j + \xi_2 B_j + i\sum_{q=1}^{2}\Phi_{(q)}^\dagger\mathcal{D}_j^{(q)}\Phi_{(q)}\right)\epsilon^{ij}. \tag{13}$$

Finite energy dictates the following asymptotic behaviour for the Higgs doublets [5]

$$\Phi_{(1)_\infty} = \frac{\phi_0}{\sqrt{2}}\begin{pmatrix} 0 \\ \exp in_{(1)}\varphi \end{pmatrix} \quad , \quad \Phi_{(2)_\infty} = \frac{\phi_0}{\sqrt{2}}\begin{pmatrix} \exp in_{(2)}\varphi \\ 0 \end{pmatrix}, \tag{14}$$

where $n_{(1)}$ and $n_{(2)}$ are integers that sum up to the topological charge of the configuration m,

$$m \equiv n_{(1)} + n_{(2)}. \tag{15}$$

Then, coming back to eq.(12) for the central charge, after Stokes' theorem, we see that

$$Z = \oint(\xi_1 A_i + \xi_2 B_i)dx^i = -4\pi\phi_0^2 m \tag{16}$$

that is, the central charge of the $N = 2$ algebra equals the topological charge of the configuration. It is now easy to find the Bogomol'nyi bound from the supersymmetry algebra (10). Indeed,

$$\{\tilde{Q}, Q\} = \int d^2x \left[(\delta\Xi^a)^\dagger(\delta\Xi^a) + (\delta\Sigma_A)^\dagger(\delta\Sigma_A) + (\delta\Sigma_B)^\dagger(\delta\Sigma_B) + \sum_{q=1}^{2}(\delta\Psi_{(q)})^\dagger(\delta\Psi_{(q)})\right] \geq 0. \tag{17}$$

the lower bound being saturated if and only if $\delta\Xi^a = \delta\Sigma_A = \delta\Sigma_B = \delta\Psi_{(q)} = 0$. Non-trivial solutions to these equations force us to choose a parameter with definite chirality, say η_+. Now, conditions

$$\delta_{\eta_+}\Xi^a = \delta_{\eta_+}\Sigma_A = \delta_{\eta_+}\Sigma_B = \delta_{\eta_+}\Psi_{(q)} = 0 \tag{18}$$

are nothing but the Bogomol'nyi equations of the theory:

$$\frac{1}{2}\epsilon^{ij}F_{ij} + \sum_{q=1}^{2}\frac{\alpha_{(q)}}{2}\Phi_{(q)}^\dagger\Phi_{(q)} - \xi_1 = 0 \quad , \quad \frac{1}{2}\epsilon^{ij}G_{ij} + \sum_{q=1}^{2}\frac{\beta_{(q)}}{2}\Phi_{(q)}^\dagger\Phi_{(q)} - \xi_2 = 0 \tag{19}$$

$$\epsilon^{ij}W_{ij}{}^a + g\sum_{q=1}^{2}\Phi_{(q)}^\dagger\tau^a\Phi_{(q)} = 0 \quad \text{and} \quad (\mathcal{D}_i^{(q)} - i\epsilon_{ij}\mathcal{D}_j^{(q)})\Phi_{(q)} = 0. \tag{20}$$

Note that, for this chiral parameter, eq.(17) implies the Bogomol'nyi bound of our model,

$$M \geq 2\pi\phi_0^2 m. \tag{21}$$

Let us remark on the fact that field configurations solving Bogomol'nyi equations break half of the supersymmetries (those generated by η_-), a common feature in all models presenting Bogomol'nyi bounds with supersymmetric extension [13]. Were we faced with an antichiral parameter, we would have obtained antisoliton solutions with broken of the supersymmetry transformation generated by η_+.

The connection of our model with realistic supersymmetric extensions of the Standard model, and its coupling with supergravity (the possible existence of string-like solutions in this last theory) remain open problems. We hope to report on these issues in a forthcoming work.

References

[1] G.G.Ross, *Grand Unified Theories*, Frontiers in Physics Vol.**60**, The Benjamin-Cummings Publishing Company (1984).

[2] Particle Data Book, Phys.Rev.**D50**(1994)1173.

[3] See for example P.Nath, R.Arnowitt and A.H.Chamseddine, *Applied $N = 1$ Supergravity*, ICTP Series on Theoretical Physics, vol.1, World Scientific (1984) and References therein.

[4] M.A.Earnshaw and M.James, Phys.Rev.**D48** (1993)5818; G.Dvali and G.Senjanovich, IC/93/63 (1993); L.Perivolaropoulos, Phys.Lett.**B316** (1993)528; H.S.La, CPT-TAMU-1/93 (hep-th/9302220).

[5] G.Bimonte and G.Lozano, Phys.Lett.**B326**(1994)270.

[6] H.B. Nielsen and P. Olesen, Nucl.Phys.**B61**(1973)45.

[7] E.B.Bogomol'nyi, Sov. Jour. Nucl. Phys. **24** (1976) 449; H.de Vega and F.A. Schaposnik, Phys. Rev. **D14** (1976) 1160.

[8] E.Witten and D.Olive, Phys.Lett.**78B**(1978)97.

[9] C.Lee, K.Lee and E.J.Weinberg, Phys.Lett.**B243**(1990)105.

[10] Z.Hlousek and D.Spector, Nucl.Phys.**B370**(1992)143; **B397**(1993)173; Phys.Lett. **B283**(1992)75; Mod.Phys.Lett.**A7**(1992)3403.

[11] J.D.Edelstein, C.Núñez and F.Schaposnik, Phys.Lett.**B329**(1994)39.

[12] J.D.Edelstein and C.Núñez, in preparation.

[13] C.M.Hull, Nucl.Phys.**B239**(1984)541.

Dressing Symmetry in the sinh–Gordon Model and the Semenov–Tian–Shansky Bracket

Guillermo Cuba* and Roman Paunov†
Centro Brasileiro de Pesquisas Fisicas
Rua Dr. Xavier Sigaud 150, Rio de Janeiro, Brazil

Received March, 1996

We calculate the Poisson bracket $\{g \overset{\otimes}{,} g\}$ of the dressing group element g which generates a generic one soliton solution from the vacuum and compare it with the Semenov–Tian-Shansky bracket. The last endows the dressing group with a structure of a Lie–Poisson group. Our conclusion is that the two brackets do not coincide. We propose two inequivalent possibilities to get a relation between them. The first suggests that the Lie–Poisson structure on the dressing group has to be modified by including the topological charge. The second exploits the fact that the dressing group elements which generate one solitons from the vacuum has a specific form.

The solitons play important role in the modern particle and solid state physics [1]. It became clear (see [2] for a review) that many nonlinear integrable equations possess soliton solutions. The study of the solitons contributed to the development of the *inverse scattering method*. The last is a powerful tool in solving the Cauchy problem for integrable equations.

In the present talk we consider soliton solutions of the sinh–Gordon equation

$$\begin{aligned} \partial_+\partial_-\varphi &= 2m^2 sh2\varphi \qquad \partial_\pm = \frac{\partial}{\partial x^\pm} \\ x^\pm &= x \pm t \end{aligned} \tag{1}$$

which differs from the sine–Gordon model by a trivial renormalization of the field φ. We can quote two reasons to study the sine–Gordon theory in two dimensions: first, the sine-Gordon model is an integrable field theory both at the classical and at the quantum level; second, the quantum sine-Gordon theory is a massive integrable perturbation of a conformally invariant model. The conformal invariance plays important role in the study of the two dimensional critical phenomena and in the string theory.

The equation (1) can be equivalently written as integrability condition of the linear system

$$(\partial_\pm + A_\pm)T(x^+, x^-, \lambda) = 0 \tag{2}$$

where $A_\pm$ are components of a connection which takes values in the Lie algebra $sl(2)$

$$A_\pm = \pm\partial_\pm\Phi + me^{\pm ad\Phi}\mathcal{E}_\pm \tag{3.a}$$

$$\mathcal{E}_\pm = \lambda^{\pm 1}\left(E^+ + E^-\right) \qquad \Phi = \frac{1}{2}\varphi H \tag{3.b}$$

and λ is the spectral parameter; H, $E^\pm$ are the generators of the $sl(2)$ Lie algebra $[H, E^\pm] = \pm 2E^\pm$, $[E^+, E^-] = H$. The 2×2 matrix T together with the normalization condition $T(0, 0, \lambda) = T(0) = \mathbf{1}$ is known as the normalized transport matrix.

*E-mail address gcubac@cbpfsu1.cat.cbpf.br
†E-mail address paunov@cbpfsu1.cat.cbpf.br

To introduce the one soliton solution we consider the variable $\epsilon^+(x^+, x^-) = \epsilon^+(\mathbf{x})$ whose dependence on the light cone variables is dictated by the relation

$$\frac{\epsilon^+(\mathbf{x}) + \mu}{\epsilon^+(\mathbf{x}) - \mu} = a \exp\{2m(\mu x^+ + \frac{x^-}{\mu})\}$$

$$a = \frac{\epsilon^+ + \mu}{\epsilon^+ - \mu}, \quad \epsilon^+ = \epsilon^+(0) \tag{4.a}$$

$$e^{-\varphi(\mathbf{x})} = -\frac{\epsilon^+(\mathbf{x})}{\mu} \tag{4.b}$$

where μ is the soliton rapidity. In what follows we shall also need the variable $\epsilon^-(\mathbf{x})$ related to ϵ^+ and μ by $\epsilon^+(\mathbf{x})\epsilon^-(\mathbf{x}) = \mu^2$.

The dressing group is a symmetry of the nonlinear integrable equations [3] which acts on the connection (3.a) by gauge transformations which preserve its form. Alternatively a dressing transformation can be introduced by its action on the normalize

$$T(\mathbf{x}, \lambda)) \quad \rightarrow \quad T^g(\mathbf{x}, \lambda) = \mathbf{g}(\mathbf{x}, \lambda) \cdot \mathbf{T}(\mathbf{x}, \lambda) \cdot \mathbf{g}^{-1}(\mathbf{0}, \lambda) \tag{5}$$

In the above expression $g(\mathbf{x}, \lambda)$ is an unimodular 2×2 matrix the elements of which are functions on the spectral parameter.

It was shown in [1], [5] that in order to ensure the covariance of the Poisson brackets under the dressing group action, the following bracket

$$\{g(\lambda) \overset{\otimes}{,} g(\zeta)\}_{STS} = \frac{1}{4}[r, g(\lambda) \otimes g(\zeta)] \tag{6.a}$$

$$r = -\frac{\lambda^2 + \zeta^2}{\lambda^2 - \zeta^2} H \otimes H - 4\frac{\lambda\zeta}{\lambda^2 - \zeta^2}(E^+ \otimes E^- + E^- \otimes E^+) \tag{6.b}$$

on the dressing group has to be postulated. The above matrix Poisson bracket is known as the Semenov-Tian-Shansky bracket.

In [6], [7], [8] the dressing group element which generates the one soliton solutions (4.a), (4.b) from the vacuum one $\varphi = 0$ was explicitly calculated. It reads

$$g(x, \lambda) = \frac{e^{\Phi(x)}}{2(\lambda - \mu)} \begin{pmatrix} \lambda + \epsilon^+(x) & \lambda + \epsilon^+(x) \\ \lambda + \epsilon^-(x) & \lambda + \epsilon^-(x) \end{pmatrix} + + \frac{e^{\Phi(x)}}{2(\lambda + \mu)} \begin{pmatrix} \lambda - \epsilon^+(x) & -\lambda + \epsilon^+(x)) \\ -\lambda + \epsilon^-(x) & \lambda - \epsilon^-(x) \end{pmatrix} \tag{7}$$

To calculate the bracket $\{g \overset{\otimes}{,} g\}$ we recall that according to [2], [9] the phase space of the one solitons is two dimensional. Choosing ϵ^+ and μ (4.a) as independent coordinates one can show that

$$\{\epsilon^+, \mu\} = -\frac{1}{2}((\epsilon^+)^2 - \mu^2) \tag{8}$$

We shall also use the λ-depending representation of $sl(2)$

$$X^0(\lambda) = \frac{1}{\lambda^2 - \mu^2}((\lambda^2 + \mu^2)H + 2\lambda\mu(E^+ - E^-))$$

$$X^{\pm}(\lambda) = \pm\frac{\lambda\mu}{\lambda^2 - \mu^2}\left(H + \left(\frac{\lambda}{\mu}\right)^{\pm 1} E^+ - \left(\frac{\mu}{\lambda}\right)^{\pm 1} E^-\right) \tag{9}$$

in which the adjoint action of (7) is diagonal: $Ad\, g(\lambda)X^k(\lambda) = g(\lambda)X^k(\lambda)g^{-1}(\lambda) = e^{k\varphi}X^k(\lambda)$, $k = 0, \pm$.

Combining (7) with (8) we get the following expression

$$\{g(\lambda) \overset{\otimes}{,} g(\zeta)\} \cdot g^{-1}(\lambda) \otimes g^{-1}(\zeta) = \frac{P_{12} - 1}{2}\{\ln\epsilon^+, \mu\}\frac{\lambda}{\mu(\lambda^2 - \mu^2)}((\mu + \epsilon^-)X^+(\lambda) + (\mu + \epsilon^+)X^-(\lambda)) \otimes X^0(\zeta) \tag{10}$$

where P_{12} is the operator which permutes the factors in the tensor product and the spectral parameters λ and ζ. We also note that in the representation (9) the classical r–matrix (6.b) reads

$$r = 2(P_{12}-1)\frac{\lambda\mu}{\lambda^2-\mu^2}\left(X^+(\lambda)-X^-(\lambda)\right)\otimes X^0(\zeta)\ldots \tag{11}$$

where we have omited the terms which do not contribute to the commutator $[r, g\otimes g]$.

Using (6.a) and (7) we observe that the following relation is valid

$$\{g(\lambda)\overset{\otimes}{,} g(\zeta)\}_\star \cdot g^{-1}(\lambda)\otimes g^{-1}(\zeta) = \frac{1}{4}(1-Ad\,h(\lambda)\otimes Ad\,h(\zeta))\cdot r \tag{12}$$

provided that

$$\{\epsilon^+, \mu\}_\star = \mu\epsilon^+\frac{\epsilon^+-\mu}{\epsilon^++\mu} \tag{13}$$

and the element $h(\lambda)$ has the same form as (7) but with $\epsilon^+ \to -\epsilon^+$. Therefore $h(\lambda)$ generates the solution $\varphi + i\pi$ from the vacuum. The last suggests that one has to modify the bracket (6.a) by a factor depending on the topological charge. On the other hand, the bracket (13) differs from (8). It is known [9] that the Hamiltonians which generate the $x^\pm$ flows are $\mathcal{H}_\pm = \pm m\mu^\pm$. Due to that, the bracket $\{\,,\,\}_\star$ produces the equation

$$\partial_+\partial_-\varphi = -m^2\frac{ch\frac{\varphi}{2}}{sh^3\frac{\varphi}{2}} \tag{14}$$

which does not seem to be integrable.

There is another possible relation between (6.a) and (10). It is discussed in details in [8]. The basic idea is that to obtain the expression (7) one has to impose the following constraints

$$c_1(\lambda) = g_{12}(\lambda)+g_{21}(\lambda) = 0 \tag{15.a}$$

$$c_2(\lambda) = g_{11}(\lambda)-g_{22}(\lambda)-\frac{\lambda^2+\mu^2}{2\lambda\mu}(g_{12}(\lambda)-g_{21}(\lambda)) = 0 \tag{15.b}$$

$$c_3(\lambda) = \frac{d\kappa}{d\lambda}(\lambda) \tag{15.c}$$

$$\kappa(\lambda) = \frac{\lambda^2}{\lambda^2-\mu^2}\left(g_{11}(\lambda)-\frac{\mu}{\lambda}(g_{12}(\lambda)-g_{21}(\lambda))-\frac{\mu^2}{\lambda^2}g_{21}(\lambda)\right) \tag{15.d}$$

on the dressing group; $g_{ij}(\lambda)$, $i,j=1,2$ are the matrix elements of the matrix $g(\lambda)$ (5). The element (7) is then reproduced together with the relation $\kappa = e^{\frac{\varphi}{2}}$ Following the general approach to the Hamiltonian systems with constraints we introduce the λ-depending "canonical" Hamiltonian $\mathcal{H}(\lambda) = \frac{f_{11}(\lambda)-f_{22}(\lambda)}{f_{12}(\lambda)-f_{21}(\lambda)} \approx \frac{1}{2}(\frac{\lambda}{\mu}+\frac{\mu}{\lambda})$ where we have used the Dirac's notation of weak identity [10]. Introducing the total Hamiltonian $\mathcal{H}_T(\lambda) = \mathcal{H}(\lambda)+\sum_1^3 u^i(\lambda)c_i(\lambda)$ we get the identity

$$\{\mathcal{H}_T(\lambda), \kappa(\zeta)\}_{STS} \approx \{\mathcal{H}(\lambda), \kappa\} \tag{16}$$

for $u^1(\lambda) = \frac{1}{32}\left(\frac{\lambda^2-\mu^2}{\lambda\mu}\right)^2(\kappa+\kappa^{-1})$ and arbitrary values of the other two Lagrange multipliers. This allows us to state that the one–soliton brackets (8), (10) arise from (6.a) after a suitable "gauge" fixing.

Acknowledgements

R. P. is grateful to the Organizing Commitee of XVI Encontro Nacional de Física de Partículas e Campos for the invitation to give the present talk in Caxambu. G. C. and R. P. highly appreciate the financial support from Capes and CNPq respectively.

References

[1] A. Newell, *Solitons in Mathematics and Physics*, SIAM, 1985
Solitons, Topics in Current Physics 17, R. K. Bullough and P. J. Caudrey eds., Springer-Verlag 1980.

[2] L. D. Faddeev and L. A. Takhtajan, *Hamiltonian Methods in the Theory of Solitons*, Springer, 1986
S. Novikov, S. Manakov, L. P. Pitaevsky and V. E. Zakharov, *Theory of Solitons*, Consultants Bureau, 1984.

[3] E. Date, M. Jimbo, M. Kashiwara and T. Miwa, *Transformation Groups for Soliton Equations*, in: Non-linear integrable systems, eds M. Jimbo and T. Miwa (World Scientific, Singapore, 1983).

[4] M. Semenov-Tian-Shansky, Publ. RIMS 21 (1985) 1237,
M. Semenov-Tian-Shansky, *Poisson Lie Groups, Quantum Duality Principle, and the Quantum Double*, hep-th@9304042

[5] O. Babelon, D. Bernard, Phys. Lett. **B260** (1991) 81,
Commun. Math. Phys. **149** (1992) 279.

[6] O. Babelon, D. Bernard, Int. J. Mod. Phys. **A8** (1993) 507.

[7] R. Paunov, Phys. Lett **B** 347(1995)63.

[8] G. Cuba and R. Paunov, *A Note on The Symplectic Structure on the Dressing Group in the sinh-Gordon Model*, hep-th/9510174.

[9] O. Babelon, D. Bernard, Phys Lett. **B317** (1993) 363.

[10] P. A. M. Dirac, *Lectures on Quantum Mechanics*, N.Y., Academic Press, 1967
M. Henneaux and C. Teitelboim, *Quantization of Gauge Systems*, Princeton University Press, N. J., 1992.

Light-front quantization of Chern-Simons systems

Leon R. Mansur, *CBPF* and Prem P. Srivastava, *IF, UERJ, Rio de Janeiro*

Received March, 1996

Light-front quantization of the Chern-Simons theory coupled to complex scalar as well as fermion field is performed in the local light-cone gauge following the Dirac procedure. The light-front Hamiltonian turns out to be simple one and the framework may be useful to construct renormalized field theory of *anyons*. The theory is shown to be relativistic inspite of the unconventional transformations of the matter and the gauge fields.

1. Introduction

Chern-Simons (CS) gauge theories[1,2] coupled to matter field have been proposed to describe excitations with fractional statistics[3,4], *anyons*, and suggested to be relevant for describing the quantized Hall effect and possibly the high-T_c superconductivity[5] where the dynamics is effectively confined to a plane. There are, however, controversies related to the quantized field theoretical formulation. The Lagrangian (path integral) formulation[5], for example, seems to give result which disagree with the canonical Hamiltonian formulation[7-10]. It is claimed that the theory though shown relativistic has angular momentum anomaly[11] or shows anyonicity only in some nonlocal gauges[10,7]. Internal algebraic inconsistency[10] of using two *local* gauge conditions[12] in the context of the Coulomb gauge has also been stressed. The anomaly is also found absent in some recent works[13,14] and doubts have been raised about the anyonicity being gauge artefact[9]. We clarify here some of the points by performing the light-front (*l.f.*) quantization[15] of the CS theory coupled to the complex scalar field in the light-cone gauge. The *l.f.* vacuum[16,17] is known to be simpler than the conventional one and the anyonic excitations and possibly some non-perturbative effects may be studied more conveniently. In the descripton of the spontaneous symmetry breaking on the *l.f.*, for example, it was found[18] that we do obtain the same physical result as that in the equal-time quantization, although achieved through a different mechanism. The conventional description requires *additional external constraints* in the theory based on physical considerations while the analogous ones on the *l.f.* were shown[18] to arise from the *self-consistency requirements* in the Hamiltonian theory itself. We conclude from our study that the abovementioned rotational anomaly should rather be interpreted as gauge artefact, that even in the present theory the application of two local gauge-fixing conditions on the phase space is totally consistent, and that the *l.f.* Hamiltonian is simpler when compared to that found in the local or nonlocal Coulomb gauge and it may be useful for constructing a renormalized theory.

2. Light-front Quantization of Chern-Simons Theory

We first discuss the gauge theory based on

$$\mathcal{L} = (\mathcal{D}^\mu \phi)(\widetilde{\mathcal{D}}_\mu \phi^*) + \frac{\kappa}{4\pi}\epsilon^{\mu\nu\rho} A_\mu \partial_\nu A_\rho$$

with

$$\mathcal{D}_\mu = (\partial_\mu + ieA_\mu)$$

$$\widetilde{\mathcal{D}}_\mu = (\partial_\mu - ieA_\mu)$$

etc. For the coordinates x^μ, and for all other vector or tensor quantities, we define the *light-front* $\pm$ *components* by $x^\pm = (x^0 \pm x^2)/\sqrt{2} = x_\mp$. We take $x^+ \equiv \tau$ to indicate the *light-front time coordinate*, x^- is the *longitudinal space coordinate* and x^1 is the *transverse* one. The conjugate momenta are

$$\pi = \widetilde{\mathcal{D}}_- \phi^*, \pi^* = \mathcal{D}_- \phi, \pi^\mu = a\epsilon^{+\mu\nu} A_\nu$$

where $\kappa = 4\pi a$. The conserved current

$$j^\mu = ie(\phi^* \mathcal{D}^\mu \phi - \phi \widetilde{\mathcal{D}}^\mu \phi^*)$$

is gauge invariant and its contravariant vector property must remain intact if the theory constructed is relativistic.

Local light-cone gauge (*l.c.g.*), $A_- = 0$, is accessible in the Lagrangian theory; it will be shown below to be accessible also on the phase space of the gauge theory. Since a *self-consistent Hamiltonian theory*[19] must not contradict the Lagrangian theory we may start by deriving first some boundary conditions from the Lagrange eqs. written in the *l.c.g.*. From $2a\partial_- A_1 = j^+$ we derive that the electric charge is given by

$$Q = \int d^2x\, j^+ = 2a \int dx^1 \left[A_1(x^- = \infty, x^1) - A_1(x^- = -\infty, x^1)\right] .$$

For nonvanishing charge, A_1 may thus *not* satisfy the periodic or the vanishing boundary conditions at infinity along x^-. We assume the *anti-periodic* boundary conditions for the gauge fields along x^- while the vanishing ones along x^1. For the scalar fields we assume vanishing boundary conditions. The canonical Hamiltonian may then be written as

$$H_c = \int d^2x \left[(\mathcal{D}_1 \phi)(\widetilde{\mathcal{D}}_1 \phi^*) - A_+ \Omega \right]$$

where

$$\Omega = ie(\pi\phi - \pi^*\phi^*) + a\epsilon^{+ij}\partial_i A_j + \partial_i \pi^i$$

and $i = -, 1$. We follow the Dirac method[19] to construct an Hamiltonian for the constrained systems (1). The primary constraints are

$$\pi^+ \approx 0, \mathsf{T}^i \equiv \pi^i - a\epsilon^{+ij} A_j \approx 0, \mathsf{T} \equiv \pi - \widetilde{\mathcal{D}}_- \phi^* \approx 0, \mathsf{T}^* \equiv \pi^* - \mathcal{D}_- \phi \approx 0.$$

The preliminary Hamiltonian is

$$H' = H_c + \int d^2x \left[u\mathsf{T} + u^*\mathsf{T}^* + u_i \mathsf{T}^i + u_+ \pi^+ \right]$$

where u, u^*, u^i, u_+ are Lagrange multiplier fields. We postulate initially the standard *equal-*τ Poisson brackets, and require the *persistency in* τ of the constraints which leads to a *secondary constraint* $\Omega \approx 0$. The Hamiltonian is then extended to include this one as well and the step repeated and we find that no new constraint is generated. The Ω and π^+ can be shown to generate gauge transformations and the constraints $\pi^+ \approx 0$ and $\Omega \approx 0$ are first class[19] while the remaining ones are second class[19]. From the Hamilton's eqs. of motion we verify that there does exist a choice of the Lagrange multiplier fields for which $A_- \approx 0$ and $dA_-/d\tau \approx 0$. The light-cone gauge $A_- \approx 0$ is thus accessible on the phase space (for a fixed τ). We add in the theory this gauge-fixing constraints so that now the set of second class constraints may be checked to be: T_m, $m = 1, 2..6$:

$$\mathsf{T}_1 \equiv \mathsf{T}^-, \mathsf{T}_2 \equiv \mathsf{T}^1, \mathsf{T}_3 \equiv \mathsf{T}, \mathsf{T}_4 \equiv \mathsf{T}^*, \mathsf{T}_5 \equiv A_-, \mathsf{T}_6 \equiv \Omega ,$$

while $\pi^+ \approx 0$ stays first class. Next the Poisson brackets are modified to define the Dirac brackets so that we may now write $\mathsf{T}_m = 0$ as strong relations. The Dirac brackets are constructed to be

$$\{f, g\}_D = \{f, g\} - \int d^2u d^2v \, \{f, \mathsf{T}_m(u)\} \, C^{-1}_{mn}(u, v) \, \{\mathsf{T}_n(v), g\}$$

where $C^{-1}(x,y)$ is the inverse[20] of the constraint matrix with the elements $C_{mn} = \{\mathsf{T}_m, \mathsf{T}_n\}$. We find that A_+ which is already absent in T_m, drops out also from H_c since $\Omega = 0$. The $\pi^+ \approx 0$ stays first class even with respect to the Dirac brackets and the multiplier u_+ is left undetermined. The variable π^+ decouples and we may choose $u_+ = 0$ so that π^+ and A_+ are eliminated. The light-front Hamiltonian then simplifies to

$$H^{l.f.}(\tau) = \int d^2x \; (\mathcal{D}_1\phi)(\tilde{\mathcal{D}}_1\phi^*) \; .$$

There is still a $U(1)$ *global* gauge symmetry generated by Q. The only *independent variables* left are ϕ and ϕ^* which satisfy the well known equal-τ *l.f. Dirac brackets*

$$\{\phi,\phi\}_D = 0, \; \{\phi^*,\phi^*\}_D = 0, \quad \{\phi(x,\tau),\phi^*(y,\tau)\}_D = K(x,y)$$

where

$$K(x-y) = -(1/4)\epsilon(x^- - y^-)\delta(x^1 - y^1).$$

We remark that we could alternatively eliminate π^+ by introducing *another local gauge-fixing weak condition* $A_+ \approx 0$ (and $dA_+/d\tau \approx 0$) which is shown to be accessible. The additional modification of brackets does not alter the Dirac brackets of the scalar field already obtained. There is thus *no inconsistency in choosing the two local and weak gauge-fixing conditions* $A_\pm \approx 0$ *on the phase space at one fixed time* τ *in the CS gauge theory.* Analogous conclusion holds also for the local Coulomb gauge in the equal-time formulation where we require $A^0 \approx 0$ and $div\vec{A} \approx 0$.

We check now the *self-consistency*[19]. From the Hamilton's eq. for ϕ we derive ($e = 1$, $\pi^* = \partial_-\phi$:)

$$\partial_-\partial_+\phi(x,\tau) = \{\pi^*(x,\tau), H(\tau)\}_D = \frac{1}{2}\mathcal{D}_1\mathcal{D}_1\phi - iA_+\partial_-\phi - \frac{i}{2}(\partial_-A_+)\phi$$

where

$$-2a\partial_-A_+ = j^1 = -ie(\phi^*\mathcal{D}_1\phi - \phi\tilde{\mathcal{D}}_1\phi^*).$$

On comparing this with the corresponding Lagrange eq.

$$\partial_+\partial_-\phi = \frac{1}{2}\mathcal{D}_1\mathcal{D}_1\phi - iA_+\partial_-\phi - \frac{i}{2}(\partial_-A_+)\phi$$

in the light-cone gauge it is suggested for convenience to rename the expression A_+ on the phase space by (the above eliminated) A_+. We thus obtain agreement also with the other Lagrange eq.

$$-2a\partial_-A_+ = j^1 = -ie(\phi^*\mathcal{D}_1\phi - \phi\tilde{\mathcal{D}}_1\phi^*).$$

The Gauss' law eq. is seen to correspond to $\Omega = 0$ and the remaining Lagrange eq. is also shown to be recovered. The Hamiltonian theory in the light-cone gauge constructed here is thus shown self-consistent. The variable A_+ has *reappeared* on the phase space and we have *effectively* $A_- = 0$ (and not $A_\pm = 0$). Similar discussion can be made in the Coulomb gauge in relation to A^0. That only the nonlocal gauges may describe[10] the fractional statistics consistently for the Lagrangian (1) is not true; it should also arise in the quantum dynamics of the simpler Hamiltonian theory on the *l.f.* or in the local Coulomb gauge. In the latter case or in the nonlocal gauges the Hamiltonian is complicated and renormalized theory seems difficult to construct. A *dual description*[7,10] may also be constructed on the *l.f.*. We can rewrite the Hamiltonian density as $\mathcal{H} = (\partial_1\hat{\phi})(\partial_1\hat{\phi}^*)$ if we use $A_1 = \partial_1\Lambda$ where

$$8a\,\Lambda(x^-,x^1) = \int d^2y\,\epsilon(x^- - y^-)\,\epsilon(x^1 - y^1)\,j^+(y)$$

and define

$$\hat{\phi} = e^{i\Lambda}\phi$$

$$\hat{\phi}^* = e^{-i\Lambda}\phi^* \; .$$

The field $\hat{\phi}$ clearly does not have the vanishing Dirac bracket (or commutator) with itself and it gives rise to the manifest fractional statistics. The theory is quantized via the correspondence of $i\{f,g\}_D$ with the commutator $[f,g]$ of the corresponding field operators. Any ambiguity in the operator ordering is resolved by the Weyl ordering.

3. Relativistic Covariance and Absence of Anomaly

The relativistic invariance of the theory above is shown[20] by checking the Poincaré algebra of the field theory space time symmetry generators. The canonical energy-momentum tensor is given by

$$\theta_c{}^{\mu\nu} = (\tilde{\mathcal{D}}^\mu\phi^*)(\partial^\nu\phi) + (\mathcal{D}^\mu\phi)(\partial^\nu\phi^*) + a\epsilon^{\sigma\mu\rho}A_\sigma\partial^\nu A_\rho - \eta^{\mu\nu}\mathcal{L}$$

where $\partial_\mu\theta_c{}^{\mu\nu} = 0$ by construction. The Lorentz generators are

$$M^{-1} = \int d^2x\left[x^-\theta_c{}^{+1} - x^1\theta_c{}^{+-} - aA_1^2\right],\ M^{+1} = x^+P^1 - \int d^2x\, x^1\theta_c{}^{++},\ M^{+-} = x^+P^- - \int d^2x\, x^-\theta_c{}^{++}.$$

The expressions of the generators as obtained on using the symmetric Belinfante tensor

$$\theta_B{}^{\mu\nu} = \left[\theta_c{}^{\mu\nu} + a\epsilon^{\lambda\mu\beta}\partial_\lambda(A_\beta A^\nu)\right],$$

or the symmetric gauge invariant one[7] differ from $\theta_c{}^{\mu\nu}$ only by a surface term whose contribuition to the Lorentz genertors vanishes. We remind that A_1 is now a dependent variable and the extra term in M^{-1} is sometimes called[11,7,9] *anomalous spin* induced on the scalar field due to the constrained dynamics generated by the C.S. term. A direct verification[20] of the closure of the Poincaré algebra on the mass shell is straightforward. The anomalous spin term does not break the relativistic invariance. We do find

$$\{\phi(x,\tau), M^{-1}(\tau)\}_D = [x^-\partial^1 - x^1\partial^-]\phi(x,\tau)$$
$$-\frac{i}{2}\phi(x,\tau)\int d^2y\epsilon(x^- - y^-)\delta(x^1 - y^1)\,A_1(y,\tau),$$
$$\{\phi(x,\tau), M^{+1}(\tau)\}_D = [x^+\partial^1 - x^1\partial^+]\phi(x,\tau),$$
$$\{\phi(x,\tau), M^{+-}(\tau)\}_D = [x^+\partial^- - x^-\partial^+]\phi(x,\tau).$$

The unusual term containing A_1 on the right hand side has been called[11,7] a *rotational anomaly* arising from the anomalous spin. Our discussion, however, shows that we may rather interpret the anomalous transformation of the scalar field in the *l.c.g.* (or in the Coulomb gauge[11,7]) as *gauge artifacts*. For example, the unusual commutators $\{M^{\mu\nu}, A_-\}_D = 0$ or $\{P^\mu, A_-\}_D = 0$ originate from the construction of the Dirac bracket on working in the *l.c.g.*. As a matter of fact A_1 also satisfies an unusual transformation,

$$\{A_1(x,\tau), M^{-1}(\tau)\}_D = (x^-\partial^1 - x^1\partial^-)A_1 - A_+ + (1/\partial_-)\,\partial_1 A_1$$

but

$$\{\partial_- A_1(x,\tau), M^{-1}(\tau)\}_D$$
$$= (x^-\partial^1 - x^1\partial^-)(\partial_- A_1) - (\partial_- A_+).$$

Since $j^+ \sim \partial_- A_1$ and $j^1 \sim \partial_- A_+$ it follows that the gauge invariant current j^μ does preserve the property of a contravariant vector in the *l.c.g.* as it should. The *anyonicity* seems not to be related to the unusual behavior under rotations of the scalar or the gauge field in non-covariant gauges but rather to the (renormalized) quantum dynamics of CS system which is described, for example, on the *l.f.* by $H^{l.f}$ and the canonical *l.f.* commutators above *or* alternatively by the *dual description* above which is more difficult for constructing a renormalized theory. A parallel discussion in the Coulomb gauge can be clearly made. A parallel discussion of the CS theory coupled to fermions can also be given[21].

References

1. S. Deser, R. Jackiw, and S. Templeton, Phys. Rev. Lett. **48** (1982) 975.
2. R. Mackenzie and F. Wilczek, Int. J. Mod. Phys. **A 3** (1988) 2827.
3. R.B. Laughlin, *Phys. Rev. Lett.* **50** (1983) 1395; **60** (1988) 2677.
4. J. Froehlich and P.A. Marchetti, Nucl. Phys. **B356** (1991) 533.
5. F. Wilczek, ed., *Fractional Statistics and Anyon Superconductivity* (World Scientific, Singapore, 1990).
6. see for example, S. Forte, Rev. Mod. Phys. **64** (1992) 193 and references therein.
7. G.W. Semenoff, Phys. Rev. Lett. **61** (1988) 517.
8. T. Matsuyama, Phys. Letts. **B 228** (1989) 99.
9. A. Foerster and H.O. Girotti, Phys. Lett. **B 230** (1989) 83.
10. R. Banerjee, A. Chatterjee, and V.V. Sreedhar, Ann. Phys. (N.Y.) **222** (1993) 254.
11. C. Hagen, Ann. Phys. (N.Y.) **157**(1984) 342.
12. See for example, P.P. Srivastava, Nuovo Cimento **64 A** (1981) 259.
13. R. Banerjee, Phys. Rev. **D48** (1993) 2905.
14. R. Amorim and J. Barcelos-Neto, UFRJ preprint, IF-UFRJ-05/94.
15. P.A.M. Dirac, Rev. Mod. Phys. **21** (1949) 392.
16. S.J. Brodsky and H.C. Pauli, *Schladming Lectures*, *SLAC*-PUB-5558/91.
17. K.G. Wilson, Nucl. Phys. B (proc. Suppl.) **17** (1990).
18. P.P. Srivastava, Nuovo Cimento **A 107** (1994) 549; **A 108** (1994)35; *Lectures*, Proceedings *XIV Encontro Nacional de Partículas e Campos, Caxambu, MG*, pgs. 154-192, 1993, *Sociedade Brasileira de Física*; hep-th@xxx.lanl.gov/ 9312064. See also 9412204, 9412205.
19. P.A.M. Dirac, *Lectures in Quantum Mechanics*, Benjamin, New York, 1964.
20. P.P. Srivastava, *Light-front Dynamics of Chern-Simons System*, ICTP Trieste preprint, IC/94/305, hep-th@xxx.lanl.gov/9412239 and ref. 21.
21. L.R.U. Manssur, *Sobre o modelo de Chern-Simons na frente de onda da luz*, Tese de Mestrado, CBPF, 1996.

Um Modelo BCS Generalizado com dois Campos Fermiônicos

L. C. Malacarne, R. S. Mendes e P. R. Veroneze
Universidade Estadual de Maringá - PR

July 31, 1996

Os materiais supercondutores tem despertado um grande interesse na ciência pura e aplicada. Em particular, são conhecidos vários tipos de supercondutores com uma grande variedade de propriedades peculiares [1]. Por outro lado, do ponto de vista teórico, a descrição da supercondutividade através do modelo BCS [2] detém o papel principal. Isto aliado ao fato de que os supercondutores a alta temperatura exibem uma estrutura planar, conduzem naturalmente a generalizações do modelo BCS [3]. A exemplo destas referências, trataremos de um modelo que contempla interações entre os planos. Neste trabalho, empregaremos o formalismo da integral de trajetória, comumente usado em teoria de campos, para obter as equações de Landau-Ginsburg [4]. Analisaremos, ainda, estas equações com apenas dois campos interagentes.

O modelo para dois campos tem sua dinâmica regida pela Hamiltoniana

$$\mathcal{H} = \sum_{j=1}^{2} \int dV \left[\sum_{s=\uparrow\downarrow} \psi_{sj}^{+} \left(\frac{-1}{2m_j} \vec{\nabla}^2 - \mu_j \right) \psi_{sj} - g_j \psi_{\uparrow j}^{+} \psi_{\downarrow j}^{+} \psi_{\downarrow j} \psi_{\uparrow j} \right] + \tag{1}$$

$$- \int dV [g_3 \psi_{\uparrow 1}^{+} \psi_{\downarrow 1}^{+} \psi_{\downarrow 2} \psi_{\uparrow 2} + g_3^{*} \psi_{\uparrow 2}^{+} \psi_{\downarrow 2}^{+} \psi_{\downarrow 1} \psi_{\uparrow 1}] .$$

O primeiro termo representa a Hamiltoniana para dois modelos BCS e o último termo dita a interação entre eles. Os campos ψ_{sj} dizem respeito aos férmions; μ_j são os potenciais químicos que fixam o número dos férmions; g_1, g_2 e g_3 são as constantes que regem as interações.

No caso da teoria BCS usual, um campo auxiliar é introduzido [5] representando os pares de Cooper do modelo. Neste trabalho, generalizamos este procedimento introduzindo mais de um campo auxiliar. A função de partição usando estes novos pares de Cooper generalizados é

$$\mathcal{Z} = \int \prod_{s,j} \mathcal{D}\bar{\psi}_{sj} \mathcal{D}\psi_{sj} \mathcal{D}\sigma_j^{*} \mathcal{D}\sigma_j \exp \left[- \int_0^{\beta} d\tau \int dV (\mathcal{L}_0 + \mathcal{L}_a + \mathcal{L}_b) \right] , \tag{2}$$

onde

$$\mathcal{L}_0 = \sum_{s,j} \bar{\psi}_{sj} \left[\frac{\partial}{\partial \tau} - \frac{1}{2m_j} \vec{\nabla}^2 - \mu_j \right] \psi_{sj} , \quad \mathcal{L}_a = - \sum_{i,j} \bar{\psi}_{\uparrow i} \bar{\psi}_{\downarrow i} g_{ij} \psi_{\downarrow j} \psi_{\uparrow j} \quad \text{e}$$

$$\mathcal{L}_b = \sum_i (\sigma_i^{*} - \sum_j c_{ij}^{*} \bar{\psi}_{\uparrow j} \bar{\psi}_{\downarrow j})(\sigma_i - \sum_l c_{il} \psi_{\downarrow l} \psi_{\uparrow l}) . \tag{3}$$

Na expressão para $\mathcal{L}_0 g_{11} = g_1$, $g_{12} = g_3$ etc. Os coeficientes c_{ij} são escolhidos de modo a eliminar os termos quárticos. Além disso, é conveniente definirmos novos campos auxiliares, $\chi_i = \sum_j c_{ji}^{*} \sigma_j$, que nos possibilitam expressar a função de partição numa forma mais simplificada,

$$\mathcal{Z} = \int \prod_{s,j} \mathcal{D}\bar{\psi}_{sj} \mathcal{D}\psi_{sj} \mathcal{D}\chi_j^{*} \mathcal{D}\chi_j \exp \left[- \int_0^{\beta} d\tau \int dV (\mathcal{L}_0 + \mathcal{L}_I) \right] , \tag{4}$$

com

$$\mathcal{L}_I = - \sum_i (\chi_i^{*} \psi_{\downarrow i} \psi_{\uparrow i} + \chi_i \bar{\psi}_{\uparrow i} \bar{\psi}_{\downarrow i}) + \sum_{i,j} \chi_i^{*} (U^{+} g_D^{-1} U)_{ij} \chi_j . \tag{5}$$

U é a matriz unitária que diagonaliza g, e g_D é composta pelos autovalores de g, isto é, $g_D = U^+ g U$. Observemos que as expressões acima já fornecem a generalização imediata para o caso de N campos.

Na expressão (4) podemos efetuar as integrações nos campos $\overline{\psi}$ e ψ, resultando em

$$Z = \int \prod_i \mathcal{D}\chi_i^* \mathcal{D}\chi_i e^{-S} , \tag{6}$$

sendo que S, a menos de termos independentes de χ_j^* e χ_j, pode ser escrita, formalmente, como

$$S = \int_0^\beta d\tau \int dV \mathcal{L}_{eff} = -\sum_i tr \ln M_i + \sum_{i,j} \chi_i^* (U^+ g_D^{-1} U)_{ij} \chi_j , \tag{7}$$

onde

$$M_j = \delta(\tau - \tau')\delta(\vec{x} - \vec{y}) \begin{pmatrix} [\frac{\partial}{\partial\tau} - \frac{1}{2m_j}\vec{\nabla}^2 - \mu_j] & -\chi_j \\ -\chi_j^* & -[-\frac{\partial}{\partial\tau} - \frac{1}{2m_j}\vec{\nabla}^2 - \mu_j] \end{pmatrix} . \tag{8}$$

O cálculo de $tr \ln M_i$ é feito usando o procedimento padrão [5], que previlegia campos fracos com variações espaciais suficientemente pequenas. Portanto, podemos escrever, no espaço das coordenadas, uma forma aproximada para $\mathcal{L}_{eff}$,

$$\mathcal{L}_{eff} = \sum_i [-a_i \chi_i^* \nabla^2 \chi_i + b_i \chi_i^* \chi_i + \frac{c_i}{2}(\chi_i^* \chi_i)^2] + \sum_{ij} \chi_i^* (U^+ g_D^{-1} U)_{ij} \chi_j , \tag{9}$$

onde

$$a_i = \frac{\beta^2 \mu_i \rho_i(0)}{24\pi^2 m_i} \zeta(3, 1/2) , b_i = -\rho_i(0) \ln(\frac{2\gamma\beta w_{D_i}}{\pi}) , c_i = \frac{\rho_i(0)\beta^2}{8\pi^2} \zeta(3, 1/2) .$$

Notemos que a ação S com a aproximação (9) é a própria ação efetiva na aproximação clássica de ordem mais baixa, portanto as equações para os campos $\chi's$, que são as equações de Landau-Ginsburg do modelo, vem a ser

$$\frac{\delta S}{\delta \chi_i^*} = -a_i \nabla^2 \chi_i + b_i \chi_i + c_i (\chi_i^* \chi_i)\chi_i + \sum_j (U^+ g_D^{-1} U)_{ij} \chi_j = 0 . \tag{10}$$

No caso homogêneo, χ_i independente da posição, temos

$$b_i \chi_i + c_i (\chi_i^* \chi_i)\chi_i + \sum_j (U^+ g_D^{-1} U)_{ij} \chi_j = 0 . \tag{11}$$

Vamos analisar as equações de Landau-Ginsburg homogênias com dois campos,

$$b_1 \chi_1 + c_1 (\chi_1^* \chi_1)\chi_1 + \frac{g_{22}}{det(g)} \chi_1 + \frac{\sqrt{g_{12} g_{21}}}{det(g)} \chi_2 = 0 \tag{12}$$

$$b_2 \chi_2 + c_2 (\chi_2^* \chi_2)\chi_2 + \frac{g_{11}}{det(g)} \chi_2 + \frac{\sqrt{g_{12} g_{21}}}{det(g)} \chi_1 = 0 .$$

Observemos primeiramente que, $g_{12} = g_{21}^* = 0$ reduz o modelo a duas teorias BCS desacopladas. Neste caso, o modelo tem uma simetria global $U(1) \times U(1)$ e daí duas temperaturas críticas de transição de fase de segunda ordem $T_{c_i} = \frac{2\gamma w_{D_i}}{\pi} \exp[-1/(\rho_i(0) g_i)]$.

Se $g_{12} = g_{21}^* \neq 0$, vemos de (12) que $\chi_1^* \chi_2 = \chi_1 \chi_2^*$, isto é, as fases de χ_1 e χ_2 são iguais a menos de um sinal. Este fato faz com que a simetria contínua do modelo seja reduzida de $U(1) \times U(1)$ para $U(1)$. Consequentemente, a quebra desta última simetria leva a existência de uma única temperatura crítica para a transição de fase de segunda ordem. De fato, se um dos parâmetros de ordem, χ_1 ou χ_2, for nulo, as equações (12) implicam que o outro também será.

As soluções analíticas gerais para as equações de Landau-Ginsburg homogêneas são muito grandes, obscurecendo a análise do mínimo de S. Desta forma, somos conduzidos a dois tipos de análises: um estudo numérico ou uma abordagem analítica para casos especiais dos parâmetros. Nós nos restringiremos ao último caso pois, como veremos, este nos possibilita visualizar as características principais do modelo.

Quando os parâmetros correspondentes aos dois campos forem iguais, podemos obter, depois de alguma análise, que a temperatura crítica é

$$T_c = \frac{2\gamma w_D}{\pi} \exp\left[-\frac{1}{\rho(0)}\left(\frac{g_1}{det(g)} - |\frac{g_3}{det(g)}|\right)\right] . \quad (13)$$

Por outro lado, quando os coeficientes das equações (12) forem distintos e usarmos que os parâmetros de ordem devem ir a zero, conjuntamente, na transição de fase de segunda ordem, obtemos um vínculo entre os coeficientes. Esta conclusão pode ser facilmente verificada quando tomamos a constante de acoplamento mútua pequena.

Vamos, agora, expor os principais resultados de nossa análise. Dois modelos BCS desacoplados exibem uma simetria $U(1) \times U(1)$, porém quando a interação quártica é incorporada a simetria é reduzida para $U(1)$. Este fato faz com que a teoria com dois campos, para um dado conjunto de parâmetros, não tenha mais que uma temperatura crítica para transição de fase de segunda ordem. Por outro lado, o fato da simetria ter sido reduzida de $U(1) \times U(1)$ para $U(1)$ impõe um vículo sobre os parâmetros do modelo.

References

[1] Anderson, P. W. and Schrieffer, J. R. ,Phys. Today, June (1991); Ginsburg, V. L., Cont. Phys. 33 (1992) 15;

[2] Bardeen, J. Cooper, L. N., Schrieffer, J.R. , Phys. Rev. 108 (1957) 1175;

[3] Z. Tesanovic, Phys. Rev. B, 36(1987)2364; S. Chakravarty, A. Sudbo, P. Anderson, S. Strong, Science, 261(1993)337;

[4] Ginsburg, V. L. and Landau, L. D., JEPT 20 (1950) 1064.

[5] Popov, V. N. it Funtional Integrals and Collective Excitations, Cambridge University Press, New York (1990);

Causalidade e leis de conservação

Manoelito M. de Souza, Gilmar de Souza Dias
Universidade Federal do Espírito Santo - Departamento de Física
*29065.900 - Vitória-ES-Brasil**

Received March, 1996

Problemas relacionados com infinitos e divergências são comuns em teoria de campo; são sinais de que o formalismo não é de todo satisfatório. Estes e outrs problemas, permitem concluir, que o formalismo usado para descreve-los não é de todo satisfatório. Estes problemas têm origem numa insuficiente implementação da causalidade e não aparecem em um formalismo, baseado em uma implementação geométrica e local (ponto a ponto) da causalidade. Este formalismos são desenvolvidos nas chamadas Variedades com Preservação Local da Causalidade ou VPLC.

Estudamos o formalismo lagrangiano e o teorema de Noether definidos nestas variedades (VPLC). Obtemos as equações de Euler-Lagrange, as correntes de Noether associadas as simetrias contínuas do lagrangiano, e suas cargas conservadas. O significado físico das leis de conservação na VPLC é discutido.

As transformações do grupo de Poincaré, o qual está contido no grupo de isometria da VPLC, são consideradas para obter o tensor momento energia e a equação da continuidade associada. É um tensor simétrico, como no formalismo usual. Estes resultados são usados para definir o momento angular e o momento linear na VPLC.

No contexto de Teoria Quântica dos Campos, obtemos os operadores momento angular e momento linear na VPLC, a partir de uma ação funcional par um campo vetorial genérico; eles são os geradores do grupo de Poincaré na VPLC. A álgebra deste geradores é determinada, bem como suas relações de comutação com o campo.

*e-mail:manoelit@cce.ufes.br

Fótons em eletrodinâmica clássica

Manoelito M de Souza, Jair Valadares Costa
Universidade Federal do Espírito Santo - Departamento de Física
*29065.900 - Vitória - ES - Brasil**

Received March, 1996

Em um formalismo com preservação local de causalidade, as equações de Maxwell, o tensor campo eletromagnético, seu tensor momento-energia e as equações de continuidade (conservação) são escritos em termos de **fótons clássicos**, que são campos clássicos, localizados, de natureza granular como os fótons da teoria quântica. O sistema é consistente e livre de singularidades.

*e-mail:manoelit@cce.ufes.br

Quantização do "fóton clássico"

Manoelito M. de Souza, Adriano Sant'ana Pedra
Universidade Federal do Espírito Santo - Departamento de Física
*29065.900 - Vitória-ES-Brasil**

Received March, 1996

A Eletrodinâmica clássica se torna uma teoria consistente quando expressa, covariantemente, em termos de fótons clássicos, isto é, interações vetoriais de massa nula, discretas e de natureza granular (localizada). Problemas com singularidades e com a equação de movimento do elétron desaparecem. A quantização, **manifestamente covariantemente e canônica**, destes campos é feita. Mostra-se que os problemas usuais, comuns a métodos de quantização manifestamente covariantes, não aparecem: a condição de calibre é implementada a nível de operadores e não de estados; não há fótons escalares e temporais, só fótons físicos; não há estados de norma negativa ou nula (salvo o vácuo). Característica deste formalismo, embora manifestamente covariante, é a ausência de gráus de liberdade não físicos.

*e-mail:manoelit@cce.ufes.br

Inconsistencies in Classical Electrodynamics

Manoelito M. de Souza
Universidade Federal do Espírito Santo
Departamento de Física
29065.900 - Vitória - ES - Brasil

Received March, 1996

The problems of Classical Electrodynamics with the electron equation of motion and with non-integrable singularity of its self-field stress tensor are well known. They are consequences, we show, of neglecting terms that are null off the charge world-line but that gives a non null contribution on its world-line. The self-field stress tensor of a point classical electron is integrable without using any kind of renormalization; there is no causality violation and no conflict with energy conservation in the electron equation of motion.

The motion [1-3] of a point classical electron is described by the Lorentz-Dirac equation (LDE), $ma = F_{ext}.V + \frac{2}{3}(\dot{a} - a^2 V)$, where m, a and V are, respectively, the electron mass, 4-vector acceleration and 4-vector velocity. F_{ext} is an external electromagnetic field; $\dot{a} := \frac{da}{d\tau}$; τ is the electron proper time. The electron charge and the speed of light are put equal to 1. The Schott term, $\frac{2}{3}\dot{a}$ is the source of problems in the LDE.

The LDE can be obtained from energy-momentum conservation in the Lienard - Wiechert solution [1,3,5-7], $A(x) = \frac{V}{\rho}\big|_{\tau_{ret}}$, *for* $\rho > 0$, in the limit of $\rho \to 0$. V is tangent to the particle world-line, $z = z(\tau)$, parameterized by its proper time τ, ($V = dz/d\tau$, and $V^2 = -1$). $\rho \equiv -V.\eta.R$, where η is the Minkowski metric tensor with $\eta_{oo} = -1$, and $R \equiv x - z(\tau)$. ρ is the invariant distance (in the charge rest frame) between $z(\tau_{ret})$, the position of the charge at the retarded time, and x, the point where its self field is observed. See figure 1. The constraints $R^2 = 0$, $R^0 > 0$, and $d\tau + K.dx = 0$ (or $K_\mu = -\frac{\partial \tau}{\partial x^\mu}$,) must be satisfied. K, defined by $K := \frac{R}{\rho}$, is a null 4-vector, $K^2 = 0$, and represents a light-cone generator, or the electromagnetic wave-front 4-vector.

The retarded Maxwell field, $F_{\mu\nu_{ret}} := \partial_\nu A_\mu - \partial_\mu A_\nu$, is given [1-3,5-7] by $F_{\mu\nu_{ret}} = \frac{1}{\rho^2}[K_\mu, V_\nu + \rho(\mathrm{a}_\nu + \mathrm{a}_K V_\nu)]$ where, for notational simplicity, we are using $[A, B] := AB - BA$, $\mathrm{a}_K := \mathrm{a}.K$.
The electron self-field stress tensor, $4\pi\Theta = F_{ret}.F_{ret} - \frac{\eta}{4}F_{ret}^2$, or

$$4\pi\rho^4\Theta = [K, \rho\mathrm{a} + V(1+\rho\mathrm{a}_K)].[K, \rho\mathrm{a} + V(1+\rho\mathrm{a}_K)] - \frac{\eta}{4}[K, \rho\mathrm{a} + V(1+\rho\mathrm{a}_K)]^2, \qquad (1)$$

may be written as $\Theta = \Theta_2 + \Theta_3 + \Theta_4$, with

$$4\pi\rho^2\Theta_2 = [K, \mathrm{a} + V\mathrm{a}_K].[K, \mathrm{a} + V\mathrm{a}_K] - \frac{\eta}{4}[K, \mathrm{a} + V\mathrm{a}_K]^2,$$

$$4\pi\rho^3\Theta_3 = [K, V].[K, \mathrm{a} + V\mathrm{a}_K] + [K, \mathrm{a} + V\mathrm{a}_K].[K, V] - \frac{\eta}{2}Tr[K, V].[K, \mathrm{a}],$$

and

$$4\pi\rho^4\Theta_4 = [K, V].[K, V] - \frac{\eta}{2}[K, V]^2.$$

The important difference among these expressions for Θ_2, Θ_3, and Θ_4, and the corresponding ones found, for example in [1,2,5-7] is that while the first ones are complete , in the sense that they keep the terms proportional to K^2, which are null (as $K^2 = 0$), in the last ones they have been dropped off. But these K^2-terms, even with $K^2 = 0$, should not be dropped from the above equations, since they are necessary for producing the correct limits when $\rho \Longrightarrow 0$. The presence of non-integrable singularities in the electron's self-field stress tensor is a major problem. Θ_2, although singular at $\rho = 0$, is nonetheless integrable. By that it is meant that $\int d^4x\Theta_2$ exist [6], while for Θ_3 and Θ_4 this is not true. Previous attempts, based on distribution theory, for taming these singularities have relied on modifications of the Maxwell theory with addition of extra terms to Θ on the electron world-line (see for example the reviews [5-7]). They redefine Θ_3 and Θ_4 at the electron world-line in order to make them integrable without changing them at $\rho > 0$ and so preserving the standard results of Classical Electrodynamics. But this is always an introduction of something strange to the theory and in an *ad hoc* way. Another unsatisfactory aspect of

this procedure is that it regularizes the above integral but leaves an unexplained and unphysical discontinuity in the flux of 4-momentum, $\int dx^4 \Theta^{\mu\nu} \partial_\nu \rho \, \delta(\rho - \varepsilon)$, through a cylindrical hypersurface $\rho = const$ enclosing the charge world-line. It is particularly interesting that, as we will show now, instead of adding anything we should actually not drop out the null K^2-terms. Their contribution (not null, in an appropriate limit) cancel the infinities. The same problem happens in the derivations of the electron equation of motion from these incomplete field expressions. The Schott term in the Lorentz-Dirac equation is its consequence; it does not appear in the equation when the full field expression is correctly used.

The constraint $R^2 = 0$ requires that x and $z(\tau_{ret})$ belong to a same light-cone; its differentiation generates $d\tau + K.dx = 0$, which defines a family of hyperplane tangent to the light-cone. $x + dx$ and $z(\tau_{ret} + d\tau)$ must also belong to a same light-cone. Together, these two constraints require that x and $z(\tau_{ret})$ belong to a same straight line, the light-cone generator, tangent to K. See figure 1 and 3. As discussed in [9], the limit $\rho \to 0$ is a critical point in the determination of the LDE; as x and z must belong to a same light-cone generator, this limit necessarily implies also on $x^\mu \to z^\mu$ or $R^\mu \to 0$.
As $K^\mu := \frac{R^\mu}{\rho}$, in this limit we have a 0/0-type of indeterminacy, which can be evaluated by the L'Hospital rule and $\frac{\partial}{\partial \tau}$. This results in $\lim_{\rho \to 0} K = V$, and $\lim_{\rho \to 0} K_\mu K^\mu = \lim_{\rho \to 0} \frac{R.R}{\rho^2} = -1$, as $\dot{\rho} = -(1 + a.R)$ and $\dot{R} = -V$. Classical electrodynamics alone with its picture of a continuous emission of radiation does not give room for a comprehension of these limiting processes. But we know that this is just an approximative description of an actually discrete quantum process.

Figure 2 portrays a classical picture of such a fundamental quantum process; it helps in the understanding of these two limiting results. In the limit of $\rho \to 0$ at $\tau = \tau_{ret}$ there are 3 distinct velocities: K, the photon 4-velocity, and V_1 and V_2, the electron initial and final 4-velocities. This is the reason for this indeterminacy at $\tau = \tau_{ret}$. At $\tau = \tau_{ret} + d\tau$ there is only V_2, and only V_1 at $\tau = \tau_{ret} - d\tau$. The role of $\frac{\partial}{\partial \tau}$ in this use of the L'Hospital rule is of changing the evaluation of the limit to a neighboring point after or before τ_{ret}. Actually, we are working with 2 simultaneous limiting processes: $\rho \to 0$ (or $x \to z(\tau_{ret})$) and $\tau \to \tau_{ret}$. See figure 3. It is remarkable that we can find vestiges of these traits of the quantum nature of the radiation emission process in a classical (Lienard-Wiechert) solution. This is food for thinking on the real physical meaning of a classical field. We repeat that in the classical picture with its idea of a continuous interaction this indeterminacy cannot be resolved as $\tau_{ret} \pm d\tau$, like τ_{ret}, are also singular points. The lesson one should learn from this is that even in a classical context, it is necessary to take into account the discrete and localized (quantum) character of the fundamental electromagnetic interaction in order to have a clear and consistent physical picture. To find the limit of something when $\rho \to 0$ will be done so many times in this letter that it is better to do it in a more systematic way. We want to find

$$\lim_{\rho \to 0} \frac{N(R)}{\rho^n}, \tag{2}$$

where $N(R)$ is a homogeneous function of R, $N(R)\big|_{R=0} = 0$. Then, we have to apply the L'Hospital rule consecutively until the indeterminacy is resolved. As $\frac{\partial \rho}{\partial \tau} = -(1 + a.R)$, the denominator of (2) at $R = 0$ will be different of zero only after the n^{th}-application of the L'Hospital rule, and then, its value will be $(-1)^n n!$
If p is the smallest integer such that $N(R)_p\big|_{R=0} \neq 0$, where $N(R)_p := \frac{d^p}{d\tau^p} N(R)$, then

$$\lim_{\rho \to 0} \frac{N(R)}{\rho^n} = \begin{cases} \infty, & \text{if } p < n \\ (-1)^n \frac{N(0)_p}{n!}, & \text{if } p = n \\ 0, & \text{if } p > n \end{cases} \tag{3}$$

Let us find the integral of the stress tensor of the electron self-field at its world-line: $\lim_{\rho \to 0} \int dx^4 \Theta$, or $\lim_{\rho \to 0} \int d\tau \rho^2 d\rho d$ in terms of retarded coordinates [5,6,13,14], $x^\mu = z^\mu + \rho K^\mu$. This can be made easier with two helpful expressions,

$$N_p = \sum_{a=0}^{p} \binom{p}{a} A_{p-a}.B_a \tag{4}$$

and

$$N_p = \sum_{a=0}^{p} \sum_{c=0}^{a} \binom{p}{a} \binom{a}{c} A_{p-a}.B_{a-c}.C_c \tag{5}$$

valid when $N(R)$ has, respectively, the forms $N_0 = A_0.B_0$, or $N_0 = A_0.B_0.C_0$, where A, B and C represent possibly distinct functions of R, and the subindices indicate the order of $\frac{d}{d\tau}$. So, for using (3-5), we just have to find the τ-derivatives of A, B and C ,that produce the first non- null term at the limit of $R \to 0$. Besides, for finding

$\lim_{\rho\to 0}\int dx^4\Theta$ we just have to consider the first term of the RHS of (1) because, as the second one is the trace of the first, its behaviour under this limit can easily be inferred. So, as $K=\frac{R}{\rho}$,

$$\lim_{\rho\to 0}\frac{\rho^2[K,\rho\mathrm{a}+V(1+\rho\mathrm{a}_K)].[K,\rho\mathrm{a}+V(1+\rho\,\mathrm{a}_K)]}{\rho^4}=\lim_{\rho\to 0}\frac{[R,\rho\mathrm{a}+V(1+\mathrm{a}.R)].[R,\rho\mathrm{a}+V(1+\mathrm{a}.R)]}{\rho^4}$$

As, $A_0=B_0=[R,\rho\,\mathrm{a}+V(1+\rho\mathrm{a}.R)]\Longrightarrow A_2=B_2=[\mathrm{a},V]+\mathcal{O}(R)$. Therefore, according to (4), for producing a non null N_p, a and p must be given by $p-a=a=2\Longrightarrow p=4=n\Longrightarrow N_4=6[\mathrm{a},V].[\mathrm{a},V]+\mathcal{O}(R)$. Then, we conclude from (3), that

$$\lim_{\rho\to 0}\frac{\rho^2[K,\rho\mathrm{a}+V(1+\rho\mathrm{a}_K)].[K,\rho\mathrm{a}+V(1+\rho\mathrm{a}_K)]}{\rho^4}=\frac{1}{4}[\mathrm{a},V].[\mathrm{a},V].$$

We have, therefore, from (1), that

$$\lim_{\rho\to 0}\int dx^4\,\Theta=\int d\tau\{[\mathrm{a},V].[\mathrm{a},V]-\frac{\eta}{4}[\mathrm{a},V]^2\}\tag{6}$$

The integrand of the RHS of (6) is the flux of 4-momentum irradiated from the electron, which is finite and depends only on the electron instantaneous velocity and acceleration. It is interesting that (6) comes entirely from the velocity term of F_{rel}, $\frac{[K,V]}{\rho^2}$, as $\lim_{\rho\to 0}\int dx^4\Theta=\lim_{\rho\to 0}\int dx^4\Theta_4$. The contribution from the other two terms just cancel to zero, $\lim_{\rho\to 0}\int dx^4\Theta_2=-\lim_{\rho\to 0}\int dx^4\Theta_3$, as can be easily verified.

The electron equation of motion

The LDE is the greatest paradox of classical field theory as it cannot simultaneously preserve both the causality and the energy conservation [1-3]. The presence of the Schott term, $\frac{2}{3}e^2\dot{a}$, is the cause of all of its pathological features, like microscopic non-causality, runaway solutions, preacceleration, and other bizarre effects [4]. On the other hand its presence is necessary for the energy-momentum conservation; without it it would be required a contradictory null radiance for an accelerated charge, as $\dot{a}\,.V+a^2=0$.

The LDE can be obtained from

$$\int\{a^\mu-F^{\mu\nu}_{ext}V_\nu\}d\tau=-\lim_{\epsilon\to 0}\int dx^4\partial_\nu\Theta^{\mu\nu}\theta(\rho-\varepsilon)=\lim_{\epsilon\to 0}\int dx^4\Theta^{\mu\nu}\partial_\nu\rho\,\delta(\rho-\varepsilon),\tag{7}$$

where the last term represents the impulse carried out by the emitted electromagnetic field in the Bhabha tube surrounding the electron world-line, which is defined by the Heaviside function, $\theta(\rho-\varepsilon)$. With the divergence theorem this middle term is transformed into the RHS, which represents the flux of 4-momentum through the cylindrical hypersurface $\rho=\varepsilon$. Let us denote it by P^μ: $P^\mu=\lim_{\epsilon\to 0}\int dx^4\Theta^{\mu\nu}\partial_\nu\rho\,\delta(\rho-\varepsilon)$. As $\partial_\nu\rho=\rho\mathrm{a}_K K_\nu+K_\nu-V_\nu$, and $\Theta=\Theta_2+\Theta_3+\Theta_4$, we can write $P^\mu:=P_0^\mu+P_1^\mu+P_2^\mu$, with

$$P_2^\mu=\lim_{\epsilon\to 0}\int dx^4\Theta_4^{\mu\nu}(K-V)_\nu\,\delta(\rho-\varepsilon),$$

$$P_1^\mu=\lim_{\epsilon\to 0}\int dx^4\{\Theta_4^{\mu\nu}K_\nu\,\rho\,\mathrm{a}_K+\Theta_3^{\mu\nu}(K-V)_\nu\}\,\delta(\varepsilon-\rho),$$

$$P_0^\mu=\lim_{\epsilon\to 0}\int dx^4\{\Theta_3^{\mu\nu}K_\nu\rho\mathrm{a}_K+\Theta_2^{\mu\nu}(K-V)_\nu\}\,\delta(\rho-\varepsilon),$$

P_1^μ and P_2^μ are both null, as we discover applying (3) with (5). The complete calculation is shown in [10,11]. For example, we see from Θ_2 that the integrand of P_2 produces (again, we do not need to consider the trace term)

$$\lim_{\rho\to 0}\frac{\rho^2[K,V].[K,V].(K-V)}{\rho^4}=\lim_{\rho\to 0}\frac{[R,V].[R,V].(R-\rho V)}{\rho^6},$$

or, schematically $\lim_{\rho\to 0}\frac{A.A.C}{\rho^3}$ with $A_0=B_0=[R,V]$, and $C_0=(R-V\rho)$. Then, $A_2=[a,V]+\mathcal{O}(\mathcal{R})$, $C_2=a+\mathcal{O}(\mathcal{R})$, and we have, from (5), the following restrictions on a and c for producing a $N(R=0)_p\neq 0$: $c=2$; $a-c=2$; and $p-a=2$ or $p=6>n=5$. Therefore, according to (3) $P_2^\mu=0$.
P_0^μ is distinguished from P_1^μ and P_2^μ for not being ρ-dependent, and not affected, consequently, by the limit of $\varepsilon\to 0$.Therefore, it is not necessary to use the L'Hospital rule on its determination. The physical meaning of this is

that the flux of 4-momentum through the cylindrical surface $\rho = \epsilon$ comes entirely from the radiated (photon) field. But, $\Theta_3^{\mu\nu} K_\nu = 0$ for $\rho > 0$. From Θ_2 with $K^2 = 0$, we have

$$4\pi\rho^2 \Theta_2^{\mu\nu}(K - V)_\nu = (\mathrm{a}_K^2 - \mathrm{a}^2) K^\mu),$$

which, gives [1,5]

$$P^\mu = \lim_{\rho \to 0} \int d^4x \Theta_2^{\mu\nu}(K - V)_\nu = -\int d\tau \frac{2}{3}\mathrm{a}^2 V^\mu,$$

the Larmor term.

With this result in equation (7) we could write the electron equation of motion, obtained from the Lienard-Wiechert solution, as

$$m\mathrm{a}^\mu - F_{ext}^{\mu\nu} V_\nu = -\frac{2}{3}\mathrm{a}^2 V^\mu, \tag{8}$$

but it is well known that this could not be a correct equation because it is not self-consistent: its LHS is orthogonal to V, $m\mathrm{a}.V = V.F_{ext}.V = 0$, while its RHS is not, $-\frac{2}{3}\mathrm{a}^2 V.V = \frac{2}{3}\mathrm{a}^2$. This seems to be paradoxical until we have a clearer idea of what is happening. We must return to equation (7). There is a subtle and very important distinction between its LHS and its RHS. Its LHS is entirely determined by the electron's instantaneous position, $z(\tau)$, while its RHS is determined by the sum of contributions from the electron self-field at all points of a cylindrical hypersurface $\rho = \epsilon$. In other words, the LHS is a description of some electron attributes (the electron is a point particle!) while the RHS is a description of some electron-self-field attributes. This distinction is missing in equation (8); it was deleted by the integration and limiting processes. When we multiply the LHS of (8) by V, we know that $(m\mathrm{a} - V.F_{ext}).V$, represents the net power of the system electron-external force, that is, the work realized by a force $m\mathrm{a} - V.F_{ext}$ which is being displaced with a velocity V. This does not work with the RHS of (8) multiplied by V because we know that the flux of radiated energy is through the cylindrical wall $\rho = \epsilon$; in order to make sense we have to use at each point x of this wall the electromagnetic wave-vector K, and not V. The contributions from the electron self field must always be calculated, like in P^μ, from the flux of electromagnetic energy-momentum through the walls of a Bhabha tube around the charge world-line, in the limit of $\rho \to 0$:

$$m\int \mathrm{a}.V d\tau = \int V.F_{ext}.V d\tau - \lim_{\epsilon \to 0} \int dx^4 K_\mu \partial_\nu \Theta^{\mu\nu} \theta(\rho - \epsilon).$$

Its LHS and the first term of its RHS are, of course, null. Observe that in the last term,V, the speed of the electron, is replaced by K the speed of the electromagnetic interaction; only in the limit of $\rho \to 0$ is that $K \to V$. We use again (3) and (5) for showing that:

$$\lim_{\epsilon \to 0} \int dx^4 K_\mu \partial_\nu \Theta^{\mu\nu} \theta(\rho - \epsilon) = 0.$$

The explicit calculation is shown in the appendix of [11]. So, there is no contradiction anymore.

The equation (8), in this sense, can be regarded as an effective equation that would be better represented as

$$m\mathrm{a}^\mu = F_{ext}^{\mu\nu} V_\nu - < \frac{2}{3}\mathrm{a}^2 V^\mu >, \tag{9}$$

where the bracketed term represents the contribution from the electron self field and must always be calculated as explained above, $< \frac{2}{3}\mathrm{a}^2 V^\mu > = P^\mu = \lim_{\epsilon \to 0} \int dx^4 \Theta^{\mu\nu} \partial_\nu \rho\, \delta(\rho - \epsilon)$.

So, there is no contradiction anymore. Thus, we have eliminated two old problems of Classical Electrodynamics: the non integrability of the stress tensor of a point electron and the causality violation in its equation of motion. And all that is softly required is an indirect recognition that an actually quantum process hides behind the classical picture described by the Lienard-Wiechert solution. Nothing else is added to the standard theory. But there are still two remaining inconsistencies in Classical Electrodynamics: the discontinuity in the flux of 4-momentum from the charge world-line, $\int dx^4 \Theta^{\mu\nu} \partial_\nu \rho\, \delta(\rho - \epsilon)$, and the divergence of the charge self field at $\rho = 0$. To overcome them requires a re-evaluation of the physical meaning of the Faraday-Maxwell concept of field with a deeper consideration of the "classical photon" concept. This is discussed in [10,12], from which we have presented here a simplified version. The complete version with its extended concept of causality and its discussion on the meaning of the Maxwell fields and its relevance to Quantum Field Theory would be too long to be included in a letter. The related immediate difference in the outcomes of these two versions appears in the equation of motion for a point electron,

$$m\mathrm{a}^\mu - < \frac{1}{4}\mathrm{a}^2 \mathrm{a}^\mu > = F_{ext}^\mu - < \frac{2\mathrm{a}^2}{3} V^\mu >, \tag{10}$$

where the second term in the RHS corresponds to the energy associated to the curvature of the the electron trajectory and it is not present in its simplified counterpart (9). The existence or not of this curvature term must be determined by experimental means and also evaluated by its theoretical implications.

References

[1] F. Rohrlich;"Classical Charged Particles". Reading, Mass. (1965).

[2] D. Jackson "Classical Electrodynamics",2nd ed., chap. 14, John Wiley & Sons, New York, NY(1975).

[3] Parrot, S., "Relativistic Electrodynamics and Differential Geometry", Springer-Verlag, New York, 1987.

[4] J. C. Eliezer, Rev. Mod. Phys., 19,148(1947).

[5] C. Teitelboim; D. Villaroel; Ch.G.Van Weert, Rev. del Nuovo Cim., vol 3, N.9,(1980).

[6] E.G.P.Rowe, Phys. Rev. D, 12, 1576(1975) and 18, 3639(1978); Nuovo Cim, B73, 226(1983).

[7] A. Lozada, J. Math. Phys., 30,1713(1989).

[8] C. Teitelboim Phys. Rev. D 1, 1572(1970).

[9] M. M. de Souza, "The Lorentz-Dirac equation and the structure of spacetime". hep-th/9505169.

[10] M. M. de Souza, "The Lorentz-Dirac equation and the physical meaning of the Maxwell fields". hep-th/9510160.

[11] M. M. de Souza, "Electrodynamics Classical Inconsistencies". hep-th/9511144.

[12] M. M. de Souza, "Causality and Self-consistency in Classical Electrodynamics". hep-th/9605014. A more pedagogical and amplified version of this letter.

[13] J.L. Synge: Ann. Mat. Pura Appl., 84, 241 (1975).

[14] R. Tabensky: Phys. Rev. D 13, 267 (1976).

Linear classical stability from three coupled real scalar fields

R. de Lima Rodrigues[a], Pedro Barbosa da Silva Filho[b] and A. N. Vaidya[c]

[a] *Departamento de Física, Universidade Federal da Paraíba*
58.109-970 - Campina Grande - PB, E-mail: cendfi76@brufpb.bitnet
[a,b] *Departamento de Ciências Exatas e da Natureza*
Universidade Federal da Paraíba,
Cajazeiras - PB, 58.900-000, Brazil
[b,c] *Instituto de Física*
Universidade Federal do Rio de Janeiro
Rio de Janeiro, RJ - 21.945-970 - Brazil

Received March, 1996

We investigate the linear classical stability of static solitons for a system of three coupled real scalar fields in 1+1 dimensions. We consider a general positive potential with a square form and show that the associated three-component normal modes are non-negatives.

1 Introduction

The soliton solutions have been investigated for field equations defined in a space-time of dimension equal or bigger than 1+1. The kink of a field theory is an example of a soliton in 1+1 dimensions [1, 2, 3, 4, 5]. It is a static, non-singular, *classically stable* and of finite localized energy solution of the motion equation. For solitons of three coupled scalar fields in 1+1 dimensions exist no general rules for finding analytic solutions, due to the fact the nonlinearity in potential leads to enlarging of difficulties to solve the field equations.

2 Solitons from three coupled scalar field

We consider the classical soliton solutions of three coupled real scalar fields in 1+1 dimensions. They are static, nonsingular classically stable and of finite localized energy solutions of the field equations.

The Lagrangian density for such nonlinear system in the natural system of units ($c = \hbar = 1$), in (1+1)dimensional space-time with Lorentz invariance is written as

$$\mathcal{L}(\rho_i, \partial_\mu \rho_i) = \frac{1}{2}\sum_{i=1}^{3}(\partial_\mu \rho_i)^2 + V(\rho_i), \quad \eta^{\mu,\nu} = \begin{pmatrix} 1 & 0 \\ 0 & -1 \end{pmatrix} \tag{1}$$

where $\partial_\mu = \frac{\partial}{\partial x^\mu}$, $x^\mu = (t, x)$ with $\mu = 0, 1$, $\rho_i = \rho_i(x, t)$, $i = 1, 2, 3$ are real scalar fields and $\eta^{\mu,\nu}$ is the metric tensor. Here the potential $V(\rho_i) = V(\rho_1, \rho_2, \rho_3)$ is any positive semidefinite function of ρ_i. The general classical configurations obey the equation bellow:

$$\frac{\partial^2}{\partial t^2}\rho_i - \frac{\partial^2}{\partial x^2}\rho_i + \frac{\partial}{\partial \rho_i}V = 0, \tag{2}$$

which, for static soliton solutions, becomes the following system of nonlinear differential equations

$$\rho_i'' = \frac{\partial}{\partial \rho_i}V, \quad (i = 1, 2, 3), \tag{3}$$

where primes represent differentiations with respect to space variable. There is in literature a trial orbit method, for finding static solutions for certain positive potentials, which constitutes a "trial and error" thecnique [2].

3 Linear Stability

Since the potential $V(\rho_i)$ is positive it can be written in the following square form, analogous to the case with only single field [6]

$$V(\rho_1,\rho_2,\rho_3)=\frac{1}{2}\sum_{i=1}^{3}U_i^2(\rho_1,\rho_2,\rho_3). \tag{4}$$

In this case we have the following Bogomol'nyi condition:

$$\rho_i'=-U(\rho_1,\rho_2,\rho_3),\quad (i=1,2,3). \tag{5}$$

Now let us analyze the classical stability of the soliton solutions in this nonlinear system, which is ensured by considering small perturbations around $\rho(x)$ and $\sigma(x)$:

$$\rho_i(x,t)=\rho_i(x)+\eta_i(x,t),\quad (i=1,2,3). \tag{6}$$

We expand the fluctuations $\eta_i(x,t)$ in terms of the normal modes,

$$\eta_i(x,t)=\sum_n \epsilon_{i,n}\eta_{i,n}(x)e^{i\omega_{i,n}t},\quad \omega_{1,n}=\omega_{2,n}=\omega_{3,n}. \tag{7}$$

Thus the stability equation for the field becomes a Schrödinger-like equation to three-component wave functions $\tilde{\Psi}_n$,

$$\mathcal{H}\tilde{\Psi}_n=\omega_n^2\tilde{\Psi}_n,\quad n=0,1,2,..., \tag{8}$$

where

$$\mathcal{H}=\begin{pmatrix} -\frac{d^2}{dx^2}+\frac{\partial^2}{\partial\rho_1^2}V & \frac{\partial^2}{\partial\rho_1\partial\rho_2}V & \frac{\partial^2}{\partial\rho_1\partial\rho_3}V \\ \frac{\partial^2}{\partial\rho_2\partial\rho_1}V & -\frac{d^2}{dx^2}+\frac{\partial^2}{\partial\rho_2^2}V & \frac{\partial^2}{\partial\rho_2\partial\rho_3}V \\ \frac{\partial^2}{\partial\rho_3\partial\rho_1}V & \frac{\partial^2}{\partial\rho_3\partial\rho_2}V & -\frac{d^2}{dx^2}+\frac{\partial^2}{\partial\rho^2}V \end{pmatrix}_{|\rho_i=\rho_i(x)},\quad \tilde{\Psi}_n=\begin{pmatrix}\eta_{1,n}(x)\\ \eta_{2,n}(x)\\ \eta_{3,n}(x)\end{pmatrix}. \tag{9}$$

Note that

$$\frac{\partial^2}{\partial\rho_i\partial\rho_j}V=\frac{\partial^2}{\partial\rho_j\partial\rho_i}V \tag{10}$$

then $\mathcal{H}$ is Hermitian. Hence the eigenvalues ω_n^2 of $\mathcal{H}$ are real.

We will now show that ${\omega_n}^2$ are non-negative. Indeed, since

$$\vec{\nabla}_\rho\times\vec{U}=0,\quad \vec{U}=\begin{pmatrix}U_1\\U_2\\U_3\end{pmatrix} \tag{11}$$

we find a bilinear form of $\mathcal{H}$ given by

$$\mathcal{H}=\mathcal{A}^+\mathcal{A}^-, \tag{12}$$

where

$$\mathcal{A}^-=\begin{pmatrix} a_1^- & -\frac{\partial}{\partial\rho_2}U_1 & -\frac{\partial}{\partial\rho_3}U_1 \\ -\frac{\partial}{\partial\rho_1}U_2 & a_2^- & -\frac{\partial}{\partial\rho_3}U_2 \\ -\frac{\partial}{\partial\rho_1}U_3 & -\frac{\partial}{\partial\rho_2}U_3 & a_3^- \end{pmatrix},\quad \mathcal{A}^+=(\mathcal{A}^-)^\dagger, \tag{13}$$

with the following first order diferential operators that appear in analysis of classical stability associated at only one single field [6]

$$a_i^-=-\frac{d}{dx}-\frac{\partial}{\partial\rho_i}U_j. \tag{14}$$

Since $a_i^+=(a_i^-)^\dagger$, we find

$$(A^+A^-)_{ii}=-\frac{d^2}{dx^2}+\frac{\partial^2}{\partial\rho_i^2}V, \tag{15}$$

which are exactly the diagonal element of $\mathcal{H}$. Therefore, it is easy to show that the linear stability is satisfied i.e. $\omega_n^2=<\mathcal{H}>=<\mathcal{A}^+\mathcal{A}^->=(\mathcal{A}^-\tilde{\Psi}_n)^\dagger(\mathcal{A}^-\tilde{\Psi}_n)\geq 0$, as was affirmed.

The ground state $\mathcal{H}$ is given by

$$\tilde{\Psi}_-^{(0)}(x)=-\vec{U} \tag{16}$$

which represents the three-component zero mode.

4 Conclusion

In this paper, we consider the classical stability analysis for three coupled real scalar fields. We have shown that the positive potentials with a square form leads the three-component normal modes to be non-negative ($\omega_n{}^2 \geq 0$, analogous to the case with only single field [6]) so that the linear stability of the Schrödinger-like equations is ensured.

Acknowledgments

This research was supported in part by CNPq.

References

[1] R. Jackiw, Rev. Mod. Phys. **49**, 681 (1977).

[2] R. Rajaraman, Phys. Rev. Lett., **42**, 200 (1979); R. Rajaraman, *Solitons and Instantons*, (North-Holland, Amsterdam, 1982).

[3] S. Coleman, *Aspects of Symmetry*, (Cambridge University, London, 1985).

[4] A. P. Balachandran, G. Marmo, B. S. Skagerstam and A. Stern, *Classical Topology and Quantum States*, (World Scientific, Singapore, 1991).

[5] E. J. Weinberg, *Annu. Rev. Nucl. Part. Sci.* **42**, 177 (1992).

[6] R. de Lima Rodrigues, *Mod. Phys. Lett* **A10**, 1309 (1995).

LISTA DE PARTICIPANTES

ADELLANE ARAUJO SOUSA - UNB
ADILSON CARLOS HERMES - UFPB
ADILSON JOSE DA SILVA - IFUSP
ADOLFO MAIA JUNIOR - UNICAMP
ADRIANO SANT'ANA PEDRA - UFES
ALBERTO ETCHEGOYEN - TANDAR
ALBERTO FRANCO DE SA SANTORO - CBPF
ALCIDES GOYA - UNB
ALDO PROCACCI - UFMG
ALEXANDRE CARLOS TORT - UFRJ
ALEXANDRE G. DE MIRANDA SCHMIDT - UFPR
ALFREDO TAKASHI SUZUKI - IFT
ALVARO DE SOUZA DUTRA - UNESP-GUAR
ALVARO FAVINHA MARTINI -
ALVARO LEONARDI AYALA FILHO - UFRGS
ANA GABRIELA GRUNFELD - LA PLATA
ANA PAULA MOURA REIS MICELI - UFRJ
ANDERSON CAMPOS FAUTH - UNICAMP
ANDRE BESSADAS PENNA-FIRME - CBPF
ANDRE LUIZ MOTA - UFMG
ANDRE TENORIO LEITE - UFRJ
ANDREA DE AZEVEDO MOREGULA - UFRJ
ANDREI DEMITCHEV - CBPF
ANDREI VICTOROVICH SOMOV - UNB
ANGELA FOERSTER - UFRGS
ANTONIO EDSON GONCALVES - UEL
ANTONIO R. PERISSINOTTO BIRAL - UNICAMP
ANTONIO ROBERTO DA SILVA - UFRJ
ANTONIO TAVARES DA COSTA JUNIOR - UFF
ARMANDO BERNUI LEO - CBPF
ARMANDO TURTELLI JUNIOR - UNICAMP
ARVIND NARAYAN VAIDYA - UFRJ
ARY ARMANDO PEREZ JUNIOR - UNICAMP
BERT SCHROER - UFES
BRUNO CARMINE CASSINO - UFJF
BRUNO G. CARNEIRO DA CUNHA - IFUSP
CARLA GOBEL BURLAMAQUI DE MELLO - CBPF
CARLOS A. A DE CARVALHO FILHO - UFRJ
CARLOS A. SANTOS DE ALMEIDA - UFCE
CARLOS ANTONIO DE SOUSA PIRES - IFT
CARLOS ENRIQUE NAVIA OJEDA - UFF
CARLOS FARINA DE SOUZA - UFRJ
CARLOS JAVIER SOLANO - CBPF
CARLOS MARIA NAON - LA PLATA
CARLOS OURIVIO ESCOBAR - IFUSP
CAROLA DOBRIGKEIT CHINELLATO - UNICAMP
CESAR PINHEIRO NATIVIDADE - UNESP-GUAR
CLAUDIO ANAEL GOMES SASAKI - CBPF
CLAUDIO GONCALVES CARVALHAES - UFF
CLAUDIO MANOEL GOMES DE SOUSA - UNB
CLISTENIS PONCE CONSTANTINIDIS - IFT
CRISTIANE GRALA ROLDAO - IFT
CRISTIANE MOURA LIMA DE ARAGAO - IFUSP
DANIEL ALBERTO GOMEZ DUMM - LA PLATA
DANIEL CARLOS CABRA - LA PLATA
DANIEL GUILHERME GOMES SASAKI - CBPF
DANIEL GUSTAVO BARCI - UFRJ
DANIEL HEBER THEODORO FRANCO - UFMG
DANIEL MULLER - IFUSP
DANIELLE MAGALHAES MORAES - UFRJ
DENIS DALMAZI - UNESP-GUAR
DENIS G. CREASOR MCKEON - U.ONTARIO
DICKSON CAPORE GOULART - UFRGS
DIONISIO BAZEIA FILHO - UFPB
DMITRI MAKSIMOVITCH GITMAN - IFUSP
EDISON HIROYUKI SHIBUYA - UNICAMP
EDUARDO CANTERA MARINO - PUC/RJ
EDUARDO GUERON - UNICAMP
EDUARDO SILVA MOREIRA LIMA - UFCE
EDUARDO SOUZA FRAGA -
EDUARDO VALENTINO TONINI - UFES
EDUARDO VASQUEZ CORREA SILVA - CBPF
ELIEZER BATISTA - IFT
EMMANUEL ARAUJO PEREIRA - UFMG
ERASMO MADUREIRA FERREIRA - UFRJ
ERICA RIBEIRO POLYCARPO - UFRJ
EUGENE LEVIN - CBPF
EUGENIO RAMOS BEZERRA DE MELLO - UFPB
EVERTON M. CARVALHO DE ABREU - UFRJ
FERNANDO M. L. DE A. JUNIOR - UFRJ
FERNANDO SILVEIRA NAVARRA - IFUSP
FERNANDO TADEU CALDEIRA BRANDT - IFUSP
FILADELFO CARDOSO SANTOS - UFRJ
FLAVIA CIRAUDO MAXIMO - PUC/RJ
FLAVIO GIMENEZ ALVARENGA - UFES
FLAVIO IMBERT DOMINGOS - UCP
FRANCISCO CARLOS PINHEIRO NUNES - UFES
FRANCISCO EUGENIO M DA SILVEIRA - IFT
FRANCISCUS JOZEF VANHECKE - UFRJ
FRANZ PETER ALVES FARIAS - UFBA
GALEN MIHAYLOV SOTKOV - UFRJ
GASTAO INACIO KREIN - IFT
GERARDO HERRERA - CBPF
GIL DA COSTA MARQUES - IFUSP
GILMAR DE SOUZA DIAS - UFES
GILVAN AUGUSTO ALVES - CBPF
GINO NOVALIS JANAMPA ANANOS - CBPF
GUILHERME DE BERREDO PEIXOTO - CBPF
GUILLERMO GONZALEZ - UNICAMP
HEBE QUEIROZ PLACIDO - UFBA
HELIO MANOEL PORTELLA - UFF
HELIO NOGIMA - UNICAMP
HENRIQUE BOSCHI FILHO - UFRJ
HERMAN JULIO MOSQUERA CUESTA - INPE
HERMES ALVES FILHO - UFRJ
HERON CARLOS DE GODOY CALDAS - UFMG
HUGH ELLIOT MONTGOMERY - FERMILAB
HUGO R. CHRISTIANSEN - LA PLATA
HUMBERTO DE MENEZES FRANCA - IFUSP
I. C. MOREIRA - UFRJ
IRAZIET DA CUNHA CHARRET - UFF
IVAN JOSE LAUTENSCHLEGUER - IFT
JAIR LUCINDA - UFPR
JAIR VALADARES COSTA -
JANILO SANTOS - UFRN
JOAO CARLOS ALVES BARATA - IFUSP
JOAO CARLOS COSTA DOS ANJOS - CBPF
JOAO JOSE CALUZI - UFES
JOAO RAMOS TORRES DE MELLO NETO - CBPF
JORGE ABEL ESPICHAN CARRILLO - UNICAMP
JORGE ANANIAS NETO - UFJF
JORGE EDUARDO CIEZA MONTALVO - UERJ
JORGE H. COLONIA BARTRA - UNICAMP
JORGE M. CARVALHO MALBOUISSON - IFUSP

JOSE ABDALLA HELAYEL-NETO - CBPF
JOSE ALEXANDRE NOGUEIRA - UFES
JOSE AUGUSTO CHINELLATO - UNICAMP
JOSE CARLOS BRUNELLI - IFUSP
JOSE DANIEL EDELSTEIN - LA PLATA
JOSE DE SA BORGES FILHO - UFRJ
JOSE FRANCISCO GOMES - IFT
JOSE HELDER LOPES - UFRJ
JOSE LUIS BOLDO - IFT
JOSE LUIZ ACEBAL FERNANDES - UFMG
JOSE LUIZ MATHEUS VALLE - CBPF
JOSE MANOEL DE SEIXAS - UFRJ
JOSE MARIANO GRACIA-BONDIA - U. C. RICA
JOSE MONTANHA NETO - UNICAMP
JOSE NOGALES - UFF
JOSE ROBERTO MARINHO - LIV_USP
JOSE R. SOARES DO NASCIMENTO - IFUSP
JOSE TADEU DE SOUZA PAES - UFPA
JUAREZ CAETANO DA SILVA - CEFET/BA
JULIANA RITA FLEITAS - UNICAMP
JULIO CESAR FABRIS - UFES
JULIO MIRANDA PUREZA - UDESC
JUSSARA M. DE MIRANDA - CBPF
KALED DECHOUM - IFUSP
LEANDRO SALAZAR DE PAULA - UFRJ
LEON RICARDO URURAHY MANSSUR - CBPF
LEONARDO FOGEL - UCP
LEONIDAS SANDOVAL JUNIOR - EXTERIOR
LOURDES(BRADESCO) - BRADESCO
LUCIENE PONTES FREITAS - IFT
LUIS ALFREDO ANCHORDOQUI - LA PLATA
LUIS ANTONIO C PEREIRA DA MOTA - CBPF
LUIS ANTONIO CABRAL - IFUSP
LUIS CARLOS MALACARNE - FUEM
LUIS EDUARDO SALTINI - IFUSP
LUIZ AMERICO DE CARVALHO - UNICAMP
LUIZ C. MARQUES DE ALBUQUERQUE - IFUSP
LUIZ CLAUDIO QUEIROZ VILAR - CBPF
LUIZ EDUARDO SILVA SOUZA - UFRJ
LUIZ FERNANDO BLOOMFIELD TORRES - UFRJ
LUIZ VICTORIO BELVEDERE - UFF
M. SCHIFFER - UNICAMP
MANOEL F. BORGES NETO - UNESP-SJRP
MANOEL M. FERREIRA JUNIOR - UNICAMP
MANOELITO MARTINS DE SOUZA - UFES
MANUEL MAXIMO B M DE OLIVEIRA - UFF
MARCELO A. LEIGUI DE OLIVEIRA - UNICAMP
MARCELO BATISTA HOTT - UNESP-GUAR
MARCELO BYRRO RIBEIRO - CNPQ
MARCELO COSTA DE LIMA - CBPF
MARCELO DE MOURA LEITE - IFUSP
MARCELO DE O. TERRA CUNHA - UNICAMP
MARCELO DE OLIVEIRA SOUZA - UENF
MARCELO EVANGELISTA DE ARAUJO - UNB
MARCELO GLEISER - D. COLLEGE
MARCELO JOSE REBOUCAS - CBPF
MARCELO MARIA DE FRANCIA - LA PLATA
MARCELO MORAES GUZZO - UNICAMP
MARCELO OTAVIO CAMINHA GOMES - IFUSP
MARCELO SAMUEL BERMAN - INPE
MARCIA GONCALVES DO AMARAL - UFF
MARCIO JOSE MENON - UNICAMP
MARCIO LIMA DE SOUZA - IFUSP
MARCO ANTONIO DE ANDRADE - CBPF
MARCONY SILVA CUNHA - CBPF
MARCOS BENEVENUTO JARDIM - UNICAMP
MARCUS VENICIUS COUGO PINTO - UFRJ
MARGARIDA M. RODRIGUES NEGRAO - UFRJ
MARIA ALINE BARROS DO VALE - UFRJ
MARIA APARECIDA B. P. GENNARI - SBF
MARIA B. DE LEONE GAY DUCATTI - UFRGS
MARIA DE FATIMA ALVES DA SILVA - UFF
MARIA LUIZA BEDRAN - UFRJ
MARIA TERESA C DOS SANTOS THOMAZ - UFF
MARINA NIELSEN - IFUSP
MARIO EVERALDO DE SOUZA - UFSE
MARIO NOVELLO - CBPF
MARTA LILIANA TROBO - LA PLATA
MARTHA CHRISTINA MOTTA DA SILVA - CBPF
MARTIN FLECK - UFRGS
MAURO SERGIO GOES NEGRAO - CBPF
MAXWEL GAMA MONTEIRO - UCP
MIKAEL BERGGREN - UFRJ
MIRIAM GANDELMAN - CBPF
MIRIAN BATISTA - UNICAMP
MOACYR HENRIQUE GOMES E. SOUZA - CBPF
N. SANTOS - ON
NATHAN BERKOVITS - IFUSP
NAZIRA ABACHE TOMIMURA - UFF
NELSON RICARDO DE FREITAS BRAGA - UFRJ
NEUSA LUCAS MARTIN - SBF
NIKOLAI KUROPATKIN - IFUSP
NOZIMAR DO COUTO - UFRJ
ODYLIO DENYS DE AGUIAR - INPE
OSCAR JOSE PINTO EBOLI - IFUSP
OSWALDO MONTEIRO DEL CIMA - CBPF
OZEMAR SOUTO VENTURA - CBPF
PATRICIO A. L. SOTOMAYOR - UNICAMP
PAULO ALEX DA SILVA CARVALHO - UNICAMP
PAULO CESAR BEGGIO - UNICAMP
PAULO CESAR DA ROCHA - UFRJ
PAULO DE FARIA BORGES - UFRJ
PAULO JOSE SENA DOS SANTOS - UFRJ
PAULO ROBERTO DE ALMEIDA SACOM - UFRJ
PAULO ROBERTO VERONEZE - FUEM
PAULO SERGIO KUHN - UFRGS
PAULO SERGIO RODRIGUES DA SILVA - IFT
PEDRO CUNHA DE HOLANDA - UNICAMP
PEDRO PACHECO DE QUEIROZ FILHO - UFRJ
PREM PRAKASH SRIVASTAVA - CBPF
R. JACKIW - MIT
RAFAEL DE LIMA RODRIGUES - UFPB
RAFAEL NUNES THESS - UCP
RAIMUNDO MUNIZ TEIXEIRA FILHO - IFUSP
RANDALL GUEDES TEIXEIRA - IFT
REGINA CELIA ARCURI - CBPF
REGINA HELENA CEZAR MALDONADO - UFF
REGINA MARIA RICOTTA - UNESP
REINALDO LUIZ CAVASSO FILHO - UFPR
RENATA ZUKANOVICH FUNCHAL - IFUSP
RENATO KLIPPERT BARCELLOS - CBPF
RENATO MELCHIADES DORIA - UCP
RENATO PORTUGAL - CBPF
RENIO DOS SANTOS MENDES - FUEM
RICARDO MORITZ CAVALCANTI - PUC/RJ
RICARDO R. LANDIM DE CARVALHO - CBPF

RITA LAVINIA TORRIANI - SBF
ROBERTO COLISTETE JUNIOR - UFES
ROBERTO PEREIRA ORTIZ - UFES
ROBERVAL WALSH BASTOS RANGEL - UFRJ
ROBSON NASCIMENTO SILVEIRA - UFES
RODOLFO ALVAN CASANA SIFUENTES - CBPF
ROGERIO DOS SANTOS GOMES - UFRJ
ROGERIO ROSENFELD - IFT
ROMAN PAUNOV - CBPF
RONALD CINTRA SHELLARD - CBPF
RONALDO SILVA THIBES - UFRJ
RUBENS FREIRE RIBEIRO - UFPB
RUBENS L. PINTO GURGEL DO AMARAL - UFF
RUDNEI DE OLIVEIRA RAMOS - UERJ
SAMUEL MACDOWELL - UFRJ
SAMUEL ROCHA DE OLIVEIRA - UNB
SANDRA LILIANA SAUTU - CBPF
SANDRO SILVA E COSTA - IFT
SANTIAGO E. PEREZ BERGLIAFFA - LA PLATA
SEBASTIAO CASSEMIRO DE F. NETO - IFUSP
SERGIO JOFFILY - CBPF
SERGIO LUIZ CARMELO BARROSO - UNICAMP
SERGIO MARTINS DE SOUZA - UFRJ
SERGIO MORAIS LIETTI - IFT
SERGIO V. DE BORBA GONCALVES - UFES
SERGUEI GAVZILOV - IFUSP
SIDINEY DE ANDRADE LEONEL - UFJF
SILVESTRE RAGUSA - IFQSC
SILVIO JOSE RABELLO - UFRJ
SILVIO PAOLO SORELLA - CBPF
SOLANGE DA FONSECA RUTZ - LNCC
SONIA GAONA JURADO - UFMG
STENIO WULCK ALVES DE MELO - UFRJ
STOIAN IVANOV ZLATEV - UFSE
TANIA GLAUCIA DARGAM - UFRJ
TATIANA DA SILVA - UFRJ
UBIRAJARA FERRAIOLO WICHOSKI - IFUSP
VAN SERGIO ALVES - UFPA
VERISSIMO MANOEL DE AQUINO - UEL
VICTOR PAULO BARROS GONCALVES - UFRGS
VITOR EMANUEL RODINO LEMES - CBPF
VITORIO ALBERTO DE LORENCI - CBPF
VLADMIR KOPENKIN - UNICAMP
WALDEMAR M. DA SILVA JUNIOR - UFF
WELLINGTON DA CRUZ - UNICAMP
WILSON OLIVEIRA - UFJF
WINDER ALEXANDER DE MOURA MELO - CBPF
WLADIMIR SEIXAS - UNESP
XIN-HENG GUO - CBPF
XUN XUE - UNB
YARA DO AMARAL COUTINHO - UFRJ
ZIELI DUTRA THOME FILHO - UFRJ